Proceedings of the VIIIth International Workshop on Heavy Quarks and Leptons HQL06

October 2006

Deutsches Museum, Munich

Editors
S. Recksiegel, A. Hoang, S. Paul

Organized by the Physics Department of the Technical University of Munich
and the Max-Planck Institute for Physics, Munich

Foreword

With the rich harvest of the two B-factories Belle and BaBar, the Cornell charm factory and the Tevatron, the field of heavy quarks is currently receiving much attention and has turned into a field of precision physics. The combination of both experimental work and theoretical efforts, have revealed almost perfect consistency with the Standard Model. In fact, the lack of significant deviations and absence of new phenomena have led to much theoretical speculations on the energy scale for the necessary extensions of the Standard Model.
In the field of leptons, the attention has strongly shifted to the sector of neutrinos. The recent observations of neutrino oscillations have opened the field for new ideas, and many new experimental efforts are either ongoing or planned. We may expect many new surprises on both the nature of the neutrino and the completion of the mixing matrix in the lepton sector.

The 2006 edition of the Conference on Heavy Quarks and Leptons (HQL2006) has been organized by the groups E18 and T31 from the Physics Department of the Technische Universität München and with the help of the Max-Planck-Institut für Physik. It was the 8^{th} edition in the biannual series, founded in 1993 by Laboratori Nazionali di Frascati with the aim to bring together experts in the fields of heavy quarks and leptons and to present the state-of-the-art of this area of research. In particular, junior physicists have been encouraged to give presentations, next to talks given by senior researchers.

The present conference took place in the impressive environment of the hall of fame ('Ehrensaal') of the German Museum of Science and Technology ('Deutsches Museum') in which statues and busts of many famous scientists from the past are on continuous display. Under the supervision of Heisenberg, Hahn, Einstein and Planck, 47 talks were presented, grouped into 9 session, which are also reflected in the organization of this collection of proceedings articles.

We would like to thank the international advisory committee for the help in building the scientific program and the effort to guarantee the high scientific level observed throughout HQL2006. We thank the speakers for their excellent presentations and their contributions to these proceedings. In fact the prices 'Heavy Quarks and Leptons Young Scientists Award' for the best presentations by a young scientist were awarded to Cecilia Tarantino (1^{st} place), Stephanie Hansmann-Menzemer (2^{nd} place) and to Andreas Weiler and Lucio Cerrito (jointly holding the 3^{rd} place)

We would like to thank the local organizing committee for their dedication to make HQL2006 a successful conference. We are indebted to the staff of the groups T31 and E18 of the Physics Department as well as to the Max-Planck-Institut für Physik (Werner-Heisenberg-Institut).

The next edition of this conference series will take place in Melbourne (Australia) in 2008. We are looking forward to many more fruitful results, possibly with first insights from the LHC.

Stephan Paul
Chairman, Organizing Committee

Acknowledgements

As always, many contributions are necessary in order to provide a smooth and successful meeting. Not all can be mentioned but a few should be spelled out.

We would like to thank the German Ministry for Education and Science (BMBF), the Max-Planck Institute für Physik and the Maier-Leibnitz Laboratory for Nuclear, Particle and Astroparticle Physics in Munich for their financial support of this conference. In addition we would like to thank the Deutsches Museum for the support and hospitality.

Special thanks go to Karin Frank, Anna-Maria Dinkelbach, Bernhard Ketzer, Moritz Hantel, Stefan Recksiegel (all TUM), Carola Reinke (MPI) and M. Loyer (Deutsches Museum) for their strong engagement and their continuous support during the planning and the running of the conference. Many thanks also go the numerous physics students from the Technische Universität, who have helped the conference going.

We thank LITEC-Computer GmbH for their donation in the context of the Young Scientists Award.

Stephan Paul
Chairman, Organizing Committee

Conference Organization

International Advisory Committee

Angel López	Univ. of Puerto Rico, USA
Ikaros Bigi	Univ. of Notre Dame, USA
Brad Cox	Univ. of Virginia, USA
Stephan Paul	TU Muenchen, Germany
Andrzej Buras	TU Muenchen, Germany
Stefano Bianco	INFN-Frascati, Italy
Konrad Kleinknecht	Univ. Mainz, Germany
Giancarlo D'Ambrosio	INFN-Napoli, Italy
Franco L. Fabbri	INFN-Frascati, Italy
Alberto Reis	CBPF, Brazil
Gianpaolo Bellini	Univ. Milano, Italy
Joel Butler	Fermilab, USA
Peter Dornan	Imperial College London, UK
Vera Luth	SLAC, USA
Hitoshi Yamamoto	Tohoku Univ. Japan
Ritchie Patterson	Cornell Univ. USA
Adam Para	Fermilab, USA
Franco Grancagnolo	INFN-Lecce, Italy

Local Organizing Committee

A. Buras	Technical University of Munich
A. Dinkelbach	
K. Frank	
J. Friedrich	
B. Ketzer	
R. Kuhn	
S. Paul	(conference chairman)
S. Recksiegel	
A. Hoang	Max-Planck Institute for Physics, Munich

Contents

Heavy Quark Spectroscopy

Heavy Quark Spectroscopy

New states: ccbar and charmed mesons	*T. Lesiak*	
Recent Results in Bottomonium Physics	*T. Pedlar (CLEO)*	
SELEX results	*J. Engelfried (Selex)*	
NRQCD and Quarkonia	*N. Brambilla*	
B lifetimes, CPV and rare decays	*A. Cano (CDF)*	(no contribution)
Charmonium Physics with PANDA	*J. Ritman*	

New charm resonances

Tadeusz Lesiak
Institute of Nuclear Physics
Polish Academy of Sciences
ul. Radzikowskiego 152
31-142 Kraków, Poland

1 Introduction

In the last five years we have witnessed a renaissance of charm spectroscopy. Several new charmed states have been observed, using data samples collected by so-called B-factories i.e. e^+e^- storage rings dedicated to the studies of CP violation in the sector of the beauty quark. These machines are running essentially at the center-of-mass (CMS) energy corresponding to the maximum of the $\Upsilon(4S)$ resonance (10.58 GeV/c^2). There are three such accelerators and detectors, which are currently taking data. The oldest one, which contributed a lot of to the heavy flavour physics in the past twenty years, is the CLEO apparatus [1,2] at the CESR [3] storage-ring (Cornell, USA). After collecting the data sample of 16 fb^{-1}, the CLEO collaboration has moved since 2003 to the lower energy working point corresponding to the maximum of the $\psi(3770)$. The other two detectors working at B-factories: the BaBar [4] at PEP-II [5] (Stanford, USA) and Belle [6] at KEKB [7] (Tsukuba, Japan) have collected in the last few years enormous data samples corresponding to 370 fb^{-1}(630 fb^{-1}), respectively. The KEKB is, in fact, the record holder as far as the luminosity is concerned with its peak value of 1.65×10^{34} cm^{-2}s^{-1}. It is worthwile to stress here that the cross-section for the continuum process $e^+e^- \to c\overline{c}$ (1.3 nb) is comparable to the one for the reaction $e^+e^- \to \Upsilon(4S) \to B\overline{B}$ (1.1 nb). As a result, B-factories can be safely considered as c-factories too. Moreover, charmed hadrons can he reconstructed here relatively easy, due the 'clean' environment provided by e^+e^- collisions.

This paper is divided into several chapters, each one of them discussing the observation of an individual new state and entitled with its name. The following new meson-like charmed hadrons are talked over: $X(3872)$, $Y(3940)$, $X(3940)$, $\chi'_{c2}(3930)$, $Y(4260)$, h_c and the $c\overline{s}$ states D_{sJ}. Then the following new observations of charmed barions will be described: $\Sigma_c(2800)$, $\Lambda_c(2940)$, $\Xi_{cx}(2980)$, $\Xi_{cx}(3077)$ and Ω_c^*.

2 X(3872)

The first new charmed resonance, marked as X(3872), was discovered by the Belle collaboration in 2003 [8] by analyzing exclusive decays[1] $B^+ \to \pi^+\pi^- J/\psi K^+, J/\psi \to l^+l^-$. The B mesons were reconstructed using two kinematical variables: the energy offset $\Delta E = \sum_i E_i - E_{beam}$ and the beam-constrained mass $M_{bc} = \sqrt{E^2_{beam} - \sum_i (\vec{p_i})^2}$, where E_i and $\vec{p_i}$ are the center-of-mass (CMS) energies and momenta of the selected B meson decay products and E_{beam} is the CMS beam energy. A very narrow peak in the invariant mass spectrum of the system $\pi^+\pi^- J/\psi$ was observed (Fig. 2) with a statistical significance above 10 σ. The mass of the resonance was determined to be $(3872.0 \pm 0.6 \pm 0.5)$ MeV/c^2 and a width below 2.3 MeV (90% C.L.), which is consistent with the detector resolution.

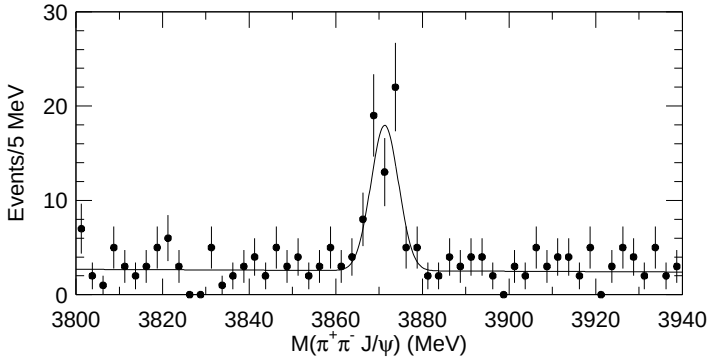

Figure 1: The mass distribution of $J/\psi\pi^+\pi^-$ for the X(3872) resonance, as measured by Belle collaboration.

The observation of $X(3872)$ was very quickly confirmed by the CDF [9], D0 [10] and BaBar [11] experiments. At first glance the $X(3872)$ would appear as an ideal candidate for one of the, unobserved yet, charmonium states. Among $(c\overline{c})$ states, the ones expected to be closest in mass to X are those belonging to the multiplets $1D$ and $2P$ multiplets [12]– [15]. However, it soon turned out that the, discussed below, properties of none of these states are in agreement with measured properties of $X(3872)$. This fact stimulated the development of several theoretical models assuming the exotic nature of this new resonance. In particular, the coincidence of the X mass with the $D^0\overline{D^{*0}}$ threshold i.e. (3871.3 ± 1.0) MeV/c^2 has prompted many theoretical speculations that X(3872) may be a so-called deuson [16]– [19] i.e. a loosely bound molecular state of these two mesons or a tetraquark i.e. a tightly bound open charm diquark-antidiquark state [20, 21]. Other models attributed the $X(3872)$ as a $(c\overline{c})$-

[1] charge conjugate modes are included everywhere, unless otherwise specified.

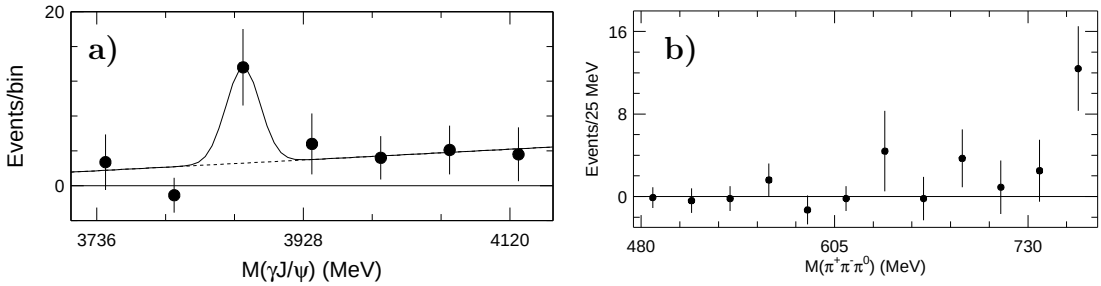

Figure 2: The yield of B mesons from the decay **a)** $B^0 \to \gamma J/\psi K$, in bins of the $\gamma J/\psi$ invariant mass and **b)** $B^0 \to \pi^+\pi^-\pi^0 J/\psi K$, in bins of the $\pi^+\pi^-\pi^0$ invariant mass, determined by the Belle collaboration from fits to the ΔE and M_{bc} distributions.

gluon hybrid meson [22], a glueball with a ($c\overline{c}$) admixture [23] or the so called threshold cusp effect [24].

The Belle collaboration, has also provided the first evidence for two new decay modes of the $X(3872)$: $X \to \gamma J/\psi$ and $X \to \pi^+\pi^-\pi^0 J/\psi$ [25], observed in exclusive B meson decays to the final states $\gamma J/\psi K$ and $\pi^+\pi^-\pi^0 J/\psi K$, respectively. The yield of the decay $B \to \gamma J/\psi K$ plotted in bins of the $\gamma J/\psi$ invariant mass (Fig. 2**a)**) exhibits an excess of 13.6 ± 4.4 events (statistical significance of 4σ). This evidence was was recently confirmed by the BaBar collaboration [26] with the signal yield of 19.2 ± 5.7 events (3.4σ). The observation of this decay establishes unambiguously that the charge-conjugation parity of the X(3872) is positive and indicates the presence of the $c\overline{c}$ component in its wave function. The partial width ratio $\Gamma(X \to \gamma J/\psi)/\Gamma(X \to \pi^+\pi^- J/\psi)$ amounts to 0.14 ± 0.05. This result is, in particular, in contradiction with the χ'_{c1} (1^{++} charmonium) assignment for X as in this case a value around 40 would be expected. The second decay mode $X \to \pi^+\pi^-\pi^0 J/\psi$ was found to be dominated by the sub-threshold decay $X \to \omega^* J/\psi$. This is motivated by the fact that the yield of B mesons plotted in bins of the $\pi^+\pi^-\pi^0$ invariant mass (Fig 2**b)**) inside of the signal region from the decay $X \to \pi^+\pi^-\pi^0 J/\psi$ is consistent with zero except for the $M(\pi^+\pi^-\pi^0) > 750$ MeV/c^2. There, the excess of 12.4 ± 4.1 events (4.3σ) is observed. The ratio of branching fractions $\mathrm{B}(X \to \pi^+\pi^-\pi^0 J/\psi)/\mathrm{B}(X \to \pi^+\pi^- J/\psi)$. was measured to be $1.0 \pm 0.4 \pm 0.3$, which implies a large violation of isospin symmetry. This in turn points at the presence of both $u\overline{u}$ and $d\overline{d}$ pairs in the X wave function. The overall properties of the above two decays are in reasonable agreement with the $D^0\overline{D}^{0*}$ molecule hypothesis.

The Belle collaboration also attempted to determine the J^{PC} quantum numbers of the X(3872) [27] by studying the angular distributions of the decay $X \to \pi^+\pi^- J/\psi$, as suggested by J.L. Rosner [28] Among the twelve possible J^{PC} assignments, half (0^{--}, 0^{+-}, 1^{--}, 1^{+-}, 2^{--} and 2^{+-}) may be discarded due to their negative charge conjugation-parity. The assignments 0^{-+} and 0^{++} are strongly disfavoured by the

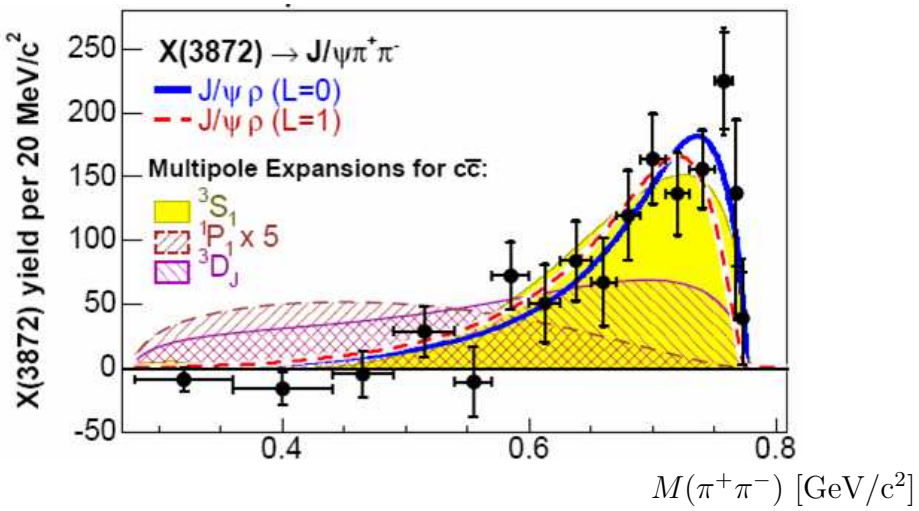

Figure 3: The dipion mass spectrum for the $X(3872)$ (data points), as measured by the CDF collaboration, together with fits to different J^{PC} hypotheses.

analysis of angular distributions. The additional two odd-parity possibilities: 1^{-+} and 2^{-+} are discarded as for them the dipion invariant mass spectrum is expected to be much softer to compare with the data. The above considerations leave only two assignments: 1^{++} and 2^{++} as the possible J^{PC} of X. The decay angular distributions and $\pi^+\pi^-$ angular distribution agree well with the 1^++ hypothesis.

The assignment 2^{++} was disfavoured by the recent observation by Belle [29] of a near-threshold enhancement in the $D^0\overline{D^0}\pi^0$ invariant mass in $B \to KD^0\overline{D^0}\pi^0$ decays. It corresponds to 23.4 ± 5.6 signal events (6.4σ) at mass $(3875.4 \pm 0.7 \pm 1.1)$ MeV/c^2 which is around two standard deviations higher than the world average for $X(3872)$ [30]. Taking for granted that the observed near-threshold enhancement is due to the $X(3872)$, the decay of a spin 2 state to three pseudoscalars ($D^0\overline{D^0}\pi^0$) would require at least one pair of them to be in a relative D wave. In such a configuration the near threshold production would be strongly suppressed by a centrifugal barrier.

The CDF collaboration [31] has recently studied the spin-parity of $X(3872)$ using a high-statistics sample of ≈ 3000 events of $X(3872) \to \pi^+\pi^- J/\psi$. The shape of the $\pi^+\pi^-$ invariant mass distribution was compared with the predictions corresponding to all relevant J^{PC} values. (Fig. 2). It was found that both 1^{++} and 2^{-+} assignments fit reasobably the data.

Collecting the above information it seems the most plausible that X(3872) is a deuson. This conjecture is supported in particular by the pattern of its decay modes and the favoured spin-parity assignment 1^{++}.

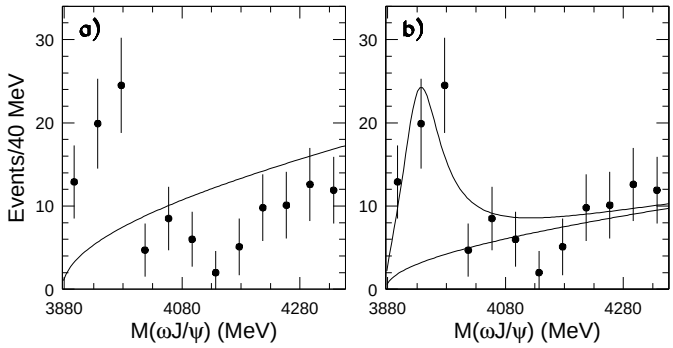

Figure 4: $B^+ \to K^+\omega J/\psi$ signal yields vs $M(\omega J/\psi)$ as determined by the Belle collaboration. The curve in (a) shows the result of a fit that includes only a phase-space-like threshold function. The curve in (b) corresponds to the result of a fit that includes an S-wave Breit-Wigner resonance term.

3 Y(3940)

In 2004 The Belle collaboration observed another new state, denoted as Y(3940) and produced in $B^+ \to K\omega J/\psi$ decays [32]. In this study events with $M(K\omega) < 1.6$ GeV/c^2 were rejected in order to remove the contribution from $K^* \to Kw$ decays. A fit to the $\omega J/\psi$ invariant-mass distribution (Fig.4) yielded a signal of 58 ± 11 events (8.1σ) corresponding to a mass of (3943$\pm$11$\pm$13) MeV/c^2 and the width (87$\pm$22$\pm$26) MeV.

Both mass and width of Y are in agreement with expectations for a radially excited charmonium state χ'_{cJ}. This interpretation is also strengthened by the observation of the corresponding $(b\overline{b})$ decay $\chi'_{b1} \to \omega\Upsilon(1S)$ [33]. Such a $(c\overline{c})$ state would, however, decay predominantly to $D\overline{D}^{(*)}$ pairs, which is not observed. Moreover, for the χ'_{cJ} hypothesis one would expect that $\mathcal{B}(B \to K\chi'_{cJ}) < \mathcal{B}(B \to K\chi_{cJ}) = 4\times10^{-4}$. Taking into account the value of the product $\mathcal{B}(B \to KY)\mathcal{B}(Y \to \omega J/\psi) = (7.1\pm1.3\pm3.1)\times 10^{-5}$, determined by Belle, this implies that $\mathcal{B}(Y \to \omega J/\psi) > 12$ %. Such a value would seem exceptionally high for any charmonium state with a mass above $D\overline{D}^{(*)}$ threshold.

The above drawbacks of the conventional charmonium interpretation of Y, in particular the lack of its decay to $D\overline{D}^{(*)}$ and a large $\mathcal{B}(Y \to \omega J/\psi)$, are in fact advantages while taking for granted the hypothesis of a $c\overline{c}$-gluon hybrid [34]. This is also supported by the lattice QCD calculations [35] which indicate that a partial width for the decay to $K\omega J/\psi$ are comparable to the value measured by Belle. However, the masses of $c\overline{c}$-gluon mesons predicted by these calculations [35]– [37] are between

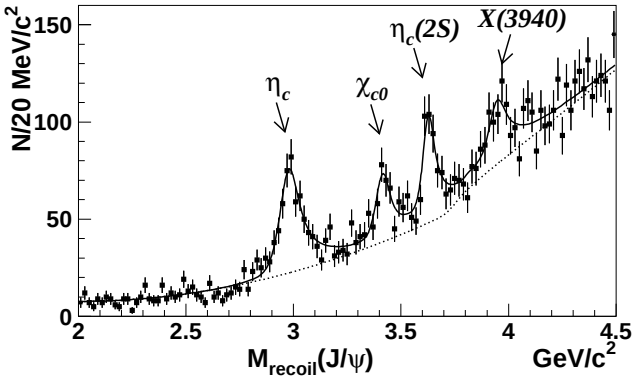

Figure 5: The distribution of masses recoiling against the reconstructed J/ψ measured by the Belle collaboration in inclusive $e^+e^- \to J/\psi X$ events. The four enhancements, from left to right, correspond to the η_c, χ_{c0}, $\eta_c(2S)$ and a new state $X(3940)$.

4300 and 4500 MeV/c^2 i.e. substantially higher than the measured value.

4 X(3940)

Yet another particle, marked as $X(3940)$ with the mass of 3940 MeV/c^2 was observed by the Belle collaboration in the process $e^+e^- \to J/\psi X$ [38]. Its signal was seen in the spectrum of the J/ψ recoil mass (Fig. 5) defined as $M_{recoil}(J/\psi) = \sqrt{(E_{CMS} - E^*_{J/\psi})^2 - (cp^*_{J/\psi})^2}/c^2$, where E_{CMS} is the center-of-mass energy of the event and $E^*_{J/\psi}$ ($p^*_{J/\psi}$) denote the CMS energy (momentum) of the J/ψ, respectively. The previous studies of this process reveiled the presence of three states: η_c, χ_{c0} and $\eta_c(2S)$. The new analysis, using significantly higher statistics, provided the observation of the fourth particle in the J/ψ recoil mass spectrum. Its mass was estimated to be $(3943 \pm 6 \pm 6)$ MeV/c^2 and and the width smaller than 52 MeV (90 % C.L.). The search for $X(3940)$ decay modes yielded the evidence for $X \to D^*\overline{D}$ ($\mathcal{B} = 96^{+45}_{-32} \pm 22$ %). No signal was observed for $X \to D\overline{D}$ ($\mathcal{B} < 41$ % (90 % C.L.)) and $X \to \omega J/\psi$ ($\mathcal{B} < 26$ % (90 % C.L.)) The properties of X(3940) match the expectations [15] of the 3^1S_0 charmonium state, denoted also as $\eta_c^{''}$.

It is appropriate to stress here that, in spite the same mass measured, it is extremely unlikely that the states $X(3940)$ and $Y(3940)$ coincide. The X(3940) decays to $D\overline{D^*}$ and does not decay to $\omega J/\psi$. for the Y(3940) the situation is reversed, as far as the above-mentioned decays are concerned.

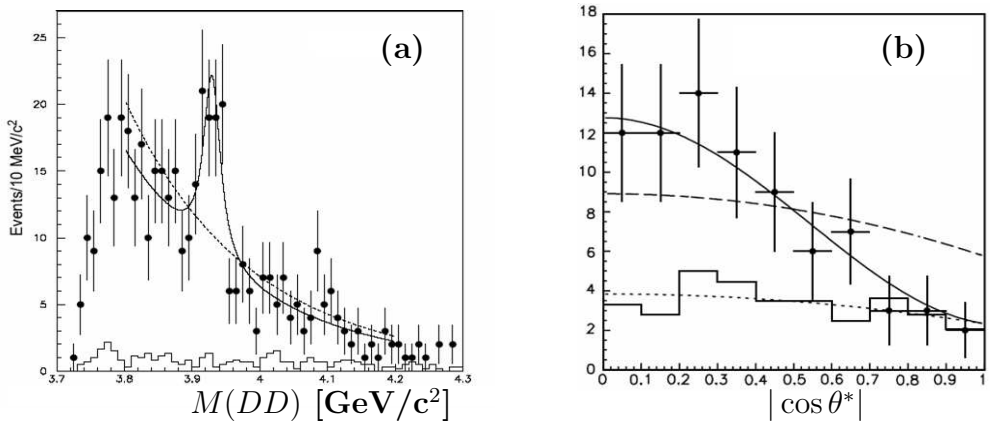

Figure 6: **(a)** Invariant mass distribution of $D\overline{D}$ pairs produced in two photon processes as measured by Belle. The solid (dashed) curve shows the fits with (without) a resonance component. The histogram corresponds to the distribution of the events from the D-mass sidebands. **(b)** The distribution of the angle θ^* of a D meson relative to the beam axis in the $\gamma\gamma$ CMS frame. The data points correspond to the $3.91 < M(D\overline{D}) < 3.95$ MeV/c^2 region. The solid histogram shows the yield of background scaled from $M(D\overline{D})$ sidebands. The solid and dashed curves represent expectations for spin-2 and spin-0 hypotheses, respectively. The dotted curve interpolates the non-peak background.

5 $\chi'_{c2}(3930)$

The Belle collaboration has also performed the search for the production of new resonances in the process $\gamma\gamma \to D\overline{D}$ [39]. Here the two-photon processes are studied in the "zero-tag" mode, where the final state electron and positron are not detected and the transverse momentum of the $D\overline{D}$ system is very small. The analysis yielded an observation of a new state, marked as $Z(3930)$, at the mass and width of $(3929\pm5\pm2)$ MeV/c^2 and $(29 \pm 10 \pm 2)$ MeV, respectively (Fig. 6 a)). The statistical significance of the signal amounted to 5.3σ. The product of the two-photon radiative width and branching fraction for the decay to $D\overline{D}$ was found to be $\Gamma_{\gamma\gamma} \times \mathcal{B}(Z(3930) \to D\overline{D}) = (0.18\pm0.05\pm0.03)$ keV. The properties of this new state match the expectations [15,40] for the radially excited $(c\overline{c})$ states χ'_{c0} and χ'_{c2}. A study of angular distribution of the D mesons in the $\gamma\gamma$ CMS frame showed that that spin-2 assignment is strongly favoured over the spin-0 hypothesis. Thus the state $Z(3930)$ can be safely interpreted as the χ'_{c2} 2^3P_2 charmonium.

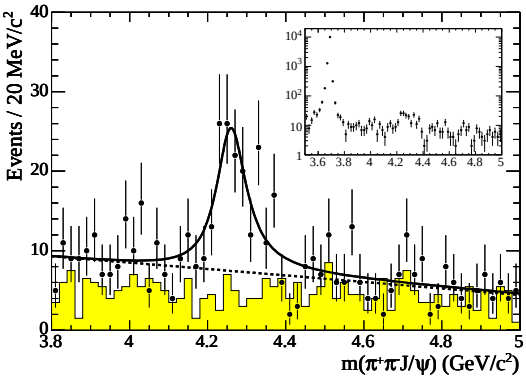

Figure 7: The $\pi^+\pi^- J/\psi$ invariant mass spectrum measured by BaBar in the range 3.8–5.0 GeV/c^2 and (inset) over a wider range that includes the $\psi(2S)$. The points represent the data and the shaded histogram corresponds to the scaled data from the J/ψ mass sidebands. The solid line shows the result of the single-resonance fit. The dashed curve represents the background component.

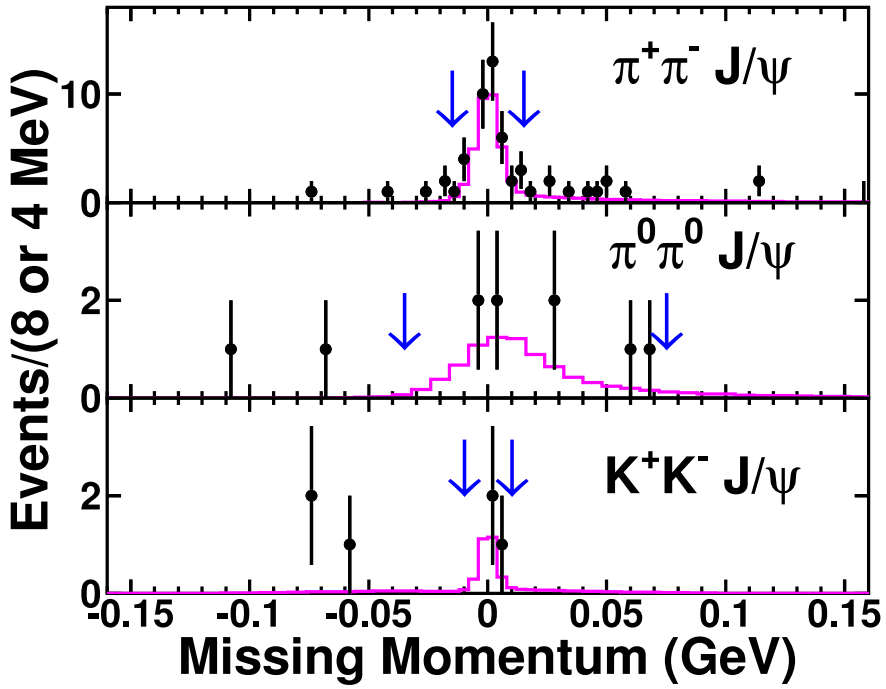

Figure 8: The missing momentum distribution measured by Cleo collaboration for $\pi^+\pi^- J/\psi$ (top), $\pi^0\pi^0 J/\psi$ (middle) and $K^+K^- J/\psi$ (bottom) in the data at $\sqrt{s} = 4.26$ GeV (data points) and the signal shape as predicted by MC simulation (histogram) scaled to the net signal size.

6 $Y(4260)$

The BaBar collaboration has studied initial-radiation (ISR) processes [41] $e^+e^- \to \gamma_{ISR}\pi^+\pi^- J/\psi$ and observed a broad resonance in the invariant mass spectrum of $\pi^+\pi^- J/\psi$ near 4.26 GeV/c^2(Fig. 7). The photon radiated from an initial e^+e^- collision is not detected directly. Since the new state, marked as $Y(4260)$, is produced in ISR events, its spin-parity is well defined as 1^{--}. The existence of $Y(4260)$ was soon confirmed by CLEO [42] and Belle [43] collaborations. The relevant parameters of this new state are collected in Table 1. It is worthwile to note that the values measured so far by three collaborations are only marginally consistent.

The CLEO collaboration has also provided the first observation of $Y(4260) \to \pi^0\pi^0 J/\psi)$ (5.1σ) and found the first evidence for $Y(4260) \to K^+K^- J/\psi)$ (3.7σ) [42] (Fig. 8). Simultaneously, the e^+e^- cross-sections at $\sqrt{s} = 4.26$ GeV were determined for $\pi^+\pi^- J/\psi$ and $\pi^0\pi^0 J/\psi$ final states to be $(58^{+12}_{-10} \pm 4)$ pb and $(23^{+12}_{-8} \pm 1)$ pb, respectively.

The observation of the $\pi^0\pi^0 J/\psi$ contradicts the hypothesis that Y is a $\chi_{cJ}\rho$ molecule [44]. The interpretation of Y as a baryonium state [45] is strongly disfavoured by the fact that the $\pi^0\pi^0 J/\psi$ rate is about half that of $\pi^+\pi^- J/\psi$. The $Y(4260)$ is located at the dip in $R(e^+e^- \to hadrons)$. Similar drop of the cross-section was also found by Belle in the exclusive reaction $e^+e^- \to D^{*+}D^{*-}$, measured as a function of the CMS energy using ISR events [46]. This dip could be accomodated as a result of $\psi(3S) - \psi(4S)$ interference, provided that $Y(4260)$ can be interpreted as the conventional charmonium state $\psi(4S)$ [47]. Then, however, the $\psi(3S)$ should exhibit a substantial coupling to $\pi^+\pi^- J/\psi$, which is not observed. Two other viable models describe the $Y(4260)$ as a tetraquark [48] or a $c\overline{c}$-gluon hybrid meson [49]–[51]. The unambiguos interpretation of $Y(4260)$ can be possibly obtained as a result of careful studies of its open-charm decays, in particular those with D meson (both S and P wave) pairs.

The BaBar collaboration has studied the exclusive production of the $D\overline{D}$ system ($D = D^0$ or D^+) through initial state radiation [52]. As seen in Fig 9, the $D\overline{D}$ mass spectrum shows a clear $\psi(3770)$ signal and two further structures, centered around 3.9 and 4.1 GeV/c^2. No evidence was found for $Y(4260) \to D\overline{D}$, leading to an upper

	BaBar	CLEO	Belle (preliminary)
Yield (significance)	125 ± 23 $(> 8\sigma)$	$14.1^{+5.2}_{-4.2}$ (4.9σ)	165^{+24+7}_{-22-23} $(> 7\sigma)$
Mass (MeV/c^2)	$4259 \pm 8^{+2}_{-6}$	$4283^{+17}_{-16} \pm 4$	$4295 \pm 10^{+11}_{-5}$
Width (MeV)	$88 \pm 23^{+6}_{-4}$	$70^{+40}_{-25} \pm 5$	133^{+26+13}_{-22-6}

Table 1: The parameters of the $Y(4260)$ resonance, as measured by BaBar, CLEO and Belle.

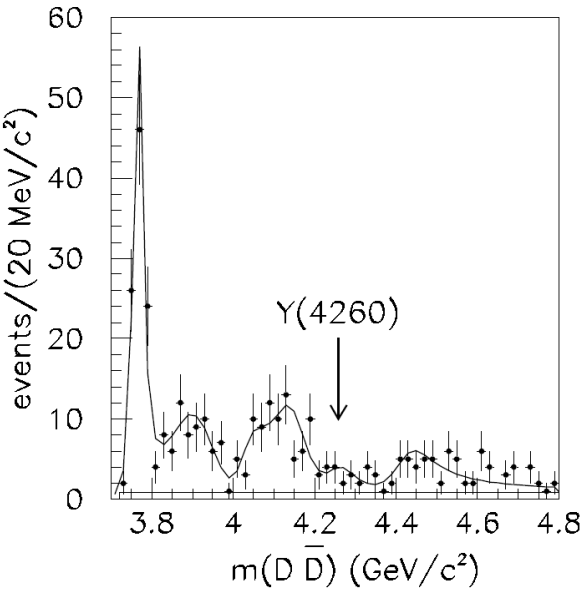

Figure 9: The $D\overline{D}$ mass spectrum for the ISR sample, as measured by BaBar. The arrow indicates the expected position of the $Y(4260)$.

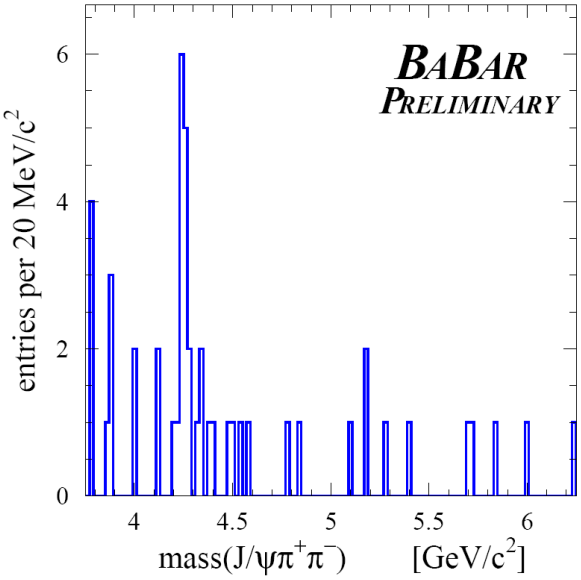

Figure 10: The $\pi^+\pi^- J/\psi$ mass spectrum for the ISR sample, as measured by BaBar in the analysis with the detection of the hard photon radiated from an initial e^+e^- collision.

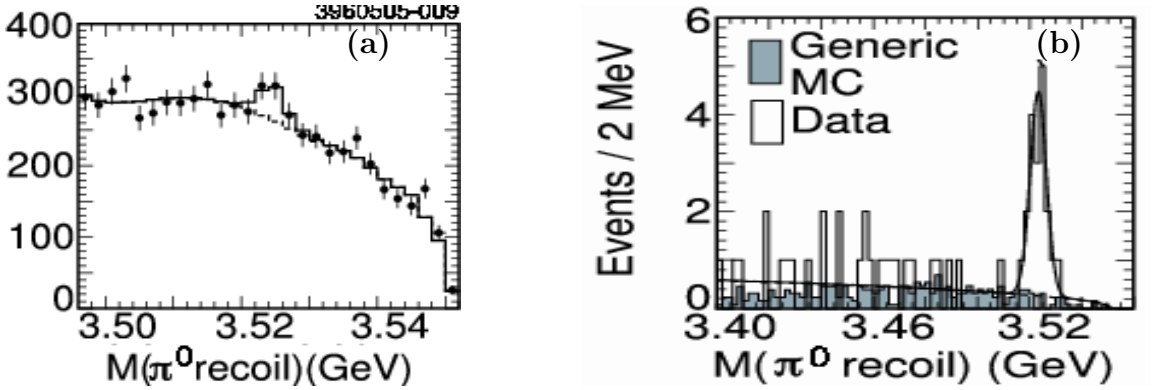

Figure 11: The recoil mass against π^0 for **(a)** inclusive (i.e. no reconstruction of the η_c) and **(b)** exclusive η_c reconstruction in the reaction $\psi(2S) \to \pi^0 h_c \to (\gamma\gamma)(\gamma\eta_c)$, as measured by CLEO collaboration.

limit $\frac{\mathcal{B}(Y(4260)\to D\overline{D})}{\mathcal{B}(Y(4260)\to \pi^+\pi^- J/\psi)} < 7.6$ (90 % C.L.). This number is over an order of magnitude smaller to compare with the value for the $\psi(3770)$ which makes the interpretation of $Y(4260)$ as a conventional $c\overline{c}$, rather doubtful.

The BaBar collaboration has also searched for the processes $e^+e^- \to (J/\psi\gamma\gamma)\gamma_{ISR}$ and $e^+e^- \to (J/\psi\pi^+\pi^-)\gamma_{ISR}$ [53], where the hard photon radiated from an initial electron-positron collision is directly detected. In the latter final state the signal of $Y(4260)$ was observed (Fig. 10). Its mass and width are consistent with the the values originally reported by BaBar in [41]. In the $(J/\psi\gamma\gamma)\gamma_{ISR}$ final state, no events were found in the $Y(4260)$ mass region in the $J/\psi\eta$, $J/\psi\pi^0$ and $\chi_{c2}\gamma$ distributions.

7 h_c

The CLEO collaboration has observed the h_c ($^1P1$) state of charmonium in the reaction $\psi(2S) \to \pi^0 h_c \to (\gamma\gamma)(\gamma\eta_c)$ [54]. The signal in the π^0 recoil mass was observed both for the inclusive reaction (Fig. 11 a)), where the decay products of the η_c are not identified, and for exclusive processes (Fig. 11 b)), in which η_c decays are reconstructed in seven hadronic decay channels ($\sim$ 10 % of all η_c decays). The results of the inclusive and exclusive analyses were combined and yielded $M(h_c) = (3524.4 \pm 0.6 \pm 0.4)$ MeV/c^2 (in agreement with [55]) and $\mathcal{B}(\psi(2S) \to \pi^0 h_c) \times \mathcal{B}(h_c \to \gamma\eta_c) = (4.0 \pm 0.8 \pm 0.7) \times 10^{-4}$. Together with the well known mass value of the ^3P_J centroid ($< M(^3P_J) >= (3525.36 \pm 0.06)$ MeV/c^2 [30]), it has allowed to determine for the first time the hyperfine splitting for the P states of charmonium: $\Delta M_{hf}(< M(^3P_J) > - M(^1P_1) = (+1.0 \pm 0.6 \pm 0.4)$ MeV/c^2. This agrees well with the simplest calculations assuming the potential composed of a vector Coulombic ($\sim r$) and a scalar confining ($\sim 1/r$) terms. They are both spin independent and as a

result the hyperfine splitting should be zero. Larger values of the ΔM_{hf} could be accomodated only after the inclusion of the higher-order corrections [56, 57], which is not confirmed by the CLEO measurement.

8 D_{sJ} mesons

The symbol D_{sJ} is often used to mark orbital excitations of the $c\overline{s}$ bound states. Four such P-wave mesons are expected in the framework of potential models, inspired by the heavy quark symmetry (HQS) [58, 59]. They can be naturally splitted in two doublets differing in the orbital momentum of light degrees of freedom (j_q). The states with $j_q = 3/2$ are predicted to be narrow and were identified as the $D_{s1}(2536)$ (Argus) and $D_{s2}(2573)$ (Cleo) in 1989 (1994), respectively. The mesons belonging to the $j_q = 1/2$ are expected to be much wider i.e. more difficult to observe.

Two candidates for such states were found in 2003. First the BaBar collaboration provided the evidence for the state $D_{sJ}(2317)^+$ (Fig. 12), decaying to $D_s^+\pi^0$ [60]. The observation by Cleo of the second state $D_{sJ}(2460)$ (Fig. 13), in the decay to $D_s^{*+}\pi^0$ [61], followed almost immediately. Both signals were found in the continuum processes $e^+e^- \to c\overline{c}$. There were soon confirmed by the Belle collaboration, together with an additional evidence of their presence in B meson exclusive decays [62]. Two other decay modes to the final states $D_s\gamma$ and $D_s\pi^+\pi^-$ (implies a spin of at least one) were observed for the $D_{sJ}(2460)^+$.

The discussed below, unexpected properties of both new mesons questioned the interpretation of both new mesons as ($c\overline{s}$, $j_q = 1/2$) bound states. First of all the widths of both the $D_{sJ}(2317)$ and $D_{sJ}(2460)$ turned out to be very small, consistent with the experimental resolution (< 4.6 MeV and < 5.5 MeV, respectively). Also their masses, measured to be below the DK (D*K) thresholds, respectively, appeared to be significantly lower to compare with HQS expectations, On the other side the study of angular distributions of the $D_{sJ}(2317)$ and $D_{sJ}(2460)$ decay products, performed by BaBar [63] and Belle [64], favoured strongly their spin-parity assignments 0^+ and 1^+, in agreement with HQS predictions. This motivated a vigorous answer from the side of theorists, proposing several exotic explanations for the two new mesons. In particular, the $D_{sJ}(2317)$ and $D_{sJ}(2460)$ were interpreted as $D^{(*)}K$ molecules [65, 66] or the chiral doublers of the D_s and D_s^* [67, 68]. Assuming that current mass predictions of HQS are wrong (they can in fact be shifted to lower values, in the presence of a strong S wave coupling to $DK^{(*)}$), both new D_{sJ} mesons could be comfortably interpreted as coventional ($c\overline{s}$) states. Provided that their predicted masses may be lowered below the respective $D^{(*)}K$ thresholds, the narrow widths of the $D_{sJ}(2317)$ and $D_{sJ}(2460)$ are naturally explained. These low masses would clearly allow the observed electromagnetic and isospin-violating decays of the the two states to be pronounced. Thus, the two new D_{sJ} mesons can be interpreted as conventional states

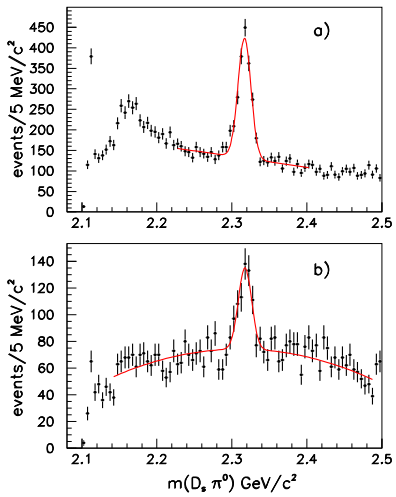

Figure 12: The $D_s^+\pi^0$ mass distributions for **(a)** the decay $D_s^+ \to K^+K^-\pi^+$ and **(b)** $D_s^+ \to K^+K^-\pi^+\pi^0$, as measured by BaBar. The solid curves represent the fits, described in [60].

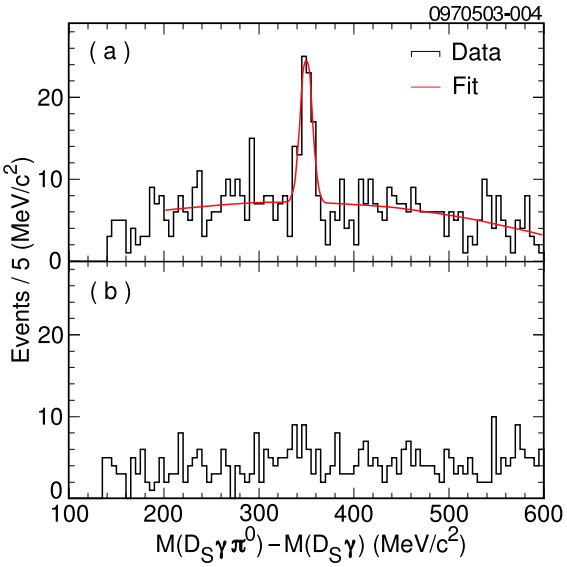

Figure 13: The mass difference $\Delta M(D_s^*\pi^0) = M(D_s\gamma\pi^0) - M(D_s\gamma)$, measured by the Cleo collaboration for **(a)** combinations where the $D_s\gamma$ system is consistent with D_s^* decay and **(b)** $D_s\gamma$ combinations selected from the D_s^* mass sideband regions.

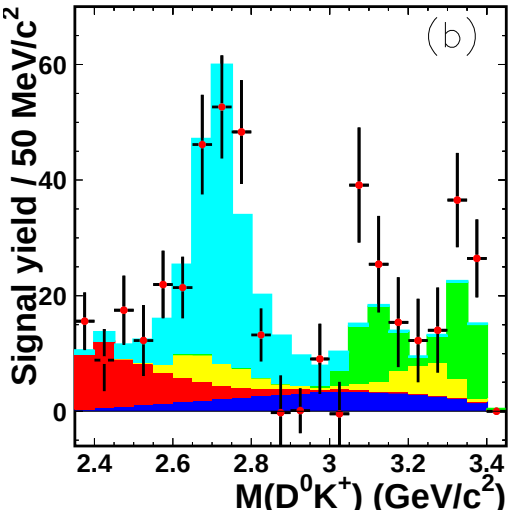

Figure 14: $B^+ \to \overline{D^0} D^0 K^+$ signal yield vs $M(D^0K^+)$ (data points) as measured by Belle. Additively superimposed histograms denote the contributions from $D_{sJ}(2700)$ (blue), $\psi(3770)$ (green), $\psi(4160)$ (yellow), threshold (red) and phase-space (navy blue) components.

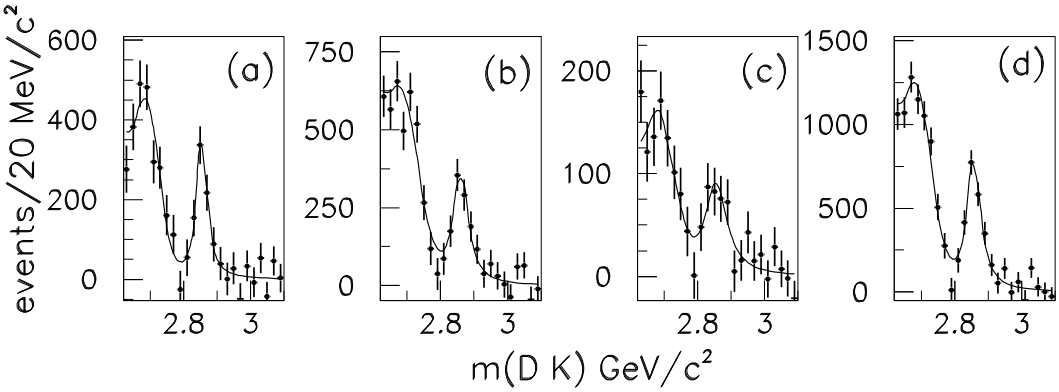

Figure 15: Background subtracted DK invariant mass distributions measured by BaBar collaboration for **(a)** $D^0(\to K^-\pi^+)K^+$, **(b)** $D^0(\to K^-\pi^+\pi^0)K^+$, **(c)** $D^+(\to K^-\pi^+\pi^+)K^0_s$ and **(d)** the sum of all modes in the 2.86 GeV/c^2 mass range. The curves are the fitted functions described in [73].

D^*_{s0} and D_{s1} ([69]– [71]).

Yet another charm-strange meson, marked as $D_{sJ}(2700)$ and produced in $B^+ \to \overline{D^0} D_{sJ}$, $D_{sJ} \to D^0 K^+$ was observed by Belle [72] (Fig. 14). This state has a mass of $M = (2715 \pm 11^{+11}_{-14})$ MeV/c^2 and a width $\Gamma = (115 \pm 20^{+36}_{-32})$ MeV and its signal corresponds to 182 ± 30 events. The study of $D_{sJ}(2700)$ helicity angle distributions strongly favours the spin parity assignment of 1^-.

Recent observations concerning the D_{sJ} family are completed by the study of three inclusive processes $e^+e^- \to D^0 K^+ X, D^0 \to K^-\pi^+$, $e^+e^- \to D^0 K^+ X, D^0 \to K^-\pi^+\pi^0$ and $e^+e^- \to D^+ K^0_s X, D^+ \to K^-\pi^+\pi^+$ performed by BaBar [73]. The distributions of DK invariant mass (Fig. 15) show a clear signal of a new charm-strange meson, marked as $D_{sJ}(2860)$, with a mass of $M = (2856.6 \pm 1.5 \pm 5.0)$ MeV/c^2 and a width $\Gamma = (47 \pm 7 \pm 10)$ MeV. The decay to two pseudoscalars implies a natural spin-parity for this state $(0^+, 1^-, ...)$ and the value $J^P = 3^-$ is predicted in [74]. According to [75], the $D_{sJ}(2860)$ could be a radial excitation of $D^*_{sJ}(2317)$. However, other assignments cannot be ruled out. Moreover, a second broad enhancement is observed around 2.69 GeV/c^2 (Fig. 15). This state was temporarily marked as $X(2690)^+$ and clearly further inputs are necessary in order to understand its origin. Its mass was determined to be $M = (2688 \pm 4 \pm 3)$ MeV/c^2 and a width $\Gamma = (112 \pm 7 \pm 36)$ MeV. It would be very interesting to check if there is any association between the $D_{sJ}(2700)$ and $X(2690)$.

9 $\Sigma_c(2800)$

The Belle collaboration has provided the first evidence [76] for an isotriplet of excited charmed baryons $\Sigma_c(2800)$ decaying into the $\Lambda_c^+\pi^-$, $\Lambda_c^+\pi^0$ and $\Lambda_c^+\pi^+$ final states. As shown in Fig. 16, clear enhancements around 0.51 GeV/c^2 are seen in the distributions of the mass difference $\Delta M(\Lambda_c^+\pi) = M(\Lambda_c^+\pi) - M(\Lambda_c^+)$ for the $\Lambda_c^+\pi^-$, $\Lambda_c^+\pi^0$, and $\Lambda_c^+\pi^+$ combinations. The mass differences ΔM together with the widths of the states $\Sigma_c(2800)$ are collected in Table 2. These states are identified as the members of the predicted Σ_{c2}, $J^P = 3/2^-$ isospin triplet [77]. The enhancement near $\Delta M = 0.43$ GeV/c^2 (cf Fig. 16), in the spectra corresponding to $\Lambda_c^+\pi^-$ and $\Lambda_c^+\pi^+$ combinations, is attributed to feed-down from the decay $\Lambda_c(2880)^+ \to \Lambda_c^+\pi^+\pi^-$, as verified by reconstructing $\Lambda_c(2880)$ in the data.

10 $\Lambda_c(2940)^+$ and $\Lambda_c(2880)^+$

The charmed baryon $\Lambda_c(2940)^+$ was first observed by the BaBar collaboration in the pD^0 final state [78] (Fig. 17). The signal at 2.88 GeV/c^2 is due to the decay $\Lambda_c(2880)^+ \to pD^0$. This comprises the first observation of the above decay channel (the baryon $\Lambda_c(2880)^+$ was first seen by CLEO in the final state $\Lambda_c^+\pi^+\pi^-$ [79]). The

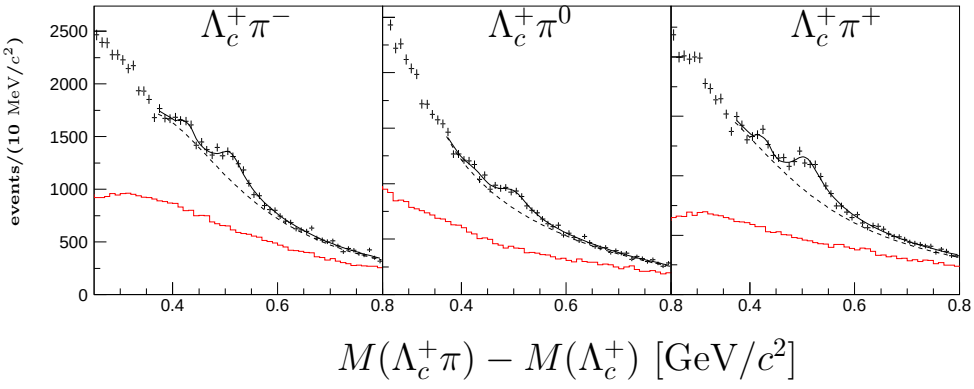

Figure 16: $M(\Lambda_c^+\pi) - M(\Lambda_c)$ distributions of the selected $\Lambda_c^+\pi^-$ (left), $\Lambda_c^+\pi^0$ (middle), and $\Lambda_c^+\pi^+$ (right) combinations. Data from the Λ_c^+ signal window (points with error bars) and normalized sidebands (histograms) are shown, together with the fits (solid curves) and their combinatorial background components (dashed).

Table 2: Parameters of the baryons $\Sigma_c(2800)^0$, $\Sigma_c(2800)^+$ and $\Sigma_c(2800)^{++}$ as measured by Belle.

State	ΔM [MeV/c^2]	Width [MeV]	Yield/10^3	Significance (σ)
$\Sigma_c(2800)^0$	$515.4^{+3.2+2.1}_{-3.1-6.0}$	61^{+18+22}_{-13-13}	$2.24^{+0.79+1.03}_{-0.55-0.50}$	8.6
$\Sigma_c(2800)^+$	$505.4^{+5.8+12.4}_{-4.6-2.0}$	62^{+37+52}_{-23-38}	$1.54^{+1.05+1.40}_{-0.57-0.88}$	6.2
$\Sigma_c(2800)^{++}$	$514.5^{+3.4+2.8}_{-3.1-4.9}$	75^{+18+22}_{-13-11}	$2.81^{+0.82+0.71}_{-0.60-0.49}$	10.0

Table 3: Parameters of the baryons $\Lambda_c(2880)^+$ and $\Lambda_c(2940)^+$, as determined by BaBar and Belle.

State	Expt.	Mass [MeV/c^2]	Width [MeV]	Yield (events)
$\Lambda_c(2880)^+$	BaBar	$2881.9 \pm 0.1 \pm 0.5$	$5.8 \pm 1.5 \pm 1.1$	2800 ± 190
$\Lambda_c(2880)^+$	Belle	$2881.2 \pm 0.2^{+0.4}_{-0.3}$	$5.5^{+0.7}_{-0.3} \pm 0.4$	$880 \pm 50 \pm 40$
$\Lambda_c(2940)^+$	BaBar	$2939.8 \pm 1.3 \pm 1.0$	$17.5 \pm 5.2 \pm 5.9$	2280 ± 310
$\Lambda_c(2940)^+$	Belle	$2937.9 \pm 1.0^{+1.8}_{-0.4}$	$10 \pm 4 \pm 5$	$210^{+70+100}_{-40-60}$

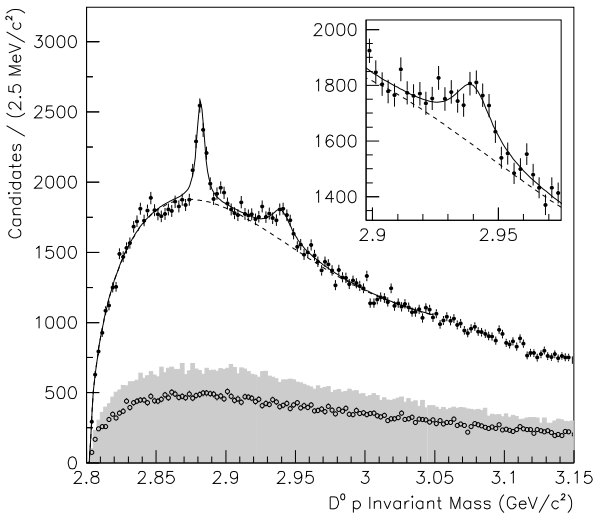

Figure 17: Invariant mass distribution of pD^0 pairs, as measured by BaBar collaboration (data points). The shaded histogram and open circles correspond to the D^0 mass sidebands and wrong-sign $p\overline{D^0}$ candidates, respectively. The inset shows the pD^0 mass spectrum in the range 2.9–2.975 GeV/c^2.

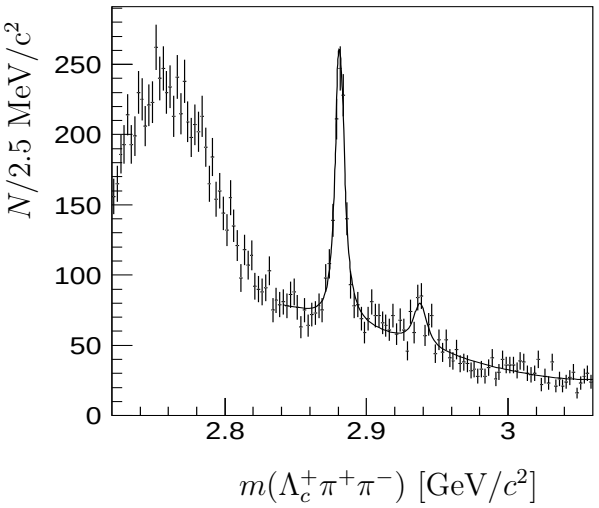

Figure 18: The invariant mass distribution of the $\Lambda_c^+\pi^+\pi^-$ combinations as measured by the Belle collaboration. The plot corresponds to the $\Sigma_c(2455)$ mass peak of the $\Lambda_c\pi^\pm$ combinations. The signals of $\Lambda_c(2765)^+$, $\Lambda_c(2880)^+$ and $\Lambda_c(2940)^+$ can be clearly distinguished.

search for a doubly-charged partner of the $\Lambda_c(2940)^+$, performed by BaBar in the final state pD^+, gave negative results [78].

The Belle collaboration has recently reported the evidence for another decay mode $\Lambda_c(2940)^+ \to \Sigma_c(2455)^{0,++}\pi^\pm$ [80] (Fig. 18). The study of angular distributions of the decay $\Lambda_c(2880)^+ \to \Sigma_c^{0,++}\pi^\pm$ strongly favours a $\Lambda_c(2880)^+$ spin assignment of $\frac{5}{2}$ over $\frac{3}{2}$ and $\frac{1}{2}$ [80].

The parameteters of both $\Lambda_c(2880)^+$ and $\Lambda_c(2940)^+$ measured by Belle and BaBar, are in good overall agreement (Table 3).

11 $\Xi_{cx}(2980)$ and $\Xi_{cx}(3077)$

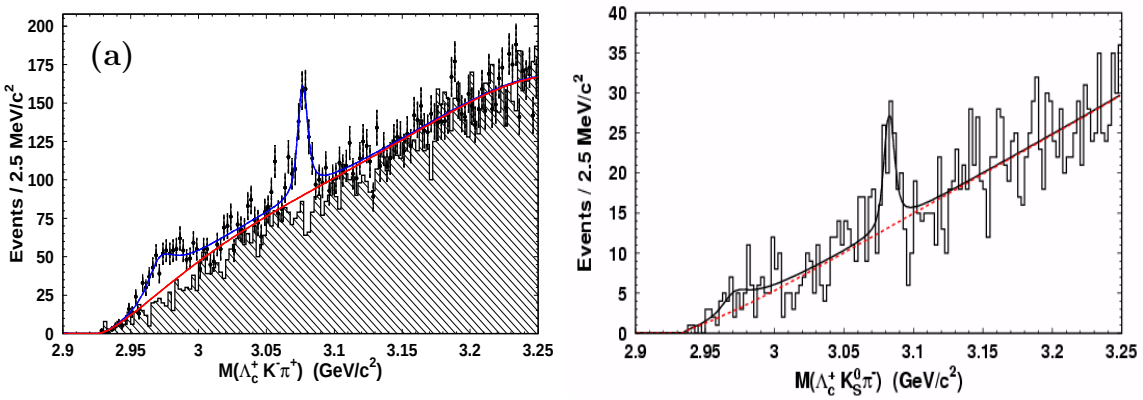

Figure 19: **(a)**: $M(\Lambda_c^+ K^-\pi^+)$ distribution (points with error bars) together with the fit (solid curve). The dashed region represents the background component corresponding to the wrong-sign combinations $\Lambda_c^+ K^+\pi^-$. **(b)**: $M(\Lambda_c^+ K_s^0\pi^+)$ distribution (points) together with the overlaid fitting curve. Both spectra were measured by the Belle collaboration.

In the beginning of this year, the Belle collaboration reported the first observation of two baryons [81], denoted as $\Xi_{cx}(2980)^+$ and $\Xi_{cx}(3077)^+$ and decaying into $\Lambda_c^+ K^-\pi^+$ (Fig. 19(a)). The existence of both new particles were quickly confirmed by BaBar [82]. Assuming that these states carry charm and strangeness, the above observation would comprise the first example of a baryonic decay in which the initial c and s quarks are carried away by two different final state particles. Most naturally, these two states would be interpreted as excited charm-strange baryons Ξ_c. This interpretation is strengthened by the positive results of the search for neutral isospin related partners of the above states (Fig. 19(b)), performed by Belle in $\Lambda_c^+ K_s^0\pi^-$ final state [81]. It yielded an evidence of the $\Xi_{cx}(3077)^0$ together with a broad enhancement near the threshold i.e. in the mass range corresponding to the $\Xi_{cx}(2980)^0$.

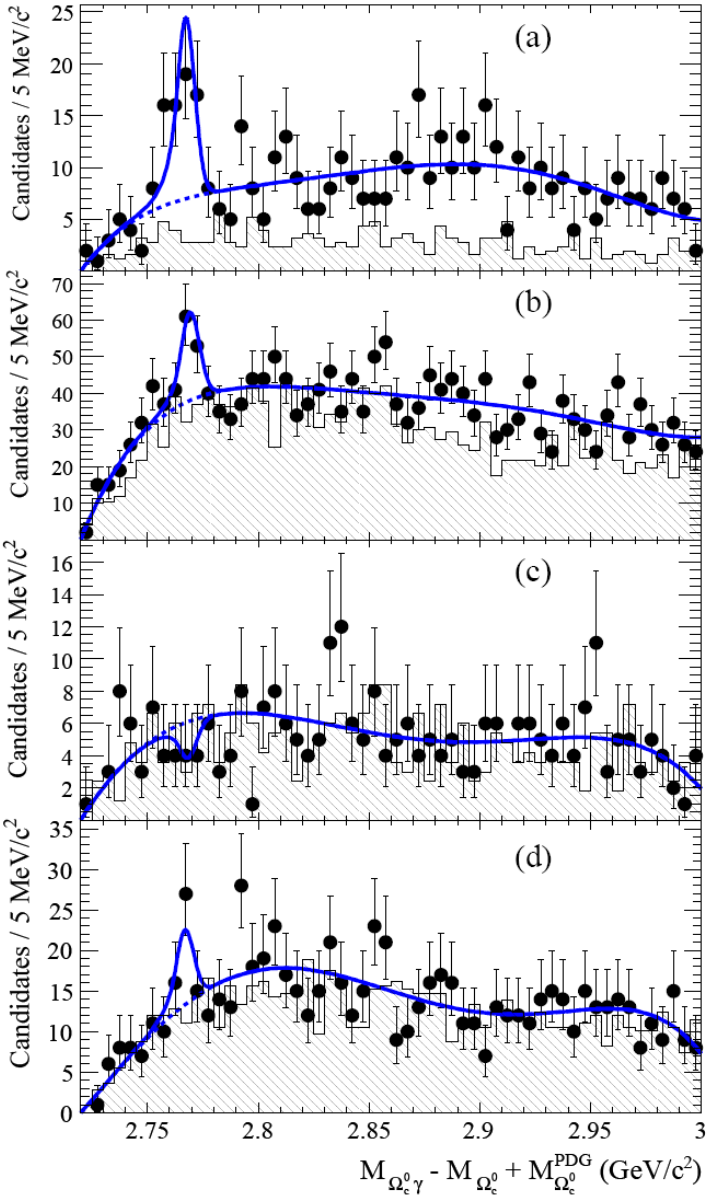

Figure 20: The invariant mass distributions of $\Omega_c^{*0} \to \Omega_c^0\gamma$ candidates with Ω_c^0 reconstructed by BaBar in the decay modes **(a)** $\Omega^-\pi^+$, **(b)** $\Omega^-\pi^+\pi^0$, **(c)** $\Omega^-\pi^+\pi^-\pi^+$ and **(d)** $\Xi^-K^-\pi^+\pi^+$. The points with error bars represent the data, the dashed line corresponds to the combinatorial background and the solid line is the sum of signal and background. The shaded histograms correspond to the mass distribution expected from the mass sideband of Ω_c^0.

The preliminary parameters of the states $\Xi_{cx}(2980)^+$ and $\Xi_{cx}(3077)^+$ are collected in Table 4.

In the $\Lambda_c^+ K^-\pi^+(\pi^+)$ final state, the SELEX collaboration [83] reported the observation of two double charmed baryon: Ξ_{cc}^+ with a mass of 3520 MeV/c^2 and Ξ_{cc}^{++} with a mass of 3460 MeV/c^2. The studies by Belle [81] and BaBar [85] show no evidence for these states. The BaBar collaboration estimated the following 95 % C.L. upper limits on the ratio of production cross-sections: $\sigma(\Xi_{cc}^+)\times\mathcal{B}(\Xi_{cc}^+ \to \Lambda_c^+ K^-\pi^+)/\sigma(\Lambda_c^+) < 2.7\times10^{-4}$ and $\sigma(\Xi_{cc}^{++})\times\mathcal{B}(\Xi_{cc}^{++} \to \Lambda_c^+ K^-\pi^+\pi^+)/\sigma(\Lambda_c^+) < 4.0\times10^{-4}$ (estimated for $p^*(\Lambda_c) > 2.3$ GeV/c, where p^* denotes the CMS momentum of the Λ_c). The Belle collaboration studied only the single-charged state which yielded $\sigma(\Xi_{cc}^+)\times\mathcal{B}(\Xi_{cc}^+ \to \Lambda_c^+ K^-\pi^+)/\sigma(\Lambda_c^+) < 1.5\times10^{-4}$ (90 % C.L.; $p^*(\Lambda_c) > 2.5$ GeV/c).

Table 4: Parameters of the new charm-strange baryons $\Xi_{cx}(2980)^{+,0}$ and $\Xi_{cx}(3077)^{+,0}$

State	Expt.	Mass (MeV/c^2)	Width (MeV)	Yield (events)	Signif. (σ)
$\Xi_{cx}(2980)^+$	BaBar	$2967.1 \pm 1.9 \pm 1.0$	$23.6 \pm 2.8 \pm 1.3$	$284 \pm 45 \pm 46$	7.0
$\Xi_{cx}(2980)^+$	Belle	$2978.5 \pm 2.1 \pm 2.0$	$43.5 \pm 7.5 \pm 7.0$	405.3 ± 50.7	5.7
$\Xi_{cx}(3077)^+$	BaBar	$3076.4 \pm 0.7 \pm 0.3$	$6.2 \pm 1.6 \pm 0.5$	$204 \pm 35 \pm 12$	8.6
$\Xi_{cx}(3077)^+$	Belle	$3076.7 \pm 0.9 \pm 0.5$	$6.2 \pm 1.2 \pm 0.8$	326.0 ± 39.6	9.2
$\Xi_{cx}(2980)^0$	Belle	$2977.1 \pm 8.8 \pm 3.5$	43.5 (fixed)	42.3 ± 23.8	1.5
$\Xi_{cx}(3077)^0$	Belle	$3082.8 \pm 1.8 \pm 1.5$	$5.2 \pm 3.1 \pm 1.8$	67.1 ± 19.9	4.4

12 Ω_c^{*0}

The baryon Ω_c^{*0} was observed by the BaBar collaboration in the radiative decay $\Omega_c^0\gamma$ [86]. This state was the last singly-charm baryon having zero orbital momentum, remaining to be experimentally detected. The Ω_c^0 was reconstructed in the decays to the final states $\Omega^-\pi^+$, $\Omega^-\pi^+\pi^0$, $\Omega^-\pi^+\pi^-\pi^+$ and $\Xi^- K^-\pi^+\pi^+$ (Fig. 20). The mass difference between Ω_c^{*0} and Ω_c^0 was measured to be $\Delta M = 70.8 \pm 1.0 \pm 1.1$ MeV/c^2. This agrees with the theoretical prediction in [87, 88] and is below that described in [89].

13 Summary

The charm physics has many features of the Sleeping Beauty. After the initial publicity of the times of November revolution, it remained a calm field aimed at filling the columns of Particle Data Group booklets with new or more accurate cross-sections,

branching ratios, lifetimes etc. It seems that B factories acted like a prince who kissed the Sleeping Beauty and waked her up right in the beginning of this century. The discovery of plethora of new charmed states has revitalized the charm physics and triggered many new theoretical ideas. Since the B factories are still collecting enormous samples of data, it is rather likely that some new exciting and charming discoveries are just around the corner.

I am very grateful to the organizers of the HQL2006 Conference for their support and all efforts in making this venue successful. Special thanks to Prof. S.Paul.

Bibliography

[1] Y. Kubota *et al.* [CLEO Collaboration], Nucl. Instrum. Meth. A **320**, 66 (1992).

[2] R. A. Briere *et al.*, CLNS-01-1742.

[3] http://www.lns.cornell.edu/public/lab-info/cesr.html

[4] B. Aubert *et al.* [BaBar Collaboration], Nucl. Instrum. Meth. A **479**, 1 (2002) [arXiv:hep-ex/0105044].

[5] http://www.slac.stanford.edu/grp/ad/ADPEPII/ADPEPII.html

[6] Nucl. Instrum. Meth. A **479** (2002) 117.

[7] S. Kurokawa, E. Kikutani, Nucl. Instrum. Methods A, **499**, 1 (2003), and other papers incl. in this vol.

[8] S. K. Choi *et al.* [Belle Collaboration], Phys. Rev. Lett. **91**, 262001 (2003) [arXiv:hep-ex/0309032].

[9] D. Acosta *et al.* [CDF II Collaboration], Phys. Rev. Lett. **93**, 072001 (2004) [arXiv:hep-ex/0312021].

[10] V. M. Abazov *et al.* [D0 Collaboration], Phys. Rev. Lett. **93**, 162002 (2004) [arXiv:hep-ex/0405004].

[11] B. Aubert *et al.* [BaBar Collaboration], Phys. Rev. D **71**, 071103 (2005) [arXiv:hep-ex/0406022].

[12] T. Barnes and S. Godfrey, Phys. Rev. D **69**, 054008 (2004) [arXiv:hep-ph/0311162].

[13] T. Barnes, S. Godfrey and E. S. Swanson, Phys. Rev. D **72**, 054026 (2005) [arXiv:hep-ph/0505002].

[14] E. J. Eichten, K. Lane and C. Quigg, Phys. Rev. D **73**, 014014 (2006) [Erratum-ibid. D **73**, 079903 (2006)] [arXiv:hep-ph/0511179].

[15] E. J. Eichten, K. Lane and C. Quigg, Phys. Rev. D **69**, 094019 (2004) [arXiv:hep-ph/0401210].

[16] F. E. Close and P. R. Page, Phys. Lett. B **578**, 119 (2004) [arXiv:hep-ph/0309253].

[17] N. A. Tornqvist, Phys. Lett. B **590**, 209 (2004) [arXiv:hep-ph/0402237].

[18] E. S. Swanson, Phys. Lett. B **588**, 189 (2004) [arXiv:hep-ph/0311229].

[19] E. S. Swanson, Phys. Lett. B **598**, 197 (2004) [arXiv:hep-ph/0406080].

[20] L. Maiani, F. Piccinini, A. D. Polosa and V. Riquer, Phys. Rev. D **71**, 014028 (2005) [arXiv:hep-ph/0412098].

[21] D. Ebert, R. N. Faustov and V. O. Galkin, Phys. Lett. B **634**, 214 (2006) [arXiv:hep-ph/0512230].

[22] B. A. Li, Phys. Lett. B **605**, 306 (2005) [arXiv:hep-ph/0410264].

[23] K. K. Seth, Phys. Lett. B **612**, 1 (2005) [arXiv:hep-ph/0411122].

[24] D. V. Bugg, Phys. Lett. B **598**, 8 (2004) [arXiv:hep-ph/0406293].

[25] K. Abe *et al.* [Belle Collaboration], arXiv:hep-ex/0505037.

[26] B. Aubert *et al.* [BaBar Collaboration], Phys. Rev. D **74**, 071101 (2006) [arXiv:hep-ex/0607050].

[27] K. Abe *et al.* [Belle Collaboration], arXiv:hep-ex/0505038.

[28] J. L. Rosner, Phys. Rev. D **70**, 094023 (2004) [arXiv:hep-ph/0408334].

[29] G. Gokhroo *et al.*, arXiv:hep-ex/0606055, accepted by Phys. Rev. Lett.

[30] W. M. Yao *et al.* [Particle Data Group], J. Phys. G **33**, 1 (2006).

[31] A. Abulencia *et al.* [CDF Collaboration], Phys. Rev. Lett. **96**, 102002 (2006) [arXiv:hep-ex/0512074].

[32] K. Abe *et al.* [Belle Collaboration], Phys. Rev. Lett. **94**, 182002 (2005) [arXiv:hep-ex/0408126].

[33] H. Severini *et al.* [CLEO Collaboration], Phys. Rev. Lett. **92**, 222002 (2004) [arXiv:hep-ex/0307034].

[34] F. E. Close and S. Godfrey, Phys. Lett. B **574**, 210 (2003) [arXiv:hep-ph/0305285].

[35] C. McNeile, C. Michael and P. Pennanen [UKQCD Collaboration], Phys. Rev. D **65**, 094505 (2002) [arXiv:hep-lat/0201006].

[36] Z. H. Mei and X. Q. Luo, Int. J. Mod. Phys. A **18**, 5713 (2003) [arXiv:hep-lat/0206012].

[37] X. Liao and T. Manke, arXiv:hep-lat/0210030.

[38] K. Abe *et al.* [Belle Collaboration], arXiv:hep-ex/0507019, submitted to Phys. Rev. Lett.

[39] S. Uehara *et al.* [Belle Collaboration], Phys. Rev. Lett. **96**, 082003 (2006) [arXiv:hep-ex/0512035].

[40] AIP Conf. Proc. **814**, 203 (2006) [Int. J. Mod. Phys. A **21**, 733 (2006)] [arXiv:hep-ph/0509327].

[41] B. Aubert *et al.* [BaBar Collaboration], Phys. Rev. Lett. **95**, 142001 (2005) [arXiv:hep-ex/0506081].

[42] T. E. Coan *et al.* [CLEO Collaboration], Phys. Rev. Lett. **96**, 162003 (2006) [arXiv:hep-ex/0602034].

[43] G. Majumder [Belle Collaboration], talk at ICHEP06 Conference, Moscow, (2006).

[44] X. Liu, X. Q. Zeng and X. Q. Li, Phys. Rev. D **72**, 054023 (2005) [arXiv:hep-ph/0507177].

[45] C. F. Qiao, Phys. Lett. B **639**, 263 (2006) [arXiv:hep-ph/0510228].

[46] K. Abe *et al.* [Belle Collaboration], arXiv:hep-ex/0608018.

[47] F. J. Llanes-Estrada, Phys. Rev. D **72**, 031503 (2005) [arXiv:hep-ph/0507035].

[48] L. Maiani, V. Riquer, F. Piccinini and A. D. Polosa, Phys. Rev. D **72**, 031502 (2005) [arXiv:hep-ph/0507062].

[49] S. L. Zhu, Phys. Lett. B **625**, 212 (2005) [arXiv:hep-ph/0507025].

[50] F. E. Close and P. R. Page, Phys. Lett. B **628**, 215 (2005) [arXiv:hep-ph/0507199].

[51] E. Kou and O. Pene, Phys. Lett. B **631**, 164 (2005) [arXiv:hep-ph/0507119].

[52] B. Aubert *et al.*, [BaBar Collaboration], preprint SLAC-PUB-11983 (BABAR-CONF-06/33).

[53] B. Aubert *et al.* [BaBar Collaboration], preprint SLAC-PUB-11971 (BABAR-CONF-06/003).

[54] J. L. Rosner *et al.* [CLEO Collaboration], Phys. Rev. Lett. **95**, 102003 (2005) [arXiv:hep-ex/0505073].

[55] D. Ebert, R. N. Faustov and V. O. Galkin, Mod. Phys. Lett. A **20**, 875 (2005) [arXiv:hep-ph/0503012].

[56] T. Appelquist, R. M. Barnett and K. D. Lane, Ann. Rev. Nucl. Part. Sci. **28**, 387 (1978).

[57] S. Godfrey and J. L. Rosner, Phys. Rev. D **66**, 014012 (2002) [arXiv:hep-ph/0205255].

[58] S. Godfrey and N. Isgur, Phys. Rev. D **32** (1985) 189.

[59] M. Di Pierro and E. Eichten, Phys. Rev. D **64**, 114004 (2001) [arXiv:hep-ph/0104208].

[60] B. Aubert *et al.* [BaBar Collaboration], Phys. Rev. Lett. **90**, 242001 (2003) [arXiv:hep-ex/0304021].

[61] D. Besson *et al.* [CLEO Collaboration], Phys. Rev. D **68**, 032002 (2003) [arXiv:hep-ex/0305100].

[62] K. Abe *et al.* [Belle Collaboration], Phys. Rev. Lett. **92**, 012002 (2004) [arXiv:hep-ex/0307052].

[63] B. Aubert *et al.* [BaBar Collaboration], Phys. Rev. Lett. **93**, 181801 (2004) [arXiv:hep-ex/0408041].

[64] K. Abe *et al.* [Belle Collaboration], preprint BELLE-CONF-0461).

[65] T. Barnes, F. E. Close and H. J. Lipkin, Phys. Rev. D **68**, 054006 (2003) [arXiv:hep-ph/0305025].

[66] A. P. Szczepaniak, Phys. Lett. B **567**, 23 (2003) [arXiv:hep-ph/0305060].

[67] M. A. Nowak, M. Rho and I. Zahed, Phys. Rev. D **48**, 4370 (1993) [arXiv:hep-ph/9209272].

[68] W. A. Bardeen and C. T. Hill, Phys. Rev. D **49**, 409 (1994) [arXiv:hep-ph/9304265].

[69] P. Colangelo, F. De Fazio and R. Ferrandes, Mod. Phys. Lett. A **19**, 2083 (2004) [arXiv:hep-ph/0407137].

[70] P. Colangelo and F. De Fazio, Phys. Lett. B **570**, 180 (2003) [arXiv:hep-ph/0305140].

[71] P. Colangelo, F. De Fazio and A. Ozpineci, Phys. Rev. D **72**, 074004 (2005) [arXiv:hep-ph/0505195].

[72] K. Abe *et al.* [Belle Collaboration], arXiv:hep-ex/0608031.

[73] B. Aubert *et al.* [BaBar Collaboration], arXiv:hep-ex/0607082.

[74] P. Colangelo, F. De Fazio and S. Nicotri, Phys. Lett. B **642**, 48 (2006) [arXiv:hep-ph/0607245].

[75] E. van Beveren and G. Rupp, Phys. Rev. Lett. **97**, 202001 (2006) [arXiv:hep-ph/0606110].

[76] R. Mizuk *et al.* [Belle Collaboration], Phys. Rev. Lett. **94**, 122002 (2005) [arXiv:hep-ex/0412069].

[77] L. A. Copley, N. Isgur and G. Karl, Phys. Rev. D **20**, 768 (1979) [Erratum-ibid. D **23**, 817 (1981)].

[78] B. Aubert *et al.* [BaBar Collaboration], arXiv:hep-ex/0603052.

[79] M. Artuso *et al.* [CLEO Collaboration], Phys. Rev. Lett. **86**, 4479 (2001) [arXiv:hep-ex/0010080].

[80] K. Abe *et al.* [Belle Collaboration], arXiv:hep-ex/0608043.

[81] R. Chistov *et al.* [BELLE Collaboration], Phys. Rev. Lett. **97**, 162001 (2006) arXiv:hep-ex/0606051.

[82] B. Aubert *et al.* [BaBar Collaboration], preprint SLAC-PUB-11980 (BABAR-CONF-06/01).

[83] M. Mattson *et al.* [SELEX Collaboration], Phys. Rev. Lett. **89**, 112001 (2002) [arXiv:hep-ex/0208014].

[84] J. S. Russ [SELEX Collaboration], arXiv:hep-ex/0209075.

[85] B. Aubert *et al.* [BaBar Collaboration], arXiv:hep-ex/0605075.

[86] B. Aubert *et al.* [BaBar Collaboration], arXiv:hep-ex/0608055, submitted to Phys. Rev. Lett.

[87] N. Mathur, R. Lewis and R. M. Woloshyn, Phys. Rev. D **66**, 014502 (2002) [arXiv:hep-ph/0203253].

[88] D. Ebert, R. N. Faustov and V. O. Galkin, Phys. Rev. D **72**, 034026 (2005) [arXiv:hep-ph/0504112].

[89] R. M. Woloshyn, Nucl. Phys. Proc. Suppl. **93**, 38 (2001) [arXiv:hep-ph/0009332].

Recent Results in Bottomonium Spectroscopy

Todd K. Pedlar
Department of Physics
Luther College
Decorah, IA, 52101 USA

1 Introduction

Nearly thirty years ago, the E288 experiment at Fermilab reported [1] the observation of a significant excess in the number of events near 9.5 GeV in the spectrum of the invariant mass of $\mu^+\mu^-$ produced in a proton beam on a nuclear target. Over the course of the subsequent two decades the spectrum of this newly-discovered heavy quarkonium system was fleshed out in some detail. Experiments which contributed to this initial survey of the system included those whose methods of production span the full spectrum of possible techniques, including the interaction of extracted hadron beams on heavy targets, electron-positron annihilation and two-photon double-bremsstrahlung from very high energy electron and positron beams. Compared to charmonium, the bottomonium spectrum below open flavor threshold is richer, offering more opportunity to flesh out the details of the interactions between heavy quarks. Despite the two decades of research on the spectrum of this beautiful system, many things remain hidden and left to be discovered. We describe the status of several studies in bottonium spectroscopy made over the course of the past several years at CLEO, BaBar and Belle.

As evidenced by the prodigious output of the Quarkonium Working Group, [2] heavy quarkonia offer an important experimental laboratory for the understanding of quark-antiquark interactions. The bottomonium system, free as it is of some of the more severe relativistic complications due to the very large mass of the bottom quark, is a particularly advantageous system to study. Among the important quantities that one would like to measure precisely in the bottomonium spectrum are the masses, hyperfine splittings, dilepton decay widths, etc. These are key inputs and checks for Lattice QCD calculations, which are steadily improving in precision. Such data, and additionally measurements of the details of the P-wave fine structure can also aid the development of QCD and potential models. Hadronic decay rates and detailed studies of angular distributions and invariant mass spectra are important in developing our theoretical understanding of hadronization.

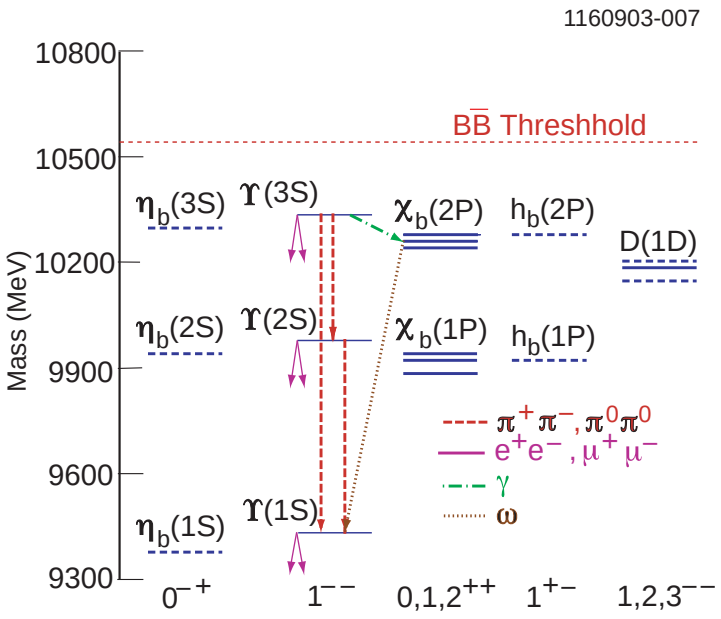

Figure 1: Schematic showing the full $b\bar{b}$ spectrum below open beauty threshold.

In each of these cases, comparison to similarly precise measurements in the charmonium system that have been performed by CLEO, E835 and other recent experiments, provide a very nice foundation for improving theoretical models that describe the dynamics of heavy quarks.

2 The Experimental Situation Circa 2001

At the beginning of 2001, the spectrum of bottomonium was known, in its gross features, relatively well (see Figure 1). Three triplet-S states, the Υ(3S), Υ(2S) and Υ(1S) had been observed, with known branching ratios to lepton pairs; two pairs of triplet-P states ($\chi_b(1P)$ and $\chi_b(2P)$) had all been observed in radiative transitions from the higher Υ(nS) states, and many had been observed to decay radiatively to lower Υ(mS) states. The masses of all nine of these states were known to varying degrees of precision. Leptonic branching ratios and/or partial widths were not all well known.

From 2001 to 2002, CLEO took data at center of mass energies on or near the three lower-lying triplet-S bottomonium resonances, expending from 1.2 to 1.5 fb^{-1} in each case. The number of Υ(nS) decays observed were approximately 22, 9 and 6 million, for Υ(1S), Υ(2S) and Υ(1S), respectively. These data samples were at the time the largest single samples of each state, representing factors of ten- to twenty-fold

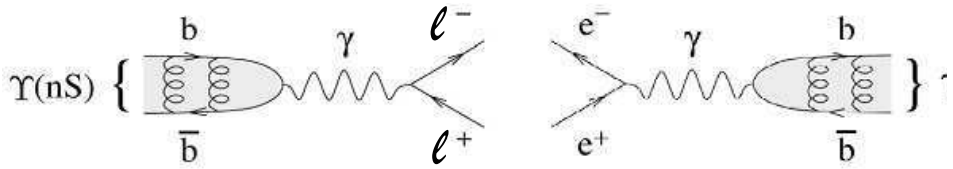

Figure 2: Schematic showing dilepton decay and production vertices involving Υ(nS).

statistical improvement.

3 New Leptonic Decay Measurements from e to τ

The leptonic partial width of a quarkonium state is one of the basic parameters calculable in LQCD, and is therefore a valuable parameter to be explored with precision. In Figure 2 are shown Feynman diagrams illustrating the heavy quarkonium production and decay vertices involving a lepton pair. At CLEO, we have recently measured leptonic widths or branching ratios for all three Υ(nS) states that lie below open-bottom threshold to all three lepton flavors (e^+e^-, [3] $\mu^+\mu^-$, [4] $\tau^+\tau^-$ [5]). We describe these measurements in chronological order.

3.1 $\mu^+\mu^-$ Branching Ratios

The branching ratios of Υ(nS) to $\mu^+\mu^-$ involve a relatively simple measurement: the observation of a final state consisting only of a high-momentum muon pair. Dominant systematic uncertainties for these measurements are the hadronic trigger efficiency, muon detection efficiency and the scale factor which is used in the background subtraction. Overall systematic uncertainties are 2.7, 3.7 and 4.1%, for the branching ratio measurements of Υ(1S), Υ(2S) and Υ(3S), respectively.

The new measurements by CLEO of these branching ratios represent, in the case of Υ(2S) and Υ(3S) in particular, substantial improvements in precision - and are significantly different than the previously-reported world average values. Because of this, these measurements have significant impact on many of the branching ratios for cascade decays that end in Υ(2S). They also impact the total widths of Υ(2S) and Υ(3S). Using the PDG2004 values for the quantity $\Gamma_{ee}\Gamma_{had}/\Gamma_{tot}$, we obtain $\Gamma(1S) = (52.8 \pm 1.8)$keV, $\Gamma(2S) = (29.0 \pm 1.6)$ keV and $\Gamma(3S) = (20.3 \pm 2.1)$keV. This should be compared with the previous [6] evaluations in the 2004 version of the PDG of $\Gamma(1S) = (53.0 \pm 1.5)$keV, $\Gamma(2S) = (43 \pm 6)$ keV and $\Gamma(3S) = (26.3 \pm 3.4)$keV.

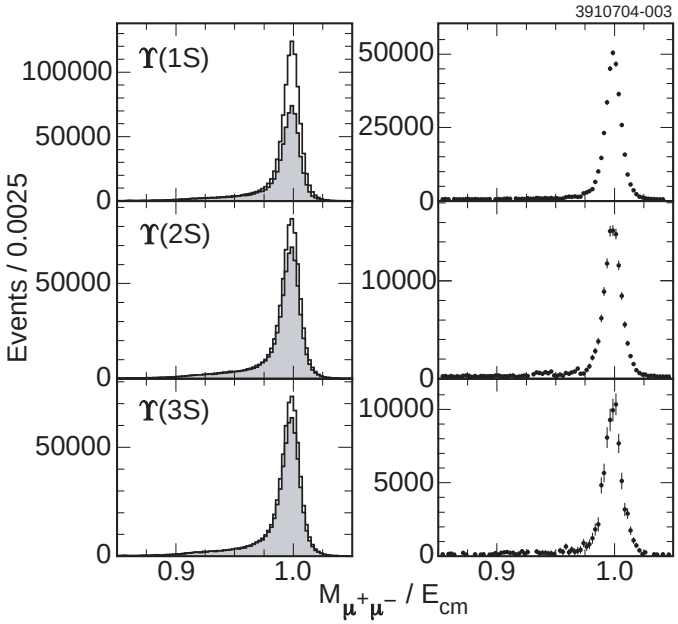

Figure 3: Reconstructed $\mu^+\mu^-$ as a function of $\mu^+\mu^-$ invariant mass for each of the three low-lying Υ(nS) states. (left) Open histogram: reconstructed events; shaded histogram: scaled off-resonance data for continuum subtraction. (right) Difference between the two histograms at left reveals the decay of Υ(nS) to $\mu^+\mu^-$.

Quantity	New CLEO Result	PDG2004
$\mathcal{B}_{\mu\mu}(\Upsilon(1S))$	$(2.49 \pm 0.02 \pm 0.07)\%$	$(2.48 \pm 0.06)\%$
$\mathcal{B}_{\mu\mu}(\Upsilon(2S))$	$(2.03 \pm 0.03 \pm 0.08)\%$	$(1.31 \pm 0.21)\%$
$\mathcal{B}_{\mu\mu}(\Upsilon(3S))$	$(2.39 \pm 0.07 \pm 0.10)\%$	$(1.81 \pm 0.17)\%$

Table 1: New measurements of $B(\Upsilon(\text{nS}) \to \mu^+\mu^-)$ from CLEO. [4]

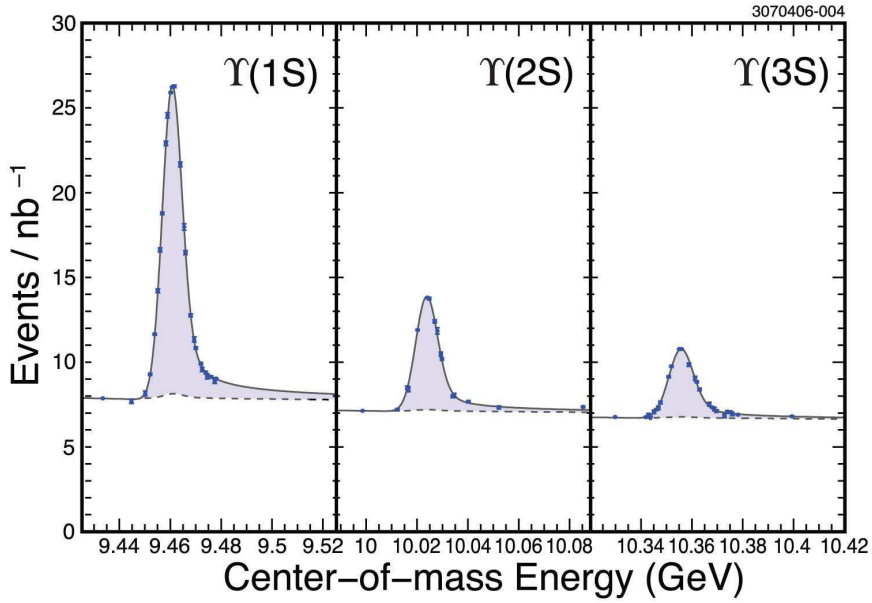

Figure 4: Hadronic yield measured by CLEO during scans of the center of mass regions near the Υ(nS) masses. The points represent the data, the solid line is the fit, and the dashed line the sum of backgrounds, which are dominantly hadronic continuum and radiative Bhabhas. The shaded area represents the yield from which Γ_{ee} is obtained. [3]

3.2 e^+e^- Partial Widths

Because at CLEO Υ(nS) states are produced at resonance by annihilation of e^+ and e^- beams, the partial width of these states to e^+e^- are not measured by studying the e^+e^- final state, but by observing the decay of these states to hadrons at various center of mass energies ($\sqrt{s}$) that span the width of the state and integrating under the excitation curve thus produced. In these measurements a systematic uncertainty of 1.5−1.8% was achieved - the chief contributing uncertainty being the 1.3% uncertainty from the overall luminosity scale. From the fit to the yields (see Figure 4) is obtained the partial width product $\Gamma_{ee}\Gamma_{had}/\Gamma_{tot}$. Applying an assumption of lepton universality, and using the recent measurement of $B(\mu^+\mu^-)$ for all three states by CLEO, [4] this product is then converted into the final results for Γ_{ee}, thus:

$$\Gamma_{ee} = \frac{\Gamma ee\Gamma_{had}/\Gamma_{tot}}{1 - 3B(\mu^+\mu^-)}.$$

The results are tabulated in Table 2. The best object for comparison to lattice calculations is the ratio of e^+e^- partial widths times the square of the mass of the state for pairs of states. For instance, we compare in Figure 5 the measured ratio

$\Gamma_{ee}\Gamma_{had}/\Gamma_{tot}(\Upsilon(1S))$:	$1.252 \pm 0.004 \pm 0.019$ keV
$\Gamma_{ee}\Gamma_{had}/\Gamma_{tot}(\Upsilon(2S))$:	$0.581 \pm 0.004 \pm 0.009$ keV
$\Gamma_{ee}\Gamma_{had}/\Gamma_{tot}(\Upsilon(3S))$:	$0.413 \pm 0.004 \pm 0.006$ keV
$\Gamma_{ee}(\Upsilon(1S))$:	$1.354 \pm 0.004 \pm 0.020$ keV
$\Gamma_{ee}(\Upsilon(2S))$:	$0.619 \pm 0.004 \pm 0.010$ keV
$\Gamma_{ee}(\Upsilon(3S))$:	$0.446 \pm 0.004 \pm 0.007$ keV
$\Gamma_{ee}(\Upsilon(2S))/\Gamma_{ee}(\Upsilon(1S))$:	$0.457 \pm 0.004 \pm 0.004$
$\Gamma_{ee}(\Upsilon(3S))/\Gamma_{ee}(\Upsilon(1S))$:	$0.329 \pm 0.003 \pm 0.003$
$\Gamma_{ee}(\Upsilon(3S))/\Gamma_{ee}(\Upsilon(2S))$:	$0.720 \pm 0.009 \pm 0.007$

Table 2: Various combinations of partial and total widths for the three triplet-S bottomonium resonances. The top three rows contain the primary measurements made by CLEO [3]. The second two sets of three rows are derived quantities using combinations of measurements and/or other experimental inputs [4, 6].

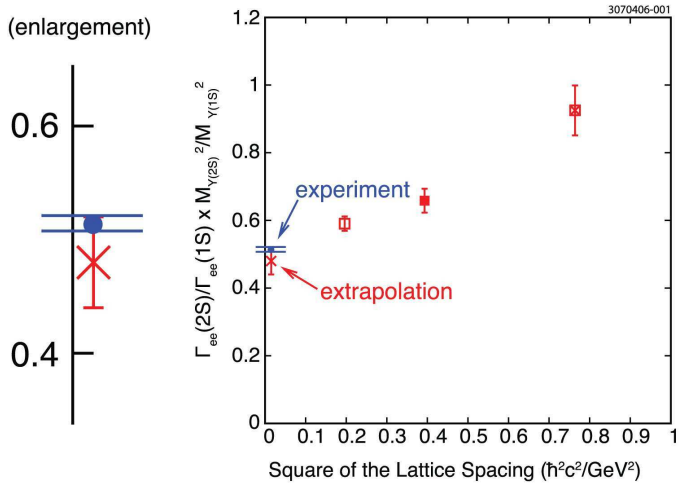

Figure 5: Comparison between the CLEO measurement and the unquenched lattice QCD calculation of the quantity $\Gamma_{ee}(2S)M^2(2S))/(\Gamma_{ee}(1S)M^2(1S))$. [3, 7]

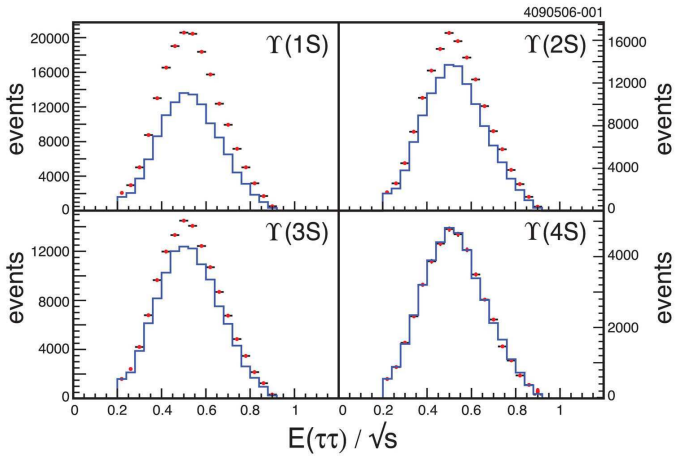

Figure 6: Ratio of observed τ pair energy to $\sqrt{s}$ for each of the four Υ(nS) resonances. The points represent the data and the solid histogram the scaled continuum. From the excess above scaled continuum, we obtain the final event yield, and subsequently $B(\tau^+\tau^-)$. The plot of data taken at the $\Upsilon(4S)$, which shows agreement between the scaled continuum and the on-resonance data is included to demonstrate the validity of the background subtraction. [5]

$\Gamma_{ee}(2S)M^2(2S))/(\Gamma_{ee}(1S)M^2(1S))$. The most recent lattice result for this quantity compares well with the experimental result, with theoretical uncertainties somewhat larger than the uncertainties of the experimental result:

$$\begin{aligned}\Gamma_{ee}(2S)M^2(2S))/(\Gamma_{ee}(1S)M^2(1S)) &= 0.514 \pm 0.007 \text{ (CLEO, [3])} \\ &= 0.48 \pm 0.05 \text{ (LGT, [7])}.\end{aligned}$$

3.3 $\tau^+\tau^-$ Branching Ratios

Prior to the CLEO result which is presented here, only the Υ(1S) decay to $\tau^+\tau^-$ was at all well measured. Υ(2S) had been observed to decay to $\tau^+\tau^-$, but Υ(3S) had never been observed in this decay mode. For this study, each τ is observed to decay via one of its one-prong decay modes. One of the benefits of this selection is a very clean final state involving just two tracks, but one which is easily distinguishable from Bhabha, Υ(nS)$\rightarrow e^+e^-$ or Υ(nS)$\rightarrow\mu^+\mu^-$ by virtue of the large missing energy in the event that is taken up by unobserved neutrinos. Furthermore, the results of this analysis are quoted as a ratio to the very well measured $\mu^+\mu^-$ branching ratios presented above, so that many systematic uncertainties are either cancelled or very greatly reduced. These new measurements are of particular interest as tests of lepton universality in the decays of Υ(nS) - they demonstrate consistency with Standard Model expectations,

	$B(\tau^+\tau^-)/B(\mu^+\mu^-)$	$B(\tau\tau)(\%)$
Υ(1S)	$1.02 \pm 0.02 \pm 0.05$	$2.54 \pm 0.04 \pm 0.12$
Υ(2S)	$1.04 \pm 0.04 \pm 0.05$	$2.11 \pm 0.07 \pm 0.13$
Υ(3S)	$1.07 \pm 0.08 \pm 0.05$	$2.55 \pm 0.19 \pm 0.15$

Table 3: Ratios of $B(\tau^+\tau^-)$ to $B(\mu^+\mu^-)$, and $B(\tau^+\tau^-)$, calculated using the most recent CLEO measurements of $B(\mu^+\mu^-)$ [4] for the three triplet-S bottomonium resonances. [5]

and represent the most precise single measurement of $B(\Upsilon(1S)\to\tau\tau)$, a very much improved value of $B(\Upsilon(2S)\to\tau\tau)$ and the first ever measurement of $B(\Upsilon(3S)\to\tau\tau)$.

4 New Studies of Hadronic Transitions

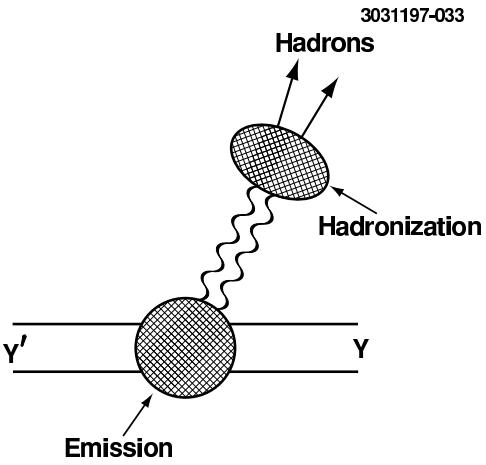

Figure 7: Schematic illustrating the transtion from one Υ(nS) state to a lower state by emission of hadrons.

Measurements of the decay rates and kinematic characteristics of hadronic transitions within the bottomonium system, which are generally understood theoretically in terms of a multipole expansion model [8], (see Figure 7) are important tools for improving our understanding of the hadronization process. Ever since the discovery of the bottomonium dipion transitions by CLEO and others, there has been a well-known difficulty in the describing the various transitions in a single theoretical framework. In particular, the $\Upsilon(3S)\to\Upsilon(1S)\pi\pi$ decays are of interest.

In the past year, both Belle and BaBar have produced interesting results involving hadronic transitions from the $\Upsilon(4S)$. Together with recent results from CLEO on

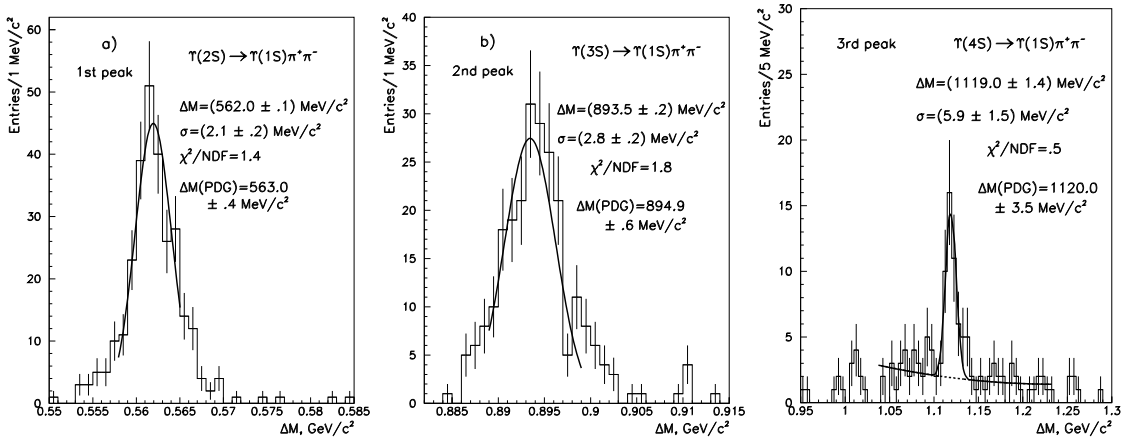

Figure 8: Plots from Belle of the quantity ΔM, the mass difference between the combination of $\mu^+\mu^-\pi^+\pi^-$ and the $\mu^+\mu^-$ alone, in the region expected for the observation of (left) Υ(2S)$\rightarrow\pi^+\pi^-\Upsilon$(1S), (center) Υ(3S)$\rightarrow\pi^+\pi^-\Upsilon$(1S) and (right) $\Upsilon(4S)\rightarrow\pi^+\pi^-\Upsilon$(1S). [9]

hadronic transitions between Υ(3S) and Υ(2S) and the lower Υ(mS) resonances, an intriguing picture is emerging concerning the distributions of dipion invariant masses.

4.1 Studies of Hadronic Transitions at Belle

The Belle study of $\Upsilon(4S)\rightarrow\pi^+\pi^-\Upsilon(1S)$, [9] was based on a sample of integrated luminosity 398 fb^{-1} (386 million $\Upsilon(4S)$ decays). In this study, the daughter Υ(1S) was observed via its decay to $\mu^+\mu^-$. After requiring a $\mu^+\mu^-$ candidate with an invariant mass in the vicinity of $M(\Upsilon(1S)) = 9.460$ GeV, an additional pair of pions of opposite charge was required, with the criterion $\Delta M \equiv \mathcal{M}(\mu^+\mu^-\pi^+\pi^-) - M(\mu^+\mu^-)$ satisfying the expectation that it be consistent with $10.580 - 9.460$ GeV $= 1.120$ GeV. A significant source of background for this analysis is the process $e^+e^-\rightarrow\gamma\mu\mu$, in which the γ converts in detector material and fakes the $\pi^+\pi^-$.

In order to obtain a yield of the desired signal events, the ΔM spectrum is fitted. Shown in Figure 8 are the signals near the appropriate ΔM regions for the observation of processes involving either the resonant decay of $\Upsilon(4S)$ or the radiative return process $e^+e^-\rightarrow\gamma\Upsilon$(3S), Υ(2S) and the subsequent decay Υ(3S), Υ(2S)$\rightarrow\pi^+\pi^-\Upsilon$(1S). After correcting for acceptance and efficiency, a branching ratio of

$$B(\Upsilon(4S)\rightarrow\pi^+\pi^-\Upsilon(1S)) = (1.1 \pm 0.2 \pm 0.4) \times 10^{-4}$$

was obtained. Using the PDG value for the full width of $\Upsilon(4S)$, they obtain a partial width

$$\Gamma(\Upsilon(4S)\rightarrow\pi^+\pi^-\Upsilon(1S)) = (2.2 \pm 1.0) \text{ keV}.$$

This value can be compared to the decay partial widths to $\pi^+\pi^-\Upsilon(1S)$ for the $\Upsilon(3S)$ and $\Upsilon(2S)$ of 8.1 ± 1.2 keV and 1.2 ± 0.2 keV, respectively.

4.2 Studies of Hadronic Transitions at BaBar

The BaBar study of $\Upsilon(4S)$ hadronic transitions was based on a sample of integrated luminosity 211 fb^{-1} (230 million $\Upsilon(4S)$ decays). Both $\Upsilon(4S)\rightarrow\pi^+\pi^-\Upsilon(1S)$ and $\Upsilon(4S)\rightarrow\pi^+\pi^-\Upsilon(2S)$ transitions were observed using a similar analysis method to that used by Belle. [10] Their selection of the $\mu^+\mu^-\pi^+\pi^-$ final state required a pair of charged particles consistent with being $\mu^+\mu^-$ and a second pair of tracks which are not consistent with being e^+e^-, in order to remove the events in which the γ produced in a radiative mu pair event converts to e^+e^- and would otherwise fake the $\pi^+\pi^-$ signal.

BaBar defines the same quantity ΔM as do their counterparts at Belle, and similarly fit the ΔM spectra obtained by selecting appropriate regions in the two-dimensional plane of $M(\mu^+\mu^-)$ vs. ΔM (see Figure 9). The two ΔM spectra used in the observation of $\Upsilon(4S)\rightarrow\pi^+\pi^-\Upsilon(1S)$ and $\Upsilon(4S)\rightarrow\pi^+\pi^-\Upsilon(2S)$ are shown in Figure 10. From the fits to the data shown are obtained yields (signal significances) of $167 \pm 19(10.3\sigma)$ and $97 \pm 15(7.3\sigma)$ for the transitions terminating in $\Upsilon(1S)$ and $\Upsilon(2S)$, respectively. (See Table 4) From these yields, the following product branching fractions are obtained:

$$B(\Upsilon(4S)\rightarrow\Upsilon(1S)\pi^+\pi^-) \times B_{\mu^+\mu^-}(\Upsilon(1S)) = (2.23 \pm 0.25 \pm 0.27) \times 10^{-6}$$
$$B(\Upsilon(4S)\rightarrow\Upsilon(2S)\pi^+\pi^-) \times B_{\mu^+\mu^-}(\Upsilon(2S)) = (1.69 \pm 0.26 \pm 0.20) \times 10^{-6}$$

These products may then, using the most recent CLEO results for $B_{\mu^+\mu^-}(\Upsilon(nS))$, [4] and a recent measurement (BaBar) of $\Gamma_{tot}(\Upsilon(4S))$, [11] be used to obtain the following partial widths $\Gamma(\Upsilon(4S)\rightarrow\Upsilon(nS)\pi^+\pi^-$:

$$\Gamma(\Upsilon(4S)\rightarrow\Upsilon(1S)\pi^+\pi^-) = 1.8 \pm 0.4 \text{ keV}$$
$$\Gamma(\Upsilon(4S)\rightarrow\Upsilon(2S)\pi^+\pi^-) = 1.7 \pm 0.5 \text{ keV}$$

4.3 Studies of Dipion Invariant Mass Spectra

It has long been known that the invariant mass distribution of the $\pi^+\pi^-$ produced in $\Upsilon(3S)\rightarrow\Upsilon(1S)\pi^+\pi^-$ is difficult to explain with a simple S-wave decay model, but it is safe to say that the theoretical description of this decay remains incomplete. CLEO has recently made measurements of the $\Upsilon(nS)\rightarrow\Upsilon(mS)\pi^+\pi^-$ transitions in

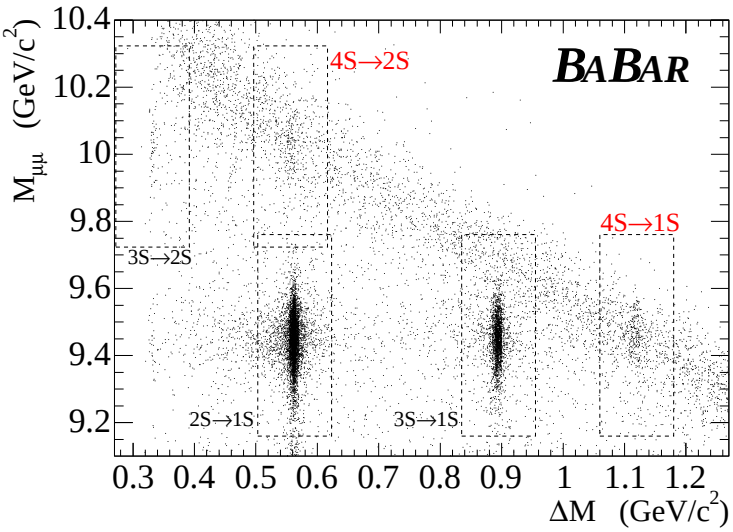

Figure 9: Two-dimensional plot from BaBar of $M(\mu^+\mu^-)$, the invariant mass of the $\mu^+\mu^-$ candidate vs. ΔM, the mass difference between the combination of $\mu^+\mu^-\pi^+\pi^-$ and the $\mu^+\mu^-$ alone. [10]

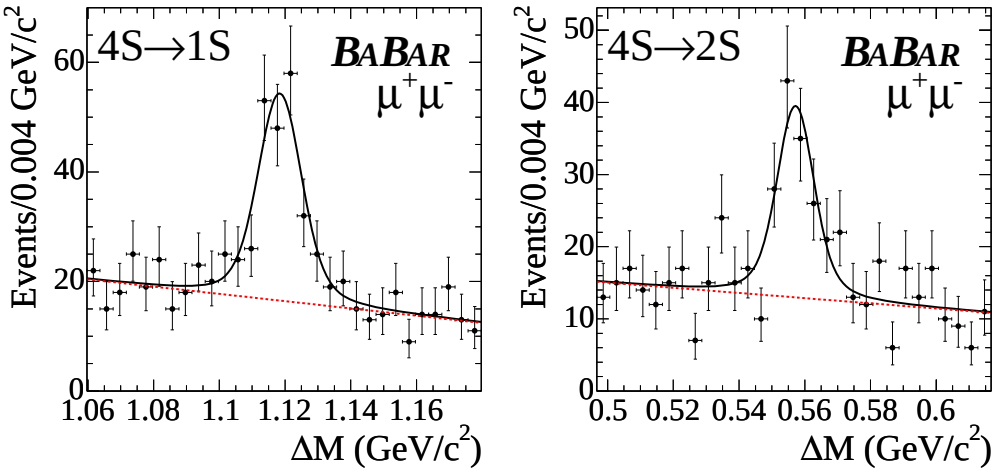

Figure 10: Plots from BaBar of the quantity ΔM, the mass difference between the combination of $\mu^+\mu^-\pi^+\pi^-$ and the $\mu^+\mu^-$ alone, in the region expected for the observation of (left) $\Upsilon(4S)\to\pi^+\pi^-\Upsilon(1S)$ and (right) $\Upsilon(4S)\to\pi^+\pi^-\Upsilon(2S)$. [10]

Experiment	Transition	$B_{\pi^+\pi^-}$ ($\times 10^{-4}$)	$\Gamma_{\pi^+\pi^-}$ (keV)
Belle	$4S \to 1S$	1.13 ± 0.45	2.3 ± 0.9
BaBar	$4S \to 1S$	0.90 ± 0.15	1.8 ± 0.4
BaBar	$4S \to 2S$	0.88 ± 0.19	1.8 ± 0.5

Table 4: Results of measurements by Belle [9] and from BaBar [10]. For ease of comparison, the branching ratios and the partial widths have been recalculated using common inputs: the PDG06 average value for $\Gamma(4S)$ [12] and the most recent CLEO results for $B(\Upsilon(\mathrm{nS}) \to \mu^+\mu^-)$. [4] Belle has since the conference updated their result, basing a new measurement on $477 fb^{-1}$ of integrated luminosity at $\Upsilon(4S)$, obtaining $B(\pi^+\pi^-) = 1.77 \pm 0.23 \times 10^{-4}$ and $\Gamma(\pi^+\pi^-) = 3.7 \pm 0.9$ keV. [13]

the most recent data sets, and observed again the familiar double-humped structure in the invariant mass of the $\pi^+\pi^-$ produced in the $\Upsilon(3\mathrm{S}) \to \Upsilon(1\mathrm{S})\pi^+\pi^-$ transition, a preliminary plot of which is shown in Figure 11.

BaBar and Belle have also made recent measurements of $\pi^+\pi^-$ invariant mass distributions in conjunction with the measurements discussed in the previous section (see Figure 11). Each of the three experiments show $\Upsilon(3\mathrm{S}) \to \Upsilon(1\mathrm{S})$ and $\Upsilon(2\mathrm{S}) \to \Upsilon(1\mathrm{S})$ distributions that agree with each other and with the previously measured distributions. Of particular interest, however, is the fact that the $\Delta n = 2$ transition reported by BaBar, namely $\Upsilon(4S) \to \Upsilon(2\mathrm{S})\pi^+\pi^-$, also shows a double-humped structure similar to the well-measured $\Upsilon(3\mathrm{S}) \to \Upsilon(1\mathrm{S})\pi^+\pi^-$ transition from CLEO. The fact that both these $\Delta n = 2$ transitions show similar $\pi^+\pi^-$ invariant mass structure may be helpful in solving the long-known puzzle of the $\Upsilon(3\mathrm{S}) \to \Upsilon(1\mathrm{S})\pi^+\pi^-$ mass distribution.

5 Conclusions

The past five years has been an active period in bottomonium spectroscopy, with several new measurements contributing to the greater understanding of the bottmonium system and heavy quark dynamics. With the missing bottomonium singlet states still to be found, and the question of a fuller explanation of hadronic transitions within the system still to be answered, there is plenty of opportunity for still more work to be done, should the opportunity arise.

6 ACKNOWLEDGMENTS

The author thanks the International and Local Conference Committees for their efforts at putting together a fabulous conference in a wonderful setting. The extensive

preparations made for a most excellent visit, a smooth conference, and a thoroughly enjoyable time for all. The author also acknowledges the support of National Science Foundation Grant No. PHY-0603831.

Bibliography

[1] S. W. Herb *et al.*, Phys. Rev. Lett. **39**, 252 (1977). See also `http://history.fnal.gov/botqrk.html` for a collection of very interst-ing documents concerning the discovery.

[2] Quarkonium Working Group Yellow Report, CERN 2005-005. See also `http://www.qwg.to.infn.it/` for more information.

[3] J. L. Rosner *et al.*(CLEO), Phys. Rev. Lett. **96**, 092003 (2006).

[4] G. S. Adams *et al.*(CLEO), Phys. Rev. Lett. **94**, 012001 (2005).

[5] D. Besson *et al.*(CLEO), Phys. Rev. Lett. **98**, 052002 (2007). hep-ex/0607019 *Accepted for publication in PRL.*

[6] S. Eidelman *et al.*(PDG),Phys. Lett. B **592** 1 (2004) and partial updates for the 2006 Edition available at `http://pdg.lbl.gov`.

[7] A. Gray *et al.*, Phys. Rev. D **72**, 094507 (2005).

[8] K. Gottfried, Phys. Rev. Lett. **40**, 598 (1978).

[9] K. Abe *et al.*(Belle), hep-ex/0512034, BELLE-CONF-510.

[10] B. Aubert *et al.*(BaBar), Phys. Rev. Lett. **96**, 232001 (2006).

[11] B. Aubert *et al.*(BaBar), Phys. Rev. D **95**, 032005 (2005).

[12] W.-M. Yao *et al.*PDG, *J. Phys. G***33** (2006) 1.

[13] K. Abe *et al.*(Belle), hep-ex/0611026.

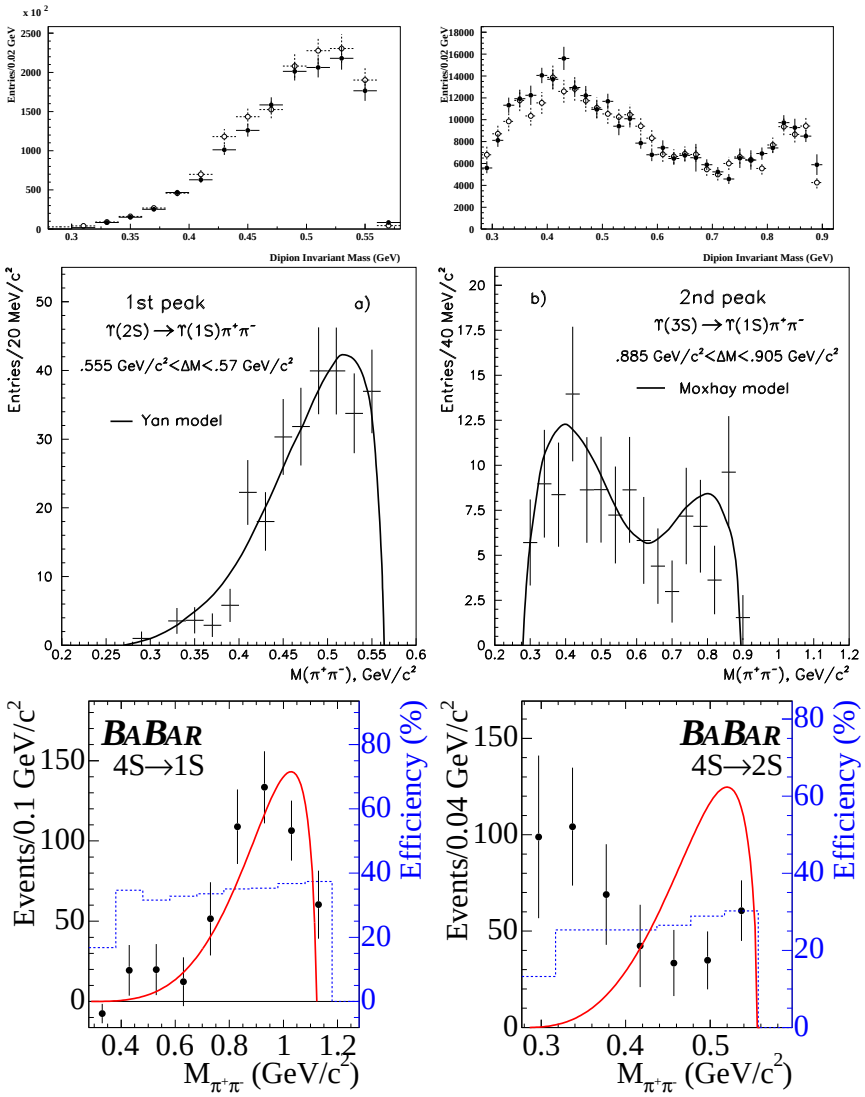

Figure 11: $\pi^+\pi^-$ invariant mass distributions in Υ(nS)$\rightarrow\Upsilon$(mS)$\pi^+\pi^-$ from (top)CLEO $2S\rightarrow 1S\pi^+\pi^-$ and $3S\rightarrow 1S\pi^+\pi^-$, (middle) Belle $4S\rightarrow 1S\pi^+\pi^-$ and $3S\rightarrow 1S\pi^+\pi^-$ [9] (bottom) BaBar $4S\rightarrow 1S\pi^+\pi^-$ and $4S\rightarrow 2S\pi^+\pi^-$. [10]

SELEX: Recent Progress in the Analysis of Charm-Strange and Double-Charm Baryons

Jürgen Engelfried[1]
Instituto de Física,
Universidad Autónoma de San Luis Potosí, Mexico
for the SELEX Collaboration

1 Introduction

SELEX (Fermilab Experiment 781) [1] employs beams of Σ^-, π^-, and protons at around 600 GeV/c to study production and decay properties of charmed baryons. It took data in the 1996/7 fixed target run and is currently analyzing those data.

Here we will focus on recently obtained results concerning the Ω_c^0 lifetime and the doubly-charmed baryons Ξ_{cc}^+ and Ξ_{cc}^{++}.

2 New Results on the Ω_c^0

SELEX observes the Ω_c^0 in three decay modes, namely $\Omega_c^0 \to \Omega^-\pi^+$, $\Omega_c^0 \to \Omega^-\pi^+\pi^+\pi^-$, and $\Omega_c^0 \to \Xi^- K^-\pi^+\pi^+$. The invariant mass distributions for these modes are shown in fig. 1. The total sample contains 107 ± 22 events, nearly half of them in $\Omega 3\pi$. At this moment we are working on the systematics of the mass and branching ratio measurements of these modes [2].

We use the $\Omega\pi$ and $\Omega 3\pi$ channels to determine the lifetime of the Ω_c^0. We calculate the reduced proper time ct, given by $ct = (L - N\sigma)/\gamma$, requiring $L/\sigma > N$ with $N = 6$, for each event within the mass region of the Ω_c^0. The proper lifetime resolution is ~ 20 fs. We make a maximum likelihood fit to a probability distribution having an exponential decay for the signal and two exponentials for the fast and slow components of the background:

$$N_s(1-\alpha)f(t)\tau^{-1}e^{-t/\tau} + \alpha N_B(\beta\tau_1^{-1}e^{-t/\tau_1} + (1-\beta)\tau_2^{-1}e^{-t/\tau_2})$$

where τ, α, β, τ_1, τ_2 are the fit parameters describing the lifetime and the relative contributions of the background to the ct distribution, and $f(t)$ is the acceptance

[1]email: jurgen@ifisica.uaslp.mx

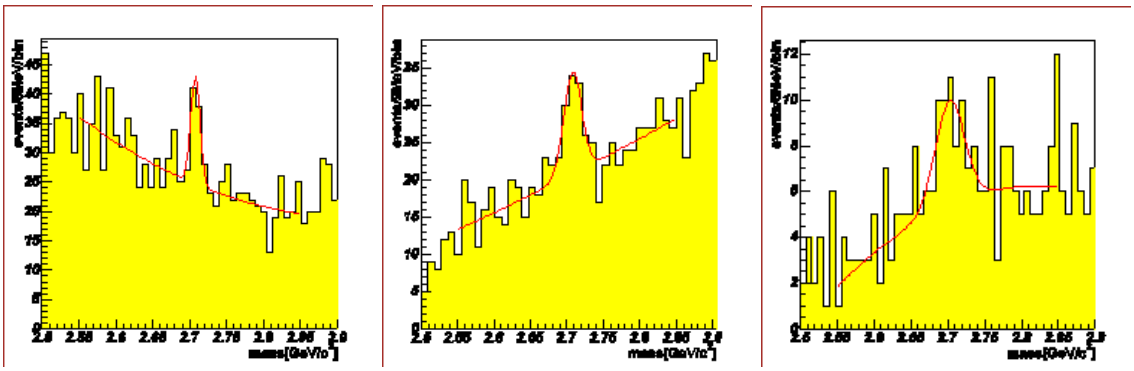

Figure 1: Invariant mass distributions for different decay modes of the Ω_c^0. Left: $\Omega^-\pi^+$, Signal: 35 ± 12 events; center: $\Omega^-\pi^+\pi^+\pi^-$, 44 ± 14 events; right: $\Xi^- K^-\pi^+\pi^+$, 28 ± 12 events

function. We do this for each mode separately, and obtain for the $\Omega\pi$ mode $\tau = 62.6 \pm 22.0\,\mathrm{fs}$ and for the $\Omega 3\pi$ mode $\tau = 65.8 \pm 16.0\,\mathrm{fs}$. Combining the two results yields $\tau_{\Omega_c} = 65 \pm 13\,(stat) \pm 9\,(sys)\,\mathrm{fs}$. More details can be found in [3]. This result should be compared to the current PDG average [4] of $69 \pm 12\,\mathrm{fs}$, using a total of 175 events from three different experiments.

3 Doubly Charmed Baryons

3.1 The Discovery of Double Charm Baryons

In 2002 the SELEX collaboration reported the first observation of a candidate for a double charm baryon, decaying as $\Lambda_c^+ K^-\pi^+$ [5, 6]. The state had a mass of $3519 \pm 2\,\mathrm{MeV}/c^2$, and its observed width was consistent with experimental resolution, less than $5\,\mathrm{MeV}/c^2$. The final state contained a charmed baryon and negative strangeness (Λ_c^+ and K^-), consistent with the Cabibbo-allowed decay of a Ξ_{cc}^+ configuration. In order to confirm the interpretation of this state as a double charm baryon, it is essential to observe the same state in some other way. Other experiments with large charm baryon samples, e.g., the FOCUS [7] and E791 fixed target charm experiments at Fermilab or the B-factories, have not confirmed the double charm signal. This is not inconsistent with the SELEX results. The report in Ref. [5] emphasized that this new state was produced by the baryon beams (Σ^-, proton) in SELEX, but not by the π^- beam. It also noted that the apparent lifetime of the state was significantly shorter than that of the Λ_c^+, which was not expected in model calculations [8]. A more detailed discussion can be found in [9].

3.2 Features and Problems in the Original Analysis, and Possible Solutions

All the signals observed so far are statistically significant, but have only a few signal events. The signals are clean, e.g. there is very little background, but the background itself is also difficult to estimate. SELEX only observes events from the baryon (Σ^-, proton) beams, and the number of observed events is larger than some production models (see for example [10, 11]) predict. As mentioned before, the lifetime seems to be very short, and no other experiment has confirmed our observations.

Another way to confirm the Ξ_{cc}^+ is to observe it in a different decay mode that also involves a final state with baryon number and charm (not anti-charm). One such mode involving only stable charged particles is the channel pD^+K^-, another one $\Xi_c^+\pi^+\pi^-$. SELEX developed a new method for a more reliable background determination. We also improved the resolution on the secondary vertex position by including the single-charm track into the vertex fit, and we redid our full analysis chain to increase our statistics. In the following we will describe these step in details.

3.3 New Analysis Features within SELEX

The Cabibbo-allowed decay of the Ξ_{cc}^+ is shown in the following figure.

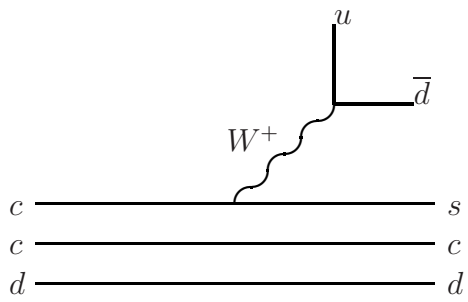

In the final state we expect a baryon, and the quarks $csdu\overline{d}$ plus eventually some pairs from the sea. We also expect a cascaded decay chain, with the first, and later the second charm quark undergoing a weak decay.

For SELEX, the easily accessible decay modes for the different doubly charmed baryons are: $\Xi_{cc}^+ \to \Lambda_c^+K^-\pi^+$, $\Xi_{cc}^+ \to pD^+K^-$, $\Xi_{cc}^+ \to \Xi_c^+\pi^-\pi^+$, $\Xi_{cc}^{++} \to \Lambda_c^+K^-\pi^+\pi^+$, $\Xi_{cc}^{++} \to pD^+K^-\pi^+$ (depending on the mass of the Ξ_{cc}^{++}), $\Xi_{cc}^{++} \to \Xi_c^+\pi^+$, $\Xi_{cc}^{++} \to \Xi_c^+\pi^+\pi^+\pi^-$, $\Omega_{cc}^+ \to \Xi_c^+K^-\pi^+$, and $\Omega_{cc}^+ \to \Xi_c^+K^-\pi^+\pi^+\pi^-$. The first two modes are already published [5, 12] by SELEX, and work on the other modes is in progress; here we will report on a first observation of the third decay mode listed.

For the background determination, we developed an event mixing method. The first decay vertex is close to the primary vertex, and we assume that all the background is purely combinatoric. We make combinatoric backgrounds by taking the first decay

vertex from one event, and the second vertex from another event; to increase statistics, we use the single-charm vertex 25 times. The resulting combinatoric background is absolutely normalized. We employed this method already in [12].

3.4 $\Xi_{cc}^+ \to \Lambda_c^+ K^- \pi^+$ – New Analysis

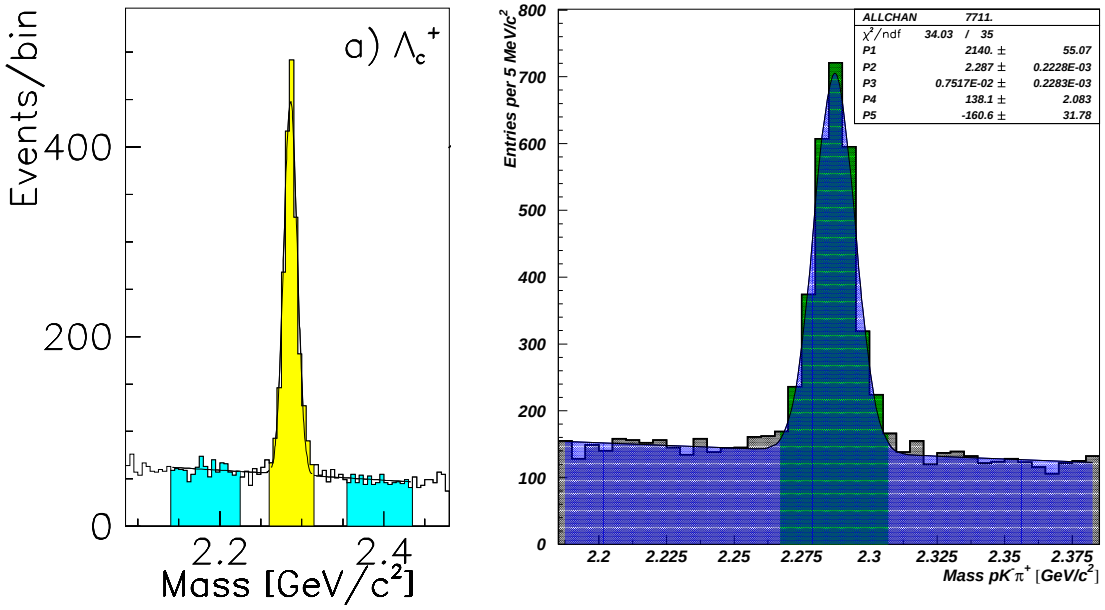

Figure 2: $\Lambda_c^+ \to pK^-\pi^+$ data sets of original (left) and new (right) analysis.

To increase our statistics, we re-analyzed our full data set with some softer cuts and with improved tracking software. In fig. 2 we show a comparison of the Λ_c^+ data set used for the analysis. The number of $\Lambda_c \to pK^-\pi^+$ candidates increased from 1630 to 2140.

We also improved the resolution of the decay vertex position of the Ξ_{cc}^+ candidate by including the vector of the Λ_c^+ into the vertex fit. This improved resolution reduces the background when applying a cut in L/σ, while keeping more signal events. It also increases the possibility of measuring the lifetime of double charm baryons.

Figure 3 shows the results of our new analysis, for various cuts in L/σ of the first decay vertex. Re-analyzing and relaxing some cuts in the single charm sample increased the number of signal events, but also resulted in a somewhat higher background level; but the background is nicely reproduced and well understood from the combinatoric analysis. The improved secondary vertex resolution yields in cleaner signals and allows access to other decay modes, which we will pursue in the future. Measuring the lifetime now seems possible, but is still challenging. As seen from the yields for different cuts in L/σ, the lifetime seems to be around $1\,\sigma$.

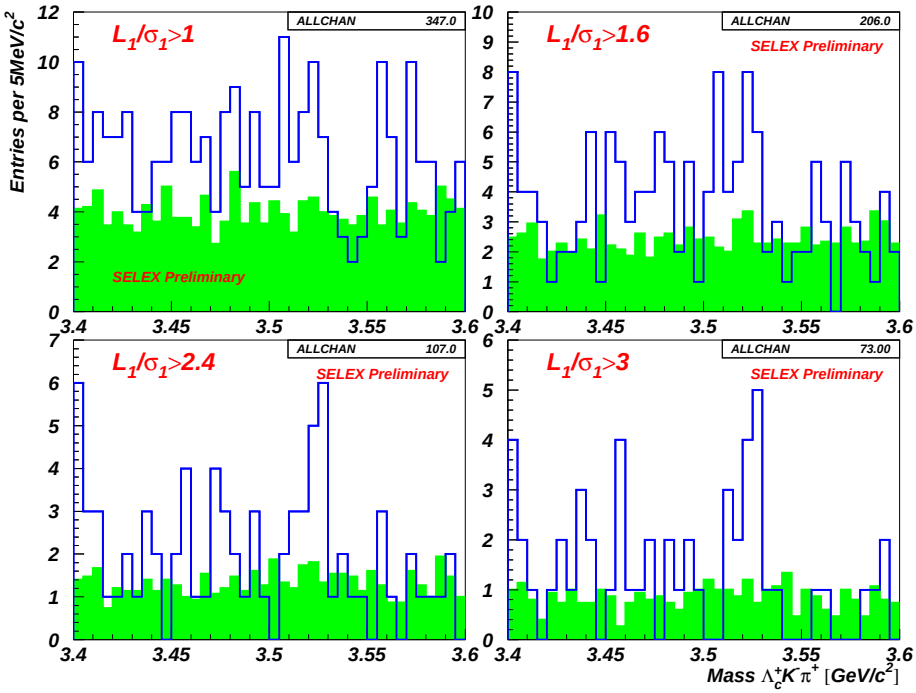

Figure 3: $\Lambda_c^+ K^- \pi^+$ ($\Lambda_c^+ \to pK^-\pi^+$) invariant mass distributions (blue) for various cuts in L/σ on the first decay vertex. In green we show the estimated combinatoric background from the event mixing procedure described in the text.

3.5 $\Xi_{cc}(3780)^{++} \to \Lambda_c^+ K^- \pi^+ \pi^+$

We also revisited with our re-analyzed data set the first double-charm baryon state we found in SELEX [6], the $\Xi_{cc}(3780)^{++}$. In fig. 4 is shown the $\Lambda_c^+ K^- \pi^+ \pi^+$ invariant mass distribution, restricting ourselves to Σ^- induced events. The peak at $3780\,\mathrm{MeV}/c^2$ is statistically significant, and is wider than our experimental resolution, as shown by Monte Carlo. The background is well described by our mixed event procedure. By removing the slower of the π^+'s, we observe that about half of the $\Xi_{cc}(3780)^{++}$ decay to $\Xi_{cc}^+(3520)$. At this moment we are finishing up the analysis for this state.

4 First Observation of $\Xi_{cc}^+ \to \Xi_c^+ \pi^+ \pi^-$

SELEX published [13] the first observation of the Cabibbo-suppressed decay of $\Xi_c^+ \to pK^-\pi^+$; this is the same final state as we used before for the reconstruction of the Λ_c^+. Our sample of Ξ_c^+ in the mode is much smaller than our Λ_c^+ sample, but the branching fraction of $\Xi_{cc}^+ \to \Xi_c^+ \pi^+ \pi^-$ should be larger than to $\Lambda_c^+ K^- \pi^+$. We applied

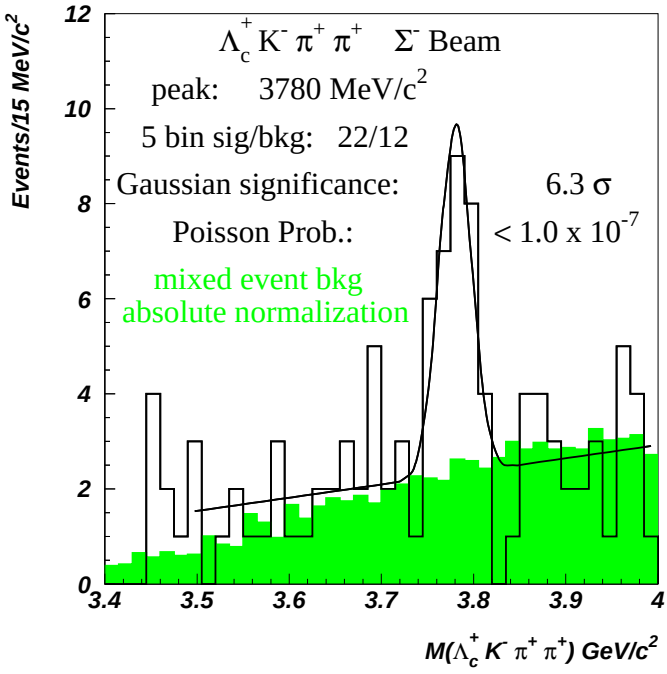

Figure 4: The $\Lambda_c^+ K^- \pi^+ \pi^+$ invariant mass distribution, for Σ^- beam only.

the same cuts and procedure as to the previously described analyzes, and obtained [14] the $\Xi_c^+ \pi^+ \pi^-$ invariant mass distribution shown in fig. 5. A clear peak at about 3520 MeV/c^2 is seen in the figure. This constitutes the first observation of this decay mode of the $\Xi_{cc}^+(3520)$.

5 Summary

SELEX is still the only experiment observing double charm baryons. We published observations on two different decays modes, $\Xi_{cc}^+ \to \Lambda_c^+ K^- \pi^+$ [5] and $\Xi_{cc}^+ \to p D^+ K^-$ [12]. After a re-analysis of our full data set, with improved efficiency and resolution, we presented here a higher-statistics observation of $\Xi_{cc}^+ \to \Lambda_c^+ K^- \pi^+$, and a re-analysis of the $\Xi_{cc}(3780)^{++}$. The new analysis also allows access to additional decay modes, and we presented here the first observation of $\Xi_{cc}^+ \to \Xi_c^+ \pi^- \pi^+$.

SELEX will continue the line of analysis, by first publishing these preliminary results. We will try to measure the lifetime of the Ξ_{cc}^+. We will also seek the isospin-partner of the Ξ_{cc}^+, the Ξ_{cc}^{++} in all corresponding decay modes around 3500 MeV/c.

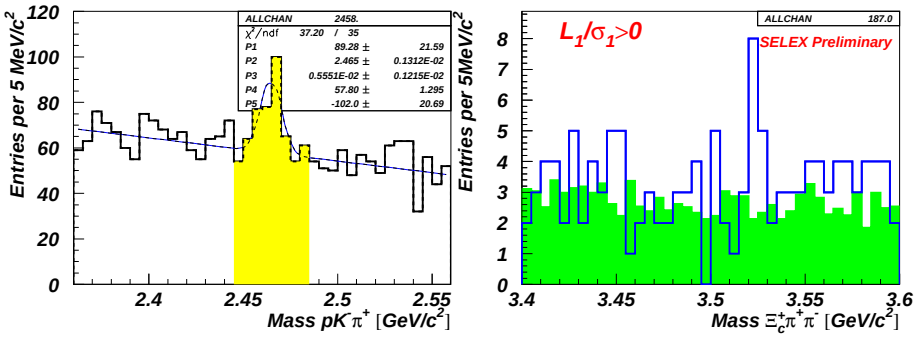

Figure 5: Left: $pK^-\pi^+$ invariant distribution and Ξ_c^+ sample (yellow) used. Right: $\Xi_c^+\pi^+\pi^-$ invariant mass distribution. The green histogram is our estimate of the combinatoric background.

6 Acknowledgment

The author thanks the organizers for the invitation to present these results at the conference. This work was supported in part by the Consejo Nacional de Ciencia y Tecnología (CONACyT), Mexico, and by a special research grant of UASLP.

Bibliography

[1] The SELEX (Fermilab E781) Collaboration: Ball State University, Bogazici University, Carnegie-Mellon University, Centro Brasileiro de Pesquisas Fisicas, Fermilab, Institute For High Energy Physics (Protvino), Institute of High Energy Physics (Beijing), Institute of Theoretical and Experimental Physics (Moscow), Max-Planck-Institute for Nuclear Physics, Moscow State University, Petersburg Nuclear Physics Institute, Tel Aviv University, Universidad Autónoma de San Luis Potosí, Universidade Federal da Paraíba, H. H. Wills Physics Laboratory, University of Bristol, University of Iowa, University of Michigan-Flint, University of Rochester, University of Rome La Sapienza and INFN, University of São Paulo, University of Trieste and INFN. `http://www-selex.fnal.gov`

[2] SELEX Collaboration, to be published.

[3] SELEX Collaboration, M.Iori, et al.: *Measurement of the* Ω_c^0 *lifetime*. Submitted to Physical Review Letters. Preprint Fermilab-Pub-07/011-E, hep-ex/0701021.

[4] Particle Data Group, W. M. Yao et al., Journal of Physics G 33, 1 (2006).

[5] SELEX Collaboration, M. Mattson et al.: *First observation of the doubly charmed baryon* Ξ_{cc}^+. Phys. Rev. Letters **89** (2002) 112001, [arXiv:hep-ex/0208014].

[6] M. Mattson, Ph.D. thesis, Carnegie Mellon University, 2002, FERMILAB-THESIS-2002-03.

[7] S. Ratti, BEACH2002, Vancouver, B.C., see also
`www.hep.vanderbilt.edu/~stenson/xicc/xicc_focus.html`

[8] B. Guberina, B. Melic, and H. Stefancic: Phys. Lett. **B484** (2000) 43.

[9] J. Engelfried: *The Experimental Discovery of Double-Charm Baryons*. Nuclear Physics A 752 (2005) 121c-128c.

[10] M. Moinester: Zeit. Phys. **A355** (1996) 349.

[11] V. Kiselev and A. Likhoded: Phys. Usp. **45** (2002) 455-506, Usp.Fiz.Nauk **172** (2002) 497-550, [arXiv:hep-ex/0103169], and references therein.

[12] SELEX Collaboration, A. Ocherashvili, et al.: *Confirmation of the double charm baryon* $\Xi_{cc}^+(3520)$ *via its decay to* pD^+K^-. Physics Letters B **628** (2005) 18. [arXiv:hep-ex/0406033].

[13] SELEX Collaboration, S.Y. Jun, et al.: *Observation of the Cabibbo-suppressed decay* $\Xi_c^+ \to pK^-\pi^+$. Phys. Rev. Letter **84** (2000) 1857-1861. [hep-ex/9907062].

[14] I. Torres, Ph.D. Thesis, Instituto de Física, Universidad Autónoma de San Luis Potosí, Mexico (2006).

NRQCD and Quarkonia

Nora Brambilla
Dipartimento di Fisica
Università di Milano and INFN,
via Celoria 16,
20133 Milan, ITALY

1 Introduction

Quarkonia play an important role in several high energy experiments. The diversity, quantity and accuracy of the data still under analysis and currently being collected is impressive and includes: data on quarkonium formation from BES at the Beijing Electron Positron Collider (BEPC), E835 at Fermilab, and CLEO at the Cornell Electron Storage Ring (CESR); clean samples of charmonia produced in B-decays, in photon-photon fusion and in initial state radiation, at the B-meson factories, BaBar at PEP-II and Belle at KEKB, including the unexpected observation of large amounts of associated $(c\overline{c})(c\overline{c})$ production and the observation of new and possibly exotics quarkonia states; the CDF and D0 experiments at Fermilab measuring heavy quarkonia production from gluon-gluon fusion in $p\overline{p}$ annihilations at 2 TeV; the Selex experiment at Fermilab with the preliminary observation of possible candidates for doubly charmed baryons; ZEUS and H1, at DESY, studying charmonia production in photon-gluon fusion; PHENIX and STAR, at RHIC, and NA60, at CERN, studying charmonia production, and suppression, in heavy-ion collisions. This has led to the discovery of new states, new production mechanisms, new decays and transitions, and in general to the collection of high statistics and precision data sample. In the near future, even larger data samples are expected from the BES-III upgraded experiment, while the B factories and the Fermilab Tevatron will continue to supply valuable data for few years. Later on, new experiments at new facilities will become operational (the LHC experiments at CERN, Panda at GSI, hopefully a Super-B factory, a Linear Collider, etc.) offering fantastic challenges and opportunities in this field. A comprehensive review of the experimental and theoretical status of heavy quarkonium physics may be found in the Cern Yellow Report prepared by the Quarkonium Working Group [1]. Many excellent reviews of the field have been presented at this meeting [2].

On the theory side, systems made by two heavy quarks are a rather unique laboratory. They are characterized by the existence of a hierarchy of energy scales in correspondence of which one can construct a hierarchy of nonrelativistic effective field theries (NR EFT), each one with less degrees of freedom left dynamical and thus

simpler. Some of these physical scales are large and may be treated in perturbation theory. The occurrence of these two facts makes two heavy quark systems accessible in QCD. In particular, the factorization of high and low energy scales realized in the EFTs allows us to study low energy QCD effects in a systematic way. Today the remarkable progress in the construction of these nonrelativistic EFTs together with the advance in lattice QCD give us well based theory tools to investigate heavy quarkonia.

Therefore, on the one hand the progress in our understanding of EFTs makes it possible to move beyond phenomenological models and to provide a systematic description from QCD of several aspects of heavy-quarkonium physics. On the other hand, the recent progress in the measurement of several heavy-quarkonium observables makes it meaningful to address the problem of their precise theoretical determination. In this situation heavy quarkonium becomes a very special and relevant system to advance our understanding of strong interactions and our control of some parameters of the Standard Model.

Here I will briefly review some of the recent developments in the construction of NR EFTs with the main emphasis on the physical applications. For some reviews see [3–6].

2 Scales and Effective Field Theories

The description of hadrons containing two heavy quarks is a rather challenging problem, which adds to the complications of the bound state in field theory those coming from the nonperturbative QCD low-energy dynamics. A simplification is provided by the nonrelativistic nature suggested by the large mass of the heavy quarks and manifest in the spectrum pattern. As nonrelativistic systems, quarkonia are characterized by three energy scales, hierarchically ordered by the heavy quark velocity in the center of mass frame $v \ll 1$: the mass m (hard scale), the momentum transfer mv (soft scale), which is proportional to the inverse of the typical size of the system r, and the binding energy mv^2 (ultrasoft scale), which is proportional to the inverse of the typical time of the system. In bottomonium $v^2 \sim 0.1$, in charmonium $v^2 \sim 0.3$, in $t\bar{t}$ $v \sim 0.15$. In perturbation theory $v \sim \alpha_{\rm s}$. Feynman diagrams will get contributions from all momentum regions associated with these scales. Since these momentum regions depend on $\alpha_{\rm s}$, each Feynman diagram contributes to a given observable with a series in $\alpha_{\rm s}$ and a non trivial counting. Besides, the $\alpha_{\rm s}$ associated to different momentum region are evaluated at different scales. For energy scales close to $\Lambda_{\rm QCD}$, the scale at which nonperturbative effects become dominant, perturbation theory breaks down and one has to rely on nonperturbative methods. Regardless of this, the nonrelativistic hierarchy $m \gg mv \gg mv^2$, $m \gg \Lambda_{\rm QCD}$ will persist also below the $\Lambda_{\rm QCD}$ threshold.

The wide span of involved energy scales makes also a lattice calculation in full QCD extremely challenging. However, it is possible to exploit the existence of a hierarchy of scales by introducing a hierarchy of nonrelativistic effective field theories. Lower energy EFTs may be constructed by systematically integrating out modes associated to energy scales not relevant for the two quark system. Such integration is made in a matching procedure that enforces the equivalence between QCD and the EFT at any given order of the expansion in v. Any prediction of the EFT is therefore a prediction of QCD with an error of the size of the neglected order in v. By integrating out the hard modes, one obtains Nonrelativistic QCD [9, 10, 13]. In such EFT, soft and ultrasoft scales are left dynamical and still their mixing complicates calculations and power counting. In the last few years the problem of systematically treating the remaining dynamical scales in an EFT framework has been addressed by several groups [11] and has now reached a good level of understanding. So one can go down one step further and integrate out also the soft scale in a matching procedure to the lowest energy and simplest EFT that can be introduced for quarkonia, where only ultrasoft degrees of freedom remain dynamical. Here I will review potential NRQCD [7, 8], for an alternative and equivalent EFT (in the case in which $\Lambda_{\rm QCD}$ is the smallest scale) see [12]. In the case in which the soft scale is of the same order of $\Lambda_{\rm QCD}$, the matching to pNRQCD is still possible but it is nonperturbative.

3 NonRelativistic QCD (NRQCD)

NRQCD [9,10] is the EFT for two heavy quarks that follows from QCD by integrating out the hard scale m. Only the upper (lower) components of the Dirac fields remain relevant for dymanical quarks (antiquarks) at energies lower than m. Thus quark and antiquarks are described in terms of two-components Pauli spinor fields. The part of the NRQCD Lagrangian bilinear in the heavy quark fields is the same as Heavy Quark Effective Field Theory (HQET) (for a review see [14]) but for the case of two heavy quarks also four fermion operators have to be considered. The Lagrangian is organized as an expansion in v and $\alpha_{\rm s}(m)$:

$$\mathcal{L}_{\rm NRQCD} = \sum_n c_n(m,\mu) \times O_n(\mu, mv, mv^2, \Lambda_{\rm QCD})/m^n. \qquad (1)$$

The NRQCD matching coefficients c_n are series in $\alpha_{\rm s}$ and encode the ultraviolet physics that has been integrated out from QCD. The low energy operators O_n are constructed out of two or four heavy quark/antiquark fields plus gluons. They are counted in powers of v. Since two scales, soft and the ultrasoft, are dynamical, the power counting in v is not unambiguous. The imaginary part of the coefficients of the 4-fermion operators contains the information on heavy quarkonium annihilations. The NRQCD heavy quarkonium Fock state is given by a series of terms, increasingly

subleading, where the leading term is a $Q\overline{Q}$ in a color singlet state and the first correction, suppressed in v, comes from a $Q\overline{Q}$ in a color octet state plus a gluon. The NRQCD Lagrangian can be used for studies of spectroscopy (on the lattice), inclusive decays and electromagnetics threshold production of heavy quarkonia.

4 potential NonRelativistic QCD (pNRQCD)

pNRQCD [3,7,8] is the EFT for two heavy quark systems that follows from NRQCD by integrating out the soft scale mv. Here the role of the potentials and the quantum mechanical nature of the problem are realized in the fact that the Schrödinger equation appears as zero order problem for the two quark states. We may distinguish two situations: 1) weakly coupled pNRQCD when $mv \gg \Lambda_{\rm QCD}$, where the matching from NRQCD to pNRQCD may be performed in perturbation theory; 2) strongly coupled pNRQCD when $mv \sim \Lambda_{\rm QCD}$, where the matching has to be nonperturbative. Recalling that $r^{-1} \sim mv$, these two situations correspond to systems with inverse typical radius smaller than or of the same order as $\Lambda_{\rm QCD}$.

4.1 Weakly coupled pNRQCD

The effective degrees of freedom that remain dynamical are: low energy $Q\overline{Q}$ (Pauli spinor) states that can be decomposed into a singlet field S and an octet field O under colour transformations, have energy of order $\Lambda_{\rm QCD}$, mv^2 and momentum $\mathbf{p}$ of order mv; low energy (ultrasoft (US)) gluons $A_\mu(\mathbf{R}, t)$ with energy and momentum of order $\Lambda_{\rm QCD}$, mv^2. All the gluon fields are multipole expanded (i.e. expanded in the quark-antiquark distance r, R being the center of mass). The Lagrangian is then given by terms of the type

$$\frac{c_k(m,\mu)}{m^k} \times V_n(r\mu', r\mu) \times O_n(\mu', mv^2, \Lambda_{\rm QCD})\, r^n. \qquad (2)$$

where the matching coefficients c_k are inherited from NRQCD and contain the logs in the quark masses, the pNRQCD potential matching coefficients V_n encode the non-analytic behaviour in r and the low energy operators O_n are constructed in terms of singlet, octet fields and ultrasoft gluons. At leading order in the multipole expansion, the singlet sector of the Lagrangian gives rise to equations of motion of the Schrödinger type. Each term in the pNRQCD Lagrangian has a definite power counting. The bulk of the interaction is carried by potential-like terms, but non-potential interactions, associated with the propagation of low energy degrees of freedom are present as well. Such retardation (or non-potential) effects start at the next-to-leading order (NLO) in the multipole expansion and are systematically encoded in the theory and typically related to nonperturbative effects [8]. There is a systematic procedure to calcolate

corrections in v to physical observables: higher order perturbative (bound state) calculations in this framework become viable. In particular the EFT can be used for a very efficient resummation of large logs (typically logs of the ratio of energy and momentum scales) using the renormalization group (RG) adapted to the case of correlated scales [12, 15]; Poincaré invariance is not lost, but shows up in some exact relations among the matching coefficients [16]. The renormalon subtraction may be implemented systematically obtaining a perturbative series better behaved and allowing a factorization of the genuine QCD nonperturbative effects.

4.2 Strongly coupled pNRQCD

In this case the matching to pNRQCD is nonperturbative. Away from threshold (precisely when heavy-light meson pair and heavy hybrids develop a mass gap of order $\Lambda_{\rm QCD}$ with respect to the energy of the $Q\overline{Q}$ pair), the quarkonium singlet field S remains as the only low energy dynamical degree of freedom in the pNRQCD Lagrangian (if no ultrasoft pions are considered), which reads [3, 19, 20]:

$$\mathcal{L}_{\rm pNRQCD} = \mathrm{S}^\dagger \left(i\partial_0 - \frac{\mathbf{p}^2}{2m} - V_S(r) \right) \mathrm{S}. \tag{3}$$

The matching potential $V_S(r)$ is a series in the expansion in the inverse of the quark masses: static, $1/m$ and $1/m^2$ terms have been calculated, see [19, 20]. They involve NRQCD matching coefficients and low energy nonperturbative parts given in terms of Wilson loops and field strengths insertions in the Wilson loop. In this regime we recover the quark potential singlet model from pNRQCD. However the potentials are calculated from QCD in the formal nonperturbative matching procedure. An actual evaluation of the low energy part requires lattice evaluation [17] or QCD vacuum models calculations [18, 27].

5 Applications

The condition $m \ll \Lambda_{\rm QCD}$ always holds and thus the first matching from QCD to NRQCD is a perturbative matching. NRQCD describes in principle all heavy quarkonia states and physical processes. However, since still the soft and the ultrasoft scales are dynamical, the power counting is not unambiguous and in some cases may differ from the perturbative inspired BBL counting [10, 34, 35]. The number of nonperturbative operators tend to increase with the order of the expansion in v, and their expectation values depend both on the quarkonium states and the US gluons. The NRQCD lattice implementation still requires the calculation of the NRQCD matching coefficients in the lattice regularization, which is still missing in many cases. Being

NRQCD a nonrenormalizable theory at the leading order Lagrangian, NRQCD lattice calculations maybe tricky.

The lowest energy EFT, pNRQCD, is simpler and as such may be more predictive. However, in the present formulation, it is valid only for states away from threshold. Since we are now integrating out also the soft scale, it is important to establish when $\Lambda_{\rm QCD}$ sets in, i.e. when we have to resort to non-perturbative methods. For low-lying resonances, it is reasonable, although not proved, to assume $mv^2 \gtrsim \Lambda_{\rm QCD}$. The system is weakly coupled and we may rely on perturbation theory, for instance, to calculate the potential. The theoretical challenge here is performing higher-order calculations and the goal is precision physics. For high-lying resonances, we assume $mv \sim \Lambda_{\rm QCD}$. The system is strongly coupled and the potential must be determined non-perturbatively, for instance, on the lattice. The theoretical challenge here is providing a consistent framework where to perform lattice calculations and the progress is measured by the advance in lattice computations. The number of nonperturbative operators maybe be greatly reduced with respect to NRQCD, since a further factorization at the soft scale is realized and nonperturbative contributions become typically only a function of the US gluons. The pNRQCD leading order strongly coupled Lagrangian is renormalizable allowing in principle a straightforward lattice implementation.

Both in NRQCD and pNRQCD a source of concern may arise from the large v^2 corrections in the charmonium case. Large (renormalon-like) perturbative contributions in the matching coefficients need to be properly taken care, resummed and subtracted.

6 QCD potentials

The QCD potentials achieve a well defined status and definition only in pNRQCD: they are the matching coefficients of the EFT and as such there is a well defined procedure to calculate them. They depend on the scale of the matching. In weakly coupled pNRQCD the soft scale is bigger than $\Lambda_{\rm QCD}$ and so the singlet and octet potentials have to be calculated in the perturbative matching. In [21] a determination of the singlet potential at three loops leading log has been obtained inside the EFT which gives the way to deal with the well known infrared singularity arising in the potential at this order [36]. From this, $\alpha_{\rm s}$ in the V regularization can be obtained, showing a dependence on the infrared behaviour of the theory at this order and for this regularization. The finite terms in the singlet static potential at three loops are not yet known but has been estimated [24]. Recently, also the logarithmic contribution at four loops has been calculated [23]. The three loop renormalization group improved calculation of the static singlet potential has been compared to the lattice calculation and found in good agreement up to about 0.25 fm [22]. The static octet potential is

known at two loops [25] and again agrees well with the lattice data [26].

At a scale μ such that $mv \sim \Lambda_{\rm QCD} \gg \mu \gg mv^2$, confinement sets in and the potentials become admixture of perturbative terms, inherited from NRQCD, which encode high-energy contributions, and non-perturbative objects. Strongly coupled pNRQCD gives us the general form of the potentials obtained in the nonperturbative matching to QCD in the form of Wilson loops and Wilson loop chromoelectric and chromomagnetic field strengths insertions [19, 20], very well suited for lattice calculations. These will be in general complex valued functions. The real part controls the spectrum and the imaginary part controls the decays.

The real part of the potential has been one of the first quantities to be calculated on the lattice (for a review see [17]). In the last year, there has been some remarkable progress. In [28], the $1/m$ potential has been calculated for the first time. The existence of this potential was first pointed out in the pNRQCD framework [19]. A $1/m$ potential is typically missing in potential model calculations. The lattice result shows that the potential has a $1/r$ behaviour, which, in the charmonium case, is of the same size as the $1/r$ Coulomb tail of the static potential and, in the bottomonium one, is about 25%. Therefore, if the $1/m$ potential has to be considered part of the leading-order quarkonium potential together with the static one, as the pNRQCD power counting suggests and the lattice seems to show, then the leading-order quarkonium potential would be, somewhat surprisingly, a flavor-dependent function. In [29], spin-dependent potentials have been calculated with unprecedented precision. In the long range, they show, for the first time, deviations from the flux-tube picture of chromoelectric confinement [27, 30]. The knowledge of the potentials in pNRQCD could provide an alternative to the direct determination of the spectrum in NRQCD lattice simulations: the quarkonium masses would be determined by solving the Schrödinger equation with the lattice potentials. The approach may present some advantages: the leading-order pNRQCD Lagrangian, differently from the NRQCD one, is renormalizable, the potentials are determined once for ever for all quarkonia, and the solution of the Schrödinger equation provides also the quarkonium wave functions, which enter in many quarkonium observables: decay widths, transitions, production cross-sections. The existence of a power counting inside the EFT selects the leading and the subleading terms in quantum-mechanical perturbation theory. Moreover, the quantum mechanical divergences (typically encountered in perturbative calculations involving iterations of the potentials, as in the case of the iterations of spin delta potentials) are absorbed by NRQCD matching coefficients. Since a factorization between the hard (in the NRQCD matching coefficients) and soft scales (in the Wilson loops or nonlocal gluon correlators) is realized and since the low energy objects are only glue dependent, confinement investigations, on the lattice and in QCD vacuum models become feasible [18, 27].

The potentials evaluated on the lattice once used in the Schrödinger equation produce the spectrum. The calculations involve only QCD parameters (at some scale

and in some scheme).

7 Precision determination of Standard Model parameters

Given the advancement in the EFTs formulation and in the lattice calculations as well as the existence of several high order perturbative bound state calculations, quarkonia may become a very appropriate system for the extraction of precise determination of the Standard Model parameters like $\alpha_{\rm s}$ and the heavy quark masses. Such precise determinations are important for physics inside and beyond the Standard Model. Inside the QWG (www.qwg.to.infn.it) there is a topical group for such studies and in the QWG YR [1] there is a dedicated chapter.

7.1 c and b mass extraction

The lowest heavy quarkonium states are suitable systems to extract a precise determination of the mass of the heavy quarks b and c. Perturbative determinations of the $\Upsilon(1S)$ and J/ψ masses have been used to extract the b and c masses. The main uncertainty in these determinations comes from nonperturbative nonpotential contributions (local and nonlocal condensates) together with possible effects due to subleading renormalons. These determinations are competitive with those coming from different systems and different approaches (for the b mass see e.g. [84]). We report some recent determinations in Tab. 7.1.

A recent analysis performed by the QWG [1] and based on all the previous determinations indicates that at the moment the mass extraction from heavy quarkonium involves an error of about 50 MeV both for the bottom (1% error) and in the charm (4% error) mass. It would be very important to be able to further reduce the error on the heavy quark masses.

7.2 Determinations of $\alpha_{\rm s}$.

Heavy quarkonia leptonic and non-leptonic inclusive and radiative decays may provide means to extract α_s. The present PDG determination of α_s from bottomonium pulls down the global α_s average noticeably [1]. Recently, using the most recent CLEO data on radiative $\Upsilon(1S)$ decays and dealing with the octet contributions within weakly coupled pNRQCD, a new determination of $\alpha_{\rm s}(M_{\Upsilon(1S)}) = 0.184^{+0.014}_{-0.013}$ has been obtained [43], which corresponds to $\alpha_{\rm s}(M_Z) = 0.119^{+0.006}_{-0.005}$ in agreement with the central value of the PDG [71] and with competitive errors.

reference	order	$\overline{m}_b(\overline{m}_b)$ (GeV)
[85]	NNNLO*	$4.210 \pm 0.090 \pm 0.025$
[86]	NNLO +charm	$4.190 \pm 0.020 \pm 0.025$
[88]	NNLO	4.24 ± 0.10
[87]	NNNLO*	4.346 ± 0.070
[89]	NNNLO*	4.20 ± 0.04
[90]	NNNLO*	4.241 ± 0.070
[91]	NNLL*	4.19 ± 0.06
reference	order	$\overline{m}_c(\overline{m}_c)$ (GeV)
[79]	NNLO	1.24 ± 0.020
[88]	NNLO	1.19 ± 0.11

Table 1: Different recent determinations of $\overline{m}_b(\overline{m}_b)$ and $\overline{m}_c(\overline{m}_c)$ in the $\overline{\rm MS}$ scheme from the bottomonium and the charmonium systems. The displayed results either use direct determinations or non-relativistic sum rules. Here and in the text, the * indicates that the theoretical input is only partially complete at that order.

7.3 Top-antitop production near threshold at ILC.

In [91, 92] the total cross section for top quark pair production close to threshold in e+e- annihilation is investigated at NNLL in the weakly coupled EFT. The summation of the large logarithms in the ratio of the energy scales is achieved with the renormalization group (for correlated scales) and significantly reduces the scale dependence of the results. Studies like these will make feasible a precise extractions of the strong coupling, the top mass and the top width at a future ILC.

8 Spectra

The NRQCD Lagrangian is well suited for lattice calculations [31]. The quark propagators are the nonrelativistic ones and since the heavy-quark mass scale has been integrated out, for NRQCD on the lattice, it is sufficient to have a lattice spacing a as coarse as $m \gg 1/a \gg mv$. A price to pay is that, by construction, the continuum limit cannot be reached. Another one is that the NRQCD Lagrangian has to be supplemented by matching coefficients calculated in lattice perturbation theory, which encode the contributions from the heavy-mass energy modes that have been integrated out. A recent unquenched determination of the bottomonium spectrum with staggered sea quarks can be found in [32]. The fact that all matching coefficients of NRQCD on the lattice are taken at their tree-level value induces a systematic error of order $\alpha_s v^2$ for the radial splittings and of order α_s for the fine and hyperfine

splittings.

Inside pNRQCD we have to consider separately systems with a small interquark radius (low-lying states) and systems with a radius comparable or bigger than the confinement scale $\Lambda_{\rm QCD}^{-1}$ (high-lying states). It is difficult to say to which group a specific resonance may belong, since there are no direct measurements of the interquark radius. Electric dipole transitions or quarkonium dissociation in a medium, once a well founded theory treatment of such processes will be given, may give a clear cut procedure. At the moment one uses the typical EFT approaches assuming that a particular scales hierarchy holds and checking then a posteriori that the prediction and the error estimated inside such framework are consistent with the data.

Low-lying $Q\overline{Q}$ states are assumed to realize the hierarchy: $m \gg mv \gg mv^2 \gtrsim \Lambda_{\rm QCD}$ and they may be described in weakly coupled pNRQCD.

B_c mass (MeV)				
[82] (expt)	[81] (lattice)	[80] (NNLO)	[79] (NNLO)	[86] (NNLO)
$6287 \pm 4.8 \pm 1.1$	$6304 \pm 12^{+12}_{-0}$	6326(29)	6324(22)	6307(17)

Table 2: Different perturbative determinations of the B_c mass compared with the experimental value and a recent lattice determination.

Once the heavy quark masses are known, one may use them to extract other quarkonium ground-state observables. The B_c mass has been calculated at NNLO in [79,80,86], see Table 2. These values agree well with the unquenched NRQCD/Fermilab method) lattice determination of [81], which shows that the B_c mass is not very sensitive to non-perturbative effects. This is confirmed by a recent measurement of the B_c in the channel $B_c \to J/\psi\,\pi$ by the CDF collaboration at the Tevatron; they obtain with 360 pb^{-1} of data $M_{B_c} = 6285.7 \pm 5.3 \pm 1.2$ MeV [82], while the latest available figure based on 1.1 fb^{-1} of data is $M_{B_c} = 6276.5 \pm 4.0 \pm 2.7$ MeV (see http://www-cdf.fnal.gov/physics/new/bottom/060525.blessed-bc-mass/).

The bottomonium and charmonium ground-state hyperfine splitting has been calculated at NLL in [93]. Combining it with the measured $\Upsilon(1S)$ mass, this determination provides a quite precise prediction for the η_b mass: $M_{\eta_b} = 9421 \pm 10^{+9}_{-8}$ MeV, where the first error is an estimate of the theoretical uncertainty and the second one reflects the uncertainty in $\alpha_{\rm s}$. Note that the discovery of the η_b may provide a very competitive source of $\alpha_{\rm s}$ at the bottom mass scale with a projected error at the M_Z scale of about 0.003. Similarly, in [94], the hyperfine splitting of the B_c was calculated at NLL accuracy: $M_{B_c^*} - M_{B_c} = 65 \pm 24^{+19}_{-16}$ MeV.

High-lying $Q\overline{Q}$ states are assumed to realize the hierarchy: $m \gg mv \sim \Lambda_{\rm QCD} \gg mv^2$. A first question is where the transition from low-lying to high-lying takes place. This is not obvious, because we cannot measure directly mv. Therefore, the answer can only be indirect and, so far, there is no clear agreement in the literature. A weak-coupling treatment for the lowest-lying bottomonium states ($n = 1$, $n = 2$ and

also for the $\Upsilon(3S)$) appears to give positive results for the masses at NNLO in [79] and at N^{3}LO* in [37]. The result is more ambiguous for the fine splittings of the bottomonium $1P$ levels in the NLO analysis of [42] and positive only for the $\Upsilon(1S)$ state in the N^{3}LO* analysis of [38].

Masses of high-lying quarkonia may be accessed either using the lattice nonperturbative potentials inside a Schrödinger equation [33] or via a direct lattice pNRQCD calculation.

9 Transitions and decays

9.1 Inclusive Decays

NRQCD gives a factorization formula for heavy quarkonium inclusive decay widths, precisely it factorizes four-fermion matching coefficients and matrix elements of four fermion operators [10]. Color singlet operator expectation values may be easily related to the square of the quarkonium wave functions (or derivatives of it) at the origin. Octet contributions remain as nonperturbative matrix elements of operators evaluated over the quarkonium states. In some situations the octet contributions may not be suppressed and become as relevant as the singlet contributions in the NRQCD power counting. In particular octet contributions may reabsorb the dependence on the infrared cut-off of the Wilson coefficients, solving the problem that arised originally in the color singlet potential model [61].

Systematic improvements are possible, either by calculating higher-order corrections in the coupling constant or by adding higher-order operators.

In order to describe electromagnetic and hadronic inclusive decay widths of heavy quarkonia, many NRQCD matrix elements are needed. The specific number depends on the order in v of the non-relativistic expansion to which the calculation is performed and on the power counting. At order mv^5 and within a conservative power counting, S- and P-wave electromagnetic and hadronic decay widths for bottomonia and charmonia below threshold depend on 46 matrix elements [34]. More are needed at order mv^7 [58–60]. Order mv^7 corrections are particularly relevant for P-wave quarkonium decays, since they are numerically as large as NLO corrections in $\alpha_{\rm s}$, which are known since long time [61] and to which the most recent data are sensitive [1, 62]. NRQCD matrix elements may be fitted to the experimental decay data [63, 64] or calculated on the lattice [65–67]. The matrix elements of color-singlet operators are related at leading order to the Schrödinger wave functions at the origin [10] and, hence, may be evaluated by means of potential models [68] or potentials calculated on the lattice [17]. However, a great part of the matrix elements remain poorly known or unknown.

In the matching coefficients large contributions in the perturbative series coming from bubble-chain diagrams may need to be resummed [69].

In lattice NRQCD in [32], the ratio $\Gamma(\Upsilon(2S) \to e^+e^-)/\Gamma(\Upsilon(1S) \to e^+e^-) \times M^2_{\Upsilon(2S)}/M^2_{\Upsilon(1S)}$ has been calculated. The result on the finest lattice compares well with the experimental one.

The imaginary part of the potential provides the NRQCD decay matrix elements in pNRQCD. For excited states, they typically factorize in a part, which is the wave function in the origin squared (or its derivatives), and in a part which contains gluon tensor-field correlators [34, 54–56]. This drastically reduces the number of non-perturbative parameters needed; in pNRQCD, these are wave functions at the origin and universal gluon tensor-field correlators, which can be calculated on the lattice. Another approach may consist in determining the correlators on one set of data (e.g. in the charmonium sector) and use them to make predictions for another (e.g. in the bottomonium sector). Following this line in [54,57], at NLO in $\alpha_{\rm s}$, but at leading order in the velocity expansion, it was predicted $\Gamma_{\rm had}(\chi_{b0}(2P))/\Gamma_{\rm had}(\chi_{b2}(2P)) \approx 4.0$ and $\Gamma_{\rm had}(\chi_{b1}(2P))/\ \Gamma_{\rm had}(\chi_{b2}(2P)) \approx 0.50$. Both determinations turned out to be consistent, within large errors, with the CLEO III data [1]. One should notice that at some order of the expansion in v, the scale $\sqrt{m\Lambda_{\rm QCD}}$ start also to contribute in pNRQCD jeopardizing in some cases the effective reduction of the nonperturbative operators [55].

For the lowest resonances, inclusive decay widths are given in weakly coupled pNRQCD by a convolution of perturbative corrections and nonlocal nonperturbative correlators. The perturbative calculation embodies large contributions and requires large logs resummation. The ratio of electromagnetic decay widths was calculated for the ground state of charmonium and bottomonium at NNLL order in [75]. In particular, they report: $\Gamma(\eta_b \to \gamma\gamma)/\Gamma(\Upsilon(1S) \to e^+e^-) = 0.502 \pm 0.068 \pm 0.014$, which is a very stable result with respect to scale variation. A partial NNLL* order analysis of the absolute width of $\Upsilon(1S) \to e^+e^-$ can be found in [76].

9.2 Electromagnetic transitions

Allowed magnetic dipole transitions between charmonium and bottomonium ground states have been considered in pNRQCD at NNLO in [40, 70]. The results are: $\Gamma(J/\psi \to \gamma\,\eta_c) = (1.5 \pm 1.0)$ keV and $\Gamma(\Upsilon(1S) \to \gamma\,\eta_b) = (k_\gamma/39\ \text{MeV})^3\ (2.50 \pm 0.25)$ eV, where the errors account for uncertainties (which are large in the charmonium case) coming from higher-order corrections. The width $\Gamma(J/\psi \to \gamma\,\eta_c)$ is consistent with [71]. Concerning $\Gamma(\Upsilon(1S) \to \gamma\,\eta_b)$, a photon energy $k_\gamma = 39$ MeV corresponds to a η_b mass of 9421 MeV. The pNRQCD calculation features a small quarkonium magnetic moment (in agreement with a recent lattice calculation [78]) and the interesting fact, related to the Poincaré invariance of the nonrelativistic EFT [16], that M1 transition of the lowest quarkonium states at relative order v^2 are completely accessible in perturbation theory [40].

In the weak-coupling regime, the magnetic-dipole hindered transition $\Upsilon(2S) \to$

$\gamma\,\eta_b$ at leading order [40] does not agree with the experimental upper bound [39]. It should be still clarified if this is related to the fact that $\Upsilon(2S)$ system belongs to the strong coupling regime or if it is due to large corrections (more relevant in the hindered case).

9.3 Semi-inclusive decays

The radiative transition $\Upsilon(1S) \to \gamma\, X$ has been considered in [72,73]. The agreement with the CLEO data of [74] is very satisfactory when one properly includes the octet contribution in pNRQCD [73]. In the same work it is found that the ratios for different n of the radiative decay widths $\Gamma(\Upsilon(nS) \to \gamma\, X)$ are better consistent with the data if $\Upsilon(1S)$ is assumed to be a weakly-coupled bound state and $\Upsilon(2S)$ and $\Upsilon(3S)$ strongly coupled ones [41].

In general in exclusive decays and for certain kinematical end points of semi-inclusive decays, NRQCD or pNRQCD should be supplemented by collinear degrees of freedom. This can be realized in the framework of Soft Collinear Effective Theory (SCET) [95].

10 Baryons with two or more heavy quarks

The SELEX collaboration at Fermilab reported evidence for five resonances that may be possibly identified with doubly charmed baryons, see the presentation of Jurgen Engelfried at this meeting [2] and [44]. Although these results have not been confirmed by other experiments (FOCUS, BELLE and BABAR) they have triggered a renewed theoretical interest in doubly heavy baryon systems.

Low-lying QQq states may be assumed to realize the hierarchy: $m \gg mv \gg \Lambda_{\rm QCD}$, where mv is the typical inverse distance between the two heavy quarks and $\Lambda_{\rm QCD}$ is the typical inverse distance between the centre-of-mass of the two heavy quarks and the light quark. At a scale μ such that $mv \gg \mu \gg \Lambda_{\rm QCD}$ the effective degrees of freedom are QQ states (in color antitriplet and sextet configurations), low-energy gluons and light quarks. The most suitable EFT at that scale is a combination of pNRQCD and HQET [45,46]. The hyperfine splittings of the doubly heavy baryon lowest states have been calculated at NLO in $\alpha_{\rm s}$ and at LO in $\Lambda_{\rm QCD}/m$ by relating them to the hyperfine splittings of the D and B mesons (this method was first proposed in [47]). In [45], the obtained values are: $M_{\Xi_{cc}^*} - M_{\Xi_{cc}} = 120 \pm 40$ MeV and $M_{\Xi_{bb}^*} - M_{\Xi_{bb}} = 34 \pm 4$ MeV, which are consistent with the quenched lattice determinations of [48, 49] and the quenched NRQCD lattice determinations of [50, 51]. Chiral corrections to the doubly heavy baryon masses, strong decay widths and electromagnetic decay widths have been considered in [52].

Also low-lying QQQ baryons can be studied in a weak coupling framework. Three

quark states can combine in four color configurations: a singlet, two octets and a decuplet, which lead to a rather rich dynamics [45]. Masses of various QQQ ground states have been calculated with a variational method in [53]: since baryons made of three heavy quarks have not been discovered so far, it may be important for future searches to remark that the baryon masses turn our to be lower than those generally obtained in strong coupling analyses.

For QQQ baryons with a typical distance of the order $\Lambda_{\rm QCD}$ inverse, the form of the static, $1/m$ and spin dependent nonperturbative potentials have been obtained in pNRQCD [45]. Up to now only the static potential has been evaluated on the lattice [17, 77].

11 Gluelump spectrum and exotic states

Gluelumps are states formed by a gluon and two heavy quarks in a octet configuration at small interquark distance [97] . The mass of such nonperturbative objects are typically measured on the lattice. The tower of hybrids static energies [96] measured in lattice NRQCD reduces to the gluelump masses for small interquark distances. In pNRQCD [8, 26] the full structure of the gluelump spectrum has been studied, obtaining model independent predictions on the shape, the pattern, the degeneracy and the multiplet structure of the hybrid static energies for small $Q\overline{Q}$ distances that well match and interpret the existing lattice data. These studies may be important both to elucidate the confinement mechanism (the gluelump masses control the behaviour of the nonperturbative glue correlators appearing in the spectrum and in the decays) and in relation to the exotic states recently observed at the B-factories. The $Y(4260)$ in the charmonium sector may be identified with an hybrid state inside such picture. A complete pNRQCD description of heavy hybrids is still missing.

12 Production

Before the advent of NRQCD, colour singlet production and colour singlet fragmentation underestimated the data on prompt quarkonium production at Fermilab by about an order of magnitude indicating that additional fragmentation contributions were missing [83]. The missing contribution was precisely the gluon fragmentation into colour-octet ${}^3S_1$ charm quark pairs. The probability to form a J/ψ particle from a pointlike $c\overline{c}$ pair in a colour octet ${}^3S_1$ state is given by a NRQCD nonperturbative matrix element which is suppressed by v^4 with respect to to the leading singlet term but is enhanced by two powers of $\alpha_{\rm s}$ in the short distance matching coefficient for producing colour-octet quark pairs. Introducing the leading colour-octet contributions, the data of CDF could be reproduced and this has been an important result of NRQCD [83]. NRQCD factorization has proved to be very successful to explain

a large variety of quarkonium production processes (for a review see the production chapter in [1] and [5]). A formal proof of the NRQCD factorization formula for heavy quarkonium production has however not yet been obtained. Recently, there has been important work in the direction of an all order proof in [98, 99]. In particular, it has been shown that a necessary condition for factorization to hold at NNLO is that the conventional octet NRQCD production matrix elements have to be redefined with Wilson lines, acquiring manifest gauge invariance.

For production, a pNRQCD formulation is not yet existing. In principle to go through a further factorization also in production, if at all possible, may reduce the number of nonperturbative matrix elements and enhance the predictive power.

Two outstanding problems exist at the moment in quarkonium production: double charmonium production in e^+e^- collisions and charmonium polarization at the Tevatron.

In [100], BELLE reports $\sigma(e^+e^- \to J/\psi+\eta_c)\,\mathrm{Br}(c\overline{c} \to > 2 \text{ charged}) = 25.6 \pm 2.8 \pm 3.4$ fb and in [101], BABAR reports $\sigma(e^+e^- \to J/\psi + \eta_c)\,\mathrm{Br}(c\overline{c} \to > 2 \text{ charged}) = 17.6 \pm 2.8^{+1.5}_{-2.1}$ fb. Originally these data were about one order of magnitude above theoretical expectations. Recently, with some errors corrected in some of the theoretical determinations, NLO corrections in α_s calculated in [102] and higher-order v^2 corrections obtained in [103], the theoretical prediction has moved closer to the experimental one. In [104], a preliminary estimate of $\sigma(e^+e^- \to J/\psi + \eta_c)$ including the above corrections gives 16.7 ± 4.2 fb.

Still open is the problem of the BELLE measurement $\sigma(e^+e^- \to J/\psi+c\overline{c})/\sigma(e^+e^- \to J/\psi+X)$, about 80%, with respect to theory calculation that gives about 10% (see [1] for a detailed discussion).

Charmonium polarization has been measured at the Tevatron by the CDF collaboration at run I with 110 pb^{-1} [105] and recently at run II with 800 pb^{-1} [106]. The data of the two runs are not consistent with each other in the 7-12 GeV region of transverse momentum, p_T, and both disagree with the NRQCD expectation of an increased polarization with increased p_T. For large p_T, NRQCD predicts that the main mechanism of charmonium production is via color-octet gluon fragmentation, the gluon being transversely polarized and most of the gluon polarization being transferred to the charmonium. The CDF data do not show any sign of transverse polarization at large p_T.

A solution to such problem may be obtained in the case in which a nonperturbative power counting is valid [34, 35].

13 Challenges

For what concerns systems close or above the open flavor threshold, a complete and satisfactory understanding of the dynamics has not been achieved so far and a corre-

sponding general NR EFT has not yet been constructed. Such systems are difficult to address also with a lattice calculation. Hence, the study of these systems is on a less secure ground than the study of states below threshold. Although in some cases one may develop an EFT owing to special dynamical conditions (as for the $X(3872)$ interpreted as a loosely bound $D^0 \overline{D}^{*0} + \overline{D}^0 D^{*0}$ molecule [107]), the study of these systems largely relies on phenomenological models [108, 109]. The major theoretical challenge here is to interpret the new states in the charmonium region discovered at the B-factories in the last few years.

Heavy ion experiments use quarkonium suppression as one of the smoking guns for quark-gluon plasma formation (cf. e.g. the media chapter in [1]). . To describe quarkonium suppression it would be important to formulate an EFT for heavy quarkonium in media and to obtain a clear definition of the heavy quark potential at finite T . Preliminary studies are ongoing with several approaches [110].

With a good control in theory and high statistic data sample available at present and future (Super-B factory) experiments, heavy quarkonia may also supply us with an alternative way of looking for new physics BSM, cf. [111] and the BSM chapter in [1].

14 Outlook

Today NR EFTs and lattice calculations allow us to investigate a wide range of heavy quarkonium observables in a controlled and systematic fashion and, therefore, learn about one of the most elusive sectors of the Standard Model: low-energy QCD.

Predictions based on non-relativistic EFTs are conceptually solid, and systematically improvable. EFTs have put quarkonium on the solid ground of QCD: quarkonium becomes a privileged window for precision measurements, new physics and confinement mechanism investigations.

Many new data on heavy-quark bound states are provided in these years by the B-factories, CLEO and the Tevatron experiments. Many more will come in the near future from BES-III, LHC and later Panda at GSI. They will show new (perhaps exotic) states, new production and decay mechanisms and they will be a great arena for new EFT tools.

15 Acknowledgments

I would like to thank the organizers for the invitation and for the perfect organization of this very enjoable conference. The support by the European Research Training Network Flavianet, contract number MRTN-CT-2006-035482 is gratefully acknowleged.

Bibliography

[1] N. Brambilla *et al.*, *Heavy quarkonium physics*, CERN-2005-005, (CERN, Geneva, 2005) [arXiv:hep-ph/0412158].

[2] See the presentations at this meeting by J. Engelfried [the SELEX Collaboration], arXiv:hep-ex/0702001; T. Lesiak, arXiv:hep-ex/0612042; T. K. Pedlar, arXiv:hep-ex/0702011; J. Ritman, arXiv:hep-ex/0702013.

[3] N. Brambilla, A. Pineda, J. Soto and A. Vairo, Rev. Mod. Phys. **77**, 1423 (2005) [arXiv:hep-ph/0410047].

[4] J. Soto, arXiv:nucl-th/0611055; A. Vairo, arXiv:hep-ph/0610251; P. Ruiz-Femenia and A. Hoang, arXiv:hep-ph/0611291; A. V. Manohar and I. W. Stewart, Nucl. Phys. Proc. Suppl. **94**, 130 (2001) [arXiv:hep-lat/0012002]; N. Brambilla, arXiv:hep-ph/0012026.

[5] G. T. Bodwin, Int. J. Mod. Phys. A **21**, 785 (2006) [arXiv:hep-ph/0509203].

[6] G. P. Lepage, arXiv:hep-ph/0506330; B. Grinstein, Int. J. Mod. Phys. A **15**, 461 (2000) [arXiv:hep-ph/9811264]; U. Van Kolck, L. J. Abu-Raddad and D. M. Cardamone, arXiv:nucl-th/0205058; A. H. Hoang, arXiv:hep-ph/0204299. I. Z. Rothstein, arXiv:hep-ph/0308266.

[7] A. Pineda and J. Soto, Nucl. Phys. Proc. Suppl. **64**, 428 (1998) [arXiv:hep-ph/9707481].

[8] N. Brambilla, A. Pineda, J. Soto and A. Vairo, Nucl. Phys. B **566**, 275 (2000) [arXiv:hep-ph/9907240].

[9] W. E. Caswell and G. P. Lepage, Phys. Lett. B **167**, 437 (1986).

[10] G. T. Bodwin, E. Braaten and G. P. Lepage, Phys. Rev. D **51**, 1125 (1995) [Erratum-ibid. D **55**, 5853 (1997)] [hep-ph/9407339].

[11] M. Beneke and V. A. Smirnov, Nucl. Phys. B **522**, 321 (1998) [arXiv:hep-ph/9711391]; B. A. Kniehl and A. A. Penin, Nucl. Phys. B **563**, 200 (1999) [arXiv:hep-ph/9907489]. M. E. Luke and A. V. Manohar, Phys. Rev. D **55**, 4129 (1997) [arXiv:hep-ph/9610534].

[12] M. E. Luke, A. V. Manohar and I. Z. Rothstein, Phys. Rev. D **61**, 074025 (2000) [arXiv:hep-ph/9910209]; A. H. Hoang and I. W. Stewart, Phys. Rev. D **67**, 114020 (2003) [arXiv:hep-ph/0209340]. A. V. Manohar and I. W. Stewart, Phys. Rev. D **62**, 014033 (2000) [arXiv:hep-ph/9912226].

[13] A. V. Manohar, Phys. Rev. D **56**, 230 (1997) [arXiv:hep-ph/9701294].

[14] M. Neubert, Phys. Rept. **245**, 259 (1994) [arXiv:hep-ph/9306320].

[15] A. Pineda, Phys. Rev. D **65**, 074007 (2002); A. Pineda and J. Soto, Phys. Lett. B **495**, 323 (2000).

[16] N. Brambilla, D. Gromes and A. Vairo, Phys. Lett. B **576**, 314 (2003); Phys. Rev. D **64**, 076010 (2001);

[17] G. S. Bali, Phys. Rept. **343**, 1 (2001) [arXiv:hep-ph/0001312].

[18] N. Brambilla and A. Vairo, arXiv:hep-ph/9904330.

[19] N. Brambilla, A. Pineda, J. Soto and A. Vairo, Phys. Rev. D **63**, 014023 (2001) [arXiv:hep-ph/0002250].

[20] A. Pineda and A. Vairo, Phys. Rev. D **63**, 054007 (2001) [Erratum-ibid. D **64**, 039902 (2001)] [arXiv:hep-ph/0009145].

[21] N. Brambilla, A. Pineda, J. Soto and A. Vairo, Phys. Rev. D **60**, 091502 (1999) [arXiv:hep-ph/9903355].

[22] A. Pineda, J. Phys. G **29**, 371 (2003) [arXiv:hep-ph/0208031].

[23] N. Brambilla, X. Garcia i Tormo, J. Soto and A. Vairo, arXiv:hep-ph/0610143.

[24] F. A. Chishtie and V. Elias, Phys. Lett. B **521**, 434 (2001) [arXiv:hep-ph/0107052].

[25] B. A. Kniehl, A. A. Penin, Y. Schroder, V. A. Smirnov and M. Steinhauser, Phys. Lett. B **607**, 96 (2005) [arXiv:hep-ph/0412083].

[26] G. S. Bali and A. Pineda, Phys. Rev. D **69**, 094001 (2004) [arXiv:hep-ph/0310130].

[27] N. Brambilla, arXiv:hep-ph/9809263; M. Baker, N. Brambilla, H. G. Dosch and A. Vairo, Phys. Rev. D **58**, 034010 (1998) [arXiv:hep-ph/9802273]. N. Brambilla and A. Vairo, Phys. Rev. D **55**, 3974 (1997) [arXiv:hep-ph/9606344]; arXiv:hep-ph/0004192. [arXiv:hep-ph/9809230]. N. Brambilla, P. Consoli and G. M. Prosperi, Phys. Rev. D **50**, 5878 (1994) [arXiv:hep-th/9401051].

[28] Y. Koma, M. Koma and H. Wittig, Phys. Rev. Lett. **97**, 122003 (2006) [arXiv:hep-lat/0607009].

[29] Y. Koma and M. Koma, arXiv:hep-lat/0609078.

[30] W. Buchmüller, Phys. Lett. B **112**, 479 (1982).

[31] G. P. Lepage, L. Magnea, C. Nakhleh, U. Magnea and K. Hornbostel, Phys. Rev. D **46**, 4052 (1992) [arXiv:hep-lat/9205007].

[32] A. Gray, I. Allison, C. T. H. Davies, E. Gulez, G. P. Lepage, J. Shigemitsu and M. Wingate, Phys. Rev. D **72**, 094507 (2005) [arXiv:hep-lat/0507013].

[33] G. S. Bali, K. Schilling and A. Wachter, Phys. Rev. D **56**, 2566 (1997) [arXiv:hep-lat/9703019].

[34] N. Brambilla, D. Eiras, A. Pineda, J. Soto and A. Vairo, Phys. Rev. D **67**, 034018 (2003) [arXiv:hep-ph/0208019].

[35] S. Fleming, I. Z. Rothstein and A. K. Leibovich, Phys. Rev. D **64**, 036002 (2001) [arXiv:hep-ph/0012062].

[36] T. Appelquist, M. Dine and I. J. Muzinich, Phys. Rev. D **17**, 2074 (1978).

[37] A. A. Penin, V. A. Smirnov and M. Steinhauser, Nucl. Phys. B **716**, 303 (2005) [arXiv:hep-ph/0501042].

[38] M. Beneke, Y. Kiyo and K. Schuller, Nucl. Phys. B **714**, 67 (2005) [arXiv:hep-ph/0501289].

[39] M. Artuso *et al.* [CLEO Collaboration], Phys. Rev. Lett. **94**, 032001 (2005) [hep-ex/0411068].

[40] N. Brambilla, Y. Jia and A. Vairo, Phys. Rev. D **73**, 054005 (2006) [arXiv:hep-ph/0512369].

[41] X. Garcia i Tormo and J. Soto, Phys. Rev. Lett. **96**, 111801 (2006) [arXiv:hep-ph/0511167].

[42] N. Brambilla and A. Vairo, Phys. Rev. D **71**, 034020 (2005) [arXiv:hep-ph/0411156].

[43] N. Brambilla, X. G. i. Tormo, J. Soto and A. Vairo, arXiv:hep-ph/0702079.

[44] A. Ocherashvili *et al.* [SELEX Collaboration], arXiv:hep-ex/0406033; M. Mattson *et al.* [SELEX Collaboration], Phys. Rev. Lett. **89**, 112001 (2002) [arXiv:hep-ex/0208014]; M. A. Moinester *et al.* [SELEX Collaboration], Czech. J. Phys. **53**, B201 (2003) [arXiv:hep-ex/0212029]; see also the SELEX web page http://www-selex.fnal.gov/Welcome.html.

[45] N. Brambilla, A. Vairo and T. Rösch, Phys. Rev. D **72**, 034021 (2005) [arXiv:hep-ph/0506065]; [arXiv:hep-ph/9507300].

[46] S. Fleming and T. Mehen, Phys. Rev. D **73**, 034502 (2006) [arXiv:hep-ph/0509313].

[47] M. J. Savage and M. B. Wise, Phys. Lett. B **248**, 177 (1990).

[48] J. M. Flynn, F. Mescia and A. S. B. Tariq [UKQCD Collaboration], JHEP **0307**, 066 (2003) [arXiv:hep-lat/0307025].

[49] R. Lewis, N. Mathur and R. M. Woloshyn, Phys. Rev. D **64**, 094509 (2001) [arXiv:hep-ph/0107037].

[50] A. Ali Khan *et al.*, Phys. Rev. D **62**, 054505 (2000) [arXiv:hep-lat/9912034].

[51] N. Mathur, R. Lewis and R. M. Woloshyn, Phys. Rev. D **66**, 014502 (2002) [arXiv:hep-ph/0203253].

[52] J. Hu and T. Mehen, Phys. Rev. D **73**, 054003 (2006) [arXiv:hep-ph/0511321].

[53] Y. Jia, arXiv:hep-ph/0607290.

[54] N. Brambilla, D. Eiras, A. Pineda, J. Soto and A. Vairo, Phys. Rev. Lett. **88**, 012003 (2002) [arXiv:hep-ph/0109130].

[55] N. Brambilla, A. Pineda, J. Soto and A. Vairo, Phys. Lett. B **580**, 60 (2004) [arXiv:hep-ph/0307159].

[56] A. Vairo, Mod. Phys. Lett. A **19**, 253 (2004) [arXiv:hep-ph/0311303].

[57] A. Vairo, Nucl. Phys. Proc. Suppl. **115**, 166 (2003) [arXiv:hep-ph/0205128].

[58] G. T. Bodwin and A. Petrelli , Phys. Rev. D **66**, 094011 (2002) [arXiv:hep-ph/0205210].

[59] J. P. Ma and Q. Wang, Phys. Lett. B **537**, 233 (2002) [arXiv:hep-ph/0203082].

[60] N. Brambilla, E. Mereghetti and A. Vairo, JHEP **0608**, 039 (2006) [arXiv:hep-ph/0604190].

[61] R. Barbieri, M. Caffo, R. Gatto and E. Remiddi, Phys. Lett. B **95**, 93 (1980); A. Petrelli, M. Cacciari, M. Greco, F. Maltoni and M. L. Mangano, Nucl. Phys. B **514**, 245 (1998) [arXiv:hep-ph/9707223].

[62] A. Vairo, AIP Conf. Proc. **756**, 101 (2005) [arXiv:hep-ph/0412331].

[63] M. L. Mangano and A. Petrelli, Phys. Lett. B **352**, 445 (1995) [arXiv:hep-ph/9503465].

[64] F. Maltoni, arXiv:hep-ph/0007003.

[65] G. T. Bodwin, D. K. Sinclair and S. Kim, Phys. Rev. Lett. **77**, 2376 (1996) [arXiv:hep-lat/9605023].

[66] G. T. Bodwin, D. K. Sinclair and S. Kim, Phys. Rev. D **65**, 054504 (2002) [arXiv:hep-lat/0107011].

[67] G. T. Bodwin, J. Lee and D. K. Sinclair, Phys. Rev. D **72**, 014009 (2005) [arXiv:hep-lat/0503032].

[68] E. J. Eichten and C. Quigg, Phys. Rev. D **52**, 1726 (1995) [arXiv:hep-ph/9503356].

[69] G.T. Bodwin and Y.Q. Chen, Phys. Rev. **D64**, 114008 (2001); Phys. Rev. **D60**, 054008 (1999).

[70] A. Vairo, arXiv:hep-ph/0608327.

[71] W. M. Yao *et al.* [Particle Data Group], J. Phys. G **33**, 1 (2006).

[72] S. Fleming and A. K. Leibovich, Phys. Rev. D **67**, 074035 (2003) [arXiv:hep-ph/0212094].

[73] X. Garcia i Tormo and J. Soto, Phys. Rev. D **72**, 054014 (2005) [arXiv:hep-ph/0507107].

[74] B. Nemati *et al.* [CLEO Collaboration], Phys. Rev. D **55**, 5273 (1997) [arXiv:hep-ex/9611020].

[75] A. A. Penin, A. Pineda, V. A. Smirnov and M. Steinhauser, Nucl. Phys. B **699**, 183 (2004) [arXiv:hep-ph/0406175].

[76] A. Pineda and A. Signer, arXiv:hep-ph/0607239.

[77] H. Suganuma, T. T. Takahashi, F. Okiharu and H. Ichie, AIP Conf. Proc. **756**, 123 (2005) [arXiv:hep-lat/0412026].

[78] J. J. Dudek, R. G. Edwards and D. G. Richards, Phys. Rev. D **73**, 074507 (2006) [arXiv:hep-ph/0601137].

[79] N. Brambilla, Y. Sumino and A. Vairo, Phys. Lett. B **513**, 381 (2001) [arXiv:hep-ph/0101305].

[80] N. Brambilla and A. Vairo, Phys. Rev. D **62**, 094019 (2000) [arXiv:hep-ph/0002075].

[81] I. F. Allison, C. T. H. Davies, A. Gray, A. S. Kronfeld, P. B. Mackenzie and J. N. Simone [HPQCD Collaboration], Phys. Rev. Lett. **94**, 172001 (2005) [arXiv:hep-lat/0411027].

[82] D. Acosta *et al.* [CDF Collaboration], Phys. Rev. Lett. **96**, 082002 (2006) [arXiv:hep-ex/0505076].

[83] M. Kramer, Prog. Part. Nucl. Phys. **47**, 141 (2001) [arXiv:hep-ph/0106120].

[84] A. X. El-Khadra and M. Luke, Ann. Rev. Nucl. Part. Sci. **52**, 201 (2002) [arXiv:hep-ph/0208114].

[85] A. Pineda, JHEP **0106**, 022 (2001) [arXiv:hep-ph/0105008].

[86] N. Brambilla, Y. Sumino and A. Vairo, Phys. Rev. D **65**, 034001 (2002) [arXiv:hep-ph/0108084].

[87] A. A. Penin and M. Steinhauser, Phys. Lett. B **538**, 335 (2002) [arXiv:hep-ph/0204290].

[88] M. Eidemüller, Phys. Rev. D **67**, 113002 (2003) [arXiv:hep-ph/0207237].

[89] T. Lee, JHEP **0310**, 044 (2003) [arXiv:hep-ph/0304185].

[90] C. Contreras, G. Cvetic and P. Gaete, Phys. Rev. D **70**, 034008 (2004) [arXiv:hep-ph/0311202].

[91] A. Pineda and A. Signer, Phys. Rev. D **73**, 111501 (2006) [arXiv:hep-ph/0601185].

[92] A. H. Hoang, A. V. Manohar, I. W. Stewart and T. Teubner, Phys. Rev. D **65**, 014014 (2002) [arXiv:hep-ph/0107144].

[93] B. A. Kniehl, A. A. Penin, A. Pineda, V. A. Smirnov and M. Steinhauser, Phys. Rev. Lett. **92**, 242001 (2004) [arXiv:hep-ph/0312086].

[94] A. A. Penin, A. Pineda, V. A. Smirnov and M. Steinhauser, Phys. Lett. B **593**, 124 (2004) [arXiv:hep-ph/0403080].

[95] C. W. Bauer, S. Fleming, D. Pirjol and I. W. Stewart, Phys. Rev. D **63**, 114020 (2001) [arXiv:hep-ph/0011336].

[96] K. J. Juge, J. Kuti and C. Morningstar, Phys. Rev. Lett. **90**, 161601 (2003) [arXiv:hep-lat/0207004].

[97] M. Foster and C. Michael [UKQCD Collaboration], Phys. Rev. D **59**, 094509 (1999) [arXiv:hep-lat/9811010].

[98] G. C. Nayak, J. W. Qiu and G. Sterman, Phys. Rev. D **72**, 114012 (2005) [arXiv:hep-ph/0509021].

[99] G. C. Nayak, J. W. Qiu and G. Sterman, arXiv:hep-ph/0608066.

[100] K. Abe *et al.* [Belle Collaboration], Phys. Rev. D **70**, 071102 (2004) [arXiv:hep-ex/0407009].

[101] B. Aubert *et al.* [BABAR Collaboration], Phys. Rev. D **72**, 031101 (2005) [arXiv:hep-ex/0506062].

[102] Y. J. Zhang, Y. j. Gao and K. T. Chao, Phys. Rev. Lett. **96**, 092001 (2006) [arXiv:hep-ph/0506076].

[103] G. T. Bodwin, D. Kang and J. Lee, Phys. Rev. D **74**, 014014 (2006) [arXiv:hep-ph/0603186].

[104] J. Lee, talk at the Quarkonium Working Group meeting (BNL, 2006), http://www.qwg.to.infn.it/WS-jun06 /WS4talks/Thursday_PM/Lee.pdf

[105] A. A. Affolder *et al.* [CDF Collaboration], Phys. Rev. Lett. **85**, 2886 (2000) [arXiv:hep-ex/0004027].

[106] M. J. Kim, talk at the Quarkonium Working Group meeting (BNL, 2006), http://www.qwg.to.infn.it/WS-jun06 /WS4talks/Thursday_AM/Kim.pdf

[107] E. Braaten and M. Kusunoki, Phys. Rev. D **69**, 074005 (2004) [arXiv:hep-ph/0311147]; Phys. Rev. D **72**, 014012 (2005) [arXiv:hep-ph/0506087].

[108] E. J. Eichten, K. Lane and C. Quigg, Phys. Rev. D **73**, 014014 (2006) [Erratum-ibid. D **73**, 079903 (2006)] [arXiv:hep-ph/0511179].

[109] E. S. Swanson, Phys. Rept. **429**, 243 (2006) [arXiv:hep-ph/0601110].

[110] A. Jakovac, P. Petreczky, K. Petrov and A. Velytsky, Phys. Rev. D **75**, 014506 (2007) [arXiv:hep-lat/0611017]; A. Jakovac, P. Petreczky, K. Petrov and A. Velytsky, Phys. Rev. D **75**, 014506 (2007) [arXiv:hep-lat/0611017]; K. Petrov, A. Jakovac, P. Petreczky and A. Velytsky, PoS **LAT2005**, 153 (2006) [arXiv:hep-lat/0509138]; M. Laine, O. Philipsen, P. Romatschke and M. Tassler, arXiv:hep-ph/0611300.

[111] M. A. Sanchis-Lozano, arXiv:hep-ph/0610046.

Charmonium Physics with PANDA at FAIR

James Ritman for the PANDA collaboration
Institute for Nuclear Physics (IKP)
Forschungszentrum Jülich
D-52425 Jülich, Germany

1 Introduction

The science goals underlying the future international Facility for Antiproton and Ion Research - FAIR - [1] that is being realized in Darmstadt span a broad range of research activities on the structure of matter. One component of this facility is directed towards studies of hadronic matter at the sub-nuclear level with beams of antiprotons. These studies focus on two key aspects: confinement of quarks and the generation of the hadron masses. These goals will be pursued by performing precision measurements of charged and neutral decay products from antiproton-proton annihilation in the charmonium mass region.

The PANDA experiment, located at an internal target position of the High Energy Storage Ring for anti-protons HESR, is one of the large installations at the future FAIR facility [2]. It is being planned by a multi-national collaboration, currently consisting of about 350 physicists from 50 institutions in 15 countries. The PANDA detector is designed as a multi-purpose setup. The cornerstones of the PANDA physics program are:

- Study of narrow charmonium states with unprecedented precision
- Search for gluonic excitations such as hybrids and glueballs in the charmonium mass region
- Investigate the properties of mesons with hidden and open charm in the nuclear medium
- Spectroscopy of double strange hypernuclei.

In addition to these topics a number of additional physics opportunties will open up as the facility achieves or exceeds the design goals for luminosity and resolution. These include electromagentic final states (e.g. wide angle Compton Scattering, EM Form-factors, etc.), D-meson spectroscopy, excited strange and charm baryon spectroscopy as well as CP violation in the D and/or Λ sectors.

In this report I will concentrate on the charmonium issues relevant to PANDA.

2 Charmonium physics with PANDA

The discovery of the J/Ψ in 1974 and subsequently other charmonium systems greatly stimulated the understanding of the strong interaction in terms of QCD. The low density of states and the small widths below the open charm threshold reduce mixing among them thereby offering unique advantages for understanding quarkonium.

Extensive studies of the Ψ states have been performed at e^+e^- machines where they can be formed directly. In contrast, formation reactions of the type $\overline{p}p \rightarrow X$ can excite charmonium states of all quantum numbers. As a result, the precision of mass and width measurements is determined by the precision of the phasespace cooled beam momentum distribution and not the (significantly poorer) detector resolution. The concept of the resonance scan is illustrated in Figure 1. In this figure

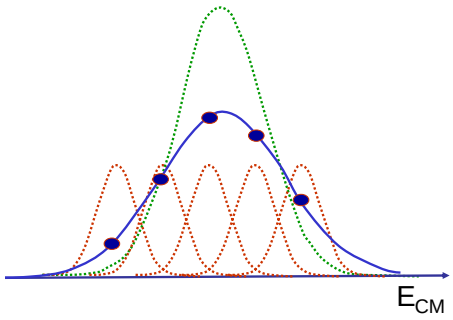

Figure 1: Schematic overview of the resonance scan technique.

the mass distribution that we would like to measure for the particle of interest is indicated by the green solid curve. The nominal beam momentum is adjusted to several discrete values. Due to the finite momentum distribution of the beam, each nominal setting of the beam momentum excites a distribution of $\sqrt{s}$ as indicated by the red dashed curves. The measured rate of a given final state is the convolution of these two distributions, as indicated by the filled points along the blue line. The power of this method is clearly seen by comparing measurements of the total decay width of the χ_{c1}. Measurements from the Crystal Ball were only able to achieve a precision $< 3.8 MeV$ [3] and newer measuremnts from BES achieved precisions of $\Gamma = 1.39^{+0.40}_{-0.38}{}^{+0.26}_{-0.77} MeV$ [4]. In contrast, E835 was able to achieve one further order of magnitude higher precision $\Gamma = 0.876 \pm 0.045 \pm 0.026 MeV$ [5].

The combination of the much better mass resolution with the ability to detect hadronic final states which have up to two orders of magnitude higher branching fractions than the $\gamma\gamma$ channel will permit high precision investigations of many open issues in the charmonium system. For instance, our knowledge of the ground state (η_c) is surprisingly poor. The existing data do not present a consistent picture, and

only a small fraction of the total decay width has been measured via specific decay channels. Furthermore, radial excitations are not simple recursion of the ground state, as observed in the hadronic decays of the Ψ states. In particular, the existing data on the first radial excitation of the ground state (η_c') leave a lot to be desired. Its discovery by BELLE [6] was an 8σ deviation from the initial claims of the Crystal Ball [7]. Furthermore, the existing data on the mass only have an accuracy of 4 MeV and there is a 50% uncertainty to the width. These results are only marginally consistent with most predictions.

The singlet-P resonance (h_c) is of extreme importance to determine the spin dependent component of the $q\overline{q}$ potential. Only two decay channels have been observed for this state, and the PDG [8] omitts this from the summary table stating that it needs confirmation. Due to the narrow width of this state ($\Gamma < 1MeV$) only $\overline{p}p$ formation experiments similar to those proposed for PANDA will be able to measure the width and perform systematic investigations of the decay modes.

The energy region above the $\overline{D}D$ threshold has until recently been very poorly explored. Since 2003 a number of narrow states in this mass region have been observed by BELLE, BABAR and CLEO. Many basic quantities of these states have yet to be determined. Furthermore, precision measurements of all ^1D and ^3D states is required to distinguish between models that have different describtions of the nature of these states.

3 The PANDA Detector

FAIR will include a storage ring for beams of phase space cooled antiprotons with unprecedented quality and intensity [9]. The antiprotons will be collected with an average rate of about 10^7/s and then stochastically cooled and stored. After 5×10^{10} antiprotons have been produced, they will be transferred to the High Energy Storage Ring HESR where internal experiments in the beam momentum range 1.5 – 15 GeV/c can be performed. Electron and stochastic phase space cooling will be available to allow for experiments with either high momentum resolution of about $\sim 10^{-5}$ at reduced luminosity or at high luminosity up to $2\times10^{32}/cm/s$ with enlarged momentum spread ($\sim 10^{-4}$).

The PANDA detector is designed as a large acceptance multi-purpose setup. The experiment will use internal targets. It is conceived to use either pellets of frozen H_2 or cluster jet targets for the $\overline{p}p$ reactions, and wire targets for the $\overline{p}A$ reactions. Pellet targets such as the one in operation at WASA at COSY [10] shoot droplets of frozen H_2 with radii 20 μm with typical separations of 1 mm transversely through the beam.

This detector facility must be able to handle high rates (10^7 annihilations/s), with good particle identification and momentum resolution for $\gamma,\ e,\ \mu,\ \pi,\ K$, and

p. Furthermore, the detector must have the ability to measure D, K^0_S, and Λ which decay at displaced vertices. Finally, a large solid angle coverage is essential for partial wave analysis of resonance states.

In order to cope with the variety of final states and the large range of particle momenta and emission angles, associated with the different physics topics, the detector has almost 4π detection capability both for charged particles and photons. A schematic overview of the detector is given in Figure 2. It is divided into two

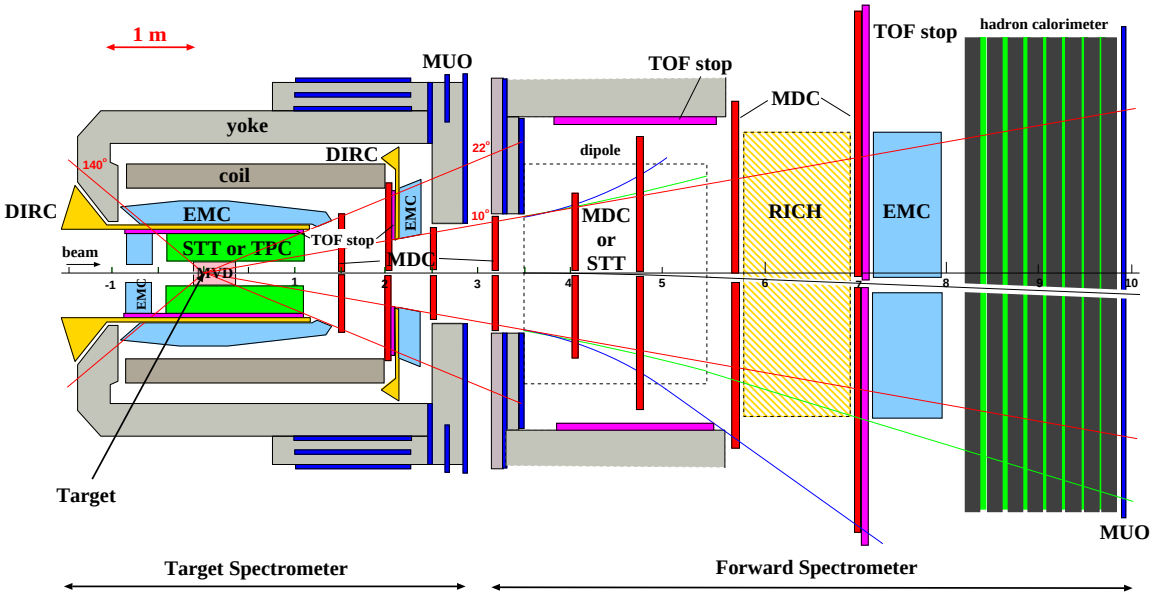

Figure 2: Schematic overview of the PANDA detector as seen from the top. The overall length is about 12 m.

sub-components, a central target spectrometer and a forward spectrometer with an overall length of 12 m of the total detector. The cylindrical structure of the target spectrometer is given by the 2 T solenoid magnetic field around the target. In sequence of increasing radii, it consists of a Micro Vertex Detector (MVD) as innermost sub-detector close to the interaction point, a central tracker built either of straw tubes (STT) or a time projection chamber (TPC) in the barrel part and mini-drift chambers (MDC) as front cap, a system of ring-imaging Cherenkov detectors for particle identification, an electromagnetic calorimeter made of $PbWO_4$ crystals, a superconducting coil, and a muon detector outside of the return yoke. The forward spectrometer consists of a 2 Tm dipole magnet with a set of multi-wire drift chambers (MDC) for tracking, a RICH detector for particle identification, electromagnetic and hadronic calorimeters for neutral and charged particles, and a muon detector as the most downstream component.

4 Physics Reach

The cross sections and branching ratios for many of the interesting channels to be measured are not known. Nevertheless estimates of events rates can be made in order to compare the physics reach of this experiment with other existing or planned experiments. Based upon the design luminosity of L= $2 \times 10^{32}/cm^2/s$, the planned operating cycle of 6 months per year, and accounting for the duty cycle, an integrated luminosity of more than $1fb^{-1}$ per year will be collected. The annihilation cross section for $\overline{p}p \rightarrow X$ can be determined by the following formula:

$$\sigma_R(s) \equiv \frac{4\pi(\hbar c)^2}{(s - 4m_p^2c^4)} \frac{B_{in}B_{out}}{1 + [2(\sqrt{s} - M_Rc^2)]^2} \quad (1)$$

Here B_{in} and B_{out} correspond to the branching ratios in and out, respectively. For instance, at the J/Ψ mass the annihilation cross section is $\sigma = 1.8 \times 10^6 pb$, corresponding to about 2×10^9 J/Ψ produced per year. The measured events rates must of course be scaled with the branching ratio and the detection efficiency of that channel. The corresponding rates for the $\Psi(3770)$ is of interest for the D-meson measurements, as well as other charomonium states above the $\overline{D}D$ threshold. In this case the branching ratio $B_{in} \equiv B(\Psi(3770) \rightarrow \overline{p}p)$ can be estimated by scaling with the total width of the state, *i.e.*$B_{in} = B(J/\Psi \rightarrow \overline{p}p) \times \Gamma_{J/\Psi}/\Gamma_{\Psi(3770)}$. Based upon this estimate there will be 4×10^6 produced $\Psi(3770)$ per year. Details of the detection efficiencies and background estimates are given in [2].

5 Conclusion

The PANDA collaboration has a rich and innovative program, of which only a small part could be presented here, that will be realized at the upcoming FAIR facility. The high mass resolution and integrated luminosity will open unique possibilities to do precision spectroscopy of the charmonium system.

.

Bibliography

[1] http://www.gsi.de/fair/index.html

[2] Technical Progress Report for PANDA, http://www-panda.gsi.de/archive/public/panda_tpr.pdf

[3] J. Gaiser *et al.*, Phys. Rev. D 34, 711 (1986).

[4] M. Ablikim *et al.*, Phys. Rev. D 71, 092002 (2005).

[5] M. Andreotti *et al.*., Nucl. Phts. B 717 34 (2005).

[6] S.K. Choi *et al.*, Phys. Rev. lett. 89, 102002 (2002).

[7] C. Edwards *et al.*, Phys. Rev. Lett. 48, 70 (1982).

[8] W.-M. Yao *et al.*, J. Phys. G: Nucl. PArt. Phys. 33 (2006) 1.

[9] The High Energy Storage Ring, http://www.fz-juelich.de/ikp/hesr/

[10] Proposal to transfer the WASA detector to COSY, nucl-ex/0411038.

Kaons

Kaons

New Results on Neutral Hyperon Decays	*R. Wanke*	
The Search for New Physics in Hyperon Decays with HyperCP	*E.C. Dukes*	(no contribution)
Rare K and B-decays	*A. Weiler*	(no contribution)
Rare K-decays (KTEV&NA48)	*M. Arenton*	
Ke4 decays and Wigner CUSP	*L. Masetti*	
New Results from KLOE	*R. Versaci*	
KL decays into n p's + gamma	*E. Cheu*	
New results on B_s at CDF	*S. Menzemer (CDF)*	

New Results on Ξ^0 Hyperon Decays

Rainer Wanke
Institut für Physik,
Universität Mainz
D-55099 Mainz, GERMANY

1 Introduction

Hyperons have been among the first non-stable elementary particles discovered and are known for more than 50 years now. In spite of this, the physics interest in hyperons is by far not yet exhausted, several important aspects are still under intense investigation. At first, as hyperons only differ by one or two strange-quarks from proton and neutron, they are ideal playgrounds to study $SU(3)_f$ symmetry breaking. Secondly, studying their decays offers unique opportunities to understand baryon structure and decay mechanisms. Last, but not least, by comparing hyperon decays to neutron decay, it is possible to measure the CKM matrix parameter $|V_{us}|$ in a complementary way with respect to kaon decays.

However, despite of their interest, most previous measurements date back to the 1960's and 70's, in particular those on the neutral Ξ^0 hyperon. Only recently new measurements have been performed, with much increased statistics and leading to a series of new results.

The two main new experiments on Ξ^0 decays are the KTeV experiment at Fermilab and NA48/1 at the CERN SPS. Both experiments were designed to measure neutral kaon decays and profit from the fact, that the Ξ^0 lifetime and decay length are of the same order as those of the K_S^0 meson. Most of the new results are coming from NA48/1. This experiment was performed in the year 2002 to measure specifically rare K_S^0 and neutral hyperon decays. During the data taking period, in total more than 2 billion of Ξ^0 decays took place in the fiducial detector volume, providing enough statistics to precisely measure also very rare Ξ^0 decays.

2 Measurement of the Ξ^0 Lifetime

The Ξ^0 lifetime, i.e. its total decay rate, is a key parameter for interpreting other measurements on Ξ^0 decays. In particular for the determination of the CKM matrix element $|V_{us}|$, as reported in the following section, the Ξ^0 lifetime is a direct input

parameter. However, the precision on the Ξ^0 lifetime is very poor. The current world average $\tau_{\Xi^0} = (2.90 \pm 0.03) \times 10^{-10}$ s [1] has less than 3% accuracy, and the last measurement dates back to 1977.

For a new, much more precise measurement the NA48/1 Collaboration has used $\Xi^0 \to \Lambda\pi^0$ decays taken with a minimum bias trigger. In total about 260 000 decays have been selected with completely negligible background. The energy spectrum of the selected events is shown in Fig. 1 (left). To be insensitive to the small residual differences between data and simulation in the spectrum, the lifetime distributions are split Ted into 10 separate bins of energy, indicated by vertical lines in Fig. 1. The fit region is shown in Fig. 1 (right). To avoid effects from the vertex resolution differences between data and simulation at the beginning of the decay region, the fit region is well separated from the final collimator. This requirement rejects about half of the statistics, leaving 133 293 events to enter the fit. The fit to the lifetime is performed using the least-squares method, with the normalisations in each energy bin left as free parameters.

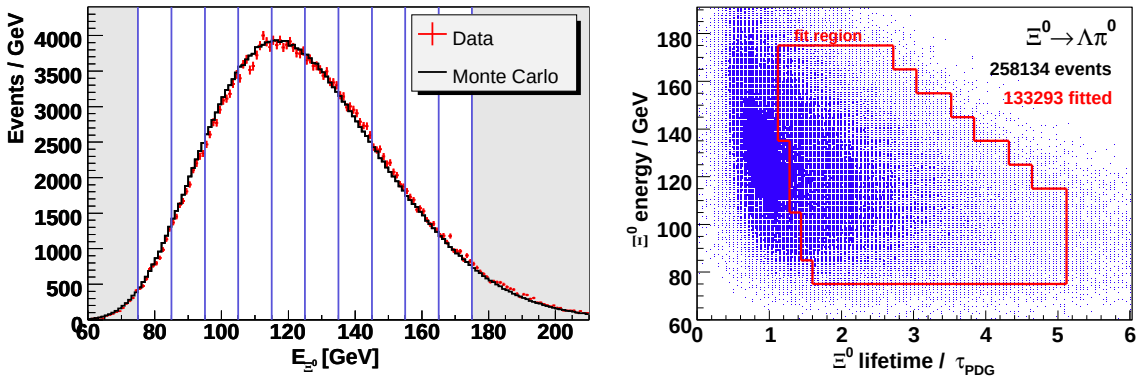

Figure 1: Left: Energy spectrum of $\Xi^0 \to \Lambda\pi^0$ data and Monte Carlo events used in the lifetime fit. Right: Energy versus proper lifetime of the selected events. Indicated is the region used in the fit.

The fit result, integrated over the separate energy bins, is shown in Fig 2. The NA48/1 collaboration obtains as preliminary result

$$\tau_{\Xi^0} = (3.082 \pm 0.013_{\text{stat}} \pm 0.012_{\text{syst}}) \cdot 10^{-10}\,\text{s}, \tag{1}$$

with the systematics being dominated by uncertainties of the detector acceptance, the nominal Ξ^0 mass, and the Ξ^0 polarisation. The result is about 2 standard deviations above the current world average and five times more precise.

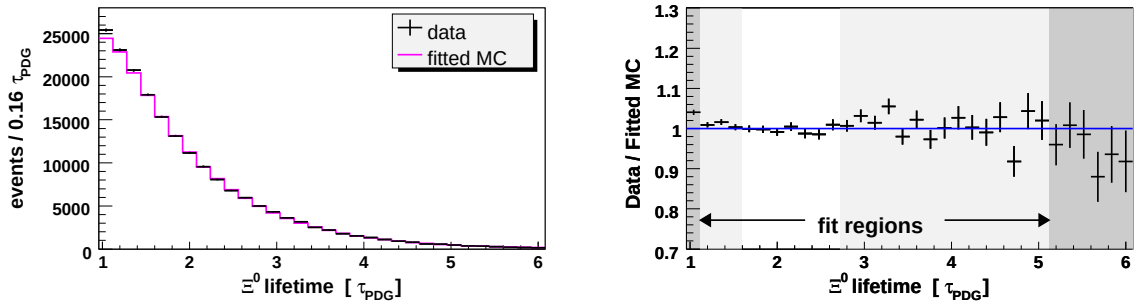

Figure 2: Fit of the Ξ^0 lifetime. Left: Comparison of data and fitted Monte Carlo simulation as function of the current PDG lifetime $\tau_{\rm PDG} = 2.90 \times 10^{-10}$ s [1]. Right: Fit residuals. The white (light grey) regions indicate the regions where the fit has been performed for all (some) energy bins.

3 Measurement of the Ξ^0 Beta Decay and Determination of $|V_{us}|$

The Ξ^0 beta decay $\Xi^0 \to \Sigma^+ e^- \overline{\nu}$ is similar to the neutron beta decay with the down-quarks exchanged by strange-quarks. The decay therefore is well suited for a measurement of the CKM parameter $|V_{us}|$ complementary to the usual determination from kaon semileptonic decays. A previous measurement has been published by the KTeV Collaboration, based on 176 events [2]. An additional preliminary KTeV result, based on 626 events, has been presented on conferences [3].

With much larger statistics, NA48/1 has now performed a precise measurement of the Ξ^0 beta decay. Since Ξ^0 semileptonic decays are the only source of Σ^+ in the neutral beam, it is sufficient to select $\Sigma^+ \to p\pi^0$ events and require an additional electron. The invariant $p\pi^0$ mass distribution of the accepted events is shown in Fig. 3, yielding 6316 $\Xi^0 \to \Sigma^+ e^- \overline{\nu}$ candidates with an estimated background contamination of about 3% mainly from in-time accidental overlaps.

Normalising to the abundant decay $\Xi^0 \to \Lambda\pi^0$, NA48/1 obtains [6]

$$\mathrm{Br}(\Xi^0 \to \Sigma^+ e^- \overline{\nu}) = (2.51 \pm 0.03_{\rm stat} \pm 0.09_{\rm syst}) \times 10^{-4} \qquad (2)$$

The systematic uncertainty is dominated by the statistical uncertainty of the determination of the trigger efficiency (±2.2%). Further contributions are the limited knowledge of the decay form factors g_1 and f_2 (±1.6%), the detector acceptance, the Ξ^0 polarisation, and the normalisation (±1.0% each).

In addition to the Ξ^0 decay, 555 $\overline{\Xi^0} \to \overline{\Sigma^+} e^+ \nu$ candidates were selected with a background of about 136 events, yielding a branching fraction of $\mathrm{Br}(\overline{\Xi^0} \to \overline{\Sigma^+} e^+ \nu) = (2.55 \pm 0.14_{\rm stat} \pm 0.10_{\rm syst}) \times 10^{-4}$ in perfect agreement with the one obtained from the Ξ^0 decay.

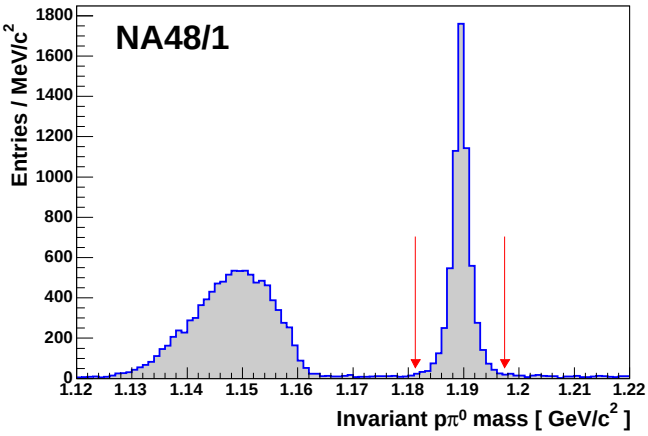

Figure 3: Invariant $p\pi^0$ mass distribution from NA48/1 $\Xi^0 \to \Sigma^+ e^- \overline{\nu}$ decays.

Using the combined result $\mathrm{Br}(\Xi^0 \to \Sigma^+ e^- \overline{\nu}) = (2.51 \pm 0.09) \times 10^{-4}$ and the new preliminary value for the Ξ^0 lifetime, the partial decay width is $\Gamma(\Xi^0 \to \Sigma^+ e^- \overline{\nu}) = (8.14 \pm 0.29) \times 10^5\ \mathrm{s}^{-1}$, from which the CKM matrix element $|V_{us}|$ can be determined. The semileptonic decay rate is given by [4]

$$\begin{aligned}\Gamma &= G_F^2\,|V_{us}|^2\,\frac{\Delta m^5}{60\pi^3}\,(1+\delta_{\mathrm{rad}}) \\ &\times \left[\left(1-\frac{3}{2}\,\beta\right)\left(|f_1|^2+|g_1|^2\right)+\frac{6}{7}\,\beta^2\left(|f_1|^2+2|g_1|^2+\mathrm{Re}(f_1 f_2^\star)+\frac{2}{3}\,|f_2^2|\right)+\delta_{q^2}\right],\end{aligned}$$

with $\Delta m = m_{\Xi^0} - m_{\Sigma^+}$ [1], $\beta = \Delta m / m_{\Xi^0}$, the radiative corrections δ_{rad}, and $\delta_{q^2}(f_1, g_1)$ taking into transfer momentum dependence of f_1 and g_1 [4]. The form factor ratios g_1/f_1 and f_2/f_1 have been measured by the KTeV Collaboration [5]. Neglecting $SU(3)$ breaking corrections for f_1, a value of

$$|V_{us}| = 0.203 \pm 0.004_{\mathrm{exp}}\ {}^{+0.022}_{-0.027}\ {}_{\text{form factors}} \tag{3}$$

is found, in good agreement with the value of 0.226 ± 0.002 obtained from kaon decays [1], but still large uncertainties from the form factor measurement.

4 First Measurements of the Decay $\Xi^0 \to \Sigma^+ \mu \nu_\mu$

Because of the small available phase space, the semimuonic Ξ^0 decay is highly suppressed with respect to its semielectronic counterpart. The first observation of the

decay was done by the KTeV Collaboration in 2005 [7]. They observe 8 signal candidates over negligible background (Fig. 4 (left)) from which they obtain a branching fraction of $\mathrm{Br}(\Xi^0 \to \Sigma^+\mu^-\overline{\nu}) = (4.7\,^{+2.0}_{-1.4} \pm 0.8) \times 10^{-6}$.

More recently, the NA48/1 Collaboration reported a preliminary measurement, based on 99 signal candidates including about 30 background events (Fig. 4 (right)), leading to a value of $\mathrm{Br}(\Xi^0 \to \Sigma^+\mu^-\overline{\nu}) = (2.2 \pm 0.3 \pm 0.2) \times 10^{-6}$.

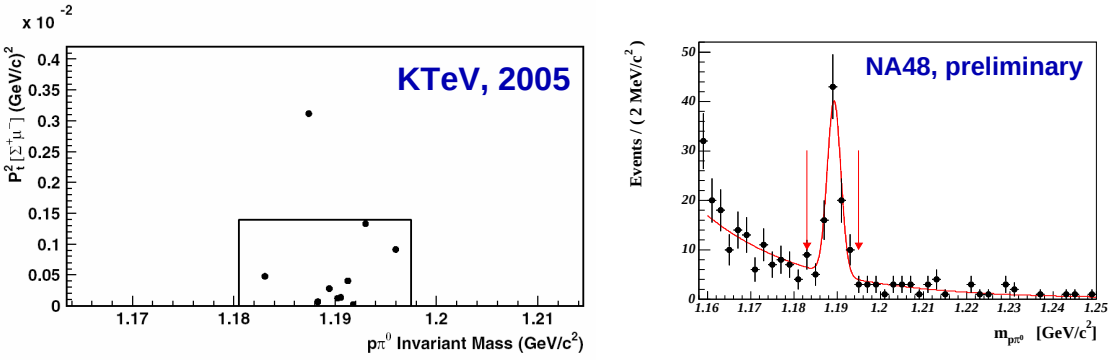

Figure 4: Invariant $p\pi^0$ mass distributions of $\Xi^0 \to \Sigma^+\mu^-\overline{\nu}$ decays measured by KTeV (left) and NA48/1 (right).

5 Weak Radiative Ξ^0 Decays

Up to this day, weak radiative hyperon decays as $\Xi^0 \to \Lambda\gamma$ and $\Xi^0 \to \Sigma^0\gamma$ are still barely understood. Several competing theoretical models exist, which give very different predictions. An excellent experimental parameter to distinguish between models is the decay asymmetry α of these decays. It is defined as

$$\frac{dN}{d\cos\Theta} = N_0(1 + \alpha\,\cos\Theta), \tag{4}$$

where Θ is the direction of the daughter baryon with respect to the polarisation of the mother in the mother rest frame. For e.g. $\Xi^0 \to \Lambda\gamma$, the decay asymmetry can then be measured by looking at the angle between the incoming Ξ^0 and the outgoing proton from the subsequent $\Lambda \to p\pi^-$ decay in the Λ rest frame (see Fig. 5) Using this method, the measurement is independent of the unknown initial Ξ^0 polarisation.

The NA48/1 experiment has selected 48314 $\Xi^0 \to \Lambda\gamma$ and 13068 $\Xi^0 \to \Sigma^0\gamma$ candidates (Fig. 6). The background contributions are 0.8% for $\Xi^0 \to \Lambda\gamma$ and about 3% for $\Xi^0 \to \Sigma^0\gamma$, respectively.

Using these data, fits to the decay asymmetries have been performed. In case of $\Xi^0 \to \Sigma^0\gamma$, where we have the subsequent decay $\Sigma^0 \to \Lambda\gamma$, the product $\cos\Theta_{\Xi\to\Sigma\gamma} \cdot$

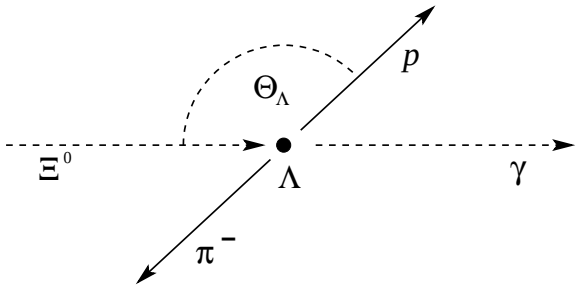

Figure 5: Definition of the angle Θ between the proton and the incoming Ξ^0 in the Lambda rest frame.

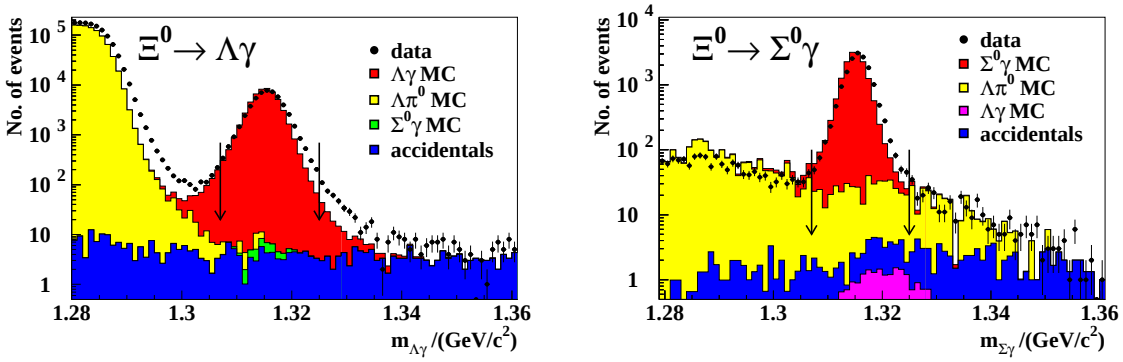

Figure 6: $\Xi^0 \to \Lambda\gamma$ (left) and $\Xi^0 \to \Sigma^0\gamma$ (right) signal together with MC expectations for signal and backgrounds.

$\cos\Theta_{\Sigma\to\Lambda\gamma}$ has to be used for the fit. Both fits show the expected linear behaviour on the angular parameters (Fig. 7)

After correcting for the well-known asymmetry of $\Lambda \to p\pi^-$, values of

$$\alpha_{\Xi^0\to\Lambda\gamma} = -0.684 \pm 0.020 \pm 0.061 \quad \text{and} \tag{5}$$

$$\alpha_{\Xi^0\to\Sigma^0\gamma} = -0.682 \pm 0.031 \pm 0.065 \tag{6}$$

are obtained, where the first error is statistical and the second systematic. These values agree with previous measurements by NA48 on $\Xi^0 \to \Lambda\gamma$ [8] and KTeV on $\Xi^0 \to \Sigma^0\gamma$ [9], but are much more precise. In particular the result on $\Xi^0 \to \Lambda\gamma$ is of high theoretical interest, as it confirms the large negative value of the decay asymmetry, which is difficult to accommodate for quark and vector meson dominance models.

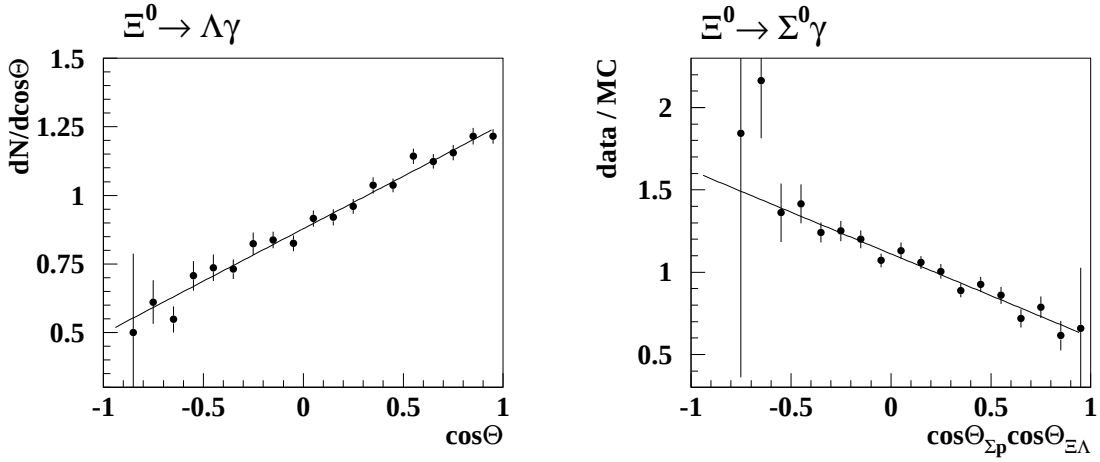

Figure 7: Fits of the decay asymmetries in $\Xi^0 \to \Lambda\gamma$ (left) and $\Xi^0 \to \Sigma^0\gamma$ (right).

Bibliography

[1] W.-M. Yao *et al.* (Particle Data Group), Jour. of Phys. G **33** (2006) 1.

[2] A. Affolder *et al.* (KTeV Collaboration), Phys. Rev. Lett. **82** (1999) 3751.

[3] A. Alavi-Harati, Proc. of DPF99, July 1999, Los Angeles, CA (hep-ex/9903031).

[4] A. Garcia and P. Kielanowski, Lect. Notes Phys. **222** (1985) 1.

[5] A. Alavi-Harati *et al.* (KTeV Collaboration), Phys. Rev. Lett. **87** (2001) 132001 (hep-ex/0105016).

[6] J.R. Batley *et al.* (NA48/1 Collaboration), Phys. Lett. B **645** (2007) 36.

[7] E. Abouzaid *et al.* (KTeV Collaboration), Phys. Rev. Lett. **95** (2005) 081801 (hep-ex/0504055).

[8] A. Lai *et al.* (NA48 Collaboration), Phys. Lett. B **584** (2004) 251 (hep-ex/0401027).

[9] A. Alavi-Harati *et al.* (KTeV Collaboration), Phys. Rev. Lett. **86** (2001) 3239 (hep-ex/0012031).

Rare K Decays

Michael Arenton
Physics Department
University of Virginia
P.O. Box 400714
Charlottesville, VA 22904, USA

1 Introduction

We review recent results on rare K decays from KTeV and NA-48. By rare decays we mean both those modes where the experiments are pushing the branching fraction measurements and limits to lower and lower values and also small branching fraction modes where experimental advances now allow their study with relatively large statistics.

2 The KTeV Experiment

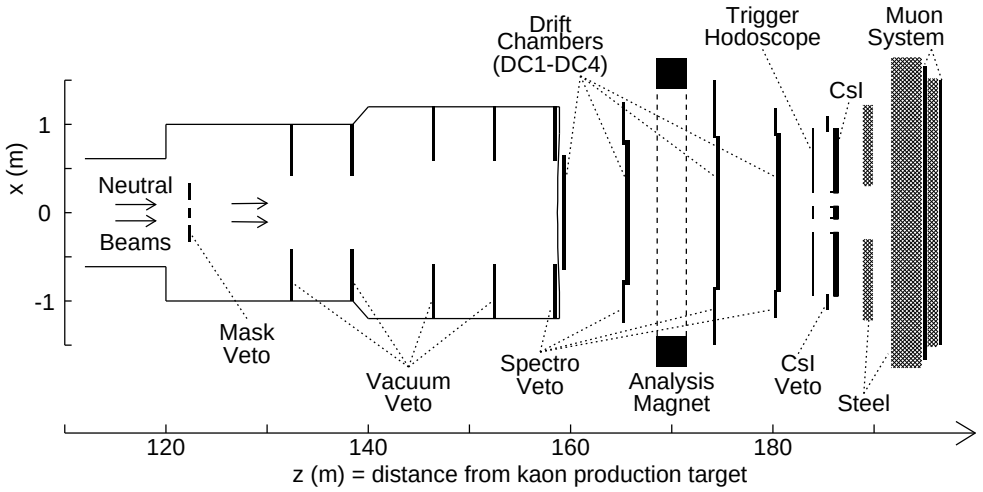

Figure 1: Plan view of KTeV E-832 configuration as used for rare decay measurements (regenerator not shown).

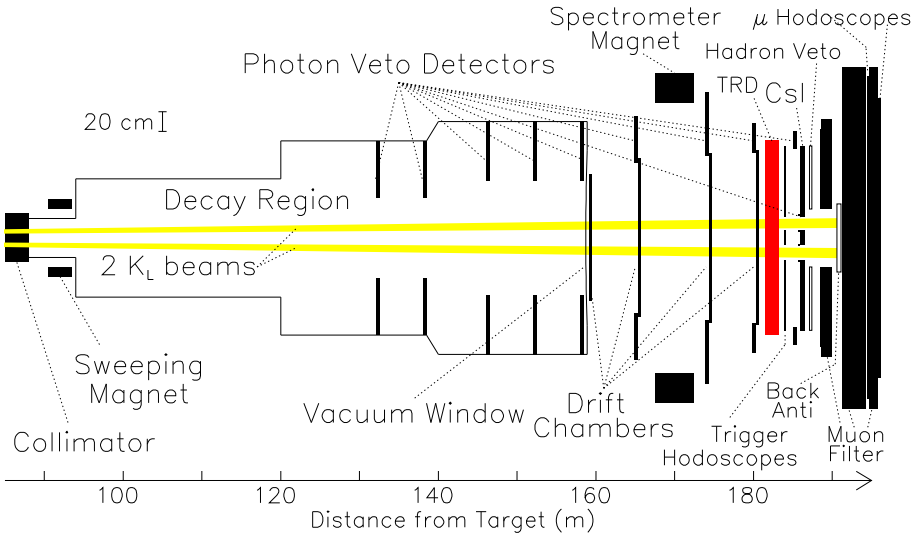

Figure 2: Plan view of KTeV E-799 configuration.

Here we give a brief description of the KTeV experiment [1] [2] . There were two configurations, E832 and E799, shown respectively in Fig. 1 and Fig. 2. . E832 was designed primarily to measure the direct CP violation parameter ϵ'/ϵ, while E799 was devoted to rare K_L decays. Two K_L beams were generated by 800 GeV/c protons on a target. In E832 a regenerator in one of the beams converted K_L to K_S. In E799 the regenerator was removed to have two K_L beams. The beams were run at higher intensity in E799. The decays took place in a large vacuum decay region.

In both configurations a magnetic spectrometer consisting of two sets of x and y drift chambers before and after an analysing magnet measured charged particles. Photons were measured in a 3100 element array of pure CsI blocks which had energy resolution of $\sigma(E)/E = 0.45\% + 2\%/\sqrt{(E)}$. This electromagnetc calorimeter was followed by layers of steel and concrete absorber and scintillators for muon identification. Several arrays of counters vetoed on the presence of charged particles or photons outside the aperture of the spectrometer and calorimeter. The E799 configuration also included a set of transition radiation detectors for improved electron identification.

There were two data taking runs for each configuration, in 1997 and 1999. The 1999 E832 run repeated the 1997 run with somewhat better running conditions to check the systematics of the ϵ'/ϵ measurement. The 1999 E799 run was devoted to increasing the sensitivity for rare decays. To this end the p_t kick of the analysing magnet was reduced to 150 MeV/c in 1999 from 200 MeV/c in 1997 to increase acceptance, particularly for 4 body decays. Also in 1999 several triggers were prescaled

to increase the data acquistion bandwidth for other triggers. E799 was sensitive to 2.5 X 10^{11} and 3.5 X $10^{11} K_L$ decays in 1997 and 1999 respectively.

3 The decay $K_L \to \pi^+\pi^-\gamma$

The decay $K_L \to \pi^+\pi^-\gamma$ proceeds through the amplitudes shown in Fig. 3. The two main contributions, of about equal magnitude, are from the CP violating Inner Bremsstralung (IB) and the CP conserving Direct Emission terms. The Direct Emission term is mostly magnetic dipole (M1) radiation. This must be modified with a form factor that is usually expressed in a ρ pole form. As well as the M1 term there might be an electric dipole (E1) term. The E1 term is especially interesting because it is CP violating. The experiments have now reached statistical levels where searching for the E1 term is possible.

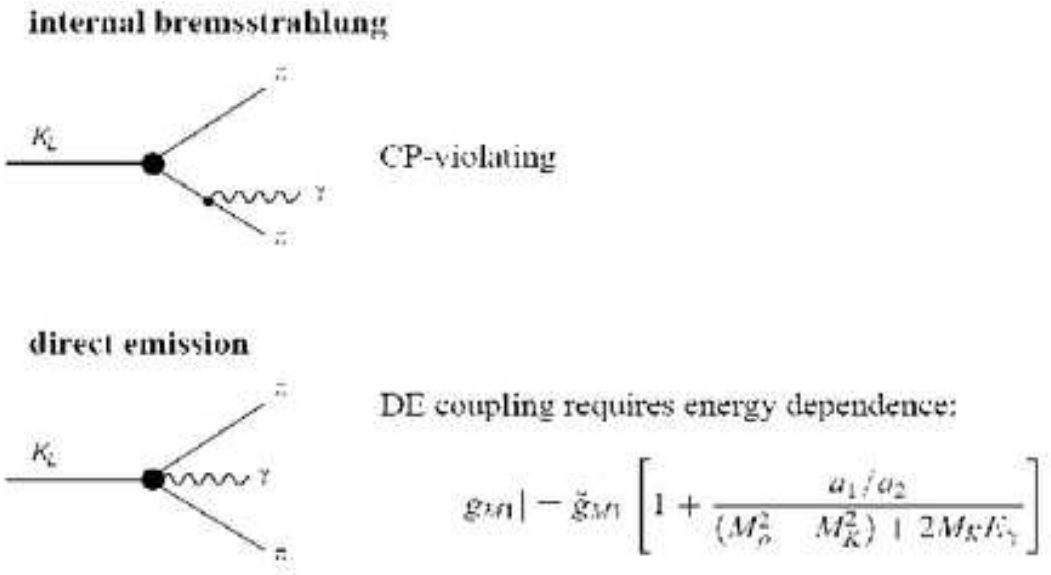

Figure 3: Amplitudes for the decay $K_L \to \pi^+\pi^-\gamma$

The KTeV results on $K_L \to \pi^+\pi^-\gamma$ [3] are based on a sample of 112,100 events over a background of 671 $\pm$ 41 events recorded in the 1997 run of E832. The amplitudes are determined from a fit to the distribution of the γ energy in the K_L rest frame which shows a falling distribution at low E_γ from IB and a broad peak at high E_γ from M1 DE. Interference of the M1 and E1 DE amplitudes would show up in the intermediate energy region. The distribution and fit are shown in figure 4. The DE form factor parameters are found to be $g_{M1} = 1.198 \pm 0.035 \pm 0.086$ and $a_1/a_2 = -0.738 \pm 0.007 \pm 0.018(GeV^2)$. The ratio of the direct emission to total

decay rate is 0.0689 ± 0.021. An upper limit for the magnitude of an E1 term is found to be $|g_{E1}| < 0.21$ at the 90% confidence level.

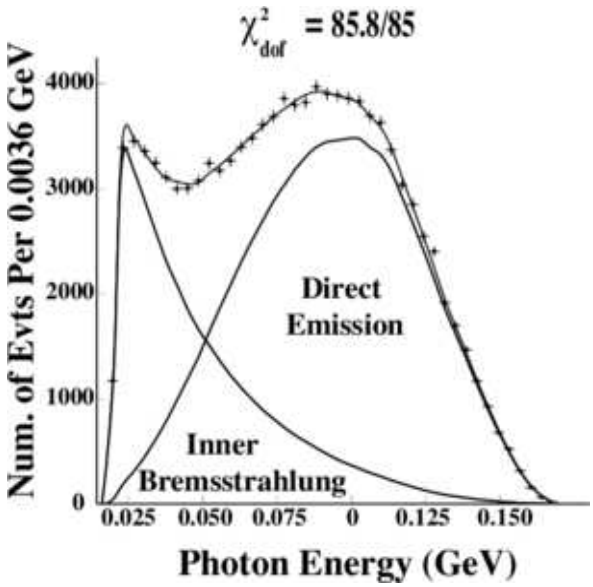

Figure 4: E_γ distribution in $K_L \to \pi^+\pi^-\gamma$ with fit results.

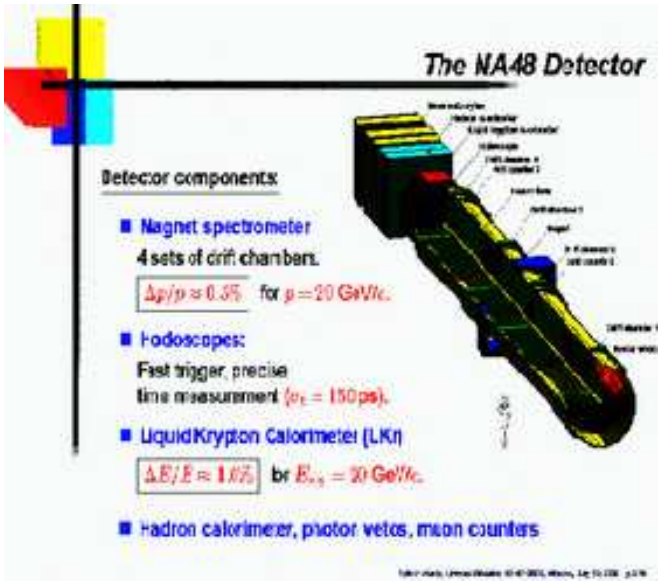

Figure 5: View of the NA48/2 detector. [5]

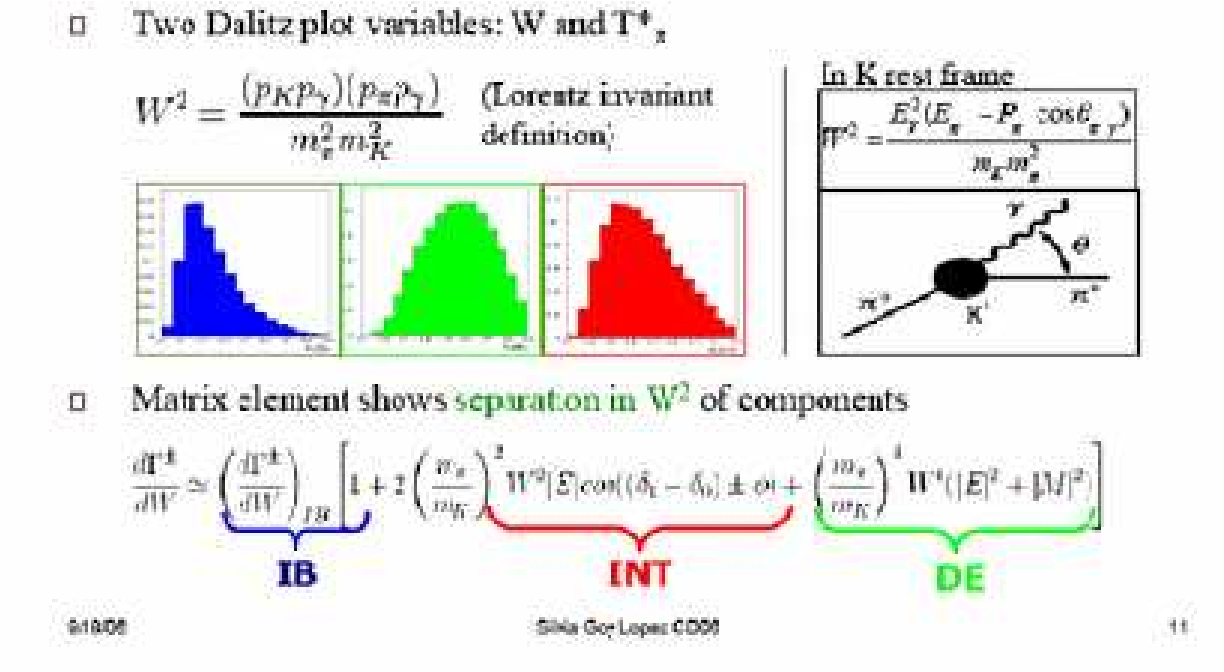

Figure 6: Variables describing the decay $K^{\pm} \to \pi^{\pm}\pi^0\gamma$ [6]

KTeV has also searched for the E1 term in the related decay mode $K_L \to \pi^+\pi^-e^+e^-$ [4]. Along with amplitudes analogous to those of $K_L \to \pi^+\pi^-\gamma$ this decay also has a term related to the K charge radius. The angular distributions of the $\pi\pi$ and ee pairs provide additonal information making this decay more sensitive to E1 contributions. We find an upper limit of $|g_{E1}|/|g_{M1}| < 0.04$ at 90% confidence level.

4 NA48 results on $K^{\pm} \to \pi^{\pm}\pi^0\gamma$

The charged kaon extension of the NA48 experiment, NA48/2, has recently presented results on the related radiative decay $K^{\pm} \to \pi^{\pm}\pi^0\gamma$. Like $K_L \to \pi^+\pi^-\gamma$ this decay has IB and DE amplitudes, but here the IB amplitude is CP conserving and much larger than DE.

The NA48/2 detector is shown in Fig. 5 [5] The NA48/2 experiment was primarily directed to searching for direct CP violation in $K^{\pm} \to 3\pi$ decays. It used simultaneous $K^{\pm}$ beams of 60 ± 3 GeV/c.

The Dalitz plot variables W^2 and T^*_π used to describe the $K^{\pm} \to \pi^{\pm}\pi^0\gamma$ decay are shown in Fig. 6. One searches for the interference term between the IB and the electric dipole direct emission. Previous experiments have not seen evidence of this interference. This analysis was based on 124,000 events, which is 30% of the available

data and 5 times the statistics of previous experiments.

In the analysis it was necessary to solve two problems that might cause distortions in the W^2 distribution that could mimic direct emission or interference terms. The first is misassignment of the γ's, which was reduced by cuts on the π^0 and $K^\pm$ masses and requirement of agreement of the charged and neutral vertices. The second is backgrounds from the $K^\pm \to \pi^\pm\pi^0$ and $K^\pm \to \pi^\pm\pi^0\pi^0$ decays with coalesed γ's, which were reduced using techniques to split coalesed γ's. In the final analysis these backgrounds were reduced to less than 1% of the direct emission level.

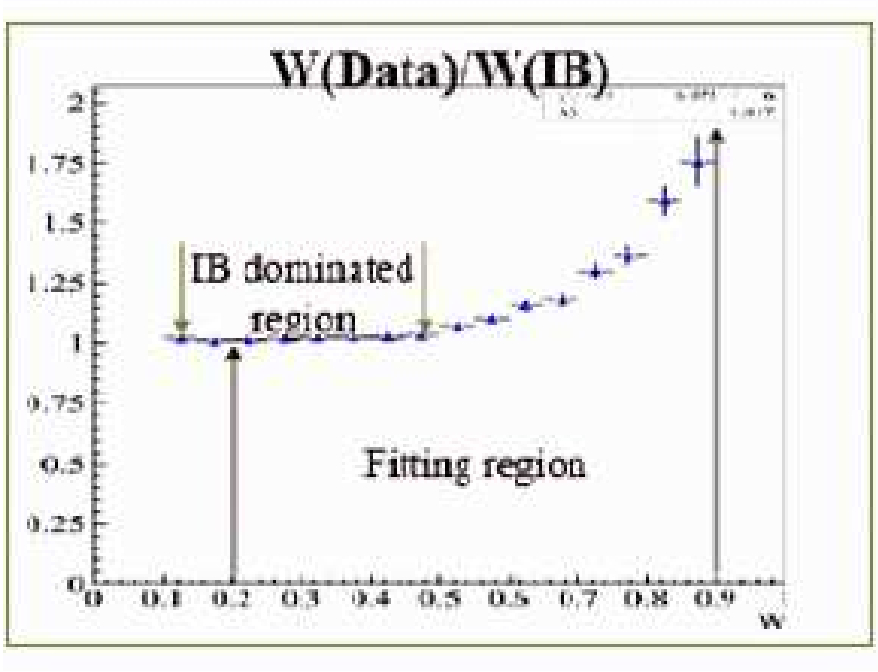

Figure 7: W distribution of NA48/2 data divided by Inner Bremmstralung shape. [6]

Fig. 7 shows the measured W distribution divided by that expected for IB alone. Clearly this deviates from unity at high W. A fit yields a preliminary result for the fraction of direct emission of $(3.35 \pm 0.35_{stat} \pm 0.25_{syst})\%$ and of the interference $(-2.67 \pm 0.81_{stat} \pm 0.73_{syst})\%$. These values are highly correlated, with a correlation coefficient of -0.92. This result is the first observation of the electric dipole interference term with high statistical certainty.

5 $K_L \to \pi^+\pi^-\pi^0\gamma$ and $K_L \to \pi^+\pi^-\pi^0 e^+e^-$

First results on the radiative decays $K_L \to \pi^+\pi^-\pi^0\gamma$ and $K_L \to \pi^+\pi^-\pi^0 e^+e^-$ have been obtained by KTeV. $K_L \to \pi^+\pi^-\pi^0\gamma$ is expected to be dominated by the inner

bremmstralung process with a theoretical branching fraction of $(1.65 \pm 0.03) \times 10^{-4}$ for $E_\gamma < 10MeV$ [7]. The direct emission contribution is expected to be very small: $BR|_{direct} = (8a_1 + a_2 - 10a_3)^2 \cdot 2 \cdot 10^{-10}$ where the a_i are unknown parameters of order 1 [8]. For $K_L \to \pi^+\pi^-\pi^0 e^+e^-$ there are no published theories. There should be IB and DE terms similar to $K_L \to \pi^+\pi^-\pi^0\gamma$ with virtual photon conversion to an e^+e^- pair. In addition there should be a charge radius amplitude.

KTeV has observed $K_L \to \pi^+\pi^-\pi^0\gamma$ both in data from E832 with $\pi^0 \to \gamma\gamma$ and from E799 with $\pi^0 \to e^+e^-\gamma$ yielding signals of 2853 and 2847 events respectively, as shown in Fig. 8. A preliminary result for the branching ratio with $E_\gamma^{cm} > 10MeV$ is $BR = (1.70 \pm 0.03_{stat} \pm 0.04_{syst} \pm 0.03_{extsyst}) \times 10^{-4}$ in good agreement with theory.

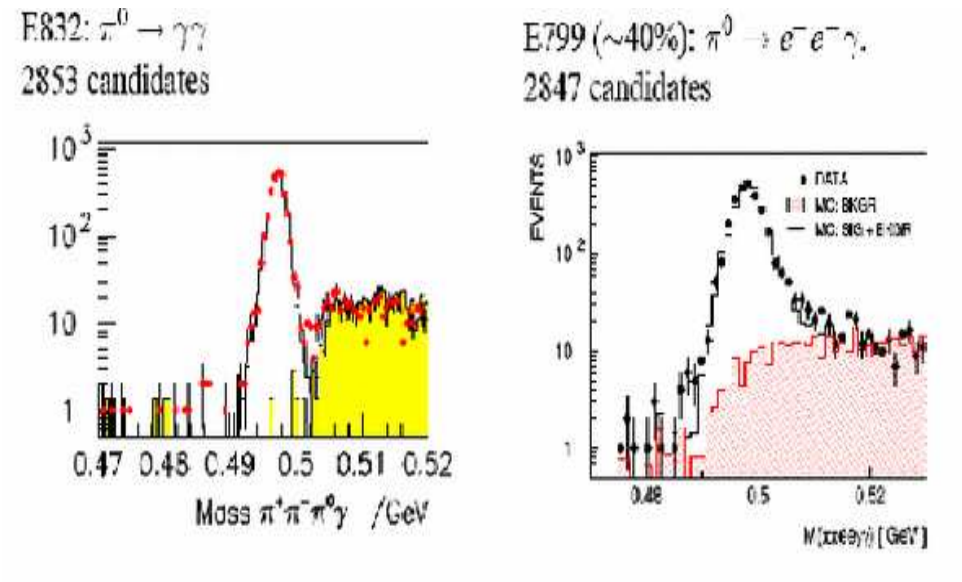

Figure 8: $\pi^+\pi^-\pi^0\gamma$ and $\pi^+\pi^-\pi^0_D\gamma$ mass distributions from E832 and E799 data.

KTeV has made a first observation of $K_L \to \pi^+\pi^-\pi^0 e^+e^-$ in the E799 data. In 40% of the data 132 candidates are observed with an estimated background level of 1.2 ± 0.9 event. This is shown in Fig. 9. The preliminary result for $E_{ee} > 20MeV$ is $BR = (1.60 \pm 0.18_{stat}) \times 10^{-7}$.

6 $K_L \to e^+e^-\gamma$

Radiative decays of the type $K_L \to \gamma^{(*)}\gamma^{(*)}$ are of interest largely because of their role in the measurement of the CKM matrix element $|V_{td}|$ from the decay $K_L \to \mu^+\mu^-$. This decay proceeds partly from a short distance coupling related to $|V_{td}|$, but also has a long distance couplling related to $K_L \to \gamma^{(*)}\gamma^{(*)}$ that must be subtracted.

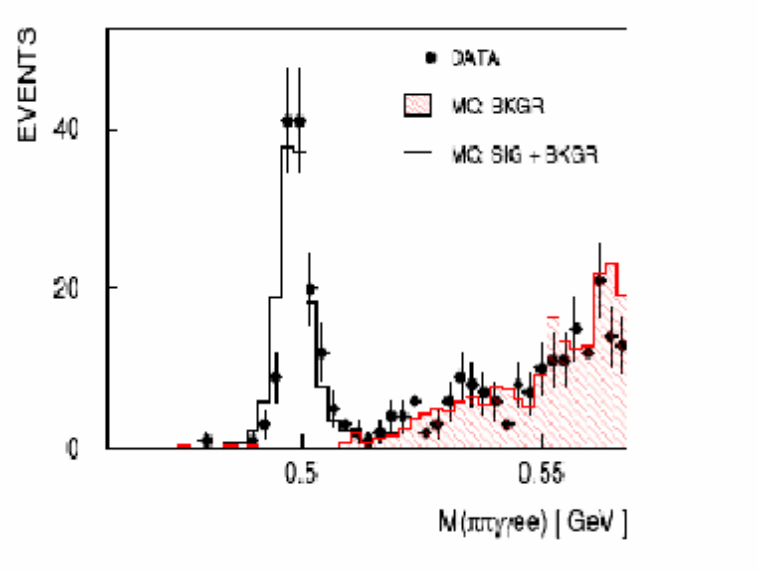

Figure 9: $\pi^+\pi^-\pi^0_D e^+e^-$ mass distribution from E799 data.

The $K_L \to \gamma^{(*)}\gamma^{(*)}$ decays have been described by two form factor models. One is the vector dominance inspired model of Bergström, Masso and Singer (BMS) [9]. The other is the chiral perturbation theory model of D'Ambrosio, Isidori and Portoles (DIP) [10]. The parameters of these models can be determined by fits to the m_{ee} distribution of the data. The BMS model contains a parameter α_{K^*}. However experiments actually determine the quantity $C\alpha_{K^*}$ where $C = (8\pi\alpha_{em})^{1/2} G_{NL} f_{K^*K\gamma} m_\rho^2/(f_{K^*} f_\rho^2 A_{\gamma\gamma})$. A number of experiments using various decay modes have presented results for α_{K^*} but are inconsistent because the values of the parameters making up C have changed over time. Therefore KTeV chooses to quote $C\alpha_{K^*}$ and compare it to $C\alpha_{K^*}$ from other experiments.

The KTeV form factor measurements are based on a sample of 83,000 $K_L \to e^+e^-\gamma$ decays. Of particular importance in the form factor fits is the handling of radiative corrections. KTeV has developed a Monte Carlo including the complete set of second order radiative diagrams.

The corrected preliminary KTeV results are a branching fraction of $(9.25 \pm 0.03_{stat} \pm 0.07_{syst} \pm 0.26_{extsyst}) \times 10^{-6}$, $C\alpha_{K^*} = -0.517 \pm 0.030_{fit} \pm 0.022_{syst}$ for the BMS model and $\alpha_{DIP} = -1.729 \pm 0.043_{fit} \pm 0.028_{syst}$ for the DIP model. A comparison of values of $C\alpha_{K^*}$ from various decay modes is shown in Fig.10.

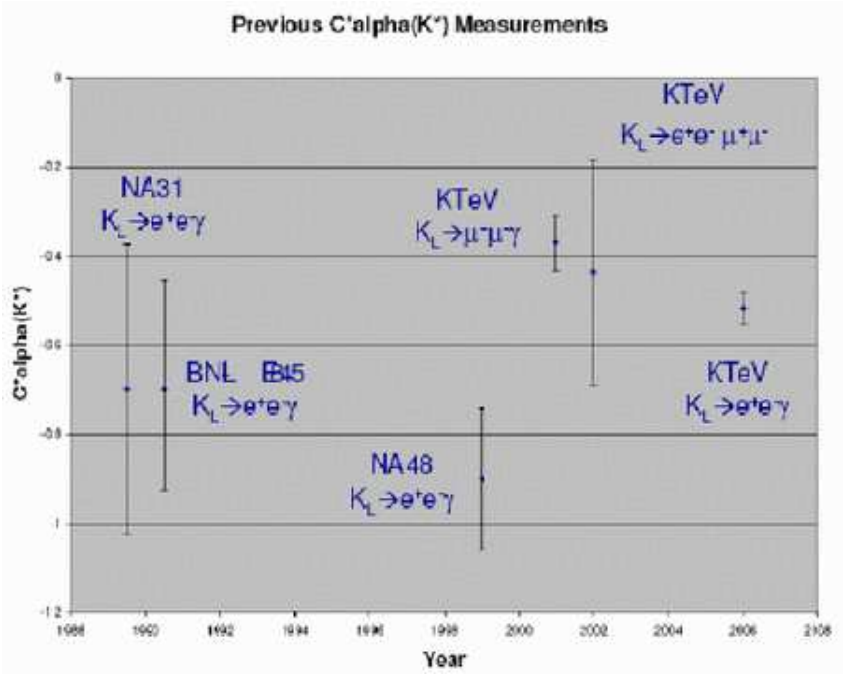

Figure 10: Results on $C\alpha_{K^*}$ from various decay modes

7 $K_L \to \pi^\pm e^\mp \nu e^+ e^-$

KTeV has made the first measurements of the decay $K_L \to \pi^\pm e^\mp \nu e^+ e^-$ [11]. This is of course related to the radiative K_{e3} decay mode $K_L \to \pi^\pm e^\mp \nu\gamma$. New tests of chiral perturbation theory are enabled by these measurements.

Because of the missing ν there are less kinematic constraints available to use in signal selection. The worst backgrounds come from $K_L \to \pi^+\pi^-\pi^0$ with π^0 decays to $e^+e^-\gamma$ or $e^+e^-e^+e^-$, $K_L \to \pi^\pm e^\mp \nu\pi^0$ with $\pi^0 \to e^+e^-\gamma$, and $K_L \to \pi^\pm e^\mp \nu\gamma$ where the γ converts in material in the spectrometer. The analysis relies heavily on the full identification power of the CsI Calorimeter and the TRD's.

A sample of 19466 candidate events is obtained with a background of about 5% from about 25% of the E799 data. A preliminary result for the branching fraction of $K_L \to \pi^\pm e^\mp \nu e^+ e^-$ with $m_{e^+e^-} > 0.005$GeV and $E_{e^+e^-} > 0.03$GeV is $(1.281 \pm 0.010_{stat} \pm 0.019_{syst} \pm 0.035_{extsyst}) \times 10^{-5}$.

A theoretical calculation in chiral perturbation theory [12] has been made of the quantity $R = \Gamma(K_L \to \pi^\pm e^\mp \nu e^+ e^-, m_{ee} > \ 0.005GeV)/\Gamma(K_L \to \pi^\pm e^\mp \nu)$. At leading order in the theory the predicted value of R is 4.06×10^{-5} whereas at next to leading order (p^4) it is 4.29×10^{-5}. The experimental result corresponds to R = $(4.54 \pm 0.15) \times 10^{-5}$ which is 3.2σ from the leading order and 1.7σ from the next to leading

order calculation.

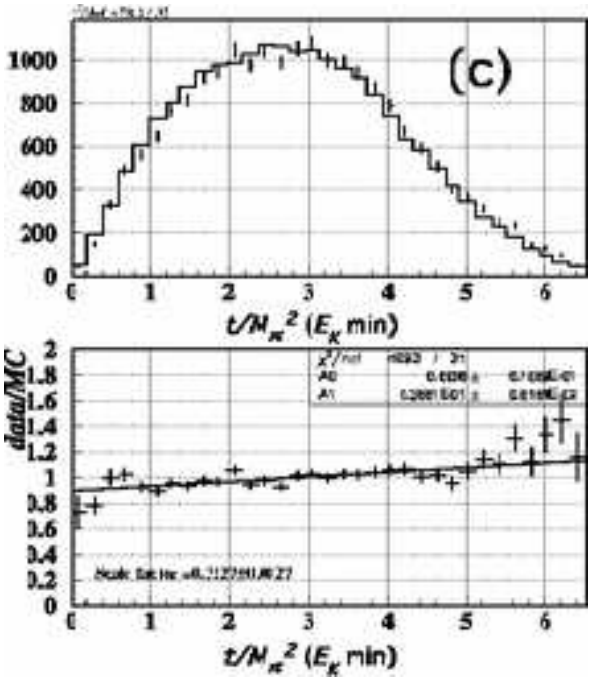

Figure 11: Distribution of the minimum solution for t. Upper plot shows data (points) and leading order χPT calculation (lines). Lower plot show the ratio of data/calcuation.

One may also examine agreement with theoretical predictions by looking at the distributions of the kinematics of the decay. One such variable is the momentum transfer t. Because of the missing ν, experimentally there are two possible solutions for t in each event. Figs. 11 and 12 show the distributions of the minimum solution for t. The points in both of these figures are the same. Fig. 11 shows a comparison to the distribution calculated with leading order chiral perturbation theory while Fig. 12 shows the comparison to next to leading order theory. One sees a better agreement with next to leading order, as shown in the ratio plots in the bottom parts of the figures, the ratio being flatter for NLO than for LO. The same conclusion is reached when the maximum solution for t is examined (not shown).

8 $\pi^0 \longrightarrow e^+e^-$

K_L decays are a copious source of "tagged" π^0's. KTeV has used these to measure the rare decay $\pi^0 \to e^+e^-$. To lowest order this is described by the diagram shown in Fig.

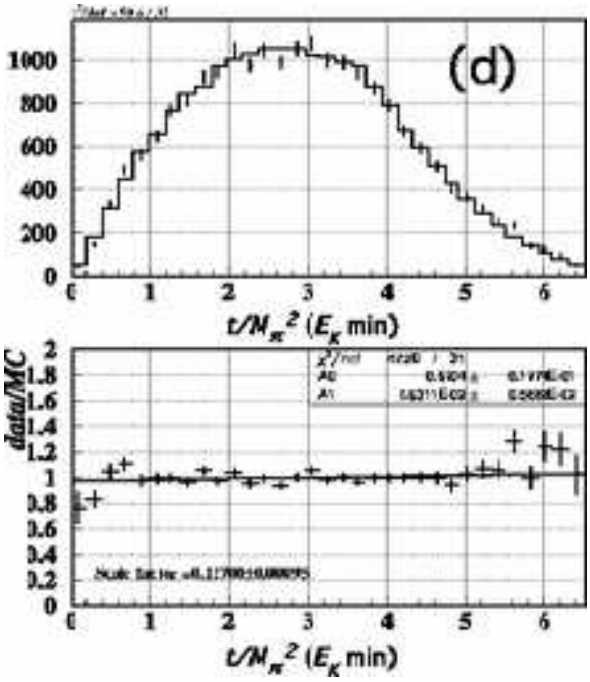

Figure 12: Distribution of the minimum solution for t. Upper plot shows data(points) and next to leading order χPT calculation (lines). Lower plots shows the ratio of data/calculation.

13 [14]. Various calculations based on vector dominance or chiral perturbation theory predict branching fractions somewhat higher than this unitarity limit [15] [16] [17] [18] [19].

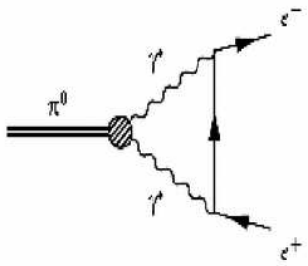

Figure 13: Lowest order diagram describing $\pi^0 \to e^+e^-$.

After appropriate analysis cuts the m_{ee} distribution shown in Fig.14 is obtained, for events of the final state $\gamma\gamma\gamma\gamma e^+e^-$ with two $\gamma\gamma$ pairs consistent with π^0's and $m_{\gamma\gamma\gamma\gamma ee}$ consistent with m_K. The peak has 794 events with a background of 53.2 ± 9.5

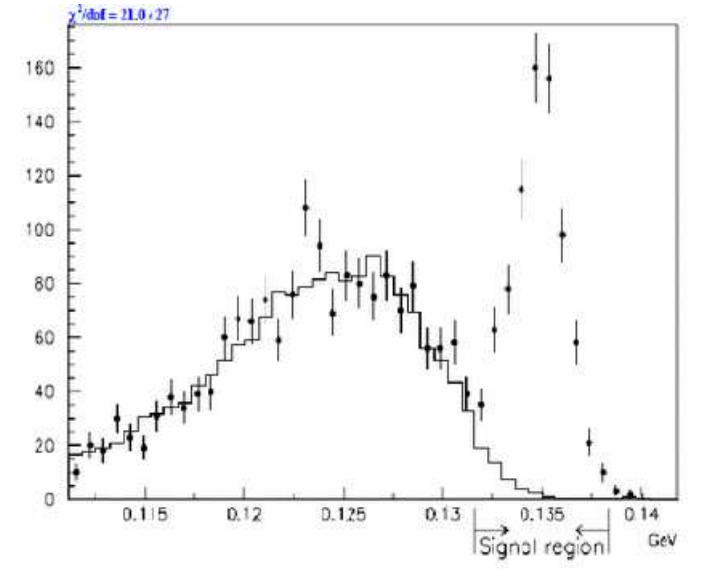

Figure 14: m_{ee} distribution after all other cuts.

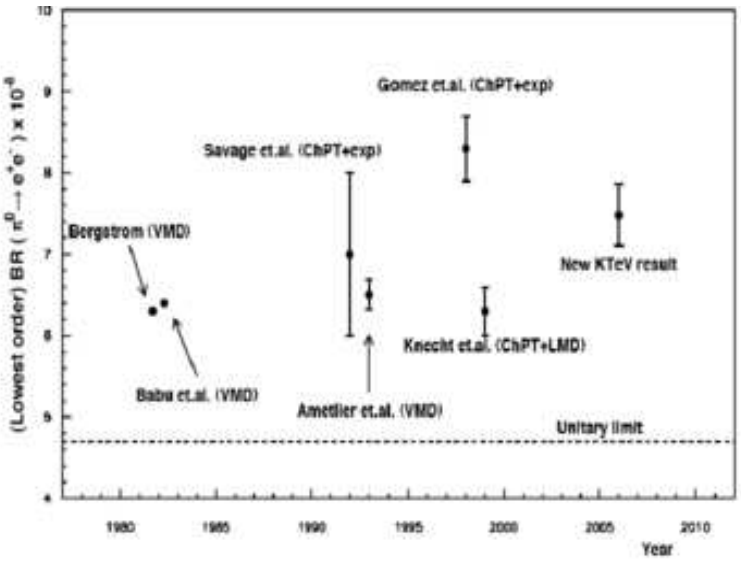

Figure 15: Comparison of the measured $\pi^0 \to e^+e^-$ branching fraction to theories of refs [15] to [19].

events. The branching fraction for $\pi^0 \to e^+e^-$ with $x > 0.95$ is $(6.56 \pm 0.26_{stat} \pm 0.10_{syst} \pm 0.19_{extsyst}) \times 10^{-8}$, where $x = m_{ee}/m_{\pi^0}$.

Fig. 15 shows this result in comparison with the unitarity limit and various theoretical calculations. This measurement is 7σ above the unitarity limit.

9 Searches for Lepton Flavor Violating Decays

KTeV has searched for the lepton flavor violating decays $K_L \to \pi^0\mu^\pm e^\mp$, $K_L \to \pi^0\pi^0\mu^\pm e^\mp$, and $\pi^0 \to \mu^\pm e^\mp$. There is nothing new to report on $K_L \to \pi^0\mu^\pm e^\mp$ but recently new preliminary results have been obtained on the latter two modes. (The π^0 decay analysis is in effect a subset of the K_L analysis.)

In the past, analyses of this sort have been done by defining a "box" in some kinematical space (usually in a 2 dimensional plot of the mass of all the particles making up the decay versus a transverse momentum that should be zero for a true decay), not looking at the data in the box while cuts to reduce backgrounds are established by studying their effects on the events near to, but outside the box, and finally opening the box and comparing the number of events found to what is expected from background evaluations. This is not in general the most sensitive procedure however, since the true signal would not usually be evenly distributed over a rectangular box.

Instead KTeV has based its analysis on a probability distribution function (PDF) formed from the distributions of mass and p_t^2. The PDF distribution for the decay mode $K_L \to \pi^0\mu^\pm e^\mp$ is shown in Fig. 16 which illustrates the search regions. The PDF distribution for $K_L \to \pi^0\pi^0\mu^\pm e^\mp$ is very similar.

Determination of the background is a key to this analysis. Initial Monte Carlo calculations indicated that backgrounds originate from several common decay modes. Because of this and the very small branching fractions being probed it was not practical to calculate background levels by Monte Carlo simulations. Instead the data itself was used, loosening some cuts so that the PDF distributions of the background could be examined and then rescaling by the effects of the final cuts. Figure 17 shows this. The result of this is predicted backgrounds of 0.44 ± 0.12 events of $K_L \to \pi^0\pi^0\mu^\pm e^\mp$ and 0.03 ± 0.02 events for $\pi^0 \to \mu^\pm e^\mp$.

When the blind region in the PDF distribution was examined no events were found. Using the Feldman-Cousins method with the predicted backgrounds and no events seen yields preliminary 90% confidence level upper limits of $BR(K_L \to \pi^0\pi^0\mu^\pm e^\mp) < 1.58 \times 10^{-10}$ and $BR(\pi^0 \to \mu^\pm e^\mp) < 3.63 \times 10^{-10}$.

10 Conclusion

Sensitive results have recently been obtained on a number of rare K decays [20]. In $K_L \to \pi^+\pi^-\gamma$ and $K_L \to \pi^+\pi^-e^+e^-$ accurate measurement of the inner bremsstrahlung and M1 direct emission components have been made and searches done for the E1

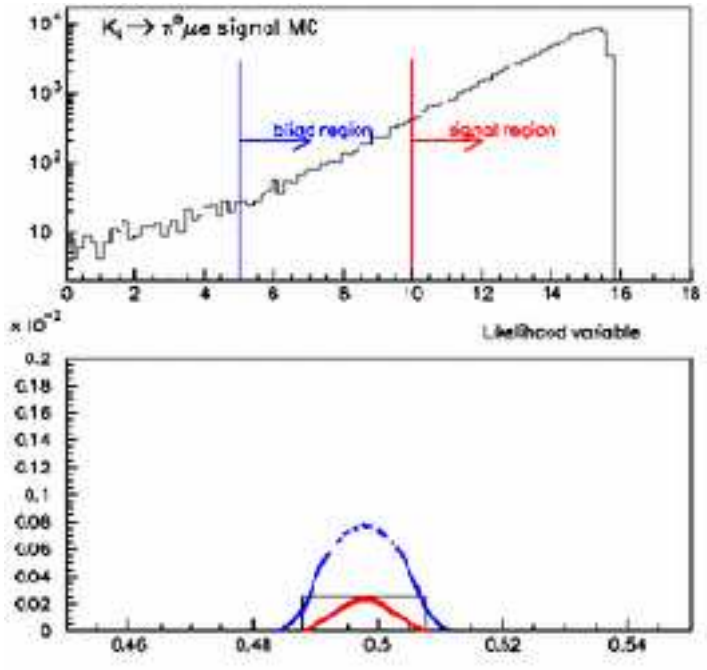

Figure 16: Signal probability distribution function for $K_L \to \pi^0 \mu e$.

amplitude. In the analogous charged decay $K^\pm \to \pi^\pm \pi^0 \gamma$ NA48/2 has found the first clear evidence for the E1 interference term. KTeV has observed the decays $K_L \to \pi^+ \pi^- \pi^0 \gamma$ and $K_L \to \pi^+ \pi^- \pi^0 e^+ e^-$. KTeV has made high statistics measurements of $K_L \to e^+ e^- \gamma$. KTeV has made the first measurements of $K_L \to \pi^\pm e^\mp \nu e^+ e^-$. KTeV has made accurate measurements of $\pi^0 \to e^+ e^-$. Finally KTeV has new results on searches for the lepton flavor violating decays $K_L \to \pi^0 \pi^0 \mu^\pm e^\mp$ and $\pi^0 \to \mu^\pm e^\mp$.

I thank my colleagues on KTeV and Augusto Ceccucci of NA48 for discussions. This work was supported by the U.S. Department of Energy

Bibliography

[1] A. Alavi-Harati *et al.* [The E799-II/KTeV Collaboration], Phys. Rev. D **61**, 072006 (2000) [arXiv:hep-ex/9907014].

[2] A. Alavi-Harati *et al.* [KTeV Collaboration]' Phys. Rev. Lett. **83**, 922 (1999) [arXiv:hep-ex/9903007].

[3] E. Abouzaid *et al.* [KTeV Collaboration], Phys. Rev. D **74**, 032004 (2006) [Erratum-ibid. D **74**, 039905 (2006)] [arXiv:hep-ex/0604035].

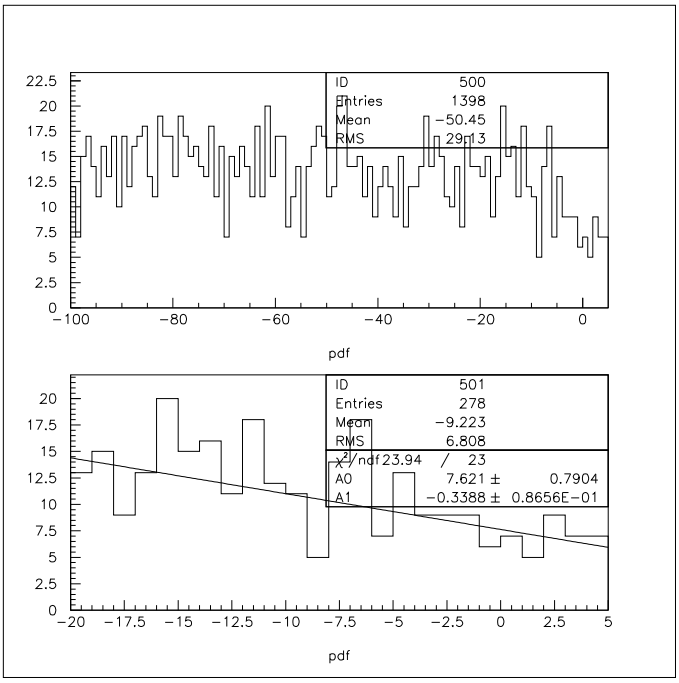

Figure 17: Signal probability distribution distributions for relaxed cut background samples. Note that the signal region is PDF > 10.

[4] E. Abouzaid *et al.* [KTeV Collaboration], Phys. Rev. Lett. **96**, 101801 (2006) [arXiv:hep-ex/0508010].

[5] R. Wanke, arXiv:hep-ex/0610066.

[6] S. Goy Lopez, talk given at 5th International Workshop on Chiral Dynamics, Theory and Experiment, Sept 18-22 2006, Durham and Chapel Hill NC, USA. to be published.
http://www.cern.ch/NA48/Welcome/images/talks/CD06/
CD06_goylopez_radiative.pdf

[7] G. D'Ambrosio, G. Ecker, G. Isidori and H. Neufeld, Z. Phys. C **76**, 301 (1997) [arXiv:hep-ph/9612412].

[8] G. Ecker, H. Neufeld and A. Pich, Nucl. Phys. B **413**, 321 (1994) [arXiv:hep-ph/9307285].

[9] L. Bergström, E. Masso and P. Singer, Phys. Lett. B **131**, 229 (1983).

[10] G. D'Ambrosio, G. Isidori and J. Portoles, Phys. Lett. B **423**, 385 (1998) [arXiv:hep-ph/9708326].

[11] K.Kotera, Thesis, Osaka University, 2006.

[12] K.Tsuji paper in preparation.

[13] E. Abouzaid *et al.* [KTeV Collaboration], Phys. Rev. D ,**75**, 012004 (2007). [arXiv:hep-ex/0610072].

[14] S. Drell, Nuovo Cim. **XI**, 693, (1959).

[15] L. Bergström, Z. Phys., **C20**, 135 (1983).

[16] M. Savage, M. Luke, and M. Wise, Phys. Lett., **B291**, 481 (1992).

[17] L. Ametller, A. Bramon, and E. Masso, Phys. Rev., **D48**, 3388 (1993).

[18] D. Gomez Dumm and A. Pich, Phys. Rev. Lett., **80**, 4633 (1998).

[19] M. Knecht*et al.*, Phys. Rev. Lett., **83**, 5230 (1999).

[20] KTeV results from other decay modes have been presented at this conference by E. Cheu.

K_{e4} decays and Wigner cusp

Lucia Masetti[1]
Institut für Physik
Universität Mainz
D-55099 Mainz, GERMANY

1 Introduction

The single-flavour quark condensate $\langle 0 \left| \overline{q} q \right| 0 \rangle$ is a fundamental parameter of χPT, determining the relative size of mass and momentum terms in the expansion. Since it can not be predicted theoretically, its value must be determined experimentally, e.g. by measuring the $\pi\pi$ scattering lengths, whose values are predicted very precisely within the framework of χPT, assuming a big quark condensate [1], or of generalised χPT, where the quark condensate is a free parameter [2].

The K^{+-}_{e4} decay is a very clean environment for the measurement of $\pi\pi$ scattering lengths, since the two pions are the only hadrons and they are produced close to threshold. The only theoretical uncertainty enters through the constraint [3] between the scattering lengths a_0^2 and a_0^0. In the $K^{\pm} \to \pi^0\pi^0\pi^{\pm}$ decay a cusp-like structure can be observed at $M_{00}^2 = 4m_{\pi^+}^2$, due to re-scattering from $K^{\pm} \to \pi^+\pi^-\pi^{\pm}$. The scattering lengths can be extracted from a fit of the M_{00}^2 distribution around the discontinuity.

2 Experimental setup

Simultaneous K^+ and K^- beams were produced by 400 GeV energy protons from the CERN SPS, impinging on a beryllium target. The kaons were deflected in a front-end achromat in order to select the momentum band of (60 ± 3) GeV/c and focused at the beginning of the detector, about 200 m downstream. For the measurements presented here, the most important detector components are the magnet spectrometer, consisting of two drift chambers before and two after a dipole magnet and the quasi-homogeneous liquid krypton electromagnetic calorimeter. The momentum of the charged particles and the energy of the photons are measured with a relative uncertainty of 1% at 20 GeV. A detailed description of the NA48/2 detector can be found in Ref. [4].

[1]Present address: Physikalisches Institut, Universität Bonn, D-53012 Bonn, GERMANY

3 $K^{\pm} \to \pi^+\pi^- e^{\pm}\nu_e$

The K_{e4}^{+-} selection consisted of geometrical criteria, like the requirement of having three tracks within the detector acceptance and building a good vertex; particle identification requirements, based mainly on the different fraction of energy deposited by pions and electrons in the electromagnetic calorimeter; kinematical cuts for background rejection, like an elliptical cut in the (p_T,$M_{3\pi}$) plane centered at (0,M_K). In order to improve the pion rejection, the electron identification also included a Linear Discriminant Analysis combining the three quantities with the highest discriminating power. Two reconstruction strategies can be applied to the K_{e4}^{+-} events: either imposing the kaon mass and extracting the kaon momentum from a quadratic equation, or imposing the kaon momentum to be the mean beam momentum (60 GeV/c along the beam axis) and extracting the kaon mass from a linear equation (see Fig. 1).

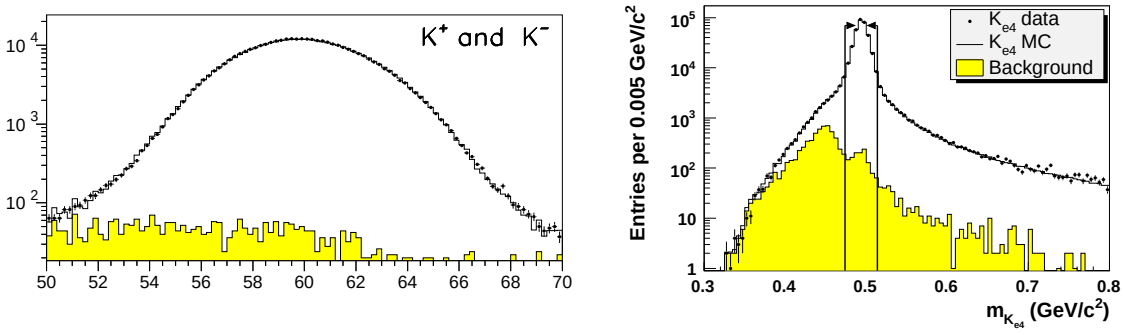

Figure 1: Kaon momentum (left) and mass (right) of the K_{e4}^{+-} events reconstructed with a quadratic or a linear equation, respectively. The data (crosses) are compared to signal MC (open histogram) plus background (yellow).

Analysing part of the 2003 data, 3.7×10^5 K_{e4}^{+-} events were selected with a background contamination below 1%. The background level was estimated from data, using the so-called "wrong sign" events, i.e. with the signature $\pi^{\pm}\pi^{\pm}e^{\mp}\nu_e$, that, at the present statistical level, can only be background, since the corresponding kaon decay violates the $\Delta S = \Delta Q$ rule and is therefore strongly suppressed [5]. The main background contributions are due to $K^{\pm} \to \pi^+\pi^-\pi^{\pm}$ events with $\pi \to e\nu$ or a pion mis-identified as an electron. The background estimate from data was cross-checked using Monte Carlo simulation (MC).

3.1 Form factors

The form factors of the K_{e4}^{+-} decay are parametrised as a function of five kinematic variables [6] (see Fig. 2): the invariant masses $M_{\pi\pi}$ and $M_{e\nu}$ and the angles θ_π, θ_e

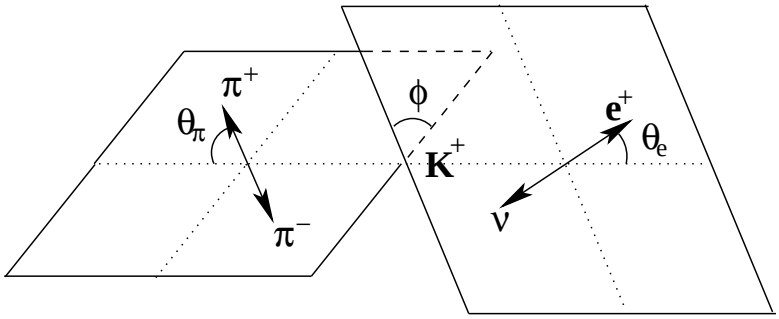

Figure 2: Topology of the K_{e4} decay.

and ϕ. The matrix element

$$T = \frac{G_F}{\sqrt{2}} V_{us}^* \overline{u}(p_\nu)\gamma_\mu(1-\gamma_5)v(p_e)(V^\mu - A^\mu)$$

contains a hadronic part, that can be described using two axial (F and G) and one vector (H) form factors [7]. After expanding them into partial waves and into a Taylor series in $q^2 = M_{\pi\pi}^2/4m_{\pi^+}^2 - 1$, the following parametrisation was used to determine the form factors from the experimental data [8, 9]:

$$\begin{aligned} F &= (f_s + f_s' q^2 + f_s'' q^4) e^{i\delta_0^0(q^2)} + f_p \cos\theta_\pi e^{i\delta_1^1(q^2)} \\ G &= (g_p + g_p' q^2) e^{i\delta_1^1(q^2)} \\ H &= h_p e^{i\delta_1^1(q^2)}. \end{aligned}$$

In a first step, ten independent five-parameter fits were performed for each bin in $M_{\pi\pi}$, comparing data and MC in four-dimensional histograms in $M_{e\nu}$, $\cos\theta_\pi$, $\cos\theta_e$ and ϕ, with 1500 equal population bins each. The second step consisted in a fit of the distributions in $M_{\pi\pi}$ (see Figs. 3,4), to extract the (constant) form factor parameters.

The polynomial expansion in q^2 was truncated according to the experimental sensitivity. The dependence on $M_{e\nu}$ and the D-wave were found to be negligible within the total uncertainty and the corresponding parameters were therefore set to zero. The $\delta = \delta_0^0 - \delta_1^1$ distribution was fitted with a one-parameter function given by the numerical solution of the Roy equations [3], in order to determine a_0^0, while a_0^2 was constrained to lie on the centre of the universal band. The following preliminary

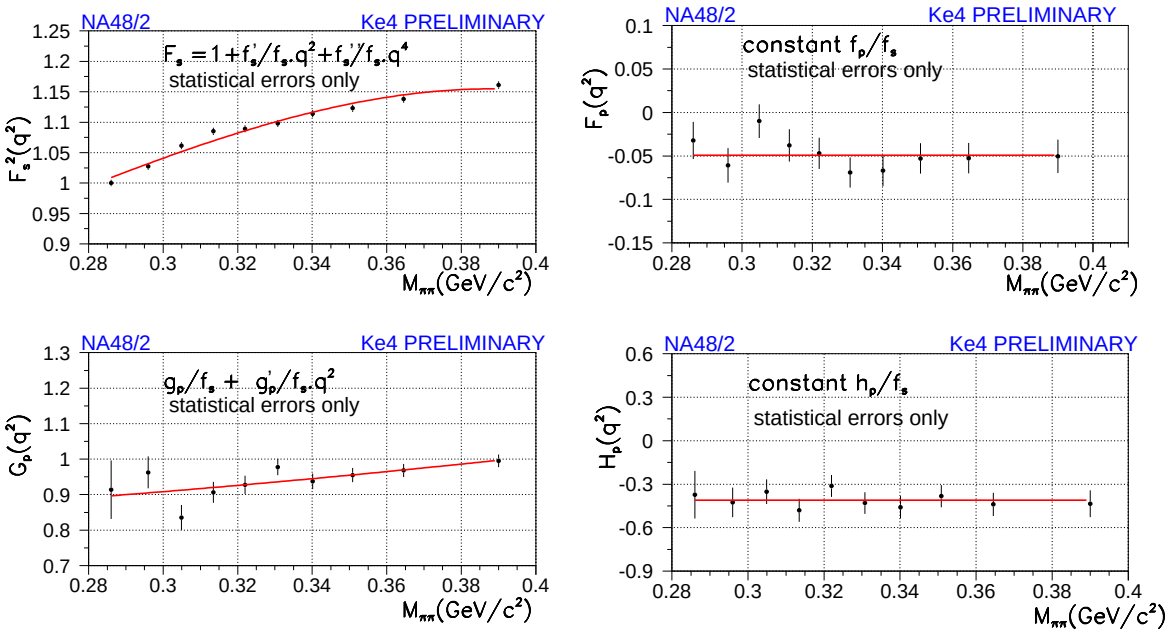

Figure 3: F, G and H dependence on $M_{\pi\pi}$. The points represent the results of the first-step fits, the lines are fitted in the second step.

result was obtained:

$$\begin{aligned}
f_s'/f_s &= 0.169 \pm 0.009_{stat} \pm 0.034_{syst} \\
f_s''/f_s &= -0.091 \pm 0.009_{stat} \pm 0.031_{syst} \\
f_p/f_s &= -0.047 \pm 0.006_{stat} \pm 0.008_{syst} \\
g_p/f_s &= 0.891 \pm 0.019_{stat} \pm 0.020_{syst} \\
g_p'/f_s &= 0.111 \pm 0.031_{stat} \pm 0.032_{syst} \\
h_p/f_s &= -0.411 \pm 0.027_{stat} \pm 0.038_{syst} \\
a_0^0 &= 0.256 \pm 0.008_{stat} \pm 0.007_{syst} \pm 0.018_{theor},
\end{aligned}$$

where the systematic uncertainty was determined by comparing two independent analyses and taking into account the effect of reconstruction method, acceptance, fit method, uncertainty on background estimate, electron-ID efficiency, radiative corrections and bias due to the neglected $M_{e\nu}$ dependence. The form factors are measured relative to f_s, which is related to the decay rate. The obtained value for a_0^0 is compatible with the χPT prediction $a_0^0 = 0.220 \pm 0.005$ [10] and with previous measurements [11, 12].

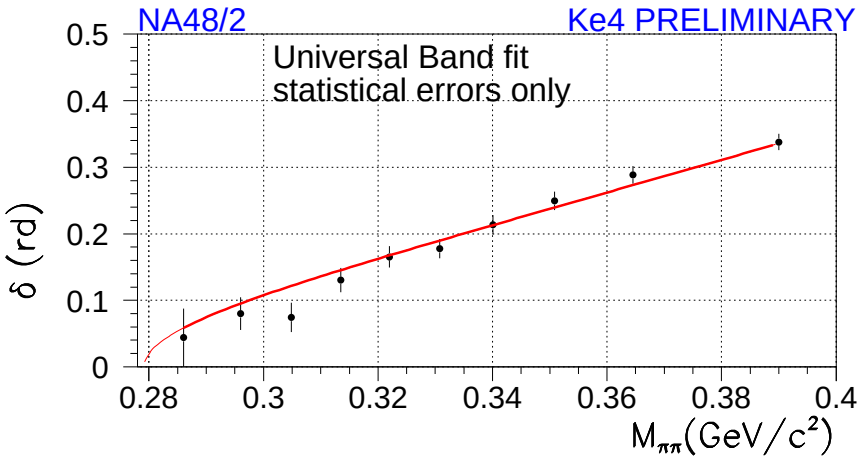

Figure 4: $\delta = \delta_0^0 - \delta_1^1$ distribution as a function of $M_{\pi\pi}$. The points represent the results of the first-step fits, the line is fitted in the second step.

4 $K^\pm \to \pi^0\pi^0 e^\pm \nu_e$

About 10,000 K_{e4}^{00} events were selected from the 2003 data and about 30,000 from the 2004 data with a background contamination of 3% and 2%, respectively. The selection criteria were similar to the ones used for the K_{e4}^{+-} events, apart from the requirement of containing one track and 4 photons compatible with two π^0s at the same vertex. The electron identification was based on the fraction of energy deposited in the electromagnetic calorimeter and on the width of the corresponding shower. The background level was estimated from data by reversing some of the selection criteria and was found to be mainly due to $K^\pm \to \pi^0\pi^0\pi^\pm$ events with a pion mis-identified as an electron (see Fig. 5).

The branching fraction was measured, as a preliminary result from the 2003 data only, normalised to $K^\pm \to \pi^0\pi^0\pi^\pm$:

$$BR(K_{e4}^{00}) \;=\; (2.587 \pm 0.026_{stat} \pm 0.019_{syst} \pm 0.029_{ext}) \times 10^{-5},$$

where the systematic uncertainty takes into account the effect of acceptance, trigger efficiency and energy measurement of the calorimeter, while the external uncertainty is due to the uncertainty on the $K^\pm \to \pi^0\pi^0\pi^\pm$ branching fraction. This result is about eight times more precise than the best previous measurement [13].

For the form factors the same formalism is used as in K_{e4}^{+-}, but, due to the symmetry of the $\pi^0\pi^0$ system, the P-wave is missing and only two parameters are left: f_s'/f_s and f_s''/f_s. Using the full data sample, the following preliminary result was obtained:

$$\begin{aligned} f_s'/f_s &= \;\; 0.129 \pm 0.036_{stat} \pm 0.020_{syst} \\ f_s''/f_s &= -0.040 \pm 0.034_{stat} \pm 0.020_{syst}, \end{aligned}$$

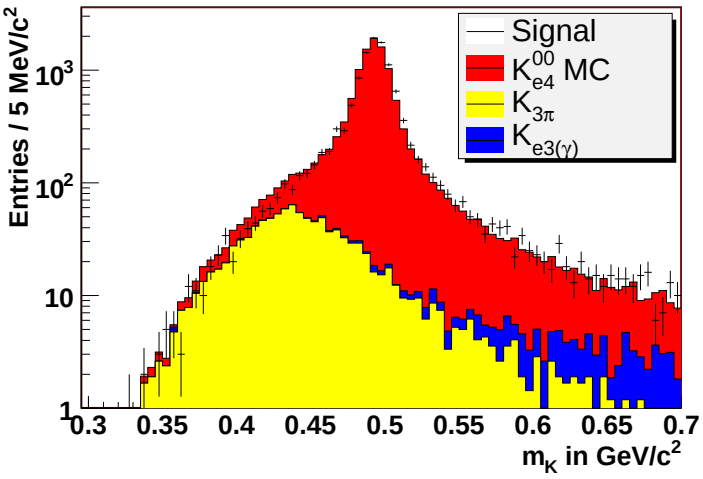

Figure 5: Invariant mass distribution in logarithmic scale of the K^{00}_{e4} events selected from the 2003 data (crosses) compared to the signal MC (red) plus physical (yellow) and accidental (blue) background.

which is compatible with the K^{+-}_{e4} result (see Fig. 6).

5 $K^{\pm} \to \pi^0\pi^0\pi^{\pm}$

From 2003 data, about 23 million $K^{\pm} \to \pi^0\pi^0\pi^{\pm}$ events were selected, with negligible background. The squared invariant mass of the $\pi^0\pi^0$ system (M^2_{00}) was computed imposing the mean vertex of the π^0s, in order to improve its resolution close to threshold. At $M^2_{00} = 4m^2_{\pi^+}$, the distribution shows evidence for a cusp-like structure (see Fig. 7, left) due to $\pi\pi$ re-scattering.

Fitting the distribution with the theoretical model presented in Ref. [14] and using the unperturbed matrix element

$$M_0 = A_0(1 + \tfrac{1}{2}g_0 u + \tfrac{1}{2}h'u^2 + \tfrac{1}{2}k'v^2),$$

the following result was obtained [15], assuming $k' = 0$ [16]:

$$\begin{aligned} g_0 &= 0.645 \pm 0.004_{stat} \pm 0.009_{syst} \\ h' &= -0.047 \pm 0.012_{stat} \pm 0.011_{syst} \\ a_2 &= -0.041 \pm 0.022_{stat} \pm 0.014_{syst} \\ a_0 - a_2 &= 0.268 \pm 0.010_{stat} \pm 0.004_{syst} \pm 0.013_{theor}, \end{aligned}$$

where the $a_0 - a_2$ measurement is dominated by the uncertainty on the theoretical model.

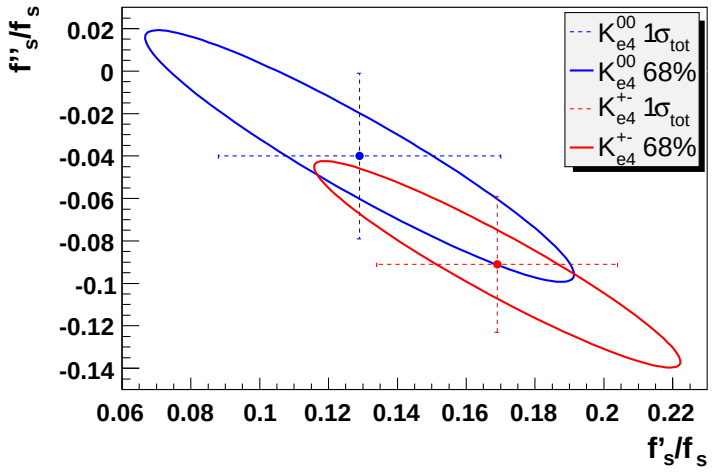

Figure 6: Comparison of the f'_s/f_s and f''_s/f_s measurements in K^{+-}_{e4} and K^{00}_{e4}.

In a further analysis, the value of k' was obtained from a fit above the cusp in the plane $\cos\theta$ vs M^2_{00}, where θ is the angle between the π^+ and the π^0 in the $\pi^0\pi^0$ centre of mass system. Evidence was found for a non-zero value of k' (see Fig. 7, right):

$$k' = 0.0097 \pm 0.0003_{stat} \pm 0.0008_{syst},$$

where the systematic uncertainty takes into account the effect of acceptance and trigger efficiency. Reweighting the MC with the obtained value of k', the standard fit of the M^2_{00} distribution with the Cabibbo-Isidori model was performed to obtain the cusp parameters, that were found to be compatible with the published values.

Bibliography

[1] G. Colangelo AIP Conf. Proc. **756**, 60 (2005).

[2] M. Knecht *et al.* Nucl. Phys. B **457**, 513 (1995).

[3] B. Ananthanarayan *et al.* Phys. Rept. **353**, 207 (2001).

[4] J. R. Batley *et al.* Phys. Lett. B **634**, 474 (2006).

[5] P. Bloch *et al.* Phys. Lett. B **60**, 393 (1976).

[6] N. Cabibbo and A. Maksymowicz Phys. Rev. **137**, B438 (1965); *Ibid.* **168**, 1926 (1968).

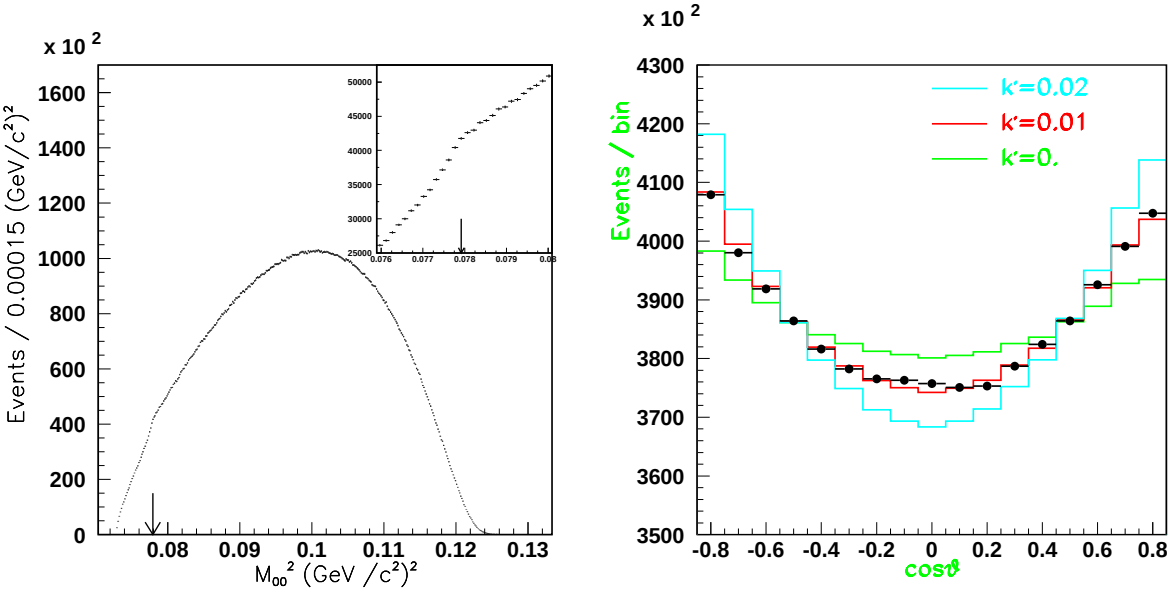

Figure 7: Left: M_{00}^2 of the selection $K^\pm \to \pi^0\pi^0\pi^\pm$ data events. The arrow indicates the position of the cusp. Right: angle between the $\pi^\pm$ and the π^0 in the $\pi^0\pi^0$ centre of mass system. The points represent the data, the three curves, the MC distribution for different values of k'

[7] J. Bijnens *et al.* 2nd DAΦNE Phisics Handbook, 315 (1995).

[8] A. Pais and S. B. Treiman Phys. Rev. **168**, 1858 (1968).

[9] G. Amoros and J. Bijnens J. Phys. G **25**, 1607 (1999).

[10] G. Colangelo *et al.* Nucl. Phys. B **603**, 125 (2001).

[11] L. Rosselet *et al.* Phys. Rev. D **15**, 574 (1977).

[12] S. Pislak *et al.* Phys. Rev. D **67**, 072004 (2003).

[13] S. Shimizu *et al.* Phys. Rev. D **70**, 037101 (2004).

[14] N. Cabibbo and G. Isidori JHEP **0503**, 021 (2005).

[15] J. R. Batley *et al.* Phys. Lett. B **633**, 173 (2006).

[16] S. Eidelman *et al.* Phys. Lett. B **592**, 1 (2004).

New results from KLOE

KLOE collaboration[1]
presented by Roberto Versaci
Laboratori Nazionali di Frascati dell'INFN
Via Enrico Fermi 40,
00044 Frascati (RM), ITALY

1 Introduction

The most precise determination of V_{us} comes from semileptonic kaon decays. We have measured with the KLOE detector at DAΦNE, the Frascati ϕ-factory, all the experimental inputs to V_{us} for both neutral and charged kaons. Using our results we extract the value of V_{us} with 0.9% fractional error, which is dominated by the theoretical error on the form factor, $f_+(0)$. A new determination of the ratio V_{us}/V_{ud} is also presented, based on our precise measurement of the absolute branching ratio for the decay $K \to \mu\nu(\gamma)$, combined with lattice results for the ratio f_K/f_π. New results on CPT symmetry and quantum mechanics test have also been achieved, which are based on the first measurement of the charged asymmetry for $K_S \to \pi e\nu$ decay and on interferometry studies using the $\phi \to K_L K_S \to \pi^+\pi^-\pi^+\pi^-$.

2 DAΦNE and KLOE

The DAΦNE e^+e^- collider operates at a total energy $\sqrt{s} = 1020$ MeV, the mass of the $\phi(1020)$-meson.

Since 2001, KLOE has collected an integrated luminosity of about 2.5 fb^{-1}. Results presented below are based on 2001-02 data for about 450 pb^{-1}.

[1]F. Ambrosino, A. Antonelli, M. Antonelli, C. Bacci, P. Beltrame, G. Bencivenni, S. Bertolucci, C. Bini, C. Bloise, S. Bocchetta, V. Bocci, F. Bossi, D. Bowring, P. Branchini, R. Caloi, P. Campana, G. Capon, T. Capussela, F. Ceradini, S. Chi, G. Chiefari, P. Ciambrone, S. Conetti, E. De Lucia, A. De Santis, P. De Simone, G. De Zorzi, S. Dell'Agnello, A. Denig, A. Di Domenico, C. Di Donato, S. Di Falco, B. Di Micco, A. Doria, M. Dreucci, G. Felici, A. Ferrari, M. L. Ferrer, G. Finocchiaro, S. Fiore, C. Forti, P. Franzini, C. Gatti, P. Gauzzi, S. Giovannella, E. Gorini, E. Graziani, M. Incagli, W. Kluge, V. Kulikov, F. Lacava, G. Lanfranchi, J. Lee-Franzini, D. Leone, M. Martini, P. Massarotti, W. Mei, S. Meola, S. Miscetti, M. Moulson, S. Müller, F. Murtas, M. Napolitano, F. Nguyen, M. Palutan, E. Pasqualucci, A. Passeri, V. Patera, F. Perfetto, L. Pontecorvo, M. Primavera, P. Santangelo, E. Santovetti, G. Saracino, B. Sciascia, A. Sciubba, F. Scuri, I. Sfiligoi, T. Spadaro, M. Testa, L. Tortora, P. Valente, B. Valeriani, G. Venanzoni, S. Veneziano, A. Ventura, R. Versaci, G. Xu.

The KLOE detector consists of a large cylindrical drift chamber surrounded by a lead/scintillating-fiber electromagnetic calorimeter. The drift chamber [1], is 4 m in diameter and 3.3 m long. The momentum resolution is $\sigma(p_T)/p_T \sim 0.4\%$. Two track vertices are reconstructed with a spatial resolution of ~ 3 mm. The calorimeter [2], composed of a barrel and two endcaps, covers 98% of the solid angle. Energy and time resolution are $\sigma(E)/E = 5.7\%/\sqrt{E[\mathrm{GeV}]}$ and $\sigma(t) = 57$ ps$/\sqrt{E[\mathrm{GeV}]} \oplus 100$ ps. A superconducting coil around the detector provides a 0.52 T magnetic field.

The KLOE trigger [3], uses calorimeter and drift chamber information. For the present analyses only the calorimeter triggers have been used. Two energy deposits above threshold, $E > 50$ MeV for the barrel and $E > 150$ MeV for the endcaps, have been required.

3 The tag mechanism

In the rest frame ϕ-mesons decay into anti-collinear $K\overline{K}$ pairs (with branching ratios $\mathrm{BR}(\phi \to K^+K^- \simeq 49\%)$ and $\mathrm{BR}(\phi \to K_SK_L \simeq 34\%)$ [4]). In the laboratory this remains approximately true because of the small crossing angle of the e^+e^- beams.

The decay products of the K and $\overline{K}$ define, event by event, two spatially well separated regions called the tag and the signal hemispeheres. Identified $\overline{K}(K)$ decays tag a $K(\overline{K})$ beam and provide an absolute count, using the total number of tags as normalization. This procedure is a unique feature of a ϕ-factory and provides the means for measuring absolute branching ratios.

Charged kaons are tagged using the two body decays $K^\pm \to \mu^\pm\nu_\mu$ and $K^\pm \to \pi^\pm\pi^0$. K_S are tagged by K_L interacting in the calorimeter (K_L-crash); K_L are tagged detecting $K_S \to \pi^+\pi^-$. For all of cases it is possible to precisely measure the tagged kaon momentum from the knowledge of the ϕ and the tagging kaon momentum.

4 K_L physics

As already stated, a pure sample of K_L mesons is selected by the identification of $K_S \to \pi^+\pi^-$ decays. K_L can either decay in the detector volume or interact in the calorimeter or escape the detector.

Branching ratios of K_L main decays

Starting from this sample, the K_L branching ratios are evaluated by counting the number of decays to each channel in the fiducial volume FV and correcting for the geometrical acceptance, the reconstruction efficiency and the background contamination.

K_L decays in charged particles are identified by selecting a decay vertex within the FV along the expected K_L flight direction, as defined by the tag. In order to discriminate among the different K_L charged modes the variable $\Delta_{\mu\pi} = |p_{miss} - E_{miss}|$ is used, where p_{miss} and E_{miss} are the missing momentum and the missing energy at the K_L decay vertex, evaluated by assigning to one track the pion mass and to the other one the muon mass. Signal counting is thus achieved by fitting the $\Delta_{\mu\pi}$ spectrum with a linear combination of four Monte Carlo shapes ($K_L \to \pi e\nu_e$, $K_L \to \pi\mu\nu_\mu$, $K_L \to \pi^+\pi^-\pi^0$, $K_L \to \pi^+\pi^-$).

To count $K_L \to \pi^0\pi^0\pi^0$ events, we exploit the time of flight capability of the calorimeter to reconstruct the neutral vertex position. Such a vertex is assumed to be along the K_L line of flight. The arrival time of each photon detected in the calorimeter is thus used to give an independent determination of L_K, the path length of the K_L. Its final value is obtained from a weighted average of the different measurements. This decay has been used also to measure the K_L lifetime, $\tau_K = 50.92 \pm 0.17 \pm 0.25$ ns, from a fit to the proper time distribution of neutral decay vertexes [5].

Since the geometrical efficiency of the FV depends on τ_K, the branching ratios measured by KLOE have been renormalized by imposing their sum plus the remaining ones ($\approx 0.86\%$ from PDG) to be equal to one. This removes the uncertainty due to τ_K, while giving at the same time a precise determination of the K_L lifetime itself. The measured branching ratios are [6]:

$$\mathrm{BR}(K_L \to \pi e\nu_e(\gamma)) = 0.4007 \pm 0.0005 \pm 0.0004 \pm 0.0014 \quad (1)$$

$$\mathrm{BR}(K_L \to \pi\mu\nu_\mu(\gamma)) = 0.2698 \pm 0.0005 \pm 0.0004 \pm 0.0014 \quad (2)$$

$$\mathrm{BR}(K_L \to \pi^+\pi^-\pi^0(\gamma)) = 0.1263 \pm 0.0004 \pm 0.0003 \pm 0.0011 \quad (3)$$

$$\mathrm{BR}(K_L \to \pi^0\pi^0\pi^0(\gamma)) = 0.1997 \pm 0.0003 \pm 0.0003 \pm 0.0019 \quad (4)$$

The corresponding lifetime is: $\tau_{K_L} = 50.72 \pm 0.11 \pm 0.13 \pm 0.33$ ns. It is in agreement with KLOE's previous measurement. The two measurements are uncorrelated and can be averaged: $\tau_{K_L} = 50.84 \pm 0.23$ ns.

$K_L \to \pi e\nu_e$ decay: branching ratio and form factor

From the K_Le3 semileptonic decays it is possible to extract the shape of the vector form factor $f_+(t)$, since extra terms in the matrix element depend on the lepton mass. The form factor is usually parametrized as

$$f_+(t) = f_+(0)\left[1 + \lambda'_+\frac{t}{m^2_{\pi^+}} + \frac{\lambda''_+}{2}\left(\frac{t}{m^2_{\pi^+}}\right)^2 + \ldots\right] \quad (5)$$

where $f_+(0)$ is evaluated from theory and t is the $K \to \pi$ four momentum transfer squared of the lepton pair invariant mass. The parameters λ',λ'' are obtained by fitting

the spectrum of $t/m^2_{\pi^+}$ K_{e3} events. The fit procedure takes into account the efficiency of the selection cuts, the resolution effects and the background contamination as a function of t. We find for a fit to $1 + \lambda'_+ t/m^2_{\pi^+}$ [7]:

$$\lambda_+ = (28.6 \pm 0.5 \pm 0.4) \times 10^{-3} \tag{6}$$

with $\chi^2/\mathrm{dof} = 330/363$ ($P(\chi^2) = 0.89$); for the quadratic term:

$$\lambda'_+ = (25.5 \pm 1.5 \pm 1.0) \times 10^{-3} \tag{7}$$

$$\lambda''_+ = (1.4 \pm 0.7 \pm 0.4) \times 10^{-3} \tag{8}$$

with $\chi^2/\mathrm{dof} = 325/362$ ($P(\chi^2) = 0.92$).

We also fit the data using a pole parametrization shape, $f_+(t)/f_+(0) = M_V^2/(M_V^2 - t)$. We obtain $M_V = (870 \pm 6 \pm 7)$ MeV ($\chi^2/\mathrm{dof} = 326/363$ with $P(\chi^2) = 0.924$).

$K_L \to \pi^+\pi^-$

KLOE has also measured the BR of the $K_L \to \pi^+\pi^-$ decay. This has been done measuring the ratio $R = \mathrm{BR}(K_L \to \pi^+\pi^-(\gamma))/\mathrm{BR}(K_L \to \pi\mu\nu_\mu(\gamma))$ and taking the value of the semileptonic branching ratio previously measured, since the tagging efficiency are very similar. The number of events has been obtained fitting the spectrum of the quantity $\sqrt{E^2_{miss} + p^2_{miss}}$ with a linear combination of the Monte Carlo shapes for signal and backgrounds corrected for the data/Monte Carlo ratio. Thus the result obtained is [8]:

$$\frac{\mathrm{BR}(K_L \to \pi^+\pi^-(\gamma)}{\mathrm{BR}(K_L \to \pi\mu\nu_\mu(\gamma))} = (0.7275 \pm 0.0042 \pm 0.0054) \times 10^{-2} \tag{9}$$

using the BR from the semileptonic decay:

$$\mathrm{BR}(K_L \to \pi^+\pi^-(\gamma)) = (1.963 \pm 0.0012 \pm 0.0017) \times 10^{-3} \tag{10}$$

This measurement, together with the measurements of the $\mathrm{BR}(K_S \to \pi^+\pi^-)$, the K_L and K_S lifetimes, can be used to determine $|\eta_{+-}|$ and $|\epsilon|$:

$$|\eta_{+-}| = (2.219 \pm 0.013) \times 10^{-3} \tag{11}$$

$$|\epsilon| = (2.216 \pm 0.013) \times 10^{-3} \tag{12}$$

where for $|\epsilon|$ we have used the world average for $Re(\epsilon'/\epsilon) = (1.67 \pm 0.26) \times 10^{-3}$ and assumed $\arg \epsilon' = \arg \epsilon$.

5 K_S decays

As already stated, a pure sample of K_S is selected by the detection of a K_L interaction in the calorimeter (K_L-crash).

$R_S^\pi = BR(K_S \to \pi^+\pi^-(\gamma))/BR(K_S \to \pi^0\pi^0)$

The ratio R_S^π is a fundamental parameter of the K_S meson. It enters into the double ratio that quantifies direct CP violation in $K \to \pi\pi$ transitions: $R_S^\pi/R_L^\pi = 1-6\Re(\epsilon'/\epsilon)$. The most precise measurement was performed by KLOE using data collected in 2000 for an integrated luminosity of 17 pb^{-1}: $R_S^\pi = 2.236 \pm 0.003 \pm 0.015$ [9]. This result was limited by systematic uncertainties. A new measurement has been performed using 410 pb^{-1} data collected in 2001 and 2002, inproving on the total error by a factor three. The K_S decays into two neutral pions are selected by requiring the presence of at least three EMC clusters with a timing compatible with the hypothesis of being due to prompt photons (within 5 $\sigma's$) and energy larger than 20 MeV. The selection of charged decays requires for two oppositely charged tracks coming from the IP. The result obtained is: $R_S^\pi = 2.2555 \pm 0.0056$ [10]. This result can be compared and averaged with the old one; weighting each by its independent errors and calculating the average systematic error with the same weigths gives [10]:

$$R_S^\pi = 2.2549 \pm 0.0054 \tag{13}$$

The result can be combined with the KLOE measurement of $\Gamma(K_S \to \pi^\mp e^\pm \nu(\overline{\nu})/\Gamma(K_S \to \pi^+\pi^-(\gamma))$ to extract the dominant K_S BRs. For the $\pi\pi$ mode we find [10]:

$$\mathrm{BR}(K_S \to \pi^+\pi^-(\gamma)) = (69.196 \pm 0.051) \times 10^{-2} \tag{14}$$

$$\mathrm{BR}(K_S \to \pi^0\pi^0) = (30.687 \pm 0.051) \times 10^{-2} \tag{15}$$

BR($K_S \to \pi e \nu$) and charge asymmetry

The measurement of the BR is an improvement (factor 4 on the total error) of KLOE's previous result [11]. It has been obtained by measuring the ratio $\mathrm{BR}(K_S \to \pi e\nu(\gamma))/\mathrm{BR}(K_S \to \pi^+\pi^-(\gamma))$ and using the KLOE's BR for the two bodies decay as normalization. The event counting is performed by fitting the $E_{miss} - p_{miss}$ spectrum with a combination of MC shapes for signal and background [12]:

$$\mathrm{BR}(K_S \to \pi^- e^+ \nu) = (3.528 \pm 0.062) \times 10^{-4} \tag{16}$$

$$\mathrm{BR}(K_S \to \pi^+ e^- \nu) = (3.517 \pm 0.058) \times 10^{-4} \tag{17}$$

$$\mathrm{BR}(K_S \to \pi e \nu) = (7.046 \pm 0.091) \times 10^{-4} \tag{18}$$

Fitting the ratio of data and MC $t/m^2_{\pi^+}$ distributions we have measured the form factor slope. The fit has been performed using only a linear parametrization, since the available statistics does not allow to be sensitive to a quadratic one. The result obtained is in agreement with the corresponding value for the linear slope of the semileptonic K_L form factor. The slope obtained is $\lambda_+ = (33.9 \pm 4.1) \times 10^{-3}$. The charge asymmetry measured is [12]:

$$A_S = \frac{\Gamma(K_S \to \pi^- e^+ \nu) - \Gamma(K_S \to \pi^+ e^- \nu)}{\Gamma(K_S \to \pi^- e^+ \nu) + \Gamma(K_S \to \pi^+ e^- \nu)} = (1.5 \pm 9.6 \pm 2.9) \times 10^{-3}. \tag{19}$$

The comparison of A_S with the corresponding for K_L allows precision tests of CP and CPT symmetries. The difference between the charge asymmetries $A_S - A_L = 4(Re\ \delta + Re\ x_-)$ signals CPT violation either in the mass matrix (δ term) or in the decay amplitudes with $\Delta S \neq \Delta Q$ (x_- term). The sum of the asymmetries $A_S + A_L = 4(Re\ \epsilon + Re\ y)$ is related to CP violation in the mass matrix (ϵ term) and to CPT violation in the decay amplitude (y term). K_S and K_L decay amplitudes allow test of the $\Delta S = \Delta Q$ rule through the quantity:

$$Re\ x_+ = \frac{1}{2}\frac{\Gamma(K_S \to \pi e\nu) - \Gamma(K_L \to \pi e\nu)}{\Gamma(K_S \to \pi e\nu) + \Gamma(K_L \to \pi e\nu)}. \tag{20}$$

The results obtained (using other quantities when needed either from KLOE when available or from PDG) are:

$$Re\ x_+ = (-0.5 \pm 3.6) \times 10^{-3} \tag{21}$$
$$Re\ x_- = (-0.8 \pm 2.5) \times 10^{-3} \tag{22}$$
$$Re\ y = (0.4 \pm 2.5) \times 10^{-3} \tag{23}$$

they are all compatible with zero. KLOE has a disposal of a statistic five time bigger, using all the data available the uncertainty on A_S can be reduced by more than a factor 5.

BR($K_S \to \pi^0\pi^0\pi^0$)

This decay is a pure CP violating process. The related CP violation parameter η_{000} is defined as the ratio of decay amplitudes: $|\eta_{000}| = A(K_S \to 3\pi^0)/A(K_L \to 3\pi^0) = \epsilon + \epsilon'_{000}$ where ϵ describes the CP violation in the mixing matrix and ϵ'_{000} is a direct CP violating term. The signal selection requires six neutral clusters coming from the interaction point. Background coming from $K_S \to \pi^0\pi^0$ + fake γ is rejected applying a kinematic fit imposing as constraints the K_S mass, the K_L four momentum and $\beta = 1$ for each photon. Two pseudo χ^2 variables are then built, ζ_3 which is based on the best 6 γ combination into 3 π^0 and ζ_2 which select four out of six γ providing the best agreement with the $K_S \to \pi^0\pi^0$ decay. Events with two charged tracks coming from the interaction point are vetoed. Using the $K_S \to \pi^0\pi^0$ branching ratio as normalization sample we obtained a 90% C.L. upper limit [13]:

$$\mathrm{BR}(K_S \to \pi^0\pi^0\pi^0) < 1.2 \times 10^{-7}. \tag{24}$$

The corresponding 90% C.L. upper limit on η_{000} is:

$$|\eta_{000}| = \frac{|A(K_S \to 3\pi^0)|}{|A(K_L \to 3\pi^0)|} < 0.018. \tag{25}$$

6 Quantum interference in kaons

KLOE at a ϕ-factory has the unique possibility for testing QM and CPT simmetry studying interference in the $\phi \to K_L K_S \to \pi^+\pi^-\pi^+\pi^-$ channel. Deviation from QM can be parametrized introducing a decoherence parameter ζ in the formula for the decay intensity [14, 15]:

$$I(|\Delta t|) \propto e^{-|\Delta t|\Gamma_L} + e^{-|\Delta t|\Gamma_S} - 2(1-\zeta)cos(\Delta m|\Delta t|)e^{\frac{\Gamma_S+\Gamma_L}{2}|\Delta t|} \tag{26}$$

The meaning and value of ζ depends on the basis used for the initial state (i.e. ζ_{SL} for $K_S K_L$ and $\zeta_{0\overline{0}}$ for $K^0\overline{K^0}$). The results have been obtained performing a fit of the Δt distribution. For the decoherence parameter we find [16]:

$$\zeta_{SL} = \quad 0.018 \pm 0.040 \pm 0.007 \qquad \chi^2/\mathrm{dof} = 29.7/32 \tag{27}$$

$$\zeta_{0\overline{0}} = \quad (0.10 \pm 0.21 \pm 0.04) \times 10^{-5} \qquad \chi^2/\mathrm{dof} = 29.6/32. \tag{28}$$

The results are consistent with zero, therefore there is not evidence for QM violation. Space-time fluctuactions at the Planck scale might induce a pure state to become mixed [17]. This results in QM and CPT violation, changing therefore the decay time distribution of the $K^0\overline{K^0}$ pair from ϕ decays. In some theoretical framework this violation can be parametrized with the quantities γ [18] or ω [19]. Again the values obtained are compatible with zero. There is no evidence for QM violation [16]:

$$\gamma = \quad (1.3^{+2.8}_{-2.4} \pm 0.4) \times 10^{-21} GeV \qquad \chi^2/dof = 33/32 \tag{29}$$

$$\Re\omega = \quad (1.1^{+8.7}_{-5.7} \pm 0.9) \times 10^{-4} \qquad \chi^2/dof = 29/31 \tag{30}$$

$$\Im\omega = \quad (3.4^{+4.8}_{-5.0} \pm 0.6) \times 10^{-4}. \tag{31}$$

Another test of CPT invariance can be performed via the Bell-Steinberger relation (BSR) [20]:

$$\left(\frac{\Gamma_S+\Gamma_L}{\Gamma_S-\Gamma_L} + i\ \mathrm{tan}\phi_{SW}\right)\left(\frac{Re(\epsilon)}{1+|\epsilon|^2} - i\ Im(\delta)\right) = \frac{1}{\Gamma_S-\Gamma_L}\sum_f A_L(f)A_S^*(f) \tag{32}$$

where $\phi_{SW} = \arctan(2(m_L - m_S)/(\Gamma_S - \Gamma_L))$. The Bell-Steinberger relation links a possible violation of CPT invariance ($m_{K^0} \neq m_{\overline{K^0}}$ or $\Gamma_{K^0} \neq \Gamma_{\overline{K^0}}$) in the time evolution of the $K^0\overline{K^0}$ system to the observable CP violating interference of K_L and K_S decays into the same final state f. Any evidence for a non vanishing $Im(\delta)$ can only be due to violation of: i) CPT invariance; ii) unitarity; iii) the time independence of M and Γ in the equation which describes the time evolution of the neutral kaon system within the Wigner-Weisskopf approximation:

$$i\frac{\partial}{\partial t}\Psi(t) = H\Psi(t) = \left(M - \frac{i}{2}\Gamma\right)\Psi(t), \tag{33}$$

where M and Γ are 2×2 time-independent Hermitian matrices and $\Psi(t)$ is a two-component state vector in the $K^0 - \overline{K^0}$ space. The result we have obtained (using all experimental inputs from KLOE where available) are [21]:

$$Re(\epsilon) = (159.6 \pm 1.3) \times 10^{-5} \tag{34}$$

$$Im(\delta) = (0.4 \pm 2.1) \times 10^{-5}. \tag{35}$$

The limits on $Im(\delta)$ and $Re(\delta)$ can be used to constrain the mass and width difference between the neutral kaons via the relation:

$$\delta = \frac{i(m_{K^0} - m_{\overline{K}^0}) + \frac{1}{2}(\Gamma_{K^0} - \Gamma_{\overline{K}^0})}{\Gamma_S - \Gamma_L} \cos\,\phi_{SW} e^{i\phi_{SW}} [1 + O(\epsilon)]. \tag{36}$$

In the limit $\Gamma_{K^0} = \Gamma_{\overline{K}^0}$ (i.e. neglecting CPT-violating effects in the decay amplitudes) we obtain the following bound at 95% C.L. on the mass difference [21]:

$$-5.3 \times 10^{-19}\ GeV < m_{K^0} - m_{\overline{K}^0} < 6.3 \times 10^{-19}\ GeV \tag{37}$$

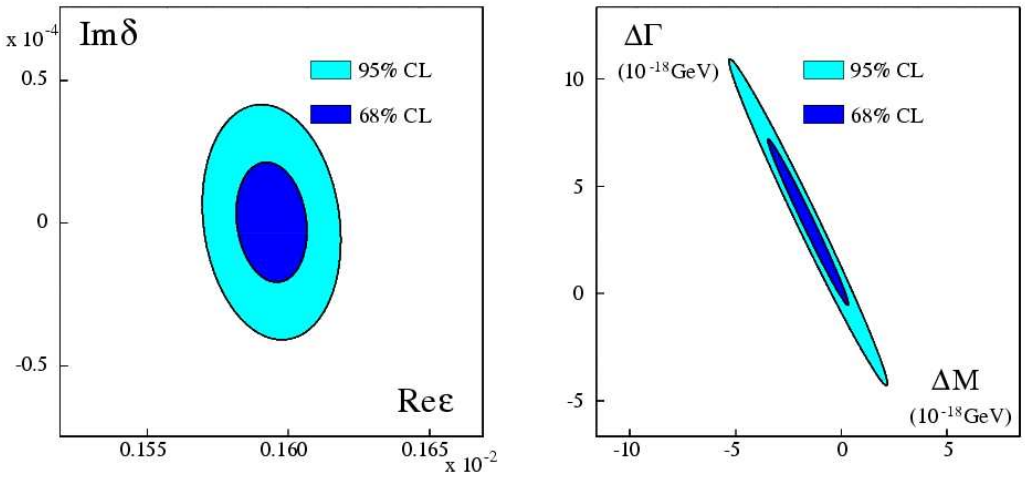

Figure 1: Left: allowed region at 68% and 95% CL in the Re(ϵ), Im(δ) plane. Right: allowed region at 68% and 95% CL in ΔM, $\Delta\Gamma$ plane.

7 Charged kaons decays

As already stated, a pure sample of $K^{\pm}$ is selected by the identification of a $K^{\mp}$ two bodies decay in the drift chamber.

Charged kaon lifetime

Together with the branching ratios of the semileptonic decays, the lifetime is one of the fundamental experimental inputs for the evaluation of V_{us}. There are two methods available for the measurement: the kaon decay length and the kaon decay time. The two methods allow cross checks and studies of systematics; their resolutions are comparable. The first requires a kaon decay vertex in the fiducial volume, then the kaon is extrapolated backward to the IP taking into account the dE/dx to evaluate its velocity. The proper time can be obtained fitting the distribution of

$$\tau^* = \sum_i \Delta T_i = \sum_i \frac{\sqrt{1-\beta_i^2}}{\beta_i c} \Delta l_i \tag{38}$$

The preliminary result we have obtained for the K^+ is:

$$\tau^+ = (12.377 \pm 0.044 \pm 0.065) ns \tag{39}$$

with $\chi^2/\mathrm{dof} = 17.7/15$. The analysis with the second method is still in progress.

Branching ratio of the charged kaon semileptonic decays

The BRs for the two semileptonic decays are obtained performing a fit of the mass squared of the charged secondary decay product (m^2_{lept}), using the MC distributions for signal and background. The mass is obtaind via a TOF measurement. Background from $\mu\nu_\mu$ decay is rejected applying a cut on the momentum of the charged secondary in the decaying kaon rest frame. The BRs have been evaluated separately for each tag sample and each charge; corrections have been applied in order to account for data-MC differences. The preliminary branching ratios obtained are:

$$\mathrm{BR}(K^\pm \to \pi^0 e^\pm \nu_e(\gamma) = (5.047 \pm 0.019 \pm 0.039) \times 10^{-2} \tag{40}$$

$$\mathrm{BR}(K^\pm \to \pi^0 \mu^\pm \nu_\mu(\gamma) = (3.310 \pm 0.016 \pm 0.045) \times 10^{-2}. \tag{41}$$

$\mathbf{BR}(K \to \mu\nu_\mu(\gamma))$

The number of signal events has been obtained performing a fit of the momentum of the charged secondary in the decaying kaon rest frame. Background has been identified as any event having a π^0 in the final state. The efficiency has been evaluated directly on data using a sample selected only with calorimeter informations. The result obtained is [22]:

$$\mathrm{BR}(K^+ \to \mu^+ \nu_\mu(\gamma)) = 0.6366 \pm 0.0009 \pm 0.0015 \tag{42}$$

8 V_{us} summary

The KLOE results on semileptonic decays on both neutral and charged kaons, can be used together with results from other experiments in order to evaluate V_{us} and check the unitarity of the first row of the CKM matrix.
Averaging over all the available experimental inputs according to the procedure specified in [23], it is possible to extract the world average:

$$V_{us} \times f_+(0) = 0.2164 \pm 0.0004 \tag{43}$$

which can be compared with the value expected from unitarity of CKM matrix using V_{ud} from [24]:

$$V_{us} \times f_+(0) = 0.2187 \pm 0.0022. \tag{44}$$

We use $f_+(0) = 0.961 \pm 0.008$, computed by Leutwyler and Roos [25]. It is also possible

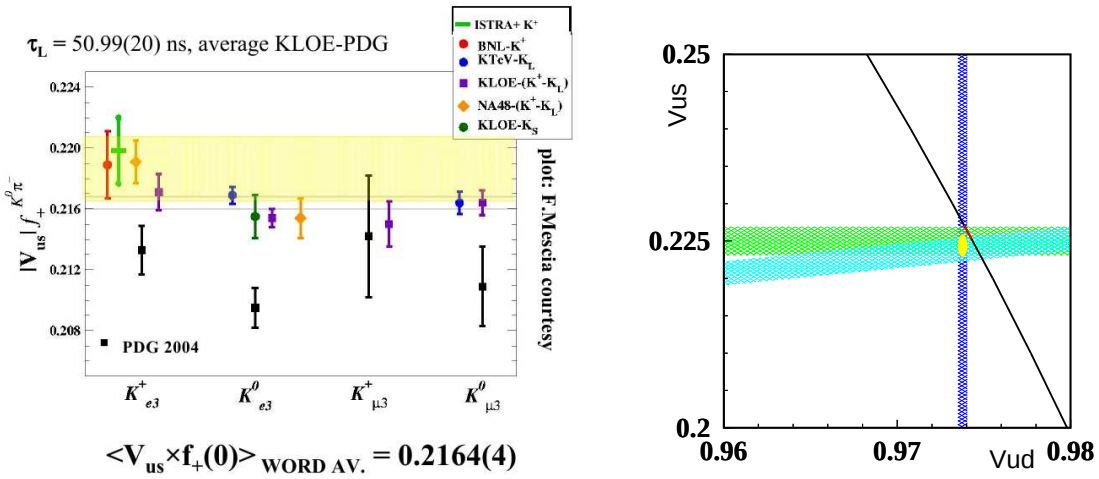

Figure 2: Left: $V_{us} \times f_+(0)$ world average. Right: $V_{us} - V_{ud}$ plane.

to use the charged kaon leptonic decay to evaluate V_{us} using lattice calculation of the ratio f_K/f_π as pointed out in [26]. Using the latest value from the MILC collaboration for the ratio of the decay constants [27] we find:

$$\frac{V_{us}}{V_{ud}} = 0.2286^{+0.0020}_{-0.0011}. \tag{45}$$

This value can be fitted together with V_{us} from kaon semileptonic decays and V_{ud} from nuclear beta decays, obtaining:

$$V_{us} = 0.2246^{+0.0009}_{-0.0013} \tag{46}$$

$$V_{ud} = 0.97377 \pm 0.00027 \tag{47}$$

with $\chi^2/dof = 0.046/2$, $P(\chi^2) = 0.97$. Imposing also the unitarity constraint (see the right panel of figure 2):

$$V_{us} = 0.2257 \pm 0.0007 \quad (48)$$
$$V_{ud} = 0.97420 \pm 0.00016 \quad (49)$$

with $\chi^2/dof = 3.94/1$, $P(\chi^2) = 0.05$.

Bibliography

[1] M. Adinolfi *et al.*, [KLOE Collaboration], *Nucl. Instrum. Meth* **A 488** 2002 51

[2] M. Adinolfi *et al.*, [KLOE Collaboration], *Nucl. Instrum. Meth* **A 482** 2002 364

[3] M. Adinolfi *et al.*, [KLOE Collaboration], *Nucl. Instrum. Meth* **A 492** 2002 134

[4] W. M. Yao *et al.* [Particle Data Group], J. Phys. G **33** (2006) 1.

[5] F. Ambrosino *et al.* [KLOE Collaboration], Phys. Lett. B **626** (2005) 15

[6] F. Ambrosino *et al.* [KLOE Collaboration], Phys. Lett. B **632** (2006) 43

[7] F. Ambrosino *et al.* [KLOE Collaboration], Phys. Lett. B **636** (2006) 166

[8] F. Ambrosino *et al.* [KLOE Collaboration], Phys. Lett. B **638** (2006) 140

[9] A. Aloisio *et al.* [KLOE Collaboration], Phys. Lett. B **538** (2002) 21

[10] F. Ambrosino *et al.* [KLOE Collaboration], Eur. Phys. J. C **48** (2006) 767

[11] A. Aloisio *et al.* [KLOE Collaboration], Phys. Lett. B **535**, 37 (2002)

[12] F. Ambrosino *et al.* [KLOE Collaboration], Phys. Lett. B **636** (2006) 173

[13] F. Ambrosino *et al.* [KLOE Collaboration], Phys. Lett. B **619** (2005) 61

[14] P. H. Eberhard, *In *Maiani, L. (ed.) et al.: The second DAPHNE physics handbook* 99-110*

[15] R. A. Bertlmann, W. Grimus and B. C. Hiesmayr, Phys. Rev. D **60** (1999) 114032

[16] F. Ambrosino *et al.* [KLOE Collaboration], Phys. Lett. B **642** (2006) 315

[17] S. W. Hawking, Commun. Math. Phys. **87**, 395 (1982)

[18] J. R. Ellis, J. S. Hagelin, D. V. Nanopoulos and M. Srednicki, Nucl. Phys. B **241** (1984) 381

[19] J. Bernabeu, N. E. Mavromatos and J. Papavassiliou, Phys. Rev. Lett. **92** (2004) 131601

[20] J. S. Bell and J. Steinberger, *Proceedings Oxford Int. Conf. on Elementary Particles* (1965)

[21] F. Ambrosino *et al.* [KLOE Collaboration], G. D'Ambrosio and G. Isidori, JHEP **12** (2006) 011

[22] F. Ambrosino *et al.* [KLOE Collaboration], Phys. Lett. B **632** (2006) 76

[23] F. Mescia, arXiv:hep-ph/0411097

[24] W. J. Marciano and A. Sirlin, Phys. Rev. Lett. **96** (2006) 032002

[25] H. Leutwyler and M. Roos, Z. Phys. C **25** (1984) 91

[26] W. J. Marciano, Phys. Rev. Lett. **93** (2004) 231803

[27] C. Bernard *et al.* [MILC Collaboration], arXiv:hep-lat/0609053

KTeV Results on Chiral Perturbation Theory

Elliott Cheu
Department of Physics
1118 E 4th Street
Tucson, AZ 85749 USA

The KTeV experiment has carried out a broad program of studies of rare kaon decays. In this paper we present results on $K_L \to \pi^0\gamma\gamma$, $K_L \to \pi^0 e^+e^-\gamma$ and $K_L \to \pi^0\pi^0\gamma$. These decays provide a window for testing chiral perturbation theory at $O(p^6)$. We find $\mathrm{BR}(K_L \to \pi^0\gamma\gamma) = (1.30 \pm 0.03) \times 10^{-6}$, $\mathrm{BR}(K_L \to \pi^0 e^+e^-\gamma) = (1.90 \pm 0.16 \pm 0.12) \times 10^{-8}$, and set the limit $\mathrm{BR}(K_L \to \pi^0\pi^0\gamma) < 2.32 \times 10^{-7}$. The KTeV measurements are competitive with or better than the world's best results in these decays.

1 Introduction

The decays $K_L \to \pi^0\gamma\gamma$, $K_L \to \pi^0 e^+e^-\gamma$ and $K_L \to \pi^0\pi^0\gamma$ can all be used as tests of chiral perturbation theory. In particular, predictions for the branching ratios of these modes show significant increases when one uses $O(p^6)$ versus $O(p^4)$ chiral perturbation theory. The first measurements of $K_L \to \pi^0\gamma\gamma$ [1, 2] were a factor of three higher than the $O(p^4)$ prediction, but were consistent with the $O(p^6)$ calculation. [3] This was also seen in the decay $K_L \to \pi^0 e^+e^-\gamma$ decay where the $O(p^4)$ prediction was inconsistent with the measurement, but consistent with the $O(p^6)$ calculation. [4] For the $K_L \to \pi^0\pi^0\gamma$ decay, the branching ratio vanishes at $O(p^4)$ chiral perturbation theory, yet is non-zero at higher order. Recent predictions for this decay range from $10^{-11} - 10^{-8}$. [5, 6]

In addition, the two decays $K_L \to \pi^0\gamma\gamma$ and $K_L \to \pi^0 e^+e^-\gamma$ are important for understanding the direct CP violating decay $K_L \to \pi^0 e^+e^-$. Three components contribute to the $K_L \to \pi^0 e^+e^-$ amplitude: direct CP violation, indirect CP violation (and an interference term), and a CP conserving term. Recent measurements of the decay $K_S \to \pi^0 e^+e^-$ [7] and $K_S \to \pi^0\mu^+\mu^-$ [8] have helped to determine the indirect CP violating contributions to $K_L \to \pi^0 e^+e^-$ and $K_L \to \pi^0\mu^+\mu^-$. The magnitude of the CP conserving contributions to $K_L \to \pi^0 l\bar{l}$ can be determined by measurements of the decay $K_L \to \pi^0\gamma\gamma$ [9, 10] and $K_L \to \pi^0 e^+e^-\gamma$. The CP conserving term is estimated to be small [11].

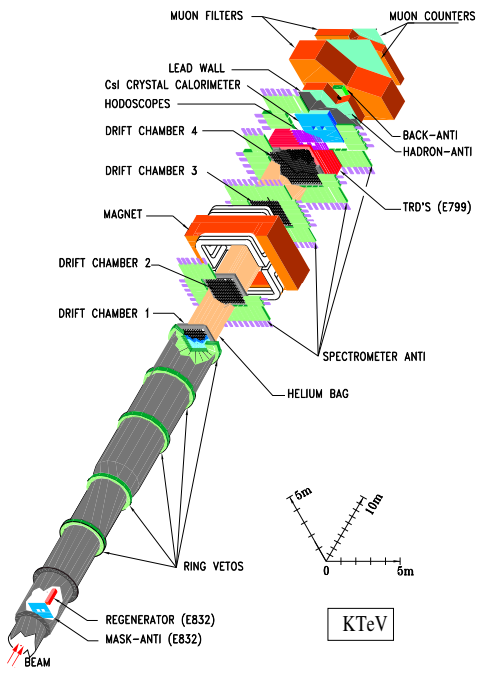

Figure 1: The KTeV detector.

2 The KTeV Experiment

The KTeV experiment, shown in Figure 1, is a Fermilab fixed target experiment. The detector ran in two different configurations: E799 and E832. The E799 configuration took advantage of a higher kaon flux to search for rare kaon decays. The E832 configuration was used primarily for a measurement of ϵ'/ϵ. The main difference between the two configurations was the use of a regenerator to produce K_S decays in the E832 configuration. The two experimental configurations also had a few other differences as noted below.

The KTeV detector contains a charged spectrometer with four drift chambers, two on either side of a large dipole magnet. At the downstream end of the detector is a two-meter square calorimeter consisting of 3100 pure CsI blocks. Following the calorimeter are 10 cm of lead and 5 meters of steel which act as a muon filter. Two planes of scintillator, used for muon detection, are located just downstream of the steel. Photon vetoes to detect the the presence of particles that would otherwise escape detection surround the spectrometer. The charged spectrometer achieves a hit resolution of better than 100 μm, while the CsI calorimeter obtains better than 1% energy resolution over the range of energies of interest. Just upstream of the CsI calorimeter is a transition radiation detector (TRD) capable of e/π separation

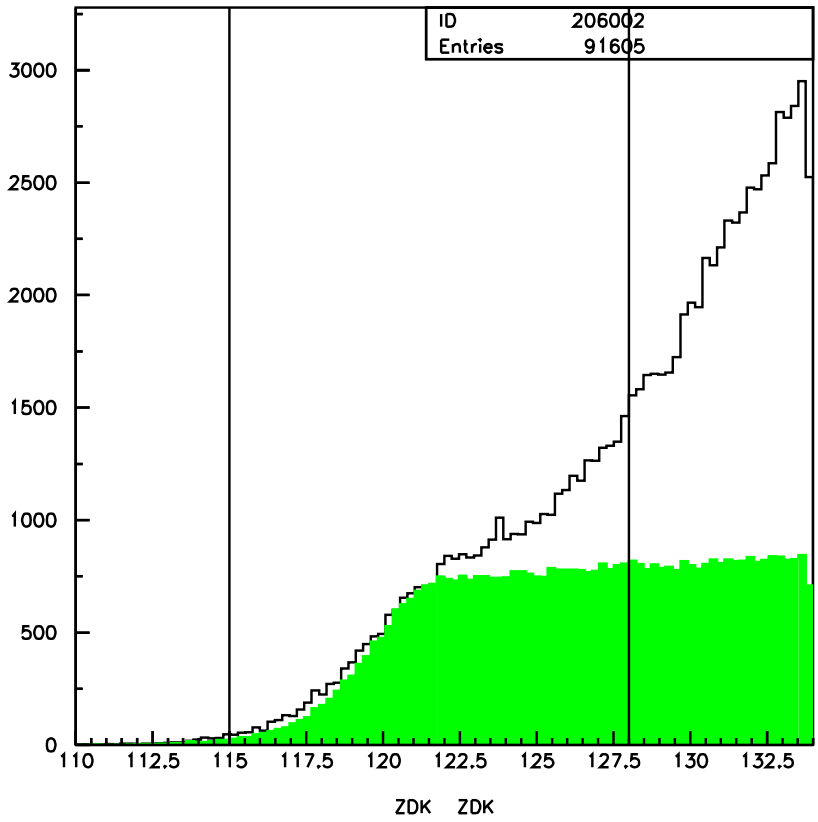

Figure 2: The kaon reconstructed decay position. The green histogram is the $K_L \to \pi^0\gamma\gamma$ Monte Carlo, while the black histogram is the $K_L \to \pi^0\pi^0\pi^0$ Monte Carlo.

of 200:1 with a 90% efficiency. The TRDs were employed during E799 running, and were moved out of the way during E832 running.

The KTeV experiment took data during a number of different periods between 1996 and 1999. In the E832 configuration, we had three different running periods: 1996, 1997 and 1999. The E799 running occurred in 1997 and 1999. Between the 1997 and 1999 runs, a number of upgrades were made to the detector to increase its reliability and to improve its live time. In addition during E799 running, the transverse kick from the magnet was reduced from 205 MeV/c to 150 MeV/c, enabling a larger acceptance for high multiplicity decay modes. For the entire E799 data set, approximately 6.6×10^{11} kaon decays occurred in the KTeV detector. This large kaon flux allows us to have an unprecedented sensitivity to a number of rare kaon decays with large multiplicity final states.

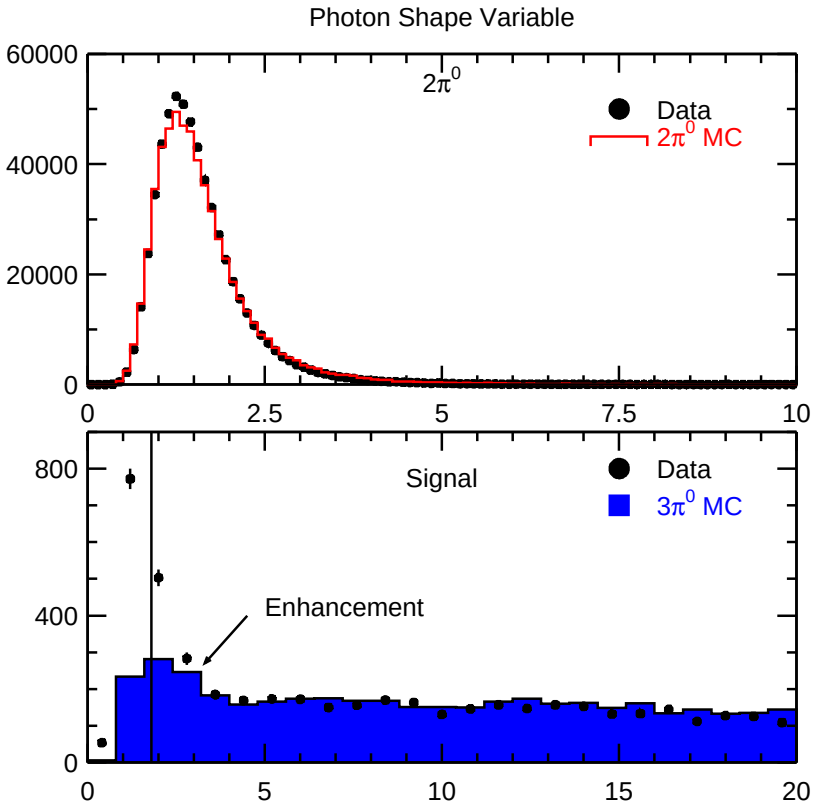

Figure 3: The photon shape variable for $K_L \to \pi^0\pi^0$ (top) and $K_L \to \pi^0\gamma\gamma$ candidates (bottom). In the top plot, the dots are the data and the red histogram is the Monte Carlo. In the bottom plot, the blue histogram represents the $K_L \to \pi^0\pi^0\pi^0$ background.

3 Measurement of $K_L \to \pi^0\gamma\gamma$

In the decay $K_L \to \pi^0\gamma\gamma$, the final state consists of four photons, two from the π^0 and two from the K_L. Our analysis requires four electromagnetic clusters in the CsI calorimeter, with no tracks or extra clusters. One can combine the four clusters in three different combinations. We choose the combination in which the two photon invariant mass reconstructs closest to the known π^0 mass.

Backgrounds to this decay originate from two main sources, $K_L \to \pi^0\pi^0$ and $K_L \to \pi^0\pi^0\pi^0$. The first background has the same topology as our signal events. However, the relatively small branching ratio for $K_L \to \pi^0\pi^0$ and kinematic cuts reduce this background to a negligible level. In particular, we look at all possible photon combinations of the four photons and reject any event in which the invariant $\gamma\gamma$ mass for both pairs of photons reconstruct near the π^0 mass.

$K_L \to \pi^0\pi^0\pi^0$ decays constitute the largest source of background to $K_L \to \pi^0\gamma\gamma$. These events can contribute to the background in three distinct ways. First, two photons from the $K_L \to \pi^0\pi^0\pi^0$ decay can miss the calorimeter, with the remaining four photons interacting in the CsI calorimeter. Another possibility is that one photon misses the calorimeter while two photons overlap in the calorimeter. Finally, all six photons can hit the calorimeter, with four of the six photons from the $K_L \to \pi^0\pi^0\pi^0$ decay overlapping in the calorimeter, producing four separate clusters in the calorimeter.

The first source of $K_L \to \pi^0\pi^0\pi^0$ background can be reduced by first eliminating events with signals in the photon vetoes. In addition, one can improve the signal to background ratio by cutting on the reconstructed z position of the event. When the energy in the calorimeter is less than the kaon energy, the event reconstructs downstream of its true decay position. This can be seen in Figure 2 where the signal events are relatively flat, while the background events show a large enhancement at the downstream end of the detector.

To get rid of events in which photons overlap in the CsI calorimeter, we define a photon shape variable. This variable uses the 3x3 array of CsI crystals containing the core of the shower and compares the energy distribution to an ideal energy distribution determined from Monte Carlo. This shape variable can be seen in Figure 3. The top plot shows the photon shape variable for $K_L \to \pi^0\pi^0$ events for both the data and the Monte Carlo, and shows good agreement between the two. The bottom plot shows the data with the $K_L \to \pi^0\pi^0\pi^0$ Monte Carlo overlaid. As can be seen, the signal events tend to peak at low values of the shape variable, while the $3\pi^0$ background is relatively flat. We require that the shape variable be less than 1.8, which removes the majority of the $3\pi^0$ events.

Because of the discrepancy between the NA48 and KTeV published results on $K_L \to \pi^0\gamma\gamma$, we reexamined the data used in our previous result. [10] We found that we underestimated the impact of a disagreement between the data and the Monte

Source of Uncertainty	Uncertainty (%)	
a_V dependence	1.5	
$3\pi^0$ background	1.3	
MC statistics		1.0
Normalization		0.9
Photon Shape	1.1	
Tracking Chambers	0.9	
$2\pi^0$ branching ratio	0.9	
Photon vetoes	0.9	
Kaon Energy	0.7	
Decay Vertex	0.4	
Total	2.9	

Table 1: Systematic errors for the $K_L \to \pi^0\gamma\gamma$ measurement

Carlo photon shape variable. This led to an underestimate of the background in our final sample. With an improved simulation of the photon shape variable, our background estimate nearly doubles, and the $K_L \to \pi^0\gamma\gamma$ branching ratio decreases.

After all cuts, the background is dominated by $K_L \to \pi^0\pi^0\pi^0$ events, with the total background constituting approximately 30% of the final events. To check that we understand the background level, we examine the data/MC overlays of the m_{π^0} distributions. Any underestimate of the $3\pi^0$ background would manifest itself as a data/MC mismatch in the tails of the m_{π^0} distributions. As shown in Figure 4, at small values of the photon shape variable, the tails agree quite well in the m_{π^0} distributions.

The systematic errors associated with this measurement are shown in Table 3. The main sources of uncertainty stem from understanding the $3\pi^0$ background and its normalization. Other sources of systematic uncertainty come from our knowledge of the photon veto system, the acceptance determination and external factors such as the measured $K_L \to \pi^0\pi^0$ branching ratios. The total systematic uncertainty is 2.9%.

After all cuts have been implemented, we find 1982 events with a background of 601 events. The reconstructed $\gamma\gamma$ mass is shown in Figure 5. The distinctive $\gamma\gamma$ shape results from coupling of the $\gamma\gamma$ system to two virtual pions, and peaks around 320 MeV/c^2. We determine the $K_L \to \pi^0\gamma\gamma$ branching ratio to be: BR($K_L \to \pi^0\gamma\gamma$) $= (1.30 \pm 0.03 \pm 0.04) \times 10^{-6}$, where the first error is statistical and the second error systematic. As shown in Figure 5, this result is compatible and competitive with the result from NA48. Our new result supercedes the previous KTeV measurement of BR($K_L \to \pi^0\gamma\gamma$), which was in nominal disagreement with the NA48 result.

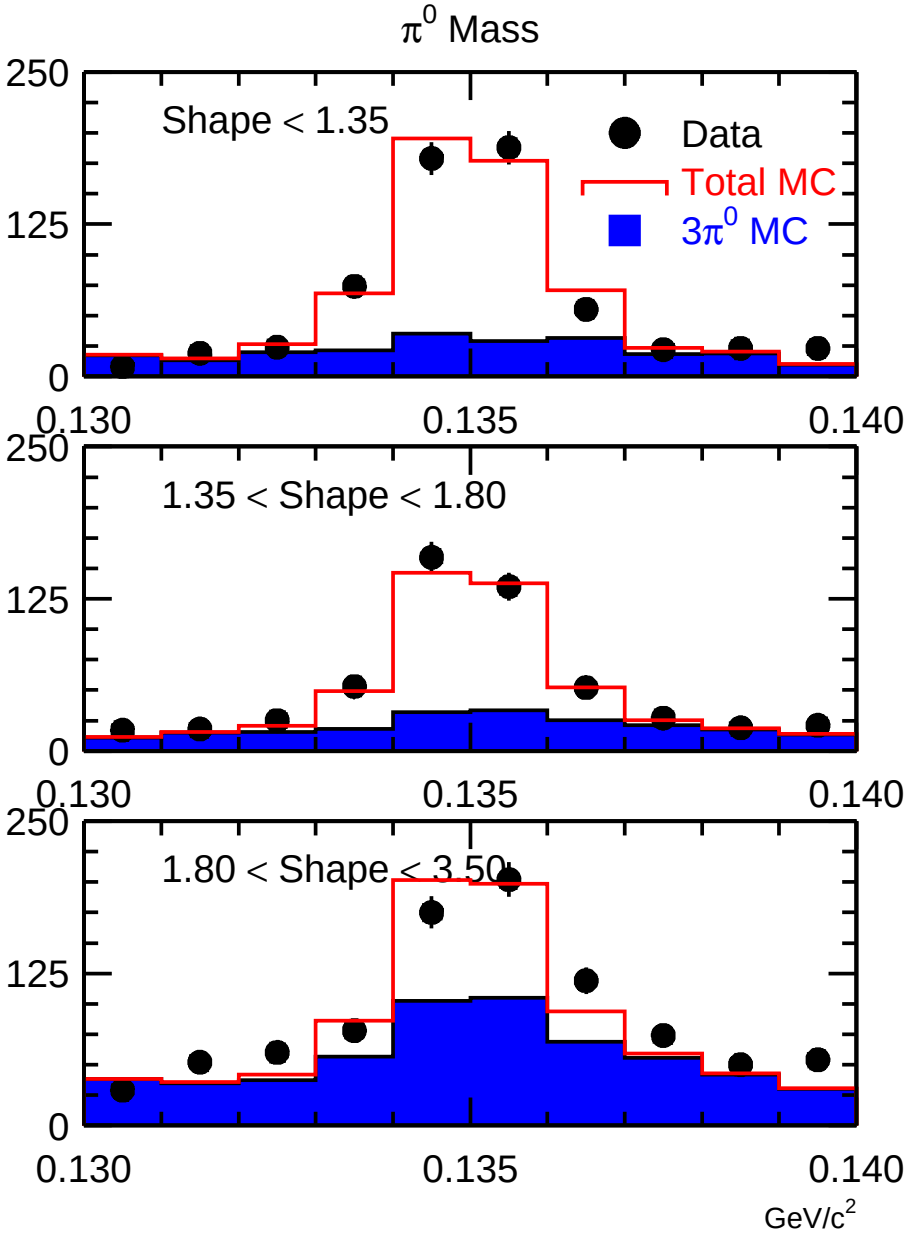

Figure 4: The reconstructed π^0 mass distribution for candidate events. The dots are the data, the red histogram the sum of the Monte Carlo, and the blue histogram the $K_L \to \pi^0\pi^0\pi^0$ background Monte Carlo. The three plots represent different regions of the photon shape variable.

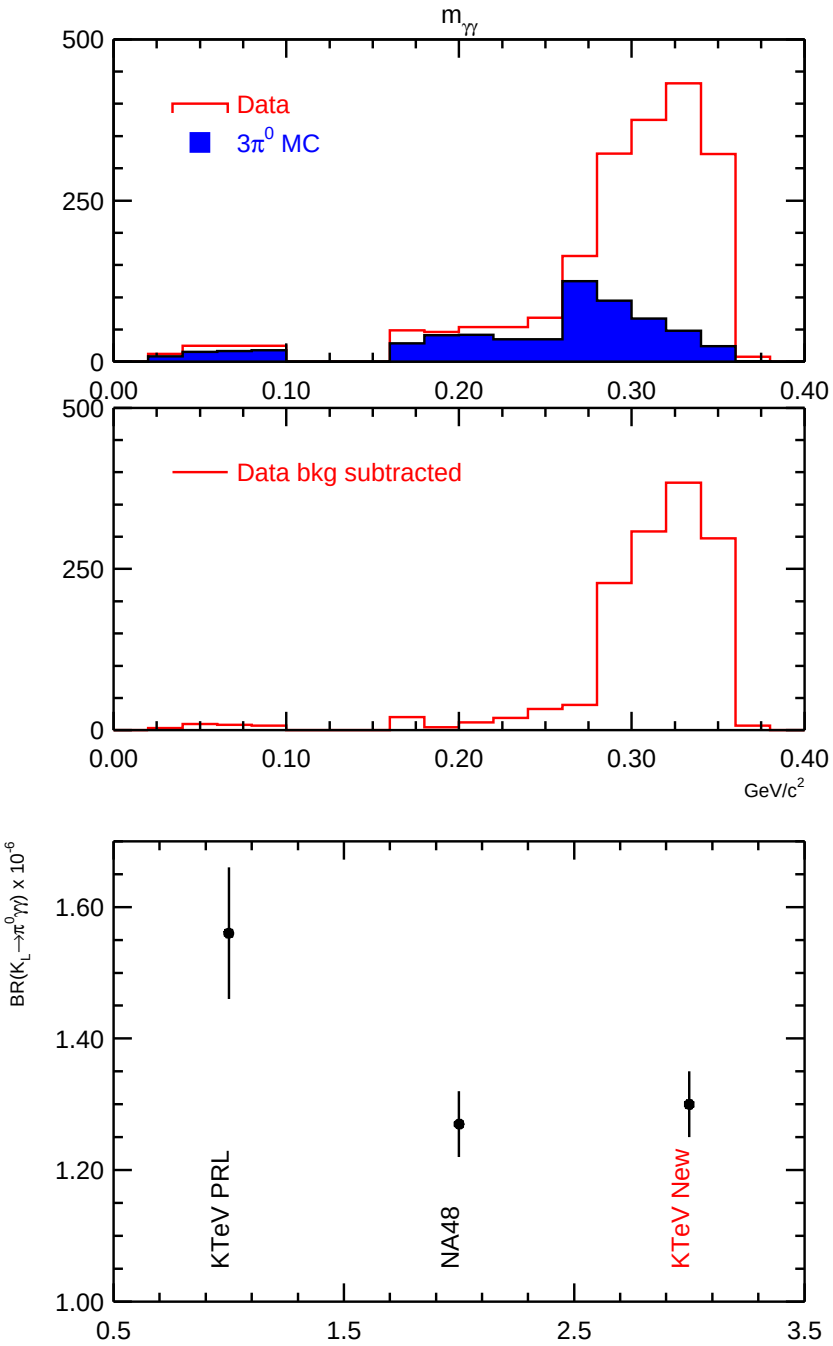

Figure 5: The top plots show the final $\gamma\gamma$ mass distribution for $K_L \to \pi^0\gamma\gamma$ candidates before and after background subtraction. The bottom plot shows the branching ratio results for the previous KTeV result, the NA48 result and our new KTeV result. The results have been rescaled using the latest PDG value for $K_L \to \pi^0\pi^0$.

4 Measurement of $K_L \to \pi^0 e^+ e^- \gamma$

The decay $K_L \to \pi^0 e^+ e^- \gamma$ produces two charged tracks in the spectrometer and three photons in the CsI calorimeter. The three photons can be combined in three different ways to form a neutral pion. We choose the combination that has the best π^0 mass. The neutral vertex is used to determine the decay position rather than the charged vertex due to its better resolution.

Like the $K_L \to \pi^0\gamma\gamma$ decay, the main backgrounds to this decay are from $K_L \to \pi^0\pi^0$ and $K_L \to \pi^0\pi^0\pi^0$. The difference is that one of the π^0 undergoes Dalitz decay to $e^+e^-\gamma$. To help reduce the background from $K_L \to \pi^0\pi^0$ decays, we formed a neural net variable using the reconstructed masses $m_{\gamma\gamma}$ and $m_{e^+e^-\gamma}$ from the second and third best combinations. We define the second and third best combinations by how far from the nominal π^0 mass the $\gamma\gamma$ combination reconstructs. The neural net variable can be seen in Figure 6. In this plot the $K_L \to \pi^0\pi^0$ events are well-separated from the signal $K_L \to \pi^0 e^+ e^- \gamma$ events. We require that the neural net variable be greater than 0.5

To reduce $K_L \to \pi^0\pi^0\pi^0$ backgrounds we also require that the photon shape variable, defined above, be small for each photon candidate. We can use the decay kinematics to help reduce the background from $K_L \to \pi^0\pi^0\pi^0$ decays. We define a variable p_L^2, which is the longitudinal momentum squared of the missing π^0 in the kaon rest frame. We perform a two-dimensional cut on the p_L^2 variable versus the three photon invariant mass, $m_{\gamma\gamma\gamma}$. This distribution is shown in Figure 6. There is good separation between the signal events, shown in blue, and the $K_L \to \pi^0\pi^0\pi^0$ background. We use a polynomial to define the cut shown in Figure 6.

After applying all cuts, we find 139 events over a background of 14.4 events as shown in Figure 7. We reconstructed 80,445 $K_L \to \pi^0\pi^0$ events used for normalization. This allows us to determine the branching ratio for $K_L \to \pi^0 e^+ e^- \gamma$ to be $\mathrm{BR}(K_L \to \pi^0 e^+ e^- \gamma) = (1.90 \pm 0.16 \pm 0.12) \times 10^{-8}$ where the first error is statistical and the second is systematic. The results from the 1997 and 1999 data sets are shown separately in Figure 7, along with the previously published result on $K_L \to \pi^0 e^+ e^- \gamma$. The published result and our new 1997 result use the same data set. Although the branching ratio results for these two results differ, the two results are statistically consistent with each other. We expect the two results to differ because of differences in selection criteria and calibration constants. As in the $K_L \to \pi^0\gamma\gamma$, the normalization mode branching ratio has decreased by approximately 8% from the value used in the published KTeV result. The systematic uncertainties are listed in Table 4. The largest systematics come from the limited Monte Carlo statistics and the dependence of the result on the parameter a_V.

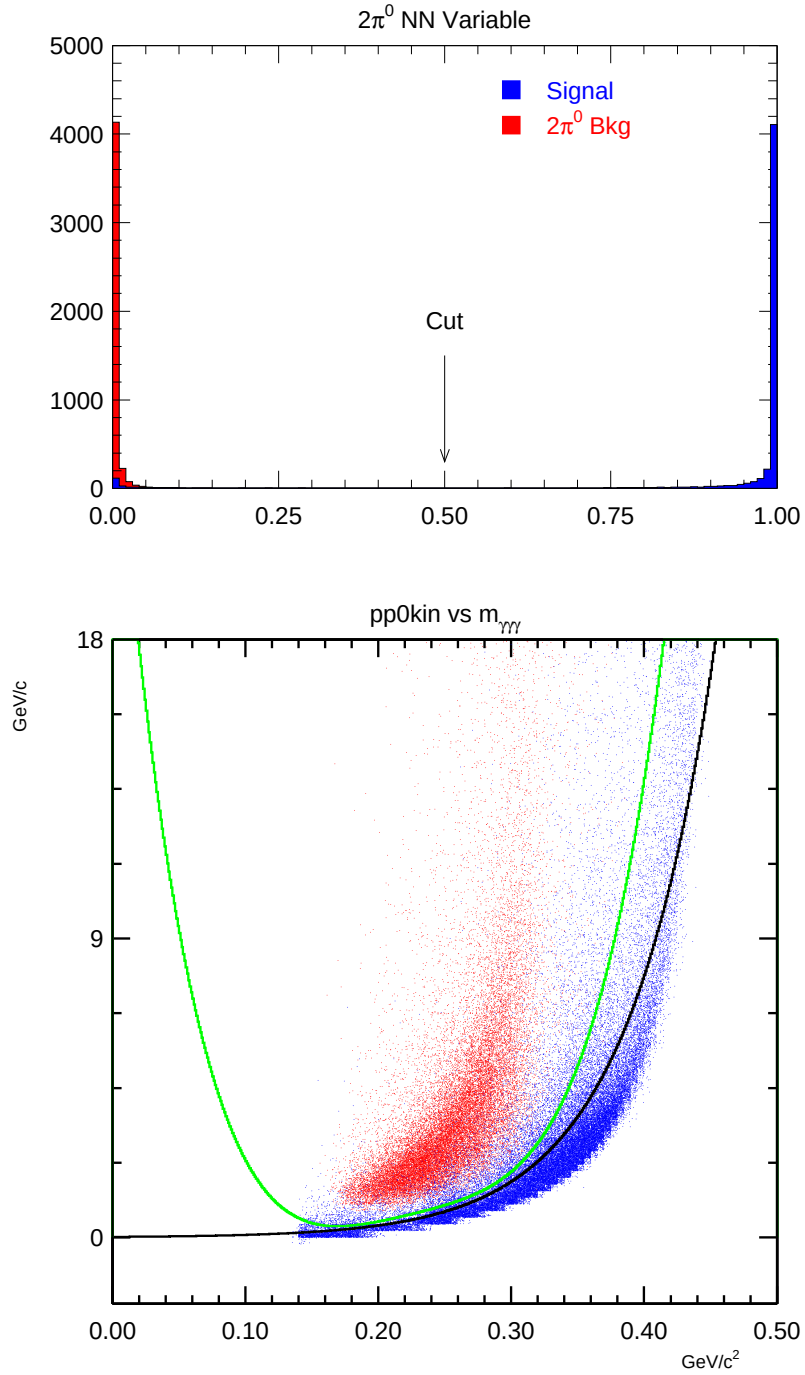

Figure 6: The variables used to reduce the $K_L \to \pi^0\pi^0$ (top) and $K_L \to \pi^0\pi^0\pi^0$ (bottom) backgrounds. The top plot shows the neural net variable for the $K_L \to \pi^0\pi^0$ background (red) and the $K_L \to \pi^0 e^+ e^- \gamma$ signal Monte Carlo. The bottom plot shows the missing momentum versus the $\gamma\gamma\gamma$ mass distribution for $K_L \to \pi^0\pi^0\pi^0$ background (red) and signal Monte Carlo (blue).

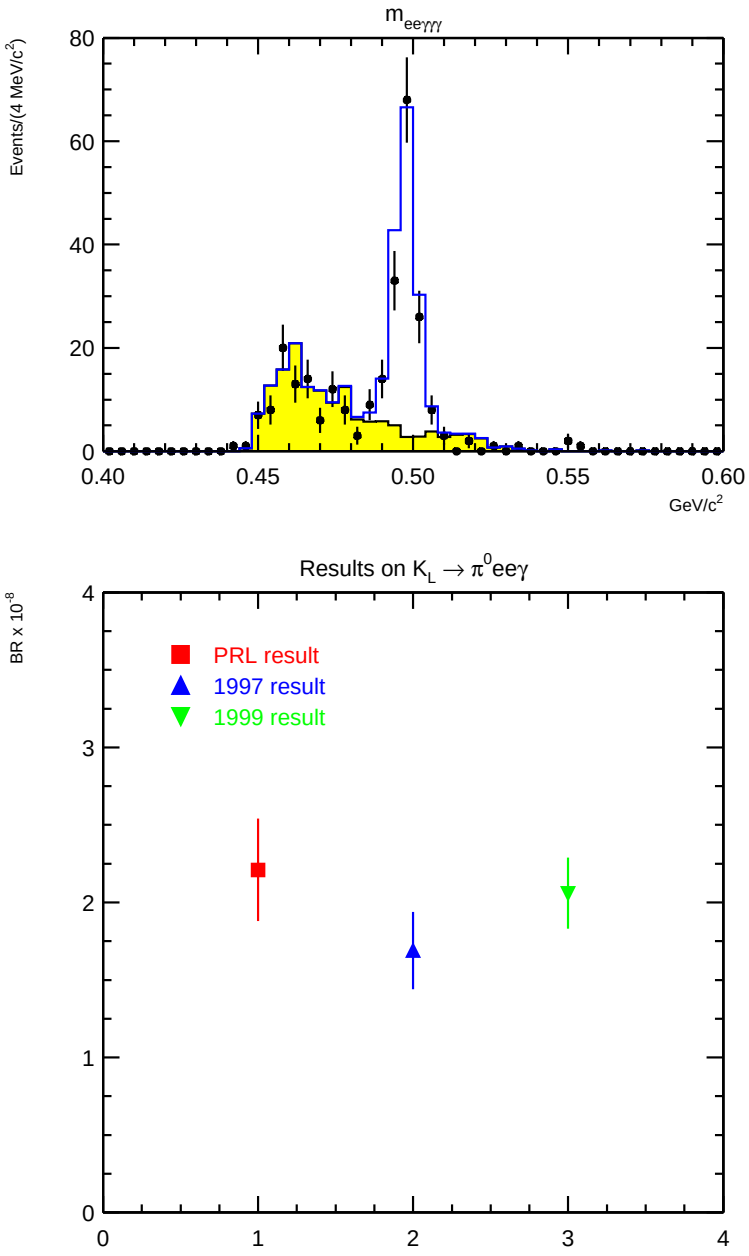

Figure 7: The $e^+e^-\gamma\gamma\gamma$ mass (top) for the combined 1997 and 1999 data sets. The dots are the data, the blue histogram is the sum of the signal plus background Monte Carlo, and the yellow histogram represents the sum of the $K_L \to \pi^0\pi^0$ and $K_L \to \pi^0\pi^0\pi^0$ backgrounds. The bottom plot shows the branching ratio results for the KTeV PRL (red) and our new 1997 (blue) and 1999 (green) analyses. The results have been rescaled using the latest PDG value for $K_L \to \pi^0\pi^0$.

Systematic	Error (%)
MC Statistics	4.2
a_V dependence	3.8
K_L and π^0 BR	2.8
$3\pi^0$ bkg	0.8
acceptance	0.4
$2\pi^0$ background	0.1
Total	6.4

Table 2: Systematic errors for the $K_L \to \pi^0 e^+ e^- \gamma$ measurement

5 Search for $K_L \to \pi^0\pi^0\gamma$

In this decay we use the π^0 Dalitz decay for one of the neutral pions. We chose this because the fully neutral mode trigger was heavily prescaled, whereas the KTeV two-track trigger was not. The final state consists of an e^+e^- pair, and three photons in the CsI calorimeter. As in the other analyses discussed in this paper, there are three possible combinations of photons for each event. Again, we choose the combination that reconstructs closest to the π^0 mass.

The main background to this decay comes from $K_L \to \pi^0\pi^0\pi^0$ events, since $K_L \to \pi^0\pi^0$ cannot contribute to the background without the addition of accidental particles. Two variables are effective in reducing the background to this mode. The first is to employ the photon shape variable described above. This reduces events in which two of the photons overlap in the calorimeter. The second varible used is the missing momentum in the kaon rest frame, p_L^2. Cutting on this variable significantly reduces the $K_L \to \pi^0\pi^0\pi^0$ background.

A unique feature of this analysis is that the normalization mode is not fully reconstructed. Rather we use $K_L \to \pi^0\pi^0\pi^0$ events in which one of the photons passes through one of the beam holes in the CsI calorimeter. This photon is kinematically constrained using the known kaon mass.

The final candidates are shown in Figures 8, where the reconstructed kaon mass is shown along the x-axis and the kaon transverse momentum squared, p_T^2, is shown on the y-axis. For the 1997 sample we chose a square signal region, while for the 1999 sample we formed a likelihood from the product of the m_K and p_T^2 probabilities. After all cuts we found no events in the 1997 sample and one event in the 1999 sample. The probability of this event to come from background is determined to be approximately 10%.

Using our $K_L \to \pi^0\pi^0\pi^0$ normalization sample, we determine an upper limit of $\mathrm{BR}(K_L \to \pi^0\pi^0\gamma) < 2.32 \times 10^{-7}$. This constitutes an improvement of about 20 over the previous limit from NA31. However, this limit is well-above the predictions for

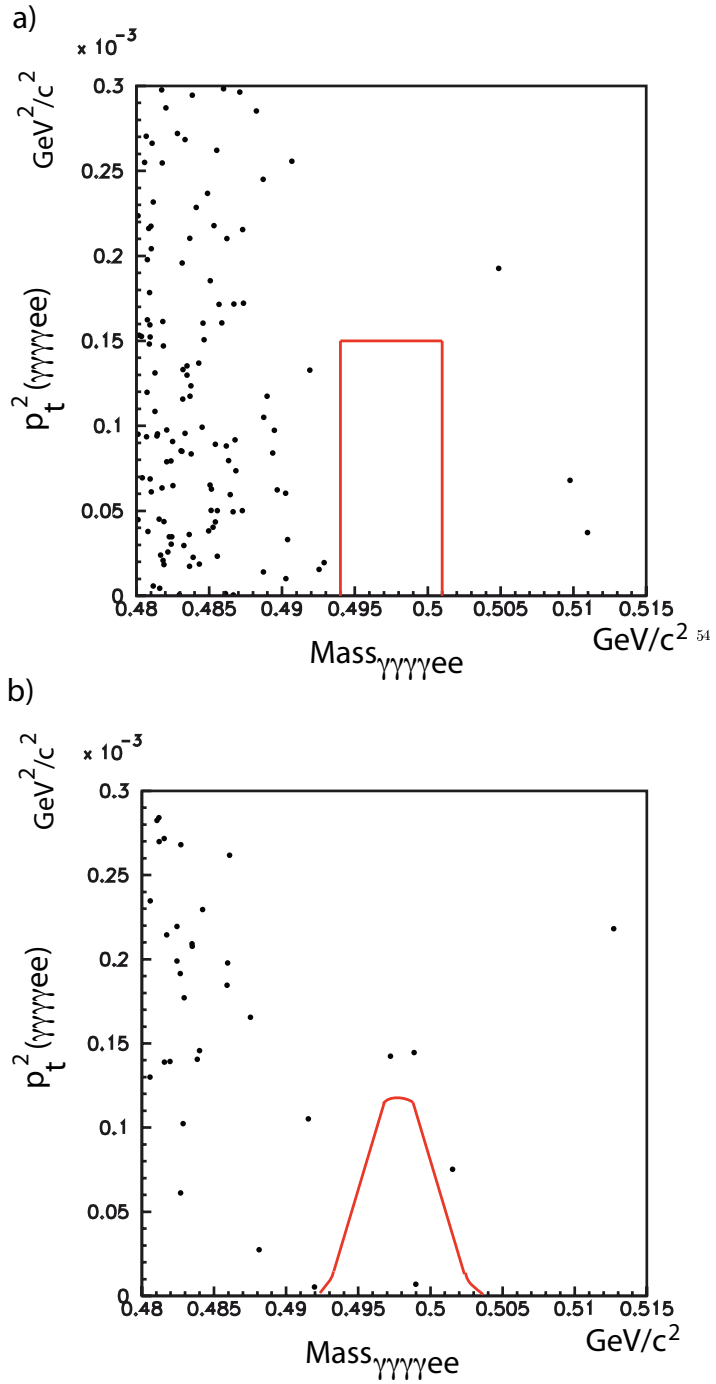

Figure 8: The p_T^2 versus kaon mass distributions for the 1997 (top) and 1999 (bottom) samples after all selection cuts have been applied. The red line represents the signal region.

this decay.

6 Summary and Conclusions

The KTeV experiment has presented three new results on $K_L \to \pi^0\gamma\gamma$, $K_L \to \pi^0 e^+ e^-\gamma$ and $K_L \to \pi^0\pi^0\gamma$. The first result is competitive with the world's best result from NA48, while the other two represent the world's best measurements on these two decays. The measured branching ratios are both inconsistent with the $O(p^4)$ predictions from chiral perturbation theory, and consistent with $O(p^6)$ chiral perturbation theory.

Bibliography

[1] G.D. Barr *et al.*, Phys. Lett. **B284**, 440 (1992).

[2] V. Papadimitriou *et al.* Phys. Rev. **D44**, 573 (1991).

[3] G. D'Ambrosio and J. Portoles, Nucl. Phys. **B492**, 417 (1997).

[4] J. Donoghue and F. Gabbiani, Phys. Rev. **D56**, 1605 (1997).

[5] P. Heiliger and L.M. Sehgal, Phys. Lett. **B307**, 182 (1993).

[6] G. Ecker, H. Neufeld and A. Pich, Nucl. Phys. **B413**, 321 (1994).

[7] J.R. Batley *et al.*, Phys. Lett. **B576**, 43 (2003).

[8] J.R. Batley *et al.*, Phys. Lett. **B599**, 197 (2004)..

[9] A. Lai *et al.*, Phys. Lett. **B536**, 229 (2002).

[10] A. Alavi-Harati *et al.*, Phys. Rev. Lett. **83**, 917 (1999).

[11] G. D'Ambrosio, G. Ecker, G. Isidori and J. Portoles, J. High Energy Physics, **08**, 004 (1998).

B_s Lifetime Difference and Mixing @ the Tevatron

S. Hansmann-Menzemer
for the CDF II & D0 Collaboration
Physikalisches Institut Heidelberg
Philosophenweg 12
69120 Heidelberg, Germany

1 Introduction

The Tevatron collider at Fermilab, operating at a center-of-mass energy of $\sqrt{s} = 1.96$ TeV has a huge $b\overline{b}$ production cross section (≈ 1 nb), which is about five orders of magnitude larger than the $b\overline{b}$ production rate at the B factories PEP and KEK, e^+e^- colliders running on the $Y(4S)$ resonance. In addition, only B^+ and B_d mesons are produced at $Y(4S)$, while higher mass b hadrons such as B_s, B_c, b baryons, B^* and p-wave B mesons are currently produced only at the Tevatron. In order to exploit the possibility to study those variety of heavy b hadrons in a busy hadronic environment, dedicated detector systems, triggers and reconstruction are crucial.
Both D0 and CDF are multipurpose detectors featuring high resolution tracking in a magnetic field and lepton identification. These detectors are symmetrical in polar and azimuthal angles around the interaction point, with approximate 4π coverage [1, 2]. The CDF and D0 experiments are able to trigger at hardware level on large track impact parameters. CDF exploits this trigger to collect a sample of fully reconstructed B mesons, enhancing the potential of its B physics program. At D0 the displaced track trigger is for the time being only used at lower bandwidth, e.g. for b tagging of potential Higgs candidates. CDF has a dedicated particle identification system composed of a time-of-flight detector and dE/dx measurements in the drift-chamber, which allows kaon-pion separation of at least 1.5 σ throughout the whole momentum range. D0 has an excellent muon system and a tracking coverage in the forward region up to a pseudo-rapidity of $\eta = 2.5$.
About 2 fb^{-1} of data has been collected in the meantime by each of the both experiments. About 8 fb^{-1} are expected till the shutdown of the Tevatron end of 2009. The results presented here are unless otherwise specified based on 1 fb^{-1} of data.

2 B_s Lifetime Difference & Mixing Phase

In the standard model (SM), the light (L) and heavy (H) eigenstates of the B_s system are expected to mix in such a way that the mass and decay width differences between them, $\Delta m_s = m_H - m_L$ and $\Delta\Gamma_s = \Gamma_L - \Gamma_H$, are sizeable. The mixing phase ϕ_s^{SM} is within the SM predicted to be small [3], and thus to a good approximation the two mass eigenstates are expected to be CP eigenstates. New phenomena may introduce a non-vanishing mixing phase ϕ_s^{NP}, leading to a reduction of the observed $\Delta\Gamma_s$ compared to the SM prediction: $\Delta\Gamma_s = \Delta\Gamma_s^{SM} \times |\cos(\phi_s^{SM} + \phi_s^{NP})|$ [3]. While the mass difference Δm_s in the B_s system has been recently measured with a high precision, as it will be described in the following section, the mixing phase has remained unknown sofar.

Several analysis have been performed at the Tevatron, to access $\Delta\Gamma_s$ and/or ϕ_s:
$B_s \to K^+K^-$ is a pure CP even state. Assuming a small CP violating phase, the measurement of the lifetime in this final state directly corresponds to the measurement of the lifetime of the B_s(light), which can then be compared to measurements of lifetimes in flavor specific eigenstates [5].
The untagged decay rate asymmetry in semileptonic B_s decays (A_{SL}^s) is another handle on the mixing parameters of the B_s system [4]:

$$A_{SL}^s = \frac{\Delta\Gamma_s}{\Delta m_s}\tan(\phi_s) \tag{1}$$

Both analysis have been performed at the Tevatron and have been discussed in the talk from Cano Ay at this conference.
A third approach is the measurement of the branching ration of $B_s \to D_s^{(*)}D_s^{(*)}$. This decay is predominantly CP even [6] and gives the largest contribution in the lifetime difference between the B_s(heavy) and B_s(light). The following relation can be obtained [3]:

$$2 * BR(B_s \to D_s^{(*)}D_S^{(*)}) \approx \frac{\Delta\Gamma_s}{\cos(\phi_s)\Gamma_s}[1 + O(\frac{\Delta\Gamma}{\Gamma_s})], \tag{2}$$

where Γ_s is the average B_s decay width. This analysis is describe in more detail in the contribution from Manfred Paulini.

The decay $B_s \to J/\Psi\phi$, through the quark process $b \to c\bar{c}s$, gives rise to both CP even and CP odd final states. It is possible to separate the two CP components of this decay, and thus to measure the lifetime difference, through a simultaneous study of the time evolution and the angular distributions of the decay products of the J/Ψ and the ϕ mesons. Moreover, with a sizeable lifetime difference, there is a sensitivity to the mixing phase through the interference terms between the CP even and CP odd waves.

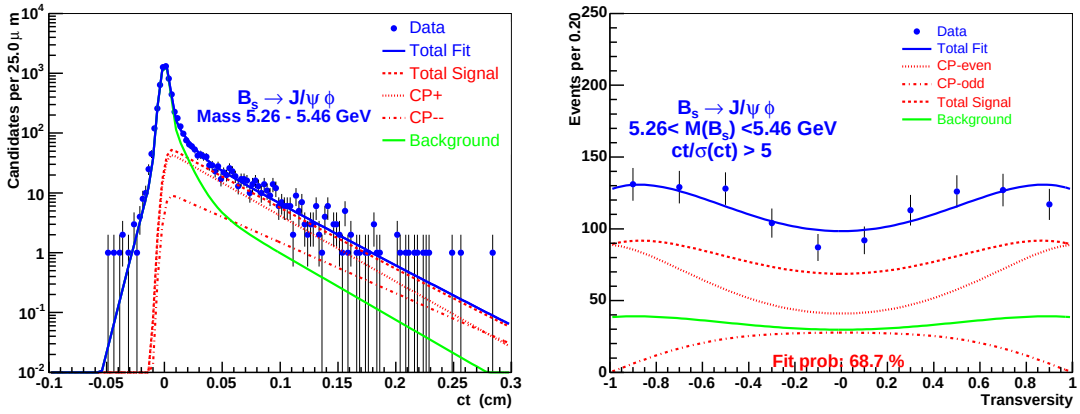

Figure 1: Lifetime and transversity angle distribution for CP even and CP odd $B_s \to J/\Psi\ \Phi$ decays of the D0 analysis.

Based on 1 fb^{-1} of D0 analyzes about 23.000 $B_s \to J/\Psi(\mu^+\mu^-)\phi(K^+K^-)$ candidates after selection cuts. A simultaneous unbinned likelihood fit is performed in terms of invariant mass, proper decay length and transversity angular variables, described in [7]. In Fig. 1 we show the projection of the fit result onto the proper decay time distribution and the onto $\cos\theta$, one of the transversity angles. Similar good agreement is observed in the projections onto the invariant mass and remaining transversity angles. A fit to the data has been performed in two ways. First the mixing phase ϕ_s has been fixed to zero, which assumes no significant New Physics contribution in ϕ_s. A non-zero decay width difference of $\Delta\Gamma_s = 0.12 \pm 0.08$ (stat.) $\pm$ 0.03 (syst.) has been obtained. This result has been compared to the result of the analysis of the $B_s \to K^+K^-$ lifetime and the branching ratio measurement, which have been briefly described above (Fig. 2). The plot contains as well the result of the angular analysis of the $B_s \to J/\Psi\phi$ mode performed by the CDF collaboration based on 380 pb^{-1} of data.
In a second fit to the D0 data, both the decay width difference $\Delta\Gamma_s$ and ϕ_s where floating parameters, which results in:

$$\Delta\Gamma_s = 0.17 \pm 0.09\ (\text{stat.}) \pm 0.03\ (\text{syst.})\ \text{ps}^{-1} \quad (3)$$

$$\phi_s = -0.79 \pm 0.56\ (\text{stat.}) \pm 0.01\ (\text{syst.}) \quad (4)$$

This is the first measurement of the mixing phase ϕ_s. The result is still dominated by statistical uncertainties. But with increasing data samples, this is a very promising analysis to probe the SM. Any sizeable phase would be a clear hint to New Physics. A combined fit of $\Delta\Gamma_s$ and ϕ_s both in the $B_s \to J/\Psi\phi$ decays and in the untagged semileptonic decay rate asymmetrie has been performed (Fig. 2).

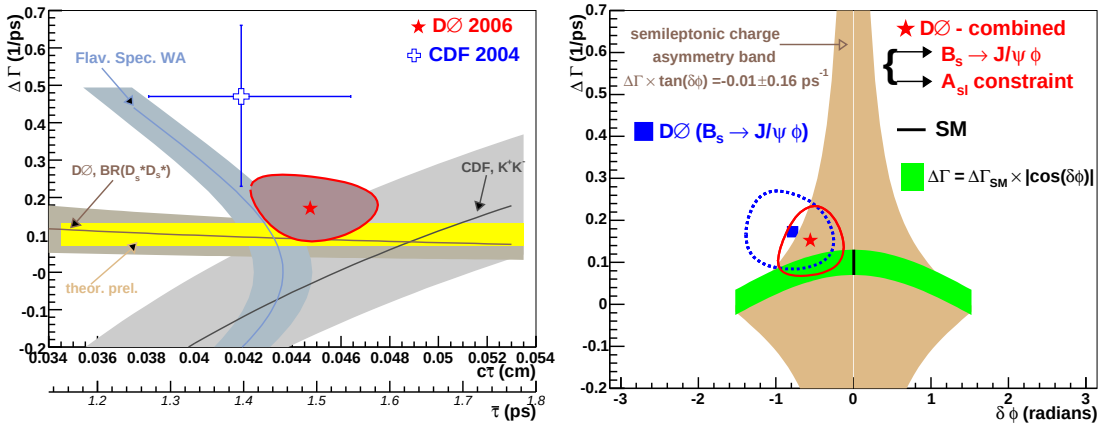

Figure 2: Left: Results of several Tevatron $\Delta\Gamma_s$ measurements superimposed with the SM theory predictions [3]. All measurements are performed under the SM assumption of a negligible CP violating phase ϕ_s. Right: D0 result for a common fit of the decay width difference $\Delta\Gamma_s$ and the CP violating phase ϕ_s superimposed with the SM expectations.

This combined fit slightly reduces the uncertainties on ϕ_s but still the analysis is at this stage statistical dominated:

$$\Delta\Gamma_s = 0.15^{+0.09}_{-0.08}\ \mathrm{ps}^{-1} \quad (5)$$

$$\phi_s = -0.56^{+0.44}_{-0.41} \quad (6)$$

For the moment all results are consistent with the SM expectations.

3 B_s Mixing

The precise determination of the $B_s - \overline{B_s}$ oscillation frequency Δm_s from a time-dependent analysis of the $B_s - \overline{B_s}$ system has been one of the most important goals for heavy flavor physics at the Tevatron. This frequency can be used to strongly improve the knowledge of the Cabbibo-Kobayashi-Maskawa (CKM) matrix, and to constraint contributions from New Physics.
The probability $\mathcal{P}$ for a B_s meson produced at time $t = 0$ to decays as a B_s ($\overline{B_s}$) at proper time t > 0 is, neglecting effects from CP violation as well as possible lifetime difference between the heavy and light B_s^0 mass eigenstates, given by

$$\mathcal{P}_{\pm}(t) = \frac{\Gamma_s}{2} e^{-\Gamma_s t}[1 \pm \cos \Delta m_s t)], \quad (7)$$

where the subscript "+" ("-") indicates that the meson decays as B_s ($\overline{B_s}$). Oscillation have been observed and well established in the B_d system. The mass difference Δm_d

is measured to be [5]

$$\Delta m_d = 0.505 \ \pm \ 0.005 \ ps^{-1}. \tag{8}$$

In the B_s system oscillation have also been established but till winter 2006 all attempts to measure Δm_s have only yielded a combined lower limit on the mixing frequency of $\Delta m_s > 14.5$ ps^{-1} at 95% confidence level (C.L.). Indirect fits constraint Δm_s to be below 24 ps^{-1} @ 95% C.L. within the SM. This spring the D0 experiment presented the first double sided 90% C.L. limit [8] and CDF shortly afterwards presented the first precision measurement on Δm_s, with a significance of the signal of about 3 σ at that time [9]. Just a few months later the CDF collaboration updated their result using the very same data, but improved analysis technics and where able to announce the observation of the $B_s - \overline{B_s}$ mixing frequency [10].
The canonical B mixing analysis proceeds as follows. The b flavor (b or $\overline{b}$ of the B meson at the time of decay) is determined from the charges of the reconstructed decay products in the final state. The proper time at which the decay occurred is determined from the transverse displacement of the B_s decay vertex with respect to the primary vertex, and the B_s transverse momentum with respect to the proton beam. Finally the production b flavor must be known in order to classify the B meson as being mixed (production and decay b flavor are different) or unmixed (production and decay b flavor are equal) at the time of its decay. Then the asymmetry can be measured and thus Δm_s be determined:

$$\mathcal{A}(t) \equiv \frac{N(t)_{unmixed} - N(t)_{mixed}}{N(t)_{unmixed} + N(t)_{mixed}} = \mathcal{D}\cos(\Delta m_s t), \tag{9}$$

where $N(t)$ are the time-dependent rates for mixed and unmixed B_s decays. $\mathcal{D}$ is the so-called dilution, a damping term which is related to the imperfect tagging. It is defined as $\mathcal{D} = 1 - P_w$, where P_w is the probability for a wrong tag.
The significance $\mathcal{S}$ of a mixing signal is given by:

$$\mathcal{S} = \sqrt{\frac{\epsilon\mathcal{D}^2}{2}}\sqrt{\frac{S}{S+B}}e^{-\frac{(\Delta m_s \sigma_{ct})^2}{2}} \tag{10}$$

S and B are the rates of signal and background events respectively. $\epsilon\mathcal{D}^2$ is the figure of merit for the flavor tagging, where ϵ is the efficiency to actually apply a tag to a given B_s candidate. σ_{ct} is the proper decay time resolution. Especially at large Δm_s values a small σ_{ct} resolution is crucial for this analysis.
We will in the following sections discuss those various ingredients to the mixing analysis and then present the result.

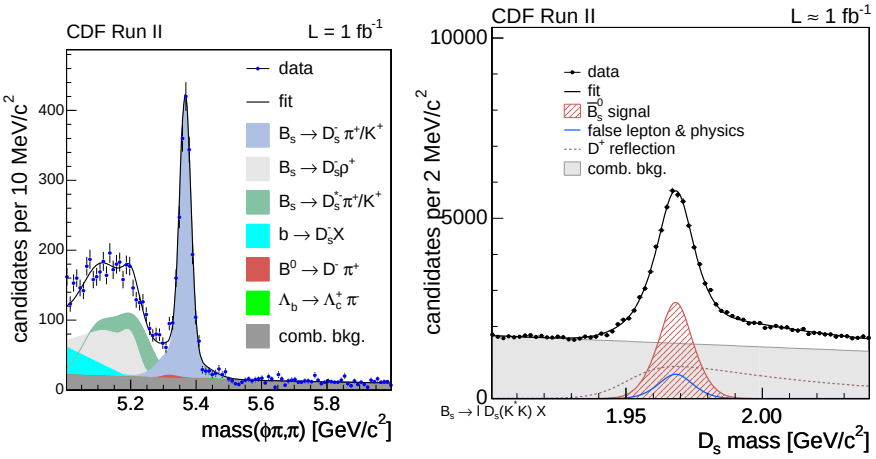

Figure 3: Left: Invariant mass distribution of $B_s \to D_s(\phi\pi)\pi$ candidates of the CDF mixing analysis. Right: D_s invariant mass distribution of $B_s \to \ell D_s X$ candidates.

3.1 Signal Yields

CDF analysis fully and partial reconstructed hadronic and semileptonic B_s candidates in events collected by the displaced track trigger. About 2000 candidates are fully reconstructed in the cleanest, so-called golden mode $B_s \to D_s(\phi\pi)\pi$. About 3200 partially reconstructed B_s candidates coming from $B_s \to D_s^*(\phi\pi)\pi$ and $B_s \to D_s^*(\phi\pi)\rho$ are reconstructed with the same signal signature. Those events have slightly worse proper decay time resolution than the fully reconstructed ones due to γ or π^0, which escaped reconstruction. 3600 B_s candidates are fully reconstructed in additional decay signatures such as $B_s \to D_s(K^*K)\pi$, $B_s \to D_s(3\pi)\pi$, $B_s \to D_s(\phi\pi)3\pi$, $B_s \to D_s(K^*K)3\pi$ and $B_s \to D_s(3\pi)3\pi$. Neural network technics have been used to enhance signal yield and to improve signal/background ratio.
A large sample of 61.500 semileptonic $B_s \to \ell D_s X$ candidates has been studied as well. Due to the missing momentum of the non reconstructed particles in this decay a correction factor derived in Monte Carlo, has been applied to scale the ℓD_s momentum to match the B_s momentum, which is needed to compute the proper decay time:

$$ct = \frac{L_{xy} M(B_s)}{p_T(B_s)} = \frac{L_{xy} M(B)}{p_T(\ell D_s)} * k. \tag{11}$$

It has turned out that the invariant ℓD_s mass is a good variable, both to reject background as well as to parameterize the k factor distribution. Low ℓD_s values are mainly background and the k factor distribution is rather broad which results in a large proper decay time uncertainty. Events with ℓD_s mass close to the B_s mass are more valuable events. They are suffering from less background and their k factor distribution is narrower.

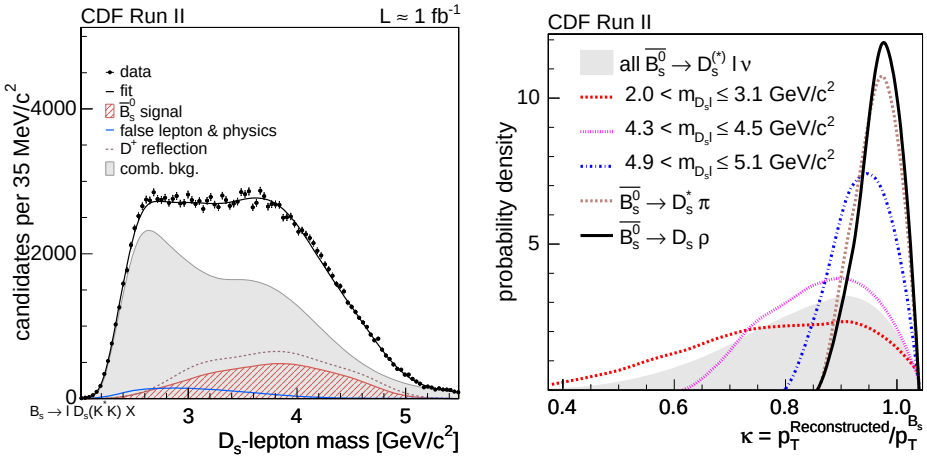

Figure 4: Left: ℓD_s invariant mass distribution of $B_s \to \ell D_s X$ candidates of the CDF analysis. K factor distribution for several ℓD_s mass values for semileptonic and partially reconstructed hadronic decays.

D0 studies exploits their excellent muon coverage and analyses a large sample of semi-muonic decays. About 27.000 $B_s \to \mu D_s(\phi\pi)X$, 12.600 $B_s \to \mu D_s(K^*K)X$ and 2.000 $B_s \to eD_s(\phi\pi)X$ candidates are analyzed. In order to get a handle on fully reconstructed candidates it is planed to use events triggered with a single muon as opposite-side tag and search for fully reconstructed B_s candidates on the non-trigger side.

3.2 Decay Length Resolution

One of the critical input to the analysis is the proper decay time resolution. It is the limiting factor of the sensitivity of the signal at large Δm_s values. For setting a limit a too optimistic proper decay time resolution estimate could potentially lead to the exclusion of Δm_s regions we are actually not sensitive to. Therefore σ_{ct} has been measured directly on data. CDF exploits prompt D decays plus tracks from the primary vertex to mimic all B decay topologies studied in this analysis. On an event-by-event basis, the decay time resolution is predicted, taking into account dependences on several variables, such as isolation, vertex χ^2 etc. D0 uses the negative tail of the lifetime distribution of prompt J/Ψ events to fit for one average σ_{ct} value applied to all events. The mean $< \sigma_{ct} >$ for hadronic events at CDF is 26 μm and for semileptonic events about 45 μm. The semileptonic events used in the D0 analysis have a resolution of a out 50-60 μm. The main difference between the D0

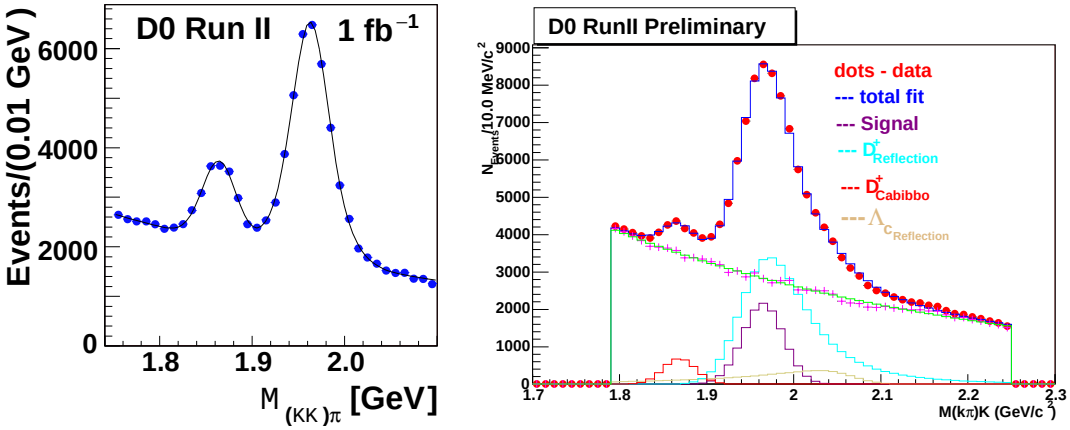

Figure 5: Left: D_s invariant mass distribution of $B_s \to \mu D_s(\phi\pi)X$ candidates of the D0 mixing analysis. Right: D_s invariant mass distribution of $B_s \to \mu D_s(K^*K)X$ candidates of the D0 mixing analysis.

and CDF semileptonic numbers is coming from the additional innermost silicon layer at a distance of about 1.2 cm from the collision point, in the CDF detector. D0 has added a similar layer to their detector recently, which is currently being commissioned. Therefore improvements in the D0 decay length resolution are expected to come soon.

3.3 Flavor Tagging

While the flavor of the B_s candidate at decay time is unambiguously defined by the charges of its daughter tracks, the flavor at production can be inferred, with a certain degree of uncertainty, by flavor tagging algorithms.
Two type of flavor tags can be applied: opposite-side and same-side flavor tags. Opposite-side tags infer the production flavor of the B_s from the decay products of the b hadron produced from the other b quark in the event. Lepton tagging algorithms are based on semileptonic b decays into an electron or muon ($b \to \ell^- X$). The charge of the lepton is thus correlated to the charge of the decaying b hadron. Jet charge tagging algorithms uses the fact that the charge of a b jet is correlated to the charge of the b quark. Kaon tagging are based on the CKM favored quark level decay sequence $b \to c \to s$. The charge of the kaon from opposite-side B decays is correlated to the b flavor. CDF combines this three tagging technics using a Neural Network approach. D0 exploits a combination of jet charge and lepton tags to determine the B_s production flavor. The performance of the opposite-side flavor tagging algorithm is measured in kinematically similar B_d and B^+ samples. The following Δm_d values have been found,

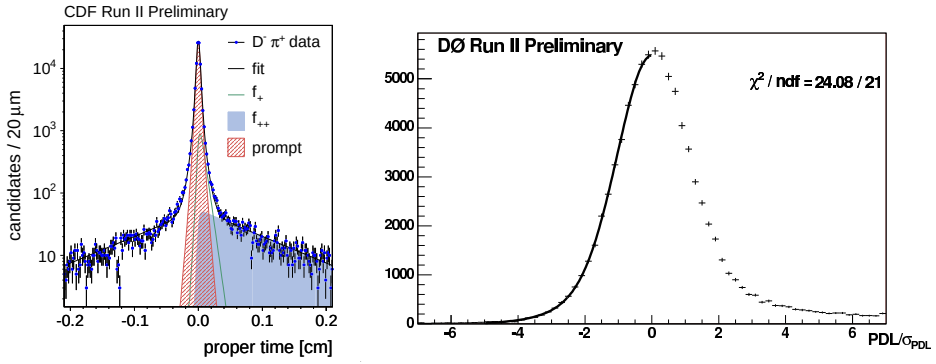

Figure 6: Left: CDF fits for vertex resolution of prompt charm decays to determine decay time resolution of B_s candidates.Right: D0 studies the negative side of the prompt J/Ψ decay time resolution.

$$\Delta m_d^{D0} = 0.506 \pm 0.020\ (\text{stat.}) \pm 0.016\ (\text{syst.})\ \text{ps}^{-1} \quad (12)$$
$$\Delta m_d^{CDF} = 0.509 \pm 0.010\ (\text{stat.}) \pm 0.016\ (\text{syst.})\ \text{ps}^{-1}, \quad (13)$$

which agree well with the world average [5].
CDF yields a combined opposite-side tagging performance of $\epsilon\mathcal{D}^2 = 1.8\%$. Mainly due to its excellent muon detector system, D0 yields a higher performance of $\epsilon\mathcal{D}^2 = 2.5\%$. Those values have to be compared to ϵD^2 of about 30% at the B factories. B flavor tagging in an hadronic environment is one of the main challenges of the Δm_s analysis. Same-side flavor tags are based on the charges of associated particles produced in the fragmentation of the b quark that produces the reconstructed B_s. Contrary to the opposite-side tagging algorithms, the performance of this tagging algorithm can not be calibrated on B_d and B^+ data, but we have to rely on Monte Carlo samples until a significant B_s mixing signal has been established.
CDF uses Neural Network technics to combined kaon particle-identification variables from dE/dx measurements in the drift-chamber and time-of-flight measurements with kinematic quantities of the kaon candidate into a single tagging variable. Tracks close in phase space to the B_s candidate are considered as same-side kaon tag candidates, and the track with the largest value of the tagging variable is selected as the tagging track. We predict the dilution of the same-side tag using simulated data samples generated with the PYTHIA [11] Monte Carlo program. Control samples of B^+ and B_d are used to validate the predictions of the simulation. The tagging power of this flavor tag is $\epsilon D^2 = 3.7/4.8\%$ for hadronic and semileptonic samples respectively. The same-side tags enlarges the CDF tagging power by a factor of 3-4. This was one of the key ingredients which pushed the analysis towards the observation of Δm_s. If both a same-side tag and an opposite-side tag are present, we combine the information from

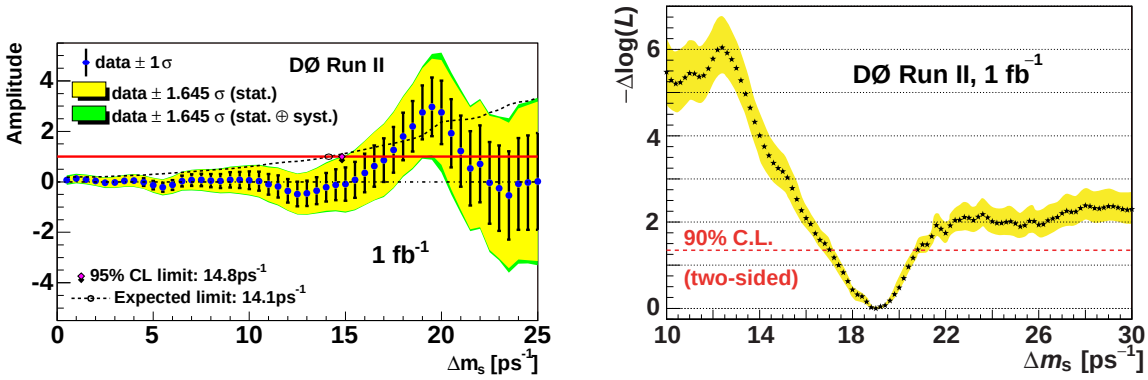

Figure 7: Left: Amplitude scan of $B_s \to \mu \mathcal{D}_s X$ candidates from D0. Right: $-\Delta \log \mathcal{L}$ distribution. The minimum is around 19 ps^{-1}, the two sided 90% C.L. is displayed.

both tags assuming they are independent.

3.4 Fit and Results

An unbinned maximum likelihood fit is utilized to search for $B_s - \overline{B_s}$ oscillations. The likelihood combines mass, proper decay time, proper decay time resolution and flavor tagging information for each candidate. Separate probability density functions are used to describe signal and each type of background. The amplitude scan method [12] was used to search for oscillations. The likelihood term describing the proper decay time of tagged B_s meson candidates in Eq. 7 is modified by introducing the amplitude $\mathcal{A}$:

$$\mathcal{L} \sim 1 \pm \mathcal{A} D \cos(\Delta m t). \tag{14}$$

Then, a scan in Δm is performed by fitting $\mathcal{A}$ for fixed values of Δm. The dilution $\mathcal{D}$ is fixed to the value obtained by the calibration process. This procedure corresponds to a Fourier transformation of the proper time space into the frequency space. In the case of infinite statistics and perfect resolution, it is expected to find $\mathcal{A} = 1$ for the true value of Δm and $\mathcal{A} = 0$ otherwise. In practice, the procedure consists in recording $(\mathcal{A}, \sigma_{\mathcal{A}})$ for each Δm hypothesis. A particular value of Δm is excluded at 95% C.L. if $\mathcal{A} + 1.645\ \sigma_{\mathcal{A}} < 1$ holds. The sensitivity of a mixing analysis is defined as the lowest Δm value for which $1.645\ \sigma_{\mathcal{A}} = 1$.

D0 Δm_s Results

The amplitude scan for the analysis of the semi-muonic $B_s \to D_s(\phi\pi)$ candidates is shown in Fig 7. The sensitivity is 14.1 ps^{-1}, the lower 95 % C.L. is 14.8 ps^{-1}. Around $\Delta m_s = 19.0$ ps^{-1} the amplitude $\mathcal{A}$ is consistent with 1 but not with 0. To

assess the significance of this deviation, the negative logarithm of the ratio of the likelihood function for $\mathcal{A} = 1$ (mixing hypothesis) and $\mathcal{A} = 0$ (no-mixing hypothesis) was utilized ($\Lambda = -\log(\mathcal{L})$). D0 placed the first double sided limit on the mixing frequency of $17 < \Delta m_s < 21$ ps^{-1}. Toy Monte Carlo studies determined the probability to find a minimum that deep in the Λ distribution in the Δm_s range 17-21 ps^{-1} for a no-mixing sample. It is found to be 5%. A preliminary update of this analysis including as well $B_s \to \mu D_s(K^*K)X$ and $B_s \to eD_s(\phi\pi)X$ candidates was not able to confirm this result.

CDF Δm_s Results

The amplitude scans for the analysis of the hadronic and semileptonic B_s candidates and the combined result are shown separately in Fig 8. The combined sensitivity is 31.3 ps^{-1}. The value of the amplitude is consistent with unity around $\Delta m_s = 17.75$ ps^{-1}, where $\mathcal{A} = 1.21 \pm 0.20$. For all other Δm_s values, the amplitude is always consistent with zero (Fig. 8). The minimum likelihood ratio Λ is at $\Delta m_s = 17.77$ ps^{-1} and has a value of -17.26. The significance of the signal in the amplitude is the probability that randomly tagged data would produce a value of Λ lower than -17.26 at any value of Δm_s. Only 28 out of 350 million generated toy experiments yielded a Λ value lower than that. This results in a p-value of 8×10^{-8}, which corresponds to a 5.4 σ signal. The fit for Δm_s, with $\mathcal{A}$ fixed to unity, finds

$$\Delta m_s = 17.77 \ \pm \ 0.10 \text{ (stat.)} \ \pm \ 0.07 \text{ (syst) ps}^{-1}. \tag{15}$$

The dominant contributions to the systematic uncertainties comes from uncertainties on the absolute scale of the decay-time measurement.
The $B_s - \overline{B_s}$ oscillations are displayed in Fig. 9. Candidates in the hadronic sample are collected in five bins of proper decay time modulo $2\pi/\Delta m_s$. In each bin, a fit for $\mathcal{A}$ is performed and the result is plotted. The curve corresponds to a cosine wave with amplitude equal to 1.28, which is the fitted value in the hadronic sample. Data are well represented by the curve.

4 Summary

Both D0 and CDF have measured the width difference $\Delta\Gamma_s$ between the light and heavy B_s mass eigenstates, which in the limit of no CP violation, coincide with the CP even and CP odd eigenstates of the B_s system. A non-zero value of $\Delta\Gamma_s$ has been found. Additionally D0 has performed a simultaneous fit to $\Delta\Gamma_s$ and the CP violating phase ϕ_s. For the time being the result of the ϕ_s is completely dominated by statistical uncertainties and well consistent with the SM. Given the amount of data,

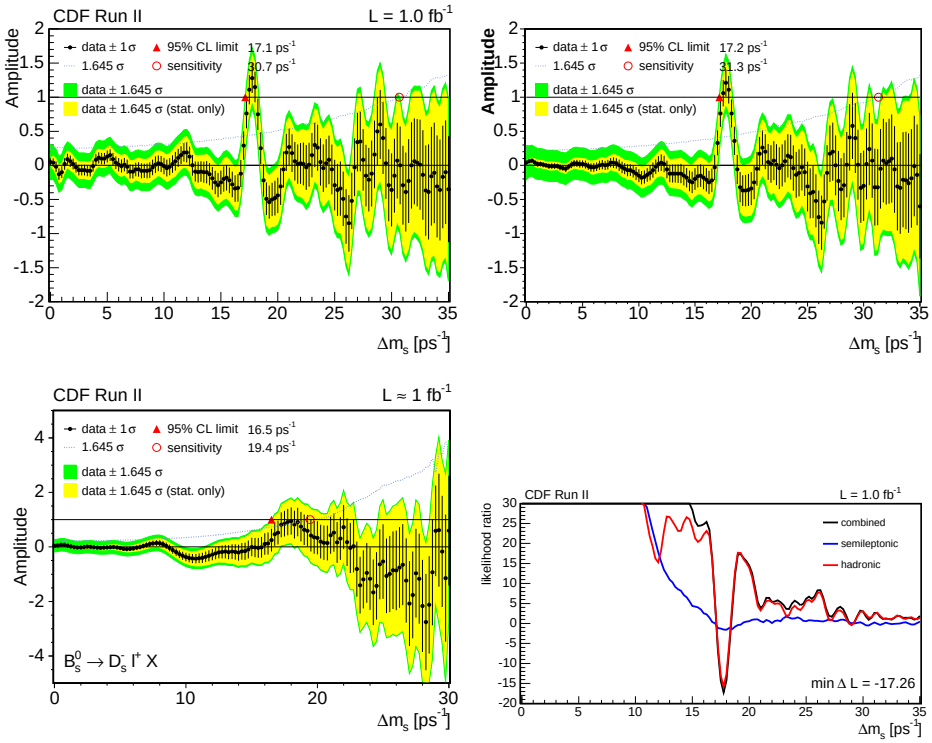

Figure 8: Left + top right: Amplitude scan of CDF hadronic and semileptonic modes separately and combined. While the semileptonic scan dominates at small Δm_s values due to its large static, the hadronic one takes over at large Δm_s values due to the better decay time resolution. Bottom right: Likelihood ration Λ distribution for combined CDF result.

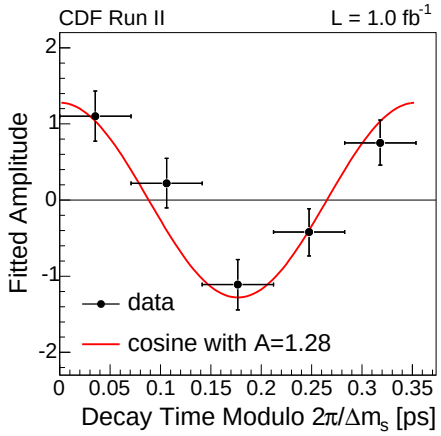

Figure 9: The CDF $B_s - \overline{B_s}$ oscillation signal (only hadronic decays) measured in five bins of proper decay time modulo the measured oscillation period $2\pi/\Delta m_s$. The curve shown is a cosine with an amplitude of 1.28, which corresponds to the observed value in the amplitude scan for the hadronic sample at $\Delta m_s = 17.77$ ps^{-1}. This plot does not represent the full statistic of the presented analysis.

expected to be collected in the next two years at the Tevatron, this analysis has the potential of being an interesting test of the SM and/or a window to New Physics.
D0 has performed a study of $B_s - \overline{B_s}$ oscillations using $B_s \to \mu^+ D_s^- (\phi\pi) X$ decays and opposite-side flavor tagging algorithms. The expected limit at 95% C.L. is 14.1 ps^{-1}. Assuming Gaussian uncertainties, a 90 % C.L. interval of $17 < \Delta m_s < 21$ ps^{-1} is set. A preliminary analysis on the same dataset including as well $B_s \to \mu^+ D_s^- (K^* K^+) X$ and $B_s \to e D_s (\phi\pi) X$ decays was not able to confirm this result.
CDF has searched for B_s flavor oscillations using hadronic and semileptonic decays. Opposite-side and for the first time at a hadron collider, same-side tags provide information about the B_s production flavor. A significant peak (probability for background fluctuation $< 8 \times 10^{-8}$) in the amplitude scan consistent with unity is observed. CDF measures the oscillating frequency to be

$$\Delta m_s \;=\; 17.77 \;\pm\; 0.10\ (\text{stat.}) \;\pm\; 0.07\ (\text{syst.})\ \text{ps}^{-1} \tag{16}$$

The $B_s - \overline{B_s}$ oscillation frequency is used to derive the ratio of $|V_{td}/V_{ts}|$,

$$|\frac{V_{td}}{V_{ts}}| \;=\; \xi \sqrt{\frac{\Delta m_d M_{B_s}}{\Delta m_s M_{B_d}}} \;=\; 0.2061 \;\pm\; 0.0007\ (\text{exp.})\ ^{+0.0081}_{-0.0060}\ (\text{theo.}), \tag{17}$$

where the following values have been used as inputs: $M_{B_d}/M_{B_s} = 0.98390$ [5] with negligible uncertainty, $\Delta m_d = 0.507 \pm 0.005$ ps^{-1} [5] and $\xi = 1.21^{+0.047}_{-0.035}$ [13].

5 Acknowledgments

I like to thank the organizers of the HQL2006 for a very enjoyable conference!

Bibliography

[1] A. Abachi *et al.,* FERMILAB-PUB-96-357-E.

[2] R. Blair *et al.,* FERMILAB-PUB-96-390-E.

[3] I. Dunietz, R. Fleischer and U. Nierste, hep-ph/0012219

[4] M. Beneke, G. Buchalla, a. Lenz and U. Nierste, Phys. Lett. B **576** (2003) 173, hep-ph/0307344

[5] S. Eidelmann *et al.,* Phys. Lett **B592**, 1.

[6] R. Alexan *et al.,* Phys. Rev. Lett. **95** 171801 (2005)

[7] T. Affolder *et al.,* Phys. Rev. Lett. **85**, 4668;
V. M. Abazov *et al.,* Phys. Rev. Lett **95**, 171801

[8] Direct Limits on the B_s Oscillation Frequency, V. M. Abazov *et al.*, The D0 Collaboration, Phys. Rev. Lett **97** (2006) 021802

[9] First precision measurement of Δm_s, A. Abulencia *et al.,* The CDF Collaboration, Phys. Rev. Lett. **97**, (2006) 062003

[10] Observation of $B_s - \overline{B_s}$ Oscillations, A. Abulencia *et al.,* The CDF Collaboration, Phys. Rev. Lett **97** 242003 (2006)

[11] T. Sjörstrand *et al.,* Computer Phys. Commun. **135**, 238 (2001).
Version 6.216 has been used here.

[12] H. G. Moser and A. Roussarie, Nucl. Instrum. Methods Phys. Res., Sect. A **384**, 491 (1997)

[13] M. Okamoto, hep-lat/0510113.

Leptonic and semi-leptonic decays

Leptonic and semi-leptonic decays

Theory of Semi-Leptonic B Decays: Exclusive and Inclusive

Thomas Mannel
Theoretische Physik I
Fachbereich Physik
Universität Siegen
57068 Siegen, Germany

1 Introduction

Semi-leptonic decays of B mesons play an important role in flavour physics. On one hand they are relatively simple as far as the effects of strong interactions are concerned (at least compared to non-leptonic decays), on the other hand they are an important ingredient for the determination of the unitarity triangle. The radius of the so-called "Unitarity Clock", the circle around the origin in the ρ-η plane, is determined by the ratio $|V_{ub}/V_{cb}|$ which is most cleanly determined from semi-leptonic decays.

The theoretical methods to evaluate the hadronic matrix elements have developed tremendously over the past fifteen years [1]. With the advent of the $1/m_b$ expansion a systematic, QCD based theory could be set up which resulted in a drastic reduction of model dependence in many theoretical calculations.

The $1/m_b$ expansion can be set up for both exclusive and inclusive decays. Any observable of a B meson decay can in general be written as

$$R = R_0 + \left(\frac{\Lambda_{\rm QCD}}{m_b}\right) R_1 + \left(\frac{\Lambda_{\rm QCD}}{m_b}\right)^2 R_2 + \left(\frac{\Lambda_{\rm QCD}}{m_b}\right)^3 R_3 + \cdots \qquad (1)$$

where the coeffcients are expressed in terms of a set of non-perturbative matrix elements with computable prefactors. The strength of the method is that the leading term may in many cases be fixed by heavy quark symmetries and hence hadronic uncertainties enter the stage only at the level of corrections.

In the following I will give a short summary on the status of these methods for inclusive as well as for exclusive decays. In the next section I shall consider exclusive semi-leptonic decays for both heavy-to-heavy and heavy-to-light decays and discuss the impact on the CKM matrix elements V_{cb} and V_{ub}. In section 3 I will consider inclusive decays and discuss the methods to extract the necessary infomation for the $1/m_b$ expansion. Finally I give a few concluding remarks.

2 Exclusive Decays

The main ingredient for a description of exclusive decays are the form factors for the decays. In general, there are two independent form factors for a $0^- \to 0^-$ transition

$$\langle M(p')|\overline{q}\gamma_\mu(1-\gamma_5)b|B(p)\rangle = f_+(q^2)(p+p')_\mu + f_-(q^2)q_\mu\,, \quad q = p - p' \tag{2}$$

and another four independent form factors for the $0^- \to 1^-$ transition.

We will concentrate here on the decay modes $B \to D\ell\overline{\nu}_\ell$ and $B \to D^*\ell\overline{\nu}_\ell$ for the heavy-to-heavy ($b \to c$) case and on $B \to \pi\ell\overline{\nu}_\ell$ for the heavy-to-light ($b \to u$) case.

2.1 $B \to D\ell\overline{\nu}_\ell$ and $B \to D^*\ell\overline{\nu}_\ell$

In the heavy mass limit the relevant kinematic variable for a heavy meson is its four-velocity $v^\mu = P_H^\mu/M_H$. For a B meson the heavy b quark roughly moves with the same velocity, i.e. its momentum p is

$$p^\mu = m_b v^\mu + k^\mu \qquad \text{with} \qquad v^\mu = \frac{P_H^\mu}{M_H} \tag{3}$$

The residual momentum k of the b quark is assumed to be small compared to m_b and hence an expansion in powers of k/m_b is possible.

Using the four velocities of the initial and final state hadrons we may write the differential rates as ($\omega = v \cdot v'$)

$$\frac{d\Gamma}{d\omega}(B \to D^*\ell\overline{\nu}_\ell) = \frac{G_F^2}{48\pi^3}|V_{cb}|^2 m_{D^*}^3(\omega^2-1)^{1/2}P(\omega)(\mathcal{F}(\omega))^2 \tag{4}$$

$$\frac{d\Gamma}{d\omega}(B \to D\ell\overline{\nu}_\ell) = \frac{G_F^2}{48\pi^3}|V_{cb}|^2 (m_B+m_D)^2 m_D^3(\omega^2-1)^{3/2}(\mathcal{G}(\omega))^2 \tag{5}$$

where we have introduced the form factors $\mathcal{F}$ and $\mathcal{G}$.

It is well known that heavy quark symmetries allow normalization statements for the form factors in heavy-to-heavy transitions at the non-recoil point $v = v'$ or $\omega = v \cdot v' = 1$ [2–4]. In addition, effective-field-theory methods allow us to calculate corrections to these normalization statements. One finds

$$\mathcal{F}(\omega) = \eta_{\rm QED}\eta_A\left[1 + \delta_{1/\mu^2} + \cdots\right] + (1-\omega)\rho^2 + \mathcal{O}((1-\omega)^2) \tag{6}$$

$$\mathcal{G}(1) = \eta_{\rm QED}\eta_V\left[1 + \mathcal{O}\left(\frac{m_B - m_D}{m_B + m_D}\right)\right] \tag{7}$$

where $\mu = m_c m_b/(m_b + m_c)$ is the parameter of Heavy-Quark-Symmetry breaking, which governs the leading non-perturbative corrections δ_{1/μ^2}, ρ is a slope parameter and η_A and η_V are the perturbative corrections to the Axial-Vector and the Vector

current due to QCD effects and $\eta_{\rm QED}$ are the QED corrections. The radiative corrections are known at the two-loop level [5], while the non-perturbative correction is estimated on the basis of a sum rule [6]; the currently best values are

$$\eta_A = 0.960 \pm 0.007\,, \quad \eta_V = 1.022 \pm 0.004\,,$$
$$\delta_{1/\mu^2} = -(8 \pm 4)\%\,, \quad \eta_{\rm QED} = 1.007 \tag{8}$$

Thus from heavy-quark symmetries one can obtain the form-factor normalization $\mathcal{F}(1)$ with an uncertainty of about 4%, while $\mathcal{G}(1)$ parametrically has a substantially larger uncertainty.

However, all the calculations based on the heavy quark limit might become obsolete, since unquenched lattice calculations become available which do not refer to the heavy mass limit [7]. These calculations compute the deviation of the two form factor from unity and the current results are

$$\mathcal{F}(1) = 0.91^{+0.03}_{-0.04} \qquad \mathcal{G}(1) = 1.074 \pm 0.018 \pm 0.016 \tag{9}$$

I is worth noticing that the uncertainty in $\mathcal{G}(1)$ is smaller than the one in $\mathcal{F}(1)$, which is currently at the same level as the the one obtained from heavy-quark considerations.

The results for the form factors may be used to obtain value for V_{cb} by extrapolating the data to the non-recoil point $v = v'$. Fig. 1 shows he current situation for this extrapolation.

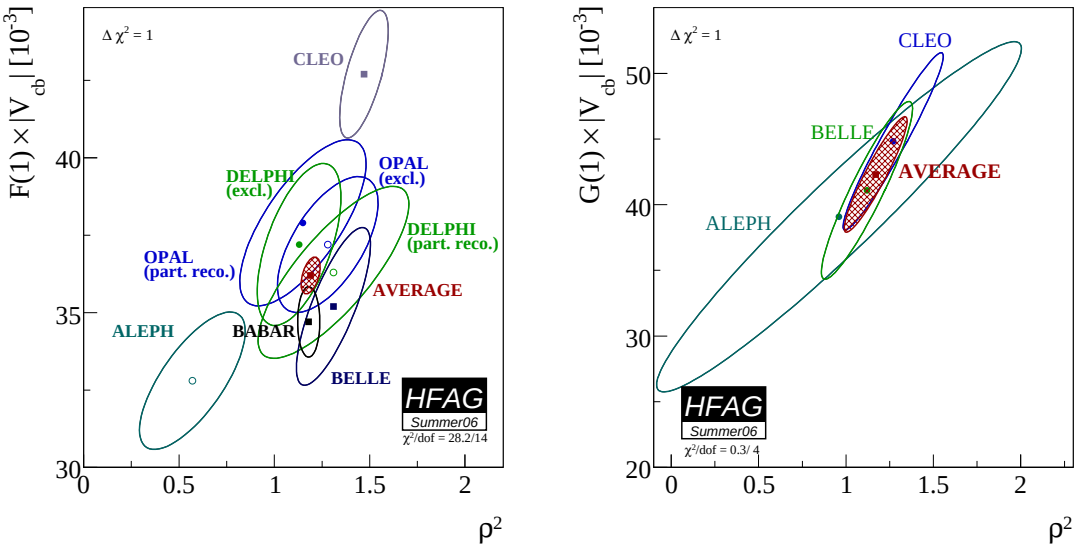

Figure 1: Measurements of $|V_{cb}|\mathcal{F}(1)$ (left) and $|V_{cb}|\mathcal{G}(1)$ versus the from factor slope. Plots are taken from [8].

From this input one extracts a value for V_{cb} from exclusive decays:

$$V_{cb,excl} = (39.4 \pm 0.87^{+1.56}_{-1.24}) \times 10^{-3} \tag{10}$$

2.2 $B \to \pi \ell \overline{\nu}_\ell$

The rate for $B \to \pi \ell \overline{\nu}_\ell$ for vanishing lepton mass is given in terms of only one form factor

$$\frac{d\Gamma}{dq^2} = \frac{G_F^2 V_{ub}}{24\pi^3} |\vec{p}_\pi|^3 |f_+(q^2)|^2 \tag{11}$$

Heavy Quark Symmetries cannot be used as efficiently as in the heavy-to-heavy case and only relative normalization statements are possible. In this case it is more convenient to make us of other methods.

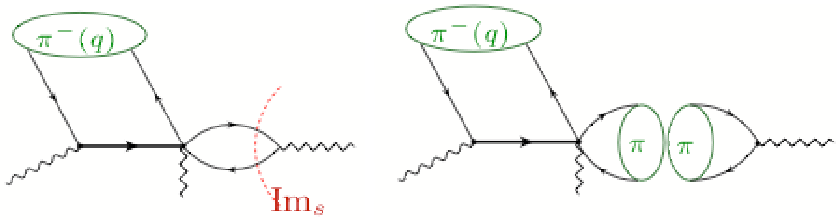

Figure 2: Feynman diagrams for the sum rule evaluation of the $B \to \pi$ form factor.

One possibility is to use QCD (light cone) sum rules [9, 10] which use dispersion relations and the light-cone expansion for the correlator

$$F_\lambda(p,q) = i \int d^4x \; e^{ipx} \langle \pi^+(q)|T\{\overline{u}\gamma_\lambda b(x) \; m_b \overline{b} i\gamma_5 d(0)\}|0\rangle \tag{12}$$

which is evaluated in the deep euclidean region using the Feynman diagrams shown in fig. 2. The imaginary part corresponding to the cut shown here is related to a sum of hadronic states which contains also the desired state.

Applying this to the $B \to \pi$ form factor one obtains an estomate for $f_B f_+(q^2)$ in the region of small q^2. The method has quite a few sources of uncertainties, which are from Higher Twists (≥ 4), from the b quark mass and renormalization scale, from the values of the condensates from the sum rule parameters (Threshold and Borel parameters) and finally from the Pion Distribution amplitude. Estimating the resulting uncertainties by varying the parameters we find [9, 10]

$$f_+(0) = 0.27 \times \left[1 \pm (5\%)_{tw>4} \pm (3\%)_{m_b,\mu} \pm (3\%)_{\langle\overline{q}q\rangle} \pm (3\%)_{s_0^B,M} \pm (8\%)_{a_{2,4}^\pi}\right] \tag{13}$$

which adds up to an uncertainty of about 15%.

Complementary information may be obtained from the lattice, since lattice simulations are restricted to large values of q^2 [11, 12]. Also for heavy-to-light decays first unquenched results become available. In fig. 3 the latice data points are shown together with a fit using a pole model [13].

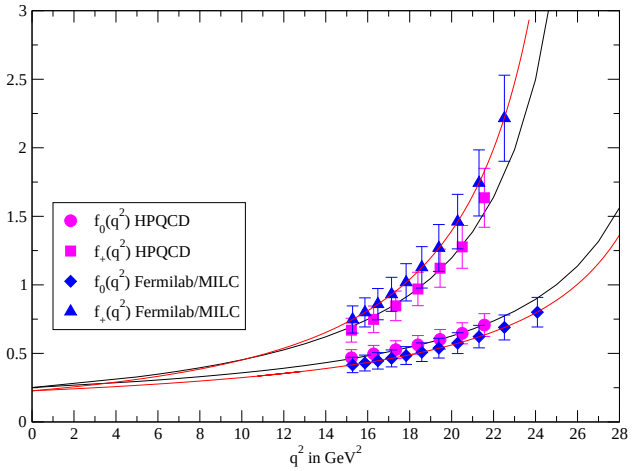

Figure 3: Lattice data for the two form factors involved in $B \to \pi$ transitions. The solid line is a fit to the data using a pole model [13].

Lattice and QCD sum rules turn out to be nicely consistent, giving us some confidence that the form factor in $B \to \pi$ is under reasonable control. Using the lattice data one obtains for the rate above $q^2 = 16\,\mathrm{GeV}^2$

$$|V_{ub}|^2 \times (1.31 \pm 0.33)\,\mathrm{ps}^{-1} \qquad \text{HPQCD} \tag{14}$$

$$|V_{ub}|^2 \times (1.80 \pm 0.48)\,\mathrm{ps}^{-1} \qquad \text{Fermilab / MILC} \tag{15}$$

Gathering the information from the various methods we yield a consistent picture for the value for V_{ub} from exclusive decays. We quote the value from QCD sum rules taken from [10]

$$|V_{ub}| = (3.41 \pm 0.12^{+0.56}_{-0.38}) \times 10^{-3} \tag{16}$$

where the first uncertainty is experimental and the second one is theoretical.

3 Inclusive Decays

The $1/m_b$ expansion for inclusive decays [14–16] is set up in a similar way as one discusses deep inelastic scattering. The total rate is proportional to

$$\begin{aligned}
\Gamma &\propto \sum_X (2\pi)^4 \delta^4(P_B - P_X) |\langle X|\mathcal{H}_{eff}|B(v)\rangle|^2 = \int d^4x\, \langle B(v)|\mathcal{H}_{eff}(x)\mathcal{H}^\dagger_{eff}(0)|B(v)\rangle \\
&= 2\,\mathrm{Im} \int d^4x\, \langle B(v)|T\{\mathcal{H}_{eff}(x)\mathcal{H}^\dagger_{eff}(0)\}|B(v)\rangle \\
&= 2\,\mathrm{Im} \int d^4x\, e^{-im_b v\cdot x} \langle B(v)|T\{\widetilde{\mathcal{H}}_{eff}(x)\widetilde{\mathcal{H}}^\dagger_{eff}(0)\}|B(v)\rangle
\end{aligned} \tag{17}$$

where in the last step we have replaced the b quark field operator by $b \to \widetilde{b} = \exp(-im_b v\cdot v)b$, which corresponds to the replacement $p_b = m_b v + k$.

The next step is to perform an operator product expansion (OPE), which is in the case at hand not in the euclidean region, but rather in the minkowskian. One obtains for the operator product

$$\int d^4x e^{im_b vx} T\{\widetilde{\mathcal{H}}_{eff}(x)\widetilde{\mathcal{H}}^\dagger_{eff}(0)\} = \sum_{n=0}^{\infty}\left(\frac{1}{2m_Q}\right)^n C_{n+3}(\mu)\mathcal{O}_{n+3} \tag{18}$$

where $\mathcal{O}_j$ represents a set of local operators of dimension j and C_j are (perturbatively computable) Wilson coefficients, encoding the short distance contributions.

Taking the forward matrix element of (18) yields an expansion for the total rate of the form

$$\Gamma = \Gamma_0 + \frac{1}{m_Q}\Gamma_1 + \frac{1}{m_Q^2}\Gamma_2 + \frac{1}{m_Q^3}\Gamma_3 + \cdots \tag{19}$$

where the non-perturbative contributions are encoded in the forward matrix elements of the local operators. The general structure of such an expansion is

- Γ_0 is the decay of a free quark ("Parton Model")
- Γ_1 vanishes due to "Luke's theorem" [17]
- Γ_2 is expressed in terms of two parameters

$$2M_H\mu_\pi^2 = -\langle H(v)|\overline{Q}_v(iD)^2Q_v|H(v)\rangle \tag{20}$$
$$2M_H\mu_G^2 = \langle H(v)|\overline{Q}_v(-i\sigma_{\mu\nu})(iD^\mu)(iD^\nu)Q_v|H(v)\rangle \tag{21}$$

  where μ_π is the kinetic energy parameter and μ_G is the chromomagnetic moment.

- Γ_3 introduces two more parameters [18]

$$2M_H\rho_D^3 = -\langle H(v)|\overline{Q}_v(iD_\mu)(ivD)(iD^\mu)Q_v|H(v)\rangle \tag{22}$$
$$2M_H\rho_{LS}^3 = \langle H(v)|\overline{Q}_v(-i\sigma_{\mu\nu})(iD^\mu)(ivD)(iD^\nu)Q_v|H(v)\rangle \tag{23}$$

  where ρ_D is the so-called Darwin Term and ρ_{LS} is the spin-orbit term

- Recently the $1/m_b^4$ contribution has been calculated at tree level for semileptonic decays [19]. This introduces five more parameters which have a simple intuitive interpretation:

  $\langle\vec{E}^2\rangle$: Expectation value of the Chromoelectric Field squared

  $\langle\vec{B}^2\rangle$: Expectation value of the Chromomagnetic Field squared

  $\langle(\vec{p}^2)^2\rangle$: Fourth power of the residual b quark momentum

  $\langle(\vec{p}^2)(\vec{\sigma}\cdot\vec{B})\rangle$: Mixed Chromomagnetic Moment and res. Momentum sqrd.

  $\langle(\vec{p}\cdot\vec{B})(\vec{\sigma}\cdot\vec{p})\rangle$: Mixed Chromomagnetic field and res. helicity

3.1 $B \to X_c \ell \overline{\nu}_\ell$

The total rate becomes schematically [20]

$$\Gamma = |V_{cb}|^2 \hat{\Gamma}_0 m_b^5(\mu)(1+A_{ew})A^{\rm pert}(r,\mu) \left[z_0(r) + z_2(r)\left(\frac{\mu_\pi^2}{m_b^2},\frac{\mu_G^2}{m_b^2}\right) + z_3(r)\left(\frac{\rho_D^3}{m_b^2},\frac{\rho_{\rm LS}^3}{m_b^2}\right) + ... \right] \quad (24)$$

where A_{ew} and $A^{\rm pert}$ are the electroweak and the perturbative QCD corrections, $r = m_c^2/m_b^2$ and $z_i(r)$ are the phase space correction factors appearing in the different orders in $1/m_b$.

The state-of-the-art for this calculation includes the $1/m_b$ Expansion at tree level up to $1/m_b^4$, the complete $\mathcal{O}(\alpha_s)$ corrections for the partonic rate $(1/m_b^0)$ and the partial $\mathcal{O}(\alpha_s^2)$, while the $\mathcal{O}(\alpha_s)$ for $1/m_b^2$ terms under consideration.

The partonic rate has a significant scheme dependence, related to the strong dependence on the heavy quark mass. It is well known that the calculation in the pole mass scheme yields sizable QCD radiative corrections. However, switching to a scheme with a suitably chosen short-distance mass reduces the size of the QCD radiative corrections by absorbing them into the mass.

There are two schemes which are commonly used. The kinetic scheme [6] defines the kinetic mass $m_{\rm kin}(\mu)$ from a sum rule for the kinetic energy of a heavy quark, while the $1S$ scheme uses a mass definition derived from a perturbative calculation of the $\Upsilon(1S)$ mass [21]. Both schemes yield a comparable precision; for simplicity I will stick to the kinetic scheme in this talk.

The extraction of V_{cb} from (24) requires (aside from the quark masses m_b and m_c) the knowledge of the Heavy Quark Expansion (HQE) parameters μ_π, μ_G, ρ_D and $\rho_{\rm LS}$. These parameters are obtained from the analysis of the leptonic energy and the hardonic invariant mass. It has been shown that the moments of these spectra can be computed reliably in HQE and hence one considers

$$\langle M_X^n \rangle = \frac{1}{\Gamma}\int dM_X\, M_X^n \int_{E_{\rm cut}} dE_\ell \frac{d^2\Gamma}{dM_x\, dE_\ell} \quad (25)$$

$$\langle E_\ell^n \rangle = \frac{1}{\Gamma}\int dM_X \int_{E_{\rm cut}} dE_\ell\, E_\ell^n \frac{d^2\Gamma}{dM_x\, dE_\ell} \quad (26)$$

Aside from extracting the HQE parameters in this way one may in addition study the dependence of the various moments on the cut energy $E_{\rm cut}$ which is the minimal lepton energy included in the integration. The fits show a very good agreement with the theoretical expectation [22], giving us some confidence that we do understand inclusive semi-leptonic decays at a precision level. In table 1 we show the fit results for the heavy quark parameters.

Using this method one can extract the value of V_{cb} to be

$$V_{cb} = 41.96 \pm 0.23_{\rm exp} \pm 0.35_{\rm HQE} \pm 0.59_{\Gamma_{sl}}) \times 10^{-3} \quad (27)$$

Quantity	Value	exp	HQE
m_b (GeV)	4.590	$\pm$ 0.025	$\pm$ 0.030
m_c (GeV)	1.142	$\pm$ 0.037	$\pm$ 0.045
μ_π^2 (GeV)^2	0.401	$\pm$ 0.019	$\pm$ 0.035
μ_G^2 (GeV)^2	0.297	$\pm$ 0.024	$\pm$ 0.046
ρ_D^3 (GeV)^3	0.174	$\pm$ 0.009	$\pm$ 0.022
$\rho_{\rm LS}^3$ (GeV)^2	-0.183	$\pm$ 0.054	$\pm$ 0.071

Table 1: Values of the HQE parameters [22]. The column "exp" contains the experimental uncertainty, while "HQE" contains the remaining uncertainy from the heavy quark expansion.

where the last uncertainty is from the experimental knowledge of the total semileptonic rate. Note that the relative theoretical uncertainty in V_{cb} is currently at the level of 2% and can possibly further reduced by including the newly calculated contribution of order $1/m_b^4$

3.2 $B \to X_u \ell \overline{\nu}_\ell$

The extaction of V_{ub} has to proceed along different lines due to the problem that in most of the phase space the $b \to u$ transitions are completely obscured by the much stronger $b \to c$ decays. Thus the analysis for V_{ub} has to make use of small corners of phase space in which the OPE described in the last section breaks down. For example, the lepton energy spectrum ($y = 2E_\ell/m_b$) close to the endpoint region $y \to 1$ becomes

$$\frac{d\Gamma}{dy} \stackrel{y\to 1}{=} \frac{G_F^2 |V_{ub}^2| m_b^5}{96\pi^3} \left[\Theta(1-y) + \frac{\mu_\pi^2 - \mu_G^2}{6m_b^2}\delta(1-y) + \frac{\mu_\pi^2}{6m_b^2}\delta'(1-y) + \cdots \right] \tag{28}$$

where the singular terms indicate a breakdown of the OPE close to $y = 1$, which yields in this case an expansion in terms of $1/[m_b(1-y)]$

It has been shown some time ago that thee singular terms can be resummed into a non-perturbative function, the so called shape function which is formally defined as [23–25]

$$2M_B f(\omega) = \langle B(v)|\overline{b}_v \delta(\omega + i(n\cdot D))|B(v)\rangle \tag{29}$$

where the second and the third moments of this function may be related to the HQE parameters μ_π and ρ_D

$$f(\omega) = \delta(\omega) + \frac{\mu_\pi^2}{6m_b^2}\delta''(\omega) - \frac{\rho_D^3}{18m_b^3}\delta'''(\omega) + \cdots \tag{30}$$

In terms of the shape function one may write the resummed rate as

$$\frac{d\Gamma}{dy} = \frac{G_F^2 |V_{ub}^2| m_b^5}{96\pi^3} \int d\omega\, \Theta(m_b(1-y)-\omega) f(\omega) \tag{31}$$

and moment expansion of this expression yields (28).

In order to obtain a precise method for the extraction of V_{ub} one needs aside from some information on the shape function (this could be taken from the rare decay $B \to X_s\gamma$, which is governed by the same shape function) also to take into account the radiative and the $1/m_b$ corrections. In order to do this one has to use "Soft Collinear Effective Theory" (SCET), since in the endpoint region the light degrees of freedom become energetic [26, 27].

It has been shown the within SCET the inclusive rates in the endpoint can be factorized according to [28]

$$d\Gamma = H \otimes J \otimes S \tag{32}$$

where the symbol $\otimes$ means a convolution. The function H contains the hard contribution related to scales of order m_b, J is the "jet function" containing the scales $\sqrt{\Lambda_{\rm QCD} m_b}$ and S is the shape function with the soft pieces with scales $\Lambda_{\rm QCD}$. Note that both m_b and $\sqrt{\Lambda_{\rm QCD} m_b}$ are perturbative scales and hence H and J are computed in perturbation theory.

Without going into further details we only quote the state-of-the-art of this kind of calculation. The next to leading terms in the $1/m_b$ expansion have been investigated in [29,30] and the QCD radiative corrections have been considered in [31]. Finally, in order to obtain quantitative predictions one needs a model for the shape functions. There are two approaches commonly used. One makes use of a model which is chosen such that the first few moments coincide with what is known from the local OPE [31] (BLNP). The second method [32] is based on the so called "dressed gluon exponentiation" (DGE) which is a QCD based model for the shape function. The results which are obtained from these two approaches are consistent [8]

$$\begin{aligned} V_{ub} &= (4.49 \pm 0.19_{\rm exp} \pm 0.27_{\rm theo}) \times 10^{-3} \qquad \text{BLNP} \\ V_{ub} &= (4.46 \pm 0.20_{\rm exp} \pm 0.20_{\rm theo}) \times 10^{-3} \qquad \text{DGE} \end{aligned}$$

Aside from the shape function dependent methods there are also shape function insensitive methods [33]. However, although these methods have a smaller theoretical uncertainty, they are using a smaller part of the phase space and hence the experimental uncertainties are larger. From this method one obtains [8]

$$V_{ub} = (5.02 \pm 0.26_{\rm exp} \pm 0.37_{\rm theo}) \times 10^{-3} \tag{33}$$

4 Conclusion

From all the checks that have been made it is fair to conclude that the theory of semi-leptonic decays is in a mature state. Current methods allow us to extract V_{cb} with an overall relative accuracy at the level of 2%. This is a remarkble progress in view of the fact that the relative uncertainty of the Cabbibo angle is also not significantly better.

For the calculations of the inclusive rates for the determination of V_{cb} only small improvements are possible, e.g. by a calculation of the contributions of order α_s/m_b^2 and by the inclusion of the newly calculated $1/m_b^4$ terms. However, the progress in the lattice calculations of the exclusive form factors is very promising and the precision of these calculations is already in competition with the heavy quark expansion method. In the near future one may expect that exclusive methods using lattice data will become more precise than the heavy quark expansion method

The determination of V_{ub} has currently a relative theoretical uncertainty of about 8%, and possible improvements of the inclusive methods are still limited either by statistics or by model dependences for e.g. the subleading shape functions. Similar to the exclusive methods are catching up due to more precise and more reliable lattice data. On this basis a future improvement to a level of 5% relative uncertainty (or maybe even better) seems to be possible.

There seems to be a systematic tendency that the exclusive values of both V_{cb} and V_{ub} come out to be lower that the inclusive values, where this effect is more pronounced for the case of V_{ub}. It is interesting to note that the somewhat lower value of V_{ub} is more compatible with the time dependent CP asymmetry measured in $B \to J/\psi K_s$. However, all these effects are well within the uncertainties, which may have been estimated a bit too optimistic, since - in particular a theoretical uncertainty - is hard to estimate.

Bibliography

[1] A textbook presentation can be found in: A. V. Manohar and M. B. Wise, Camb. Monogr. Part. Phys. Nucl. Phys. Cosmol. **10** (2000) 1.

[2] N. Isgur and M. B. Wise, Phys. Lett. B **237**, 527 (1990).

[3] N. Isgur and M. B. Wise, Phys. Lett. B **232**, 113 (1989).

[4] M. A. Shifman and M. B. Voloshin, Sov. J. Nucl. Phys. **47**, 511 (1988).

[5] A. Czarnecki and K. Melnikov, Nucl. Phys. B **505**, 65 (1997) [arXiv:hep-ph/9703277].

[6] I. I. Y. Bigi, M. A. Shifman, N. G. Uraltsev and A. I. Vainshtein, Phys. Rev. D **52**, 196 (1995) [arXiv:hep-ph/9405410].

[7] S. Hashimoto, A. X. El-Khadra, A. S. Kronfeld, P. B. Mackenzie, S. M. Ryan and J. N. Simone, Phys. Rev. D **61**:014502 (2000).

[8] Heavy Flavor Averaging Group, http://www.slac.stanford.edu/xorg/hfag/

[9] A. Khodjamirian, R. Ruckl, S. Weinzierl, C. W. Winhart and O. I. Yakovlev, Phys. Rev. D **62**, 114002 (2000) [arXiv:hep-ph/0001297].

[10] P. Ball and R. Zwicky, Phys. Rev. D **71**, 014015 (2005) [arXiv:hep-ph/0406232].

[11] M. Okamoto *et al.* (Fermilab/MILC), Nucl. Phys. Proc. Suppl. **140**:461 (2005) [arXiv:hep-lat/0409116].

[12] J. Shigemitsu *et al.* (HPQCD), Nucl. Phys. Proc. Suppl. **140**:464 (2005) [arXiv:hep-lat/0408019].

[13] D. Becirevic and A. B. Kaidalov, Phys. Lett. **B478**:417 (2000).

[14] I. I. Y. Bigi, M. A. Shifman, N. G. Uraltsev and A. I. Vainshtein, Phys. Rev. Lett. **71**, 496 (1993). [arXiv:hep-ph/9304225].

[15] A. V. Manohar and M. B. Wise, Phys. Rev. D **49**, 1310 (1994) [arXiv:hep-ph/9308246].

[16] T. Mannel, Nucl. Phys. B **413**, 396 (1994) [arXiv:hep-ph/9308262].

[17] M. E. Luke, Phys. Lett. B **252**, 447 (1990).

[18] M. Gremm and A. Kapustin, Phys. Rev. D **55**, 6924 (1997) [arXiv:hep-ph/9603448].

[19] B. M. Dassinger, T. Mannel and S. Turczyk, arXiv:hep-ph/0611168.

[20] D. Benson, I. I. Bigi, T. Mannel and N. Uraltsev, Nucl. Phys. B **665**, 367 (2003) [arXiv:hep-ph/0302262].

[21] A. H. Hoang, Z. Ligeti and A. V. Manohar, Phys. Rev. D **59**, 074017 (1999) [arXiv:hep-ph/9811239].

[22] O. Buchmüller, contribution to this conference.

[23] M. Neubert, Phys. Rev. D **49**, 3392 (1994) [arXiv:hep-ph/9311325].

[24] I. I. Y. Bigi, M. A. Shifman, N. G. Uraltsev and A. I. Vainshtein, Int. J. Mod. Phys. A **9**, 2467 (1994) [arXiv:hep-ph/9312359].

[25] T. Mannel and M. Neubert, Phys. Rev. D **50**, 2037 (1994) [arXiv:hep-ph/9402288].

[26] C. W. Bauer, S. Fleming, D. Pirjol and I. W. Stewart, Phys. Rev. D **63**, 114020 (2001) [arXiv:hep-ph/0011336].

[27] M. Beneke, A. P. Chapovsky, M. Diehl and T. Feldmann, Nucl. Phys. B **643**, 431 (2002) [arXiv:hep-ph/0206152].

[28] G. P. Korchemsky and G. Sterman, Phys. Lett. B **340**, 96 (1994) [arXiv:hep-ph/9407344].

[29] C. W. Bauer, M. Luke and T. Mannel, Phys. Lett. B **543**, 261 (2002) [arXiv:hep-ph/0205150].

[30] M. Beneke, F. Campanario, T. Mannel and B. D. Pecjak, JHEP **0506**, 071 (2005) [arXiv:hep-ph/0411395].

[31] S. W. Bosch, B. O. Lange, M. Neubert and G. Paz, Nucl. Phys. B **699**, 335 (2004) [arXiv:hep-ph/0402094].

[32] E. Gardi, JHEP **0502**, 053 (2005) [arXiv:hep-ph/0501257].

[33] C. W. Bauer, Z. Ligeti and M. E. Luke, Phys. Rev. D **64**, 113004 (2001) [arXiv:hep-ph/0107074].

Charmless B Decays

Wolfgang Gradl (from the BABAR Collaboration)
The University of Edinburgh
School of Physics
Edinburgh EH9 3JZ, UK

1 Introduction

Rare charmless hadronic B decays are a good testing ground for the standard model. The dominant amplitudes contributing to this class of B decays are CKM suppressed tree diagrams and $b \to s$ or $b \to d$ loop diagrams ('penguins'). These decays can be used to study interfering standard model (SM) amplitudes and CP violation. They are sensitive to the presence of new particles in the loops, and they provide valuable information to constrain theoretical models of B decays.

The B factories *BABAR* at SLAC and Belle at KEK produce B mesons in the reaction $e^+e^- \to \Upsilon(4S) \to B\overline{B}$. So far they have collected integrated luminosities of about $406\,\mathrm{fb}^{-1}$ and $600\,\mathrm{fb}^{-1}$, respectively. The results presented here are based on subsets of about 200–$500\,\mathrm{fb}^{-1}$ and are preliminary unless a journal reference is given.

2 ΔS from rare decays

The time-dependent CP asymmetry in B decays is observed as an asymmetry between B^0 and $\overline{B}^0$ decay rates into CP eigenstates f

$$\mathcal{A}_{cp}(\Delta t) = \frac{\Gamma(\overline{B}^0 \to f) - \Gamma(B^0 \to f)}{\Gamma(\overline{B}^0 \to f) + \Gamma(B^0 \to f)} = S_f \sin \Delta m_d \Delta t - C_f \cos \Delta m_d \Delta t,$$

where $\Delta m_d = 0.502 \pm 0.007\ \mathrm{ps}^{-1}$ and Δt is the time difference between the decays of the two neutral B mesons in the event. The coefficients S_f and C_f depend on the final state f; for the 'golden' decay $B^0 \to J/\psi K^0_s$, for example, which proceeds via a $b \to c\bar{c}s$ transition, only one weak phase enters, and $S_{J/\psi K^0_S} = \sin 2\beta$, $C_{J/\psi K^0_S} = 0$. Here, $\beta \equiv \phi_1$ is one of the angles of the unitarity triangle of the CKM matrix.

In general, the presence of more than one contributing amplitude for the decay can introduce additional phases, so that S_f measured in such a decay deviates from the simple $\sin 2\beta$. Apart from standard-model amplitudes, particles beyond the standard

model may contribute in loop diagrams. There are intriguing hints in experimental data that S_f is smaller than $\sin 2\beta$ in B decays involving the transition $b \to q\bar{q}s$, like $B^0 \to \phi K^0$, $B^0 \to \eta' K^0$, or $B^0 \to \pi^0 K^0$ (see Fig. 1). However, for each of these final states the SM contribution to $\Delta S_f \equiv S_f - \sin 2\beta$ from sub-dominant amplitudes needs to be determined in order to draw a conclusion about the presence of any new physics. Typically, models prefer $\Delta S_f > 0$ [1, 2], while for the final state $\eta' K^0_S$, a small, negative ΔS_f is expected [3]. Measuring B decays which are related to the ones above by approximate SU(3) flavour or isospin symmetries helps to constrain the standard-model expectation for ΔS_f.

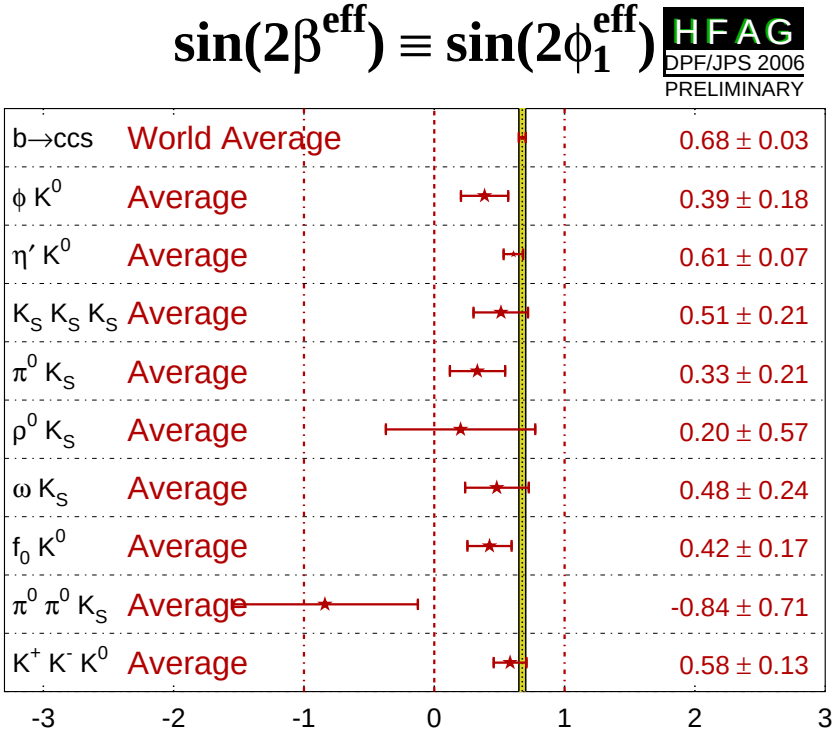

Figure 1: Average of S_f in the different $b \to q\bar{q}s$ decays [4].

2.1 $B^0 \to \phi K^0$

The sub-dominant amplitudes contributing to $B^0 \to \phi K^0$ can be constrained using SU(3) flavor relations [5]. This requires branching fraction measurements for eleven

decay channels ($K^{*0}\overline{K}^0, \overline{K}^{*0}K^0$, and hh' with $h = \rho^0, \omega, \phi$ and $h' = \pi^0, \eta, \eta'$). *BABAR* has measured an upper limit for the sum $\mathcal{B}(K^{*0}\overline{K}^0) + \mathcal{B}(\overline{K}^{*0}K^0) < 1.9 \times 10^{-6}$ [6] and an updated upper limit for $\phi\pi^0$ of $\mathcal{B}(\phi\pi^0) < 2.8 \times 10^{-7}$ [7]. Together with the already known upper limits or branching fractions for the other decays in this list, this allows one to place a bound on $|\Delta S_{\phi K^0}| < 0.43$ [6].

2.2 $B^0 \to \eta' K^0$

The decays $B^0 \to \eta^{(\prime)}\pi^0, \eta'\eta$ can be used to constrain the SM pollution in $B^0 \to \eta' K^0$, The expected branching fractions are between 0.2 and 1×10^{-6} for $\eta^{(\prime)}\pi^0$ and 0.3 - 2×10^{-6} for $\eta'\eta$. Using 211 fb^{-1} of data, *BABAR* sets the following upper limits [8] at 90% confidence level (C.L.) in units of 10^{-6}: $\mathcal{B}(B^0 \to \eta\pi^0) < 1.3$, $\mathcal{B}(B^0 \to \eta'\eta) < 1.7$, $\mathcal{B}(B^0 \to \eta'\pi^0) < 2.1$, while Belle [9] measures $\mathcal{B}(B^0 \to \eta'\pi^0) = (2.79^{+1.02+0.25}_{-0.96-0.34}) \times 10^{-6}$ with 386×10^6 analysed $B\overline{B}$ pairs. With these new upper limits, the standard model expectation for $\Delta S_{\eta' K^0_S}$ is $-0.046 < \Delta S_{\eta' K^0_S} < 0.094$ [10]. A similar improvement for the measurement of $\sin 2\alpha$ in $B^0 \to \pi^+\pi^-$ is expected. Belle also measure $\mathcal{B}(B^+ \to \eta'\pi^+) = (1.76^{+0.67+0.15}_{-0.62-0.14}) \times 10^{-6}$ and a charge asymmetry in this channel of $\mathcal{A}_{ch} = 0.20^{+0.37}_{-0.36} \pm 0.04$.

2.3 Pure penguin decays

There is special interest in decays which only proceed via the $b \to s\overline{s}s$ penguin transitions. The $b \to u$ amplitudes can only contribute through rescattering. This drastically reduces the standard model 'pollution' in these decays, making them a very clean probe for the presence of new particles in the loop. An example for this class of decays is $B^0 \to K^0_S K^0_S K^0_S$, in which the CP violating parameters S and C have been measured by both *BABAR* [11] and Belle [12], with an average of $S = 0.51 \pm 0.21$, $C = -0.23 \pm 0.15$. *BABAR* has also searched for the related decay $B^0 \to K^0_S K^0_S K^0_L$. The non-resonant contribution (besides $B^0 \to \phi(K^0_S K^0_L)K^0_S$) to this final state has not been studied before and might be large [13]. Assuming a uniform Dalitz distribution and analysing 211 fb^{-1}, *BABAR* [14] sets a 90% CL upper limit of $\mathcal{B}(B^0 \to K^0_S K^0_S K^0_L) < 7.4 \times 10^{-6}$. Due to a low product of efficiency and daughter branching fraction, this decay is therefore of limited use for the understanding of CP violation in $b \to q\overline{q}s$ decays.

3 Measurements related to α

Decays containing a $b \to u$ transition can be used to measure the angle $\alpha \equiv \phi_2$ in the unitarity triangle. In general several amplitudes with different weak phases contribute to these decays, only allowing the direct measurement of an effective parameter α_{eff}.

There are several methods to extract the true angle α in presence of this 'pollution.' Updated results for the decays $B \to \rho\rho$, have been presented by Christos Touramanis at this conference.

Another new decay studied by *BABAR* and Belle is $B^0 \to a_1^\pm \pi^\mp$, from which α can be extracted up to a four-fold ambiguity. Exploiting isospin or approximate SU(3) flavor symmetries this ambiguity can be overcome [15]. This needs also the measurement of related axial–vector decays, from which a model-dependent measurement of α can be derived. *BABAR* searches for $B^0 \to a_1^\pm \pi^\mp$ in $211\,\mathrm{fb}^{-1}$ and measures [16] a branching fraction of $\mathcal{B}(B^0 \to a_1^\pm \pi^\mp) = (33.2 \pm 3.8 \pm 3.0) \times 10^{-6}$, assuming $\mathcal{B}(a_1^+ \to (3\pi)^+) = 1$. With about the same luminosity, Belle measures a slightly larger branching fraction of $(48.6 \pm 4.1 \pm 3.9) \times 10^{-6}$ [17]. The next step is to extend this analysis to measure time-dependent CP violation in this decay.

BABAR also searched for the related decay $B^0 \to a_1^+ \rho^-$, which also could be used to measure α. In addition, B decays to 5π are an important background for the $B \to \rho\rho$ analyses. In $100\,\mathrm{fb}^{-1}$ no significant signal was seen; assuming a fully longitudinal polarisation, the analysis sets a 90% C.L. upper limit of $\mathcal{B}(B^0 \to a_1^+ \rho^-)\mathcal{B}(a_1^+ \to (3\pi)^+) < 61 \times 10^{-6}$ [18].

4 Charmless vector-vector decays

For tree-dominated B decays into two vector mesons, helicity conservation arguments together with factorisation suggest that the longitudinal polarisation fraction f_L is $f_L \sim 1 - m_V^2/m_B^2$, close to unity. Experimentally, this is seen in decays such as $B \to \rho\rho$, where $f_L \approx 0.95$ is observed. However, there seems to be a pattern emerging where f_L is smaller than the expectation in decays dominated by loop diagrams. This was first seen in the decays $B \to \phi K^*$, where f_L is near 0.5 with an uncertainty of about 0.04 [19, 20].

In the following sections, we describe a number of recent *BABAR* measurements for several of these vector-vector decays.

4.1 Decays involving an ω meson

To establish whether tree-induced decays generally have a large f_L, *BABAR* has searched for the related decays $B \to \omega V$ [21], where $V = \rho, K^*, \omega, \phi$. The results are summarised in Table 1. The only decay with a significant observed yield is $B^+ \to \omega\rho^+$ with $\mathcal{B}(B^+ \to \omega\rho^+) = (10.6 \pm 2.1^{+1.6}_{-1.0}) \times 10^{-6}$. The polarisation f_L is floated in the fit and a large value of $f_L = 0.82 \pm 0.11 \pm 0.02$ is found, as expected for a tree-dominated decay.

4.2 $B \to \rho K^*$

Conversely, the decays $B \to \rho K^*$ are penguin-dominated; some are known to have significant branching fractions and f_L can be measured. *BABAR* has published updated measurements of branching fractions, charge asymmetries and polarisation fractions [22].

$B^+ \to \rho^+ K^{*0}$

The decay $B^+ \to \rho^+ K^{*0}$ is particularly interesting because no tree diagram is thought to contribute to this decay. *BABAR* has a new measurement of the branching fraction, CP asymmetry and polarisation for this decay. The measured branching fraction is $\mathcal{B}(\rho^+ K^{*0}) = (9.6 \pm 1.7\,\mathrm{m}1.5) \times 10^{-6}$, $\mathcal{A}_{ch}(\rho^+ K^{*0}) = -0.01 \pm 0.16 \pm 0.02$. The observed polarisation is $f_L = 0.52 \pm 0.10 \pm 0.04$, as expected for a pure penguin decay and in good agreement with ϕK^*.

$B^+ \to \rho^0 K^{*+}$ and $B^0 \to \rho^0 K^{*0}$

The decays $B^+ \to \rho^0 K^{*+}$ and $B^0 \to \rho^0 K^{*0}$ are theoretically less clean because there is a Cabibbo-suppressed tree diagram contributing in addition to the penguin present for all $B \to \rho K^*$ decays. In addition, $B^+ \to \rho^0 K^{*+}$ is experimentally more challenging because of the smaller branching fraction.

For $B^+ \to \rho^0 K^{*+}$, *BABAR* measures a branching fraction of $(3.6^{+1.7}_{-1.6} \pm 0.8) \times 10^{-6}$, with a significance of only 2.6σ. The value of f_L determined by the fit is $f_L = 0.9 \pm 0.2$ although this is not considered a measurement for this decay, as the signal itself is not significant.

$B^0 \to \rho^0 K^{*0}$ is observed with a significance of 5.3σ; the branching fraction is $(5.6 \pm 0.9 \pm 1.3) \times 10^{-6}$ and $f_L = 0.57 \pm 0.09 \pm 0.08$.

	$\mathcal{B}(10^{-6})$	$S(\sigma)$	$\mathcal{B}$ U.L $\times 10^{-6}$	f_L	$\mathcal{A}_{ch}$
ωK^{*0}	$2.4 \pm 1.1 \pm 0.7$	2.4	4.2	$0.71^{+0.27}_{-0.24}$	–
ωK^{*+}	$0.6^{+1.4+1.1}_{-1.2-0.9}$	0.4	3.4	0.7 fixed	–
$\omega\rho^0$	$-0.6 \pm 0.7^{+0.8}_{-0.3}$	0.6	1.5	0.9 fixed	–
$\omega f_0(980)$	$0.9 \pm 0.4^{+0.2}_{-0.1}$	2.8	1.5	–	–
$\omega\rho^+$	$10.6 \pm 2.1^{+1.6}_{-1.0}$	5.7	–	$0.82 \pm 0.11 \pm 0.02$	$0.04 \pm 0.13 \pm 0.02$
$\omega\omega$	$1.8^{+1.3}_{-0.9} \pm 0.4$	2.1	4.0	0.79 ± 0.34	–
$\omega\phi$	$0.1 \pm 0.5 \pm 0.1$	0.3	1.2	0.88 fixed	–

Table 1: Results of the *BABAR* ωX analysis: measured branching fraction $\mathcal{B}$, significance including systematic uncertainties S, 90% C.L. upper limit, measured or assumed longitudinal polarisation f_L, charge asymmetry $\mathcal{A}_{ch}$.

	$\mathcal{B}(10^{-6})$	
	BABAR	BELLE
$B^0 \to \eta K^{*0}$	$16.5 \pm 1.1 \pm 0.8$	$15.9 \pm 1.2 \pm 0.9$
$B^+ \to \eta K^{*+}$	$18.9 \pm 1.8 \pm 1.3$	$19.7^{+2.0}_{-1.9} \pm 1.4$
$B^+ \to \eta \rho^+$	–	$4.1^{+1.4}_{-1.3} \pm 0.34$
$B^0 \to \eta \rho^0$	–	< 1.9
$B^0 \to \eta (K\pi)^{*0}_0$	$11.0 \pm 1.6 \pm 1.5$	–
$B^+ \to \eta (K\pi)^{*+}_0$	$18.2 \pm 2.6 \pm 2.6$	–
$B^0 \to \eta K^{*0}_2$	$9.6 \pm 1.8 \pm 1.1$	–
$B^+ \to \eta K^{*+}_2$	$9.1 \pm 2.7 \pm 1.4$	–

Table 2: Branching fractions for the decays $B \to \eta K^*$, $\eta\rho$, and $\eta(K\pi)$.

5 $B \to \eta^{(\prime)} K^{(*)}$

In B decays to final states comprising $\eta^{(\prime)} K^{(*)}$, the effect of the η–η' mixing angle combines with differing interference in the penguin diagrams to suppress the final states ηK and $\eta' K^*$, and enhance the final states $\eta' K$ and ηK^*. This pattern has now been experimentally established with rather precise measurements of the branching fractions for $\eta' K$ and ηK^* and the observation of the decays $\eta' K^*$. These decays are also important in light of measuring S in $B^0 \to \eta' K^0$.

5.1 $B \to \eta' K$

Belle's measurements for the branching fractions of $B \to \eta'\pi$ [9] were already mentioned above. The same analysis also obtains updated branching fraction measurements for the decays $B \to \eta' K$, with the results $\mathcal{B}(B^0 \to \eta' K^0) = (58.9^{+3.6}_{-3.5} \pm 4.3) \times 10^{-6}$, $\mathcal{B}(B^+ \to \eta' K^+) = (69.2 \pm 2.2 \pm 3.7) \times 10^{-6}$, $\mathcal{A}_{ch}(B^+ \to \eta' K^+) = 0.028 \pm 0.028 \pm 0.021$.

5.2 $B \to \eta K^*$ and $B \to \eta\rho$

BABAR [23] and Belle [24] have published updated results for the decays $B \to \eta K^*(892)$. Belle also observes the decay $B^+ \to \eta\rho^+$ and obtains an upper limit for $B^0 \to eta\rho^0$. These results confirm earlier measurements of $B \to \eta K^*$ and $\eta\rho$. *BABAR* also analyses the mass region $1035 < m_{K\pi} < 1535$ MeV of the $K\pi$ system and obtains branching fractions for the spin-0 ($\eta(K\pi)^*_0$) and spin-2 (ηK^*_2) contributions. For these two final states no predictions exist so far. The branching fraction results are summarised in Table 2.

	BABAR $\mathcal{B}(10^{-6})$	BELLE $\mathcal{B}(10^{-6})$
$\pi^+\ \pi^-$	$5.4 \pm 0.4 \pm 0.3$	$5.1 \pm 0.2 \pm 0.2$
$K^+\ \pi^-$	$18.6 \pm 0.6 \pm 0.6$	$20.0 \pm 0.4^{+0.9}_{-0.8}$
$K^+\ K^-$	< 0.40	—
$B^0 \to \pi^0\pi^0$	$1.48 \pm 0.26 \pm 0.12$	$2.3^{+0.4+0.2}_{-0.5-0.3}$
$B^+ \to \pi^+\pi^0$	$5.12 \pm 0.47 \pm 0.29$	$6.6 \pm 0.4^{+0.4}_{-0.5}$
$B^\pm \to K^\pm\pi^0$	$13.3 \pm 0.56 \pm 0.64$	$12.4 \pm 0.5^{+0.7}_{-0.6}$
$B^+ \to K^0\pi^+$	$23.9 \pm 1.1 \pm 1.0$	$22.9^{+0.8}_{-0.7} \pm 1.3$
$B^+ \to \overline{K}^0 K^+$	$1.61 \pm 0.44 \pm 0.09$	$1.22^{+0.33+0.13}_{-0.28-0.16}$
$B^0 \to \overline{K}^0 K^0$	$1.08 \pm 0.28 \pm 0.11$	$0.86^{+0.24}_{-0.21} \pm 0.09$
$B^0 \to K^0_S\pi^0$	$10.5 \pm 0.7 \pm 0.5$	$9.2^{+0.7+0.6}_{-0.6-0.7}$

Table 3: Branching fraction results for $B \to \pi\pi, \pi K, KK$

5.3 $B \to \eta' K^*$ and $B \to \eta'\rho$

BABAR [25] finds evidence for the decays $B \to \eta' K^*$ in $211\,\text{fb}^{-1}$ and measures branching fractions of $\mathcal{B}(B^+ \to \eta' K^{*+}) = (4.9^{+1.9}_{-1.7} \pm 0.8) \times 10^{-6}$ and $\mathcal{B}(B^0 \to \eta' K^{*0}) = (3.8 \pm 1.1 \pm 0.5) \times 10^{-6}$. For the related decays into $\eta'\rho$, only $B^+ \to \eta'\rho^+$ is seen with $\mathcal{B}(B^+ \to \eta'\rho^+) = (8.7^{+3.1+2.3}_{-2.8-1.3}) \times 10^{-6}$, while $B^0 \to \eta'\rho^0$ is small with a 90% C.L. upper limit of $\mathcal{B}(B^0 \to \eta'\rho^0) < 3.7 \times 10^{-6}$. The direct CP asymmetries in the decays with a significant signal are compatible with zero. Theoretical predictions using SU(3) flavor symmetry [26], QCD factorisation [27], and perturbative QCD factorisation [28] agree within errors with the observed branching fractions. The observation of small branching fractions for $B \to \eta' K^*$ confirms the pattern of enhanced and suppressed decays to $\eta^{(\prime)} K^{(*)}$.

6 $B \to \pi\pi, \pi K, KK$

Updated branching fraction measurements for the two-body decays $B \to \pi\pi, \pi K$, and KK from *BABAR* [29–32] and Belle [33, 33–35] are summarised in Table 3. Both experiments observe the decays $B^+ \to \overline{K}^0 K^+$ and $B^0 \to \overline{K}^0 K^0$ with a statistical significance $> 5\sigma$; decays with $b \to d$ hadronic penguins have now been observed.

BABAR also studied time dependent CP violation in $B^0 \to \overline{K}^0 K^0$ [31] (reconstructed as $B^0 \to K^0_S K^0_S$) which is a pure $b \to d\bar{s}s$ penguin decay. Via flavour SU(3) symmetry, this decay also allows an estimate of the penguin contribution in $B^0 \to \pi^0\pi^0$. Direct CP asymmetry is expected to be zero. The result of the time-dependent fit is $S = -1.28^{+0.80+0.11}_{-0.73-0.16}$ and $C = -0.40 \pm 0.41 \pm 0.06$.

6.1 $B \to \eta'\eta' K$, $\phi\phi K$

Motivated by the large branching fraction for $B \to \eta' K$ and the observation that final states $P^0 P^0 X^0$ are CP eigenstates [36], *BABAR* searched for the decays $B \to \eta'\eta' K$. No significant signal was found in $211\,\text{fb}^{-1}$, and the upper limits on the branching fractions of $\mathcal{B}(\eta'\eta' K^+) < 25 \times 10^{-6}$ and $\mathcal{B}(\eta'\eta' K^0) < 31 \times 10^{-6}$ are set [37].

BELLE searched for the decays $B \to \phi\phi K$. In these, direct CP violation could be enhanced in the interference between decays via the η_c and non-SM decays. In the analysis [38], charmless decays are selected by requiring that $m_{\phi\phi}$ is below the charm threshold. For these charmless decays, the observed branching fractions are $\mathcal{B}(\phi\phi K^+) = (3.2^{+0.6}_{-0.5} \pm 0.3) \times 10^{-6}$, $\mathcal{B}(\phi\phi K^0) = (2.3^{+1.0}_{-0.7} \pm 0.2) \times 10^{-6}$. The measured direct CP asymmetries are compatible with zero.

7 Summary

Charmless hadronic B decays provide a rich field for tests of QCD and the standard model of electroweak interactions. They allow to constrain the SM contribution to ΔS_f in loop-dominated B decays and precision tests of QCD models. The B factories have produced a large number of new and updated measurements. With the currently analysed statistics, decays with branching fractions of the order of 10^{-6} are within experimental reach.

Bibliography

[1] M. Beneke, Phys. Lett. **B620**, 143 (2005), hep-ph/0505075.

[2] H.-Y. Cheng, C.-K. Chua, and A. Soni, Phys. Rev. **D72**, 014006 (2005), hep-ph/0502235.

[3] A. R. Williamson and J. Zupan, Phys. Rev. **D74**, 014003 (2006), hep-ph/0601214.

[4] HFAG, http://www.slac.stanford.edu/xorg/hfag, 2006.

[5] Y. Grossman *et al.*, Phys. Rev. **D68**, 015004 (2003), hep-ph/0303171.

[6] *BABAR*, B. Aubert *et al.*, Phys. Rev. **D74**, 072008 (2006), hep-ex/0606050.

[7] *BABAR*, B. Aubert *et al.*, Phys. Rev. **D74**, 011102 (2006), hep-ex/0605037.

[8] *BABAR*, B. Aubert *et al.*, Phys. Rev. **D73**, 071102 (2006), hep-ex/0603013.

[9] Belle, J. Schumann *et al.*, Phys. Rev. Lett. **97**, 061802 (2006), hep-ex/0603001.

[10] M. Gronau, J. L. Rosner, and J. Zupan, Phys. Rev. **D74**, 093003 (2006), hep-ph/0608085.

[11] *BABAR*, B. Aubert *et al.*, (2006), hep-ex/0607108.

[12] Belle, K. F. Chen *et al.*, (2006), hep-ex/0608039.

[13] H.-Y. Cheng, C.-K. Chua, and A. Soni, Phys. Rev. **D72**, 094003 (2005), hep-ph/0506268.

[14] *BABAR*, B. Aubert *et al.*, Phys. Rev. **D74**, 032005 (2006), hep-ex/0606031.

[15] M. Gronau and J. Zupan, Phys. Rev. **D73**, 057502 (2006), hep-ph/0512148.

[16] *BABAR*, B. Aubert *et al.*, Phys. Rev. Lett. **97**, 051802 (2006), hep-ex/0603050.

[17] Belle, K. Abe *et al.*, (2005), hep-ex/0507096.

[18] *BABAR*, B. Aubert *et al.*, Phys. Rev. **D74**, 031104 (2006), hep-ex/0605024.

[19] *BABAR*, B. Aubert *et al.*, Phys. Rev. Lett. **93**, 231804 (2004), hep-ex/0408017.

[20] Belle, K. F. Chen *et al.*, Phys. Rev. Lett. **94**, 221804 (2005), hep-ex/0503013.

[21] *BABAR*, B. Aubert *et al.*, Phys. Rev. **D74**, 051102 (2006), hep-ex/0605017.

[22] *BABAR*, B. Aubert *et al.*, Phys. Rev. Lett. **97**, 201801 (2006), hep-ex/0607057.

[23] Belle, K. Abe *et al.*, (2006), hep-ex/0608034.

[24] *BABAR*, B. Aubert *et al.*, Phys. Rev. Lett. **97**, 201802 (2006), hep-ex/0608005.

[25] *BABAR*, B. Aubert *et al.*, (2006), hep-ex/0607109.

[26] C.-W. Chiang *et al.*, Phys. Rev. **D69**, 034001 (2004), hep-ph/0307395.

[27] M. Beneke and M. Neubert, Nucl. Phys. **B675**, 333 (2003), hep-ph/0308039.

[28] X. Liu *et al.*, Phys. Rev. **D73**, 074002 (2006), hep-ph/0509362.

[29] *BABAR*, B. Aubert *et al.*, (2006), hep-ex/0608003.

[30] *BABAR*, B. Aubert *et al.*, (2006), hep-ex/0607106.

[31] *BABAR*, B. Aubert *et al.*, Phys. Rev. Lett. **97**, 171805 (2006), hep-ex/0608036.

[32] *BABAR*, B. Aubert *et al.*, (2006), hep-ex/0607096.

[33] Belle, K. Abe *et al.*, (2006), hep-ex/0609015.

[34] Belle, K. Abe *et al.*, Phys. Rev. Lett. **94**, 181803 (2005), hep-ex/0408101.

[35] Belle, K. Abe *et al.*, (2006), hep-ex/0608049.

[36] T. Gershon and M. Hazumi, Phys. Lett. **B596**, 163 (2004), hep-ph/0402097.

[37] *BABAR*, B. Aubert *et al.*, Phys. Rev. **D74**, 031105 (2006), hep-ex/0605008.

[38] Belle, K. Abe *et al.*, (2006), hep-ex/0609016.

Leptonic and Semileptonic *D*-Decays

Hanna Mahlke
Laboratory of Elementary-Particle Physics
Cornell University
Ithaca, NY 14853
USA

1 Introduction

The study of semileptonic and leptonic decays allows the determination of fundamental parameters of the Standard Model (SM), which are related to the elements of the Cabibbo-Kabayashi-Maskawa matrix. Examples of these processes are shown in Fig. 1.

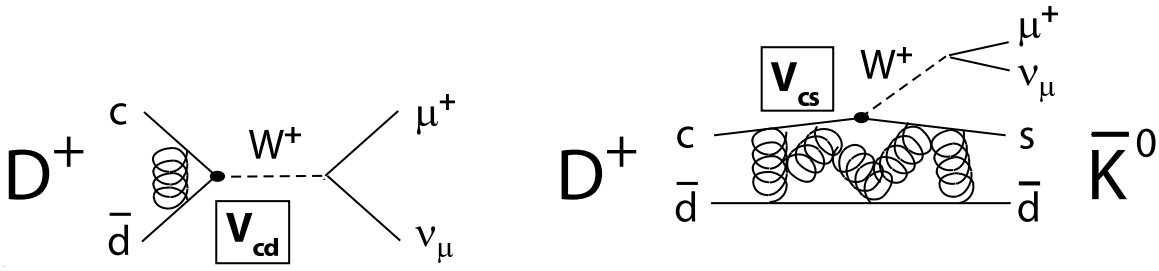

Figure 1: Diagrams for the reactions $D^+ \to \mu^+\nu_\mu$ and $D^+ \to \overline{K}^0\mu^+\nu_\mu$.

The strong interaction of the participating quarks introduces a complication because its effect is challenging to estimate accurately. Theory's difficulty in calculating phenomena rooted in strong physics seriously hamper some measurements related to weak physics in the B sector that need such input, for example extracting V_{ub} from semileptonic and leptonic B decays, or V_{td} from $B^0 - \overline{B^0}$ mixing. Theory tools have become available, but they require calibration or verification. The similarity of the charm and the bottom quark allow to test the same methods in D decay, where the quantities in question can be determined to excellent accuracy because the corresponding CKM matrix elements are well-constrained from other sources. In addition to being of interest in their own right, experimental charm results thus have a much larger impact on the field.

This presentation discusses leptonic and semileptonic D and D_s decays, where results from the BaBar, Belle, CLEO, and FOCUS collaborations are reported. The challenge in all these cases, aside from signal purity and background concerns in general, is to cleanly identify decays with neutrinos and to determine the kinematic properties of the undetected particle through external constraints.

The CLEO experiment benefits from the clean experimental environment that arises from running at or slightly above production threshold, $e^+e^- \to \psi(3770) \to D\overline{D}$ or $e^+e^- \to D_s^*\overline{D}_s \to \gamma D_s\overline{D}_s$. Identifying one of the $D_{[s]}$ by reconstructing its decay to a well-identified final state ("tagging") already guarantees a second $D_{[s]}$ in the event, which is then analyzed for a particular reaction. Because of the known final state in the first step, it is also possible to not require a tag, but to add all reconstructed tracks and showers to infer the neutrino momentum. Finally, and of particular importance, the experimental set-up also allows to count the number of produced decays accurately, thereby facilitating absolute normalization.

The B factories usually use the continuum process $e^+e^- \to c\overline{c}$ at center-of-mass energies near the $\Upsilon(4S)$. They obtain D mesons via the decay chain $D^* \to \pi_s D$, where π_s is a slow pion to mark the D flavor. It is possible to analyze both D^+ and D^0 in this way, but in practice, this method is mostly applied to $D^{*+} \to \pi_s^+ D^0$, which also has the most favorable branching fraction. Since determining the number of D decays produced in fragmentation is difficult, measurements are often performed relative to another $D_{[s]}$ decay mode. Tagging in this case means that the presence of one reconstructed D meson from $e^+e^- \to c\overline{c}$ does imply a second charm particle in the event (which then is the signal side). Even in the absence of a way to normalize the rate, it is still possible to compare the shape of kinematic distributions with theoretical predictions, for example form factor shapes (see below).

2 Leptonic Decays

Leptonic D decays proceed through annihilation of the constituent quarks into a W, followed by its decay into a lepton and the corresponding neutrino. The partial width for $\ell = e, \mu$, and τ is given by

$$\Gamma(D^+ \to \ell^+\nu_\ell) = \frac{1}{8\pi} G_F^2 f_D^2 m_\ell^2 M_D \left(1 - \frac{m_\ell^2}{M_D^2}\right)^2 |V_{cd}|^2, \quad (1)$$

where f_D is the D meson decay constant and m_ℓ and M_D are the lepton and D meson masses. G_F is the Fermi coupling constant. For D_s decay, the mass of the D_s, the decay constant of f_{D_s}, and V_{cs} are used instead. A similar formula applies for $B_{[s]}$ decays. The quantities determined in leptonic $D_{[s]}$ decays are the charm decay constant, given that the masses and the CKM elements are well-measured. The decay constant describes the strong interaction surrounding the annihilation process.

Experimental accuracy in the few-percent range is crucial to validate calculations of the decay constant in both the charm and the bottom sector. Further goals are: comparing the lepton species to put limits on physics beyond the Standard Model, and determining f_{D_s}/f_D, where some technical uncertainties cancel. The Standard Model predicts the following ratios for the production rate of $\tau : \mu : e$:

$$D \to \ell\nu_\ell : \quad 9.72 : 1 : 0.00002, \qquad D_s \to \ell\nu_\ell : \quad 2.65 : 1 : 0.00002. \tag{2}$$

In principle, it is possible to determine the decay constants from decays to all three lepton species. A few experimental considerations to take into account: $D^+_{[s]} \to e^+\nu_e$ is beyond current experimental reach (low branching fraction due to helicity suppression). $D^+_{[s]} \to \tau^+\nu_\tau$ is most copiously produced, but the observed rate is lowered, and the measurement complicated by, the subsequent decay of the τ, which involves at least one more neutrino. $D^+_{[s]} \to \mu^+\nu_\mu$ is therefore the experimentally accessible.

2.1 Leptonic D decays

CLEO studied the decay $D^+ \to \mu^+\nu_\mu$ in $281\,\mathrm{pb}^{-1}$ of $\psi(3770)$ data using the tagging technique [1]. The decay is identified with a single muon-like track on the signal side, and candidate events are required to have a missing mass squared near zero. The missing mass squared is calculated using the beam energy E_{beam}, the muon energy and momentum E_{μ^+} and p_{μ^+}, and the momentum p_D of the D: $MM^2 = (E_{\mathrm{beam}} - E_{\mu^+})^2 - (-p_{D^-} - p_{\mu^+})^2$, which for signal events corresponds to the neutrino mass. The signal distribution is shown in Fig. 2. Fifty signal candidates are found, with 2.8 background events (mostly D^+ decay to $\pi^+\pi^0$, $\tau^+(\to \pi^+\nu)$, and $K^0\pi^+$ tails from the well-separated peak at higher MM^2) expected. This allows measurement of the branching fraction $\mathcal{B}(D^+ \to \mu^+\nu_\mu) = (4.4 \pm 0.7 \pm 0.1) \times 10^{-4}$ and hence $f_D = (222.6 \pm 16.7^{+2.8}_{-3.4})\,\mathrm{MeV}$, with V_{cd} as an external input. With the SM ratios from Eqn. 2 applied to the measured branching fraction $\mathcal{B}(D^+ \to \mu^+\nu_\mu)$, one expects $\mathcal{B}(D^+ \to e^+\nu_e) \sim 1 \times 10^{-8}$ and $\mathcal{B}(D^+ \to \tau^+\nu_\tau) \sim 2 \times 10^{-3}$. Slight modification of the signal side selection criteria gives access to $\ell = e,\ \tau$, by asking for either an electron-like track (no events seen, $\mathcal{B}(D^+ \to e^+\nu_e) < 2.4 \times 10^{-5}$), or by asking for a pion track and a missing mass shifted away from zero, signalling the decay $\tau \to \pi\nu$ (no significant signal, $\mathcal{B}(D^+ \to \tau^+\nu_\tau) < 3.1 \times 10^{-3}$).

2.2 Leptonic D_s decays

Both BaBar and CLEO have recently studied leptonic D_s decays. BaBar bases their study on $230\,\mathrm{fb}^{-1}$ of data in the $\Upsilon(4S)$ region. They use kinematic constraints, require an identified D^0, D^+, D^{*+}, or D_s^+, and use the signal side decay chain $D_s^{*+} \to \gamma D_s^+$, $D_s^+ \to \mu^+\nu_\mu$ to provide a clean D_s sample [4] (extra particles may be present in

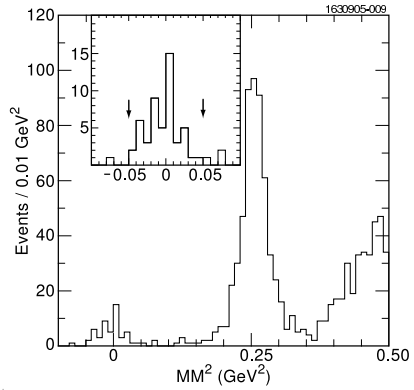

Figure 2: $D^+ \to \mu^+\nu_\mu$: reconstructed neutrino mass for signal events [1].

the event). The neutrino momentum is inferred from all other measured reaction products. The signal distribution is the $D_s^*-D_s$ mass difference $m(\gamma\mu^+\nu_\mu)-m(\mu^+\nu_\mu)$, shown in Fig. 3. Since the D_s^* production rate is not precisely known, BaBar determine the ratio relative to $D_s^+ \to (K^+K^-)\pi^+$ with $m(K^+K^-)$ in the ϕ mass region ($\pm 2\Gamma_\phi$), $\Gamma(D_s^+ \to \mu^+\nu_\mu)/\Gamma(D_s^+ \to \phi\pi^+)$. With $\mathcal{B}(D_s^+ \to \phi\pi^+) = (4.71 \pm 0.46)\%$ [5] they arrive at $\mathcal{B}(D_s^+ \to \mu^+\nu_\mu) = (6.74 \pm 0.83 \pm 0.26 \pm 0.66) \times 10^{-3}$, where the third error is due to the normalization uncertainty. This leads to $f_{D_s} = (283 \pm 17 \pm 7 \pm 14)\,\mathrm{MeV}$.

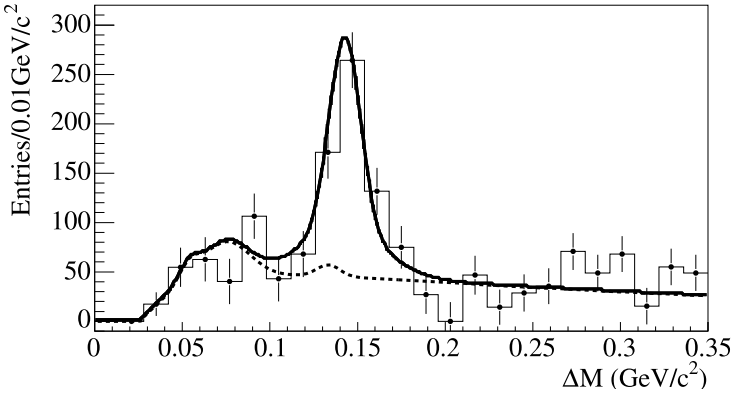

Figure 3: BaBar's signal distribution $\Delta M = m(\gamma\mu^+\nu_\mu) - m(\mu^+\nu_\mu)$ for the decay $D_s^+ \to \mu^+\nu_\mu$ detected in $D_s^* \to \gamma D_s$ [4]. The structure at $\Delta M \sim 0.07\,\mathrm{MeV}/c^2$ is due to the decay $D_s^* \to \pi^0 D_s$; the peak underneath the signal in the background shape is due to $D_s^+ \to \tau\nu_\tau$.

CLEO's analysis relies on $\sim 200\,\mathrm{pb}^{-1}$ of data taken at a center-of-mass energy of 4170 MeV. The decay chain is $e^+e^- \to D_s^*\overline{D}_s \to (\gamma D_s)\overline{D}_s$. One D_s is tagged, the

other is analyzed for the signal decay. Two strategies are used.

A. As above, the missing mass squared is examined to identify the signal. The lone signal side track is required to not be an electron but instead to be muonic or pionic. An energy requirement of 300 MeV accepts 99% of all muon tracks and 60% of all pion tracks. We distinguish cases with an energy deposition below 300 MeV in the calorimeter (typical for $D_s^+ \to \mu^+\nu_\mu$, but possible for $\tau \to \pi\nu_\tau$) from those that have above 300 MeV (in which case the track is likely to be a pion from $\tau \to \pi\nu_\tau$). The data show a clear enhancement in the expected $D_s^+ \to \mu^+\nu_\mu$ signal region. The $D_s^+ \to \tau\nu_\tau$ events are more spread out due to the presence of the additional, unreconstructed, neutrino, but signal events are seen as well. The signatures for $\ell = \mu$ and τ overlap, hence the summed distribution is fit for the two branching fractions, where the SM ratio for the two is assumed. CLEO's preliminary result, combining the two, is $\mathcal{B}(D_s^+ \to \mu^+\nu_\mu) = (0.664 \pm 0.076 \pm 0.028)$, or $f_{D_s} = (282 \pm 16 \pm 7)$ MeV. If the track is required to be consistent with an electron, no candidates are found, resulting in an upper limit of $\mathcal{B}(D_s^+ \to e^+\nu_e) < 3.1 \times 10^{-4}$.

B. The second approach, based on the same data, uses the decay chain $\tau \to e\overline{\nu}_e\nu_\tau$. Its product with the $D_s^+ \to \tau^+\nu_\tau$ branching fraction ($\sim 6-7\%$) is about 1.3%, to be compared with the inclusive semileptonic branching ratio $D_s^+ \to Xe^+\nu_e \sim 8\%$. The analysis procedure demands a sole electron-like track on the signal side, and limits the energy not associated with the other identified decay products in the calorimeter to be less than 400 MeV. No additional energy deposition is expected for signal events other than the transition photon from $D_s^*\overline{D}_s \to (\gamma D_s)\overline{D}_s$, upon which no selection requirements are placed, and showers resulting from interactions of the decay products of the tag side with the detector material. The signal distribution, together with background estimates from Monte Carlo simulations, is presented in Fig. 4. This analysis leads to $\mathcal{B}(D_s^+ \to \tau^+\nu_\tau) = (6.3 \pm 0.8 \pm 0.5)\%$ and $f_{D_s} = (278 \pm 17 \pm 12)$ MeV (both preliminary). Since the two measurements are complementary, one can form the average $f_{D_s} = (280 \pm 12 \pm 6)$ MeV and also use them to measure the ratio $\mathcal{B}(D_s^+ \to \tau^+\nu_\tau) : \mathcal{B}(D_s^+ \to \mu^+\nu_\mu) = (9.9 \pm 1.9)$, consistent with the SM expectation of 9.72.

2.3 Leptonic Decays: Summary

A visual comparison of current experimental and theoretical progress on the decay constants is given in Fig. 5. In summary: f_D from $D^+ \to \mu^+\nu_\mu$ is measured to a total relative error of 8%; the decays to e and τ are presently not experimentally accessible, although the current upper limit gives rise to the hope that a signal will soon be within reach for τ. The decay constant f_{D_s} has been measured in $D_s^+ \to \mu^+\nu_\mu$ (BaBar, CLEO) and $D_s^+ \to \tau^+\nu_\tau$ (CLEO) to an accuracy of 5-8%. The precision of theoretical calculations are in this region as well. However, the dominant experimental uncertainty is still statistical, which is – in principle – much easier to improve upon than systematic errors such as those theory is in the process of overcoming.

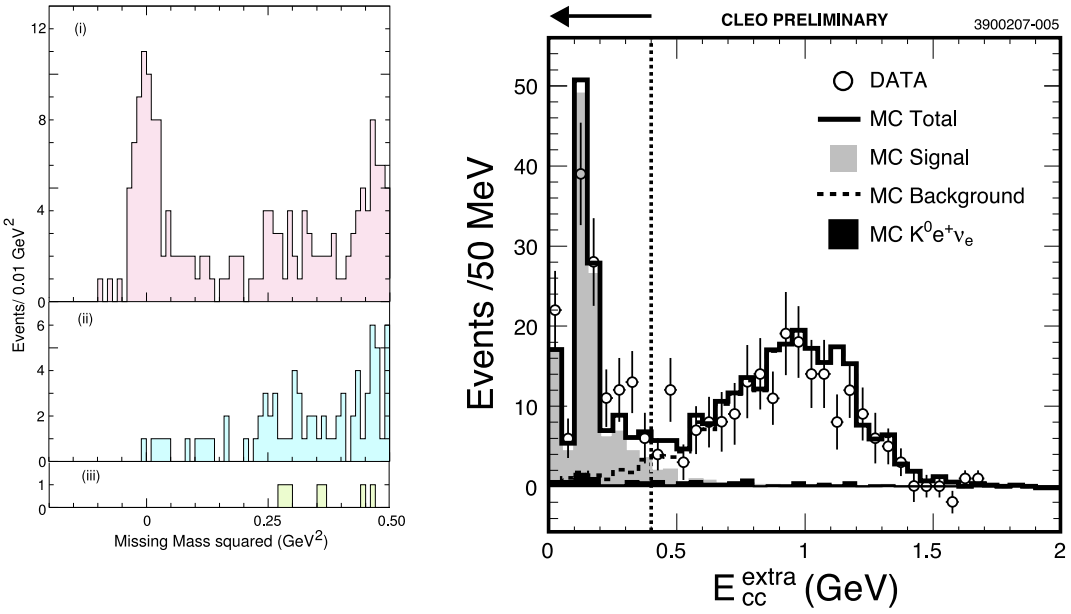

Figure 4: CLEO data on leptonic D_s decays (preliminary). Left: Missing-mass-squared distributions from data corresponding to (i) $D_s^+ \to \mu^+\nu_\mu + \tau^+\nu_\tau$, (ii) $D_s^+ \to \tau^+\nu_\tau$, (iii) $D_s^+ \to e\nu_e$. Right: $D_s^+ \to \tau^+\nu_\tau$: Energy deposited in the calorimeter for tagged D_s events and a single electron-like track on the signal side *not* accounted for by the tag or the electron candidate. The circles are data; the curves are MC predictions for signal as well as several semileptonic background sources.

3 Semileptonic Decays

Semileptonic decays $D \to h\ell\nu_\ell$ provide yet another scenario within which to study the impact of strong force. The underlying weak process at the quark level, for instance $c \to W^*q$ with $W^* \to e\nu$, can be calculated, but the observed rate is modified by the QCD interaction between the participant as well as the spectator quarks, which clouds the simple picture.

3.1 Branching fractions

The current experimental uncertainty on the $D \to K, \pi e\nu$ branching fractions is in the percent regime, thereby posing a challenge to the precision of the LQCD predictions [12].

The search is on for rarer modes, and CLEO have improved considerably upon previously achieved accuracy in many modes (Table 1). $D^+ \to \eta e^+\nu$ has been observed for the first time ($> 5\sigma$), as has the first multi-body semileptonic decay: $D^0 \to$

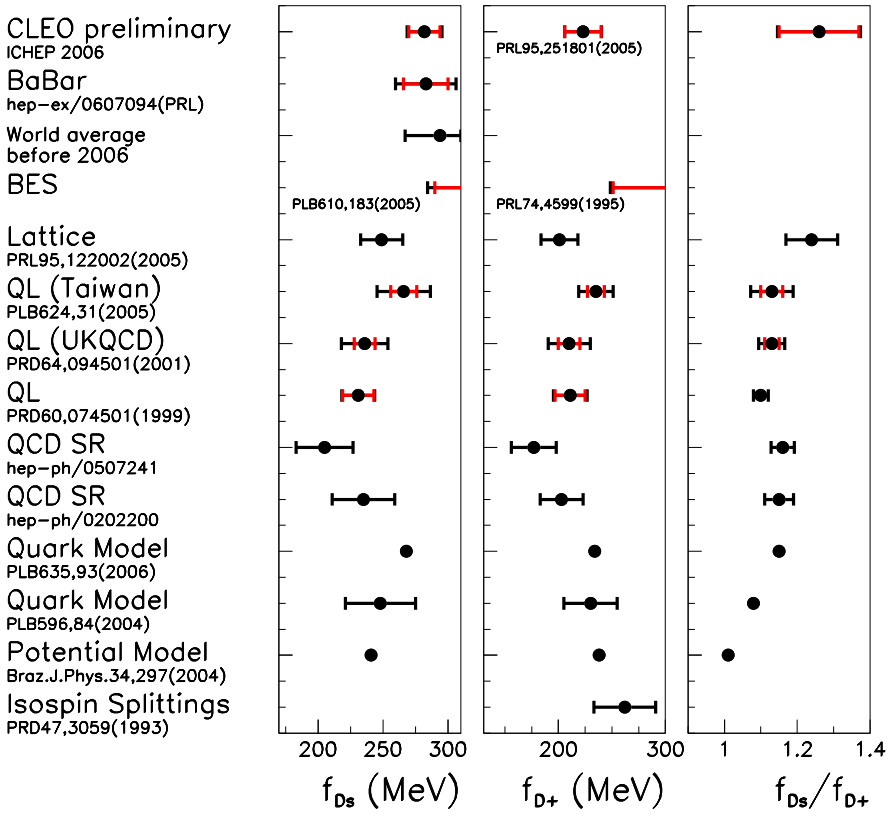

Figure 5: Recent experimental and theoretical results on f_D and f_{D_s}.

$K^-\pi^+\pi^-e^+\nu_e$ ($> 4\sigma$), which is found to mostly proceed via $K_1(1270)^- \to K^-\pi^+\pi^-$. The uncertainties on $D^+ \to \omega e^+\nu$ branching fraction have been halved, and the upper limits on the branching fractions $D^+ \to \eta', \phi e^+\nu$ have been tightened by two orders of magnitude. Once an $\eta' e\nu_e$ signal is observed this will allow a comparison with predictions for the ratio $D \to \eta : D \to \eta'$.

3.2 Form factors

Decay to a pseudoscalar

The dynamics of semileptonic $D \to h\ell\nu_\ell$ decays can for the case of a pseudoscalar hadron in the final state in the limit of small lepton masses be described as follows:

$$\frac{d\Gamma}{dq^2} \propto \left|f_+^h(q^2)\right|^2 \times p_h^3 \times |V_{cq}|^2, \tag{3}$$

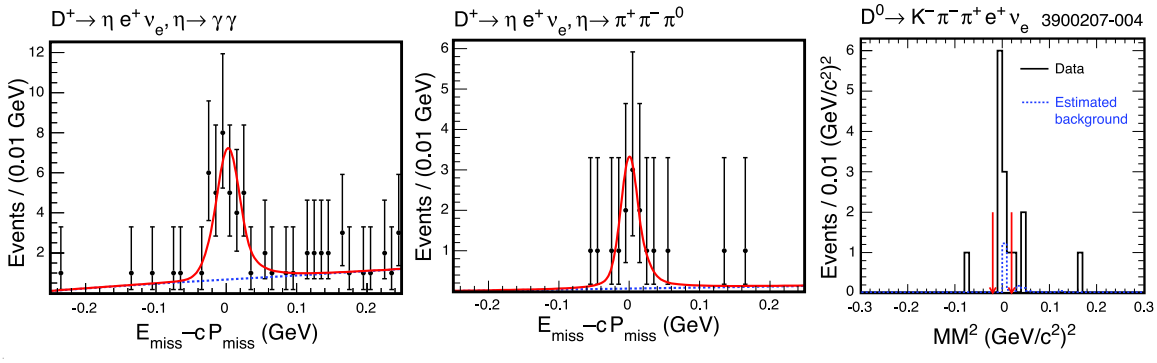

Figure 6: Preliminary CLEO results: Signal distributions for $D^+ \to \eta e^+ \nu$ for $\eta \to \gamma\gamma$ (left) and $\eta \to \pi^+\pi^-\pi^0$ (middle); $D^0 \to K^-\pi^+\pi^- e^+\nu$.

where q^2 is the momentum transfer to the W^*, $f_+^h(q^2)$ is the form factor function describing the probability to end up with a hadron of type h in the final state for a given q^2, p_h is the momentum of the outgoing hadron, and V_{cq} is the appropriate CKM matrix element.

Theoretical predictions for the form factor shape can be tested against the q^2 distribution in data, corrected for the q^2-dependent detection efficiency. This is detailed further below. The normalization is determined by the product $|V_{cq}| \times f_+(0)$. Due to the precision with which V_{cs} and V_{cd} are determined in other experiments $(2-4\%)$, a measurement of $|V_{cq}| \times f_+(0)$ determines $f_+(0)$.

Examples of form factor determinations are displayed in Fig. 7. The simplest reasonable parametrization of the pseudoscalar form factor is the single pole shape, $\sim 1/(1 - q^2/M^2_{\rm pole})$ [10], where the nominal setting of the parameter is $M_{\rm pole} = M(D_s^*)[M(D^*)]$ for $h = K[\pi]$. More sophisticated models are the modified pole model,

$$f_+^h(q^2) = \frac{f_+^h(0)}{(1 - \alpha q^2/M^2_{\rm pole}) \times (1 - q^2/M^2_{\rm pole})}, \qquad (4)$$

or, recently, the Hill series parametrization [11]. BaBar [13], Belle [15], CLEO [6], and FOCUS [14] compare their various results for $D \to \pi, K\ell\nu$ data for $D = D^{+,0}$ with the models and find reasonable agreement with all of them. In particular the Belle and CLEO measurements boast superb statistics and an excellent q^2 resolution. In general it is found that unquenched LQCD predicts the form factor shape a little too high especially for $D \to \pi$ [6, 15], but has achieved useful uncertainty, as visually evident from the agreement between the data points and the curve obtained from an interpolation between LQCD predictions at several q^2 points, Fig. 7. Fitting the predicted LQCD data points to the modified pole model shape, thereby extracting $f_+(0)$ and α, allows a comparison within this model between theory and the experiments.

This is presented for $f_+(0)$ in Fig. 8.

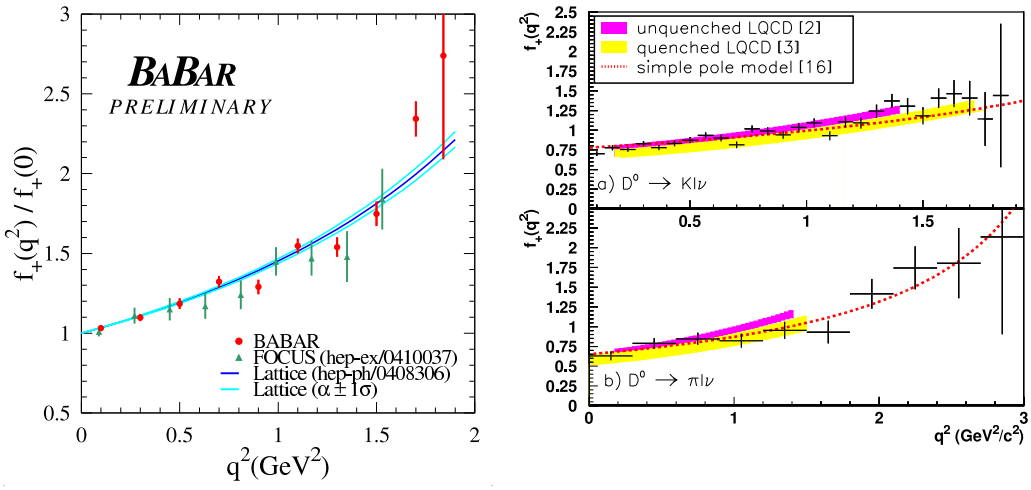

Figure 7: Form factor shapes. Left (from Ref. [13]): BaBar ($D \to Ke\nu_e$, points) and FOCUS [14] (triangles, $D \to K\mu\nu_\mu$) data and an unquenched LQCD calculation [12] (band). Right (from Ref. [15]): Belle results on $D \to K$ (top) and $D \to \pi$ (bottom), with unquenched [12] and quenched [16] LQCD predictions overlaid.

Alternatively, using $f_+^{D\to\pi} = 0.64 \pm 0.03 \pm 0.06$ and $f_+^{D\to K} = 0.73 \pm 0.03 \pm 0.07$ from LQCD [12], the CKM matrix elements are found to be in good agreement with current world averages. However, the uncertainties ($\sim 10\%$ relative) on the form factor magnitudes dominate. This constitutes a check of the LQCD calculation.

Decay to a vector

For a vector hadron in the final state, such as $D \to K^* e\nu$ (Cabibbo-favored) or $D \to \rho e\nu$ (Cabibbo-suppressed), more form factor functions enter the stage. The decay amplitude can be described in a parameter-free way using helicity basis form factors as specified in Ref. [17]. However, the helicity form factors are hard to calculate; a more traditional approach is to just assume spectroscopic pole dominance and cast the expression for the amplitude into linear combinations of the following functions:

$$A_i(q^2) = \frac{A_i(0)}{1 - q^2/M_{A_i}^2}(i = 1, 2), V(q^2) = \frac{V(0)}{1 - q^2/M_V^2}. \quad (5)$$

The pole masses are often fixed to be $M_V = 2.1\,\text{GeV}$, $M_{A_{1,2}} = 2.5\,\text{GeV}$. If one then defines $R_V = V(0)/A_1(0)$ and $R_2 = A_2(0)/A_1(0)$, one ends up with only two free parameters, albeit at the expense of an assumed shape. The parameter-free approach in Ref. [17] circumvents this.

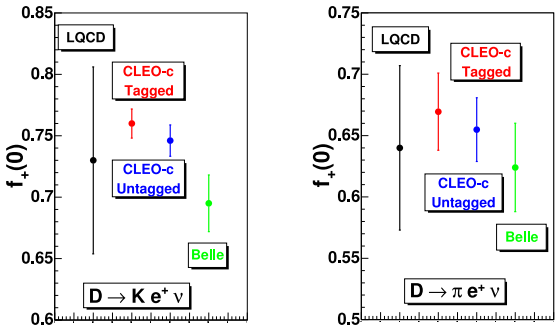

Figure 8: Comparison of form factor normalization for $D \to K$ and $D \to \pi$ obtained by unquenched LQCD [12], two CLEO [6] analyses, and Belle [15].

An analysis of $D^+ \to K^-\pi^+e^+\nu$ CLEO data uses a projective weighting technique, by which the expected shapes from helicity form factor contributions are fit to the data, thereby extracting the (bin-wise) amplitude for each of the form factors [18]. When the spectroscopic form factors as given in Eqn. 5, translated into helicity form factors, are overlaid, good agreement is found (Fig. 9). Additional conclusions are that a term describing interference with a non-resonant s-wave $K\pi$ component is necessary, and that no evidence is found for d- or f-wave contributions.

A recent preliminary study by BaBar [19] of $D_s^+ \to \phi e^+\nu$, using about 13×10^3 signal events in $78.5\,\mathrm{pb}^{-1}$, not only exhibits a beautifully precise measurement but also confirms an earlier FOCUS result. This actually resolves a controversy: The ratios R_V and R_2 for $D^+ \to K^*e^+\nu$ and $D_s^+ \to \phi e^+\nu$ are expected to be similar because the CKM matrix element involved is V_{cs} in both cases, and the only remaining difference is then the spectator quark flavor ($\overline{d}$ *vs.* $\overline{s}$). Agreement within 10% is expected. This was not borne out by earlier data, which was not inconsistent for R_V but disagreed for R_2, except for a FOCUS measurement [20] that had R_2^ϕ in agreement with the world average of $R_2^{K^*}$.

CLEO has presented preliminary results for the first Cabibbo-suppressed pseudoscalar $\to$ vector form factor measurement, $D \to \rho e\nu$. A clear signal for both isospin states is observed, making it possible to bin in kinematic distributions. The branching fractions from the $281\,\mathrm{pb}^{-1}$ data sample are found to be in good agreement with previous results (which are dominated by the CLEO-c results from the $56\,\mathrm{pb}^{-1}$ sample, see Table 1), as is the partial width $D^0 \to \rho^- e^+\nu = (0.41 \pm 0.03 \pm 0.02) \times 10^{-2}$. A simulatenous fit to $D^+ \to \rho^0 e^+\nu_e$ and $D^0 \to \rho^- e^+\nu_e$ (linked through isospin) results in the following determinations: $R_V^\rho = 1.40 \pm 0.25 \pm 0.03$, $R_2^\rho = 0.57 \pm 0.18 \pm 0.06$.

$D \to \rho e\nu$ and $D \to K^*e\nu$ studies are important to the B sector for example by aiding in the extraction of $|V_{ub}|^2/|V_{ts}|^2$ through $d\Gamma(B \to \rho e\nu) : d\Gamma(B \to K^*\ell\ell)$ [9],

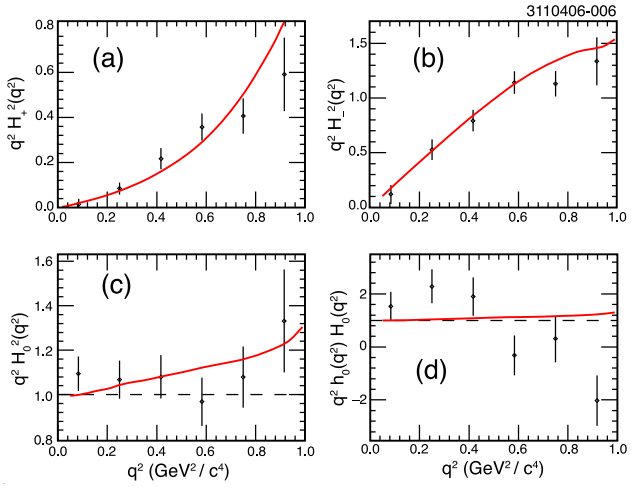

Figure 9: $D \to K\pi e\nu$ [18]: Four parameter-free helicity-basis form factor products as extracted in CLEO data, overlaid with form factors constructed from spectroscopic pole model shapes using $R_0 = 1.505$, $R_2 = 0.875$, and s-wave parameters $\mathcal{A} = 0.33$ and $\delta = 39°$.

which requires either measurement of the $B \to \rho$ and $B \to K^*$ form factors or a calculation validated by the corresponding D decays.

3.3 Inclusive semileptonic decays

CLEO has determined the semileptonic inclusive branching fraction $D \to Xe^+\nu_e$ for both charged and neutral D mesons [21]. The measured branching fractions $\mathcal{B}(D^0 \to Xe^+\nu_e) = (6.46 \pm 0.17 \pm 0.13)\%$, $\mathcal{B}(D^+ \to Xe^+\nu_e) = (16.13 \pm 0.20 \pm 0.33)\%$ agree well with the sum of all exclusive modes, although there is room for as-yet-unobserved exclusive decays at the level of $\mathcal{B} \sim 10^{-3}$. Isospin symmetry is observed within errors for the inclusive semileptonic partial widths, $\Gamma_{D^+}/\Gamma_{D^0} = 0.985 \pm 0.028 \pm 0.015$.

Aside from the branching fraction, a quantity of interest is the electron momentum spectrum. Without weak annihilation contributions ($D^+ \to gW^+ \to Xe^+\nu$) agreement between the spectra from D^+ and D^0 is expected. Weak annihilation would modify the upper end of the electron spectrum. Within uncertainties, the D^0 and D^+ distributions agree (Fig. 11).

3.4 Semileptonic decays: Summary

Many new results on D branching fractions and $D \to P, V$ and $D_s \to V$ form factors have become available. Of particular interest are the shape and the normalization of the form factor functions. Experimental accuracy is at present still consistent with

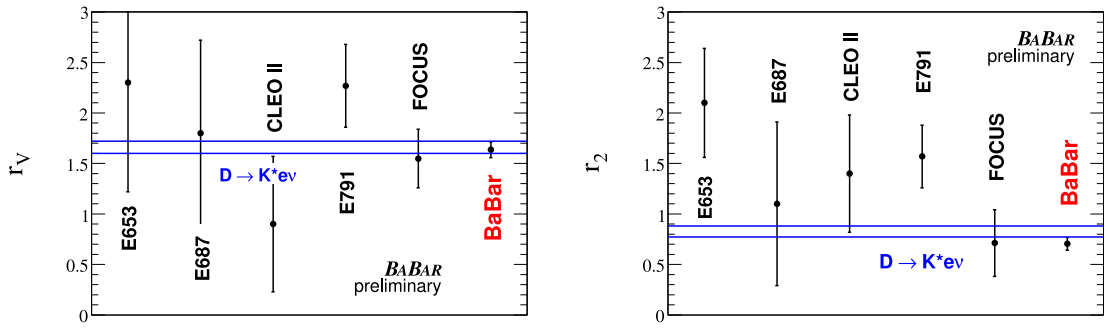

Figure 10: Comparison of form factor parameters R_2 (left) and R_V (right) for $D \to K^*$ and $D_s \to \phi$ semileptonic decays, from Ref. [19]. The data points all represent $D_s \to \phi$ analyses. The lines give the $\pm 1\sigma$ band for an average of experimental $D \to K^*$ results.

most calculations on the market; this may change as the experimental and theoretical uncertainties decrease.

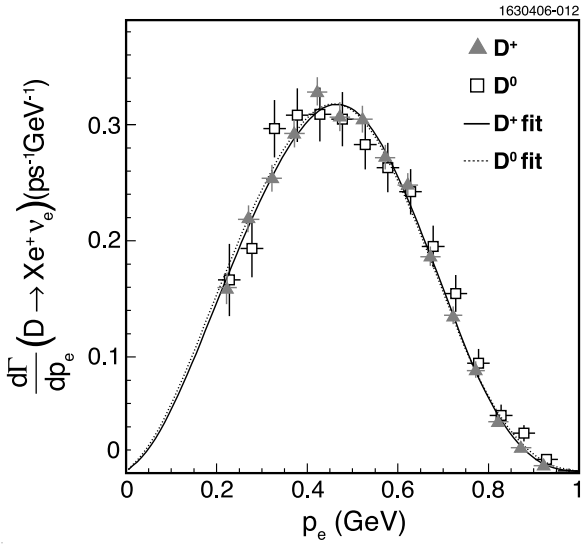

Figure 11: Electron momentum spectrum in $D \to Xe^+\nu_e$ for charged and neutral D mesons [21].

4 Conclusions

Precise results in the D sector have improved our comprehension of the QCD effects accompanying weak interactions and allowed to sharpen theoretical tools. Thanks to the similarity of the heavy quarks c and b, common calculation techniques can be applied to the estimation of D and B decay properties. Further progress in the D sector and consequently the B sector is in sight as data samples with modern detectors are being enlarged.

5 Acknowledgements

I would like to thank the conference organizers for an enjoyable conference at a exceptionally interesting venue. I am further indebted to many of my colleagues on CLEO, BaBar, Belle and FOCUS for helpful discussions. This work was supported by the US National Science Foundation under cooperative agreement PHY-0202078.

Decay	result (10^{-2})	PDG06 (10^{-2})	PDG04 (10^{-2})
$D^+ \to \overline{K}^0 \ell^+ \nu$	T: $8.86 \pm 0.17 \pm 0.20$	8.9 ± 0.4	6.8 ± 0.8
	U: $8.75 \pm 0.13 \pm 0.30$		
$D^0 \to K^- \ell^+ \nu$	T: $3.58 \pm 0.05 \pm 0.05$	3.41 ± 0.09	3.43 ± 0.14
	U: $3.56 \pm 0.03 \pm 0.11$		
	Belle: $3.45 \pm 0.07 \pm 0.20$		
$D^+ \to \pi^0 \ell^+ \nu$	T: $0.397 \pm 0.027 \pm 0.028$	0.44 ± 0.07	0.31 ± 0.15
	U: $0.383 \pm 0.025 \pm 0.016$		
$D^0 \to \pi^+ \ell^+ \nu$	T: $0.309 \pm 0.012 \pm 0.006$	0.27 ± 0.02	0.36 ± 0.06
	U: $0.301 \pm 0.011 \pm 0.010$		
	Belle: $0.255 \pm 0.019 \pm 0.016$		
$D^+ \to \rho^0 \ell \nu$	T: $0.232 \pm 0.020 \pm 0.012$	0.24 ± 0.04	0.31 ± 0.06
$D^0 \to \rho^+ \ell \nu$	T: $0.156 \pm 0.016 \pm 0.009$	0.19 ± 0.04	–
Decay	CLEO result (10^{-4})	PDG06 (10^{-4})	PDG04 (10^{-4})
$D^+ \to \omega \ell^+ \nu$	$14.9 \pm 2.7 \pm 0.5$	16^{+7}_{-6}	–
$D^+ \to \phi \ell^+ \nu$	< 2 (90% CL)	< 209	< 209
$D^+ \to \eta \ell^+ \nu$	$12.9 \pm 1.9 \pm 0.7$	< 70	< 50
$D^+ \to \eta' \ell^+ \nu$	< 3 (90% CL)	< 110	< 110
$D^0 \to K^- \pi^+ \pi^- \ell^+ \nu$	$2.9^{+1.9}_{-1.0} \pm 0.5$	< 12	< 12
$D^0 \to K_1(1270) \ell^+ \nu$	$2.2^{+1.4}_{-1.0} \pm 0.2$	–	–

Table 1: CLEO's preliminary [6] and Belle's published [15] measurements for D semileptonic branching fractions, and comparison with PDG06 [7] as well as PDG04 [8]. The PDG06 results include CLEO's published numbers based on $56\,\mathrm{pb}^{-1}$ of data taken at the $\psi(3770)$. "T" and "U" stand for CLEO's "tagged" and "untagged" analyses, respectively, and the corresponding entries are not to be averaged because of sample overlap. CLEO's results are all obtained with $\ell = e$, Belle's with $\ell = e$ or μ, and the PDG numbers are averaged over e and μ, where available.

Bibliography

[1] M. Artuso *et al.* [CLEO Collaboration], Phys. Rev. Lett. **95**, 251801 (2005) [arXiv:hep-ex/0508057].

[2] P. Rubin *et al.* [CLEO Collaboration], Phys. Rev. D **73**, 112005 (2006) [arXiv:hep-ex/0604043].

[3] S. Stone (CLEO Collaboration), contributed to the *33rd International Conference on High-Energy Physics (ICHEP06)*, Moscow, Russia, July 28 - August 2, 2006, arXiv:hep-ex/0610026.

[4] B. Aubert *et al.* [BABAR Collaboration], arXiv:hep-ex/0607094 (submitted to Phys. Rev. Lett.).

[5] B. Aubert *et al.* [BaBar Collaboration], Phys. Rev. D **71**, 091104 (2005) [arXiv:hep-ex/0502041]; B. Aubert *et al.* [BABAR Collaboration], Phys. Rev. D **74**, 031103 (2006) [arXiv:hep-ex/0605036].

[6] Y. Gao [CLEO Collaboration], contributed to the *33rd International Conference on High-Energy Physics (ICHEP06)*, Moscow, Russia, July 28 - August 2, 2006.

[7] W. M. Yao *et al.* [Particle Data Group], J. Phys. G **33**, 1 (2006).

[8] S. Eidelman *et al.* [Particle Data Group], Phys. Lett. B **592**, 1 (2004).

[9] B. Grinstein and D. Pirjol, Phys. Lett. B **549**, 314 (2002) [arXiv:hep-ph/0209211].

[10] See *e.g.* P. L. Frabetti *et al.* [E687 Collaboration], Phys. Lett. B **364**, 127 (1995).

[11] T. Becher and R. J. Hill, Phys. Lett. B **633**, 61 (2006) [arXiv:hep-ph/0509090].

[12] C. Aubin *et al.*, Phys. Rev. Lett. **95**, 122002 (2005) [arXiv:hep-lat/0506030].

[13] B. Aubert *et al.* [BABAR Collaboration], contributed to the *33rd International Conference on High-Energy Physics (ICHEP06)*, Moscow, Russia, July 28 - August 2, 2006, arXiv:hep-ex/0607077.

[14] J. M. Link *et al.* [FOCUS Collaboration], Phys. Lett. B **607**, 233 (2005) [arXiv:hep-ex/0410037].

[15] L. Widhalm *et al.*, Phys. Rev. Lett. **97**, 061804 (2006) [arXiv:hep-ex/0604049].

[16] A. Abada, D. Becirevic, P. Boucaud, J. P. Leroy, V. Lubicz and F. Mescia, Nucl. Phys. B **619**, 565 (2001) [arXiv:hep-lat/0011065].

[17] J. M. Link *et al.* [FOCUS Collaboration], Phys. Lett. B **633**, 183 (2006) [arXiv:hep-ex/0509027].

[18] M. R. Shepherd *et al.* [CLEO Collaboration], Phys. Rev. D **74**, 052001 (2006) [arXiv:hep-ex/0606010].

[19] B. Aubert *et al.* [BABAR Collaboration], contributed to the *33rd International Conference on High-Energy Physics (ICHEP06)*, Moscow, Russia, July 28 - August 2, 2006, arXiv:hep-ex/0607085.

[20] J. M. Link *et al.* [FOCUS Collaboration], Phys. Lett. B **586**, 183 (2004) [arXiv:hep-ex/0401001].

[21] N.E. Adam *et al.* [CLEO Collaboration], Phys. Rev. Lett. **97**, 251801 (2006) [arXiv:hep-ex/0604044].

Review of Exclusive $B \to D^{(*,**)}l\nu$ Decays – Branching Fractions, Form-factors and $|V_{cb}|$

A. E. Snyder
Stanford Linear Accelerator Center (SLAC)
Menlo Park, CA, USA 94041

1 Introduction

This paper reviews semileptonic decays of B-mesons to states containing charm mesons, *i.e.*, D, D^*, D^{**} and possible non-resonant $D^{(*)}n\pi$ states as well. The paper covers measurement of branching fractions, form-factors and, most importantly, the magnitude of the CKM matrix element V_{cb}.

I will not attempt a comprehensive review, but will concentrate on reasonably fresh results and consider mostly exclusive measurements. I will also comment on the consistency of the results and what needs to be done to resolve the apparent conflicts.

2 Physics and motivation

At the parton level (see Figure 1) the decay rate is simply related to $|V_{cb}|$ by

$$\Gamma = \frac{G_F^2}{192\pi^3} m_b^5 |V_{cb}|^2 \tag{1}$$

at tree level. A slightly more complicated formula applies if higher order QCD (loop corrections) are considered [1]. It's still thought to be theoretical clean at the parton level, but the parton level process cannot be measured.

Experiment can only measure at the hadron level. There are two general approaches to measuring the decay rate: inclusive measurements in which one sums over the possible final states X_c and exclusive in which one selects a particular state, such as $X_c = D^{*+}$. In the latter case one has to account for the probability (represented by form-factors) that the c-quark and the spectator quark combine to form the selected final state particle. The form-factors depend on the momentum transfer $q^2 = (P_l + P_\nu)^2$ and the formula that relates the decay rate to $|V_{cb}|$ depends on the final state selected.

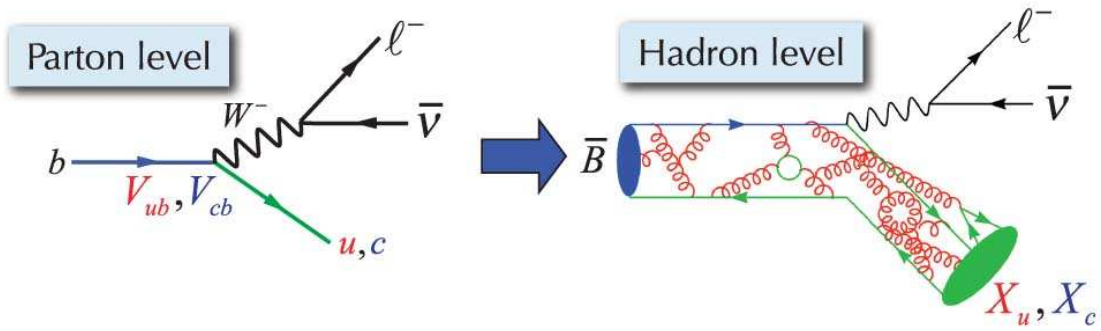

Figure 1: Parton level and hadronic level diagrams for semi-leptonic B decay.

3 $B \to Dl\nu$

The decay rate for $B \to Dl\nu$ is given by

$$\frac{d\Gamma}{dw} = \frac{G_F^2}{48\pi^3}|V_{cb}|^2(m_B + m_D)^2 m_D^3 (w^2-1)^{\frac{3}{2}}\mathcal{F}_D^2(w) \tag{2}$$

where the convention is to use

$$w = \frac{m_B^2 + m_D^2 - q^2}{2m_B m_D} = \frac{E_D^*}{m_D} \tag{3}$$

instead of q^2 and $\mathcal{F}_\mathcal{D}$ is the form-factor. Because this is $0^- \to 0^-$ transition only one form-factor is needed.

In the heavy quark symmetry (HQS) limit (*i.e.* for infinite c- and b-quark masses) $\mathcal{F}_\mathcal{D}(w=1) = 1$. However, as quarks are not infinitely heavy, a correction is needed. Lattice QCD calculations of Hashimoto and collaborators finds $\mathcal{F}_\mathcal{D}(w=1) = 1.069 \pm 0.026$ [2]. Because $\mathcal{F}_\mathcal{D}(1)$ may change as theory matures, it is common practice to give the experimentally measured quantity $\mathcal{F}_\mathcal{D}(1) \times |V_{cb}|$.

To extrapolate to $w = 1$ (or equivalently integrate over the full w range with normalization at $w = 1$ imposed) the shape of $\mathcal{F}_\mathcal{D}(w)$ is also needed. In principle this could be measured, but the rate at $w = 1$ vanishes, so some theoretical input that constrains the form-factor shape has to be deployed.

The most popular (though not the first) $\mathcal{F}_\mathcal{D}$ parameterization is that of Caprini, Lelloch and Neubert (CLN) [3] based on Heavy Quark Effective Theory (HQET) and using dispersion relations to constrain the parameterization. The CLN parametrization for $\mathcal{F}_\mathcal{D}(w)$ is

$$\mathcal{F}_D(w) = \mathcal{F}_\mathcal{D}(1) \times (1 - 8\rho^2 z + (51\rho^2 - 10)z^2 + (252\rho^2 - 84)z^3 \tag{4}$$

where $z \equiv (\sqrt{w+1} - \sqrt{2})/(\sqrt{w+1} + \sqrt{2})$ is an improved expansion variable (that converges faster than $w-1$).

Some other parameterizations are provide by Boyd, Grinstein and Lebid (BGL) [4] and LeyYaonac, Oliver and Raynal (LeYor) [5].

In all these parameterizations we are left with only one parameter to fit – ρ^2 – which is the derivative of $\mathcal{F}_{\mathcal{D}}(w)$ *w.r.t.* w at $w = 1$.

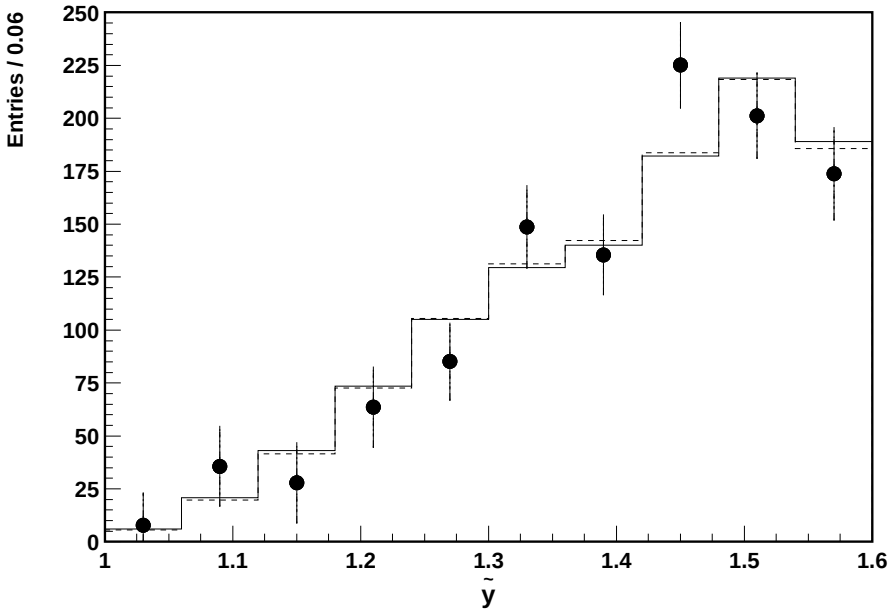

Figure 2: Background subtracted w-distribution (called $\hat{y}$ here) as measured by BELLE. Points are data and histograms are fits.

The $D \to Dl\nu$ analysis has been carried out by the CLEO [6] and BELLE [7] collaborations. CLEO used both $\overline{B}^- \to D^0 l^- \overline{\nu}$ and $B^- \to D^+ l^- \overline{\nu}$ modes, while BELLE only used the $B^- \to D^+ l^- \overline{\nu}$. Figure 2 shows the background subtracted w-distribution obtained by BELLE (note in BELLE's notation w is called $\hat{y}$). The signal is extracted using the discriminating variable $cos\theta_{BY}$ defined and described in detail in section 4.

They fit by minimizing χ^2 given by

$$\chi^2 = \sum_i \left(\frac{N_i^{obs} - \sum_j \varepsilon_{ij} N_j(N, \rho^2)}{\sigma_i} \right)^2 \tag{5}$$

where N_j is the number predicted based on Eq.(2) and ε_{ij} is the efficiency for an event truly in bin i to be detected in bin j. The errors σ_i includes both the uncertainty in the observation and the uncertainty in the efficiency matrix ε_{ij}

Exp	$\mathcal{B}(B^- \to D^0 l^- \overline{\nu})(\%)$	ρ^2(CLN)	$\mathcal{F}(1) \times \lvert V_{cb}\rvert(10^{-3})$
CLEO	$2.21 \pm 0.13 \pm 0.19$	1.27 ± 0.25	$44.8 \pm 5.8 \pm 3.$
BELLE	$2.13 \pm 0.12 \pm 0.39$	1.12 ± 0.22	$41.1 \pm 4.4 \pm 5.1$
HFAG	2.12 ± 0.20	1.17 ± 0.18	42.4 ± 4.5

Table 1: CLEO and BELLE results for branching fraction, ρ^2 and $|V_{cb}|$ and HFAG averages

The fit parameters are the number of events N and the slope parameter ρ^2. The fit using the CLN parameterization (Eq.(4)) is shown as solid histogram in the figure. The dashed histogram represents the result when a simple linear parameterization is used instead of CLN. The two fits are not distinguishable.

CLEO does something similar. The results of both experiments is given table 1 along with the HFAG averages[1] as of summer 2006.

The BELLE and CLEO results are consistent. The uncertainties are large and BELLE assigns a more conservative systematic than CLEO.

4 $B \to D^* l\nu$

The analysis of $B \to D^* l\nu$ is more complex than $Dl\nu$. There are three form-factors called A_1, A_2 and V. To separate them an analysis in the three angles (θ_l, θ_V and χ) and w is needed. The angles are defined in Figure 3.

The decay rate in terms of the four kinematic variables w, θ_l, θ_V and χ is given by

$$\frac{d\Gamma}{dw\ dcos_l\ dcos_V\ d\chi} = K|V_{cb}|^2 q^2 p_{D^*} \times \tag{6}$$

$$\{H_+^2(1-cos\theta_l)^2 sin^2\theta_V + H_-^2(1+cos\theta_l)^2 sin^2\theta_V + 4H_0^2 sin^2\theta_l cos^2\theta_V$$

$$-2H_+H_- sin^2\theta_l sin^2\theta_V cos2\chi - 4H_0(H_+(1-cos\theta_l) - H_-(1+cos\theta_l))\, sin\theta_V cos\theta_V cos\chi\} \tag{7}$$

where $H_\pm$ and H_0 are helicity amplitudes related to the form-factors by

$$H_\pm = -(m_B + m_{D^*})A_1(w) \pm \frac{2p_{D^*}m_B}{m_B + m_{D^*}} V(w) \tag{8}$$

$$H_0 = -\frac{m_B + m_{D^*}}{m_{D^*}\sqrt{q^2}}(m_{D^*}(wm_B - m_{D^*})A_1(w) - \frac{4m_B^2 p_{D^*}^2}{(m_B + m_{D^*})^2})A_2(w). \tag{9}$$

[1]HFAG averages in includes older result from ALEPH

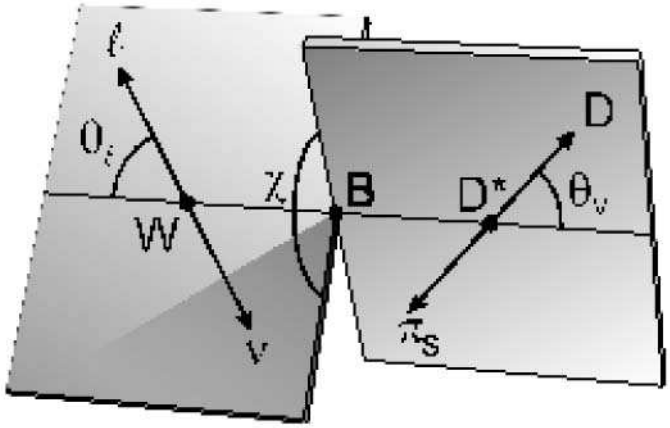

Figure 3: Definition of the angles θ_l, θ_V and χ that describe the decay $B \to D^* l\nu$.

In principle, by doing a spin-parity analysis in bins of w the form-factors could be measured without any model dependence. In practice the statistics are inadequate and we have to resort to some parameterization.

HQET relates the three form-factors describing the decay to a single common form-factor called the Isgur-Wise function. The relationships are

$$A_2(w) = \frac{R_2(w)}{R_*^2} \frac{2}{w+1} A_1(w) \tag{10}$$

$$V(w) = \frac{R_1(w)}{R_*^2} \frac{2}{w+1} A_1(w) \tag{11}$$

$$A_1(w) = R_* \frac{w+1}{2} h_{A_1}(w) \to R_* \frac{w+1}{2} \xi(w) \tag{12}$$

where $R_* = 2\sqrt{m_B m_{D*}}/(m_B + m_{D^*})$.

The CLN [3] formalism is again the most popular. They provide the w dependence of $R_1(w)$ and $R_2(w)$ and a parameterization in terms of the slope ρ^2 at $w = 1$ of the common form-factor $h_{A_1}(w)$. In fitting for the form-factors the intercepts $R_1(w = 1)$, $R_2(w = 1)$ and ρ^2 are taken as the independent parameters.

The CLN parameterizations are

$$R_1(w) = 1.27 - 0.12(w-1) + 0.05(w-1)^2, \tag{13}$$

$$R_2(w) = 0.79 + 0.15(w-1) - 0.04(w-1)^2 \tag{14}$$

for the form-factor ratio parameters and

$$h_{A_1}(w) = h_{A_1}(1)(1 - 8\rho^2 z + (53\rho^2 - 15)z^2 - (231\rho^2 - 91)z^3 \tag{15}$$

for the common 'Isgure-Wise' like form-factor.

Outside the heavy quark limit where $h_{A_1}(w) = \xi(w)$ and the value at $w = 1$ is 1.0, $h_{A_1}(w = 1)$ has to be taken from theory. The best estimate comes from lattice QCD [2]. It is $0.919^{+0.030}_{-0.035}$.

BABAR measures the decay rates as function of θ_l, θ_V, χ and w. Because of the missing neutrino these cannot be directly obtained from the measured tracks. Thus, a partial reconstruction technique, (illustrated in Figure 4), which allows a reasonable accurate approximation to be made, is used. Using the kinematic constraints expressed in Figure 4 the cosine of the angle between the B direction and the direction of the lepton-D^* system ($\mathbf{P}_Y = \mathbf{P}_{D*} + \mathbf{P}_l$) can be obtained as follows:

$$cos\theta_{BY} = \frac{2E_B E_{D^*+l} - m_B^2 - m_{D^*+l}^2}{2|\mathbf{P}_{D^*}||\mathbf{P}_Y|} \tag{16}$$

where lepton and D^* momenta are measured and $|\mathbf{P}_B|$ can be estimated from the beam energies. Note the same construction is used for $Dl\nu$ with, of course, $D \to D^*$

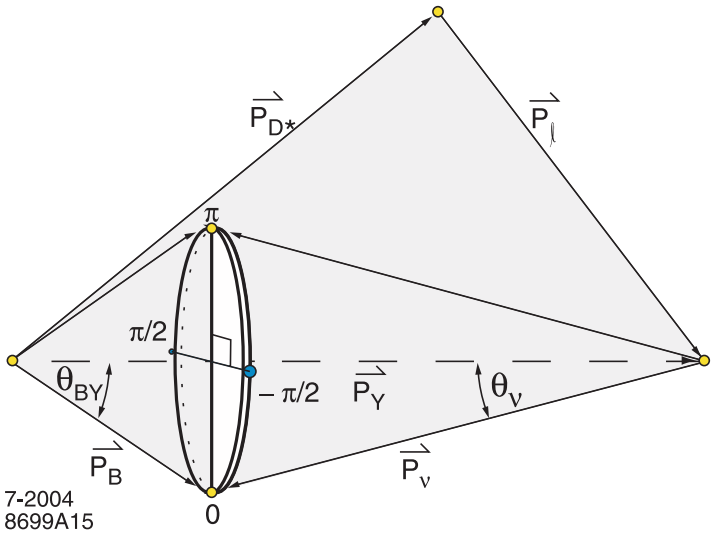

Figure 4: Kinematics of $B \to D^* l\nu$ that allow $cos\theta_{BY}$ to be reconstructed.

The azimuthal angle ϕ_{BY} of $\mathbf{P}_B$ around the Y direction is undetermined. The kinematic variables $cos\theta_l$, $cos\theta_V$, χ and w can be calculated for any choice of ϕ_{BY}. Averaging over ϕ_{BY} gives reasonable estimators of their values. BABAR uses points

at $\phi_{BY} = 0,\ \pi,\ \pm\pi/2$ weighted by the B production angular distribution ($\propto sin^2\theta_B$) to perform this average.

Only and CLEO [9] and BABAR [10, 11] have attempted form-factor measurements. BABAR uses two method: a likelihood fit to the full $4-d$ distribution of the kinematics variables ($w,\ \theta_l,\ \theta_V,\ \chi$) and a simultaneous fit to the one-dimensional w, $cos\theta_l$ and $cos\theta_V$ projections. CLEO also does a 4-d likelihood fit. I'll describe the BABAR methods in some detail.

For the $4-d$ likelihood fit it's difficult to construct the full, correlated PDF (including efficiency and resolution) for the measured variables $w,\ \theta_l,\ \theta_V$ and χ, so BABAR resorts to the 'integral method' that avoids the need to know this complicated PDF. With the integral method only the integral of the efficiency and the theoretical PDF Eq.(6) are needed.

The extended likelihood (include resolution) is given by

$$log\mathcal{L} = \sum_e log\tilde{F}(\tilde{\Omega}_e|\mu) - \int d\tilde{\Omega}\tilde{F}(\tilde{\Omega}|\mu) \tag{17}$$

where $\tilde{\Omega}$ represents measured quantities and $\tilde{F}(\tilde{\Omega}|\mu)$ represents their PDF for parameters μ. The sum is over events. Using the approximation

$$\tilde{F}(\tilde{\Omega}|\mu) \approx F(\tilde{\Omega}|\mu) \times \frac{\tilde{F}(\tilde{\Omega}|\mu_{mc})}{F(\tilde{\Omega}|\mu_{mc})} \tag{18}$$

we obtain

$$log\mathcal{L} \approx \sum logF(\tilde{\Omega}_e|\mu) - \tilde{I}(\mu, \mu_{mc}) \tag{19}$$

with

$$\tilde{I}(\mu, \mu_{mc}) = \int d\tilde{\Omega}F(\tilde{\Omega}, \mu) \times \left(\frac{\tilde{F}(\tilde{\Omega}|\mu_{mc})}{F(\tilde{\Omega}|\mu_{mc})}\right) \tag{20}$$

which can be obtained by Monte Carlo integration as

$$\tilde{I}(\mu, \mu_{mc}) \approx \frac{1}{N_{mc}} \sum \frac{F(\tilde{\Omega}_{imc}|\mu)}{F(\tilde{\Omega}_{imc}|\mu_{mc})}. \tag{21}$$

It can be shown that for μ_{true} equal μ_{mc}, the result of this approximation is unbiased. The procedure can be iterated by re-weighting to get $\mu_{mc} \approx \mu_{fit}$ which is close enough. Extra contributions to the error from MC statistics need to be evaluated, but knowledge of $4-d$ efficiency-resolution function is not required. Background is subtracted event-by-event using MC events to avoid breaking the factorization that leads to Eq.(19).

Since there is no explicit PDF $\tilde{F}$ constructed, the MC is re-weighted to fitted values of $R_1(1),\ R_2(1)$ and ρ^2 (histogram) and compared to the data (points) to see

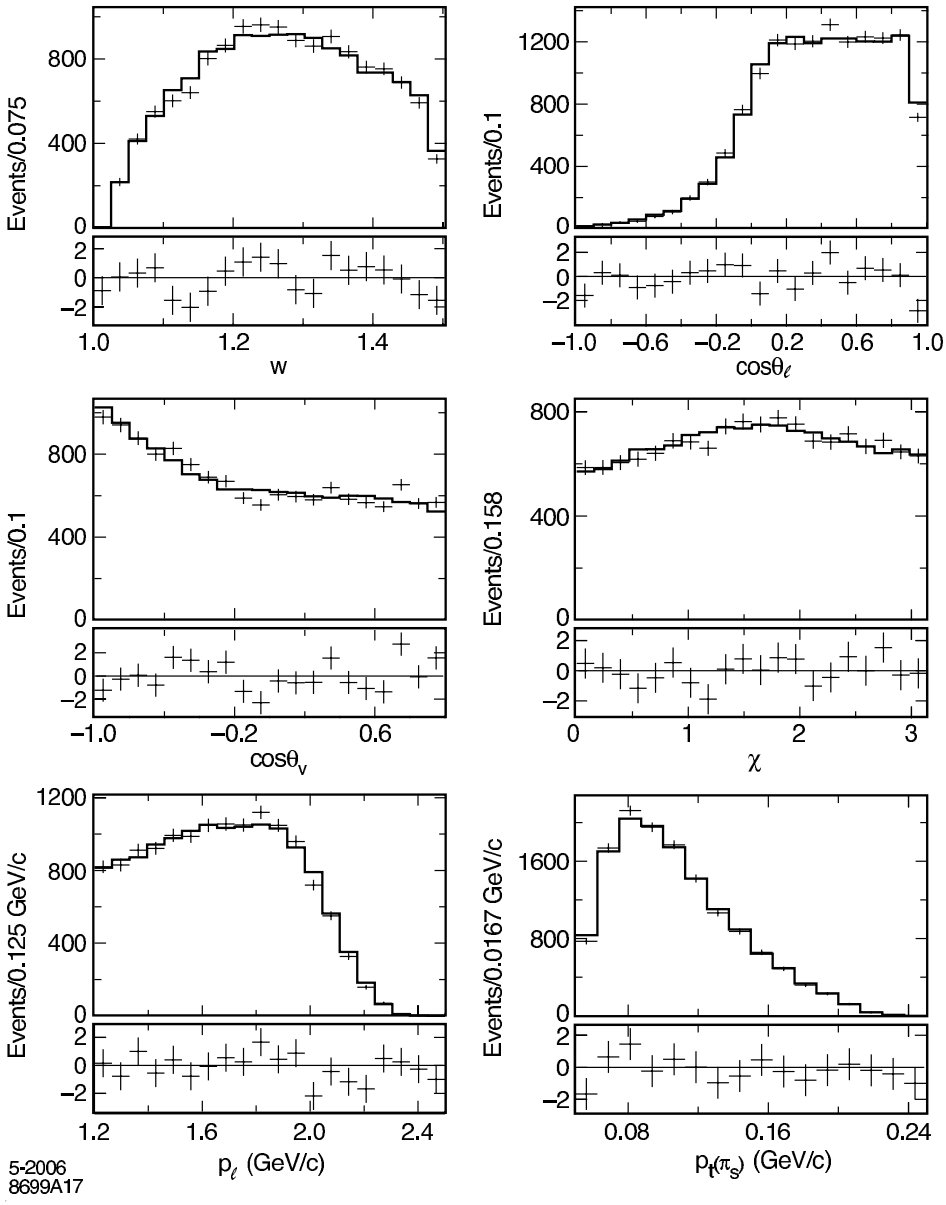

Figure 5: Distribution of w, $cos\theta_l$, $cos\theta_V$, χ as well as lepton momentum p_l and "slow" pion momentum $p_t(\pi_s)$.

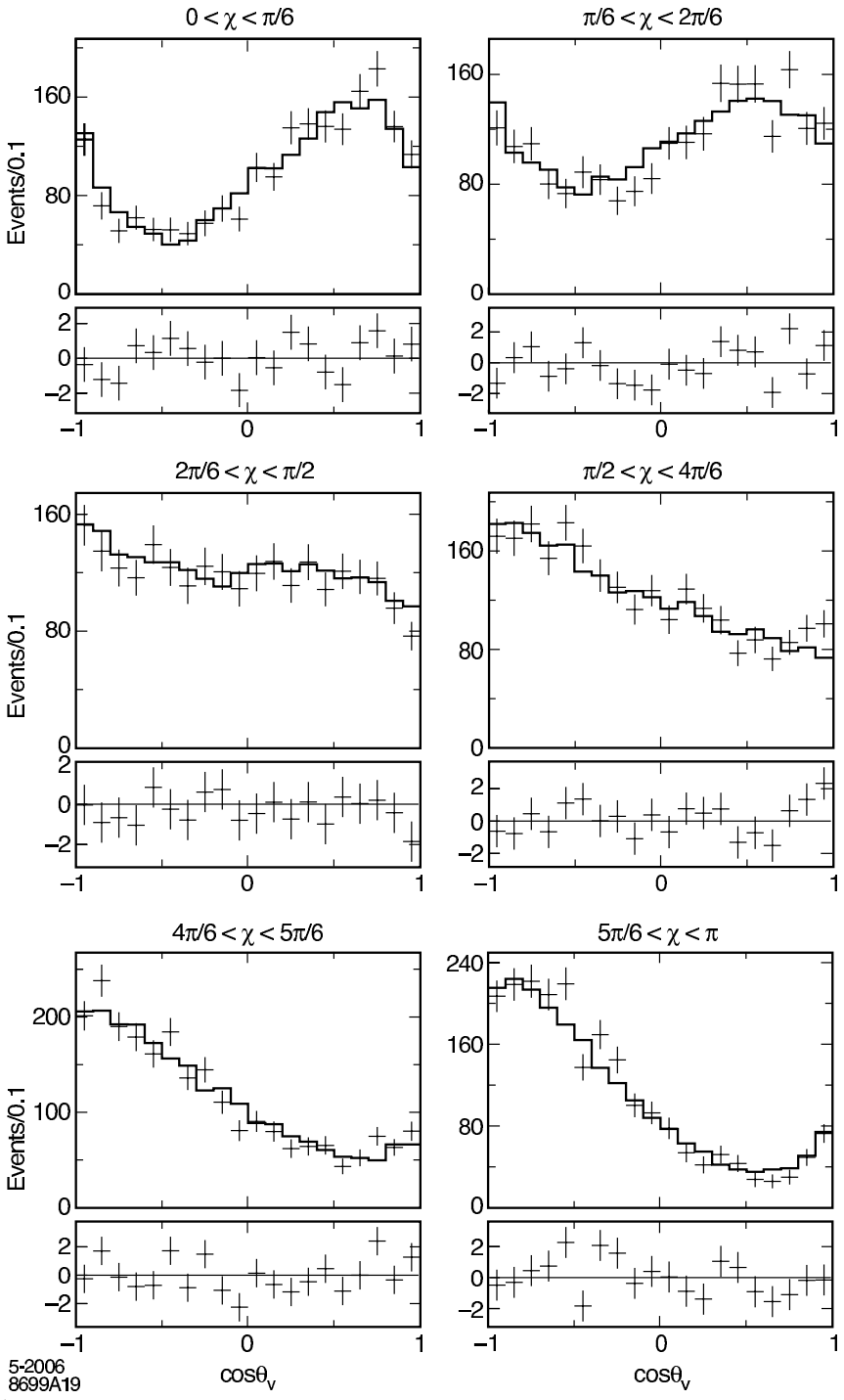

Figure 6: Distribution of χ for six cuts on $cos\theta_V$.

if fit is good. Figure 5 shows the four projects and Figure 6 shows the χ projection for six bins of $cos\theta_V$. The agreement with the fit represented by re-weight MC is excellent and reproduces even the details of the interference in the χ vs. $cos\theta_V$ plots.

The results[2] are

$$R_1(w) = 1.396 \pm 0.046 \pm 0.027 \tag{22}$$

$$R_2(w) = 0.885 \pm 0.046 \pm 0.013 \tag{23}$$

$$\rho^2 = 1.145 \pm 0.066 \pm 0.035 \tag{24}$$

The BABAR results are consistent with the pioneering CLEO measurement of $R_1 = 1.18 \pm 0.30 \pm 0.12$, $R_2 = 0.71 \pm 0.22 \pm 0.07$. The slope parameter ρ^2 also agrees when equivalent parameterizations of $h_{A_1}(w)$ are used. The values are also consistent with theoretical expectations. Since, $|V_{cb}|$ is highly sensitive to R_1 and R_2, this measurement leads to substantial reduction in the error achievable on it.

The second BABAR method works with projections in w, $cos\theta_l$ and $cos\theta_V$. The dihedral angle χ is not used because it has little sensitivity when one integrates over the other angles. The projection method is not as statistical powerful for the form-factors as the full $4-d$ fit, however, it has the advantage that the background can be estimated and removed in a manner that is nearly independent of the MC. This allows higher multiplicity D-decays to be used. The $4-d$ method only used the $D \to K\pi$ in order to keep the systematic error from dependence on MC simulation of the background shape under control.

The projection method divides each variable into ten bins and fits the $cos\theta_{BY}$ distribution in each bin to obtain estimates of the signal and background *in that bin*. The shape of the $cos\theta_{BY}$ distribution for background and signal is taken from MC and whenever possible from data control samples, but no assumption about the shape of the background distributions in w, $cos\theta_l$ or $cos\theta_V$ is used. Thus the resulting projection plots are only weakly dependent on the MC simulation.

Figure 7 shows the results of simultaneous fits to the projection plots. The projection distributions are correlated since they share the same events; this correlation is taken into account in the fitting procedure. The triangles represent that data, the yellow the signal and the other colors the results of the $\cos\theta_{BY}$ fits for the background. The χ projection is not fit, but is only shown for completeness. The fits look good.

For BABAR's final result they combine the results of the two method. The results are

$$\mathcal{F}(1)|V_{cb} = (34.68 \pm 0.32 \pm 1.15) \times 10^{-3} \tag{25}$$

[2]These are for so called baseline case where $R_1(w) = R_1(1)$ and $R_2(w) = R_2(1)$ are taken to be constant. The results using the CLN or other predictions for the w dependence of R_1 and R_2 are not much different.

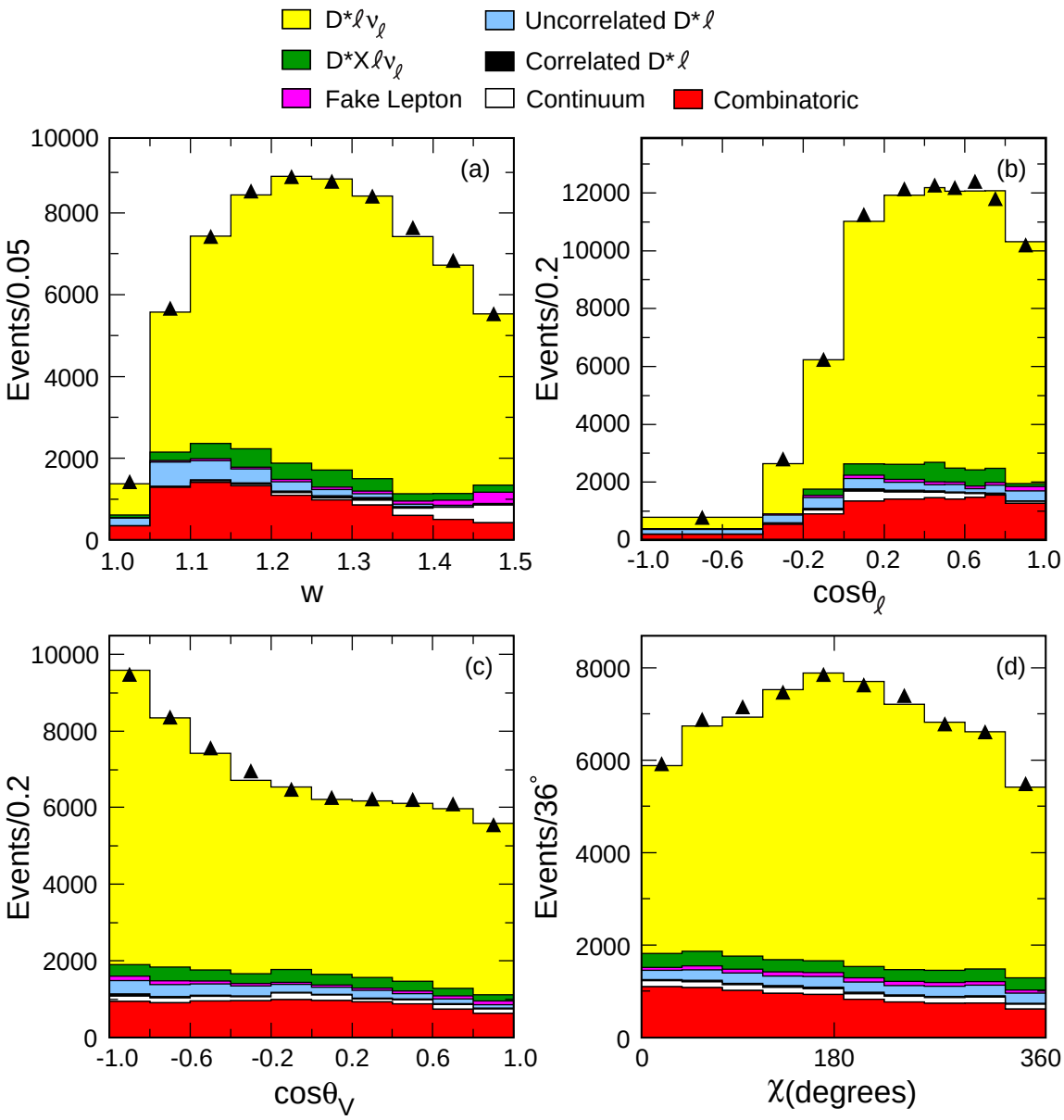

Figure 7: Projection results for w, $cos\theta_l$, $cos\theta_V$. The angle χ was not part of the fit.

$$\rho^2 = 1.179 \pm 0.048 \pm 0.028 \quad (26)$$

$$R_1 = 1.417 \pm 0.061 \pm 0.044 \quad (27)$$

$$R_2 = 0.836 \pm 0.037 \pm 0.022 \quad (28)$$

where errors are statistical and systematic respectively. In this case the CLN form (Eqs. 13-14) for $R_1(w)$ and $R_2(w)$ has been used.

This currently yields the best exclusive measurement of $|V_{cb}| = (37.74 \pm 0.35 \pm 1.24^{+1.32}_{-1.44}) \times 10^{-3}$. The additional error is from the theoretical predictions of $\mathcal{F}(1)$.

HFAG has averaged the $|V_{cb}| - \rho^2$ results from six experiments. The summer 2006 average, which includes the BABAR improvement of R_1 and R_2 to the results of other experiments, is shown in Figure 8. The poor χ^2 (28/14) is mostly due to the CLEO and ALEPH measurements. While BABAR is the single best measurement, the others make a significant contribution to the world average.

There is a persistent conflict between the $D^*l\nu$ branching fraction measured with charged and neutral B-mesons. In PDG 2006 average is $5.34 \pm 0.20\%$ for neutrals and $6.5 \pm 0.5\%$ for charged B's. This difference would represent isospin violation, which is *apriori* very unlikely. At this point it's only $\sim 2\sigma$, so we can hope the difference will "regress-to-the-mean" as new measurements come in.

BELLE [12] has used a "recoil" technique to measure both $D^{*0}l^+\nu$ and $D^{*0}l\nu$ recoiling against a fully reconstructed B^- or $\overline{B}^0$. While the sample is quite small, this method substantially reduces the background and thus potentially the systematic errors. BELLE has not yet fully exploited this potential as they do not give a systematic error on these branching fractions.

Figure 9 shows BELLE's missing mass plots. The branching fractions they obtain are

$$B(\overline{B}^0 \to D^*l\nu) = 4.7 \pm 0.24\%, \; B(B^+ \to D^*l\nu) = 6.06 \pm 0.25\% \quad (29)$$

which is $\sim 4\sigma$ discrepancy, ...but of course only the statistical error is taken into account. This method has the potential to shed considerable light on the issue, if the systematic uncertainties can be understood.

5 Higher mass states: D^{**}, $D^{(*)}\pi$, etc.

One might ask *w.r.t* the semi-leptonic decays to the higher mass charm states "why bother?" It seems unlikely anything very exciting will be found.

One answer might be simply "because they're there." In general, it's good idea to try to understand the decay modes of particles like the B as completely as possible...and you'll never know what might be lurking there, if you don't look...we need to see what we can see (see Figure 10).

A more practical answer is "engineering." The so-called $\mathcal{D}^{**}$ states and $D^*n\pi$ are the dominant backgrounds to $Dl\nu$ and $D^*l\nu$ and the lack of understanding of these

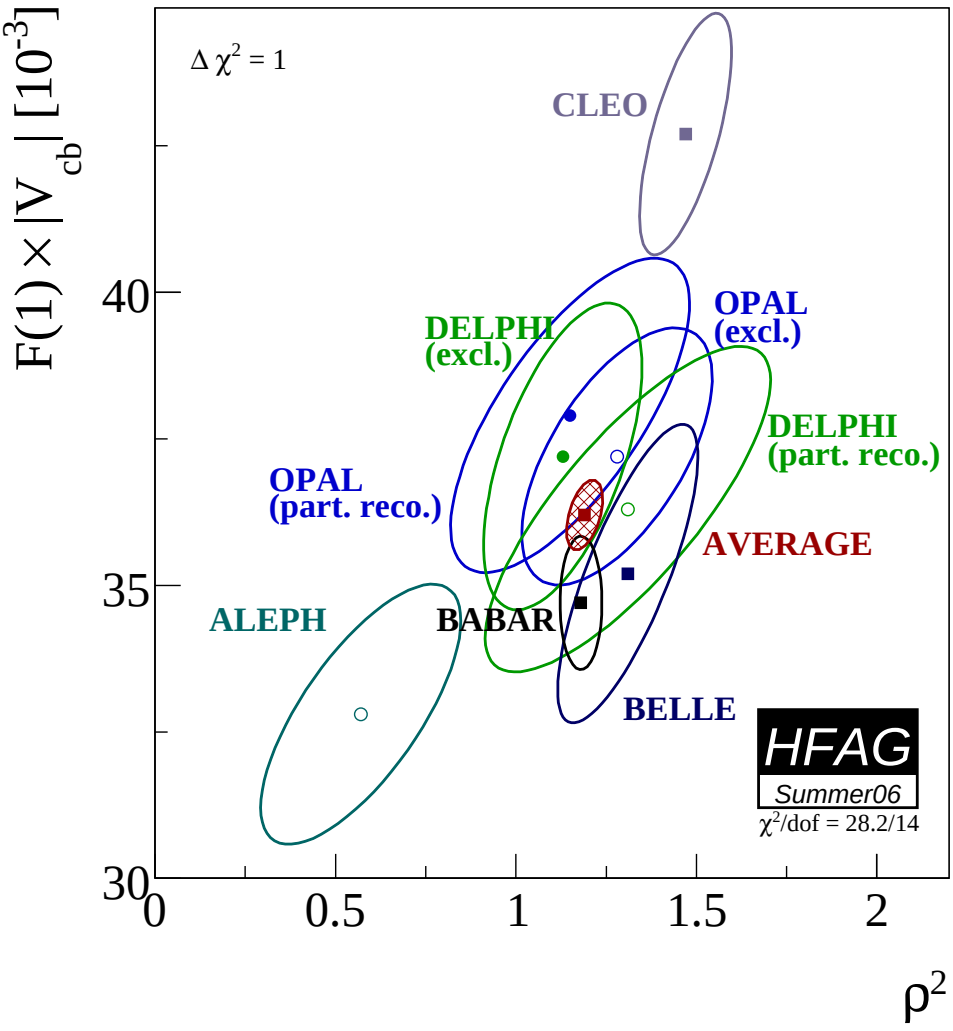

Figure 8: Summer '06 plot of $\mathcal{F}(1)|V_{cb}|$ vs. ρ^2 from HFAG.

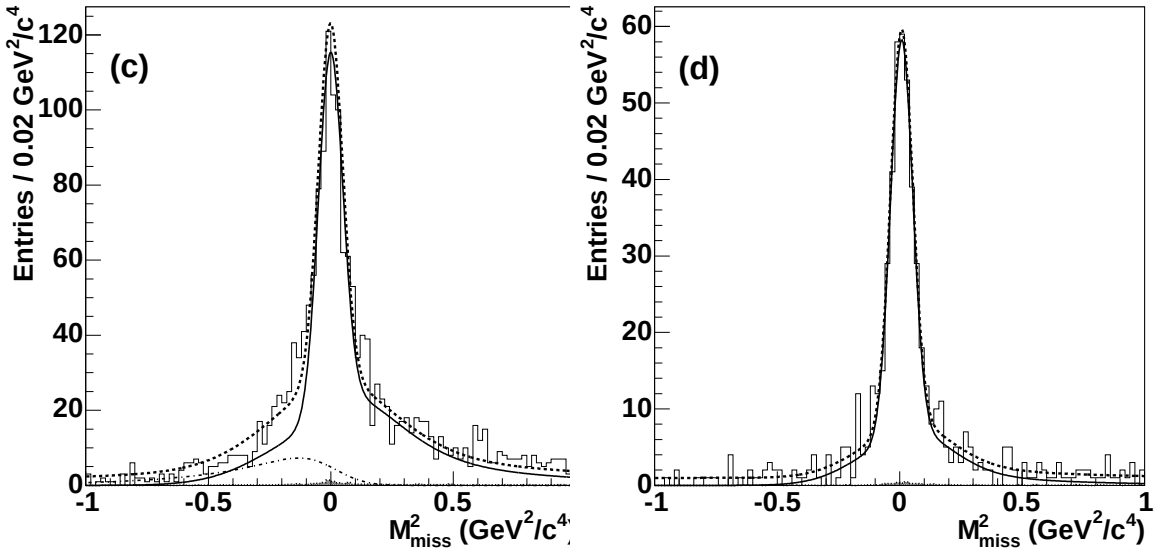

Figure 9: Missing mass against $D^* l\nu$ in $B^{\pm}$ recoil sample (left) and in B^0 sample (right).

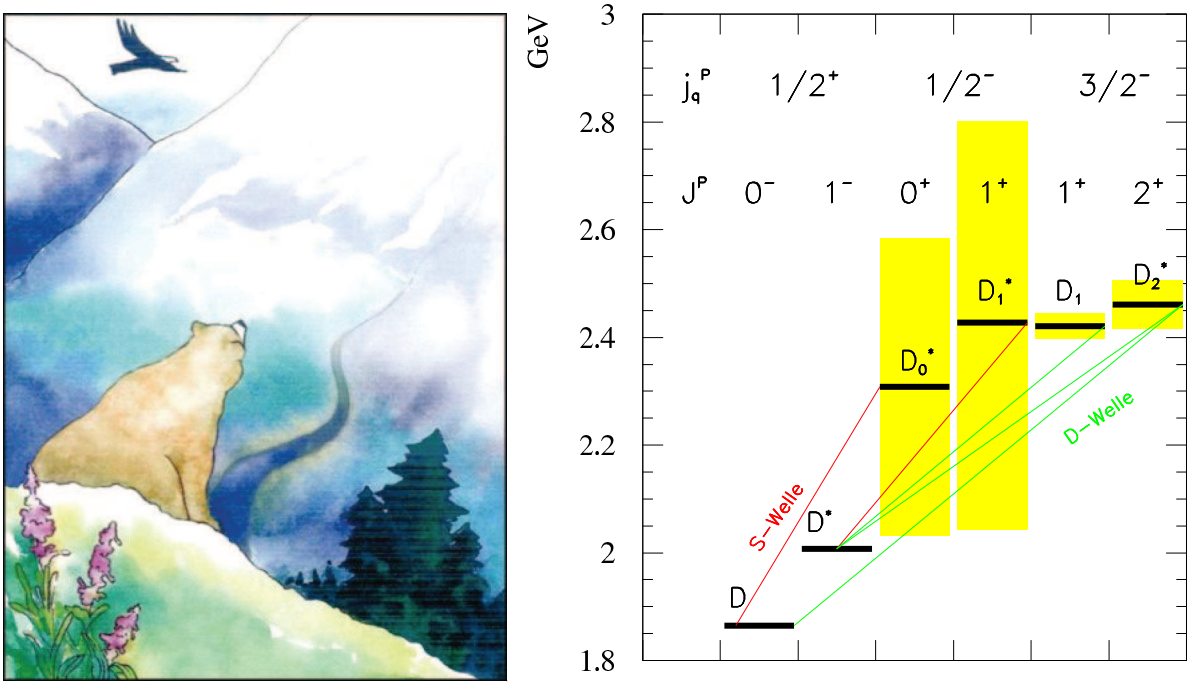

Figure 10: "...to see what he could see...and high mass charm states we might see... [13]

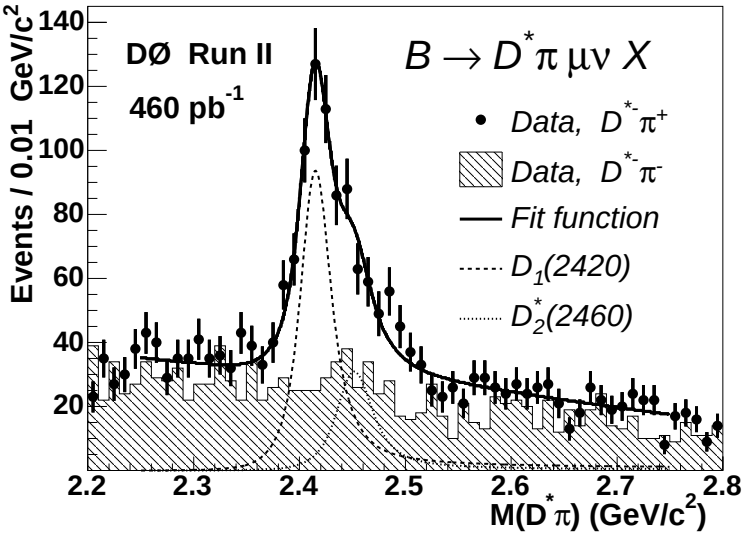

Figure 11: $D^*\pi$ mass distribution from D^0.

backgrounds is a major source of systematic error for V_{cb}, ρ^2 and the form-factor ratios R_1 and R_2.

HQET also makes predictions about the form-factors of excited D-mesons and perhaps lattice QCD can too. Measurements in the high mass sector can test the theory that underlies the extraction of $|V_{cb}|$ and are of some interest in themselves.

What could be there? In terms of resonance, this also shown in Figure 10 where the predictions for the resonant structure based on HQET are given. There are two narrow resonances – the $D_1(2420)$ and the $D_2^*(2460)$ which should be relatively easy to detect and, in fact, are already seen in semi-leptonic B-decay. The wide D_0^* and D_1^* will be hard to distinguish from the non-resonant $D^{(*,**)} n\pi$ contributions.

The D0 experiment [14] has observed the narrow states in $B \to D^*\pi l\nu + X$. The measurement does not strictly correspond to exclusive $D^*\pi$ though that's likely to be a major component of the signal. The $D^*\pi$ mass plot is displayed in Figure 11. The $D_2(2460)$ corresponds to the shoulder on the right side of the bump. Only the product production×branching fraction are directly measured, they are

$$B \to \overline{D}_1 l\nu,\ \overline{D}_1^0 \to D^{*-}\pi^+ = 0.087 \pm 0.007 \pm 0.014, \tag{30}$$

$$B \to \overline{D}_2 l\nu,\ \overline{D}_2^{*0} \to D^{*-}\pi^+ = 0.035 \pm 0.007 \pm 0.008, \tag{31}$$

$$ratio\ \overline{D}_2^{*0}/\overline{D}_1^0 = 0.39 \pm 0.09 \pm 0.12. \tag{32}$$

Using $b \to B^- = 0.39 \pm 0.09 \pm 0.12$ and isospin symmetry, the absolute branching fractions can be estimated as $0.33 \pm 0.06\%$ for the D_1 and $0.44 \pm 0.16\%$ for the D_2^*.

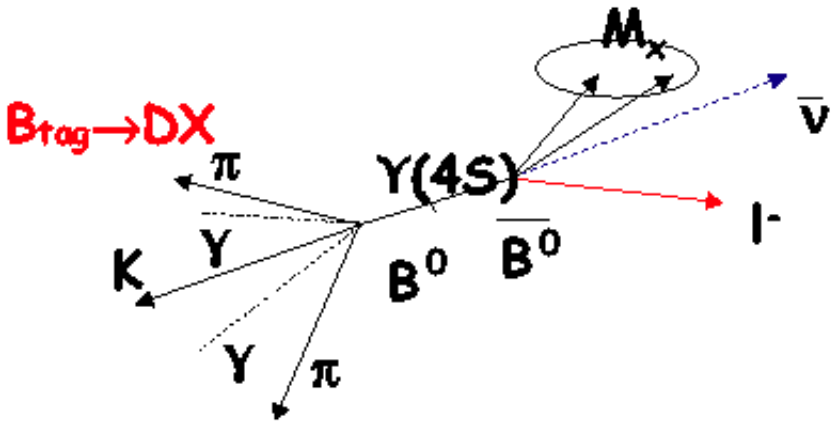

Figure 12: Illustration of reconstruction missing mass M_{miss} in the system recoiling against a fully reconstructed B and some hadrons (represented by M_X). For the exclusive channels of interest M_X is composed of $D^{(*)}\pi$ and $M_{miss} = M_\nu = 0$ for signal.

The OPAL [15] collaboration does a similar measurement, but is unable to see the D_2. They get

$$\mathcal{B}(b \to \overline{B}) \times \mathcal{B}(D_1^0 l^- \overline{\nu}) \times \mathcal{B}(D^{*+}\pi^-) = (2.64 \pm 0.79 \pm 0.39) \times 10^{-3}. \qquad (33)$$

For the D_2 they get $(0.26 \pm 0.59 \pm 0.35) \times 10^{-3}$ which is consistent with zero.

BABAR [16] also makes a measurement of the higher mass states using an inclusive method that also yields estimate of $Dl\nu$ and $D^*l\nu$. This is done looking at the semi-leptonic decays recoiling against a fully reconstructed B.

Using a recoil tagged sample, the distributions of the missing mass against Dl, shown in Figure 13, can be constructed. The decay modes $Dl\nu$, $D^*l\nu$ and the modes $D^(*)n\pi$ have different shapes in missing mass, so the missing mass distribution can be used to disentangle them. Roughly speaking, $Dl\nu$ is peaked at zero, $D^*l\nu$ peaks a bit higher ($\sim 0.8GeV$) and the rest is broad.

While missing mass is the most powerful variable for discriminating these decay contributions, there is also discriminating power in the lepton momentum (p_l) spectrum and in the number of extra tracks not used reconstructing the Dl. BABAR extracts the relative branching fractions of these three components by fitting simultaneously to the missing mass, p_l and extra-track distributions using PDFs determined by the data and validated with the Monte Carlo. The results are normalized to the semi-leptonic decay rate ($B \to DXl\nu$). Small contributions from baryons in the final state are missing.

The results are summarized in Table 5. If I use semi-leptonic branching fractions from the 2006 PDG (neglecting small non-$DXl\nu$ contributions) to estimate absolute

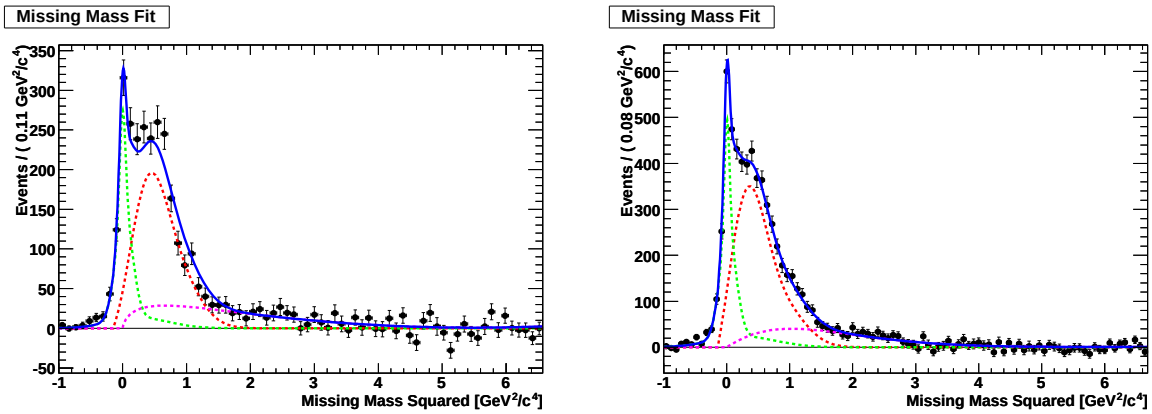

Figure 13: Missing mass against Dl in full recoil tagged events. Left is B^0 decays and right charged B decays.

branching fractions for $D^*l\nu$, I get $6.34 \pm 0.2\%$ for charged B's and $5.58 \pm 0.32\%$ for the neutrals. I've only kept the statistical errors. Under the assumption that most systematics are common, this is again a $\sim 2\sigma$ descrepency...however not all the systematics are common so the discrepancy may not really be that large.

The BELLE paper [12] also contains results on the higher mass states $D\pi l\nu$ and $D^*\pi l\nu$. In fact, these are the main results of their paper and the $D^*l\nu$ decays are not the focus of the analysis. This technique also employs recoil tagged sample (see Figure 12 again), but looks at the missing mass recoiling against the specific states. Figure 14 show the missing mass distribution obtained for the four $D^{(*)}\pi$ modes reconstructed. The signal in these plots appears at zero. There is little background in the $D^*\pi$ modes and even in the $D\pi$ modes the signals are evident.

The branching fractions obtained are

$$B(D^+\pi^-l^-\overline{\nu}) = 0.54 \pm 0.07 \pm 0.07 \pm 0.06\%, \tag{34}$$

$$B(D^0\pi^+l^-\overline{\nu}) = 0.33 \pm 0.06 \pm 0.06 \pm 0.03\%, \tag{35}$$

$$B(D^{*+}\pi^-l^-\overline{\nu}) = 0.67 \pm 0.11 \pm 0.09 \pm 0.03\%, \tag{36}$$

$$B(D^{*0}\pi^+l^-\overline{\nu}) = 0.65 \pm 0.12 \pm 0.08 \pm 0.05\%, \tag{37}$$

where in addition to the usual systematic uncertainties there is an additional contribution from using the $Dl\nu$ and $D^*l\nu$ to normalize the results. The higher mass contribution to the total branching fraction should be $\sim 10.4 - 2.1 - 5.3 = 3\%$. BELLE's observed $D^*\pi$ contribution to B^0 decays is $\approx (0.98 \pm 0.13\%)$ which accounts for only $\sim 1/3$. If we assume [3] the total isospin of the $D\pi$ system is $1/2$ then

[3] This is in fact a good assumption, no other isospin is possible given the $c\overline{q}$ produced must be $I = 1/2$.

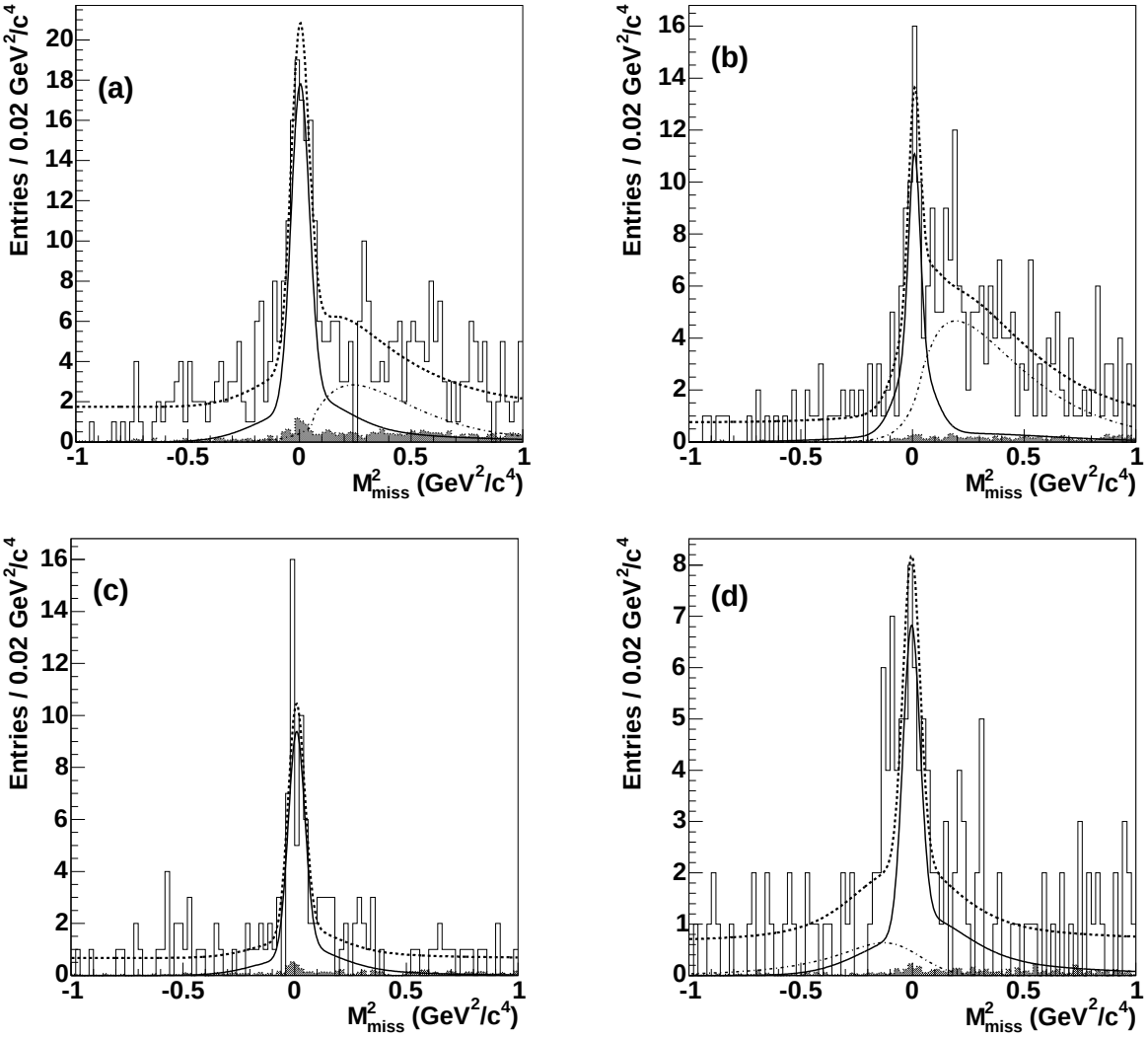

Figure 14: Missing mass against $D^*\pi$ in full recoil tagged events. The modes considered are (a) $D^+\pi^-l^-\overline{\nu}$, (b) $D^0\pi^+l^-\overline{\nu}$, (c) $D^{*+}\pi^-l^-\overline{\nu}$ and (d) $D^{*0}\pi l^-\overline{\nu}$.

Ratio	$B^-(\%)$	$B^0(\%)$
$Dl\nu$	$22.7 \pm 1.4 \pm 1.5$	$21.5 \pm 1.6 \pm 1.3$
$D^* l\nu$	$58.2 \pm 1.8 \pm 3.0$	$53.7 \pm 3.1 \pm 3.6$
$D^{*,**} n\pi l\nu$	$19.1 \pm 1.3 \pm 1.9$	$24.8 \pm 3.2 \pm 3.0$

Table 2: Ratios of $Dl\nu$, $D^* l\nu$ and $D^{*,**} n\pi$ to $DXl\nu$ for charged and neutral B-mesons.

there should be 1/2 as many again in the unobserved charge D with π^0 modes for a total, of 1.5 ± 0.2 thus accounting for $\sim 1/2$ of the missing modes. The same argument applies to the charged B, where the estimate $D\pi$ branching fraction corrected for isospin is 1.8 ± 0.20. So it seems, like there must be some contribution from states with two pions. Both of these are consistent with BABAR's estimate using the Dl missing mass.

Using isospin to relate B^0 and B^+ modes we could average to produce a somewhat more accurate estimate. However, considering the unsettled state of $D^* l\nu$ branching fractions, it's probably best to just settle for the statement that $D^{(*)}\pi$ can account for $\sim 1/2$ the decays with hadronic masses $m_{had} > m_{D^*}$.

Another interesting number is the ratio $R = D\pi/D^*\pi$. To estimate this I average the BELLE's numbers for B^0 and B^+ and assume systematics cancel in the ratio. I find $R = 1.58 \pm 0.26$ (stat error only).

Using D0's estimate of the branching fraction to the narrow state D_1^0 (see above), I find that $\sim 35\%$ of $D^*\pi$ are from this narrow state. This suggest that some narrow states might be visible in BELLE's recoil samples.

These are very beautiful measurements. Given that there's still a percent of so in other modes it would be interesting to measure modes like $D^*\pi\pi$.

6 What to do?

- We need to resolve the discrepancy between $D^* l\nu$ measured in B^0 and B^+ decays!
  - Isospin violation is most unlikely
  - It's only $\sim 2\sigma$, so may be we're just chasing a fluctuation
  - Could there be high-spin, high-mass states that can mimic $D^{*0} l\nu$ modes?
    - Try to get solid theory predictions for spin 2 states implemented in MC and seek parameters that might cause such a problem, *i.e.,* investigate the theoretical constraints on the high mass states.
    - Example of "D^{**}" faking $D^* l\nu$ is shown in Figure 15

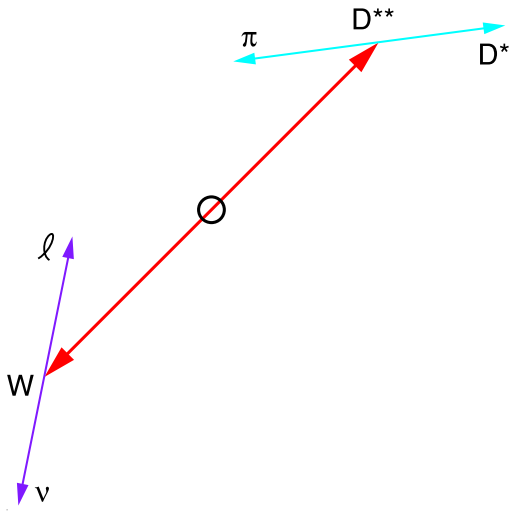

Figure 15: Possible fake $D^*l\nu$ from a $D^{**}l\nu$ decay – a neutrino goes "forward" and π goes "backward" the missing mass gets small and the event mimics $D^*l\nu$. Any decay with ν and π moving the same direction will produce a successful $cos\theta_B Y$ construction with just a slightly higher neutrino momentum. The number of D^{**} decays near this configuration will be influenced by the D^{**} form-factors.

  - Maybe slow pions from $D^* \to D\pi$ decays not well understood?
    - This is not a likely explanation as there aren't many events produced at low w (high q^2) so they should not affect branching fraction too much
    - Try using $D^+\pi^0$ decay instead of $D^0\pi^+$ to see if the same answer is obtained with a different slow π efficiency
    - Repeat BELLE style missing mass analysis for $D^*l\nu$ with careful attention to systematics and background. Hopefully many systematics would cancel in the charge to neutral B ratios

- $D\pi l\nu$ accounts for about half the missing modes. What is the rest?
  - Measure $D^*\pi\pi$. Is this possible with current statistics?
  - Wide states are hard. They need a full spin-parity analysis to extract phase shifts – an analysis that is not feasible with the current generation of B factories

- Test HQET. Needs higher precision form-factor measurements and ultimately model independent measurements

7 Summary

We already know quite a bit. The HFAG world average is $\mathcal{F}(1)_{cb}$ is $36.2 \pm 0.6 \times 10^{-3}$. The form-factor parameters R_1 and R_2 have been measured to be 1.42 ± 0.07 and 0.84 ± 0.043, respectively. Two narrow contributions to the high mass region are known at the $10 - 20\%$ level. It's been established that $D\pi$ (resonant+wide+nonresonant) can account of $\sim 1/2$ of the branching fraction to higher mass states.

The biggest outstanding problem is *tensione* between the $D^* l\nu$ decay in B^0 ($\sim 5\%$) and B^+ decay ($\sim 6\%$). However, it's only $\sim 2\sigma$, so it probably will resolve itself in due course – which is not to say we shouldn't look for a systematic problem in the meanwhile.

While $R_1 - R_2$ are well enough measured for current $|V_{cb}|$ measurements given the other errors and the theory errors. Improved measurements could probe the HQET based theoretical assumptions.

Bibliography

[1] M.R. Ahmady et al, KEK Theory Group, hep-ph/0109061.

[2] Hashimoto et al., Phys. Rev. **D66** (2002) 01450 [hep-lat/9810056].

[3] I. Caprini, L. Lellouch and M. Neubert, Nucl. Phys. B **530**, 153 (1998) [hep-ph/9712417].

[4] C. G. Boyd, B. Grinstein and R. F. Lebed, Nucl. Phys. B **461**, 493 (1996) [hep-ph/9508211].

[5] A. Le Yaouanc, L. Oliver and J. C. Raynal, Phys. Rev. D **67**, 114009 (2003) [hep-ph/0210233].

[6] CLEO, Phys. Rev. Lett.82:3746,1999, CLNS 98/1594 hep-ex/9902005

[7] BELLE, Phys.Lett. B526 (2002) 258-268, [hep-ex/0111082]

[8] N. Isgur and M. B. Wise, "Weak transition form-factors between heavy mesons," Phys. Lett. B **237**, 527 (1990).

[9] J.E. Duboscq *et.al.* (CLEO Collaboration), Phys. Rev. Lett. **76**, 3898 (1996).

[10] B. Aubert *et.al.* (BABAR Collaboration), Phys. Rev. **D74**, 092004 (2006).

[11] B. Aubert *et.al.* (BABAR Collaboration), ICHEP 2006, hep-ph/0607076

[12] D. Liventsev *et al.*, Phys. Rev. D **72**, 051109 (2005).

[13] American folk/children's song "The bear went over the mountain" – traditional – sung in the backseat until the adults go insane!

[14] V. M. Abazov *et al.* (D0 Collaboration), Phys. Rev. Lett. **95**, 171803 (2005), hep-ex/0507046.

[15] G. Abbiendi *et al.* (OPAL Collaboration), Eur. Phys. J. C **30**, 467 (2003), hep-ex/0301018.

[16] "Measurement of the Relative Branching Fractions of $\overline{B} \to D/D^*/D^{**} l^- \overline{\nu}_l$ Decays in Events with a Fully Reconstructed B Meson," hep-ex/0703027, submitted to PRD-RC.

[17] L. da Ponte, Trans. N. Y. Acad. Sci., **3**, 27 (1795).

Semileptonic b to u transition

Eunil Won
Department of Physics
Korea University
136-713 Seoul, Korea

1 Introduction

The parameter $|V_{ub}|$ is one of the smallest and least known elements of the Cabibbo-Kobayashi-Maskawa (CKM) quark-mixing matrix. A precise determination of $|V_{ub}|$ would significantly improve the constraints on the unitarity triangle and provide a stringent test of the Standard Model mechanism for CP violation. With the CKM angle ϕ_3, $|V_{ub}|$ can constrain the unitarity triangle from tree level processes alone.

Experimental studies of charmless semileptonic B decays can be broadly categorized into inclusive and exclusive measurements depending on how the final states are treated. The inclusive method measures the decay rate $\Gamma(B \to X_u \ell\nu)$, where X_u is known as the hadronic system that does not contain charm-quark. On the other hand, the exclusive method measures the decay rates for exclusive final states such as $B \to \pi\ell\nu$ and $\rho\ell\nu$. Two methods give not only different efficiencies and signal-to-background ratios, but also different theoretical calculations to be used in order to extract $|V_{ub}|$. Using both approaches and comparing the results will help us verify the robustness of the theoretical error estimation, which dominates the current uncertainty in the determination of $|V_{ub}|$. Progress in last few years will be summarized in this presentation.

2 Inclusive determination of $|V_{ub}|$

The inclusive semileptonic decay rates in the quark level depend only on CKM matrix element and the quark mass, as shown in the following equation

$$\Gamma(b \to u\ell\overline{\nu}) = \frac{G_F^2}{192\pi^2}|V_{ub}|^2 m_b^5 \tag{1}$$

where G_F is the Fermi constant and m_b is the b-quark mass. The hadronic level is easy to calculate with the framework of operator product expansion (OPE) [1] and

the $|V_{ub}|$ can be parametrized as

$$|V_{ub}| = 0.00424 \left\{ \frac{\mathcal{B}(B \to X_u \ell\nu)}{0.02} \frac{1.61\text{ps}}{\tau_b} \right\}^{\frac{1}{2}} \times (1.0 \pm 0.012_{\text{QCD}} \pm 0.022_{\text{HQE}}) \qquad (2)$$

where the first error comes from the uncertainty in the calculation of quantum chromodynamics (QCD), perturbative and non-perturbative quantities and the 2nd from the uncertainty in the heavy quark expansion (HQE), sensitive to m_b. This formulation [2] has been updated in ICHEP06. The main problem in the inclusive method is the background from the b to c decays because the rate is approximately 50 times larger, namely

$$\Gamma(b \to c\ell\nu) \sim 50\Gamma(b \to u\ell\nu). \qquad (3)$$

One may attempt to remove this large background by applying kinematic selection criteria but once the signal to background ratio becomes controllable, the OPE is known to fail in such limited phase space. In the theory side, in order to overcome this problem, various different techniques have been developed. For example, a non-perturbative shape function [3] (SF) is developed to extrapolate to the full phase space. The shape function is the lightcone momentum distribution function of the b-quark inside the meson. The detailed shape is not known theoretically from the first principle and even phenominologically, the low-tail part is least known. The shape function is needed to be determined from experimental data. The other approach is called dressed gluon exponentiation (DGE) [4] according to the factorization properties of the fully differential width in inclusive decays Sudakov logarithms exponentiate in moment space. The third approach [5] measures the ratio of $|V_{ub}|/|V_{ts}|$ with the photon energy spectrum in $b \to s\gamma$ decay mode. This technique is interesting as the only residual shape function dependence remain at the end.

- Lepton Endpoint Analysis

The theoretical calculations allow for the extraction of the observed partial $B \to X_u \ell\nu$ decay rate above a certain lepton momentum to the total inclusive $B \to X_u \ell\nu$ decay rate using the measured shape function parameters and a subsequent translation of the total decay rate to $|V_{ub}|$. The experimental study was pioneered by the CLEO collaboration [6] and the recent work was carried out by the BaBar collaboration [7]. Fig. 1 (a), (b), and (c) show the electron energy spectra for various cases. Open circles in Fig. 1 (a) show the on-resonance data and closed circles with a curve in Fig. 1 (a) show the off-resonance data where non-$B\overline{B}$ background is included. The triangles in Fig. 1 (b) show the data after the non $B\overline{B}$ background subtraction and the histogram in Fig. 1 (b) show the simulated $B\overline{B}$ background. Closed squares and the histogram in Fig. 1 (c) show the data and the simulated signal after all background subtraction,

respectively. It is obvious that the subtraction of backgrounds is extremely crucial in this kind of analysis. The shaded region in Fig. 1 (c) is used for the final extraction of the $|V_{ub}|$. In the mean time, the partial branching fraction can be obtained from the background subtracted data and the summary from three experiment is listed in Table 1. Note that the Belle's result has the lowest cut on E_ℓ.

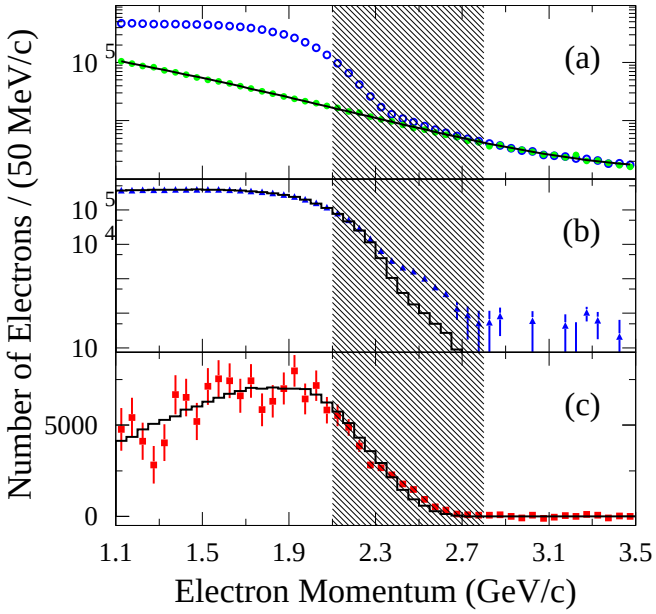

Figure 1: The distribution of electron momentum is shown [7]. Open circles in (a) show the on-resonance data and closed circles with a curve in (a) show the off-resonance data where non-$B\overline{B}$ background is included. The triangles in (b) show the data after the non $B\overline{B}$ background subtraction and the histogram (b) show the simulated $B\overline{B}$ background. Closed squares and the histogram in (c) show the data and the simulated signal after all background subtraction, respectively.

- Measurements of m_X, P_+, and q^2

In this analysis, the measurements are made with a sample of events where the hadronic decay mode of the tagging side B meson, B_{tag}, is fully reconstructed, while the semileptonic decay of the signal side B meson, B_{sig}, is identified by the presence of a high momentum electron or muon. B denotes both charged and neutral B mesons. This method allows the construction of the invariant masses of the hadronic (M_X) and leptonic ($\sqrt{q^2}$) system in the semileptonic decay, and the variable $P_+ =$

Table 1: Summary of the partial branching fraction of $B \to X_u \ell\nu$ given the lepton energy cut.

data	$\Delta\mathcal{B}(10^{-4})$	E_l (GeV)
CLEO 9/fb	$2.30 \pm 0.15 \pm 0.35$	2.1
Belle 27/fb	$8.47 \pm 0.37 \pm 1.53$	1.9
BaBar 80/fb	$5.72 \pm 0.41 \pm 0.65$	2.0

$E_X - |\vec{p}_X|$ where E_X is the energy and $|\vec{p}_X|$ the magnitude of the three-momentum of the hadronic system. These inclusive kinematic variables can be used to separate the $B \to X_u \ell\nu$ decays from the much more abundant $B \to X_c \ell\nu$ decays. Three competing kinematic regions were proposed by theoretical studies [3,8], based on the three kinematic variables, and are directly compared by this analysis.

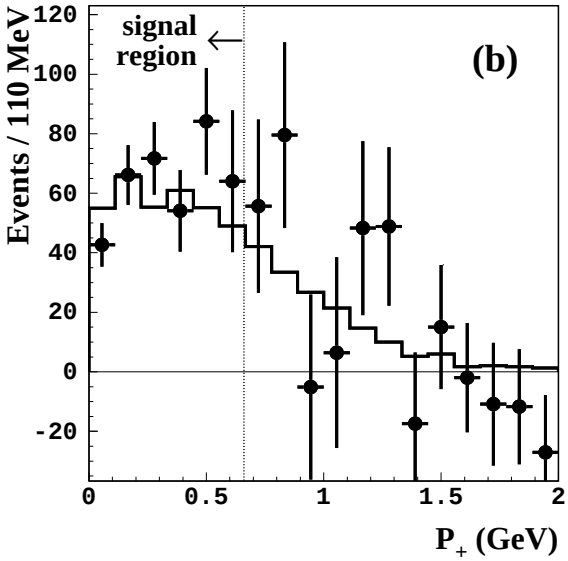

Figure 2: The P_+ distribution (symbols with error bars) after subtracting $B \to X_c \ell\nu$ background, with fitted $B \to X_u \ell\nu$ contribution (histogram).

The value of $|V_{ub}|$ is extracted using recent theoretical calculation [3,8] that include all the current known contributions. Results from the Belle experiment using a data set of 253/fb [9] is the first one to use P_+. Figure 2 show the distribution of the variable P_+. Signal region is defined by $P_X < 0.66$ GeV and shows a clear indication of enhancement of the signal in Fig. 2. BaBar did also similar analysis but only with M_X and q^2 [10]. The measured partial branching fractions from both experiments for different phase space values are summarized in Table 2. Note that the errors are

Table 2: Summary of the partial branching fraction of $B \to X_u \ell\nu$ given the lepton energy cut.

data	Phase Space	$\Delta\mathcal{B}$ (10^{-4})
Belle 253/fb	$M_X < 1.7$	$12.4 \pm 1.1 \pm 1.0$
	$M_X < 1.7$, $q^2 > 8$	$8.4 \pm 0.8 \pm 1.0$
	$P_+ < 0.66$	$11.0 \pm 1.0 \pm 1.6$
BaBar 211/fb	$M_X < 1.7$, $q^2 > 8$	$8.7 \pm 0.9 \pm 0.9$ (preliminary)

larger than those appeared in the endpoint analyses results.

- Extraction of $|V_{ub}|$

In order to extract the $|V_{ub}|$ from the partial branching fraction measurements described so far, one has to know the distribution of the shape function. The photon energy spectrum in $B \to X_s\gamma$ provides access to such distribution function of the b quark inside the B meson [11]. The knowledge of this shape function is a crucial input to the extraction of $|V_{ub}|$ from inclusive semileptonic $B \to X_u \ell\nu$ measurements. Both Belle and Babar fit the spectrum to theoretical predictions in order to extract the $|V_{ub}|$.

Using the heavy quark parameter values $m_b(\mathrm{SF}) = 4.60 \pm 0.04$ GeV and $\mu_\pi^2(\mathrm{SF}) = 0.20 \pm 0.04$ GeV^2, the value of $|V_{ub}|$ from various experimental results is extracted within "BLNP" framework [3]. This is done by the heavy flavour averaging group [12] (HFAG) and the result is

$$|V_{ub}|_{\mathrm{BLNP}} = (4.49 \pm 0.19_{\mathrm{exp}} \pm 0.27_{\mathrm{theory}}) \times 10^{-3}. \quad (4)$$

Note that the total error in percentage is

$$\delta|V_{ub}|_{\mathrm{BLNP}} = \pm 7.3\% \quad (5)$$

and the result indicates that the precision of the measurement is still limited by theoretical uncertainty but the value of the error is not far from the experimental error. The individual result from experiments is shown in Fig. 3. Note that the best measurement is from the endpoint analysis at present. Contributions to the experimental and theoretical errors can be found in Table 3. The contribution from sub-leading SF, for example, is known to be hard to reduce from the present value.

One can also extract $|V_{ub}|$ using the DGE framework [4]. This is also done by HFAG and the result is

$$|V_{ub}|_{\mathrm{DGE}} = (4.46 \pm 0.20_{\mathrm{exp}} \pm 0.20_{\mathrm{theory}}) \times 10^{-3}. \quad (6)$$

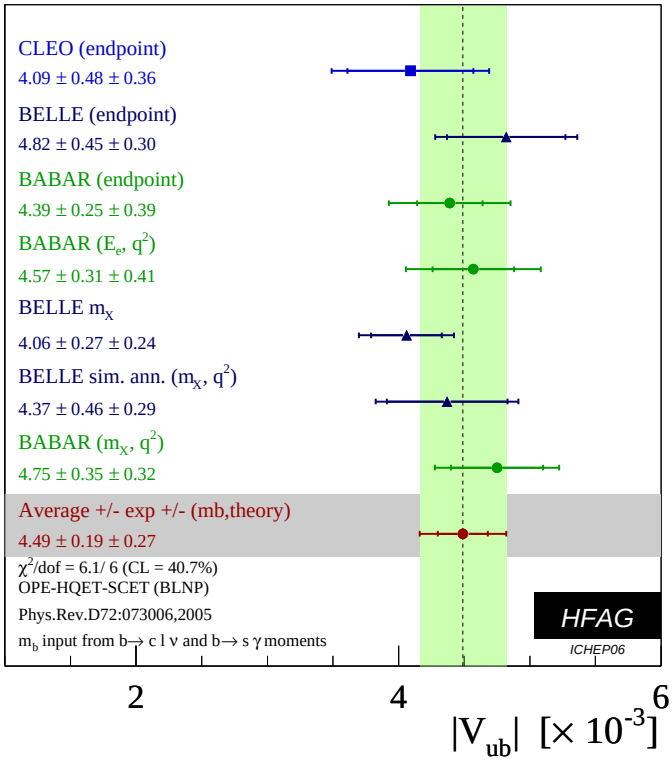

Figure 3: Summary of the measurements of $|V_{ub}|$ within BLNP framework from various experiments are shown. The averaged value is $|V_{ub}|_{\rm BLNP} = (4.49 \pm 0.19_{\rm exp} \pm 0.27_{\rm theory}) \times 10^{-3}$.

with the parameter $m_b(\overline{\rm MS}) = 4.20 \pm 0.04$ GeV. Note that the result is in good agreement with the result with BLNP method, and is remarkable as two theoretical methods use rather different approach in their calculations. The contribution of the error is also listed in Table 4. The sharing of the error is also similar to the case of the BLNP framework. One thing to note is that the weak annihilation is not taken into account in this case.

On the other hand, BaBar explored alternative methods in obtaining $|V_{ub}|$. Leibovich, Low, and Rothstein (LLR) [5] have presented a prescription to extract $|V_{ub}|$ with reduced model dependence from either the lepton energy or the hadronic mass m_X [13]. The calculations of LLR are accurate up to corrections of order α_s^2 and $(\Lambda m_B/(\zeta m_b))^2$, where ζ is the experimental maximum hadronic mass up to which the $B \to X_u \ell \nu$ decay rate is determined and $\Lambda \sim \Lambda_{\rm QCD}$. This method combines the hadronic mass spectrum, integrated below ζ, with the high-energy end of the measured differential $B \to X_s \gamma$ photon energy spectrum via the calculations of LLR. The measured $|V_{ub}|$ as a function of ζ is shown in Fig. 4. The small arrow indicates the

Table 3: Summary of the contributions to the experimental and theoretical errors of $|V_{ub}|$ in the BLNP framework.

Source	contribution (%)
statistical	2.2
Expt. systematic	2.8
$b \to c\ell\nu$ model	1.9
$b \to u\ell\nu$ model	1.6
HQ parameters	4.2
sub-leading SF	3.8
Weak Annihilation	1.9

Table 4: Summary of the contributions to the experimental and theoretical errors of $|V_{ub}|$ in the DGE framework.

Source	contribution (%)
statistical	1.8
Expt. systematic	2.5
$b \to c\ell\nu$ model	2.3
$b \to u\ell\nu$ model	2.3
m_b (R_CUT)	1.2
α_s (R_CUT)	1.0
Total semiloptonic width	3.0
DGE theory	2.9

value of ζ that is used for the cut, $\zeta = 0.67$ GeV/c^2. At this point, the measured value becomes

$$|V_{ub}| = (4.43 \pm 0.38_{\rm stat} \pm 0.25_{\rm syst} \pm 0.29_{\rm th}) \times 10^{-3}. \quad (7)$$

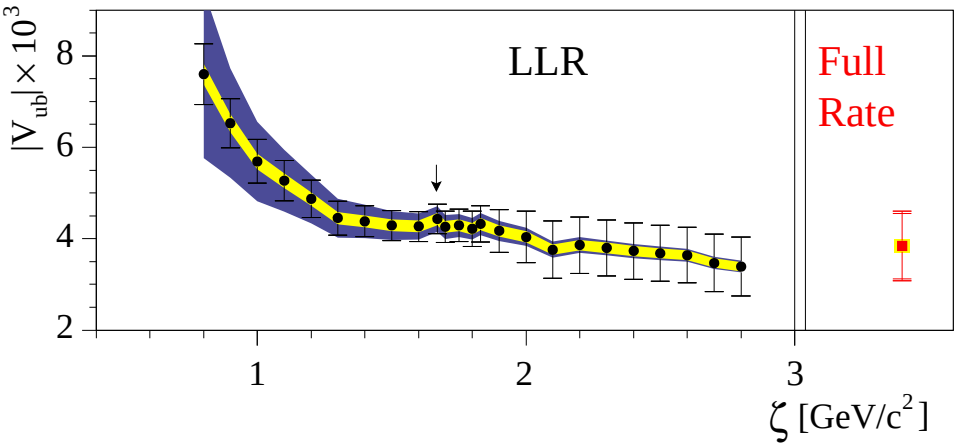

Figure 4: $|V_{ub}|$ as a function of ζ with the LLR method (left) and for the determination with the full rate measurement (right). The error bars indicate the statistical uncertainty. They are correlated between the points and get larger for larger ζ due to larger background from $B \to X_c \ell\nu$. The total shaded are illustrates the theoretical uncertainty; the inner light shaded area indicates the perturbative share of the uncertainty. The arrow indicates $\zeta = 1.67$ GeV/c^2.

Another approach that BaBar chooses to reduce the model dependence is to measure the $B \to X_u \ell\nu$ rate over the entire M_X spectrum. Since no extrapolation is necessary to obtain the full rate, systematic uncertainties from m_b and Fermi motion are much reduced. Perturbative corrections are known to order α_s. The rate of $B \to X_u \ell\nu$ is extracted from the hadronic mass spectrum up to $\zeta = 2.5$ GeV/c^2 which corresponds to about 96 % of the simulated hadronic mass spectrum, and find $|V_{ub}| = (3.84 \pm 0.70_{\rm stat} \pm 0.30_{\rm syst} \pm 0.10_{\rm th}) \times 10^{-3}$, using the average B lifetime of $\tau_B = (1.604 \pm 0.012)$ ps. The current uncertainties on the $B \to X_s\gamma$ photon energy spectrum limit the sensitivity with which the behavior at high ζ can be probed. These two new results are consistent with previous measurements but have substantially smaller uncertainties from m_b and the modeling for Fermi motion of the b quark inside the B meson. Both techniques are based on theoretical calculations that are distinct from other calculations normally employed to extract $|V_{ub}|$ and, thus, provide a complementary determination of $|V_{ub}|$.

3 Exclusive determination of $|V_{ub}|$

In this section, we discuss the extraction of $|V_{ub}|$ from exclusive decays such as $B \to (\pi, \rho, \omega)\ell\nu$. For $B^0 \to \pi^-\ell^+\nu$ decays, the differential decay rate becomes

$$\frac{d\Gamma(B \to \pi\ell\nu)}{dq^2} = \frac{G_F^2}{24\pi^3}|V_{ub}|^2 p_\pi^3 |f_+(q^2)|^2 \tag{8}$$

where $f_+(q^2)$ is a form factor and q^2 is the squared invariant mass of the $\ell^+\nu$ system. Only shape of $f_+(q^2)$ can be measured experimentally. Its normalization is provided by theoretical calculations which currently suffer from relatively large uncertainties and, often, do not agree with each other. As a result, the normalization of the $f_+(q^2)$ form factor is the largest source of uncertainly in the extraction of $|V_{ub}|$ from the $B^0 \to \pi^-\ell^+\nu$ branching fraction. Values of $f_+(q^2)$ for $B^0 \to \pi^-\ell^+\nu$ decays are provided by unquenched [14,15] and quenched [16] lattice QCD calculations, presently reliable only at high q^2 (> 16 GeV^2/c^4), and by Light Cone Sum Rules calculations [17] (LCSR) based on approximations only valid at low q^2 (< 16 GeV^2/c^4), as well as by a quark model [18]. The QCD theoretical predictions are at present more precise for $B^0 \to \pi^-\ell^+\nu$ decays than for other exclusive $B \to X_u\ell\nu$ decays. Experimental data can be used to discriminate between the various calculations by measuring the $f_+(q^2)$ shape precisely, thereby leading to a smaller theoretical uncertainty on $|V_{ub}|$.

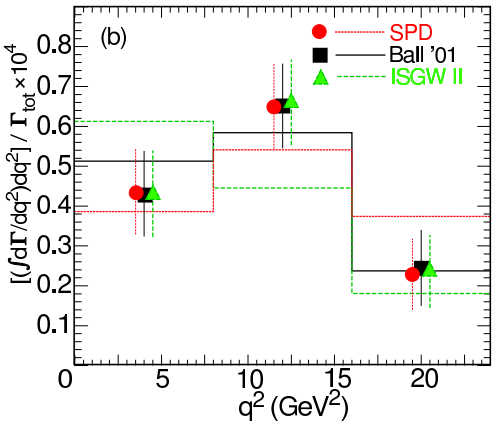

Figure 5: Fit to $d\Gamma/dq^2$ on exclusive $B \to \pi^-\ell^+\nu$ decays.

For the recoiling the other side of the B meson, we may require nothing (untagged) or require indication of semileptonic decay ($D^{(*)}\ell\nu$ tag), and require hadronic decay (full reconstruction tag). We review recent progress on experimental studies with different tagging methods listed above.

- Untagged $B \to \pi\ell\nu$

CLEO pioneered the measurement of V_{ub} with exclusive decays [19]. They perform a simultaneous maximum likelihood fit in ΔE and $M_{m\ell\nu}$ to seven sub-modes: $\pi^{\pm}$, π^0, $\rho^{\pm}$, $\omega/\eta \to pi^+\pi^-\pi^0$, and $\eta \to \gamma\gamma$. In the fit they used isospin symmetry to constrain the semileptonic widths $\Gamma^{\rm SL}(\pi^{\pm}) = 2\Gamma^{\rm SL}$ (π^0) and $\Gamma^{\rm SL}(\rho^{\pm}) = 2\Gamma^{\rm SL}$ (ρ^0) $\sim 2\Gamma^{\rm SL}$ (ω), where the final approximate equality is inspired by constituent quark symmetry. Signals for π and ρ are extracted separately in three q^2 bins. Given form factors from theory, they extracted $|V_{ub}|$ from a fit to $d\Gamma/dq^2$, and it is shown in Fig. 5. From their fit, we see that ISGW2 [18] is least favored. Combining $B \to \pi\ell\nu$ and $B \to \rho\ell\nu$ results, CLEO found that

$$|V_{ub}| = (3.17 \pm 0.17({\rm stat})^{+0.16}_{-0.17}({\rm syst})^{+0.53}_{-0.39}({\rm theo}) \pm 0.03_{\rm FF}) \times 10^{-3}. \quad (9)$$

BaBar also did similar but improved analysis [20]. More accurate value of q^2 was obtained in the so-called Y-average frame where the pseudo-particle Y has a four-momentum defined by $P_Y \equiv (P_\pi + P_\ell)$. The angle θ_{YT} between the directions of the p^*_B and p^*_Y momenta in the $\Upsilon(4S)$ rest frame can be determined assuming energy-momentum conservation in a semileptonic $B \to Y\nu$ decay. The use of the Y-averaged frame yields a q^2 resolution that is approximately 20 % bettern than what is obatined in the usual $\Upsilon(4S)$ frame where the B meson is assumed to be at rest. They also fit the $\Delta\mathcal{B}/\mathcal{B}$ spectrum using a probability density function based on the $f_+(q^2, \alpha)$ parametrization of Becirevic-Kaidalov [21] (BK). The normalized $\Delta\mathcal{B}/\mathcal{B}$ distribution is shown in Fig. 6, together with the result of a $f_+(q^2)$ shape fit using the BK parametrization and theoretical prediction. The obtain a value of $\alpha = 0.53$ $\pm$ 0.05 $\pm$ 0.04. BaBar data are clearly incompatible with the ISGW2 quark model, which is in agreement with what CLEO data indicated before. The extraction of $|V_{ub}|$ is carried out from the partial branching fractions using $|V_{ub}| = \sqrt{\Delta\mathcal{B}/(\tau^0_B \Delta\zeta)}$, where $\tau^0_B = (1.536 \pm 0.014)$ ps is the B^0 lifetime and $\Delta\zeta$ is the normalized partial decay rate predicted by various form factor calculations. For the LCSR calculations with $q^2 <$ 16 GeV^2/c^4, $|V_{ub}| = (3.6 \pm 0.1 \pm 0.1\ ^{+0.6}_{-0.4}) \times 10^{-3}$ is obtained. For the HPQCD and and FNAL lattice calculations with $q^2 > 16$ GeV^2/c^4, $|V_{ub}| = (4.1 \pm 0.2 \pm 0.2\ ^{+0.6}_{-0.4})$ $\times 10^{-3}$ and $|V_{ub}| = (3.6 \pm 0.2 \pm 0.2\ ^{+0.6}_{-0.4}) \times 10^{-3}$ are obtained, respectively. Note that all are in good agreement within given uncertainty and this gives us confidence in exclusive measurement of $|V_{ub}|$.

- $D^{(*)}\ell\nu$ tag

Belle presented measurements of $B^0 \to \pi^-/\rho^-\ell^+\nu$ and $B^+ \to \pi^0/\rho^0\ell^+\nu$ decays using $B \to D^{(*)}\ell\nu$ tagging [22]. They reconstruct the entire decay chain from the

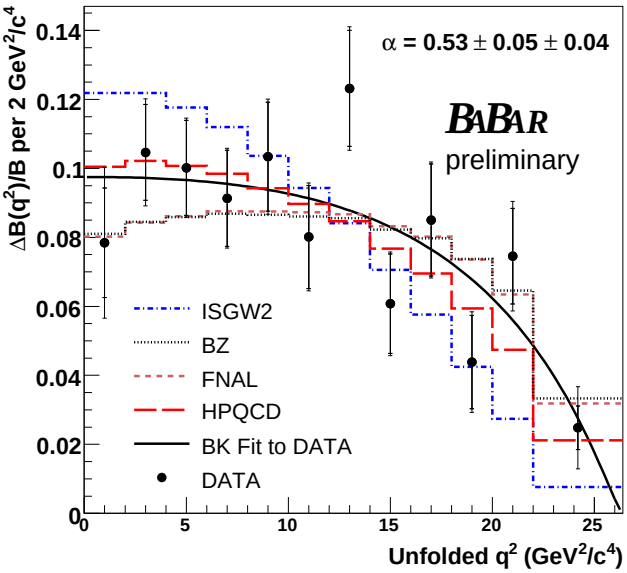

Figure 6: Differential decay rate formula fitted to the normalized partial $\Delta\mathcal{B}/\mathcal{B}$ spectrum in 12 bins of q^2. The smaller error bars are statistical only while the larger error bars include statistical and systematic uncertainties. The BK parametrization (solid black curve) reproduces the data quite well (χ^2=8.8 for 11 degrees of freedom) with the parameter $\alpha = 0.53 \pm 0.05 \pm 0.04$. The data are also compared to LCSR calculations (dotted line), unquenched LQCD calculations (long dashed line and short dashed line) and the ISGW2 quark model (dash-dot line).

$\Upsilon(4S) \to B_{\rm sig}B_{\rm tag}$, $B_{\rm sig} \to \pi/\rho\ell\nu$ and $B_{\rm tag} \to D^{(*)}\ell\nu$ tag with several $D^{(*)}$ sub-modes. The back-to-back correlation of the two B mesons in the $\Upsilon(4S)$ rest frame allows us to constrain the kinematics of the double semileptonic decay. The signal is reconstructed in four modes, $B^0 \to \pi^-/\rho^-\ell^+\nu$ and $B^+ \to \pi^0/\rho^0\ell^+\nu$. Yields and branching fractions are extracted from a simultaneous fit of the B^0 and B^+ samples in three intervals of q^2, accounting for cross-feed between modes as well as other backgrounds. Belle applied this methods to $B \to \pi/\rho\ell\nu$ decays for the first time, and have succeeded in reconstructing these decays with significantly improved signal-to-noise ratios compared to the ν-reconstruction method. With the data of 253 fb^{-1}, Belle extracted branching fractions and $|V_{ub}|$. Figure 7 shows the q^2 distribution for the decay $B^0 \to \pi^-/\rho^-\ell^+\nu$. The error bars are too large to reject any of form factor models for the moment. Table 5 summarized the results with two different lattice calculations. This gives about 13 % experimental uncertainty on $|V_{ub}|$, currently dominated by the statistical error of 11 %. By accumulating more integrated luminosity, a measurement with errors

Table 5: Summary of $|V_{ub}|$ measurements by the Belle collaboration with different lattice calculations.

	q^2 GeV^2/c^4	$\|V_{ub}\| \times 10^{-3}$
FNAL	> 16	$3.60 \pm 0.41 \pm 0.20 \pm {}^{0.62}_{-0.41}$
HPQCD	> 16	$4.03 \pm 0.46 \pm 0.22 \pm {}^{0.59}_{-0.41}$

below 10 % is feasible. With improvements to unquenched LQCD calculations, the present method may provide a precise determination of $|V_{ub}|$.

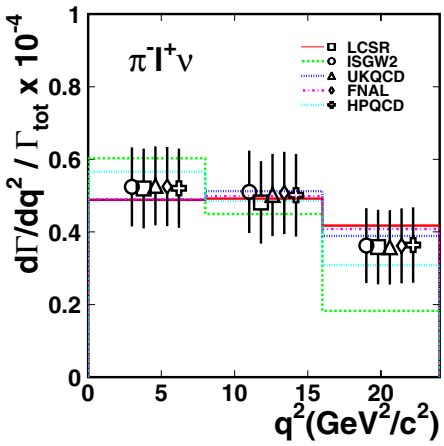

Figure 7: Extracted q^2 distribution for $B^0 \to \pi^- \ell^+ \nu$ decays. Data points are shown for different form factor models used to estimate the detection efficiency. Lines are for the best fit of the form factor shapes to the obtained q^2 distribution.

The BaBar collaboration also did similar analysis [23] based on 211 fb^{-1} of data. They also included the hadronic decay of B mesons for tagging. The detailed techniques are similar to what to be explained later. The summary of the measurement of $|V_{ub}|$ can be found in Table 6. All the results are in good agreement with the results from the Belle experiment.

- Full reconstruction tag

In this method [25], Belle fully reconstructs one of the two B mesons from $\Upsilon(4S)$ decay ($B_{\rm tag}$) in one of the following hadronic decay modes, $B^- \to D^{(*)0}\pi^-$, $B^- \to D^{(*)0}\rho^-$, $B^- \to D^{(*)0}a_1^-$, $B^- \to D^{(*)0}D_s^{(*)-}$, $B^0 \to D^{(*)+}\pi^-$, $B^0 \to D^{(*)+}\rho^-$, $B^0 \to D^{(*)+}a_1^-$, or $B^0 \to D^{(*)+}D_s^{(*)-}$. As was done in other B meson analyses, decays are identified on the basis of the proximity of the beam-energy constrained mass $M_{\rm bc}$

Table 6: Summary of $|V_{ub}|$ measurements by the BaBar collaboration with different theoretical calculations.

	q^2 GeV^2/c^4	$\|V_{ub}\| \times 10^{-3}$
Ball-Zwicky	< 16	$3.2 \pm 0.2 \pm 0.1\ ^{+0.5}_{-0.4}$
HPQCD	> 16	$4.5 \pm 0.5 \pm 0.3\ ^{+0.7}_{-0.5}$
FNAL	> 16	$4.0 \pm 0.5 \pm 0.3\ ^{+0.7}_{-0.5}$
APE [24]	> 16	$4.1 \pm 0.5 \pm 0.3\ ^{+1.6}_{-0.7}$

and ΔE to their nominal values of the B meson rest mass and zero, respectively. If multiple tag candidates are found, the one with values of $M_{\rm bc}$ and ΔE closest to nominal is chosen. Events with a $B_{\rm tag}$ satisfying the selections $M_{\rm bc} > 5.27$ GeV/c^2 and $-0.08 < \Delta E < 0.06$ GeV are retained. The charge of the $B_{\rm tag}$ candidate is necessarily restricted to $Q_{\rm tag} = 0$ or $Q_{\rm tag} \pm 1$ by demanding that it is consistent with one of the above decay modes. Reconstructed charged tracks and electromagnetic clusters which are not associated with the $B_{\rm tag}$ candidate are used to search for the signal B meson decays of interest recoiling against the $B_{\rm tag}$. After all cuts to enhance the signal are applied, remaining data are projected as a function of missing mass squared ($M_{\rm miss}$), as shown in Fig. 8. As is demonstrated in the figure, a high purity signal can be obtained with this method. A preliminary branching fractions are obtained as

$$\mathcal{B}(B \to \pi^- \ell\nu) = 1.49 \pm 0.26({\rm stat}) \pm 0.06({\rm syst}) \times 10^{-4}, \quad (10)$$

$$\mathcal{B}(B \to \pi^0 \ell\nu) = 0.86 \pm 0.17({\rm stat}) \pm 0.06({\rm syst}) \times 10^{-4}. \quad (11)$$

Whilst the statistical precision of these measurements is limited at present, the potential power of the full reconstruction tagging method, when it can be used with larger accumulated B-factory data samples in the future, can clearly be seen.

4 Conclusions

We have discussed recent progress in measurements of $|V_{ub}|$. At present, the total error from the inclusive measurement is approximately 7 %. The theoretical uncertainty in it is still larger than the experimental uncertainty, but not by a lot anymore. The shape function, describing the Fermi motion of the b-quark inside the meson still remains a big issue in extracting $|V_{ub}|$, but different approaches produce consistent numerical values indicating the problem is well understood. Also, BaBar's new approach based on Leibovich, Low and Rothstein [5] may look promising in future as it has residual SF dependence only.

The exclusive measurements of $|V_{ub}|$ gives the total error to be greater than 10 % at present and the form factor is the main issue in this field. The untagged analyses

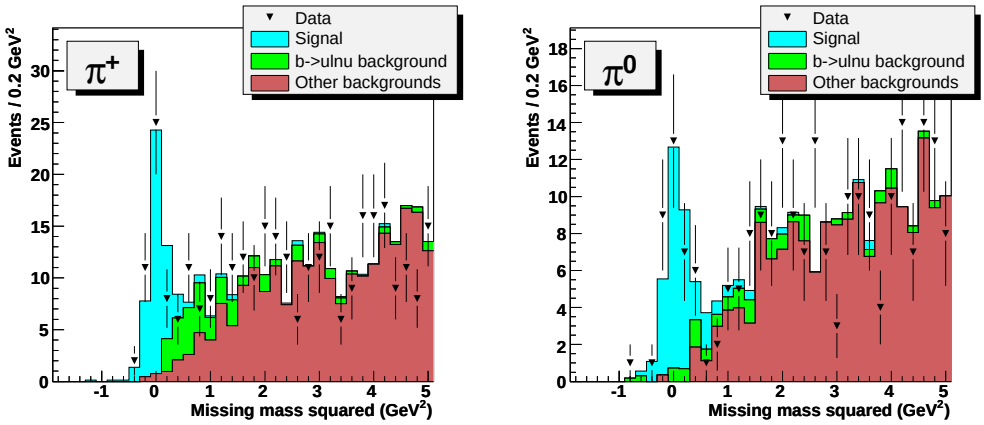

Figure 8: Missing mass squared ($M^2_{\rm miss}$) distributions after all cuts, for $B \to \pi^+ \ell\nu$ on the left and $B \to \pi^0 \ell\nu$ on the right. Data is indicated by the points with error bars. The blue histogram (lightest shade in greyscale) show the fitted prediction based on the LCSR model. The green histogram (middle shade in greyscale) shows the fitted $b \to u\ell\nu$ background contribution. The crimson histogram (darkest shade in greyscale) shows the fitted background contribution from other sources.

are the most precise ones at present. The theoretical uncertainty is still dominant in exclusive measurements.

I am grateful to Masahiro Morii from the BaBar experiment who kindly provided complete information on their experimental results.

Bibliography

[1] J. Chay, H. Georgi, and B. Grinstein, Phys. Lett. B **247**, 399 (1990); M. A. Shifman and M. B. Voloshin, Sov. J. Nucl. Phys. **41**, 120 (1985); I. I. Bigi *et al.*, Phys. Lett. B **293**, 430 (1992); **297**, 430(E) (1992); Phys. Rev. Lett. **71**, 496 (1993); A. V. Manohar and M. B. Wise, Phys. Rev. D **49**, 1310 (1994).

[2] N. Uraltsev, Int. J. Mod. Phys. A **14**, 4641 (1999); A. H. Hoang, Z. Ligeti, and A. V. Manohar, Phys. Rev. D **59**, 074017 (1999); T. van Ritbergen, Phys. Lett. B **454**, 353 (1999).

[3] B. O. Lange, M. Neubert and G. Paz, Phys. Rev. D **72**, 073006 (2005);

[4] J. R. Anderson and E. Gardi, J. High Energy Phys. **0601**, 097 (2006).

[5] A. K. Leibovich, I. Low and I. Z. Rothstein, Phys. Lett. B **486**, 86 (2000).

[6] The CLEO collaboration, Phys. Rev. Lett. **88**, 231803 (2002).

[7] The BaBar collaboration, Phys. Rev. D **73**, 012006 (2006).

[8] C. W. Bauer, Z. Ligeti and M. E. Luke, Phys. Rev. D **64**, 113004 (2001).

[9] The Belle collaboration, Phys. Rev. Lett. **95**, 241801 (2005).

[10] The BaBar collaboration, hep-ex/0507017.

[11] M. Neubert, Eur. Phys. J. C **40**, 165 (2005); Phys. Lett. B **612**, 13 (2005); S. W. Bosch, M. Neubert, and G. Paz, J. High Energy Phys. **11**, 073 (2004).

[12] htp://www.slac.stanford.edu/xorg/hfag.

[13] The BaBar collaboration, Phys. Rev. Lett. **96**, 222801 (2006).

[14] The HPQCD collaboration, E. Gulez *et al.*, Phys. Rev. **D73**, 074502 (2006).

[15] The FNAL collaboration, M. Okamoto *et al.*, Nucl. Phys. Proc. Suppl. **140** 461 (2005).

[16] A. Abada *et al.*, Nucl. Phys. **D619**, 565 (2001).

[17] P. Ball, R. Zwicky, Phys. Rev. **D71**, 014015 (2005).

[18] D. Scora, N. Isgur, Phys. Rev. **D52**, 2783 (1995).

[19] The CLEO collaboration, Phys. Rev. **D68**, 072003 (2003).

[20] The BaBar collaboration, hep-ex/0607060.

[21] D. Becirevic and A. B. Kaidalov, Phys. Lett. **B478**, 417 (2000).

[22] The Belle collaboration, hep-ex/0604024.

[23] The BaBar collaboration, hep-ex/0607089.

[24] A. Abada *et al.*, Nucl. Phys. **B619**, 565 (2001).

[25] The Belle collaboration, hep-ex/0610054.

Flavour Physics in the Littlest Higgs Model with T-Parity

Cecilia Tarantino
Physik Department,
Technische Universität München,
D-85748 Garching, Germany

We present the results of an extensive analysis of flavour physics in both quark and lepton sectors, in the Littlest Higgs model with T-parity (LHT). In the quark sector, we identify some interesting scenarios for new mirror quark masses and V_{Hd} mixing matrix that satisfy the existing experimental constraints from K and B physics and simultaneously allow large New Physics effects in rare decays and CP-violating observables. In the lepton sector, where flavour violation in the Standard Model is highly suppressed by small neutrino masses, LHT effects turn out to be naturally huge and could be seen in the near future measurements of lepton flavour violating decays.

1 The LHT Model

The Standard Model (SM) is in excellent agreement with the results of particle physics experiments, in particular with the electroweak (ew) precision measurements, thus suggesting that the SM cutoff scale is at least as large as 10 TeV. Having such a relatively high cutoff, however, the SM requires an unsatisfactory fine-tuning to yield a correct ($\approx 10^2$ GeV) scale for the squared Higgs mass, whose corrections are quadratic and therefore highly sensitive to the cutoff. This *little hierarchy problem* has been one of the main motivations to elaborate models of physics beyond the SM. While Supersymmetry is at present the leading candidate, different proposals have been formulated more recently. Among them, Little Higgs models play an important role, being perturbatively computable up to about 10 TeV and with a rather small number of parameters, although their predictivity can be weakened by a certain sensitivity to the unknown ultra-violet (UV) completion of these models.

In Little Higgs models [1] the Higgs is naturally light as it is identified with a Nambu-Goldstone boson (NGB) of a spontaneously broken global symmetry. An exact NGB, however, would have only derivative interactions. Gauge and Yukawa interactions of the Higgs have to be incorporated. This can be done without generating quadratically divergent one-loop contributions to the Higgs mass, through the

so-called *collective symmetry breaking*. Collective symmetry breaking (SB) has the peculiarity of generating the Higgs mass only when two or more couplings in the Lagrangian are non-vanishing, thus avoiding one-loop quadratic divergences. This mechanism is diagrammatically realized through the contributions of new particles with masses around 1 TeV, that cancel the SM quadratic divergences.

The most economical, in matter content, Little Higgs model is the Littlest Higgs (LH) [2], where the global group $SU(5)$ is spontaneously broken into $SO(5)$ at the scale $f \approx \mathcal{O}(1\,\text{TeV})$ and the ew sector of the SM is embedded in an $SU(5)/SO(5)$ non-linear sigma model. Gauge and Yukawa Higgs interactions are introduced by gauging the subgroup of $SU(5)$: $[SU(2) \times U(1)]_1 \times [SU(2) \times U(1)]_2$, with gauge couplings respectively equal to g_1, g_1', g_2, g_2'. The key feature for the realization of collective SB is that the two gauge factors commute with a different $SU(3)$ global symmetry subgroup of $SU(5)$, that prevents the Higgs from becoming massive when the couplings of one of the two gauge factors vanish. Consequently, quadratic corrections to the squared Higgs mass involve two couplings and cannot appear at one-loop. In the LH model, the new particles appearing at the TeV scales are the heavy gauge bosons $(W_H^\pm, Z_H, A_H)$ the heavy top (T) and the scalar triplet Φ.

In the LH model, significant corrections to ew observables come from tree-level heavy gauge boson contributions and the triplet vacuum expectation value (vev) which breaks the custodial $SU(2)$ symmetry. Consequently, ew precision tests are satisfied only for quite large values of the New Physics (NP) scale $f \geq 2-3\,\text{TeV}$ [3,4], unable to solve the little hierarchy problem. Motivated by reconciling the LH model with ew precision tests, Cheng and Low [5] proposed to enlarge the symmetry structure of the theory by introducing a discrete symmetry called T-parity. T-parity acts as an automorphism which exchanges the $[SU(2) \times U(1)]_1$ and $[SU(2) \times U(1)]_2$ gauge factors. The invariance of the theory under this automorphism implies $g_1 = g_2$ and $g_1' = g_2'$. Furthermore, T-parity explicitly forbids the tree-level contributions of heavy gauge bosons and the interactions that induced the triplet vev. The custodial $SU(2)$ symmetry is restored and the compatibility with ew precision data is obtained already for smaller values of the NP scale, $f \geq 500\,\text{GeV}$ [6]. Another important consequence is that particle fields are T-even or T-odd under T-parity. The SM particles and the heavy top T_+ are T-even, while the heavy gauge bosons $W_H^\pm, Z_H, A_H$ and the scalar triplet Φ are T-odd. Additional T-odd particles are required by T-parity: the odd heavy top T_- and the so-called mirror fermions, i.e., fermions corresponding to the SM ones but with opposite T-parity and $\mathcal{O}(1\,\text{TeV})$ mass. Mirror fermions are characterized by new flavour interactions with SM fermions and heavy gauge bosons, which involve two new unitary mixing matrices, in the quark sector, analogous to the Cabibbo-Kobayashi-Maskawa (CKM) matrix V_{CKM} [7]. They are V_{Hd} and V_{Hu}, respectively involved when the SM quark is of down- or up-type, and satisfying $V_{Hu}^\dagger V_{Hd} = V_{CKM}$ [8]. Similarly, two new mixing matrices, $V_{H\ell}$ and $V_{H\nu}$, appear in the lepton sector, respectively involved when the SM lepton is charged or a neutrino

and related to the PMNS matrix [9] through $V_{H\nu}^\dagger V_{H\ell} = V_{PMNS}^\dagger$. Both V_{Hd} and $V_{H\ell}$ contain 3 angles, like V_{CKM} and V_{PMNS}, but 3 (non-Majorana) phases [10], i.e. two additional phases relative to the SM matrices, that cannot be rotated away in this case.

Because of these new mixing matrices, the LHT model does not belong to the Minimal Flavour Violation (MFV) class of models [11, 12] and significant effects in flavour observables are possible. Other LHT peculiarities are the rather small number of new particles and parameters (the SB scale f, the parameter x_L describing T_+ mass and interactions, the mirror fermion masses and V_{Hd} and $V_{H\ell}$ parameters) and the absence of new operators in addition to the SM ones. On the other hand, one has to recall that Little Higgs models are low energy non-linear sigma models, whose unknown UV-completion introduces a theoretical uncertainty reflected by a left-over logarithmic cut-off dependence [13, 14] in $\Delta F = 1$ processes.

2 LHT Flavour Analysis

Several studies of flavour physics in the LH model without T-parity have been performed in the last four years [15]. Without T-parity, mirror fermions and new sources of flavour and CP-violation are absent, the LH model is a MFV model and NP contributions result to be very small.

More recently, flavour physics analyses have been also performed in the LHT model, for both quark [8, 14, 16] and lepton sectors [17, 18]. In this model, new mirror fermion interactions can yield large NP effects, mainly in K and B rare and CP-violating decays and in lepton flavour violating decays.

2.1 LHT Analysis in the Quark Sector

In [14, 16] we have studied in the LHT model B and K meson mixings, CP-violation, rare decays and the radiative decay $B \to X_s\gamma$. We have imposed well known experimental constraints and estimated LHT effects in those observables that are not yet measured or still very uncertain. We have considered several scenarios for the structure of the V_{Hd} matrix and the mass spectrum of mirror quarks in order to gain a global view over possible LHT signatures. The parameters f and x_L have been fixed to $f = 1\,\text{TeV}$ and $x_L = 0.5$ in accordance with ew precision tests [6]. The CKM parameters entering the analysis have been taken from tree level decays only, where NP effects can be neglected. In order to simplify the numerical analysis we have set all non-perturbative parameters to their central values, while allowing ΔM_K, ε_K, ΔM_d, ΔM_s, $\Delta M_s/\Delta M_d$ and $S_{\psi K_S}$ to differ from their experimental values by $\pm 50\%$, $\pm 40\%$, $\pm 40\%$, $\pm 40\%$, $\pm 20\%$ and $\pm 8\%$, respectively. This rather conservative choice guarantees that important effects are not missed.

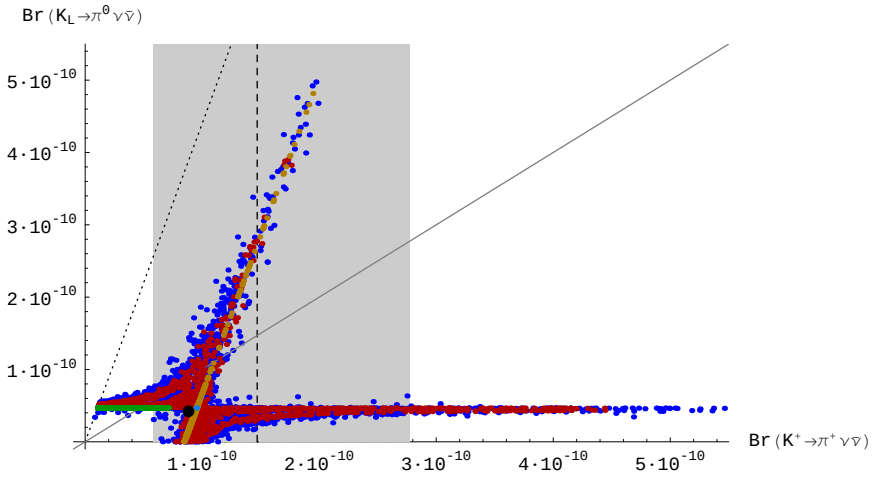

Figure 1: *$Br(K_L \to \pi^0\nu\overline{\nu})$ as a function of $Br(K^+ \to \pi^+\nu\overline{\nu})$. The shaded area represents the experimental 1σ-range for $Br(K^+ \to \pi^+\nu\overline{\nu})$. The model-independent Grossman-Nir bound [19] is displayed by the dotted line, while the solid line separates the two areas where $Br(K_L \to \pi^0\nu\overline{\nu})$ is larger or smaller than $Br(K^+ \to \pi^+\nu\overline{\nu})$.*

Two interesting scenarios have been identified. In the first one (B-scenario) large enhancements in B physics are possible, while in the second one (K-scenario) important effects appear in K observables. They are both characterized by the quasi-degeneracy of the first two mirror quark generations ($m_{H1} \simeq m_{H2} \simeq 500\,\text{GeV}$, $m_{H3} \simeq 1000\,\text{GeV}$), as required by ΔM_K and ε_K constraints. The new mixing angles in V_{Hd} are chosen to satisfy the hierarchy $s^d_{23}\bar{l}\bar{l}s^d_{13} \leq s^d_{12}$ in B-scenario and the hierarchy $s^d_{23} \simeq s^d_{13} < s^d_{12} = 1/\sqrt{2}$ in K-scenario. Moreover, the two additional phases of V_{Hd}, whose impact is numerically small, have been set to zero. In addition, in order to explore all possible LHT effects, we have performed a general scan over mirror quark masses and V_{Hd} parameters. In the following scatter plots, B- and K-scenarios and general scan are respectively displayed as green, brown and blue points, while red points correspond to a less general scan over V_{Hd} parameters at fixed mirror masses ($m_{H1} = 400\,\text{GeV}$, $m_{H2} = 500\,\text{GeV}$, $m_{H3} = 600\,\text{GeV}$).

The main results of our LHT analysis [14, 16] in the quark sector are:

- The most evident departures from the SM predictions are found for CP-violating observables that are strongly suppressed in the SM. These are the branching ratio for $K_L \to \pi^0\nu\overline{\nu}$ (Fig. 1) and the CP-asymmetry $S_{\psi\phi}$, that can be enhanced by an order of magnitude relative to the SM predictions. Large departures from SM expectations are also possible for $Br(K_L \to \pi^0\ell^+\ell^-)$ (Fig. 2), $Br(K^+ \to \pi^+\nu\overline{\nu})$ (Fig. 1) and the semileptonic CP-asymmetry A^s_{SL}, that can be enhanced

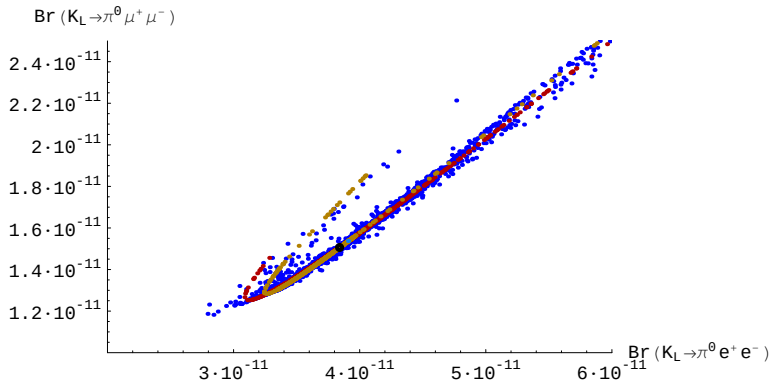

Figure 2: $Br(K_L \to \pi^0\mu^+\mu^-)$ *as a function of* $Br(K_L \to \pi^0 e^+ e^-)$.

by an order of magnitude w.r.t the SM.

- The branching ratios for $B_{s,d} \to \mu^+\mu^-$ and $B \to X_{s,d}\nu\overline{\nu}$, instead, are modified by at most 50% and 35%, respectively, and the effects of new electroweak penguins in $B \to \pi K$ are small, in agreement with the recent data. The new physics effects in $B \to X_{s,d}\gamma$ and $B \to X_{s,d}\ell^+\ell^-$ turn out to be below 5% and 15%, respectively, so that agreement with the data can easily be obtained.

- Small, but still significant effects have been found in $B_{s,d}$ mass differences. In particular, a 7% suppression of ΔM_s is possible, thus improving the compatibility with the recent experimental measurement [20].

- The possible "discrepancy" [21–23] between the values of $\sin 2\beta$ following directly from $A_{\rm CP}(B_d \to \psi K_S)$ and indirectly from the analysis of the unitarity triangle involving only tree-level processes, and in particular $|V_{ub}|$, can be cured within the LHT model thanks to a new phase $\varphi_{B_d} \simeq -5^o$.

- The universality of new physics effects, characteristic for MFV models, can be largely broken, in particular between K and $B_{s,d}$ systems. NP effects, in fact, are typically larger in K system where the SM contribution is CKM-suppressed. In particular, sizable departures from MFV relations between $\Delta M_{s,d}$ and $Br(B_{s,d} \to \mu^+\mu^-)$ and between $S_{\psi K_S}$ and the $K \to \pi\nu\overline{\nu}$ decay rates are possible.

decay	$f = 1000\,\text{GeV}$	$f = 500\,\text{GeV}$	exp. upper bound
$\mu \to e\gamma$	$1.2 \cdot 10^{-11}$ $(1 \cdot 10^{-11})$	$1.2 \cdot 10^{-11}$ $(1 \cdot 10^{-11})$	$1.2 \cdot 10^{-11}$ [24]
$\mu^- \to e^-e^+e^-$	$1.0 \cdot 10^{-12}$ $(1 \cdot 10^{-12})$	$1.0 \cdot 10^{-12}$ $(1 \cdot 10^{-12})$	$1.0 \cdot 10^{-12}$ [25]
$\mu\text{Ti} \to e\text{Ti}$	$2 \cdot 10^{-10}$ $(5 \cdot 10^{-12})$	$4 \cdot 10^{-11}$ $(5 \cdot 10^{-12})$	$4.3 \cdot 10^{-12}$ [26]
$\tau \to e\gamma$	$8 \cdot 10^{-10}$ $(7 \cdot 10^{-10})$	$2 \cdot 10^{-8}$ $(2 \cdot 10^{-8})$	$1.1 \cdot 10^{-7}$ [27]
$\tau \to \mu\gamma$	$8 \cdot 10^{-10}$ $(8 \cdot 10^{-10})$	$2 \cdot 10^{-8}$ $(2 \cdot 10^{-8})$	$4.5 \cdot 10^{-8}$ [28]
$\tau^- \to e^-e^+e^-$	$7 \cdot 10^{-10}$ $(6 \cdot 10^{-10})$	$7 \cdot 10^{-8}$ $(7 \cdot 10^{-8})$	$2.0 \cdot 10^{-7}$ [29]
$\tau^- \to \mu^-\mu^+\mu^-$	$7 \cdot 10^{-10}$ $(6 \cdot 10^{-10})$	$7 \cdot 10^{-8}$ $(6 \cdot 10^{-8})$	$1.9 \cdot 10^{-7}$ [29]
$\tau^- \to e^-\mu^+\mu^-$	$5 \cdot 10^{-10}$ $(5 \cdot 10^{-10})$	$6 \cdot 10^{-8}$ $(6 \cdot 10^{-8})$	$2.0 \cdot 10^{-7}$ [30]
$\tau^- \to \mu^-e^+e^-$	$5 \cdot 10^{-10}$ $(5 \cdot 10^{-10})$	$6 \cdot 10^{-8}$ $(5 \cdot 10^{-8})$	$1.9 \cdot 10^{-7}$ [30]
$\tau^- \to \mu^-e^+\mu^-$	$5 \cdot 10^{-14}$ $(3 \cdot 10^{-14})$	$5 \cdot 10^{-14}$ $(5 \cdot 10^{-14})$	$1.3 \cdot 10^{-7}$ [29]
$\tau^- \to e^-\mu^+e^-$	$5 \cdot 10^{-14}$ $(3 \cdot 10^{-14})$	$5 \cdot 10^{-14}$ $(4 \cdot 10^{-14})$	$1.1 \cdot 10^{-7}$ [29]
$\tau \to \mu\pi$	$2 \cdot 10^{-9}$ $(2 \cdot 10^{-9})$	$2 \cdot 10^{-7}$ $(1 \cdot 10^{-7})$	$4.1 \cdot 10^{-7}$ [31]
$\tau \to e\pi$	$2 \cdot 10^{-9}$ $(2 \cdot 10^{-9})$	$2 \cdot 10^{-7}$ $(1 \cdot 10^{-7})$	$1.9 \cdot 10^{-7}$ [31]
$\tau \to \mu\eta$	$6 \cdot 10^{-10}$ $(6 \cdot 10^{-10})$	$6 \cdot 10^{-8}$ $(5 \cdot 10^{-8})$	$1.5 \cdot 10^{-7}$ [31]
$\tau \to e\eta$	$6 \cdot 10^{-10}$ $(6 \cdot 10^{-10})$	$6 \cdot 10^{-8}$ $(5 \cdot 10^{-8})$	$2.4 \cdot 10^{-7}$ [31]
$\tau \to \mu\eta'$	$7 \cdot 10^{-10}$ $(7 \cdot 10^{-10})$	$8 \cdot 10^{-8}$ $(8 \cdot 10^{-8})$	$4.7 \cdot 10^{-7}$ [31]
$\tau \to e\eta'$	$7 \cdot 10^{-10}$ $(7 \cdot 10^{-10})$	$8 \cdot 10^{-8}$ $(7 \cdot 10^{-8})$	$1.0 \cdot 10^{-6}$ [31]
$K_L \to \mu e$	$4 \cdot 10^{-13}$ $(2 \cdot 10^{-13})$	$3 \cdot 10^{-14}$ $(3 \cdot 10^{-14})$	$4.7 \cdot 10^{-12}$ [32]
$K_L \to \pi^0\mu e$	$4 \cdot 10^{-15}$ $(2 \cdot 10^{-15})$	$5 \cdot 10^{-16}$ $(5 \cdot 10^{-16})$	$6.2 \cdot 10^{-9}$ [33]
$B_d \to \mu e$	$5 \cdot 10^{-16}$ $(2 \cdot 10^{-16})$	$9 \cdot 10^{-17}$ $(9 \cdot 10^{-17})$	$1.7 \cdot 10^{-7}$ [34]
$B_s \to \mu e$	$5 \cdot 10^{-15}$ $(2 \cdot 10^{-15})$	$9 \cdot 10^{-16}$ $(9 \cdot 10^{-16})$	$6.1 \cdot 10^{-6}$ [35]
$B_d \to \tau e$	$3 \cdot 10^{-11}$ $(2 \cdot 10^{-11})$	$3 \cdot 10^{-10}$ $(2 \cdot 10^{-10})$	$1.1 \cdot 10^{-4}$ [36]
$B_s \to \tau e$	$2 \cdot 10^{-10}$ $(2 \cdot 10^{-10})$	$3 \cdot 10^{-9}$ $(2 \cdot 10^{-9})$	—
$B_d \to \tau\mu$	$3 \cdot 10^{-11}$ $(3 \cdot 10^{-11})$	$3 \cdot 10^{-10}$ $(3 \cdot 10^{-10})$	$3.8 \cdot 10^{-5}$ [36]
$B_s \to \tau\mu$	$2 \cdot 10^{-10}$ $(2 \cdot 10^{-10})$	$3 \cdot 10^{-9}$ $(3 \cdot 10^{-9})$	—

Table 1: *Upper bounds on LFV decay branching ratios in the LHT model, for two different values of the scale f, after imposing the constraints on $\mu \to e\gamma$ and $\mu^- \to e^-e^+e^-$. The numbers given in brackets are obtained after imposing the additional constraint $R(\mu Ti \to e Ti) < 5 \cdot 10^{-12}$. The current experimental upper bounds are also given.*

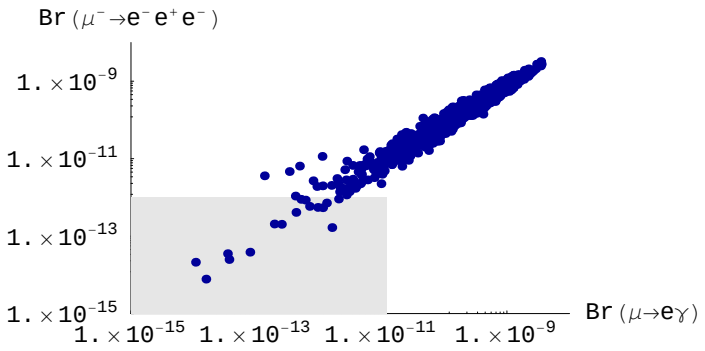

Figure 3: *Correlation between the branching ratios for $\mu \to e\gamma$ and $\mu^- \to e^-e^+e^-$ from a general scan over the LHT parameters. The shaded area represents present experimental upper bounds.*

2.2 LHT Analysis in the Lepton Sector

In contrast to rare K and B decays, where the SM contributions play an important and often dominant role in the LHT model, the smallness of ordinary neutrino masses assures that mirror fermion contributions to lepton flavour violating (LFV) processes are by far the dominant effects. Moreover, the absence of QCD corrections and hadronic matrix elements allows in most cases to make predictions entirely within perturbation theory.

In [18] we have studied the most interesting LFV processes: $\ell_i \to \ell_j\gamma$, $\tau \to \ell P$ (with $P = \pi, \eta, \eta'$), $\mu^- \to e^-e^+e^-$, the six three-body decays $\tau^- \to l_i^- l_j^+ l_k^-$ and the rate for $\mu - e$ conversion in nuclei. We have also calculated the rates for $K_{L,S} \to \mu e$, $K_{L,S} \to \pi^0\mu e$, $B_{d,s} \to \mu e$, $B_{d,s} \to \tau e$ and $B_{d,s} \to \tau\mu$.

At variance with meson decays, the number of flavour violating decays in the lepton sector, for which significant experimental constraints exist, is rather limited. Basically only the upper bounds on $Br(\mu \to e\gamma)$, $Br(\mu^- \to e^-e^+e^-)$, $Br(K_L \to \mu e)$ and $R(\mu\mathrm{Ti} \to e\mathrm{Ti})$ can be used in our analysis. The situation may change significantly in the coming years thanks to near future experiments [26, 37–39]. Meanwhile, we have estimated LHT effects, imposing the experimental bounds mentioned above and scanning over mirror lepton masses in the range $[300\,\mathrm{GeV}, 1500\,\mathrm{GeV}]$ and over the parameters of the $V_{H\ell}$ mixing matrix, with the symmetry breaking scale f fixed to $f = 1\,\mathrm{TeV}$ or $f = 500\,\mathrm{GeV}$ in accordance with ew precision tests [6].

We have found that essentially all the rates considered can reach or approach present experimental upper bounds, as shown in table 1. In particular, in order to suppress the $\mu \to e\gamma$ and $\mu^- \to e^-e^+e^-$ decay rates below the experimental upper bounds (see Fig. 3), the $V_{H\ell}$ mixing matrix has to be rather hierarchical, unless mirror

ratio	LHT	MSSM (dipole)	MSSM (Higgs)
$\frac{Br(\mu^-\to e^-e^+e^-)}{Br(\mu\to e\gamma)}$	$0.4\ldots2.5$	$\sim 6\cdot10^{-3}$	$\sim 6\cdot10^{-3}$
$\frac{Br(\tau^-\to e^-e^+e^-)}{Br(\tau\to e\gamma)}$	$0.4\ldots2.3$	$\sim 1\cdot10^{-2}$	$\sim 1\cdot10^{-2}$
$\frac{Br(\tau^-\to \mu^-\mu^+\mu^-)}{Br(\tau\to \mu\gamma)}$	$0.4\ldots2.3$	$\sim 2\cdot10^{-3}$	< 0.2
$\frac{Br(\tau^-\to e^-\mu^+\mu^-)}{Br(\tau\to e\gamma)}$	$0.3\ldots1.6$	$\sim 2\cdot10^{-3}$	< 0.1
$\frac{Br(\tau^-\to \mu^-e^+e^-)}{Br(\tau\to \mu\gamma)}$	$0.3\ldots1.6$	$\sim 1\cdot10^{-2}$	$\sim 1\cdot10^{-2}$
$\frac{Br(\tau^-\to e^-e^+e^-)}{Br(\tau^-\to e^-\mu^+\mu^-)}$	$1.3\ldots1.7$	~ 5	$0.1\ldots5$
$\frac{Br(\tau^-\to \mu^-\mu^+\mu^-)}{Br(\tau^-\to \mu^-e^+e^-)}$	$1.2\ldots1.6$	~ 0.2	$0.2\ldots20$
$\frac{R(\mu\mathrm{Ti}\to e\mathrm{Ti})}{Br(\mu\to e\gamma)}$	$10^{-2}\ldots10^{2}$	$\sim 5\cdot10^{-3}$	$> 5\cdot10^{-3}$

Table 2: *Comparison of various ratios of branching ratios in the LHT model and in the MSSM without and with significant Higgs contributions.*

leptons are quasi-degenerate.

Moreover, following the strategy proposed in [40–42] in the supersymmetric framework, we have identified certain correlations between branching ratios that are less parameter dependent than the individual branching ratios and could provide a clear signature of the model. In particular, we find that the ratios $Br(\ell_i\to\ell_j\ell_j\ell_j)/Br(\ell_i\to\ell_j\gamma)$, $Br(\ell_i\to\ell_j\ell_j\ell_j)/Br(\ell_i\to\ell_j\ell_k\ell_k)$ and $Br(\ell_i\to\ell_j\ell_k\ell_k)/Br(\ell_i\to\ell_j\gamma)$ could allow for a transparent distinction between the LHT model and the MSSM (see Table 2).

Finally, we have studied the muon anomalous magnetic moment finding that, even for values of the NP scale f as low as 500 GeV, $a_\mu^{\mathrm{LHT}} < 1.2\cdot10^{-10}$. This value is roughly a factor 5 below the current experimental uncertainty [43], implying that the possible discrepancy between the SM prediction and the data cannot be solved in the LHT model.

I would like to thank the organizers of the interesting and pleasant conference *Heavy Quarks and Leptons* realized in Munich. Special thanks go to the other authors of the work presented here: Monika Blanke, Andrzej J. Buras, Björn Duling, Anton Poschenrieder, Stefan Recksiegel, Selma Uhlig and Andreas Weiler.

Bibliography

[1] N. Arkani-Hamed, A. G. Cohen and H. Georgi, Phys. Lett. B **513** (2001) 232 [arXiv:hep-ph/0105239].

[2] N. Arkani-Hamed, A. G. Cohen, E. Katz and A. E. Nelson, JHEP **0207** (2002) 034 [arXiv:hep-ph/0206021].

[3] T. Han, H. E. Logan, B. McElrath and L. T. Wang, Phys. Rev. D **67** (2003) 095004 [arXiv:hep-ph/0301040].

[4] C. Csaki, J. Hubisz, G. D. Kribs, P. Meade and J. Terning, Phys. Rev. D **67** (2003) 115002 [arXiv:hep-ph/0211124].

[5] H. C. Cheng and I. Low, JHEP **0309** (2003) 051 [arXiv:hep-ph/0308199]. H. C. Cheng and I. Low, JHEP **0408** (2004) 061 [arXiv:hep-ph/0405243].

[6] J. Hubisz, P. Meade, A. Noble and M. Perelstein, JHEP **0601** (2006) 135 [arXiv:hep-ph/0506042].

[7] N. Cabibbo, Phys. Rev. Lett. **10** (1963) 531. M. Kobayashi and T. Maskawa, Prog. Theor. Phys. **49** (1973) 652.

[8] J. Hubisz, S. J. Lee and G. Paz, JHEP **0606** (2006) 041 [arXiv:hep-ph/0512169].

[9] B. Pontecorvo, Sov. Phys. JETP **6** (1957) 429 [Zh. Eksp. Teor. Fiz. **33** (1957) 549]; Sov. Phys. JETP **7** (1958) 172 [Zh. Eksp. Teor. Fiz. **34** (1957) 247]; Z. Maki, M. Nakagawa and S. Sakata, Prog. Theor. Phys. **28** (1962) 870.

[10] M. Blanke, A. J. Buras, A. Poschenrieder, S. Recksiegel, C. Tarantino, S. Uhlig and A. Weiler, Phys. Lett. B (2007), doi: 10.1016/j.physletb.2007.01.037 [arXiv:hep-ph/0609284].

[11] A. J. Buras, P. Gambino, M. Gorbahn, S. Jager and L. Silvestrini, Phys. Lett. B **500** (2001) 161 [arXiv:hep-ph/0007085]. A. J. Buras, Acta Phys. Polon. B **34** (2003) 5615 [arXiv:hep-ph/0310208].

[12] G. D'Ambrosio, G. F. Giudice, G. Isidori and A. Strumia, Nucl. Phys. B **645** (2002) 155 [arXiv:hep-ph/0207036].

[13] A. J. Buras, A. Poschenrieder, S. Uhlig and W. A. Bardeen, JHEP **0611** (2006) 062 [arXiv:hep-ph/0607189].

[14] M. Blanke, A. J. Buras, A. Poschenrieder, S. Recksiegel, C. Tarantino, S. Uhlig and A. Weiler, JHEP **0701** (2007) 066 [arXiv:hep-ph/0610298].

[15] A. J. Buras, A. Poschenrieder and S. Uhlig, Nucl. Phys. B **716** (2005) 173 [arXiv:hep-ph/0410309]. A. J. Buras, A. Poschenrieder and S. Uhlig, arXiv:hep-ph/0501230. A. J. Buras, A. Poschenrieder, S. Uhlig and W. A. Bardeen, JHEP **0611** (2006) 062 [arXiv:hep-ph/0607189]. S. R. Choudhury, N. Gaur,

A. Goyal and N. Mahajan, Phys. Lett. B **601** (2004) 164 [arXiv:hep-ph/0407050]. J. Y. Lee, JHEP **0412** (2004) 065 [arXiv:hep-ph/0408362]. S. Fajfer and S. Prelovsek, Phys. Rev. D **73** (2006) 054026 [arXiv:hep-ph/0511048]. W. j. Huo and S. h. Zhu, Phys. Rev. D **68** (2003) 097301 [arXiv:hep-ph/0306029].

[16] M. Blanke, A. J. Buras, A. Poschenrieder, C. Tarantino, S. Uhlig and A. Weiler, JHEP **0612** (2006) 003 [arXiv:hep-ph/0605214].

[17] S. R. Choudhury, A. S. Cornell, A. Deandrea, N. Gaur and A. Goyal, arXiv:hep-ph/0612327.

[18] M. Blanke, A. J. Buras, B. Duling, A. Poschenrieder and C. Tarantino, arXiv:hep-ph/0702136.

[19] Y. Grossman and Y. Nir, Phys. Lett. B **398** (1997) 163 [arXiv:hep-ph/9701313].

[20] A. Abulencia *et al.* [CDF Collaboration], arXiv:hep-ex/0609040. D. Lucchesi [CDF and D0 Collaborations], FERMILAB-CONF-06-262-E *Presented at Workshop on Theory, Phenomenology and Experiments in Heavy Flavor Physics, Capri, May 2006.*

[21] M. Bona *et al.* [UTfit Collaboration], JHEP **0603** (2006) 080 [arXiv:hep-ph/0509219]. M. Bona *et al.* [UTfit Collaboration], Phys. Rev. Lett. **97** (2006) 151803 [arXiv:hep-ph/0605213]. http://utfit.roma1.infn.it.

[22] J. Charles *et al.* [CKMfitter Group], Eur. Phys. J. C **41** (2005) 1 [arXiv:hep-ph/0406184]. http://www.slac.stanford.edu/xorg/ckmfitter/.

[23] M. Blanke, A. J. Buras, D. Guadagnoli and C. Tarantino, JHEP **0610** (2006) 003 [arXiv:hep-ph/0604057].

[24] M. L. Brooks *et al.* [MEGA Collaboration], Phys. Rev. Lett. **83** (1999) 1521 [arXiv:hep-ex/9905013].

[25] U. Bellgardt *et al.* [SINDRUM Collaboration], Nucl. Phys. B **299** (1988) 1.

[26] C. Dohmen *et al.* [SINDRUM II Collaboration.], Phys. Lett. B **317**, 631 (1993).

[27] B. Aubert *et al.* [BABAR Collaboration], Phys. Rev. Lett. **96** (2006) 041801 [arXiv:hep-ex/0508012].

[28] [Belle Collaboration], arXiv:hep-ex/0609049.

[29] B. Aubert *et al.* [BABAR Collaboration], Phys. Rev. Lett. **92** (2004) 121801 [arXiv:hep-ex/0312027].

[30] Y. Yusa *et al.* [Belle Collaboration], Phys. Lett. B **589** (2004) 103 [arXiv:hep-ex/0403039].

[31] Y. Enari *et al.* [Belle Collaboration], Phys. Lett. B **622** (2005) 218 [arXiv:hep-ex/0503041].

[32] D. Ambrose *et al.* [BNL Collaboration], Phys. Rev. Lett. **81** (1998) 5734 [arXiv:hep-ex/9811038].

[33] K. Arisaka *et al.*, Phys. Lett. B **432** (1998) 230.

[34] M. C. Chang *et al.* [BELLE Collaboration], Phys. Rev. D **68** (2003) 111101 [arXiv:hep-ex/0309069].

[35] F. Abe *et al.* [CDF Collaboration], Phys. Rev. Lett. **81** (1998) 5742.

[36] A. Bornheim *et al.* [CLEO Collaboration], Phys. Rev. Lett. **93** (2004) 241802 [arXiv:hep-ex/0408011].

[37] S. Yamada, Nucl. Phys. Proc. Suppl. **144** (2005) 185; http://meg.web.psi.ch/.

[38] M. A. Giorgi *et al.* [SuperB Group], INFN Roadmap Report, March 2006.

[39] Y. Mori *et al.* [PRISM/PRIME working group], LOI at J-PARC 50-GeV PS, LOI-25, http://psux1.kek.jp/~jhf-np/LOIlist/LOIlist.html.

[40] J. R. Ellis, J. Hisano, M. Raidal and Y. Shimizu, Phys. Rev. D **66** (2002) 115013 [arXiv:hep-ph/0206110].

[41] E. Arganda and M. J. Herrero, Phys. Rev. D **73** (2006) 055003 [arXiv:hep-ph/0510405].

[42] P. Paradisi, JHEP **0510** (2005) 006 [arXiv:hep-ph/0505046]. P. Paradisi, JHEP **0602** (2006) 050 [arXiv:hep-ph/0508054]. P. Paradisi, JHEP **0608** (2006) 047 [arXiv:hep-ph/0601100].

[43] G. W. Bennett *et al.* [Muon G-2 Collaboration], Phys. Rev. D **73** (2006) 072003 [arXiv:hep-ex/0602035].

D Physics

Svjetlana Fajfer[1]*, Jernej Kamenik and Saša Prelovšek*
Department of Physics, University of Ljubljana
and J. Stefan Institute
1000 Ljubljana, Slovenia

Abstract

Recently a lot of new experimental results on open charm hadrons have appeared. In particular many D meson resonances have been discovered. We discuss strong decays of positive and negative parity charmed mesons within heavy meson chiral perturbation theory and study the impact of excited charm states on the determination of the effective meson couplings [1]. Motivated by recent experimental results we also reconsider semileptonic $D \to Pl\nu_l$ and $D \to Vl\nu_l$ decays within a model which combines heavy quark symmetry and properties of the chiral Lagrangian. Using limits of soft collinear effective theory and heavy quark effective theory we parametrize the semileptonic form factors. We include excited charm meson states in our Lagrangians and determine their impact on the charm meson semileptonic form factors. In some scenarios of new physics an up-like heavy quark appears, which induces FCNC at tree level for the $c \to uZ$ transitions. We investigate FCNC effects in D rare decays in particular the $c \to ul^+l^-$ transition which might occur in $D^+ \to \pi^+l^+l^-$ and $D^0 \to \rho^0 l^+ l^-$.

1 Strong decays of positive and negative parity charmed mesons

The strong and electromagnetic transitions of positive and negative parity charmed mesons have already been studied within a variety of approaches (see references [8] - [23] given in [1]). In ref. [2] the chiral loop corrections to the $D^* \to D\pi$ and $D* \to D\gamma$ decays were calculated and a numerical extraction of the one-loop bare couplings was first performed. Since this calculation preceded the discovery of even-parity meson states, it did not involve loop contributions containing the even-parity meson states. The ratios of the radiative and strong decay widths, and the isospin violating decay $D_s^* \to D_s\pi^0$ were used to extract the relevant couplings. However, since that time, the experimental situation has improved and therefore we consider the chiral loop contributions to the strong decays of the even and odd parity charmed meson states

[1]talk given by S. Fajfer

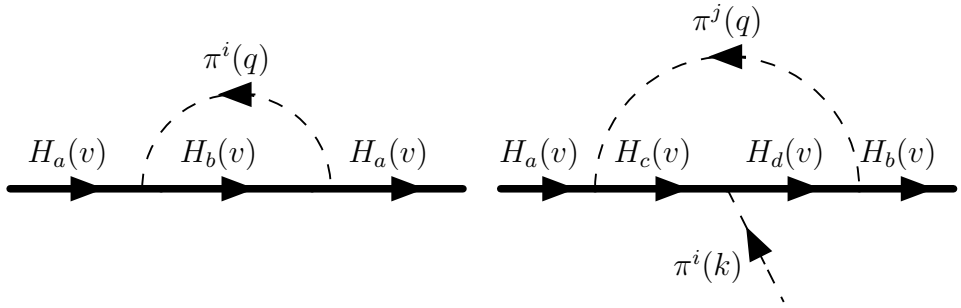

Figure 1: Sunrise (left) and sunrise road (right) topology diagrams

using HHχPT. In our calculation we consider the strong decay modes D^{*+}, D^{*0}, D_0^{*+} D_0^{*0} and $D_1^{\prime 0}$ (given in Table 1 of [1])

The existing data on the decay widths enable us to constrain the leading order parameters: the $D^*D\pi$ coupling g, $D_0^*D\pi$ coupling h, and the coupling $\tilde{g}$ which enters in the interaction of even parity charmed mesons and the light pseudo-Goldstone bosons. Although the coupling $\tilde{g}$ is not yet experimentally constrained, it moderatelly affects the decay amplitudes which we investigate.

Due to the divergences coming from the chiral loops one needs to include the appropriate counterterms. Therefore we construct a full operator basis of the relevant counterterms and include it into our effective theory Lagrangian. The details of the Heavy hadron chiral perturbation theory HHχPT we use is given in [1]. First we determine wavefunction renormalization of the relevant heavy meson fields considering the effects of the chiral loops given by the left diagram in Fig. 1. Then we calculate loop corrections for the $PP^*\pi$, $P_0P_1^*\pi$ and $P_0P\pi$ vertexes. At zeroth order in $1/m_Q$ expansion these are identical to the $P^*P^*\pi$, $P_1^*P_1^*\pi$ and $P_1^*P^*\pi$ couplings respectively due to heavy quark spin symmetry (right diagram in Fig. 1).

Using known experimental values for the decay widths of D^{+*}, D_0^{+*}, D_0^{0*} and $D_1^{\prime}$, and the upper bound on the width of D^{0*} one can extract the values for the bare couplings g, h and $\tilde{g}$ from a fit to the data. The decay rates are namely given by

$$\Gamma(P_a^* \to \pi^i P_b) = \frac{|g^{\text{eff.}}_{P_a^* P_b \pi^i}|^2}{6\pi f^2} |\vec{k}_{\pi^i}|^3, \tag{1}$$

and a similar expression (up to polarization averaging phase space factors) for $\Gamma(P_0 \to \pi P)$ and $\Gamma(P_1^* \to \pi P^*)$ with g coupling replaced by h and $|\vec{k}_\pi|^3$ replaced by $E_\pi^2|\vec{k}_\pi|$. Here $\vec{k}_\pi$ is the three-momentum vector of the outgoing pion and E_π its energy. The renormalization condition for the couplings can be written as

$$g^{\text{eff.}}_{P_a^* P_b \pi^i} = g \frac{\sqrt{Z_{2P_a}}\sqrt{Z_{2P_b^*}}\sqrt{Z_{2\pi^i}}}{\sqrt{Z_{1P_a P_b^* \pi^i}}} = g Z^g_{P_a^* P_b \pi^i} \tag{2}$$

Calculation scheme	g	$\lvert h\rvert$	$\tilde{g}$
Leading order	0.61	0.52	-0.15
One-loop without positive parity states	0.53		
One-loop with positive parity states	0.66	0.47	-0.06

Table 1: Summary of our results for the effective couplings as explained in the text. The listed best-fit values for the one-loop calculated bare couplings were obtained by neglecting counterterms' contributions at the regularization scale $\mu \simeq 1$ GeV.

with similar expressions for the h and $\tilde{g}$ couplings.

We perform a fit with a renormalization scale set to $\mu \simeq 1$ GeV [2] and we neglect counterterm contributions altogether. Our choice of the renormalization scale in dimensional regularization is arbitrary and depends on the renormalization scheme. Therefore any quantitative estimate made with such a procedure cannot be considered meaningful without also thoroughly investigating counterterm, quark mass and scale dependencies. We perform a Monte-Carlo randomized least-squares fit for all the three couplings in the prescribed regions [1] using the experimental values for the decay rates to compute χ^2 and using values from PDG [6] for the masses of final state heavy and light mesons. In the case of excited D_0^* and D_1' mesons, we also assume saturation of the measured decay widths with the strong decay channels to ground state charmed mesons and pions ($D_0^* \to D\pi$ and $D_1' \to D^*\pi$).

Due to the rather large mass splitting between positive in negative parity states Δ_{SH}, we find that the perturbative expansion holds for scales below $\mu \leq 1$ GeV, while these new strongly scale dependent corrections become large at higher renormalization scales. From the data for the four decay widths we obtain the best-fitted values for the bare couplings, which we summarize in Table 1. We are able to determine all the three couplings since the contributions proportional to the coupling $\tilde{g}$ appear indirectly, through the loop corrections.

Since we consider decay modes with the pion in the final state, we do not expect sizable contribution of the counterterms. Namely, the counterterms which appear in our study are proportional to the light quark masses, and not to the strange quark mass [2]. The effects of counterterm contributions in the decay modes we analyze, are nevertheless estimated by making the random distribution of the relevant counterterm couplings (see [1]). The counterterm contributions of order $\mathcal{O}(1)$ can spread the best fitted values of g, $|h|$ by roughly 15% and $\tilde{g}$ by as much as 60%. Similarly, up to 20% shifts in the renormalization scale modify the fitted values for the g and $|h|$ by less than 10% while $\tilde{g}$ may even change sign at high renormalization scales. Combined with the estimated 20% uncertainty due to discrepancies in the measured excited heavy meson masses, we consider these are the dominant sources of error in our determination of the couplings. One should keep in mind however that without better experimental

data and/or lattice QCD inputs, the phenomenology of strong decays of charmed mesons presented above ultimately cannot be considered reliable at this stage.

A full calculation of the strong decay couplings should also contain, in addition to the calculated contributions, the relevant $1/m_H$ corrections as discussed in ref [3]. There, the next to leading terms $(1/m_H)$ were included in the study of charm meson mass spectrum. Due to the very large number of unknown couplings the combination of $1/m_H$ and chiral corrections does not seem to be possible for the decay modes we consider. In addition, recent studies of the lattice QCD groups [4, 5] indicate that the $1/m_H$ corrections do not contribute significantly to their determined values of the strong couplings, and we therefore assume the same to be true in our calculations of chiral corrections.

Due to computational problems associated with the chiral limit, lattice QCD studies perform calculations at large light quark masses and then employ a chiral extrapolation $m_\pi \to 0$ of their results. Our analysis of such chiral extrapolation of the coupling g shows that the full loop contributions of excited charmed mesons give sizable effects in modifying the slope and curvature in the limit $m_\pi \to 0$. We argue that this is due to the inclusion of hard pion momentum scales inside chiral loop integrals containing the large mass splitting between charmed mesons of opposite parity Δ_{SH} which does not vanish in the chiral limit. If we instead impose physically motivated approximations for these contributions - we expand them in terms of $1/\Delta_{SH}$ - the effects reduce mainly to the changes in the determined values of the bare couplings, used in the extrapolation, with explicit h contributions shrinking to the order of 5%. Consequently one can infer on the good convergence of the $1/\Delta_{SH}$ expansion.

As a summary of our results, we point out that chiral loop corrections in strong charm meson decays can be kept under control, but they give important contributions and are relevant for the precise extraction of the strong coupling constants g, h and $\tilde{g}$.

2 Charm meson resonances in D semileptonic decays

The knowledge of the form factors which describe the weak *heavy* $\to$ *light* semileptonic transitions is very important for the accurate determination of the CKM parameters from the experimentally measured exclusive decay rates. Usually, the attention has been devoted to B decays and the determination of the phase of the V_{ub} CKM matrix element. At the same time in the charm sector, the most accurate determination of the size of V_{cs} and V_{cd} matrix elements is not from a direct measurement, mainly due to theoretical uncertainties in the calculations of the relevant form factors' shapes.

Recently, there have been new interesting results on D-meson semileptonic decays.

The CLEO and FOCUS collaborations have studied semileptonic decays $D^0 \to \pi^- \ell^+ \nu$ and $D^0 \to K^- \ell^+ \nu$ [7, 8]. Their data provide new information on the $D^0 \to \pi^- \ell^+ \nu$ and $D^0 \to K^- \ell^+ \nu$ form factors. Usually in D semileptonic decays a simple pole parametrization was used in the past. The results of Refs. [7, 8] for the single pole parameters required by the fit of their data, however, suggest pole masses, which are inconsistent with the physical masses of the lowest lying charm meson resonances. In their analyses they also utilized a modified pole fit as suggested in [9] and their results indeed suggest the existence of contributions beyond the lowest lying charm meson resonances [7].

In addition to these results new experimental studies of charm meson resonances have provided a lot of new information on the charm sector [10–13] which we can now apply to D and D_s semileptonic decays.

The purpose of our studies [14–16] is to accommodate contributions of the newly discovered and theoretically predicted charm mesons in form factors which are parametrized using constraints coming from heavy quark effective theory (HQET) limit for the region of q^2_{max} and in the $q^2 \simeq 0$ region using results of soft collinear effective theory (SCET). We restrain our discussion to the leading chiral and $1/m_H$ terms in the expansion.

The standard decomposition of the current matrix elements relevant to semileptonic decays between a heavy pseudoscalar meson state $|H(p_H)\rangle$ with momentum p^ν_H and a light pseudoscalar meson state $|P(p_P)\rangle$ with momentum p^μ_P is in terms of two scalar functions of the exchanged momentum squared $q^2 = (p_H - p_P)^2$ – the form factors $F_+(q^2)$ and $F_0(q^2)$. Here F_+ denotes the vector form factor and it is dominated by vector meson resonances, while F_0 denotes the scalar form factor and is expected to be dominated by scalar meson resonance exchange [17, 18]. In order that the matrix elements are finite at $q^2 = 0$, the form factors must also satisfy the relation $F_+(0) = F_0(0)$.

The transition of $|H(p_H)\rangle$ to light vector meson $|V(p_V, \epsilon_V)\rangle$ with momentum p^ν_V and polarization vector ϵ^ν_V is similarly parameterized in terms of four form factors V, A_0, A_1 and A_2, again functions of the exchanged momentum squared $q^2 = (p_H - p_V)^2$. Here V denotes the vector form factor and is expected to be dominated by vector meson resonance exchange, the axial A_1 and A_2 form factors are expected to be dominated by axial resonances, while A_0 denotes the pseudoscalar form factor and is expected to be dominated by pseudoscalar meson resonance exchange [18]. As in previous case in order that the matrix elements are finite at $q^2 = 0$, the form factors must also satisfy the well known relation $A_0(0) + A_1(0)(m_H + m_V)/2m_V - A_2(0)(m_H - m_V)/2m_V = 0$.

Next we follow the analysis of Ref. [9], where the F_+ form factor in $H \to P$ transitions is given as a sum of two pole contributions, while the F_0 form factor is written as a single pole. This parametrization includes all known properties of form factors at large m_H. Using a relation which connects the form factors within large

energy release approach [19] the authors in Ref. [9] propose the following form factor parametrization

$$F_+(q^2) = \frac{F(0)}{(1-x)(1-ax)}, \qquad F_0(q^2) = \frac{F(0)}{1-bx}, \tag{3}$$

where $x = q^2/m^2_{H^*}$.

Utilizing the same approach we propose a general parametrization of the heavy to light vector form factors, which also takes into account all the known scaling and resonance properties of the form factors [15, 16] As already mentioned, there exist the well known HQET scaling laws in the limit of zero recoil [20] while in the SCET limit $q^2 \to 0$ one obtains that all four $H \to V$ form factors can be related to only two universal SCET scaling functions [19].

The starting point is the vector form factor V, which is dominated by the pole at $t = m^2_{H^*}$ when considering the part of the phase space that is close to the zero recoil. For the *heavy* $\to$ *light* transitions this situation is expected to be realized near the zero recoil where also the HQET scaling applies. On the other hand, in the region of large recoils, SCET dictates the scaling described in [19]. In the full analogy with the discussion made in Refs. [9, 21], the vector form factor consequently receives contributions from two poles and can be written as

$$V(q^2) = \frac{V(0)}{(1-x)(1-ax)}, \tag{4}$$

where $x = q^2/m^2_{H^*}$ ensures, that the form factor is dominated by the physical H^* pole, while a measures the contribution of higher states which are parametrized by another effective pole at $m^2_{\rm eff} = m^2_{H^*}/a$.

An interesting and useful feature one gets from the SCET is the relation between V and A_1 [19, 22–24] at $q^2 \approx 0$. When combined with our result (4), it imposes a single pole structure on A_1. We can thus continue in the same line of argument and write

$$A_1(q^2) = \xi \frac{V(0)}{1-b'x}. \tag{5}$$

Here $\xi = m^2_H/(m_H + m_V)^2$ is the proportionality factor between A_1 and V from the SCET relation, while b' measures the contribution of resonant states with spin-parity assignment 1^+ which are parametrized by the effective pole at $m^2_{H'^*_{\rm eff}} = m^2_{H^*}/b'$. It can be readily checked that also A_1, when parametrized in this way, satisfies all the scaling constraints.

Next we parametrize the A_0 form factor, which is completely independent of all the others so far as it is dominated by the pseudoscalar pole and is proportional to a different universal function in SCET. To satisfy both HQET and SCET scaling laws we parametrize it as

$$A_0(q^2) = \frac{A_0(0)}{(1-y)(1-a'y)}, \tag{6}$$

where $y = q^2/m_H^2$ ensures the physical 0^- pole dominance at small recoils and a' again parametrizes the contribution of higher pseudoscalar states by an effective pole at $m^2_{H'_{\rm eff}} = m_H^2/a'$. The resemblance to V is obvious and due to the same kind of analysis [9] although the parameters appearing in the two form factors are completely unrelated.

Finally for the A_2 form factor, due to the pole behavior of the A_1 form factor on one hand and different HQET scaling at $q^2_{\rm max}$ on the other hand, we have to go beyond a simple pole formulation. Thus we impose

$$A_2(q^2) = \frac{A_2(0)}{(1-b'x)(1-b''x)}, \tag{7}$$

which again satisfies all constraints. Due to the relations between the form factors we only gain one parameter in this formulation, b''. This however causes the contribution of the 1^+ resonances to be shared between the two effective poles in this form factor.

At the end we have parametrized the four $H \to V$ vector form factors in terms of the six parameters $V(0)$, $A_0(0)$, a, a', b' and b'' ($A_2(0)$ is fixed by the kinematical constraint).

In our heavy meson chiral theory (HMχT) calculations we use the leading order heavy meson chiral Lagrangian in which we include additional charm meson resonances. The details of this framework are given in [14] and [15]. We first calculate values of the form factors in the small recoil region. The presence of charm meson resonances in our Lagrangian affects the values of the form factors at $q^2_{\rm max}$ and induces saturation of the second poles in the parameterizations of the $F_+(q^2)$, $V(q^2)$ and $A_0(q^2)$ form factors by the next radial excitations of $D^*_{(s)}$ and $D_{(s)}$ mesons respectively. Although the D mesons mat not be considered heavy enough, we employ these parameterizations with model matching conditions at $q^2_{\rm max}$. Using HQET parameterization of the current matrix elements [14, 15], which is especially suitable for HMχT calculations of the form factors near zero recoil, we are able to extract consistently the contributions of individual resonances from our Lagrangian to the various $D \to P$ and $D \to V$ form factors. We use physical pole masses of excited state charmed mesons in the extrapolation, giving for the pole parameters $a = m^2_{H^*}/m^2_{H'^*}$, $a' = m_H^2/m^2_{H'}$, $b' = m^2_{H^*}/m^2_{H_A}$. Although in the general parameterization of the form factors the extra poles in F_+, V and $A_{0,1,2}$ parametrized all the neglected higher resonances beyond the ground state heavy meson spin doublets $(0^-, 1^-)$, we are here saturating those by a single nearest resonance. The single pole q^2 behavior of the $A_1(q^2)$ form factor is explained by the presence of a single 1^+ state relevant to each decay, while in $A_2(q^2)$ in addition to these states one might also account for their next radial excitations. However, due to the lack of data on their presence we assume their masses being much higher than the first 1^+ states and we neglect their effects, setting effectively $b'' = 0$.

The values of the new model parameters appearing in $D \to Pl\nu_l$ decay amplitudes [14] are determined by fitting the model predictions to known experimental values of branching ratios $\mathcal{B}(D^0 \to K^-\ell^+\nu)$, $\mathcal{B}(D^+ \to \overline{K}^0\ell^+\nu)$, $\mathcal{B}(D^0 \to \pi^-\ell^+\nu)$, $\mathcal{B}(D^+ \to \pi^0\ell^+\nu)$, $\mathcal{B}(D_s^+ \to \eta\ell^+\nu)$ and $\mathcal{B}(D_s^+ \to \eta'\ell^+\nu)$ [6]. In our calculations of decay widths we neglect the lepton mass, so the form factor F_0, which is proportional to q^μ, does not contribute. For the decay width we then use the integral formula proposed in [25] with the flavor mixing parametrization of the weak current defined in [14].

Similarly in the case of $D \to Vl\nu_l$ transitions we have to fix additional model parameters [15] and we again use known experimental values of branching ratios $\mathcal{B}(D_0 \to K^{*-}\ell^+\nu)$, $\mathcal{B}(D_s^+ \to \Phi\ell^+\nu)$, $\mathcal{B}(D^+ \to \rho^0\ell^+\nu)$, $\mathcal{B}(D^+ \to K^{*0}\ell^+\nu)$, as well as partial decay width ratios $\Gamma_L/\Gamma_T(D^+ \to K^{*0}\ell^+\nu)$ and $\Gamma_+/\Gamma_-(D^+ \to K^{*0}\ell^+\nu)$ [6]. We calculate the decay rates for polarized final light vector mesons using helicity amplitudes $H_{+,-,0}$ as in for example [26]. By neglecting the lepton masses we again arrive at the integral expressions from [25] with the flavor mixing parametrization of the weak current defined in [15].

We first draw the q^2 dependence of the F_+ and F_0 form factors for the $D^0 \to K^-$, $D^0 \to \pi^-$ and $D_s \to K^0$ transitions. The results are depicted in Fig. 2. Our model results, when extrapolated with the double pole parameterization, agree well with previous theoretical [27, 28] and experimental [7, 8] studies whereas the single pole extrapolation does not give satisfactory results. Note that without the scalar resonance, one only gets a soft pion contribution to the F_0 form factor. This gives for the q^2 dependence of F_0 a constant value for all transitions, which largely disagrees with lattice QCD results [28] as well as heavily violates known form factor relations.

We also calculate the branching ratios for all the relevant $D \to P$ semileptonic decays and compare the predictions of our model with experimental data from PDG. The results are summarized in Table 2. For comparison we also include the results for the rates obtained with our approach for $F_+(q^2_{\rm max})$ but using a single pole fit. It is very interesting that our model extrapolated with a double pole gives branching ratios for $D \to P\ell\nu_\ell$ in rather good agreement with experimental results for the already measured decay rates. It is also obvious that the single pole fit gives the rates up to a factor of two larger than the experimental results. Only for decays to η and η' as given in Table 2, an agreement with experiment of the double pole version of the model is not better but worse than for the single pole case.

We next draw the q^2 dependence of all the form factors for the $D^0 \to K^{-*}$, $D^0 \to \rho^-$ and $D_s \to \phi$ transitions. The results are depicted in Fig. 3. Our extrapolated results for the shapes of the $D \to V$ semileptonic form factors agree well with existing theoretical studies [26, 27, 29, 30], while currently no experimental determination of the form factors' shapes in these decays exists.

We complete our study by calculating branching ratios and partial decay width ratios also for all relevant $D \to V\ell\nu_\ell$ decays. They are listed in Table 3 together with

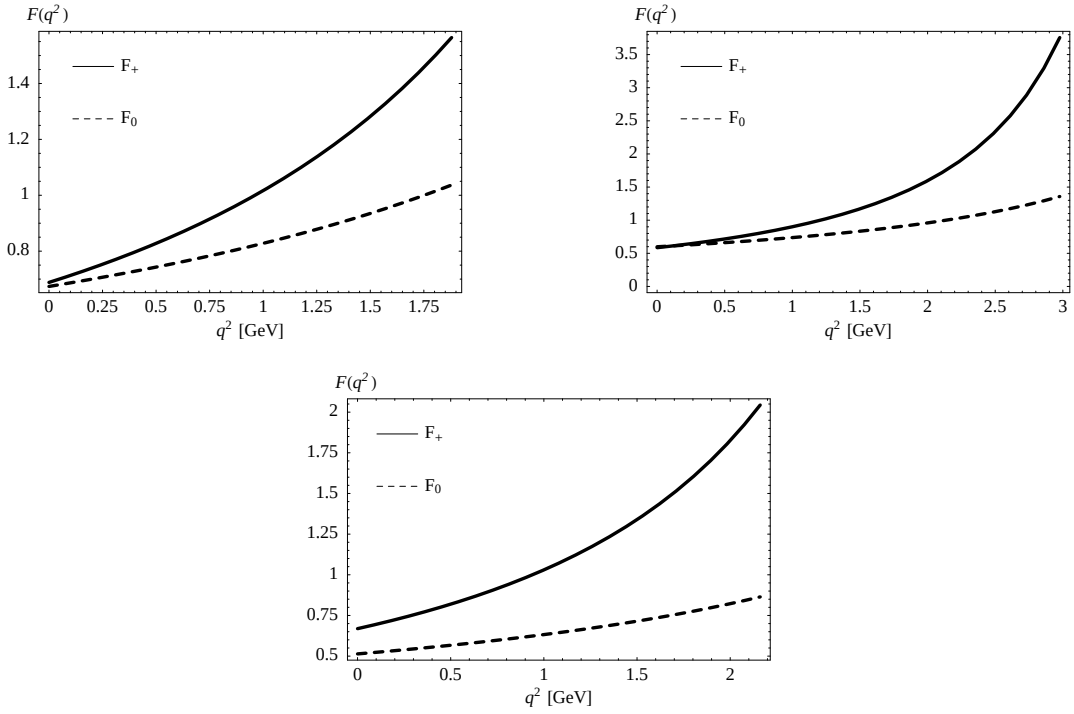

Figure 2: q^2 dependence of the $D^0 \to K^-$ (upper left), $D^0 \to \pi^-$ (upper right) and $D_s \to K^0$ (lower) transition form factors.

Decay	$\mathcal{B}$ (Mod. double pole) [%]	$\mathcal{B}$ (Mod. single pole) [%]	$\mathcal{B}$ (Exp. PDG) [%]
$D^0 \to K^-$	3.4	4.9	3.43 ± 0.14
$D^0 \to \pi^-$	0.27	0.56	0.36 ± 0.06
$D_s^+ \to \eta$	1.7	2.5	2.5 ± 0.7
$D_s^+ \to \eta'$	0.61	0.74	0.89 ± 0.33
$D^+ \to \overline{K}^0$	9.4	12.4	6.8 ± 0.8
$D^+ \to \pi^0$	0.33	0.70	0.31 ± 0.15
$D^+ \to \eta$	0.10	0.15	< 0.5
$D^+ \to \eta'$	0.016	0.019	< 1.1
$D_s^+ \to K^0$	0.20	0.32	

Table 2: The branching ratios for the $D \to P$ semileptonic decays. Comparison of our model fit with experiment as explained in the text.

known experimentally measured values.

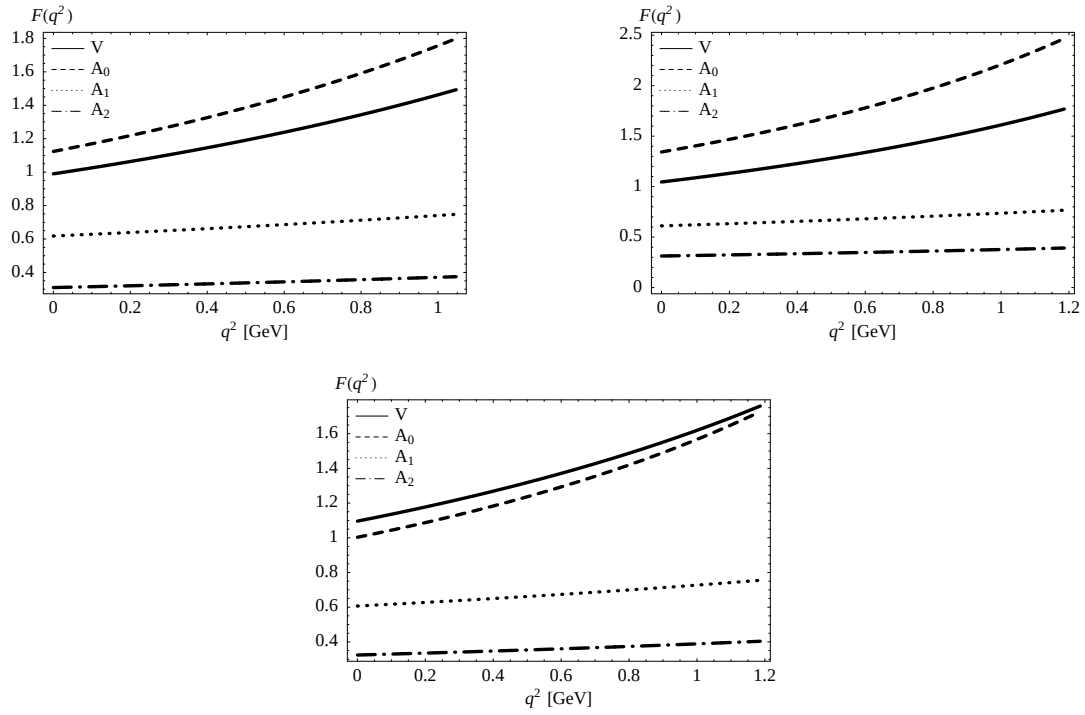

Figure 3: q^2 dependence of the $D^0 \to K^{*-}$ (upper left), $D^0 \to \rho^-$ (upper right) and $D_s \to \phi$ (lower) transition form factors.

3 Search for new physics in rare D decays

At low-energies new physics is usually expected in the down-like quark sector. Numerous studies of new physics effects were performed in the $s \to d$, $b \to s(d)$, $\overline{s}d \leftrightarrow \overline{d}s$, $\overline{b}d \leftrightarrow \overline{d}b$ and $\overline{b}s \leftrightarrow \overline{s}b$ transitions.

Decay	$\mathcal{B}$ (Mod.) [%]	$\mathcal{B}$ (Exp.) [%]	Γ_L/Γ_T (Mod.)	Γ_+/Γ_- (Mod.)
$D_0 \to K^*$	2.2	2.15 ± 0.35 [6]	1.14	0.22
$D_0 \to \rho$	0.20	$0.194 \pm 0.039 \pm 0.013$ [31]	1.11	0.14
$D^+ \to K_0^*$	5.6	5.73 ± 0.35 [6]	1.13	0.22
$D^+ \to \rho_0$	0.25	0.25 ± 0.08 [6]	1.11	0.14
$D^+ \to \omega$	0.25	$0.17 \pm 0.06 \pm 0.01$ [31]	1.10	0.14
$D_s \to \Phi$	2.4	2.0 ± 0.5 [6]	1.08	0.21
$D_s \to K_0^*$	0.22		1.03	0.13

Table 3: The branching ratios and partial decay width ratios for the $D \to V$ semileptonic decays. Comparison of our model fit with experiment as explained in the text.

However, searches for new physics in the up-like quark sector at low energies were not so attractive. Reasons are following: a)flavor changing neutral current processes at loop level in the standard model suffer from the GIM cancellation leading to very small effects in the $c \to u$ transitions. The GIM mechanism acts in many extensions of the standard model too, making contributions of new physics insignificant. b) Most of the charm meson processes, where $c \to u$ and $c\overline{u} \leftrightarrow \overline{c}u$ transitions might occur are dominated by the standard model long-distance contributions [33] - [41].

On the experimental side there are many studies of rare charm meson decays. The first observed rare D meson decay was the radiative weak decay $D \to \phi\gamma$. Its rate $BR(D \to \phi\gamma) = 2.6^{+0.7}_{-0.6} \times 10^{-5}$ has been measured by Belle collaboration [42] and hopefully other radiative weak charm decays will be observed soon [43].

In the standard model (SM) [33] the contribution coming from the penguin diagrams in c $\to$ uγ transition gives branching ratio of order 10^{-18}. The QCD corrected effective Lagrangian [44] gives BR(c $\to$ uγ) $\simeq 3 \times 10^{-8}$. A variety of models beyond SM were investigated and it was found that the gluino exchange diagrams [45] within general minimal supersymmetric SM (MSSM) might lead to the enhancement

$$\frac{\mathrm{BR(c \to u\gamma)_{MSSM}}}{\mathrm{BR(c \to u\gamma)_{SM}}} \simeq 10^2. \tag{8}$$

Within SM the $c \to ul^+l^-$ amplitude is given by the γ and Z penguin diagrams and W box diagram. It is dominated by the light quark contributions in the loop. The leading order rate for the inclusive $c \to ul^+l^-$ calculated within SM [39] was found to be suppressed by QCD corrections [34]. The inclusion of the renormalization group equations for the Wilson coefficients gave an additional significant suppression [40] leading to the rates $\Gamma(c \to ue^+e^-)/\Gamma_{D^0} = 2.4 \times 10^{-10}$ and $\Gamma(c \to u\mu^+\mu^-)/\Gamma_{D^0} = 0.5 \times 10^{-10}$. These transitions are largely driven by virtual photon at low dilepton mass m_{ll}.

The leading contribution to $c \to ul^+l^-$ in general MSSM with conserved R parity comes from the one-loop diagram with gluino and squarks in the loop [34, 39, 45]. It proceeds via virtual photon and significantly enhances the $c \to ul^+l^-$ spectrum at small dilepton mass m_{ll}. The authors of Ref. [34] have investigated supersymmetric (SUSY) extension of the SM with R parity breaking and they found that it can modify the rate. Using most resent CLEO [43] results for the $D^+ \to \pi^+\mu^+\mu^-$ one can set the bound for the product of the relevant parameters entering the R parity violating $\tilde{\lambda}'_{22k}\tilde{\lambda}'_{21k} \simeq 0.001$ (assuming that the mass of squark $M_{\tilde{D}_k} \simeq 100$ GeV). This bound gives the rates $BR_R(c \to ue^+e^-) \simeq 1.6 \times 10^{-8}$ and $BR_R(c \to u\mu^+\mu^-) \simeq 1.8 \times 10^{-8}$.

Some of models of new physics (NP) contain an extra up-like heavy quark inducing flavor changing neutral currents at tree level for the up-quark sector [32, 46, 47, 49, 50]. The isospin component of the weak neutral current is given in [32] as

$$J^\mu_{W^3} = \frac{1}{2}\overline{U}^m_L\gamma^\mu\Omega U^m_L - \frac{1}{2}\overline{D}^m_L\gamma^\mu D^m_L \tag{9}$$

with $L = \frac{1}{2}(1-\gamma_5)$ and mass eigenstates $U_L^m = (u_L, c_L, t_L, T_L)^T$, $D_L^m = (d_L, s_L, b_L)^T$. The neutral current for the down-like quarks is the same as in the SM, while there are tree-level flavor changing transitions between up-quarks if $\Omega \neq I$. The elements of 4×4 matrix Ω can be constrained by CKM unitarity violations currently allowed by experimental data. Even more stringent bound on cuZ coupling Ω_{uc} comes from the present bound on Δm in $D^0 - \overline{D}^0$ transition. It gives $|\Omega_{uc}| \leq 0.0004$ and we use the upper bound to determine the maximal effect on rare D decays in what follows. In this case the dilepton mass distribution of the $c \to u l^+ l^-$ differential branching ratio can be enhanced by two orders of magnitude in comparison with SM (see Fig. 4).

A particular version of the model with tree-level up-quark FCNC transitions is the Littlest Higgs model [51]. In this case the magnitude of the relevant $c \to uZ$ coupling $\Omega_{cu} = |V_{ub}||V_{cb}|v^2/f^2 \leq 10^{-5}$ is even further constrained via the scale $f \geq \mathcal{O}(1\ \mathrm{TeV})$ by the precision electro-weak data. The smallness of Ω_{uc} implies that the effect of this particular model on $c \to u l^+ l^-$ decay and relevant rare D decays is insignificant [32].

The study of exclusive D meson rare decay modes is very difficult due to the dominance of the long distance effects [33] - [38]. The inclusive $c \to u l^+ l^-$ can be tested in the rare decays $D \to \mu^+ \mu^-$, $D \to P(V) l^+ l^-$ [34, 35, 39].

The branching ratio for the rare decay $D \to \mu^+ \mu^-$ is very small in the SM. The detailed treatment of this decay rate [34] gives $Br(D \to \mu^+ \mu^-) \simeq 3 \times 10^{-13}$ [34]. This decay rate can be enhanced within a study which considers SUSY with R parity breaking effects [34, 41]. Using the bound $\tilde{\lambda}'_{22k}\tilde{\lambda}'_{21k} \simeq 0.001$ one obtains the limit $Br(D \to \mu^+ \mu^-)_R \simeq 4 \times 10^{-7}$.

The $D \to P(V) l^+ l^-$ decays offer another possibility to study the $c \to u l^+ l^-$ transition in charm sector. The most appropriate decay modes for the experimental searches are $D^+ \to \pi^+ l^+ l^-$ and $D^0 \to \rho^0 e^+ e^-$. In the following we present the possible maximal effect on these decays coming from a general class of models with tree level cuZ coupling at its upper bound $|\Omega_{uc}| = 0.0004$. We already pointed out that in the Littlest Higgs model, which is a particular version of these models, the coupling Ω_{uc} is constrained to be smaller and the effects on rare D decays are insignificant [32].

The calculations of the long distance contributions in the decays $D^+ \to \pi^+ l^+ l^-$ and $D^0 \to \rho^0 l^+ l^-$ are presented in Refs. [32, 38, 39]. The contributions of the intermediate vector resonances $V_0 = \rho^0, \omega, \phi$ with $V_0 \to l^+ l^-$ constitute an important long-distance contribution to the hadronic decay, which may shadow interesting short-distance contribution induced by $c \to u l^+ l^-$ transition.

Our determination of short and long distance contributions to $D^+ \to \pi^+ l^+ l^-$ takes advantage of the available experimental data [32]. This is a fortunate circumstance for this particular decay since the analogous experimental input is not available for determination of the other $D \to X l^+ l^-$ rates in a similar way. The rate resulting from the amplitudes (14) and (19) of [32] with $|\Omega_{uc}| = 0.0004$ are given in Fig. 5 and Table 4.

We are unable to determine the amplitude of the long-distance contribution to

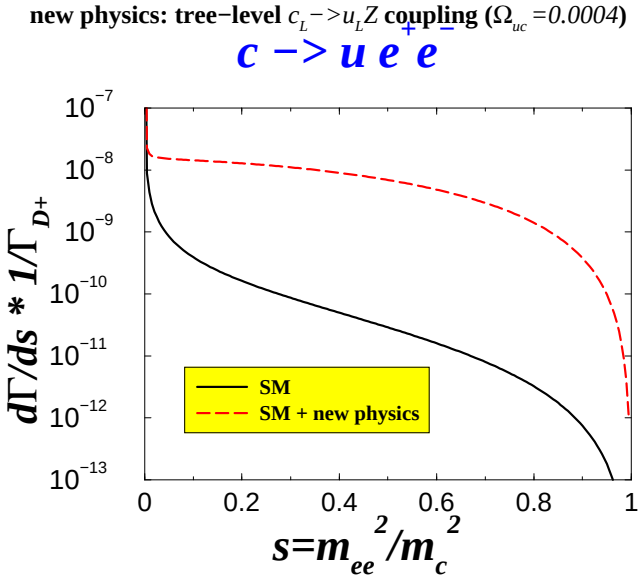

Figure 4: The dilepton mass distribution dBr/dm_{ee}^2 for the inclusive decay $c \to ul^+l^-$ as a function of the dilepton mass square $m_{ee}^2 = (p_+ + p_-)^2$.

$D^0 \to \rho^0 V_0 \to \rho^0 l^+ l^-$ using the measured rates for $D^0 \to \rho^0 V_0$ since only the rate of $D^0 \to \rho^0 \phi$ is known experimentally. We are forced to use a model [38], developed to describe all $D \to V l^+ l^-$ and $D \to V\gamma$ decays, and the resulting rates are presented in Fig. 6 and Table 4.

Therefore, the total rates for $D \to X l^+ l^-$ are dominated by the long distance resonant contributions at dilepton mass $m_{ll} = m_\rho,\ m_\omega,\ m_\phi$ and even the largest contributions from new physics are not expected to affect the total rate significantly [34, 39]. New physics could only modify the SM differential spectrum at low m_{ll} below ρ or spectrum at high m_{ll} above ϕ. In the case of $D \to \pi l^+ l^-$ differential decay distribution there is a broad region at high m_{ll} (see Fig. 5), which presents a unique possibility to study $c \to ul^+l^-$ transition [32, 39].

The non-zero forward-backward asymmetry in $D \to \rho l^+ l^-$ decay arises only when $C_{10} \neq 0$ (assuming $m_l \to 0$). The enhancement of the C_{10} in the NP models [32] is due to the tree-level $\overline{u}_L \gamma_\mu c_L Z^\mu$ coupling and leads to nonzero asymmetry $A_{FB}(m_{ll}^2)$ shown in Fig. 7. The forward-backward asymmetry for $D^0 \to \rho^0 l^+ l^-$ vanishes in SM ($C_{10} \simeq 0$), while it is reaching $\mathcal{O}(10^{-2})$ in NP model with the extra up-like quark as shown in Fig. 7. Such asymmetry is still small and difficult to be seen in the present or planned experiments given that the rate itself is already small.

We have investigated impact of the tree-level flavor changing neutral transition $c \to uZ$ on the rare D meson decay observables. However, the most suitable $D^+ \to$

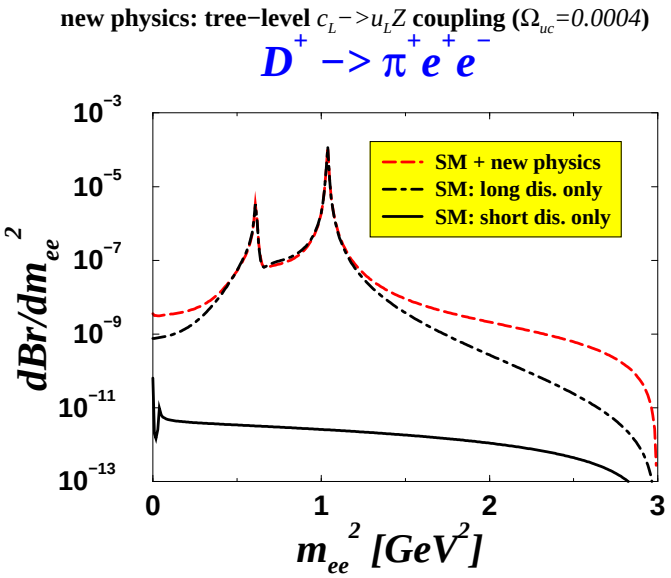

Figure 5: The dilepton mass distribution dBr/dm_{ee}^2 for $D^+ \to \pi^+ e^+ e^-$.

$\pi^+ l^+ l^-$ and $D^0 \to \rho^0 l^+ l^-$ decays are found to be dominated by the SM long distance contributions. Only small enhancement of the differential mass distribution can be seen in the case of $D^+ \to \pi^+ l^+ l^-$ decay at high dilepton mass and tiny forward backward asymmetry can be induced by new physics in $D^0 \to \rho^0 l^+ l^-$ decay.

We conclude that the NP scenarios which contain an extra singlet heavy up-like quark, have rather small effects on the charm meson observables.

Br	short distance contribution only		total rate $\simeq$ long distance contr.	experiment
	SM	SM + NP		
$D^+ \to \pi^+ e^+ e^-$	6×10^{-12}	8×10^{-9}	1.9×10^{-6}	$< 7.4 \times 10^{-6}$
$D^+ \to \pi^+ \mu^+ \mu^-$	6×10^{-12}	8×10^{-9}	1.9×10^{-6}	$< 8.8 \times 10^{-6}$
$D^0 \to \rho^0 e^+ e^-$	negligible	5×10^{-10}	1.6×10^{-7}	$< 1.0 \times 10^{-4}$
$D^0 \to \rho^0 \mu^+ \mu^-$	negligible	5×10^{-10}	1.5×10^{-7}	$< 2.2 \times 10^{-5}$

Table 4: Branching ratios for the decays in which $c \to u l^+ l^-$ transition can be probed.

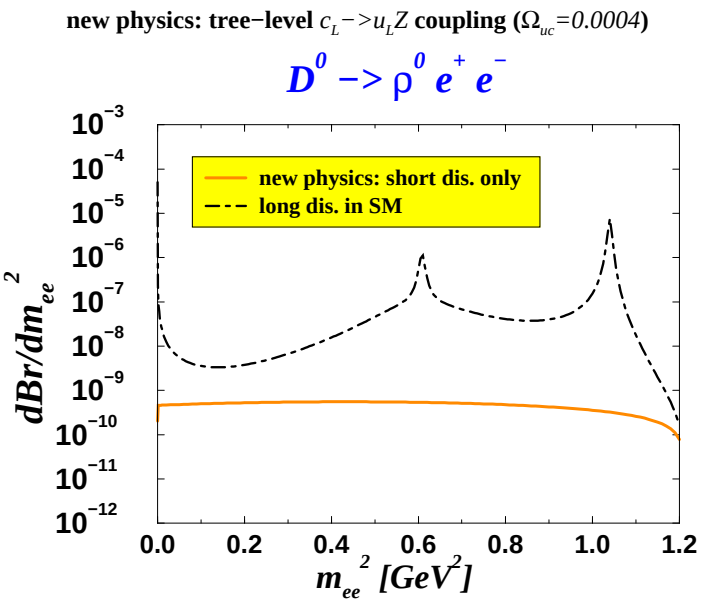

Figure 6: The dilepton mass distribution for $D^0 \to \rho^0 e^+ e^-$.

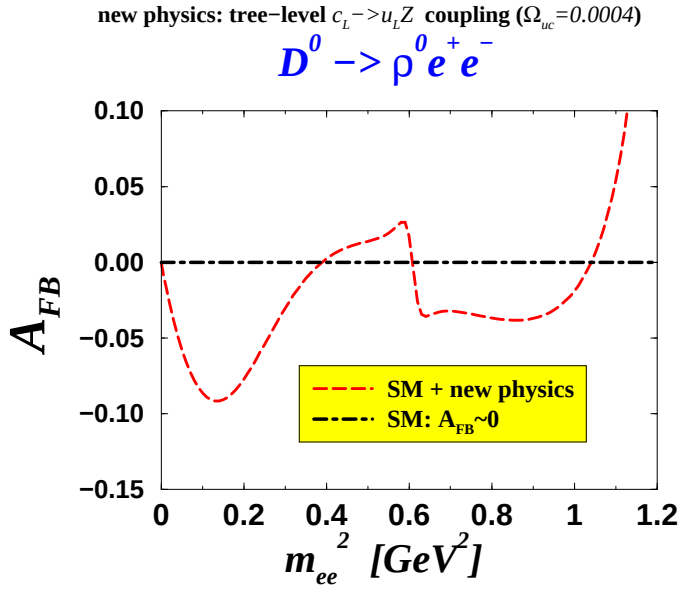

Figure 7: The forward-backward asymmetry for $D^0 \to \rho^0 e^+ e^-$.

Bibliography

[1] S. Fajfer and J. Kamenik, Phys. Rev. D **74**, 074023 (2006).

[2] I.W. Stewart, Nucl. Phys. B **529**, 62 (1998).

[3] T. Mehen and R. Springer, Phys. Rev. D **72**, 034006 (2005).

[4] A. Abada et al., J. High Enegry Phys. 02, 016, (2004).

[5] C. McNeile, C. Michael, and G. Thompson (UKQCD), Phys. Rev D **70**, 054501 (2004).

[6] W.-M. Yao et al., Journal of Physics G 33, 1 (2006).

[7] Huang, et al., Phys. Rev. Lett. **94**, 011802 (2005).

[8] J. M. Link, et al., Phys. Lett. B **607**, 233 (2005).

[9] D. Becirevic, and A. B. Kaidalov, Phys. Lett. B **478**, 417 (2000).

[10] B. Aubert, et al., Phys. Rev. Lett. **90**, 242001 (2003).

[11] E. W. Vaandering (2004), hep-ex/0406044.

[12] D. Besson, et al., AIP Conf. Proc. **698**, 497 (2004).

[13] A. V. Evdokimov, et al., Phys. Rev. Lett. **93**, 242001 (2004).

[14] S. Fajfer, and J. Kamenik, Phys. Rev. D **71**, 014020 (2005).

[15] S. Fajfer, and J. Kamenik, Phys. Rev. **72**, 034029 (2005).

[16] S. Fajfer, and J. Kamenik, Phys. Rev. **72**, 057503 (2006).

[17] R. E. Marshak, Riazuddin, and C. P. Ryan, *Theory of Weak Interactions in Particle Physics*, vol. XXIV of *Interscience Monographs and Texts in Physics and Astronomy*, Wiley-Interscience, New York, 1969.

[18] M. Wirbel, B. Stech, and M. Bauer, Z. Phys. C **29**, 637 (1985).

[19] J. Charles, A. Le Yaouanc, L. Oliver, O. Pene, and J. C. Raynal, Phys. Rev. D **60**, 014001 (1999).

[20] N. Isgur, and M. B. Wise, Phys. Rev. D **42**, 2388 (1990).

[21] R. J. Hill (2005), hep-ph/0505129.

[22] D. Ebert, R. N. Faustov, and V. O. Galkin, Phys. Rev. D **64**, 094022 (2001).

[23] G. Burdman, and G. Hiller, Phys. Rev. D **63**, 113008 (2001).

[24] R. J. Hill (2004), hep-ph/0411073.

[25] B. Bajc, S. Fajfer, and R. J. Oakes, Phys. Rev. D **53**, 4957 (1996).

[26] P. Ball, V. M. Braun, and H. G. Dosch, Phys. Rev. **D44**, 3567–3581 (1991).

[27] D. Melikhov, and B. Stech, Phys. Rev. D **62**, 014006 (2000).

[28] C. Aubin, et al. (2004), hep-ph/0408306.

[29] A. Abada, et al., Nucl. Phys. Proc. Suppl. B **119**, 625 (2003).

[30] P. Ball, Phys. Rev. D **48**, 3190 (1993).

[31] S. Blusk (2005), hep-ex/0505035.

[32] S. Fajfer and Sasa Prelovsek, Phys. Rev.D **73**, 054026 (2006).

[33] G. Burdman, E. Golowich, J. Hewett and S. Pakvasa, Phys. Rev. D **52**, 6383 (1995).

[34] G. Burdman, E. Golowich, J. Hewett and S. Pakvasa, Phys. Rev. D **66**, 014009 (2002).

[35] G. Burdman and I. Shipsey, Ann. Rev. Nucl. Part. Sci. **53** 431 (2003).

[36] S. Pakvasa, Nucl. Phys.B Proc. Suppl. **142**, 115 (2005).
Durham, England, Apr 2003, hep-ph/030626.

[37] S. Fajfer, S. Prelovsek, P. Singer, Eur. Phys. J.C **6**, 471 (1999).

[38] S. Fajfer, S. Prelovsek, P. Singer, Phys. Rev. D **58**, 094038 (1998).

[39] S. Fajfer, S. Prelovsek, P. Singer, Phys. Rev.D **64**, 114009 (2001).

[40] S. Fajfer, P. Singer, J. Zupan, Eur. Phys.J.C **27**, 201 (2003).

[41] S. Bianco, F.L. Fabbri, D. Benson and I. Bigi, Riv. Nuovo Cim. 26 N **7**, 1 2003.

[42] O. Tajima *et al.*, BELLE Collaboration, Phys. Rev. Lett. **92**, 101803 (2004).

[43] Q. He *et al.*, CLEO Collaboration, Phys. Rev. Lett.**95**, 221802 (2005).

[44] C. Greub, T. Hurth, M. Misiak and D. Wyler, Phys. Lett. B **382**, 415 (1996); Q. Ho Kim and X.Y. Pham, Phys. Rev. D **61**, 013008 (2000).

[45] S. Prelovsek and D. Wyler, Phys. Lett.B **500**, 304 (2001).

[46] V. Barger, M. S. Berger and R.J. N. Phillips, Phys. Rev. D **52**, 1663 (1995).

[47] P. Langacker and D. London, Phys. Rev. D **38**, 886 (1988).

[48] F. del Aguila and J. Santiago, JHEP **03**, 010 (2002).

[49] S.A. Abel, J. Santiago, M. Masip, JHEP **04**, 057 (2003).

[50] K. Higuchi and K. Yamamoto, Phys. Rev. D **62**, 03005 (2000).

[51] Lae Yong Lee, JHEP **0412**, 065 (2004).

Review of Charm Sector Mixing and CP Violation

David Asner
Physics Department
Carleton University,
1125 Colonel By Drive
Ottawa, Ontario, Canada, K1S 5B6

The phenomenology of $D^0 - \overline{D}^0$ mixing and CP violation is briefly described. Recent experimental results from BABAR, Belle, CDF, and CLEO-c are reviewed. No evidence for mixing or CP violation is found, and limits are set for the mixing parameters x, y, x', y', and several CP-violating parameters. Results are compared to theoretical predictions. Finally, future prospects at BESIII, LHC-b and a Super B-factory are discussed.

1 BRIEF HISTORY

The search for D^0–$\overline{D}^0$ mixing began following the discover of the D^0 meson at SPEAR [1]. The earliest searches for charm mixing were 'indirect', searching for like-sign muons rather than fully reconstructing D^0 mesons. The first direct searches recontructed the D^0, usually from a D^{*+} to tag the initial flavor, and searched for the wrong-sign final state $K^+\pi^-$. After experimental sensitivity to the expected doubly-Cabibbo suppressed (DCS) decay $D^0 \to K^+\pi^-$ was attained the search for charm mixing required a time-dependent analysis to disentangle the DCS decay ($D^0 \to K^+\pi^-$) and mixing followed by Cabibbo favored decay ($D^0 \to \overline{D}^0 \to K^+\pi^-$) amplitudes.

1.1 Indirect Searches for D^0–$\overline{D}^0$

Inclusive measurements of lepton pairs at muon or neutrino, or beam dump experiments can be used as a probe of charm mixing. Following the subtraction of the number of like-sign leptons from background sources and estimating the amount of charm produced these experiments constrain the amount of mixing. The results of indirect searches for D^0–$\overline{D}^0$ are summarized in Tab. 1. The best indirect limits were obtained by the experiment E615 where a 225 GeV pion beam was incident on a tungsten target. They searched for the reaction

$$\pi N \to D^0\overline{D}^0 \to (K^-\mu^+\nu)D^0 \to (K^-\mu^+\nu)^2 \quad (1)$$

Table 1: Indirect Searches for D^0–$\overline{D}^0$.

Experiment	Mixing Technique	90% C.L.
EMC (1981) [2]	$\mu^+ N \to \mu^+(\mu^+\mu^+)X$	20%
CCFRS (1982) [3]	$\pi^-\text{Fe} \to \mu^+\mu^+$	4.4%
BDMS (1985) [4]	$\mu^+ N \to \mu^+\mu^-\mu^- X$	1.2%
CDHS (1985) [5]	$\nu N \to \mu^-\mu^-$	$5.1 \pm 2.3\%$
	$\overline{\nu} N \to \mu^+\mu^+$	$3.2 \pm 1.2\%$
E615 (1986) [6]	$\pi^- W \to \mu^-\mu^-$	0.56%
E744 (1988) [7]	$\nu N \to \mu^-\mu^-$,	$< 9\%$
	$\overline{\nu} N \to \mu^+\mu^+$	

where only the final state muons were detected. The largest source of background was random μ pairs produced by other pion interactions in the same rf bucket. The angle between the π beam and one of the μ^+ distinguishes this background from D^0–$\overline{D}^0$ mixing. E615 observed 3973 like sign muon pairs with invariant mass greater than 2.0 GeV/c^2. Using their model of the angular dependence of charm hadroproduction, they set an upper limit on the contribution due to mixing of 63 events at the 90% confidence level. The estimate of $D\overline{D}$ production cross section is obtained by assuming that each $\overline{D}^0$ is accompanied by a D^0 or a D^+ with equal probability. Therefore $\sigma(D^0\overline{D}^0) = \frac{1}{2}\sigma(D^0) = 3.8 \pm 0.5 \mu b/\text{nucleon}$ where $\sigma(D^0)$ is an average of published cross sections from other hadroproduction experiments. The final limit obtained is $R_M < 0.56\%$ which corresponds to $x, y < 11\%$, all at the 90% confidence level.

1.2 Earlier Studies of $D^0 \to K^+\pi^-$

Experiments performed at e^+e^- storage rings or using photon or pion beams have used the decay chain $D^{*+} \to D^0\pi^+, D^0 \to K^\mp\pi^\pm$ where the charge of the pion from D^{*+} decay tags the production flavor of the D^0. Prior to the first reliable observation of $D^0 \to K^+\pi^-$ by CLEO II.V [8] many experiments searched for the 'wrong sign' decay. The limits from several experiments are given in Tab. 2.

The CLEO collaboration reported first observation of $D^0 \to K^+\pi^-$ in 1993 [19], however the decay-time resolution was not sufficient to distinguish DCS decay from mixing. In 1997, the E791 collaboration reported the first study of the time evolution of $D^0 \to K^+\pi^-$ and $K^+\pi^-\pi^+\pi^-$ [20]. The sensitivity to the time-integrated rate is somewhat less than the CLEO result but precise decay time resolution allows constraints to be placed on D^0–$\overline{D}^0$ mixing. The constraints on mixing parameters

Table 2: Experimental Searches for $D^0 \to K^+\pi^-$. The number of Cabibbo-favored (CF) $D^{*+} \to D^0\pi^+$, $D^0 \to K^-\pi^+$ is given in the second column. In the third column the limits on the mixing rate R_M before (after) 1990 are at 90% (95%) C.L.

Experiment	#CF	R_M
SPEAR (1977) [9]	~ 250	$< 16\%$
SPEAR (1977) [10]	~ 150	$< 18\%$
E87 (1980) [11]	~ 143	$< 11\%$
ACCMOR (1983) [12]	~ 10's	$< 7\%$
DELCO (1985) [13]	~ 100	$< 8.1\%$
HRS (1986) [14]	~ 70	$< 4\%$
ARGUS (1987) [15]	224	$< 1.4\%$
CLEO I.5 [16]	420	$R < 1.1\%$
E691 (1988) [17]	~ 1550	$< 0.65\%$
E687 (1994) [18]	~ 1000	-
CLEO II (1993) [19]	~ 6600	$R = 0.77 \pm 0.35\%$
E791 (1997) [20]	~ 5200	0.21 ± 0.09
Aleph (1998) [21]	~ 1000	$< 3.6\%$
CLEO II.V (2000) [8]	~ 13500	
FOCUS (2001) [22, 23]	~ 37k	$< 0.61\%$
BaBar (2003) [24]	~ 120k	$< 0.16\%$
Belle (2005) [26]	~ 227k	$< 0.046\%$
CDF (2006) [27]	~ 495k	-

obtained without the assumption of CP conservation were considerably weaker.

In 1999, E791 published [28] the first measurement of $y = (0.83 \pm 2.9 \pm 1.0)\%$ using the decays $D^0 \to K^+K^-$. Both CLEO II.V and the E831/FOCUS collaboration accumulated about 10 times the statistics of E791 in the singly-Cabibbo suppressed decay mode, $D^0 \to K^+K^-$. E831/FOCUS and CLEO II.V achieved a statistical precision of $\sim 1.4\%$ [29] and $\sim 2.5\%$ [30], respectively

2 CPV IN CHARM SECTOR

The violation of charge-parity (CP) in charm decay requires two amplitudes with different strong and weak phases that interfere to produce CP violating effects. There are three distinct types of CP violation: (1) CP violation from a non-vanishing relative phase between the mass and width components of the mixing matrix usually called "indirect"; (2) Direct CP violation due to the two decay amplitudes having different weak phases; (3) Interference between decays with and without mixing. The CP conserving phase shift is usually generated by QCD final state interactions (FSI) which

Table 3: CP Violation Results for D^0: All numbers are given in percent.

D^0 A_{CP}	E791	FOCUS	CLEO	BaBar	Belle	CDF
$K^+\pi^-$ [8, 23–25]		$18\pm14\pm4$	2^{+19}_{-20}	9.5 ± 10.3	2.3 ± 4.7	
$K^+\pi^-\pi^0$ [35, 36]			9^{+25}_{-22}		-0.6 ± 5.3	
K^-K^+ [28, 30, 37, 38]	$-1.0\pm4.9\pm1.2$	$-0.1\pm2.2\pm1.5$	$0.0\pm2.2\pm0.8$		0.2 ± 0.7	$1.0\pm1.3\pm0.6$
$\pi^-\pi^+$ [28, 30, 37, 38]	$-4.9\pm7.8\pm3.0$	$4.8\pm3.9\pm2.5$	$1.9\pm3.2\pm0.8$			$2.0\pm1.2\pm0.6$
$\pi^0\pi^0$ [39]			0.1 ± 4.8			
$K^0_SK^0_S$ [39]			-23 ± 19			
$K^0_S\pi^0$ [39]			0.1 ± 1.3			
$K^0_S\pi^+\pi^-$ [40]			$-0.9 \pm 2.1^{+1.6}_{-5.7}$			
$K^0_S\phi$ [41]			2.8 ± 9.4			
$K^-\pi^+\pi^0$ [42]			-3.1 ± 8.6			
$\pi^+\pi^-\pi^0$ [43]			$-1^{+9}_{-7}\pm5$			
$K^+\pi^-\pi^+\pi^-$ [36]					-1.8 ± 4.4	
$K^+K^-\pi^+\pi^-$ [44]		$-8.2\pm5.6\pm4.7$				

are large in the charm sector. In the Standard Model (SM), the relative weak phase is typically between tree level and penguin amplitudes. Extensions to the Standard Model introduce additional amplitudes with weak phases that can contribute to CP violation.

For charm decays, within the SM, the effective weak phase is highly diluted, $\sim \mathcal{O}(\lambda^4)$, and it can arise only in *singly-Cabibbo-suppressed* transitions, where one expects asymmetries to reach the $\mathcal{O}(0.1\%)$ level; significantly larger values would indicate new physics. *Any* asymmetry in *Cabibbo-allowed or doubly-suppressed* channels requires the intervention of new physics – except for $D^\pm \to K^0_S\pi^\pm$ [31], where the CP impurity in the K^0_S induces an asymmetry of 3.3×10^{-3}. Note that in going from Cabibbo-allowed to Cabibbo singly- and doubly- suppressed channels, the SM rate is *suppressed* by factors of about twenty and four hundred, respectively. This suppression enhances the visibility of new physics.

Decays to final states of *more than* two pseudoscalar or one pseudoscalar and one vector meson contain more dynamical information than given by their widths; their distributions as described by Dalitz plots [48] or T-odd moments can exhibit CP asymmetries that might be considerably larger than those for the width [49].

Most CP violation results are from the FNAL fixed target experiments E791 and FOCUS, and the CLEO experiment and search for direct CP violation. The CP

Table 4: CP Violation Results for D^+: All numbers are given in percent.

D^+ A_{CP}	E791	FOCUS	BaBar
$K^0_S\pi^+$ [34]		-1.6±1.5±0.9	
$K^0_S K^+$ [34]		6.9±6.0±1.8	
$K^+K^-\pi^+$ [37, 45–47]	-1.4±2.9	0.6±1.1±0.5	1.4±1.0±0.8
$\phi\pi^+$ [45]	-2.8±3.6		
K^*K^+ [45, 47]	-1.0±5.0		0.9±1.7±0.7
$\pi^-\pi^+\pi^+$ [45]	-1.7±4.2		
$K^0_S K^+\pi^+\pi^-$ [44]		-4.2±6.4±2.2	

violation asymmetry is defined as $A_{CP} \equiv \frac{\Gamma(D\to f)-\Gamma(\overline{D}\to\overline{f})}{\Gamma(D\to f)+\Gamma(\overline{D}\to\overline{f})}$. A few results from CLEO, BaBar and Belle experiments consider CP violation in mixing. The results tabulated in Tab. 3 and Tab. 4 show no evidence for CP violation. This is consistent with Standard Model expectations.

3 $D^0-\overline{D}^0$ MIXING

The formalism describing $D^0-\overline{D}^0$ mixing is given in several papers [31, 32]. The time evolution of a particle produced as a D^0 or $\overline{D}^0$, in the limit of CP conservation, is governed by four parameters: $x = \Delta m/\Gamma$ and $y = \Delta\Gamma/2\Gamma$ which characterize the mixing matrix, δ the relative strong phase between Cabibbo favored (CF) and doubly-Cabibbo suppressed (DCS) amplitudes ($\delta_{K\pi}$ refers specifically to the $K\pi$ final state) and R_D the DCS decay rate relative to the CF decay rate. The mixing rate R_M is defined as $\frac{1}{2}(x^2+y^2)$. A D^0 can evolve into a $\overline{D}^0$ through on-shell intermediate states, such as K^+K^- with mass, $m_{K^+K^-} = m_{D^0}$, or through off-shell intermediate states, such as those that might be present due to new physics. This evolution through the former (latter) states is parametrized by the dimensionless variables $-iy$ (x).

Time-dependent analyses are not feasible at CLEO-c; however, the quantum-coherent $D^0\overline{D}^0$ state provides time-integrated sensitivity to x, y at $\mathcal{O}(1\%)$ level and $\cos\delta_{K\pi} \sim 0.1$ in 1 fb^{-1} of data at the $\psi(3770)$. Due to quantum correlations in the $C = -1$ and $C = +1$ $D^0\overline{D}^0$ pairs produced in the reactions $e^+e^- \to D^0\overline{D}^0(\pi^0)$ and $e^+e^- \to D^0\overline{D}^0\gamma(\pi^0)$, respectively [33], the time-integrated $D^0\overline{D}^0$ decay rates are sensitive to interference between amplitudes for indistinguishable final states. The size of this interference is governed by the relevant amplitude ratios and can include contributions from D^0-$\overline{D}^0$ mixing.

3.1 $D^0 - \overline{D}^0$ Mixing Formalism and Results

Standard Model based predictions for x and y, as well as a variety of non-Standard Model expectations, span several orders of magnitude [31, 50]. Several non-Standard Models predict $|x| > 0.01$. Contributions to x at this level could result from the presence of new particles with masses as high as 100-1000 TeV [51, 52]. The Standard Model short-distance contribution to x is determined by the box diagram in which two virtual quarks and two virtual W bosons are exchanged. Short distance contributions to y are expected to be less than x. Both x and y are beyond current experimental sensitivity. Long distance effects are expected to be larger but are difficult to estimate due to the large number of resonances near the D^0 pole. It is likely that x and y contribute similarly to mixing in the Standard Model.

The parameters x and y can be measured in a variety of ways. The most precise constraints are obtained by exploiting the time-dependence of D decays. Previous attempts to measure x and y include: the measurement of the wrong sign semileptonic branching ratio $D^0 \to K\ell\nu$ [53–57] which is sensitive to the mixing rate $R_M = \frac{x^2+y^2}{2}$; decay rates to CP eigenstates $D^0 \to K^+K^-, \pi^+\pi^-$ [29, 30, 58–61] which are sensitive to y; and the wrong sign $D^0 \to K^+\pi^-$ [8, 23, 24, 26] hadronic branching ratio which measures $x'^2 = (y\sin\delta_{K\pi} + x\cos\delta_{K\pi})^2$ and $y' = y\cos\delta_{K\pi} - x\sin\delta_{K\pi}$.

It is usual to normalize the wrong-sign decay distributions to the integrated rate of right-sign decays and to express time in units of the precisely measured D^0 mean lifetime, $\overline{\tau}_{D^0} = 1/\Gamma = 2/(\Gamma_1 + \Gamma_2)$. Starting from a pure $|D^0\rangle$ or $|\overline{D}^0\rangle$ state at $t = 0$, the time-dependent rates of production of the wrong-sign final states relative to the integrated right-sign states are then

$$r(t) \;=\; \left|\frac{q}{p}\right|^2 \left|g_+(t)\,\chi_f^{-1} + \,g_-(t)\,\right|^2 \tag{2}$$

and

$$\overline{r}(t) \;=\; \left|\frac{p}{q}\right|^2 \left|g_+(t)\,\chi_{\overline{f}} + \,g_-(t)\,\right|^2 , \tag{3}$$

where

$$\chi_f \equiv q\overline{A}_f/pA_f\,, \quad \chi_{\overline{f}} \equiv q\overline{A}_{\overline{f}}/pA_{\overline{f}}\,, \tag{4}$$

q and p are complex coefficients relating flavor eigenstates to mass eigenstates, $\mathcal{A}_f$ ($\overline{\mathcal{A}}_f$) and $\mathcal{A}_{\overline{f}}$ ($\overline{\mathcal{A}}_{\overline{f}}$) are amplitudes for a pure D^0 ($\overline{D}^0$) state to decay to f and $\overline{f}$, respectively, and

$$g_\pm(t) = \frac{1}{2}\left(e^{-iz_1t} \pm e^{-iz_2t}\right)\,, \quad z_{1,2} = \frac{\lambda_{1,2}}{\Gamma}\,. \tag{5}$$

Note that a change in the convention for the relative phase of D^0 and $\overline{D}^0$ would cancel between q/p and $\overline{A}_f/A_f$ and leave χ_f invariant.

Table 5: Results for R_M in D^0 semileptonic decays.

Exper.	Final state(s)	R_M (90 (95)% C.L.)
Belle [57]	$K^{(*)+}e^-\overline{\nu}_e$	$<1.0\times10^{-3}$
CLEO [56]	$K^{(*)+}e^-\overline{\nu}_e$	$<7.8\times10^{-3}$
BaBar [55]	$K^{(*)+}e^-\overline{\nu}_e$	$<4.2(4.6)\times10^{-3}$
FOCUS [54]	$K^+\mu^-\overline{\nu}_\mu$	$<1.01(1.31)\times10^{-3}$
E791 [53]	$K^+\ell^-\overline{\nu}_\ell$	$<5.0\times10^{-3}$

Semileptonic

In semileptonic D decays, $A_f = \overline{A}_{\overline{f}} = 0$ in the Standard Model. Then in the limit of weak mixing, where $|ix+y|l\bar{l}1$, $r(t)$ is given by

$$r(t) = |g_-(t)|^2 \left|\frac{q}{p}\right|^2 \approx \frac{e^{-t}}{4}(x^2+y^2)\,t^2 \left|\frac{q}{p}\right|^2 . \tag{6}$$

For $\overline{r}(t)$ one replaces q/p here with p/q. In the limit of CP conservation, $r(t) = \overline{r}(t)$, and the time-integrated mixing rate relative to the time-integrated right-sign decay rate is

$$R_M = \int_0^\infty r(t)dt = \left|\frac{q}{p}\right|^2 \frac{x^2+y^2}{2+x^2-y^2} \approx \frac{1}{2}(x^2+y^2)\,. \tag{7}$$

Table 5 summarizes results from semileptonic decays.

Hadronic

Consider the final state $f = K^+\pi^-$, where A_f is doubly-Cabibbo suppressed. The ratio of decay amplitudes is

$$\frac{A_f}{\overline{A}_f} = -\sqrt{R_D}\,e^{-i\delta}, \qquad \left|\frac{A_f}{\overline{A}_f}\right| \sim O(\tan^2\theta_c)\,, \tag{8}$$

where R_D is the doubly Cabibbo suppressed decay rate relative to the Cabibbo-favored (CF) rate, the minus sign originates from the sign of V_{us} relative to V_{cd}, and δ is the phase difference between DCS and CF processes not attributed to the first-order electroweak spectator diagram.

The violation of CP in the mixing amplitude, the decay amplitude, and the interference between mixing and decay, is characterized by the real-valued parameters A_M, A_D, and ϕ.

Table 6: Results for R in $D^0 \to K^+\pi^-$.

Exper.	$R(\times 10^{-3})$	$A_D(\%)$
CDF [27]	$4.05 \pm 0.21 \pm 0.11$	—
Belle [26]	$3.77 \pm 0.08 \pm 0.05$	—
FOCUS [23]	$4.29 \pm 0.63 \pm 0.28$	$18.0 \pm 14.0 \pm 4.1$
BaBar [24]	$3.57 \pm 0.22 \pm 0.27$	$9.5 \pm 6.1 \pm 8.3$
CLEO [8]	$3.32^{+0.63}_{-0.65} \pm 0.40$	$2^{+19}_{-20} \pm 1$

Table 7: Results from studies of the time dependent $r(t)$.

Exper.	y' (95% C.L.)	$x'^2/2$ (95% C.L.)
Belle [26]	$-2.8 < y' < 2.1$ %	< 0.036 %
FOCUS [23]	$-11.2 < y' < 6.7$ %	< 0.40 %
BaBar [24]	$-5.6 < y' < 3.9$ %	< 0.11 %
CLEO [8]	$-5.8 < y' < 1.0$ %	< 0.041 %

In the limit of CP conservation, A_M, A_D, and ϕ are all zero, and then

$$r(t) = \overline{r}(t) = e^{-t}\left(R_D + \sqrt{R_D}\, y' t + \frac{1}{2} R_M\, t^2\right) , \tag{9}$$

and the time-integrated wrong-sign rate relative to the integrated right-sign rate is

$$R = \int_0^\infty r(t)\, dt = R_D + \sqrt{R_D}\, y' + R_M\, . \tag{10}$$

Here

$$y' \equiv\ y\cos\delta - x\sin\delta, \quad x' \equiv x\cos\delta + y\sin\delta\, , \tag{11}$$

and R_M is the mixing rate relative to the time-integrated right-sign rate.

The ratio R is the most readily accessible experimental quantity. Table 6 gives recent measurements of R in $D^0 \to K^+\pi^-$ decay. The average of these results, $R = (0.380 \pm 0.008)\,\%$, is about two standard deviations from the average of earlier, less precise results, $R = (0.81 \pm 0.23)\,\%$, which we have omitted.

The contributions to R—allowing for CP violation—can be extracted by fitting the $D^0 \to K^+\pi^-$ and $\overline{D}^0 \to K^-\pi^+$ decay rates. Table 6 gives the constraints on A_D

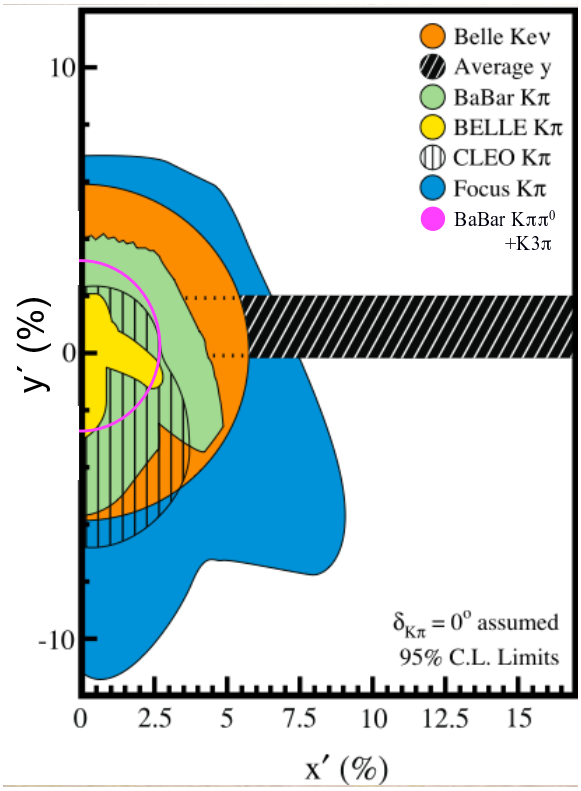

Figure 1: Allowed regions in the x',y' plane. The allowed region for y is the average of the results from E791 [58], FOCUS [29], CLEO [30], BaBar [61], and Belle [59,60]. Also shown is the limit from $D^0 \to K^{(*)}\ell\nu$ from Belle [57] and limits from $D \to K\pi$ from CLEO [8], BaBar [24], Belle [26] and FOCUS [23]. We assume $\delta = 0$ to place the y results.

with $x' = y' = 0$. Table 7 summarizes the results for y' and $x'^2/2$. Figure 1 shows the two-dimensional allowed regions. No meaningful constraints on A_M and ϕ have been reported.

Extraction of the amplitudes x and y from the results in Tab. 7 requires knowledge of the relative strong phase δ, a subject of theoretical discussion [62–65]. In most cases, it appears difficult for theory to accommodate $\delta > 25°$, although the judicious placement of a $K\pi$ resonance could allow δ to be as large as 40°.

In $D^0 \to K^0_S\pi^+\pi^-$, the DCS and CF decay amplitudes populate the same Dalitz plot, which allows direct measurement of the relative strong phase. CLEO has measured the relative phase between $D^0 \to K^*(892)^+\pi^-$ and $D^0 \to K^*(892)^-\pi^+$ to be $(189 \pm 10 \pm 3^{+15}_{-5})°$ [66], consistent with the 180° expected from Cabibbo factors and a small strong phase.

Table 8: Results for R in $D^0 \to K^{(*)+}\pi^-(n\pi)$.

Exper.	D^0 final state	$R(\%)$
BaBar [70]	$K^+\pi^-\pi^0$	$0.214 \pm 0.008 \pm 0.008$
Belle [36]	$K^+\pi^-\pi^+\pi^-$	$0.320 \pm 0.019^{+0.018}_{-0.013}$
Belle [36]	$K^+\pi^-\pi^0$	$0.229 \pm 0.017^{+0.013}_{-0.009}$
CLEO [66]	$K^{*+}\pi^-$	$0.5 \pm 0.2^{+0.6}_{-0.1}$
CLEO [67]	$K^+\pi^-\pi^+\pi^-$	$0.41^{+0.12}_{-0.11} \pm 0.04$
CLEO [35]	$K^+\pi^-\pi^0$	$0.43^{+0.11}_{-0.10} \pm 0.07$
E791 [20]	$K^+\pi^-\pi^+\pi^-$	$0.68^{+0.34}_{-0.33} \pm 0.07$

Multibody

There are several results for R measured in multibody final states with nonzero strangeness. Here R, defined in Eqn. 10, becomes an average over the Dalitz space, weighted by experimental efficiencies and acceptance. Table 8 summarizes the results.

For multibody final states, Eqn.8-10 apply to one point in the Dalitz space. Although x and y do not vary across the space, knowledge of the resonant substructure is needed to extrapolate the strong phase difference δ from point to point. Both the sign and magnitude of x and y (rather than x'^2 and y') may be measured using the time-dependent resonant substructure of multibody D^0 decays. CLEO has performed a time-dependent Dalitz-plot analysis of $D^0 \to K^0_S\pi^+\pi^-$, and reports $(-4.5 < x < 9.3)\%$ and $(-6.4 < y < 3.6)\%$ at the 95% confidence level, without phase or sign ambiguity [68] . Recently, BaBar has searched for mixing in the multibody decays $D^0 \to K^+\pi^-\pi^0$ [70] and $D^0 \to K^+\pi^-\pi^+\pi^-$ [69]. The combined result is $R_M = (0.020^{+0.011}_{-0.010})\%$ or $R_M < 0.042\%$ at the 95% confidence level.

CP Eigenstates

When the final state f is a CP eigenstate, there is no distinction between f and $\overline{f}$, and then $A_f = A_{\overline{f}}$ and $\overline{A}_{\overline{f}} = \overline{A}_f$.

The quantity y may be measured by comparing the rate for decays to non-CP eigenstates such as $D^0 \to K^-\pi^+$ with decays to CP eigenstates such as $D^0 \to K^+K^-$ [65]. A positive y would make K^+K^- decays appear to have a shorter lifetime than $K^-\pi^+$ decays. The decay rate for a D^0 into a CP eigenstate is not described by a just single exponential in the presence of CP violation. However, in the limit of weak mixing, where $|ix + y|\, l\bar{l}1$, and small CP violation, where $|A_M|$, $|A_D|$, and $|\sin\phi|\, l\bar{l}1$, the time dependence of decays to CP eigenstates is proportional to a single

Table 9: Results for y from $D^0 \to K^+K^-$ and $\pi^+\pi^-$. Belle [60] and BaBar [61] also measure A_Γ to be $(-2.0 \pm 6.3 \pm 3.0)$ and $(-8 \pm 6 \pm 2) \times 10^{-3}$.

Exper.	D^0 final state(s)	$y_{CP}(\%)$
Belle [60]	K^+K^-	$1.15 \pm 0.69 \pm 0.38$
BaBar [61]	$K^+K^-, \pi^+\pi^-$	$0.8 \pm 0.4^{+0.5}_{-0.4}$
CLEO [30]	$K^+K^-, \pi^+\pi^-$	$-1.1 \pm 2.5 \pm 1.4$
Belle [59]	K^+K^-	$-0.5 \pm 1.0^{+0.7}_{-0.8}$
FOCUS [29]	K^+K^-	$3.4 \pm 1.4 \pm 0.7$
E791 [28]	K^+K^-	$0.8 \pm 2.9 \pm 1.0$
Average		0.90 ± 0.42

exponential:

$$r_\pm(t) \propto \exp\left(-[1 \pm \left|\tfrac{p}{q}\right|(y\cos\phi - x\sin\phi)]t\right), \tag{12}$$

$$\overline{r}_\pm(t) \propto \exp\left(-[1 \pm \left|\tfrac{q}{p}\right|(y\cos\phi + x\sin\phi)]t\right),$$

$$r_\pm(t) + \overline{r}_\pm(t) \propto e^{-(1\pm y_{CP})t}. \tag{13}$$

When equal numbers of D^0 and $\overline{D}^0$ are produced

$$y_{CP} = y\cos\phi \left[\tfrac{1}{2}\left(\left|\tfrac{p}{q}\right| + \left|\tfrac{q}{p}\right|\right)\right] \tag{14}$$

$$-x\sin\phi \left[\tfrac{1}{2}\left(\left|\tfrac{p}{q}\right| - \left|\tfrac{q}{p}\right|\right)\right] \tag{15}$$

The possibility of CP violation has been considered in the limit of weak mixing and small CP violation. In this limit there is no sensitivity to CP violation in direct decay. Allowing for CP violation in interference and mixing Belle [60] and BaBar [61] have measured A_Γ, where

$$A_\Gamma \equiv \frac{r_\pm(t) - \overline{r}_\pm(t)}{r_\pm(t) - \overline{r}_\pm(t)} \approx A_M\, y\cos\phi - x\sin\phi. \tag{16}$$

In the limit of CP conservation, $y = y_{CP}$.

All measurements of y and A_Γ are relative to the $D^0 \to K^-\pi^+$ decay rate. Table 9 summarizes the current status of measurements. The average of the six y_{CP} measurements is $0.90 \pm 0.42\,\%$.

Table 10: CLEO-c preliminary results from time-integrated yields at $\psi(3770) \to D\overline{D}$. Errors are statistical only. Systematic uncertainties are anticipated to be smaller.

Parameter	CLEO-c [75]	Other results (%)
y	-0.058 ± 0.066	0.90 ± 0.42
$\cos\delta_{K\pi}$	1.09 ± 0.66	—
R_M	$(1.7 \pm 1.5) \times 10^{-3}$	< 0.1 (95% C.L.)
$x^2/2$	$< 0.44\%$ (95% C.L.)	< 0.036 (95% C.L.)

Coherent $D^0 - \overline{D}^0$ Analyses

Measurements of R_D, $\cos\delta$, x, and y can be made simultaneously in a combined fit to the single-tag (ST) and double-tag (DT) yields or individually by a series of "targeted" analyses [71, 72].

The "comprehensive" analysis simultaneously measures mixing and DCS parameters by examining various ST and DT rates. Due to quantum correlations in the $C = -1$ and $C = +1$ $D^0\overline{D}^0$ pairs produced in the reactions $e^+e^- \to D^0\overline{D}^0(\pi^0)$ and $e^+e^- \to D^0\overline{D}^0\gamma(\pi^0)$, respectively, the time-integrated $D^0\overline{D}^0$ decay rates are sensitive to interference between amplitudes for indistinguishable final states. The size of this interference is governed by the relevant amplitude ratios and can include contributions from D^0-$\overline{D}^0$ mixing.

The following categories of final states are considered:
f or $\overline{f}$: Hadronic states accessed from either D^0 or $\overline{D}^0$ decay but that are not CP eigenstates. An example is $K^-\pi^+$, which results from Cabibbo-favored D^0 transitions or DCS $\overline{D}^0$ transitions.
ℓ^+ or ℓ^-: Semileptonic or purely leptonic final states, which, in the absence of mixing, tag unambiguously the flavor of the parent D.
S_+ or S_-: CP-even and CP-odd eigenstates, respectively.

The decay rates for $D^0\overline{D}^0$ pairs to all possible combinations of the above categories of final states are calculated in Ref. [63], for both $C = -1$ and $C = +1$, reproducing the work of Refs. [62, 73, 74]. Such $D^0\overline{D}^0$ combinations, where both D final states are specified, are double tags. In addition, the rates for single tags, where either the D^0 or $\overline{D}^0$ is identified and the other neutral D decays generically are given in Ref. [63].

CLEO-c has reported preliminary results using 281 pb^{-1} of $e^+e^- \to \psi(3770)$ data [75], where the quantum coherent $D^0\overline{D}^0$ pairs are in the $C = -1$ state. The values of y, R_M, and $\cos\delta$ are determined from a combined fit to the ST (hadronic only) and DT yields. The hadronic final states included in the analysis are $K^-\pi^+$ (f), $K^+\pi^-$ ($\overline{f}$), K^-K^+ ($S+$), $\pi^+\pi^-$ (S_+), $K^0_S\pi^0\pi^0$ (S_+), and $K^0_S\pi^0$ (S_-). Both of the two flavored final states, $K^-\pi^+$ and $K^+\pi^-$, can be reached via CF or DCS transitions.

Semileptonic DT yields are also included, where one D is fully reconstructed in one of the hadronic modes listed above, and the other D is partially reconstructed, requiring that only the electron be found. When the electron is accompanied by a flavor tag ($D \to K^-\pi^+$ or $K^+\pi^-$), only the "right-sign" DT sample, where the electron and kaon charges are the same, is used. Extraction of the DCS "wrong-sign" semileptonic yield is not feasible with the current CLEO-c data sample, and the parameter R_D is constrained to the world average. Table 10 shows the results of the fit to the CLEO-c data.

4 SUMMARY OF CHARM MIXING

The 95% C.L. allowed region in x' versus y' are plotted in Fig. 1. The most stringent limits are from Belle constrain mixing in $D^0 \to K^+\pi^-$ to be $x'^2 < 2.7\%$ and $(-1.0\% < y' < 0.7\%$ [26] at 95% confidence level (C.L.). This result excludes $x'^2 = y' =$ at the 96.9% C.L. Other results are enticing too. The most recent limits from BaBar [69, 70] constrains D mixing in the multibody processes $D^0 \to K^+\pi^-\pi^0$ and $D^0 \to K^+\pi^-\pi^+\pi^-$ to be $R_M = (0.020^{+0.011}_{-0.010})\%$ or $R_M < 4.2 \times 10^{-4}$ at 95% C.L. Here the no mixing solution is excluded at the 97.9% C.L. Furthermore, the average of the six y_{CP} measurements from E791 [58], FOCUS [29], CLEO [30], BaBar [61], and Belle [59,60] is $0.90 \pm 0.42\,\%$. This could be an indication that the observation of $D^0 - \overline{D}^0$ mixing is just around the corner. Of course, it is noteworthy that earlier measurements also indicated hints of a mixing signal. In 1997, E791 reported $R_M = (0.21 \pm 0.09 \pm 0.02)\%$ [20], in 2000 CLEO II.V reported $y' = (-2.5 \pm 1.5 \pm 0.3)\%$ [8], and in 2002 FOCUS reported $y = (3.4 \pm 1.4 \pm 0.7)\%$ [29].

5 FUTURE PROSPECTS

To make significant improvement compared to the current experimental limits, an ideal charm experiment would provide a huge sample ($\sim$ 100 times the existing datasets), well understood backgrounds, efficient charged and neutral reconstruction, near 4π solid angle acceptance, particle ID for clean data samples, and precise lifetime measurements. Most of these attributes also characterise a good beauty experiment.

There are four experiments at various stages of development with significant potential for charm physics, two at e^+, e^- colliders (BESIII and Super-B), and two at hadron machines (LHCb and PANDA); two are beauty experiments, and only one a dedicated charm experiment.

BESIII [76, 77] will accumulate data at charm threshold and expects to integrate 20 times the data sample of CLEO-c.

A Super-B factory [78] would not only produce $\sim 1.5 \times 10^{10}$ $B\overline{B}$ meson pairs but also a similar number of τ pairs and about 7×10^{10} charm mesons per year. The

possibility of running near charm threshold is being considered for the ILC inspired design. A month or two of operation in this mode would be sufficient to increase the world data sample of coherently produced $D^0-\overline{D}^0$ (including BESIII) by an order of magnitude [79].

LHCb is the dedicated B physics experiment at the LHC, due to start its first physics run in 2008. It is expected to accumulate very high statistics in charged two and four body D^0 decays, for instance writing to tape 400,000 wrong-sign $K^{\pm}\pi^{\mp}$ decays per year [80]. An upgraded experiment is also being considered with the potential to increase these statistics by a further order of magnitude [81].

PANDA [82] is a fixed target experiment at the FAIR anti-proton storage ring. PANDA has a rich QCD and charm physics program including charmonium spectroscopy and an open charm studies. PANDA expects to produce about 100 charmed pairs per second around $\psi(4040)$. For a reconstruction efficiency of 30% ($S/B \sim 3$) [83] this corresponds to $\sim 20M$ reconstructed $D^0 \to K^-\pi^+$ in a year of $10^7 s$.

Bibliography

[1] G. Goldhaber *et al.*, Phys. Rev. Lett. **37**, 255 (1976).

[2] J. J. Aubert *et al.* [European Muon Collaboration], Phys. Lett. B **106**, 419 (1981).

[3] A. Bodek *et al.*, Phys. Lett. B **113**, 82 (1982).

[4] A. Argento *et al.*, Phys. Lett. B **158**, 531 (1985).

[5] H. Burkhardt *et al.*, Z. Phys. C **31**, 39 (1986).

[6] C. Biino *et al.*, Phys. Rev. Lett. **56**, 1027 (1986).

[7] B. A. Schumm *et al.*, Phys. Rev. Lett. **60**, 1618 (1988).

[8] R. Godang *et al.* [CLEO Collaboration], Phys. Rev. Lett. **84**, 5038 (2000).

[9] G. J. Feldman *et al.*, Phys. Rev. Lett. **38**, 1313 (1977).

[10] G. Goldhaber *et al.*, Phys. Lett. B **69**, 503 (1977).

[11] P. Avery *et al.*, Phys. Rev. Lett. **44**, 1309 (1980)

[12] R. Bailey *et al.* [ACCMOR Collaboration], Phys. Lett. B **132**, 237 (1983).

[13] H. Yamamoto *et al.*, Phys. Rev. Lett. **54**, 522 (1985).

[14] S. Abachi *et al.* [HRS Collaboration], Phys. Lett. B **182**, 101 (1986).

[15] H. Albrecht *et al.* [ARGUS Collaboration], Phys. Lett. B **199**, 447 (1987).

[16] R. Ammar *et al.* [CLEO Collaboration], Phys. Rev. D **44**, 3383 (1991).

[17] J. C. Anjos *et al.* [E691 Collaboration], Phys. Rev. Lett. **60**, 1239 (1988).

[18] P. L. Frabetti *et al.* [E687 Collaboration], Phys. Rev. D **50**, 2953 (1994).

[19] D. Cinabro *et al.* [CLEO Collaboration], Phys. Rev. Lett. **72**, 1406 (1994).

[20] E. M. Aitala *et al.* [E791 Collaboration], Phys. Rev. D **57**, 13 (1998).

[21] R. Barate *et al.* [ALEPH Collaboration], Phys. Lett. B **436**, 211 (1998).

[22] J. M. Link *et al.* [FOCUS Collaboration], Phys. Rev. Lett. **86**, 2955 (2001).

[23] J. M. Link *et al.* [FOCUS Collaboration], Phys. Lett. B **618**, 23 (2005).

[24] B. Aubert *et al.* [BABAR Collaboration], Phys. Rev. Lett. **91**, 171801 (2003).

[25] K. Abe *et al.* [BELLE Collaboration], Phys. Rev. Lett. **94**, 071801 (2005).

[26] L. M. Zhang *et al.* [BELLE Collaboration], Phys. Rev. Lett. **96**, 151801 (2006).

[27] A. Abulencia *et al.* [CDF Collaboration], Phys. Rev. D **74**, 031109 (2006).

[28] E. M. Aitala *et al.* [E791 Collaboration], Phys. Lett. B **421**, 405 (1998).

[29] J. M. Link *et al.* [FOCUS Collaboration], Phys. Lett. B **485**, 62 (2000).

[30] S. E. Csorna *et al.* [CLEO Collaboration], Phys. Rev. D **65**, 092001 (2002).

[31] S. Bianco, F. L. Fabbri, D. Benson and I. Bigi, Riv. Nuovo Cim. **26N7**, 1 (2003).

[32] See review by D. Asner on page 728-733 of W. M. Yao *et al.* [Particle Data Group], J. Phys. G **33**, 1 (2006).

[33] M. Goldhaber and J. L. Rosner, Phys. Rev. D **15**, 1254 (1977).

[34] J. M. Link *et al.* [FOCUS Collaboration], Phys. Rev. Lett. **88**, 041602 (2002) [Erratum-ibid. **88**, 159903 (2002)].

[35] G. Brandenburg *et al.* [CLEO Collaboration], Phys. Rev. Lett. **87**, 071802 (2001).

[36] X. C. Tian *et al.* [Belle Collaboration], Phys. Rev. Lett. **95**, 231801 (2005).

[37] J. M. Link *et al.* [FOCUS Collaboration], Phys. Lett. B **491**, 232 (2000) [Erratum-ibid. B **495**, 443 (2000)].

[38] D. Acosta *et al.* [CDF Collaboration], Phys. Rev. Lett. **94**, 122001 (2005).

[39] G. Bonvicini *et al.* [CLEO Collaboration], Phys. Rev. D **63**, 071101 (2001).

[40] D. M. Asner *et al.* [CLEO Collaboration], arXiv:hep-ex/0311033.

[41] J. Bartelt *et al.* [CLEO Collaboration], Phys. Rev. D **52**, 4860 (1995). 5B

[42] S. Kopp *et al.* [CLEO Collaboration], Phys. Rev. D **63**, 092001 (2001).

[43] D. Cronin-Hennessy *et al.* [CLEO Collaboration], Phys. Rev. D **72**, 031102 (2005).

[44] J. M. Link *et al.* [FOCUS Collaboration], Phys. Lett. B **622**, 239 (2005).

[45] E. M. Aitala *et al.* [E791 Collaboration], Phys. Lett. B **403**, 377 (1997).

[46] S. Malvezzi, AIP Conf. Proc. **549** (2002) 569.

[47] B. Aubert *et al.* [BABAR Collaboration], Phys. Rev. D **71**, 091101 (2005).

[48] See review by D. Asner on page 713-716 of W. M. Yao *et al.* [Particle Data Group], J. Phys. G **33**, 1 (2006).

[49] I. I. Bigi, A. I. Sanda, *CP Violation*, Cambridge University Press, 2000.

[50] H. N. Nelson, arXiv:hep-ex/9908021; A. A. Petrov, eConf **C030603**, MEC05 (2003) [arXiv:hep-ph/0311371]; I. I. Y. Bigi and N. G. Uraltsev, Nucl. Phys. B **592**, 92 (2001); Z. Ligeti, AIP Conf. Proc. **618**, 298 (2002); A. F. Falk, Y. Grossman, Z. Ligeti and A. A. Petrov, Phys. Rev. D **65**, 054034 (2002); C. K. Chua and W. S. Hou, arXiv:hep-ph/0110106.

[51] M. Leurer, Y. Nir and N. Seiberg, Nucl. Phys. B **420**, 468 (1994).

[52] N. Arkani-Hamed, L. Hall, D. Smith and N. Weiner, Phys. Rev. D **61**, 116003 (2000).

[53] E. M. Aitala *et al.* [E791 Collaboration], Phys. Rev. Lett. **77**, 2384 (1996).

[54] M. G. Hosack, UMI-30-71944

[55] B. Aubert *et al.* [BABAR Collaboration], Phys. Rev. D **70**, 091102 (2004).

[56] C. Cawlfield *et al.* [CLEO Collaboration], Phys. Rev. D **71**, 077101 (2005)

[57] K. Abe *et al.* [Belle Collaboration], Phys. Rev. D **72**, 071101 (2005).

[58] E. M. Aitala *et al.* [E791 Collaboration], Phys. Rev. Lett. **83**, 32 (1999).

[59] K. Abe *et al.* [Belle Collaboration], Phys. Rev. Lett. **88**, 162001 (2002) [arXiv:hep-ex/0111026].

[60] K. Abe *et al.* [BELLE Collaboration], arXiv:hep-ex/0308034.

[61] B. Aubert *et al.* [BABAR Collaboration], Phys. Rev. Lett. **91**, 121801 (2003).

[62] M. Gronau, Y. Grossman and J. L. Rosner, Phys. Lett. B **508**, 37 (2001).

[63] D. M. Asner and W. M. Sun, Phys. Rev. D **73**, 034024 (2006)

[64] L. L. M. Chau and H. Y. M. Cheng, Phys. Lett. B **333**, 514 (1994). T. E. Browder and S. Pakvasa, Phys. Lett. B **383**, 475 (1996); A. F. Falk, Y. Nir and A. A. Petrov, JHEP **9912**, 019 (1999); G. Blaylock, A. Seiden and Y. Nir, Phys. Lett. B **355**, 555 (1995).

[65] S. Bergmann *et al.*, Phys. Lett. B **486**, 418 (2000)

[66] H. Muramatsu *et al.* [CLEO Collaboration], Phys. Rev. Lett. **89**, 251802 (2002) [Erratum-ibid. **90**, 059901 (2003)].

[67] S. A. Dytman *et al.* [CLEO Collaboration], Phys. Rev. D **64**, 111101 (2001).

[68] D. M. Asner *et al.* [CLEO Collaboration], Phys. Rev. D **72**, 012001 (2005).

[69] B. Aubert *et al.* [BABAR Collaboration], arXiv:hep-ex/0607090.

[70] B. Aubert *et al.* [BABAR Collaboration], Phys. Rev. Lett. **97**, 221803 (2006).

[71] R. A. Briere *et al.*, CLNS-01-1742 (2001).

[72] G. Cavoto *et al.*, `hep-ph/0603019`.

[73] D. Atwood and A. A. Petrov, Phys. Rev. D **71**, 054032 (2005).

[74] Z. Z. Xing, Phys. Rev. D **55**, 196 (1997).

[75] W. M. Sun [CLEO Collaboration], AIP Conf. Proc. **842**, 693 (2006).

[76] F. A. Harris for the BES Collaboration arXiv:physics/0606059.

[77] H. Li for the BES Collaboration Nucl. Phys. Proc. Suppl. **162**, 312 (2006).

[78] A. Bevan, in the proceedings of Beauty 2006.

[79] D. M. Asner, arXiv:hep-ex/0605040.

[80] R. Muresan, in the proceedings of Beauty 2006.

[81] F. Muheim, in the proceedings of Beauty 2006.

[82] [PANDA Collaboration] http://www-panda.gsi.de/auto/_home.htm

[83] A. Sokolov, A. Gillitzer and J. Ritman, AIP Conf. Proc. **796** (2005) 63.

CP violation

CP violation

CP Violation and B Physics at the LHC

Robert Fleischer
Theory Division, Department of Physics, CERN
CH-1211 Geneva 23, SWITZERLAND

Abstract

In this decade, there are huge efforts to explore B-meson decays, which provide an interesting playground for stringent tests of the Standard-Model description of the quark-flavour sector and the CP violation residing there. Thanks to the e^+e^- B factories at KEK and SLAC, CP violation is now a well-established phenomenon in the B-meson system, and recently, also B_s^0–$\overline{B}_s^0$ mixing could be measured at the Tevatron. The decays of B_s^0 mesons are the key target of the B-physics programme at the LHC, and will be the focus of this presentation, discussing the theoretical aspects of various benchmark channels and the question of how much space for new-physics effects in their observables is left by the recent experimental results.

1 Setting the Stage

In the Standard Model (SM), the phenomenon of CP violation can be accommodated in an efficient way through a complex phase entering the quark-mixing matrix, which governs the strength of the charged-current interactions of the quarks [1]. This Kobayashi–Maskawa (KM) mechanism of CP violation is the subject of detailed investigations in this decade. The main interest in the study of CP violation and flavour physics in general is due to the fact that new physics (NP) typically leads to new patterns in the flavour sector. This is actually the case in several specific extensions of the SM, such as SUSY scenarios, left–right-symmetric models, models with extra Z' bosons, scenarios with extra dimensions, or "little Higgs" scenarios. Moreover, also the observed neutrino masses point towards an origin lying beyond the SM, raising now also the question of having CP violation in the neutrino sector and its connection with the quark-flavour physics. Finally, the baryon asymmetry of the Universe also suggests new sources of CP violation. These could be associated with very high energy scales, where a particularly interesting scenario is provided by "leptogenesis" [2], involving typically new CP-violating sources in the decays of heavy

Majorana neutrinos. On the other hand, new CP-violating effects arising in the NP scenarios listed above could in fact be accessible in the laboratory.

Before searching for signals of NP, we have first to understand the SM picture. Here the key problem is due to the impact of strong interactions, leading to "hadronic" uncertainties. A famous example is the quantitiy $\mathrm{Re}(\varepsilon'/\varepsilon)_K$, which measures the direct CP violation in neutral K decays (for an overview, see [3]). In the kaon system, where CP violation was discovered in 1964 [4], clean tests of the SM are offered by the decays $K^+ \to \pi^+\nu\overline{\nu}$ and $K_{\rm L} \to \pi^0\nu\overline{\nu}$, where the hadronic pieces can be fixed through $K \to \pi\ell\overline{\nu}$ modes. These rare decays are absent at the tree level of the SM, i.e. originate there exclusively from loop processes, with resulting tiny branching ratios at the 10^{-10} level (for a recent review, see [5]). Experimental studies of these channels are therefore very challenging. Nevertheless, there are plans to measure $K^+ \to \pi^+\nu\overline{\nu}$ at the SPS (CERN) [6], and efforts to explore $K_{\rm L} \to \pi^0\nu\overline{\nu}$ at the E391 (KEK/J-PARC) experiment.

The B-meson system is a particularly promising probe for the testing of the quark-flavour sector of the SM, and will be the focus of this presentation. It offers various strategies, i.e. simply speaking, there are many B decays that we can exploit, and we may search for clean SM relations that could be spoiled through the impact of NP. There are two kinds of experimental facilities, where B-meson decays can be studied:

- The "B factories", which are asymmetric e^+e^- colliders operated at the $\Upsilon(4S)$ resonance, producing only $B_d^0\overline{B}_d^0$ and $B_u^+B_u^-$ pairs: PEP-II with the Babar experiment (SLAC) and KEK-B with the Belle experiment (KEK) have by now produced altogether $\mathcal{O}(10^9)$ $B\overline{B}$ pairs, establishing CP violation in the B system and leading to many other interesting results. There are currently discussions of a super-B factory, with an increase of luminosity by two orders of magnitude [7].

- Hadron colliders produce, in addition to B_d and B_u, also B_s mesons,[1] as well as B_c and Λ_b transitions. The Tevatron experiments CDF and D0 have reported first $B_{(s)}$-decay results. The physics potential of the B_s system can be fully exploited at the LHC, starting operation in autumn 2007. Here ATLAS and CMS can also address some B physics topics, although these studies are the main target of the dedicated B-decay experiment LHCb.

The central target of these explorations is the well-known unitarity triangle (UT) of the Cabibbo–Kobyashi–Maskawa (CKM) matrix with its three angles α, β and γ. Its apex is given by the generalized Wolfenstein parameters [9]

$$\overline{\rho} \equiv (1-\lambda^2/2)\rho, \quad \overline{\eta} \equiv (1-\lambda^2/2)\eta. \tag{1}$$

The key processes for the exploration of CP violation are given by non-leptonic decays of B mesons, where only quarks are present in the final states. In these

[1] Recently, data were taken by Belle at $\Upsilon(5S)$, allowing also access to B_s decays [8].

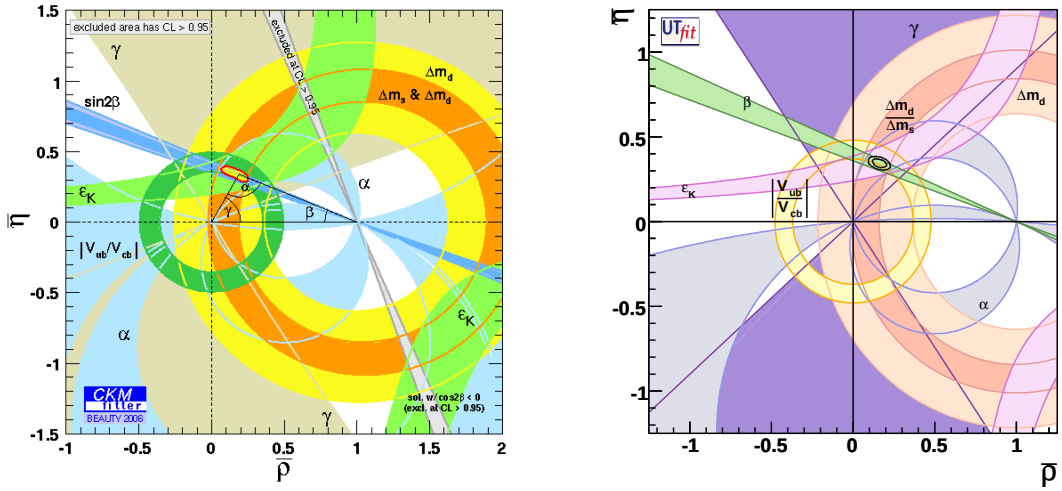

Figure 1: Analyses of the CKMfitter and UTfit collaborations [20, 21].

transitions, CP-violating asymmetries can be generated through interference effects. Depending on the flavour content of their final states, non-leptonic B decays receive contributions from tree and penguin topologies, where we distinguish between QCD and electroweak (EW) penguins in the latter case. The calculation of the decay amplitudes, which can be written by means of the operator product expansion as follows [10]:

$$A(B \to f) \sim \sum_k \underbrace{C_k(\mu)}_{\text{pert. QCD}} \times \underbrace{\langle f|Q_k(\mu)|B\rangle}_{\text{“unknown”}}, \tag{2}$$

remains a theoretical challenge, despite interesting recent progress [11].

However, for the exploration of CP violation, the calculation of the hadronic matrix elements $\langle f|Q_k(\mu)|B\rangle$ of local four-quark operators can actually be circumvented. This feature is crucial for a stringent testing of the CP-violating flavour sector of the SM. To this end, we may follow two avenues:

- Amplitude relations allow us in fortunate cases to eliminate the hadronic matrix elements. Here we distinguish between exact relations, using pure “tree” decays of the kind $B^\pm \to K^\pm D$ [12,13] or $B_c^\pm \to D_s^\pm D$ [14], and relations, which follow from the flavour symmetries of strong interactions, i.e. isospin or $SU(3)_{\rm F}$, and typically involve $B_{(s)} \to \pi\pi, \pi K, KK$ modes [15].

- In decays of neutral B_q mesons ($q \in \{d, s\}$), the interference between B_q^0–$\overline{B}_q^0$ mixing and $B_q^0, \overline{B}_q^0 \to f$ decay processes leads to “mixing-induced” CP violation. If one CKM amplitude dominates the decay, the essentially “unknown” hadronic

matrix elements cancel. The key application of this important feature is the measurement of $\sin 2\beta$ through the "golden" decay $B_d^0 \to J/\psi K_S$ [16].

Following these lines, various processes and strategies emerge for the exploration of CP violation in the B-meson system (for a more detailed discussion, see [17]). In particular, decays with a very different dynamics allow us to probe the same quantities of the UT. These studies are complemented by rare decays of B and K mesons [18], which originate from loop processes in the SM model and show interesting correlations with the CP violation in the B system. In the presence of NP, discrepancies should show up in the resulting roadmap of quark-flavour physics.

In Fig. 1, we show the current status of the UT [19] emerging from the comprehensive – and continuously updated – analyses by the "CKM Fitter Group" [20] and the "UTfit collaboration" [21]. We observe that there is impressive global agreement with the KM mechanism. However, there is also some tension present, as the straight line representing the measurement of $(\sin 2\beta)_{\psi K_S}$ is now on the lower side of the UT side R_b measured through $|V_{ub}/V_{cb}|$. We shall return to this topic in Section 2.2. Let us next discuss the interpretation of the B-factory data in more detail.

2 A Brief Look at the Current B-Factory Data

There are two popular avenues for NP to manifest itself in the B-factory data: through effects entering at the decay amplitude level, or through B_q^0–$\overline{B}_q^0$ mixing.

2.1 New Physics at the Decay Amplitude Level

If a given decay is dominated by SM tree processes, we have typically small effects through NP contributions to its transition amplitude. On the other hand, we may have potentially large NP effects in the penguin sector through new particles in the loops or new contributions at the tree level (this may happen, for instance, in SUSY or models with extra Z' bosons). The search for such signals of NP in the B-factory data has been a hot topic for several years.

CP Violation in $b \to s$ Penguin Modes

A particularly interesting probe of NP is the decay $B_d^0 \to \phi K_S$. It is caused by $\overline{b} \to \overline{s}s\overline{s}$ quark-level processes, i.e. receives only contributions from penguin topologies. The corresponding final state is CP-odd, and the time-dependent CP asymmetry takes

the following form:[2]

$$\frac{\Gamma(B_d^0(t) \to \phi K_{\rm S}) - \Gamma(\overline{B}_d^0(t) \to \phi K_{\rm S})}{\Gamma(B_d^0(t) \to \phi K_{\rm S}) + \Gamma(\overline{B}_d^0(t) \to \phi K_{\rm S})} = \mathcal{A}_{\rm CP}^{\rm dir}(B_d \to \phi K_{\rm S})\,\cos(\Delta M_d t) + \mathcal{A}_{\rm CP}^{\rm mix}(B_d \to \phi K_{\rm S})\,\sin(\Delta M_d t), \tag{3}$$

where $\mathcal{A}_{\rm CP}^{\rm dir}(B_d \to \phi K_{\rm S})$ and $\mathcal{A}_{\rm CP}^{\rm mix}(B_d \to \phi K_{\rm S})$ denote the direct and mixing-induced CP asymmetries, respectively. Thanks to the weak phase structure of the $B_d^0 \to \phi K_{\rm S}$ decay amplitude in the SM, we obtain the following expressions [17]:

$$\mathcal{A}_{\rm CP}^{\rm dir}(B_d \to \phi K_{\rm S}) = 0 + \mathcal{O}(\lambda^2) \tag{4}$$

$$\mathcal{A}_{\rm CP}^{\rm mix}(B_d \to \phi K_{\rm S}) = -\sin\phi_d + \mathcal{O}(\lambda^2), \tag{5}$$

where ϕ_d is the B_d^0–$\overline{B}_d^0$ mixing phase and the doubly Cabibbo-suppressed $\mathcal{O}(\lambda^2)$ terms describe hadronic corrections. Since the mixing-induced CP asymmetry of the $B_d \to J/\psi K_{\rm S}$ channel measures also $-\sin\phi_d$, we arrive at the following SM relation [22,23]:

$$-(\sin 2\beta)_{\phi K_{\rm S}} \equiv \mathcal{A}_{\rm CP}^{\rm mix}(B_d \to \phi K_{\rm S}) = \mathcal{A}_{\rm CP}^{\rm mix}(B_d \to J/\psi K_{\rm S}) + \mathcal{O}(\lambda^2), \tag{6}$$

which offers an interesting test of the SM. Since $B_d \to \phi K_{\rm S}$ is dominated, in the SM, by QCD penguin processes and receives significant contributions from EW penguins as well, the relations in (4) and (6) may well be affected by NP effects. This follows through field-theoretical estimates for generic NP in the TeV regime [24], and is also the case for several specific extensions of the SM (see, e.g., [25]). Concerning the current experimental status [26], it can be summarized through the averages obtained by the "Heavy Flavour Averaging Group" [27]:

$$(\sin 2\beta)_{\phi K_{\rm S}} = 0.39 \pm 0.18, \quad \mathcal{A}_{\rm CP}^{\rm dir}(B_d \to \phi K_{\rm S}) = 0.01 \pm 0.13. \tag{7}$$

During the recent years, the Belle results for $(\sin 2\beta)_{\phi K_{\rm S}}$ have moved quite a bit towards the SM reference value of

$$-\mathcal{A}_{\rm CP}^{\rm mix}(B_d \to J/\psi K_{\rm S}) \equiv (\sin 2\beta)_{\psi K_{\rm S}} = 0.674 \pm 0.026, \tag{8}$$

and are now, within the errors, in agreement with the BaBar findings. Interestingly, the mixing-induced CP asymmetries of other $b \to s$ penguin modes show the same trend of having central values that are smaller than 0.674 [27]. This feature may in fact be due to the presence of NP contributions to the corresponding decay amplitudes. However, the large uncertainties do not yet allow us to draw definite conclusions.

[2] We shall use a similar sign convention also for self-tagging neutral B_d and charged B decays.

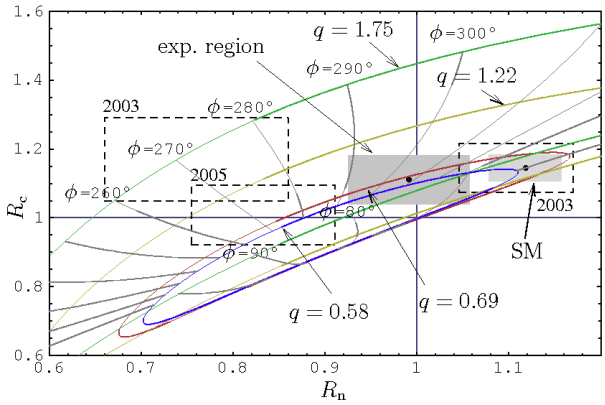

Figure 2: The situation in the R_n–R_c plane, as discussed in the text.

The $B \to \pi K$ Puzzle

Another hot topic is the exploration of $B \to \pi K$ decays. Thanks to the B factories, we could obtain valuable insights into these decays, raising the possibility of having a modified EW penguin sector through the impact of NP, which has received a lot of attention in the literature (see, e.g., [28]). Here we shall discuss key results of the very recent analysis performed in [29], following closely the strategy developed in [30]. The starting point is given by $B \to \pi\pi$ modes. Using the $SU(3)$ flavour symmetry of strong interactions and another plausible dynamical assumption,[3] the data for the $B \to \pi\pi$ system can be converted into the hadronic parameters of the $B \to \pi K$ modes, thereby allowing us to calculate their observables in the SM. Moreover, also γ can be extracted, with the result

$$\gamma = \left(70.0^{+3.8}_{-4.3}\right)^\circ , \tag{9}$$

which is in agreement with the SM fits of the UT [20, 21].

As far as the $B \to \pi K$ observables with tiny EW penguin contributions are concerned, perfect agreement between the SM expectation and the experimental data is found. Concerning the $B \to \pi K$ observables receiving sizeable contributions from EW penguins, we distinguish between CP-conserving and CP-violating observables. In the former case, the key quantities are given by the following ratios of CP-averaged

[3]Consistency checks of these working assumptions can be performed, which are all supported by the current data.

$B \to \pi K$ branching ratios [31]:

$$R_{\rm c} \equiv 2\left[\frac{{\rm BR}(B^+ \to \pi^0 K^+) + {\rm BR}(B^- \to \pi^0 K^-)}{{\rm BR}(B^+ \to \pi^+ K^0) + {\rm BR}(B^- \to \pi^- \overline{K}^0)}\right] = 1.11 \pm 0.07 \qquad (10)$$

$$R_{\rm n} \equiv \frac{1}{2}\left[\frac{{\rm BR}(B_d^0 \to \pi^- K^+) + {\rm BR}(\overline{B}_d^0 \to \pi^+ K^-)}{{\rm BR}(B_d^0 \to \pi^0 K^0) + {\rm BR}(\overline{B}_d^0 \to \pi^0 \overline{K}^0)}\right] = 0.99 \pm 0.07, \qquad (11)$$

where also the most recent experimental averages are indicated [27]. In these quantities, the EW penguin effects enter in colour-allowed form through the modes involving neutral pions, and are theoretically described by a parameter q, which measures the "strength" of the EW penguin with respect to the tree contributions, and a CP-violating phase ϕ. In the SM, the $SU(3)$ flavour symmetry allows a prediction of $q = 0.60$ [32], and ϕ *vanishes.* As is known for many years (see, for instance, [33]), EW penguin topologies offer an interesting avenue for NP to manifest itself in the B-factory data. In the case of CP-violating NP effects of this kind, ϕ would take a value different from zero. In Fig. 2, we show the situation in the $R_{\rm n}$–$R_{\rm c}$ plane. Here the various contours correspond to different values of q, and the position on the contour is parametrized through the CP-violating phase ϕ. We observe that the SM prediction (on the right-hand side) is very stable in time, having now significantly reduced errors. On the other hand, the B-factory data have moved quite a bit towards the SM, thereby reducing the "$B \to \pi K$ puzzle" for the CP-averaged branching ratios, which emerged already in 2000 [34]. In comparison with the situation of the $B \to \pi K$ observables with tiny EW penguin contributions, the agreement between the new data for the $R_{\rm c,n}$ and their SM predictions is not as perfect. However, a case for a modified EW penguin sector cannot be made through the new measurements of these quantities.

Let us now have a closer look at the CP asymmetries of the $B_d^0 \to \pi^0 K_{\rm S}$ and $B^\pm \to \pi^0 K^\pm$ channels. As can be seen in Fig. 3, SM predictions for the CP-violating observables of $B_d^0 \to \pi^0 K_{\rm S}$ are obtained that are much sharper than the current B-factory data. In particular $\mathcal{A}_{\rm CP}^{\rm mix}(B_d \to \pi^0 K_{\rm S})$ offers a very interesting quantity. We also see that the experimental central values can be reached for large *positive* values of ϕ. For the new input data, the non-vanishing difference

$$\Delta A \equiv \mathcal{A}_{\rm CP}^{\rm dir}(B^\pm \to \pi^0 K^\pm) - \mathcal{A}_{\rm CP}^{\rm dir}(B_d \to \pi^\mp K^\pm) \stackrel{\rm exp}{=} -0.140 \pm 0.030 \qquad (12)$$

is likely to be generated through hadronic effects, i.e. not through the impact of physics beyond the SM. A similar conclusion was drawn in [35], where it was also noted that the measured values of $R_{\rm c}$ and $R_{\rm n}$ are now in accordance with the SM.

Performing, finally, a simultaneous fit to $R_{\rm n}$, $R_{\rm c}$ and the CP-violating $B_d \to \pi^0 K_{\rm S}$ asymmetries yields

$$q = 1.7^{+0.5}_{-1.3}, \quad \phi = +\left(73^{+6}_{-18}\right)^\circ. \qquad (13)$$

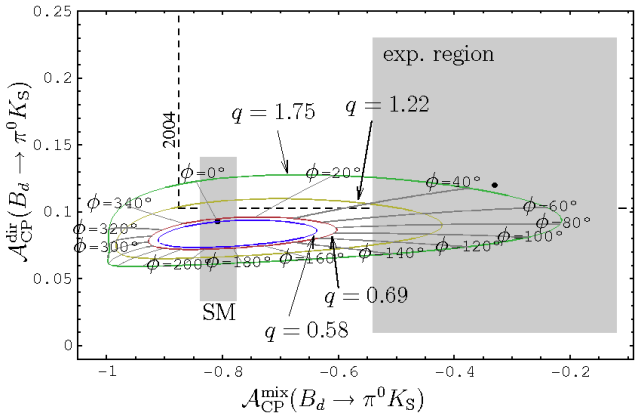

Figure 3: The situation in the $\mathcal{A}_{\rm CP}^{\rm mix}(B_d \to \pi^0 K_{\rm S})$–$\mathcal{A}_{\rm CP}^{\rm dir}(B_d \to \pi^0 K_{\rm S})$ plane.

Interestingly, these parameters – in particular the large *positive* phase – would also allow us to accommodate the experimental values of $(\sin 2\beta)_{\phi K_{\rm S}}$ and the CP asymmetries of other $b \to s$ penguin modes with central values smaller than $(\sin 2\beta)_{\psi K_{\rm S}}$. The large value of q would be excluded by constraints from rare decays in simple scenarios where NP enters only through Z penguins [30], but could still be accommodated in other scenarios, e.g. in models with leptophobic Z' bosons.

2.2 New Physics in B_d^0–$\overline{B}_d^0$ Mixing

In the SM, B_d^0–$\overline{B}_d^0$ mixing is governed by box diagrams with internal top-quark exchances and is, therefore, a strongly suppressed loop phenomenon. In the presence of NP, we may get new contributions through NP particles in the box topologies, or new contributions at the tree level (e.g. SUSY, Z' models). In this case, the off-diagonal element of the mass matrix is modified as follows [36]:

$$M_{12}^{(d)} = M_{12}^{d,{\rm SM}} \left(1 + \kappa_d e^{i\sigma_d}\right), \tag{14}$$

where the real parameter κ_d is a measure of the strength of NP with respect to the SM, and σ_d a CP-violating NP phase. The mass difference ΔM_d between the two mass eigenstates and the mixing phase ϕ_d are then modified as

$$\Delta M_d = \Delta M_d^{\rm SM} + \Delta M_d^{\rm NP} = \Delta M_d^{\rm SM} \left|1 + \kappa_d e^{i\sigma_d}\right| \tag{15}$$

$$\phi_d = \phi_d^{\rm SM} + \phi_d^{\rm NP} = \phi_d^{\rm SM} + \arg(1 + \kappa_d e^{i\sigma_d}), \tag{16}$$

where $\phi_d^{\rm SM} = 2\beta$.

Using the B-factory data to measure ΔM_d and to extract the NP phase $\phi_d^{\rm NP}$, two sets of contours can be fixed in the σ_d–κ_d plane. In the former case, the SM

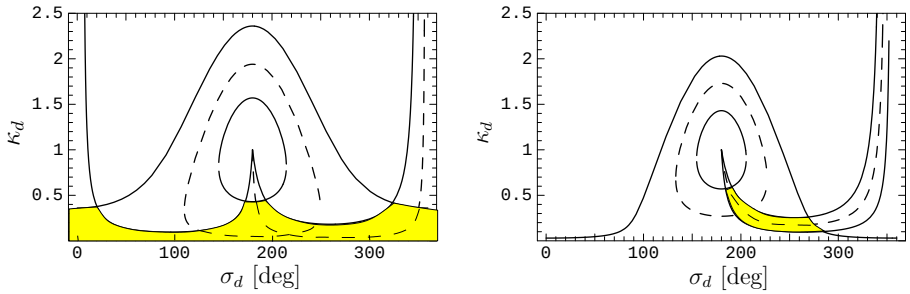

Figure 4: Left panel: allowed region (yellow/grey) in the σ_d–κ_d plane in a scenario with the JLQCD lattice results and $\phi_d^{\rm NP}|_{\rm excl}$. Right panel: ditto for the scenario with the (HP+JL)QCD lattice results and $\phi_d^{\rm NP}|_{\rm incl}$.

value $\Delta M_d^{\rm SM}$ is required. It involves the CKM parameter $|V_{td}^* V_{tb}|$, which is governed by γ in the corresponding numerical analysis if the unitarity of the CKM matrix is used. Moreover, information about the hadronic parameter $f_{B_d}^2 \hat{B}_{B_d}$ is needed, where f_{B_d} is the decay constant of the B_d^0 mesons and B_{B_d} the "bag" parameter of B_d^0–$\overline{B}_d^0$ mixing, usually coming from lattice QCD [37]. For the purpose of comparison, we use two benchmark sets of such results for these quantities [36]: the JLQCD results for two flavours of dynamical light Wilson quarks [38], and a combination of f_{B_d} as determined by the HPQCD collaboration [39] for three dynamical flavours with the JLQCD result for $\hat{B}_{B_d}$ [(HP+JL)QCD] [40].

For the determination of the NP phase $\phi_d^{\rm NP} = \phi_d - \phi_d^{\rm SM}$, we use

$$\phi_d = (42.4 \pm 2)^\circ, \tag{17}$$

which follows from the CP violation in $B_d \to J/\psi K^{(*)}$ decays [27], and fix the "true" value of $\phi_d^{\rm SM} = 2\beta$ with the help of the data for tree processes. This can simply be done through trigonometrical relations between the side $R_b \propto |V_{ub}/V_{cb}|$ of the UT and its angle γ, which are determined through semileptonic $b \to u\ell\overline{\nu}_\ell$ decays and $B \to DK$ modes, respectively. A numerical analysis shows, that the value of $\phi_d^{\rm NP}$ is actually governed by $R_b \propto |V_{ub}/V_{cb}|$, while $(\gamma)_{DK}$, which suffers currently from large uncertainties [41], plays only a minor rôle, in contrast to the SM analysis of ΔM_d. Unfortunately, we are facing a discrepancy between the determinations of $|V_{ub}|$ from exclusive and inclusive decays [42, 43], which has to be resolved in the future. The corresponding NP phases read as follows:

$$\phi_d^{\rm NP}|_{\rm excl} = -(3.4 \pm 7.9)^\circ, \quad \phi_d^{\rm NP}|_{\rm incl} = -(11.0 \pm 4.3)^\circ, \tag{18}$$

where the latter result corresponds to the "tension" in the fits of the UT discussed in the context with Fig. 1. The resulting situation in the σ_d–κ_d plane is shown in Fig. 4, where the hill-like structures correspond to the constraints from ΔM_d, which are complementary to those of $\phi_d^{\rm NP}$. We observe that the measurement of CP

violation in $B_d \to J/\psi K^{(*)}$ decays has a dramatic impact on the allowed region in NP parameter space; the right panel may indicate the presence of NP, although no definite conclusions can be drawn at the moment. It will be interesting to monitor this effect in the future. In order to detect such CP-violating NP contributions, things are much more promising in the B_s system.

3 Key Targets of B-Physics Studies at the LHC

The exploration of B-meson decays at hadron colliders – and the LHC in particular – is characterized through a high statistics and the access the B_s-meson system, which offers a physics programme that is to a large extent complementary to that of the e^+e^- B factories operating at the $\Upsilon(4S)$ resonance.

3.1 General Features of the B_s System

For B_s^0-mesons, we expect – within the SM – a mass difference $\Delta M_s = \mathcal{O}(20\,\mathrm{ps}^{-1})$, which is much larger than the experimental value of $\Delta M_d = 0.5\,\mathrm{ps}^{-1}$. Consequently, the B_s^0–$\overline{B}_s^0$ oscillations are very rapid, thereby making it very challenging to resolve them experimentally.

Whereas the difference between the decay widths of the mass eigenstates of the B_d^0-meson system is negligible, its counterpart $\Delta\Gamma_s/\Gamma_s$ in the B_s^0-meson system is expected to be of $\mathcal{O}(10\%)$ [44]. Recently, the first results for $\Delta\Gamma_s$ were reported from the Tevatron, using the $B_s^0 \to J/\psi\phi$ channel [45]:

$$\frac{\Delta\Gamma_s}{\Gamma_s} = \begin{cases} 0.65^{+0.25}_{-0.33} \pm 0.01 & \text{(CDF [46])} \\ 0.24^{+0.28+0.03}_{-0.38-0.04} & \text{(D0 [47]).} \end{cases} \tag{19}$$

It will be interesting to follow the evolution of the data for this quantity; at the LHC, we expect a precision of about 0.01 after one year of taking data [48, 49]. The width difference $\Delta\Gamma_s$ offers studies of CP violation through "untagged" rates of the following form:

$$\langle \Gamma(B_s(t) \to f) \rangle \equiv \Gamma(B_s^0(t) \to f) + \Gamma(\overline{B_s^0}(t) \to f), \tag{20}$$

which are interesting in terms of efficiency, acceptance and purity. If both B_s^0 and $\overline{B}_s^0$ states may decay into the final state f, the rapidly oscillating $\Delta M_s t$ terms cancel. Various "untagged" strategies exploiting this feature were proposed (see [45] and [50]–[53]); we will discuss an example in Section 3.3.

Finally, the CP-violating phase of B_s^0–$\overline{B}_s^0$ mixing is tiny in the SM:

$$\phi_s^{\mathrm{SM}} = -2\lambda^2\eta \approx -2^\circ, \tag{21}$$

which is very interesting for the search of signals of NP [53–55] (see Section 3.3).

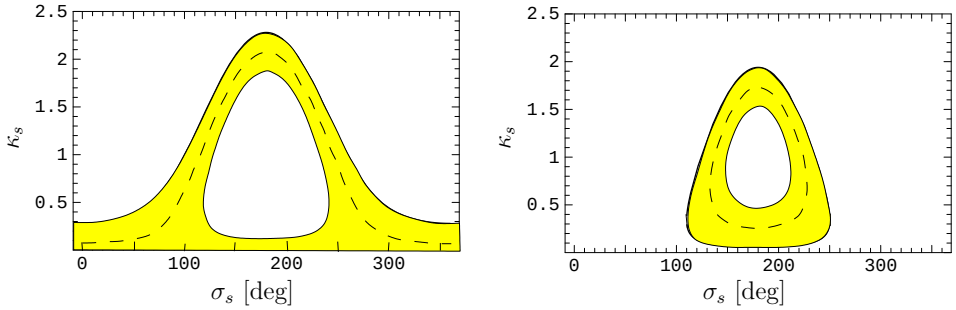

Figure 5: The allowed regions (yellow/grey) in the σ_s–κ_s plane. Left panel: JLQCD lattice results. Right panel: (HP+JL)QCD lattice results.

3.2 Hot News of 2006: Measurement of ΔM_s

For many years, only lower bounds on ΔM_s were available from the LEP (CERN) experiments and SLD (SLAC) [56]. In 2006, the value of ΔM_s could eventually be pinned down at the Tevatron [57]: the D0 collaboration reported a two-sided bound

$$17\,\text{ps}^{-1} < \Delta M_s < 21\,\text{ps}^{-1} \quad (90\%\ \text{C.L.}), \tag{22}$$

corresponding to a $2.5\,\sigma$ signal at $\Delta M_s = 19\,\text{ps}^{-1}$ [58], and CDF announced the following result [59]:

$$\Delta M_s = [17.77 \pm 0.10(\text{stat}) \pm 0.07(\text{syst})]\ \text{ps}^{-1}, \tag{23}$$

which corresponds to a signal at the $5\,\sigma$ level. These new experimental results have immediately triggered a lot of theoretical activity (see, e.g., [60, 61]).

Let us here follow once again the analysis performed in [36]. In order to explore the allowed region in NP parameter space that follows from the measurements at the Tevatron, we have just to make the substitution $d \to s$ in (14). Using the unitarity of the CKM matrix and the Wolfenstein expansion, the CKM factor entering the SM expression for ΔM_s takes the simple form

$$|V_{ts}^* V_{tb}| = |V_{cb}| \left[1 + \mathcal{O}(\lambda^2)\right]. \tag{24}$$

Consequently, in contrast to the SM analysis of ΔM_d, no information on γ and R_b is needed in this expression, which is an important advantage. The accuracy of the SM prediction of ΔM_s is hence limited by the hadronic parameter $f_{B_s}\hat{B}_{B_s}^{1/2}$. Recently, the HPQCD collaboration has reported the result $\Delta M_s^{\rm SM} = 20.3(3.0)(0.8)\,\text{ps}^{-1}$ [62], which lies between the $\Delta M_s^{\rm SM}|_{\rm JLQCD} = (16.1 \pm 2.8)\,\text{ps}^{-1}$ and $\Delta M_s^{\rm SM}|_{\rm (HP+JL)QCD} = (23.4 \pm 3.8)\,\text{ps}^{-1}$ results entering Fig. 5. In this figure, which corresponds to Fig. 4, we show the allowed regions in the σ_s–κ_s plane. We see that the measurement of ΔM_s leaves ample space for the NP parameters σ_s and κ_s. The experimental errors are

already significantly smaller than the theoretical ones. Any more precise statement about the presence or absence of NP in the mass difference ΔM_s requires the reduction of the theoretical lattice QCD uncertainties.

As discussed in [36], the situation is not much better for constraints on NP through $\Delta M_s/\Delta M_d$. In the analysis of this ratio an $SU(3)$-breaking parameter

$$\xi \equiv \frac{f_{B_s}\hat{B}_{B_s}^{1/2}}{f_{B_d}\hat{B}_{B_d}^{1/2}} \tag{25}$$

enters, which has a reduced theoretical uncertainty in comparison with the individual values of the $f_{B_q}\hat{B}_{B_q}^{1/2}$. Usually, $\Delta M_s/\Delta M_d$ is used for the determination of the side $R_t \propto |V_{td}/V_{cb}| = |V_{td}/V_{ts}|\,[1+\mathcal{O}(\lambda^2)]$ of the UT. Alternatively, applying the unitarity of the CKM matrix, the following quantity can be determined:

$$\frac{\rho_s}{\rho_d} = \lambda^2 \underbrace{\left[1 - 2R_b\cos\gamma + R_b^2\right]}_{=R_t^2}\left[1+\mathcal{O}(\lambda^2)\right]\frac{1}{\xi^2}\frac{M_{B_d}}{M_{B_s}}\frac{\Delta M_s}{\Delta M_d}, \tag{26}$$

where the ratio on the left-hand side equals 1 in the SM. For the current data, γ is the major source of uncertainty, in addition to the hadronic parameter ξ. Thanks to precision measurements of γ at LHCb, the CKM and lattice uncertainties should be of the same order of magnitude by 2010. However, unless the central values move dramatically, we would still get a result in agreement with 1 [36]. This case could correspond to the SM, but could also have NP contributions that enter in the same manner in ΔM_s and ΔM_d. Consequently, we would still be left with a rather unsatisfactory situation concerning the search for signals of NP through (26), even after a couple of years taking data at LHCb.

As in the case of the B_d-meson system discussed in Section 2.2, the allowed region in the σ_s–κ_s plane will be dramatically reduced as soon as measurements of CP violation in the B_s-meson system become available. The "golden" channel in this respect is given by $B_s^0 \to J/\psi\phi$, which is our next topic.

3.3 The Decay $B_s^0 \to J/\psi\phi$

This mode is the counterpart of the $B_d^0 \to J/\psi K_{\rm S}$ transition, where we have just to replace the down quark by a strange quark. The structures of the corresponding decay amplitudes are completely analogous to each other. However, there is also an important difference with respect to $B_d^0 \to J/\psi K_{\rm S}$, since the final state of $B_s^0 \to J/\psi\phi$ contains two vector mesons and is, hence, an admixture of different CP eigenstates. Using the angular distribution of the $J/\psi[\to \ell^+\ell^-]\phi[\to\ K^+K^-]$ decay products, the CP eigenstates can be disentangled [63] and the time-dependent decay rates calculated [45, 53]. As in the case of $B_d^0 \to J/\psi K_{\rm S}$, the hadronic matrix elements cancel then

in the mixing-induced observables. For the practical implementation, a set of three linear polarization amplitudes is usually used: $A_0(t)$ and $A_\parallel(t)$ correspond to CP-even final-state configurations, whereas $A_\perp(t)$ describes a CP-odd final-state configuration.

It is instructive to illustrate how this works by having a closer look at the one-angle distribution, which takes the following form [45, 53]:

$$\frac{d\Gamma(B_s^0(t) \to J/\psi\phi)}{d\cos\Theta} \propto \left(|A_0(t)|^2 + |A_\parallel(t)|^2\right)\frac{3}{8}\left(1+\cos^2\Theta\right) + |A_\perp(t)|^2\frac{3}{4}\sin^2\Theta. \quad (27)$$

Here Θ is defined as the angle between the momentum of the ℓ^+ and the normal to the decay plane of the K^+K^- system in the J/ψ rest frame. The time-dependent measurement of the angular dependence allows us to extract the following observables:

$$P_+(t) \equiv |A_0(t)|^2 + |A_\parallel(t)|^2, \quad P_-(t) \equiv |A_\perp(t)|^2, \quad (28)$$

where $P_+(t)$ and $P_-(t)$ refer to the CP-even and CP-odd final-state configurations, respectively. If we consider the case of having an initially, i.e. at time $t = 0$, present $\overline{B}_s^0$ meson, the CP-conjugate quantities $\overline{P}_\pm(t)$ can be extracted as well. Using an *untagged* data sample, the untagged rates

$$P_\pm(t) + \overline{P}_\pm(t) \propto \left[(1 \pm \cos\phi_s)e^{-\Gamma_{\rm L}t} + (1 \mp \cos\phi_s)e^{-\Gamma_{\rm H}t}\right] \quad (29)$$

can be determined, while a *tagged* data sample allows us to measure the CP-violating asymmetries

$$\frac{P_\pm(t) - \overline{P}_\pm(t)}{P_\pm(t) + \overline{P}_\pm(t)} = \pm\left[\frac{2\,\sin(\Delta M_s t)\sin\phi_s}{(1 \pm \cos\phi_s)e^{+\Delta\Gamma_s t/2} + (1 \mp \cos\phi_s)e^{-\Delta\Gamma_s t/2}}\right]. \quad (30)$$

In the presence of CP-violating NP contributions to B_s^0–$\overline{B}_s^0$ mixing, we obtain

$$\phi_s = -2\lambda^2 R_b \sin\gamma + \phi_s^{\rm NP} \approx -2^\circ + \phi_s^{\rm NP} \approx \phi_s^{\rm NP}. \quad (31)$$

Consequently, NP of this kind would be indicated by the following features:

- The *untagged* observables depend on *two* exponentials;
- *sizeable* values of the CP-violating asymmetries.

It should be emphasized that this avenue to search for NP signals does *not* have to rely on lattice QCD results, in contrast the analyses of ΔM_s discussed above.

These general features hold also for the full three-angle distribution [45, 53]: it is much more involved than the one-angle case, but provides also additional information through interference terms of the form

$$\mathrm{Re}\{A_0^*(t)A_\parallel(t)\}, \quad \mathrm{Im}\{A_f^*(t)A_\perp(t)\}\,(f \in \{0, \|\}). \quad (32)$$

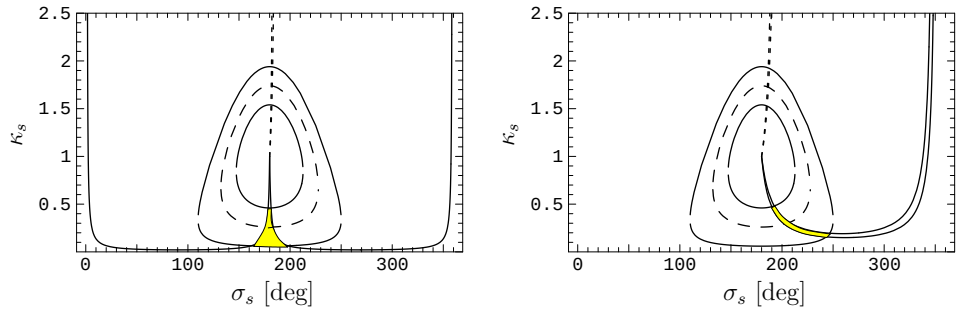

Figure 6: Illustration of the impact of measurements of CP violation in $B_s^0 \to J/\psi\phi$ for the two 2010 scenarios i) [left panel] and ii) [right panel] discussed in the text.

From an experimental point of view, there is no experimental draw-back with respect to the one-angle case. Following these lines, $\Delta\Gamma_s$ (see (19)) and ϕ_s can be extracted. Recently, the D0 collaboration has reported first results for the measurement of ϕ_s through the untagged, time-dependent three-angle $B_s^0 \to J/\psi\phi$ distribution [64]:

$$\phi_s = -0.79 \pm 0.56\,(\text{stat.})^{+0.14}_{-0.01}\,(\text{syst.}) = -(45 \pm 32^{+1}_{-8})^\circ. \tag{33}$$

This phase is therefore not yet stringently constrained. However, it will be very accessible at the LHC, where the following picture is expected with nominal one year data [49]: if ϕ_s takes its SM value, a $2\,\sigma$ measurement will be possible at LHCb ($2\,\text{fb}^{-1}$), ATLAS and CMS expect uncertainties of $\mathcal{O}(0.1)$ ($10\,\text{fb}^{-1}$) [65]. At some point, also in view of LHCb upgrade plans [66], we have to include hadronic penguin uncertainties. This can be done with the help of the $B_d^0 \to J/\psi\rho^0$ decay [67].

In order to illustrate the impact of measurements of CP violation in $B_s^0 \to J/\psi\phi$, let us discuss two scenarios for the year 2010 [36]:

i) $(\sin\phi_s)_{\text{exp}} = -0.04 \pm 0.02$: this case corresponds to the SM;

ii) $(\sin\phi_s)_{\text{exp}} = -0.20 \pm 0.02$: such a measurement would give a NP signal at the $10\,\sigma$ level. This scenario corresponds to a simple translation of the "tension" in the UT fits discussed above for $\kappa_s = \kappa_d$, $\sigma_s = \sigma_d$, and demonstrates the power of the B_s system to search for NP.

We see that it will be very challenging to establish NP effects in B_s^0–$\overline{B}_s^0$ mixing without new CP-violating contributions to this phenomenon. However, the data still leave a lot of space for such effects in specific scenarios (e.g. SUSY, extra Z' and little Higgs models [36, 60, 68]), which could be detected at the LHC. It will be very exciting to follow the corresponding measurements after the start of this new collider.

3.4 Further Benchmark Decays for LHCb

This experiment has a very rich physics programme (for an experimental overview, see [48]). Besides many other interesting aspects, there are two major lines of research:

1. Precision measurements of γ:
   On the one hand, there are strategies using pure tree decays: $B_s^0 \to D_s^{\mp} K^{\pm}$ [$\sigma_\gamma \sim 14^\circ$], $B_d^0 \to D^0 K^*$ [$\sigma_\gamma \sim 8^\circ$], $B^{\pm} \to D^0 K^{\pm}$ [$\sigma_\gamma \sim 5^\circ$], where we have also indicated the expected sensitivities after one year of taking data [48]. These numbers should be compared with the current B-factory data, yielding

$$\gamma|_{D^{(*)}K^{(*)}} = \begin{cases} (62^{+38}_{-24})^\circ & \text{(CKMfitter)} \\ (82 \pm 20)^\circ & \text{(UTfit).} \end{cases} \tag{34}$$

   These extractions are very robust with respect to NP effects. On the other hand, γ can also be extracted from B-meson decays with penguin contributions: $B_s^0 \to K^+K^-$ and $B_d^0 \to \pi^+\pi^-$ [$\sigma_\gamma \sim 5^\circ$], $B_s^0 \to D_s^+ D_s^-$ and $B_d^0 \to D_d^+ D_d^-$. The key question is whether discrepancies will arise in these determinations.

2. Analyses of rare decays, which are absent at the SM tree level:
   prominent examples are $B_{s,d}^0 \to \mu^+\mu^-$, $B_d^0 \to K^{*0}\mu^+\mu^-$ and $B_s^0 \to \phi\mu^+\mu^-$. In order to complement the studies of $B_d^0 \to \phi K_{\rm S}$ at the B factories discussed in Section 2.1, $B_s^0 \to \phi\phi$ is a very interesting mode for LHCb.

Let us next have a closer look at some of these decays.

CP Violation in $B_s \to D_s^{\pm} K^{\mp}$ and $B_d \to D^{\pm}\pi^{\mp}$

The pure tree decays $B_s \to D_s^{\pm} K^{\mp}$ [69] and $B_d \to D^{\pm}\pi^{\mp}$ [70] can be treated on the same theoretical basis, and provide new strategies to determine γ [71]. Following this paper, we write these modes as $B_q \to D_q \overline{u}_q$. Their characteristic feature is that both a B_q^0 and a $\overline{B}_q^0$ meson may decay into the same final state $D_q\overline{u}_q$. Consequently, interference effects between B_q^0–$\overline{B}_q^0$ mixing and decay processes arise, which involve the CP-violating phase combination $\phi_q + \gamma$.

In the case of $q = s$, i.e. $D_s \in \{D_s^+, D_s^{*+}, ...\}$ and $u_s \in \{K^+, K^{*+}, ...\}$, these interference effects are governed by a hadronic parameter $X_s e^{i\delta_s} \propto R_b \approx 0.4$, where $R_b \propto |V_{ub}/V_{cb}|$ is the usual UT side, and hence are large. On the other hand, for $q = d$, i.e. $D_d \in \{D^+, D^{*+}, ...\}$ and $u_d \in \{\pi^+, \rho^+, ...\}$, the interference effects are described by $X_d e^{i\delta_d} \propto -\lambda^2 R_b \approx -0.02$, and hence are tiny.

Measuring the $\cos(\Delta M_q t)$ and $\sin(\Delta M_q t)$ terms of the time-dependent $B_q \to D_q\overline{u}_q$ rates, a theoretically clean determination of $\phi_q + \gamma$ is possible [69, 70]. Since the ϕ_q can be determined separately, γ can be extracted. However, in the practical implementation, there are problems: we encounter an eightfold discrete ambiguity

for $\phi_q + \gamma$, which is very disturbing for the search of NP, and in the $q = d$ case, an additional input is required to extract X_d since $\mathcal{O}(X_d^2)$ interference effects would otherwise have to be resolved, which is impossible. Performing a combined analysis of the $B_s^0 \to D_s^+ K^-$ and $B_d^0 \to D^+\pi^-$ decays, these problems can be solved [71]. This strategy exploits the fact that these transitions are related to each other through the U-spin symmetry of strong interactions,[4] allowing us to simplify the hadronic sector. Following these lines, an unambiguous value of γ can be extracted from the observables. To this end, X_d has actually not to be fixed, and X_s may only enter through a $1 + X_s^2$ correction, which is determined through untagged B_s rates. The first studies for LHCb are very promising [72], and are currently further refined.

The $B_s \to K^+K^-$, $B_d \to \pi^+\pi^-$ System

The decay $B_s^0 \to K^+K^-$ is a $\overline{b} \to \overline{s}$ transition, and involves tree and penguin amplitudes, as $B_d^0 \to \pi^+\pi^-$ [73]. However, because of the different CKM structure, the latter topologies play actually the dominant rôle in $B_s^0 \to K^+K^-$, whereas the major contribution to $B_d^0 \to \pi^+\pi^-$ is due to the tree amplitude. In the SM, we may write

$$A(B_d^0 \to \pi^+\pi^-) \propto \left[e^{i\gamma} - de^{i\theta}\right] \tag{35}$$

$$A(B_s^0 \to K^+K^-) \propto \left[e^{i\gamma} + \left(\frac{1-\lambda^2}{\lambda^2}\right) d' e^{i\theta'}\right], \tag{36}$$

where the CP-conserving hadronic parameters $de^{i\theta}$ and $d'e^{i\theta'}$ describe – sloppily speaking – the ratios of penguin to tree contributions. The direct and mixing-induced CP asymmetries take then the following general form:

$$\mathcal{A}_{\rm CP}^{\rm dir}(B_d \to \pi^+\pi^-) = G_1(d,\theta;\gamma), \quad \mathcal{A}_{\rm CP}^{\rm mix}(B_d \to \pi^+\pi^-) = G_2(d,\theta;\gamma,\phi_d) \tag{37}$$

$$\mathcal{A}_{\rm CP}^{\rm dir}(B_s \to K^+K^-) = G_1'(d',\theta';\gamma), \quad \mathcal{A}_{\rm CP}^{\rm mix}(B_s \to K^+K^-) = G_2'(d',\theta';\gamma,\phi_s). \tag{38}$$

Since ϕ_d is already known (see (17)) and ϕ_s is negligibly small in the SM – or can be determined through $B_s^0 \to J/\psi\phi$ should CP-violating NP contributions to B_s^0–$\overline{B}_s^0$ mixing make it sizeable – we may convert the measured values of $\mathcal{A}_{\rm CP}^{\rm dir}(B_d \to \pi^+\pi^-)$, $\mathcal{A}_{\rm CP}^{\rm mix}(B_d \to \pi^+\pi^-)$ and $\mathcal{A}_{\rm CP}^{\rm dir}(B_s \to K^+K^-)$, $\mathcal{A}_{\rm CP}^{\rm mix}(B_s \to K^+K^-)$ into *theoretically clean* contours in the γ–d and γ–d' planes, respectively. In Fig. 7, we show these contours (solid and dot-dashed) for an example, which is inspired by the current B-factory data [29].

A closer look at the corresponding Feynman diagrams shows that $B_d^0 \to \pi^+\pi^-$ is actually related to $B_s^0 \to K^+K^-$ through the interchange of all down and strange

[4] The U spin is an $SU(2)$ subgroup of the $SU(3)_{\rm F}$ flavour-symmetry group of QCD, connecting d and s quarks in analogy to the isospin symmetry, which relates d and u quarks to each other.

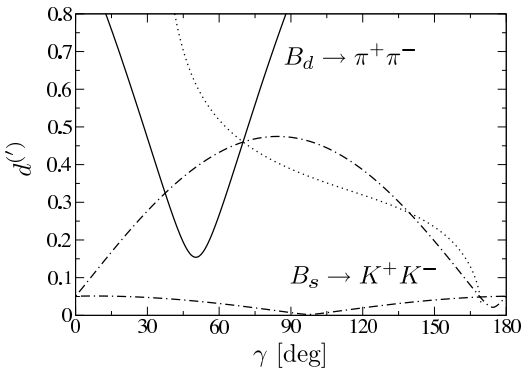

Figure 7: The contours in the γ–$d^{(\prime)}$ plane for an example with $d = d' = 0.46$, $\theta = \theta' = 155°$, $\phi_d = 42.4°$, $\phi_s = -2°$, $\gamma = 70°$, which corresponds to the CP asymmetries $\mathcal{A}_{\rm CP}^{\rm dir}(B_d \to \pi^+\pi^-) = -0.24$ and $\mathcal{A}_{\rm CP}^{\rm mix}(B_d \to \pi^+\pi^-) = +0.59$, as well as $\mathcal{A}_{\rm CP}^{\rm dir}(B_s \to K^+K^-) = +0.09$ and $\mathcal{A}_{\rm CP}^{\rm mix}(B_s \to K^+K^-) = -0.23$.

quarks. Consequently, each decay topology contributing to $B_d^0 \to \pi^+\pi^-$ has a counterpart in $B_s^0 \to K^+K^-$ and vice versa, and the corresponding hadronic parameters can be related to each other with the help of the U-spin flavour symmetry of strong interactions, implying the following relations [73]:

$$d' = d, \quad \theta' = \theta. \tag{39}$$

Applying the former, we may extract γ and d through the intersections of the theoretically clean γ–d and γ–d' contours. In the example of Fig. 7, a twofold ambiguity arises from the solid and dot-dashed curves. However, as discussed in [73], it can be resolved with the help of the dotted contour, thereby leaving us with the "true" solution of $\gamma = 70°$ in this case. Moreover, we may determine θ and θ', which allow an interesting internal consistency check of the second U-spin relation in (39).

This strategy is very promising from an experimental point of view for LHCb, where an accuracy for γ of a few degrees can be achieved [74]. As far as possible U-spin-breaking corrections to $d' = d$ are concerned, they enter the determination of γ through a relative shift of the γ–d and γ–d' contours; their impact on the extracted value of γ therefore depends on the form of these curves, which is fixed through the measured observables. In the examples discussed in [73] and Fig. 7, the extracted value of γ would be very stable with respect to such effects. It should also be noted that the U-spin relations in (39) are particularly robust since they involve only ratios of hadronic amplitudes, where all $SU(3)$-breaking decay constants and form factors cancel in factorization and also chirally enhanced terms would not lead to U-spin-breaking corrections [73].

As a by-product of the $B \to \pi\pi, \pi K$ strategy developed in [30], the observables of the $B_s^0 \to K^+K^-$ decay can be predicted in the SM. The most recent data yield

the following numbers [29]:

$$\mathcal{A}_{\rm CP}^{\rm dir}(B_s \to K^+K^-)|_{\rm SM} = 0.093 \pm 0.015 \quad (40)$$
$$\mathcal{A}_{\rm CP}^{\rm mix}(B_s \to K^+K^-)|_{\rm SM} = -0.234^{+0.017}_{-0.014}. \quad (41)$$

In the case of the CP-averaged branching ratio, an $SU(3)$-breaking form-factor ratio enters the prediction, thereby increasing the uncertainties. Using the result of a QCD sum-rule calculation [75] yields the prediction [29]

$$\mathrm{BR}(B_s \to K^+K^-) = (28^{+7}_{-5}) \times 10^{-6}. \quad (42)$$

The $B_s^0 \to K^+K^-$ mode was recently observed by CDF [76]; the most recent experimental update for the CP-averaged branching ratio reads as follows [77]:

$$\mathrm{BR}(B_s \to K^+K^-) = (24.4 \pm 1.4 \pm 4.6) \times 10^{-6}. \quad (43)$$

Within the uncertainties, (42) is in nice agreement with (43), which is another support of the working hypotheses underlying the $B \to \pi K$ analysis discussed in Section 2.1.

The Rare Decays $B_{s,d} \to \mu^+\mu^-$

In the SM, these decays originate from Z penguins and box diagrams, and the corresponding low-energy effective Hamiltonian takes the following form [10]:

$$\mathcal{H}_{\rm eff} = -\frac{G_{\rm F}}{\sqrt{2}}\left[\frac{\alpha}{2\pi \sin^2\Theta_{\rm W}}\right] V_{tb}^* V_{tq} \eta_Y Y_0(x_t) (\overline{b}q)_{\rm V-A} (\overline{\mu}\mu)_{\rm V-A} + \text{h.c.}, \quad (44)$$

where α denotes the QED coupling and $\Theta_{\rm W}$ is the Weinberg angle. The short-distance physics is described by $Y(x_t) \equiv \eta_Y Y_0(x_t)$, where $\eta_Y = 1.012$ is a perturbative QCD correction [78], and the Inami–Lim function $Y_0(x_t)$ describes the top-quark mass dependence. We observe that only the matrix element $\langle 0|(\overline{b}q)_{\rm V-A}|B_q^0\rangle$ is required. Since here the vector-current piece vanishes, as the B_q^0 is a pseudoscalar meson, this matrix element is simply given by the decay constant f_{B_q}. Consequently, we arrive at a very favourable situation with respect to the hadronic matrix elements. Since, moreover, NLO QCD corrections were calculated, and long-distance contributions are expected to play a negligible rôle [78], the $B_q^0 \to \mu^+\mu^-$ modes belong to the cleanest rare B decays.

Using also the data for the mass differences ΔM_q to reduce the hadronic uncertainties,[5] the following SM predictions were obtained in [61]:

$$\mathrm{BR}(B_s \to \mu^+\mu^-) = (3.35 \pm 0.32) \times 10^{-9} \quad (45)$$
$$\mathrm{BR}(B_d \to \mu^+\mu^-) = (1.03 \pm 0.09) \times 10^{-10}. \quad (46)$$

[5] This input allows us to replace the decay constants f_{B_q} through the bag parameters $\hat{B}_{B_q}$.

The upper bounds (95% C.L.) from the CDF collaboration read as follows [79]:

$$\mathrm{BR}(B_s \to \mu^+\mu^-) < 1.0 \times 10^{-7}, \quad \mathrm{BR}(B_d \to \mu^+\mu^-) < 3.0 \times 10^{-8}, \tag{47}$$

while the D0 collaboration finds the following 90% C.L. (95% C.L.) upper limit [80]:

$$\mathrm{BR}(B_s \to \mu^+\mu^-) < 1.9\ (2.3) \times 10^{-7}. \tag{48}$$

Consequently, there is still a long way to go within the SM. However, in this case, LHCb expects a $3\,\sigma$ observation for $B_s \to \mu^+\mu^-$ with already nominal one year data ($2\,\mathrm{fb}^{-1}$) [49]. This decay is also very interesting for ATLAS and CMS, where detailed background studies are currently in progress [65]. Things could actually be much more exciting, as NP effects may significantly enhance $\mathrm{BR}(B_s \to \mu^+\mu^-)$. For instance, in SUSY, this enhancement may be dramatic as $\mathrm{BR} \sim (\tan\beta)^6$, where β is here the ratio of the two Higgs vacuum expectation values and not the UT angle β (for recent analyses, see, e.g., [81]), and in scenarios with a modified EW penguin sector a sizeable enhancement is possible (see, e.g., [30]).

The Rare Decay $B_d^0 \to K^{*0}\mu^+\mu^-$

The key observable for NP searches provided by this decay is the following forward–backward asymmetry:

$$A_{\mathrm{FB}}(\hat{s}) = \frac{1}{\mathrm{d}\Gamma/\mathrm{d}\hat{s}} \left[\int_0^{+1} \mathrm{d}(\cos\theta) \frac{\mathrm{d}^2\Gamma}{\mathrm{d}\hat{s}\,\mathrm{d}(\cos\theta)} - \int_{-1}^{0} \mathrm{d}(\cos\theta) \frac{\mathrm{d}^2\Gamma}{\mathrm{d}\hat{s}\,\mathrm{d}(\cos\theta)} \right]. \tag{49}$$

Here θ is the angle between the B_d^0 momentum and that of the μ^+ in the dilepton centre-of-mass system, and $\hat{s} \equiv s/M_B^2$ with $s = (p_{\mu^+} + p_{\mu^-})^2$. A particularly interesting kinematical point is characterized by

$$A_{\mathrm{FB}}(\hat{s}_0)|_{\mathrm{SM}} = 0, \tag{50}$$

as $\hat{s}_0$ is quite robust with respect to hadronic uncertainties (see, e.g., [82]). In SUSY extensions of the SM, $A_{\mathrm{FB}}(\hat{s})$ could take opposite sign or take a dependence on $\hat{s}$ without a zero point [83]. The current B-factory data for the inclusive $b \to s\ell^+\ell^-$ branching ratios and the integrated forward–backward asymmetries are in accordance with the SM, but suffer still from large uncertainties. This situation will improve dramatically at the LHC. Here LHCb will collect about 4400 decays/year, yielding $\Delta\hat{s}_0 = 0.06$ after one year, and ATLAS expects to collect about 1000 $B^0 \to K^{*0}\mu^+\mu^-$ decays per year [48]. Moreover, also other $b \to s\mu^+\mu^-$ modes are currently under study, such as $\Lambda_b \to \Lambda\mu^+\mu^-$ and $B_s^0 \to \phi\mu^+\mu^-$.

4 Conclusions and Outlook

We have seen tremendous progress in B physics during the recent years, which was made possible through a fruitful interplay between theory and experiment. Altogether, the e^+e^- B factories have already produced $\mathcal{O}(10^9)$ $B\overline{B}$ pairs, and the Tevatron has recently succeeded in observing B_s^0–$\overline{B}_s^0$ mixing. The data agree globally with the KM mechanism of CP violation in an impressive manner, but we have also hints for discrepancies, which could be first signals of NP. Unfortunately, definite conclusions cannot yet be drawn as the uncertainties are still too large.

Exciting new perspectives for B physics and the exploration of CP violation will emerge through the start of the LHC in the autumn of 2007, with its dedicated B-decay experiment LHCb. Thanks to the large statistics that can be collected there and the full exploitation of the physics potential of the B_s-meson system, we will be able to enter a new territory in the exploration of CP violation at the LHC. The golden channel to search for CP-violating NP contributions to B_s^0–$\overline{B}_s^0$ mixing is $B_s^0 \to J/\psi\phi$, where the recent measurement of ΔM_s still leaves ample space for such effects both in terms of the general NP parameters and in specific extensions of the SM. In contrast to the theoretical interpretation of ΔM_s, the corresponding CP asymmetries have not to rely on non-perturbative lattice QCD calculations. The two major lines of the broad research programme of LHCb are precision measurements of γ, which is a key ingredient for NP searches, and powerful analyses of various rare B decays, offering also sensitive probes for physics beyond the SM. The implementation of this programme will lead to much more stringent consistency checks of the KM mechanism, where also measurements of the rare kaon decays $K^+ \to \pi^+\nu\overline{\nu}$ and $K_{\rm L} \to \pi^0\nu\overline{\nu}$ would be very welcome.

These studies of CP violation and flavour physics play also an outstanding rôle in the context with the major targets of the physics programme of the LHC. Here the main goal of the ATLAS and CMS experiments is to explore electroweak symmetry breaking, in particular the question of whether this is actually caused by the Higgs mechanism, to produce and observe new particles, and then to go back to the deep questions of particle physics, such as the origin of dark matter and the baryon asymmetry of the Universe. It is obvious that there should be a very fruitful interplay between these "direct" studies of NP and the "indirect" information provided by flavour physics, including the B-meson system, but also K, D and top physics as well as the flavour physics in the lepton sector.[6] I have no doubts that the next years will be extremely exciting!

I am grateful to the workshop organizers for the invitation to this interesting meeting at such a nice location, and would also like to thank my co-authors for the enjoyable collaborations on topics addressed in this talk.

[6] This synergy is the topic of a CERN Workshop: http://flavlhc.web.cern.ch/flavlhc/.

Bibliography

[1] M. Kobayashi and T. Maskawa, Prog. Theor. Phys. **49**, 652 (1973).

[2] W. Buchmüller, R. D. Peccei and T. Yanagida, Ann. Rev. Nucl. Part. Sci. **55**, 311 (2005).

[3] A. J. Buras and M. Jamin, JHEP **0401**, 048 (2004).

[4] J. H. Christenson *et al.*, Phys. Rev. Lett. **13**, 138 (1964).

[5] A. J. Buras, F. Schwab and S. Uhlig, hep-ph/0405132.

[6] G. Ruggiero, talk at this workshop.

[7] T. Iijima, talk at this workshop.

[8] K. Abe *et al.* [Belle Collaboration], hep-ex/0610003.

[9] L. Wolfenstein, Phys. Rev. Lett. **51**, 1945 (1983); A. J. Buras, M. E. Lautenbacher and G. Ostermaier, Phys. Rev. D **50**, 3433 (1994).

[10] G. Buchalla, A. J. Buras and M. E. Lautenbacher, Rev. Mod. Phys. **68**, 1125 (1996).

[11] M. Beneke, talk at this workshop [hep-ph/0612353].

[12] M. Gronau and D. Wyler, Phys. Lett. B **265**, 172 (1991).

[13] D. Atwood, I. Dunietz and A. Soni, Phys. Rev. Lett. **78**, 3257 (1997); Phys. Rev. D **63**, 036005 (2001).

[14] R. Fleischer and D. Wyler, Phys. Rev. D **62**, 057503 (2000).

[15] M. Gronau, J. L. Rosner and D. London, Phys. Rev. Lett. **73**, 21 (1994); M. Gronau, O. F. Hernandez, D. London and J. L. Rosner, Phys. Rev. D **50**, 4529 (1994).

[16] A. B. Carter and A. I. Sanda, Phys. Rev. Lett. **45**, 952 (1980); Phys. Rev. D **23**, 1567 (1981); I. I. Bigi and A. I. Sanda, Nucl. Phys. B **193**, 85 (1981).

[17] R. Fleischer, lectures given at the 2005 European School of High-Energy Physics, Kitzbühel, Austria, 21 August – 3 September 2005 [hep-ph/0608010].

[18] A. Weiler, talk at this workshop.

[19] A. Stocchi, talk at this workshop.

[20] J. Charles *et al.* [CKMfitter Group], Eur. Phys. J. C **41**, 1 (2005); for the most recent updates, see http://ckmfitter.in2p3.fr/.

[21] M. Bona *et al.* [UTfit Collaboration], JHEP **0507**, 028 (2005); for the most recent updates, see http://utfit.roma1.infn.it/.

[22] R. Fleischer, Int. J. Mod. Phys. A **12**, 2459 (1997).

[23] Y. Grossman and M. P. Worah, Phys. Lett. B **395**, 241 (1997).

[24] R. Fleischer and T. Mannel, Phys. Lett. B **511**, 240 (2001).

[25] M. Ciuchini, E. Franco, A. Masiero and L. Silvestrini, eConf **C0304052**, WG307 (2003); V. Barger, C. W. Chiang, P. Langacker and H. S. Lee, Phys. Lett. B **598**, 218 (2004).

[26] G. Dubois–Felsmann, talk at this workshop.

[27] Heavy Flavour Averaging Group [E. Barberio *et al.*], hep-ex/0603003; for online updates, see http://www.slac.stanford.edu/xorg/hfag.

[28] T. Yoshikawa, Phys. Rev. D **68**, 054023 (2003); M. Gronau and J. L. Rosner, Phys. Lett. B **572**, 43 (2003); M. Beneke and M. Neubert, Nucl. Phys. B **675**, 333 (2003); V. Barger, C. W. Chiang, P. Langacker and H. S. Lee, Phys. Lett. B **598**, 218 (2004); Y. L. Wu and Y. F. Zhou, Phys. Rev. D **72**, 034037 (2005).

[29] R. Fleischer, S. Recksiegel and F. Schwab, CERN-PH-TH/2007-044, to appear in Eur. Phys. J. C [hep-ph/0702275].

[30] A. J. Buras, R. Fleischer, S. Recksiegel and F. Schwab, Phys. Rev. Lett. **92**, 101804 (2004); Nucl. Phys. B **697**, 133 (2004); Eur. Phys. J. C **45**, 701 (2006).

[31] A. J. Buras and R. Fleischer, Eur. Phys. J. C **11**, 93 (1999).

[32] M. Neubert and J. L. Rosner, Phys. Rev. Lett. **81**, 5076 (1998).

[33] R. Fleischer and T. Mannel, hep-ph/9706261; Y. Grossman, M. Neubert and A. L. Kagan, JHEP **9910**, 029 (1999).

[34] A. J. Buras and R. Fleischer, Eur. Phys. J. C **16**, 97 (2000).

[35] M. Gronau and J. L. Rosner, Phys. Rev. D **74**, 057503 (2006); M. Gronau and J. L. Rosner, Phys. Lett. B **644**, 237 (2007).

[36] P. Ball and R. Fleischer, Eur. Phys. J. C **48**, 413 (2006).

[37] V. Lubicz, talk at this workshop [hep-ph/0702204].

[38] S. Aoki *et al.* [JLQCD collaboration], Phys. Rev. Lett. **91**, 212001 (2003).

[39] A. Gray *et al.* [HPQCD collaboration], Phys. Rev. Lett. **95**, 212001 (2005).

[40] M. Okamoto, PoS **LAT2005**, 013 (2005).

[41] H. Yamamoto, talk at this workshop.

[42] O. Buchmüller, talk at this workshop.

[43] T. Mannel, talk at this workshop.

[44] A. Lenz, talk at this workshop [hep-ph/0612176].

[45] A. S. Dighe, I. Dunietz and R. Fleischer, Eur. Phys. J. C **6**, 647 (1999).

[46] D. Acosta *et al.* [CDF Collaboration], Phys. Rev. Lett. **94**, 101803 (2005).

[47] V. M. Abazov *et al.* [D0 Collaboration], Phys. Rev. Lett. **95**, 171801 (2005).

[48] A. Schopper, Proceedings of FPCP 2006, Vancouver, British Columbia, Canada, 9–12 April 2006, pp 042 [hep-ex/0605113].

[49] T. Nakada, talk at CKM 2006, Nagoya, Japan, 12–16 December 2006.

[50] I. Dunietz, Phys. Rev. D **52**, 3048 (1995).

[51] R. Fleischer and I. Dunietz, Phys. Rev. D **55**, 259 (1997).

[52] R. Fleischer and I. Dunietz, Phys. Lett. B **387**, 361 (1996).

[53] I. Dunietz, R. Fleischer and U. Nierste, Phys. Rev. D **63**, 114015 (2001).

[54] Y. Nir and D. J. Silverman, Nucl. Phys. B **345**, 301 (1990).

[55] G. C. Branco, T. Morozumi, P. A. Parada and M. N. Rebelo, Phys. Rev. D **48**, 1167 (1993).

[56] *B* Oscillations Working Group: http://lepbosc.web.cern.ch/LEPBOSC/.

[57] S. Menzemer, talk at this workshop.

[58] V. M. Abazov *et al.* [D0 Collaboration], Phys. Rev. Lett. **97**, 021802 (2006).

[59] A. Abulencia *et al.* [CDF Collaboration], Phys. Rev. Lett. **97**, 242003 (2006).

[60] M. Carena *et al.*, Phys. Rev. D **74**, 015009 (2006); M. Ciuchini and L. Silvestrini, Phys. Rev. Lett. **97**, 021803 (2006); M. Endo and S. Mishima, Phys. Lett. B **640**, 205 (2006); Z. Ligeti, M. Papucci and G. Perez, Phys. Rev. Lett. **97**, 101801 (2006); J. Foster, K.I. Okumura and L. Roszkowski, Phys. Lett. B **641**, 452 (2006); Y. Grossman, Y. Nir and G. Raz, Phys. Rev. Lett. **97**, 151801 (2006); S. Baek, J. H. Jeon and C. S. Kim, Phys. Lett. B **641**, 183 (2006); M. Blanke and A. J. Buras, hep-ph/0610037.

[61] M. Blanke, A. J. Buras, D. Guadagnoli and C. Tarantino, JHEP **0610**, 003 (2006).

[62] E. Dalgic *et al.* [HPQCD collaboration], hep-lat/0610104.

[63] A. S. Dighe, I. Dunietz, H. J. Lipkin and J. L. Rosner, Phys. Lett. B **369**, 144 (1996).

[64] V. M. Abazov *et al.* [D0 Collaboration], hep-ex/0701012.

[65] Maria Smizanska and Thomas Speer, private communications.

[66] F. Muheim, hep-ex/0703006.

[67] R. Fleischer, Phys. Rev. D **60**, 073008 (1999).

[68] M. Blanke *et al.*, JHEP **0701**, 066 (2007); C. Tarantino, talk at this workshop [hep-ph/0702152].

[69] R. Aleksan, I. Dunietz and B. Kayser, Z. Phys. C **54**, 653 (1992).

[70] I. Dunietz and R. G. Sachs, Phys. Rev. D **37**, 3186 (1988) [E: D **39**, 3515 (1989)]; I. Dunietz, Phys. Lett. B **427**, 179 (1998); D. A. Suprun, C. W. Chiang and J. L. Rosner, Phys. Rev. D **65**, 054025 (2002).

[71] R. Fleischer, Nucl. Phys. B **671**, 459 (2003).

[72] G. Wilkinson, in G. Cavoto *et al.*, Proceedings of CKM 2005 (WG5), San Diego, California, 15–18 March 2005 [hep-ph/0603019], and private communication.

[73] R. Fleischer, Phys. Lett. B **459**, 306 (1999).

[74] G. Balbi *et al.*, CERN-LHCb/2003-123 and 124; R. Antunes Nobrega *et al.* [LHCb Collaboration], *Reoptimized LHCb Detector, Design and Performance*, Technical Design Report 9, CERN/LHCC 2003-030; J. Nardulli, talk at CKM 2006, Nagoya, Japan, 12–16 December 2006.

[75] A. Khodjamirian, T. Mannel and M. Melcher, Phys. Rev. D **70**, 094002 (2004).

[76] A. Abulencia *et al.* [CDF Collaboration], Phys. Rev. Lett. **97**, 211802 (2006).

[77] G. Punzi, talk at CKM 2006, Nagoya, Japan, 12–16 December 2006.

[78] G. Buchalla and A. J. Buras, Nucl. Phys. B **400**, 225 (1993) and B **548**, 309 (1999); M. Misiak and J. Urban, Phys. Lett. B **451**, 161 (1999).

[79] CDF Collaboration, CDF Public Note 8176 (2006) [http://www-cdf.fnal.gov].

[80] D0 Collaboration, D0note 5009-CONF (2006) [http://www-d0.fnal.gov].

[81] J. Foster, K. Okumura and L. Roszkowski, Phys. Lett. B **641**, 452 (2006); G. Isidori and P. Paradisi, Phys. Lett. B **639**, 499 (2006).

[82] G. Burdman, Phys. Rev. D **57**, 4254 (1998); M. Beneke, T. Feldmann and D. Seidel, Eur. Phys. J. C **41**, 173 (2005); A. Ali, G. Kramer and G. h. Zhu, Eur. Phys. J. C **47**, 625 (2006).

[83] A. Ali, P. Ball, L. T. Handoko and G. Hiller, Phys. Rev. D **61**, 074024 (2000).

$K \to 3\pi$ decay results by NA48/2 at CERN SPS

Gianluca Lamanna
Department of Physics and INFN
University of Pisa
I-56127 PISA, ITALY

1 Introduction

CP violation plays an important role in particle physics since its discovery 40 years ago [1]. For more than 20 years this phenomenon appeared as confined in a particular sector of particle physics, through the mixing between states of opposite CP in the neutral kaons. The unambiguous discovery in the late 1990s, after the early indication by NA31 [2], of direct CP violation in $K \to 2\pi$ decay, by the NA48 [3] and KTEV [4] experiments and the discovery of CP violation, in its various forms, in the neutral B meson system [5] represented important breakthrough in the understanding of the particles dynamics. A complete as possible study of the tiny effects due to the violation of this symmetry in all the systems where it can be carried out, represents an important window on the contribution of new physics beyond the Standard Model: in fact new effects could appear, in particular in the heavy quark loops which are the core of the mechanism allowing the CP violation in the mesons decay. In the kaon sector the most promising places, besides ε'/ε, where this kind of contributions could play some role are the rates of GIM suppressed rare decays and the charge asymmetry between charged kaons. In particular the $K \to 3\pi$ asymmetry could give a strong qualitative indication of the validity of the CKM description of the direct CP violation or reveal the existence of possible sources outside this paradigm.

In principle Direct CP violation in $K^{\pm}$ can be detected comparing the different decay amplitudes in the 3π mode:

$$|A(K^+ \to \pi^+\pi^+\pi^-)| \neq |A(K^- \to \pi^-\pi^+\pi^-)|$$

Experimentally the easiest way to study the difference between the charge conjugate modes is to compare the shape of the *Dalitz Plot* distribution instead of the decay rates. The small phase space in the three pion decay mode allows to expand the matrix element in terms of the, so called, *Dalitz variables* u and v:

$$u = \frac{(s_3 - s_0)}{m_\pi^2} \qquad v = \frac{(s_2 - s_1)}{m_\pi^2}$$

Asymmetry	*# of events*	*Experiment*
$A_g^0 = (19 \pm 125) \cdot 10^{-4}$	115K	CERN PS(1975) [6]
$A_g^0 = (2 \pm 19) \cdot 10^{-4}$	620K	Protvino IHEP (2005) [7]
$A_g^c = (-70 \pm 53) \cdot 10^{-4}$	3.2M	BNL AGS (1970) [8]
$A_g^c = (22 \pm 15 \pm 37) \cdot 10^{-4}$	54M	HyperCP (2000) prelim [9]

Table 1: Summary of the experimental situation both in "neutral" (A_g^0) and in "charged" (A_g^c) mode, before the NA48/2 results

These variables are defined using the Lorentz invariant $s_i = (p_K - p_i)^2$, where p_K is the kaon four momentum and p_i are the pion four momenta ($i = 1, 2, 3$ the latter being "odd" pion) and $s_0 = (s_1 + s_2 + s_3)/3$. Exploiting the Dalitz variables the matrix element can be written as:

$$|M(u, v)|^2 \sim 1 + gu + hu^2 + kv^2 + ... \tag{1}$$

where g,h,k are the linear and quadratic slope parameters. Using the fact that $|g| >> |h|, |k|$, the CP violation parameter

$$A_g = \frac{g^+ - g-}{g^+ + g^-} \tag{2}$$

is defined using only the linear slopes given in (1). Being g^+ relative to K^+ decay while g^- to K^-, the parameter defined above is different from 0 only if an asymmetry exists between the matrix element describing kaon decay of opposite charge. Theoretical predictions for the A_g parameter both in the $K \to \pi^\pm\pi^0\pi^0$ (A_g^n, the so called "neutral" mode) and in the $K \to \pi^\pm\pi^+\pi^-$ (A_g^c, the so called "charged" mode), are very difficult and the available predictions varying from 10^{-6} to few 10^{-5} are unreliable; calculations in the framework of theories beyond the standard model predict a substantial enhancement of this parameter up to the level of few 10^{-4}. Several experiments in the past have searched for asymmetry both in "charged" and "neutral" mode. The sensitivity reached so far is at level of 10^{-3}, as summarized in table 1. The main goals of the NA48/2 experiment are to reach the sensitivity of 10^{-4} both in "neutral" and in "charged" mode, to investigate the possibility of non standard model contributions to the CP violation in charged kaon decays, thus covering the gap existing between the experimental results and the SM theoretical predictions. The large amount of $K \to 3\pi$ collected by NA48/2 experiment, allows a very precise measurement of the Dalitz plot parameters and, as recently shown [10], the study of the neutral Dalitz plot density allows to extract important informations about the pion scattering length.

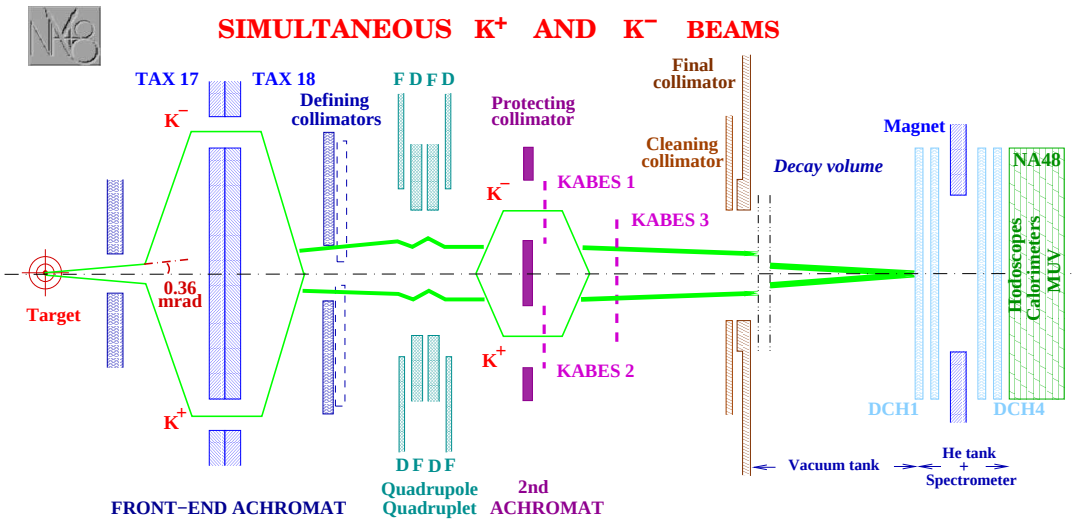

Figure 1: The NA48/2 beam line and detector. Not in scale.

2 Beams and detectors

The simultaneous collection of K^+ and K^- decay with the same apparatus is an essential point of the asymmetry measurement. A novel high intensity beam line was designed in the high energy hall (ECN3) at CERN SPS (fig. 1). The charged particles (kaons, pions, muons and electrons) are produced by 400 GeV high intensity protons beam($\sim 7 \cdot 10^{11}$ protons per pulse), from the SPS accelerator, with a 40 cm long and 2 mm in diameter beryllium target with an angle of zero degrees. A magnetic device, called *first achromat*, selects the momentum of the beam in the range $(60 \pm 3) GeV/c$, splitting the two charges. After being recombined the beams are focused by a quadruplet of quadruples, before another splitting in the *second achromat*. The second achromat houses the first detector along the beam line, called KABES [11], a spectrometer measuring the particles' momentum with a resolution of $\sim 1\%$ (this detector is used studying rare decays). The two charged beams, recombined again along the beam axis, contain $\sim 6.4 \cdot 10^7$ particles per 4.8 s spill, with a charge ratio $K^+/K^- \sim 1.8$ (irrelevant for the charge asymmetry measurement) and 12 times more pions with respect to the kaons: however the pions decay products remain into the beam pipe, because of the small momentum and do not cross the detectors. The decay region is housed in an evacuated tube $\sim 114m$ long and $\sim 2m$ in diameter. The beams in the decay region are superimposed within 1 mm with a total width of $\sim 5mm$, so that both K^+ and K^- decays illuminate with the same acceptance the same detector. The central detector is based on the old NA48 detector, described elsewhere [12]. For the asymmetry and Dalitz plot parameters measurement the

two main detector are the spectrometer and the LKr calorimeter. The magnetic spectrometer works with a $p_T = 120 MeV/c$ kick and the resolution in momentum (GeV/c) is $\sigma_p/p = 1.0\% + 0.044\%$. In order to manage the higher intensity with respect to the previous NA48 runs, the drift chambers read out has been rebuilt. In order to collect the gammas coming from the neutral pions decay a Liquid Krypton (LKr) calorimeter with a resolution in energy (GeV) of

$$\frac{\sigma_E}{E} = \frac{3.2\%}{\sqrt{E}} + \frac{9\%}{E} + 0.42\%$$

is employed. The very good resolution in the reconstructed kaon mass (1.7 MeV/c^2 for $K^\pm \to \pi^\pm\pi^+\pi^-$ and 0.9 MeV/c^2 for $K^\pm \to \pi^\pm\pi^0\pi^0$) allows a precise calibration and monitoring of the characteristics and performances of the apparatus. The data collection is based on a multilevel trigger system. The first level (L1) uses the information coming from a plastic scintillator hodoscope and from a dedicated LKr readout, in which the number of peaks in the calorimeter's energy deposit are computed. The second level (L2) is based on processors for a fast DCH reconstruction. In particular the number of reconstructed vertexes with 2 or 3 tracks, is used to collect $K^\pm \to \pi^\pm\pi^+\pi^-$ events and the missing one-track mass, assuming the nominal kaon momentum (60 GeV) and direction (z axis), is used to collect $K^\pm \to \pi^\pm\pi^0\pi^0$, rejecting the main $K^\pm \to \pi^\pm\pi^0$ background. NA48/2 collected data during two runs in 2003 and 2004, for a total of ~ 100 days of data taking. About $18 \cdot 10^9$ triggers have been registered on tape, for a total of more than 200 TB.

3 Charge asymmetry measurement strategy

The asymmetry method is based on the comparison between the u projection of the Dalitz plot distribution, in order to extract the difference between the matrix element linear components. This difference, defined as $\Delta g = g^+ - g^-$, can be extracted considering the ratio between the density in the u distribution for K^+ and K^- decays. The ratio between the two distribution can be written as:

$$R(u) = \frac{N_{K^+}}{N_{K^-}} \propto \frac{1 + (g + \Delta g)u + hu^2}{1 + gu + hu^2} \tag{3}$$

where $g = (g^+ + g^-)/2$. From Δg the asymmetry parameter A_g can be easily evaluated using the relation $A_g \sim \Delta g/2g$. The simultaneous collection of decays coming from beams with similar momentum spectrum and a similar detection efficiency and acceptance of the decay products, are fundamental points to control the instrumental charge asymmetry. However, the presence of magnetic fields both in the beam sector (achromat) and in the detector (spectrometer magnet) could introduce an intrinsic charge dependent acceptance of the apparatus. To equalize this asymmetry the main

magnetic fields were frequently reversed during the data taking. During the 2003 run the magnet spectrometer polarity was reversed every day while the achromat magnets polarities every week. In the 2004 run the reversal was more frequent: every about 3 hours for the analyzing magnet and 1 day for the beam transport line magnets. It is possible to redefine the ratio in (3) taking into account the magnetic field alternation. For instance, for a given achromat polarities, the ratios:

$$R_J(u) = \frac{N^{B^-}_{K^+}}{N^{B^+}_{K^-}} \ , \qquad R_S(u) = \frac{N^{B^+}_{K^+}}{N^{B^-}_{K^-}} \tag{4}$$

are defined using the same side of the spectrometer, in the sense that the numerator and the denominator in these ratios contain particles deflected in the same direction. The subscripts J and S represent the particles bending direction according to the geographic position of the Jura (J) and Saleve (S) mountains, respectively on the left and right side, with respect to the NA48/2 beam line direction. Considering the possible achromat polarity, four independent ratios can be built exploiting the four different field combinations: instead of the single ratio (3), a *quadruple ratio* can be defined as:

$$R(u) = R_{US}R_{UJ}R_{DS}R_{DJ} \sim \overline{R}\left(\frac{1+(g+\Delta g)u+hu^2}{1+gu+hu^2}\right)^4 \tag{5}$$

where U and D stand for the path, up or down, followed by K^+ in the achromat system, and $\overline{R}$ is an inessential normalization constant. This method is independent on the relative size of the four samples collected with different fields configuration and on the K^+ and K^- flux difference. In the value of Δg extracted from the quadruple ratio (5), the benefits due to the polarity reversal are fully exploited and the main systematic biases due to instrumental asymmetries cancel out. In particular in the quadruple ratio there is a three fold cancellation:

- local detector bias (left-right asymmetry), thanks to the fact that each single ratio is defined in the same side of the detector;
- beam local biases, because in each single ratio the path followed by the particle through the achromat is the same;
- global time variation, because the decays from both charges are collected at the same time (this is not true for the same single ratio in which the numerator and the denominator are collected in different period).

The result remains sensitive only to the time variation of the detector with a characteristic time smaller than the inversion period of the magnetic field, if this effect is charge asymmetric and u dependent. Other systematics biases induced by effects

not canceled by the magnetic field alternation of the magnetic fields (for instance the Earth's magnetic field in the decay region and any misalignment of the spectrometer) have been carefully corrected. The intrinsic cancellation of instrumental asymmetries in the quadruple ratio allows to avoid the use of a MonteCarlo simulation. Nevertheless a GEANT3 based MonteCarlo, including the full geometry description and time variations of beam characteristics, DCH inefficiency and spectrometer alignment, is used for systematics studies and as a cross-check of the result.

3.1 Results in $K^{\pm} \to \pi^{\pm}\pi^0\pi^0$

The reconstruction in the "neutral" mode is based on LKr to construct the u variable and on the spectrometer to define the event charge and close the kinematics. The possibility to define the u variable using the π^0's only is a strong point in this kind of analysis, because of the charge independence of them. Anyway an alternative u reconstruction can be done using the DCH and the KABES informations, to obtain a result, useful as cross-check, with different systematic effects. The fiducial region of the detectors is chosen to avoid edge effects. In particular in order to symmetrize the small difference in the spectrometer acceptance between decays coming from K^+ and K^- beams, the spectrometer's inner radial cut is chosen according to the actual beam position, periodically measured as the average of the reconstructed transverse vertex position using three charged pion events. The decay vertex is reconstructed from the γ impact point position on the LKr, for each π^0, by using the formula:

$$Z_{ij} = \frac{1}{m_{\pi^0}} \sqrt{E_i E_j d_{ij}^2} \tag{6}$$

Among all the possible γ pair, the correct pairing is chosen minimizing the difference between the two π^0's vertexes. The final vertex is obtained as arithmetic average. The kaon invariant mass is obtained including the charged pion measurement from the DCH, in order to reduce the events background by requiring $|M_{K^{\pm}} - M_{PDG}| < 6MeV/c^2$. A total of $59.3 \cdot 10^6$ K^+ and $32 \cdot 10^6$ K^- events has been selected; In plot 2 the reconstructed Dalitz Plot is shown. The photon position on the LKr is corrected to take in to account the calorimeter projectivity. The measurement of the charged momentum, slightly biased by variable DCH misalignment, is corrected exploiting the condition $M_{K^+} = M_{K^-}$ in the $K^{\pm} \to \pi^{\pm}\pi^+\pi^-$. Using the same decay mode the magnetic field inversion is monitored online at level of 10^{-3} studying the reconstructed kaon mass with respect to the nominal (PDG) kaon mass. The effect of the residual magnetic field in the decay region (the so called *Blue Field*), mostly due to the earth magnetic field, is corrected using the maps obtained from a direct measurement before the data taking. Several sources of potential systematic bias have been considered. The effect due to the acceptance has been evaluated studying the stability of the result varying the cuts definition. The MC has been used to

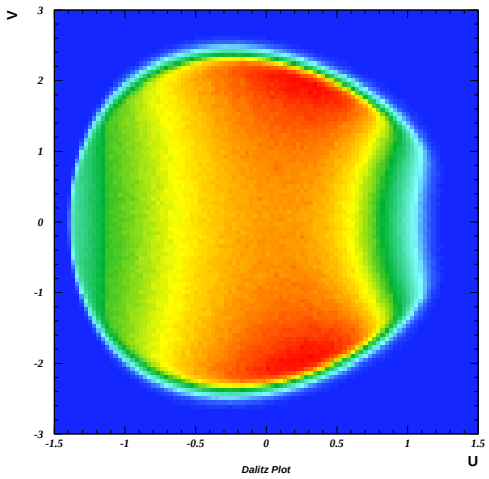

Figure 2: Dalitz plot distribution for $K^{\pm} \to \pi^{\pm}\pi^0\pi^0$

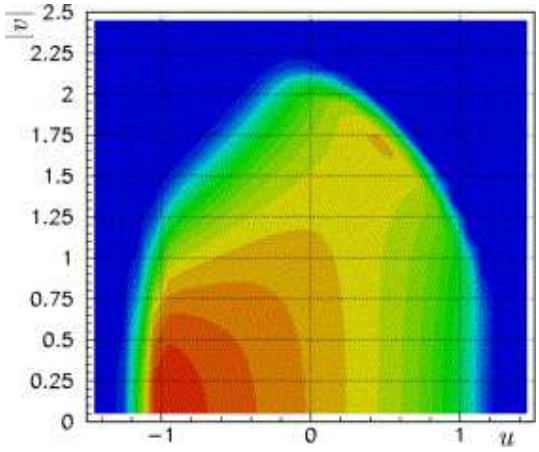

Figure 3: Dalitz plot distribution for $K^{\pm} \to \pi^{\pm}\pi^+\pi^-$

study the contribution of the pion decay in flight to the total systematics error. The contribution to the systematics of the online trigger system has been carefully studied. The efficiencies of the L1 and L2, have been evaluated using data collected with control triggers uncorrelated with the main trigger. In the neutral mode the L1 is essentially obtained with a coincidence between a signal (Q1) coming from the scintillating hodoscope and a signal (NTPEAK) compatible with a deposition of four clusters in the LKr. The L2 (MBX) is based on the algorithm that rejects the $\pi^{\pm}\pi^0$. The main source of systematics comes from the neutral part of the L1 trigger (NTPEAK) being limited by the number of events in the control sample. In table 2 a summary of systematics is shown. The preliminary result in the slope difference using the whole statistics is:

$$\Delta g = (2.7 \pm 2.0_{stat} \pm 1.2_{syst} \pm 0.3_{ext}) \times 10^{-4}$$

where the external error is due to the $\sim 3\%$ error [13] on the knowledge[1] of the g value. The resulting charge asymmetry parameter is:

$$A_g^n = (2.1 \pm 1.6_{stat} \pm 1.0_{syst} \pm 0.2_{ext}) \times 10^{-4} = (2.1 \pm 1.9) \times 10^{-4}$$

This result is fully compatible with the SM prediction and is almost one order of magnitude better than the previous measurements [6] [7].

[1]This contribution becomes negligible using the new g_0 measurement [14]

Systematic effect	*Effect on* $\Delta g \cdot 10^{-4}$
U calculation & fitting	± 0.2
LKr non linearity	± 0.1
Shower overlapping	± 0.5
Pion decay	± 0.2
Spectrometer Alignment & Momentum scale	$< \pm 0.1$
Accidentals	± 0.2
L1 Trigger: Q1	± 0.1
L1 Trigger: NTPEAK	± 0.8
L2 Trigger	± 0.6
Total systematic uncertainty	± 1.2

Table 2: Systematics in $K^{\pm} \to \pi^{\pm}\pi^0\pi^0$

3.2 Results in $K^{\pm} \to \pi^{\pm}\pi^+\pi^-$

The offline reconstruction of the $K^{\pm} \to \pi^{\pm}\pi^+\pi^-$ is totally based on the Spectrometer. The decay vertex is obtained extrapolating the track segment from the first two chambers from the spectrometer to the decay volume, taking into account the presence of the Blue Field in the decay region. The track momentum is rescaled, to compensate the variation of the DCH alignment, as described above. In the three charged pion mode the chambers' acceptance and the spectrometer performance are most critical with respect to the neutral case where the spectrometer is used only to tag the event. In particular the beam pipe crossing the chambers determines the main difference in the acceptance between the two beams for which the beam optic can not control the transverse position better than $\sim 1mm$. The cut centered on the actual beam position (at level of the first and last chamber) must be applied to all the pions, resulting in a reduction of $\sim 12\%$ of the whole statistics. In plot 3 the reconstructed Dalitz Plot is shown. The only relevant physical background come from the pion decay in flight. More than $2 \cdot 10^9$ K^+ and $1.1 \cdot 10^9$ K^- decays are collected in this channel. The main systematics in the charged mode comes from the pion decay in flight as reported in table 3 where the contributions to the systematic error are summarized. A simpler fitting function can be used in the charged mode case with respect to (5) to extract the Δg value, exploiting the relative smallness of the measured g:

$$R(u) \propto \overline{R}(1 + \Delta g u)^4$$

The preliminary result, based on the 2003+2004 data taking, is:

$$\Delta g = (0.6 \pm 0.7_{stat} \pm 0.7_{syst}) \times 10^{-4}$$

Systematic effect	*Effect on* $\Delta g \cdot 10^{-4}$
Spectrometer alignment	± 0.1
Momentum scale	± 0.1
Acceptance and Geometry	± 0.2
Pion decay	± 0.4
Accidentals	± 0.2
Resolution effects	± 0.3
L1 Trigger: Q1	± 0.3
L2 Trigger	± 0.3
Total systematic uncertainty	± 0.7

Table 3: Systematics in $K^{\pm} \to \pi^{\pm}\pi^{+}\pi^{-}$

leading to a charge asymmetry parameter of

$$A_g^c = (-1.3 \pm 1.5_{stat} \pm 1.7_{syst}) \times 10^{-4} = (-1.3 \pm 2.3) \times 10^{-4}$$

Also in this case the goal to increase by a factor 10 the sensitivity with respect to the previous measurement has been reached. The reason for a similar precision of asymmetry results in "neutral" and "charged" mode, in spite of the different statistics, lies in the fact that the Dalitz Plot density is most favourable in the "neutral" mode.

4 Dalitz plot parameters measurement in $K^{\pm} \to \pi^{\pm}\pi^{0}\pi^{0}$

In fig. 4 the $\pi^0\pi^0$ invariant mass square (M_{00}^2) distribution (proportional to the u distribution) is shown. The change of slopes, seen for the first time by NA48/2 at $M_{00}^2 = (2m_{\pi^+})^2$, can not be explained by the simple matrix element parametrization given in (1). This structure has been interpreted by Cabibbo [10] as due to the rescattering process $\pi^+\pi^- \to \pi^0\pi^0$ coming from the $K^{\pm} \to \pi^{\pm}\pi^{+}\pi^{-}$ decay. In fact the $K^{\pm} \to \pi^{\pm}\pi^{0}\pi^{0}$ amplitude can be written as the sum of two terms (just considering the first rescattering order): the direct $\pi^0\pi^0$ emission $\mathcal{M}_0$, parametrized by the standard polynomial expansion, and the terms due to the rescattering process $\mathcal{M}_1$. This last term, proportional to the difference $(a_0 - a_2)$ between the pionic scattering length for I=0 and I=2, is real below the threshold of $2m_{\pi^+}$ and imaginary above. The total amplitude can be written as:

$$\mathcal{M}^2 = \begin{cases} (\mathcal{M}_0)^2 + (\mathcal{M}_1)^2 + 2 \cdot \mathcal{M}_0\mathcal{M}_1 & s_{\pi\pi} < 4m_{\pi^+}^2 \\ (\mathcal{M}_0)^2 + |\mathcal{M}_1^2| & s_{\pi\pi} > 4m_{\pi^+}^2 \end{cases} \quad (7)$$

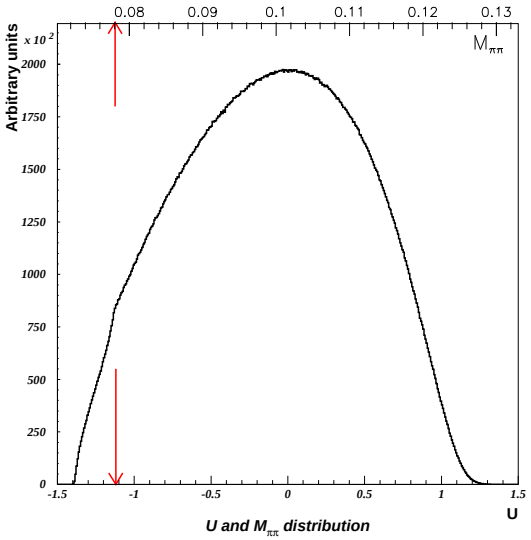

Figure 4: U distribution for $K^{\pm} \to \pi^{\pm}\pi^0\pi^0$. The $\pi^0\pi^0$ invariant mass square (M_{00}^2) is related to the u variable by $u = (M_{00}^2 - s_0)/m_{\pi}^2$. In the arrow position (corresponding to $(2m_{\pi^+})^2$) it is possible to see the "cusp" structure.

The $\mathcal{M}_0\mathcal{M}_1$ term gives a destructive interference below threshold. Other rescattering diagrams can be included in a systematic way as shown by Cabibbo and Isidori [15]. Fitting data with only the $\mathcal{M}_{\prime}$ term yields a fair agreement only above the $2m_{\pi^+}$ threshold, because of the anomaly introduced by the pions strong rescattering in the M_{00}^2 distribution, while the standard expansion is not enough to explain the complex dynamics contributing to the whole decay amplitude. Using the Cabibbo one-loop model, the fit quality increase giving a χ^2 of 420.1 for 148 degree of freedom, as shown in fig. 6 . Including the two-loop Cabibbo-Isidori approach the χ^2 becomes more reasonable (158.8 for 146 degree of freedom). Near the threshold the relative pions velocity decreases and the possibility to have electromagnetic $\pi^+\pi^-$ bound states increases. However the description of the so called pionic atoms (pionium) needs particular care, because of the Coulomb interaction correction and the critical experimental resolution (the fit obtained including the pionium is shown in the third plot in fig. 6). For that reason we prefer to exclude 7 bins around the threshold position to perform the final fit (last plot in fig.6) in which we have a χ^2 of 145.5 for 139 degree of freedom. The results [16], based on $23 \cdot 10^6$ events collected in 2003, are obtained setting k, the quadratic v slope, to 0:

$$g^0 = 0.645 \pm 0.004_{stat} \pm 0.009_{syst}$$

$$h^{'} = -0.047 \pm 0.012_{stat} \pm 0.011_{syst}$$

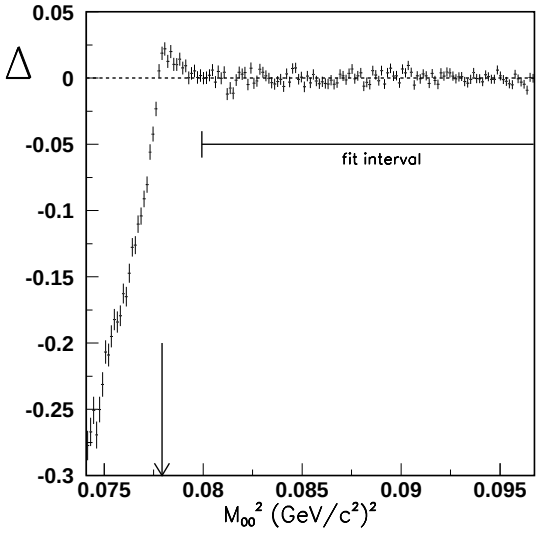

Figure 5: $\Delta = (data - fit)/data$ is shown as a function of $M_{\pi^0\pi^0}$. The cusp threshold is indicated by an arrow. The fit χ^2 is reasonable only if the fit is restricted to the indicated fit interval.

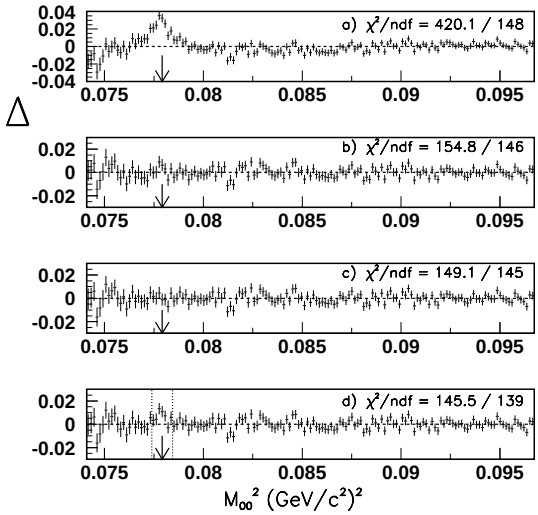

Figure 6: The application of the rescattering hypothesis improves the quality of the fit (see text)

	NA48/2 results	PDG06
g	$(-21.131 \pm 0.009_{stat} \pm 0.012_{syst})\%$	$(-21.54 \pm 0.35)\%$
h	$(1.829 \pm 0.015_{stat} \pm 0.036_{syst})\%$	$(1.2 \pm 0.8)\%$
k	$(-0.467 \pm 0.005_{stat} \pm 0.011_{syst})\%$	$(-1.01 \pm 0.34)\%$

Table 4: Results for Dalitz Plot parameter in charged mode.

where $h' + (1/4)g^2 = h$. The data are compatible with a non zero value for the k parameter, never measured before. The value of the fit

$$k = 0.0097 \pm 0.0003_{stat} \pm 0.0008_{syst}$$

is still preliminary. The $(a_0 - a_2)$ value is not affected by the $k \neq 0$ term, but the g and h values change respectively by $\sim 2\%$ and $\sim 25\%$.

5 Dalitz plot parameters measurement in $K^\pm \to \pi^\pm\pi^+\pi^-$

Thanks to the huge statistics collected in $K^\pm \to \pi^\pm\pi^+\pi^-$ decay and to the well tuned MC, very precise measurement of the Dalitz plot parameters can be performed. The

pion rescattering effects can influence the matrix element also in the "charged" mode but, being on the border of the Dalitz Plot, is not so evident like in the "neutral" mode. The goal of the first and preliminary study presented here is to measure the parameters in the standard polynomial expansion verifying the validity of (1). The parameters (g,h,k) are obtained minimizing the

$$\chi^2(g,h,k,N) = \sum_{u,v} \frac{(F_{data} - NF_{MC})^2}{\delta F_{data}^2 + N^2 F_{MC}^2}$$

where F represents the population (in data or in MC) in the (u,v) bin. The MC population is obtained adding the 4 components corresponding to the four possible terms in (1). The relative weights, obtained from the fit, are the polynomial expansion parameters. The coulomb correction is applied to take into account the pion electromagnetic interaction. The main contributions to the systematic uncertainty, at this analysis stage, come from the momentum scale in the charged pions measurement, the kaon momentum spectrum in the MC and trigger inefficiencies. The preliminary result is based on $0.47 \cdot 10^9$ events collected in the 2003 run. In table 4 the results are presented and the agreement with the PDG06 values is shown. The previous measurements, by experiments made in 70s, are one order of magnitude less precise with respect to the NA48/2 measurement, based on 1/4 of the whole statistics.

6 Conclusions

The main goal of the NA48/2 experiment was to measure, with a precision at level of 10^{-4} the charge asymmetry parameter A_g, both in $K^\pm \to \pi^\pm\pi^+\pi^-$ and in $K^\pm \to \pi^\pm\pi^0\pi^0$ decays. The preliminary results obtained in the "neutral" (A_g^n) and "charged" (A_g^c) mode:

$$A_g^n = (2.1 \pm 1.6_{stat} \pm 1.0_{syst} \pm 0.2_{ext}) \times 10^{-4} = (2.1 \pm 1.9) \times 10^{-4}$$

$$A_g^c = (-1.3 \pm 1.5_{stat} \pm 1.7_{syst}) \times 10^{-4} = (-1.3 \pm 2.3) \times 10^{-4}$$

are compatible with the SM predictions and with our previous results based on partial samples [17] [18].

In $K^\pm \to \pi^\pm\pi^0\pi^0$ the standard polynomial matrix element expansion is not enough to describe the observed $\pi^0\pi^0$ invariant mass spectrum. Taking into account the rescattering processes, whose contributions are proportional to the $(a_0 - a_2)$ term the corresponding slope are found to be (setting k=0)

$$g^0 = 0.645 \pm 0.004_{stat} \pm 0.009_{syst} \qquad h' = -0.047 \pm 0.012_{stat} \pm 0.011_{syst}$$

However a $\sim 1\%$ for the k quadratic slope is obtained with a complete fit (preliminary result).

In the charged mode the standard polynomial fit has been employed. The Dalitz plot parameters have been remeasured with higher precision with respect to the previous old measurement.

Bibliography

[1] J. H. Christenson et al. *Phys. Rev. Lett.* **13**, 138 (1964)

[2] G. Barr et al. (NA31), *Phys. Lett. B* **317**, 233 (1993)

[3] A. Lai et al (NA48), *Eur, Phys. J. C* **22**, 231 (2001)
J. R. Batley et al. (NA48), *Phys. Lett. B 544*, 97 (2002)

[4] A. Alavi-Harati et al. (KTeV) *Phys. Rev. D* **67**, 012005 (2003), Erratum: *Phys. Rev. D* **70**, 079904 (2004)

[5] K. Abe et al. (Belle), *Phys. Rev. Lett.* **93**, 021601 (2004)
B. Aubert et al. (Babar), *Phys. Rev. Lett.* **93**, 131801 (2004)

[6] K. M. Smith *et al.*, Nucl. Phys. B **60** (1973) 411.

[7] G. A. Akopdzhanov *et al.*, Eur. Phys. J. C **40** (2005) 343 [arXiv:hep-ex/0406008].

[8] W. T. Ford, P. A. Piroue, R. S. Remmel, A. J. S. Smith and P. A. Souder, Phys. Rev. Lett. **25** (1970) 1370.

[9] W. S. Choong, Ph.D. thesis, Berkeley (2000) LBNL-47014

[10] N. Cabibbo, Phys. Rev. Lett. **93** (2004) 121801 [arXiv:hep-ph/0405001].

[11] B. Peyaud, Nucl. Instrum. Meth. A **535** (2004) 247.

[12] V. Fanti et al. (NA48) *Phys. Lett. B* **465**, 335 (1999)

[13] S. Eidelman *et al.* [Particle Data Group], Phys. Lett. B **592** (2004) 1.

[14] W. M. Yao *et al.* [Particle Data Group], J. Phys. G **33** (2006) 1.

[15] N. Cabibbo and G. Isidori, JHEP **0503** (2005) 021 [arXiv:hep-ph/0502130].

[16] J. R. Batley *et al.* [NA48/2 Collaboration], Phys. Lett. B **633** (2006) 173 [arXiv:hep-ex/0511056].

[17] J. R. Batley *et al.* [NA48 Collaboration], Phys. Lett. B **638**, 22 (2006) [arXiv:hep-ex/0606007] cern-ph-ep-2006-006.

[18] J. R. Batley *et al.* [NA48/2 Collaboration], Phys. Lett. B **634** (2006) 474 [arXiv:hep-ex/0602014].

The NA48/3 Experiment at CERN

GiuseppeRuggiero
CERN
PH Department
Geneva, Switzerland

1 Introduction

The $K^+ \to \pi^+ \nu\overline{\nu}$ decay is a flavour changing neutral current process which proceeds through box and purely electroweak penguin diagrams. The short distance contributions largely dominate in the matrix element, while c-quark contributions have been evaluated at NNLO order giving an uncertainty of about 5% [1]. This is the only source of theoretical error because the hadronic matrix element can be parametrized in terms of the branching ratio of the $K^+ \to \pi^0 e^+ \nu$ decay, which is well known experimentally [5]. The computed value is $(8.0 \pm 1.1) \times 10^{-11}$, where the error is dominated by the uncertainty in the knowledge of the CKM matrix elements. Such extreme theoretical clarity, unique in K and B physics, makes this decay, together with the $K_L \to \pi^0 \nu\overline{\nu}$ decay, extremely sensitive to new physics contributions both in MVF and non-MFV scenarios [2–4]. As a by-product, it allows also a measurement of the CKM element V_{td} independent on the value extracted from B oscillation measurements.

Up to now 3 $K^+ \to \pi^+ \nu\overline{\nu}$ events have been observed [6], but a 10% accuracy measurement of the branchig ratio is required to provide a significative test of new physics scenarios. This is the goal of the proposed NA48/3 experiment at CERN-SPS [7]. It aims to collect about 80 $K^+ \to \pi^+ \nu\overline{\nu}$ events keeping the background contamination at the level of 10%.

2 The P-326 proposal

The NA48/3 experiment will be based on the NA48 apparatus at CERN and will make use of the same CERN-SPS beam line which produced the kaon beam for the NA48 experiment. The R&D program for this experiment, started in 2006, will continue in 2007. The data taking should start in 2010.

The layout of the experiment is shown in figure 1. The goal of the experiment can be achieved by exploiting a decay in flight technique which allows 10% signal

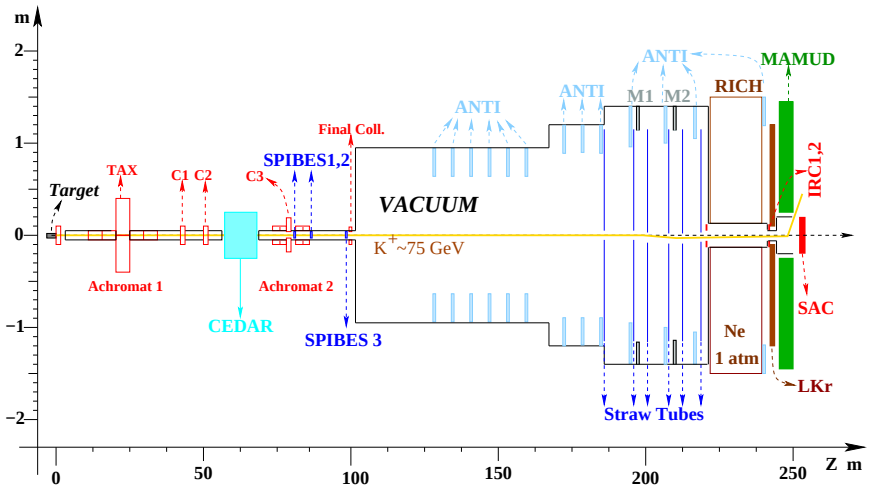

Figure 1: Layout of the experiment.

acceptance and by using a beam line able to provide of the order of 10^{13} kaon decays.

The experimental signature of a $K^+ \to \pi^+\nu\overline{\nu}$ is one reconstructed positive track in the downstream detector. A beam and a pion tracking detectors provide a precise reconstruction of the kinematics, since the squared missing mass allows a kinematical separation between the signal and more than 90% of the total background, as shown in figure 2. In particular two signal regions can be defined where the backgrounds from $K^+ \to \pi^+\pi^0$ and $K^+ \to \mu^+\nu_\mu$ enter only because of non-gaussian tails in the squared missing mass resolution. The kinematics alone cannot provide a 10^{13} background rejection. A system of calorimeters for photon vetoes, muon veto and a RICH for positron, pion and muon separation is designed to fulfill these needs. Moreover, the detector layout gives redundancy both in kinematics reconstruction and particle identification allowing the background estimation directly from data.

2.1 The beam line

An intense 400 GeV/c proton beam extracted from the SPS produces a secondary charged beam by impinging on a Be target. A 100 m long beam line selects a 75 GeV/c momentum beam with 1% RMS momentum bite and an average rate of about 800 MHz integrated over an area of 16 cm^2. However, since the beam is composed by 6% of K^+ and 94% of π^+, e^+ and protons, the kaon decay rate downstream to the final collimator is only about 6 MHz. Some MHz of accidentals coming from the beam, mainly composed by muon, accompany the kaon decays, resulting in a total $\sim$11 MHz average rate seen by the downstream detectors integrated on their surface.

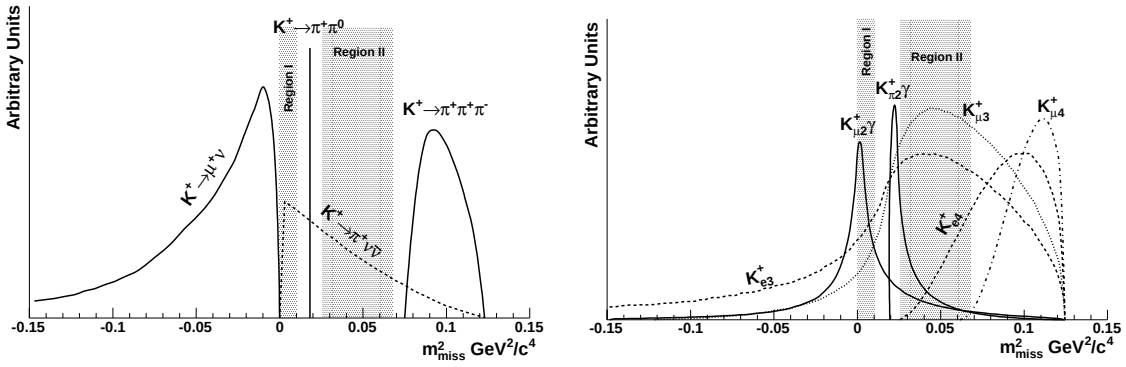

Figure 2: Squared missing mass for Kaon decays. The squared missing mass is defined as the square of the difference between the 4-momentum of the kaon and of the decayed track in the hypothesis that it is a pion.

Thanks to a significant increase of the secondary beam acceptance with respect to the beam used in NA48/2, the beam line is able to provide about 5×10^{12} K^+ decays in a 60 m decay region, in 100 days of run at 60% of efficiency, which is a very realistic estimate based on the decennial NA48 experience at the SPS. As a consequence the experiment will be able to collect $O(100)$ Standard Model events in two years of data taking.

Since the experiment uses an unseparated charged beam, a differential Cerenkov counter, the CEDAR [8], is required to provide the kaon identification. This detector is available at CERN, but upgrades are needed to adapt it to the new beam conditions. The R&D is started with a test beam run in November 2006, mainly devoted to the study of the timing capability.

The precise kinematical reconstruction requires a beam tracker highly performing in terms of time and spatial resolution and able to sustain a particle rate of about 60 MHz cm^{-2}. To limit the amount of interactions one is faced with severe constraints on the material budget. The detector under study consists of three Si pixels stations $36 \times 48\,\mathrm{mm}^2$ large, made up by $300 \times 300\,\mu\mathrm{m}^2$ pixels each of them composed by a $200\,\mu$m thick Si sensor and a chip $100\,\mu$m thick, bump-bonded on the sensor and built using a $0.13\,\mu$m CMOS technology. The characteristics of the detector and a careful design of the readout chip should provide 200 ps time resolution per station, enough for an efficient tagging of the kaon track. A mis-tagging of the kaon, in fact, may be source of background because it spoils the kinematical resolution of the squared missing mass. The design of the readout chip and the project of a cooling system is under way. Radiation damage tests on sensor prototypes took place in 2006.

Downstream of the beam tracker, the decay region consists of the existing 80 m long iron tube of NA48. Tests performed in 2006 demonstrated that one is able to

achieve a vacuum level of less than 10^{-5} mbar after a substantial improvement of the pumping system. Fluka [9] and Geant3 [10] based simulations showed that such a vacuum is enough to keep the background from the interaction of the particles with the residual gas at a fraction of one event.

2.2 The downstream detectors

Since the multiple scattering is the main limitation to the kinematics reconstruction, the minimization of the material budget is the driven parameter for the downstream spectrometer. As a consequence, the proposed detector is made by six straw chambers which can be placed directly in the same vacuum of the decay region. Two magnets space pairs of chambers, providing redundant measurements of the particle momentum. The R&D program is started in 2006 and a reduced-size prototype will be built for the end of 2007. Each chamber consists of tubes assembled in a way to ensure up to four views for a single hit reconstruction and the 36 μm thick mylar foil which forms the 1 cm diameter tubes allows the chamber thickness not to exceed 0.5% radiation lentgh. Moreover the overall resolution on hit position must be within 100 μm. Tests on gas leakage and tube expansion started in 2006 are in progress and preliminary results indicate no major problem in the use of the straws in vacuum, providing a suitable control of their mechanical stability. The layers must be packed to leave an octagonal 10 cm diameter hole in the middle of the chamber to let the intense undecayed beam to pass through. The center of each station must be displaced in the bending plane of the magnets according to the path of the 75 GeV/c positive beam. This arrangement allows the individual chambers to be used as a veto for negative particles up to 60 GeV/c, needed for the rejection of backgrounds like $K^+ \to \pi^+\pi^- e^+\nu$ and $K^+ \to \pi^+\pi^+\pi^-$. Each station will operate at about 45 KHz per tube on average, but, due to the beam halo, the region close to the hole will suffer up to 0.5 MHz rate.

A 18 m long RICH located after the spectrometer and filled with Ne at atmospheric pressure is the core of the particle identification. A 11 cm radius beam pipe crosses the RICH and two tilted mirrors at the end reflect the Cerenkov light toward an array of about 2000 phototubes placed in the focal plane. Because of the Cerenkov threshold, the RICH is able to identify pions with momentum greater than 15 GeV/c. Simulations showed that up to 40 photo electrons can be collected per track. Using phototubes of 1 cm diameter a better than 3σ separation for tracks with momentum below 35 GeV/c is achievable, where the size of the phototubes is the main limitation to the Cerenkov angle resolution. As a by-product the detector has also the function of an auxiliary spectrometer. The RICH must work also as a timing detector for the downstream track with a requested time resolution of 100 ps. The timing performances depend on the phototubes. To this purposes a set of phototubes were tested on a Cerenkov device during a test beam performed at CERN in November

2006. The construction and test of a full-length prototype of the RICH is planned for 2007.

A combination of calorimeters covering up to 50 mrad serves to identify the photons produced in kaon decays. Thirteen ring-shaped calorimeters cover the angular region between 10 and 50 mrad. They should guarantee the detection of photons down to 50 MeV with 10^{-4} inefficiency at most and must be placed in vacuum. Tests on prototypes of detectors built using lead scintillator tiles and scintillating fibers are scheduled for 2007 using a $\gamma-$tagged facility at LNF. Moreover tests on the out-gassing rate performed at CERN in 2006 showed the possibility to place these calorimeters directly in the high vacuum of the decay region. The existing NA48 liquid Kripton calorimeter (LKr) [11] covers the region between 1 and 10 mrad. A data analysis performed on $K^+ \to \pi^+\pi^0$ decays collected by NA48/2 in 2004 shows that the inefficiency of the LKr is lower than 10^{-5} for photons with energy greater than 10 GeV. A test run was performed in October 2006 at the SPS using the NA48 apparatus. This run used a well known momentum electron beam which passed through the NA48 apparatus, making photon bremsstrahlung in the detector material. These data allows the LKr inefficiency below 10 GeV to be addressed. First results indicate that the LKr matches our requests in terms of efficiency on the overall photon energy range. Finally a program of consolidation and update of the readout electronics of the LKr is under way. Two rings calorimeter (IRCs) around the beam pipe and a 20×20 cm^2 calorimeter (SAC) behind the muon veto cover the low angle region. Only photons with energy larger than 10 GeV/c illuminate these detectors, making a 10^{-5} inefficiency achievable. A SAC prototype based on shashlyk technology was built and tested with electrons on the NA48 beam line in 2006.

A 6 m long hadronic sampling calorimeter (MAMUD) provides a 10^5 rejection of muons. It is composed by 8 sections divided in 19 iron planes 2 cm thick separated by planes of extruded scintillators. The longitudinal shower development allows the separation between pion and muon. The detector should be used also as a fast trigger for muons. A 20×30 cm^2 aperture in the center lets the beam to pass through. Two coils provide a 5 Tm magnetic field integral in the hole to deflect the beam out of the acceptance of the SAC.

3 Performances

A preliminary analysis using Geant3 and Geant4 [12] based simulations of the apparatus gives an acceptance of about 17%, showing that the target of 10% of signal acceptance is safely achievable even taking into account additional losses occurring in a real data taking. The use of the RICH constrains the accepted pion tracks within the $(15, 35)$ GeV/c momentum range. The higher cut is an important loss of signal acceptance, but assures that events like $K^+ \to \pi^+\pi^0$ deposit at least 40 GeV of

	Total	Region I	Region II
Signal	65	16	49
$K^+ \to \pi^+\pi^0$	2.7	1.7	1.0
$K^+ \to \mu^+\nu$	1.2	1.1	< 0.1
$K^+ \to e^+\pi^-\pi^+\nu$	2	*negligible*	2
Other three track decays	1	*negligible*	1
$K^+ \to \pi^+\pi^0\gamma$	1.3	*negligible*	1.3
$K^+ \to \mu^+\nu\gamma$	0.4	0.2	0.2
K_{e3}, $K_{\mu 3}$, others	*negligible*	–	–
Total background	8.6	3.0	5.6

Table 1: List of the expected signal events and the expected background events from kaon decays per year of data taking.

electromagnetic energy, making their rejection easier.

Main sources of background have been considered and the results per year of data taking are shown in table 1. Just a simply counting of the signal and background events in the signal regions indicates that the 10% background level is nearly achievable.

4 Conclusions

The ultra-rare $K \to \pi\nu\nu$ decay is a unique environment where to search for new physics. The NA48/3 experiment at CERN-SPS proposes to follow this road by collecting $O(100)$ events of the $K^+ \to \pi^+\nu\overline{\nu}$ decay. The overall experimental design requires a sophisticated technology for which an intense R&D program is started. Actually we are designing an experiment able to reach a 10^{-12} sensitivity per event employing existing infrastructures and detectors at CERN.

Bibliography

[1] A. J. Buras, M. Gorbahn, U. Haisch and U. Nierste, JHEP **0611**, 002 (2006) HEP-PH 0603079.

[2] G. D'Ambrosio, G. F. Giudice, G. Isidori and A. Strumia, Nucl. Phys. B **645**, 155 (2002) HEP-PH 0207036.

[3] G. Isidori, F. Mescia, P. Paradisi, C. Smith and S. Trine, JHEP **0608**, 064 (2006) HEP-PH 0604074.

[4] M. Blanke, A. J. Buras, A. Poschenrieder, S. Recksiegel, C. Tarantino, S. Uhlig and A. Weiler, HEP-PH 0610298.

[5] W. M. Yao *et al.* [Particle Data Group], J. Phys. G **33** (2006) 1. JPHGB,G33,1.

[6] V. V. Anisimovsky *et al.* [E949 Collaboration], Phys. Rev. Lett. **93**, 031801 (2004) HEP-EX 0403036.

[7] G. Anelli *et al.*, CERN-SPSC-2005-013, SPSC-P-326.

[8] G. Bovet *et al.*, CERN Report: CERN 82-12(1982).

[9] A. Ferrari, P. R. Sala, A. Fasso and J. Ranft, CERN-2005-010.

[10] CERN Program Library Long Writeup, W5013 (1993).

[11] G. Unal, NA48 Collaboration, in: IX International Conference on Calorimetry, October 2000, Annecy, France, HEP-EX 0012011.

[12] J. Allison *et al.*, IEEE Trans. Nucl. Sci. **53**, 270 (2006). IETNA,53,270.

Searches for Permanent Electric Dipole Moments

Klaus Jungmann
Kernfysisch Versneller Instituut
University of Groningen
NL-9747 AA Groningen, THE NETHERLANDS

1 Introduction

The Standard Model (SM) of particle physics provides a theoretical framework which allows to describe all observations in particle physics to date. Even those recent observations in neutrino physics which strongly indicate the existence of neutrino oscillations can be accommodated with small modification. However, contrary to this the great success of the SM there remains a number of most intriguing questions in modern physics to which the SM can not provide further clues about the underlying physical processes, although the facts are can be described often to very high accuracy. Among those puzzling issue are the existence of exactly three generations of fundamental particles, i.e. quarks and leptons, and the hierarchy of the masses of these fundamental fermions. In addition, the electro-weak SM has a rather large number of some 27 free parameters, which all need to be extracted from experiments [1].

In modern physics - and in particular in the SM - symmetries play an important and central role. We know that global symmetries relate to conservation laws and local symmetries give forces [2]. Within the SM the physical origin of the observed breaking of discrete symmetries in weak interactions, e.g. of parity (P), of time reversal (T) and of combined charge conjugation and parity (CP), remains unrevealed, although the experimental findings can be well described.

In order to gain deeper insights into the not well understood aspects of fundamental physics, a number of speculative models beyond the present standard theory have been proposed. Those include such which involve Left-Right symmetry, fundamental fermion compositeness, new particles, leptoquarks, supersymmetry, supergravity, technicolor and many more. Interesting candidates for an all encompassing quantum field theory are string or membrane (M) theories which among other features may include supersymmetry in their low energy limit. Independent of their mathematical elegance and partial appeal all of these speculative theories will remain without status in physics unless secure experimental evidence for them being reality can be gained in future. Experimental searches for predicted unique features of those models - such as breaking of discrete symmetries - are therefore essential to steer the development

of theory towards a better and deeper understanding of fundamental laws in nature. Such experiments must be carried out not only at high energy accelerators, but also in complementary approaches at lower energies. Typically the low energy experiments in this context fall into the realm of atomic physics and of high precision measurements. Searches for permanent Electric Dipole Moments (EDMs), are an important subset of such low energy precision particle physics experiments.

2 Discrete Symmetries

A permanent electric dipole moment (EDM) of any fundamental particle or quantum system violates both parity (P) and time reversal (T) symmetries [3] and if one assumes unbroken combined CPT symmetry, it also violates CP. The violation of P is well established in physics and its accurate description has contributed significantly to the credibility of the SM. The observation of neutral currents together with the observation of parity non-conservation in atoms were important to verify the validity of the SM. The fact that physics over several orders of magnitude in momentum transfer - from atoms to highest energy scattering - yields the same electro-weak parameters may be viewed as one of the biggest successes in physics to date. However, at the level of highest precision electro-weak experiments questions arose, which ultimately may call for a refinement.

2.1 Parity

The running of the weak mixing angle $sin^2\Theta_W$ appears not to be in good agreement with observations [4]. If the value of $sin^2\Theta_W$ is fixed at the Z^0-pole, deep inelastic electron scattering at several GeV appears to yield a considerably higher value. A new round of experiments is being started with the Q_{weak} experiment [6] at the Jefferson Laboratory in the USA. For atomic parity violation [5] in principle higher experimental accuracy will be possible from experiments using Fr isotopes [7, 8] or single Ba or Ra ions in radio frequency traps [9]. Experiments with Fr atoms in magneto-optical traps were started at INFN Legnaro, Italy, and at Stony Brook, USA. Pioneering work on single Ba ions has been started at the University of Washington, Seattle, USA, and based on this experience a Ra ion experiment has been started at KVI, Groningen, The Netherlands. The full exploitation of the advantage of larger weak effects in these heavy atom systems (compared to Cs) due to their high power dependence on the nuclear charge, will require improved atomic wave function calculations, as the observation of weak effects is always through an interference of weak and electromagnetic effects. [10]

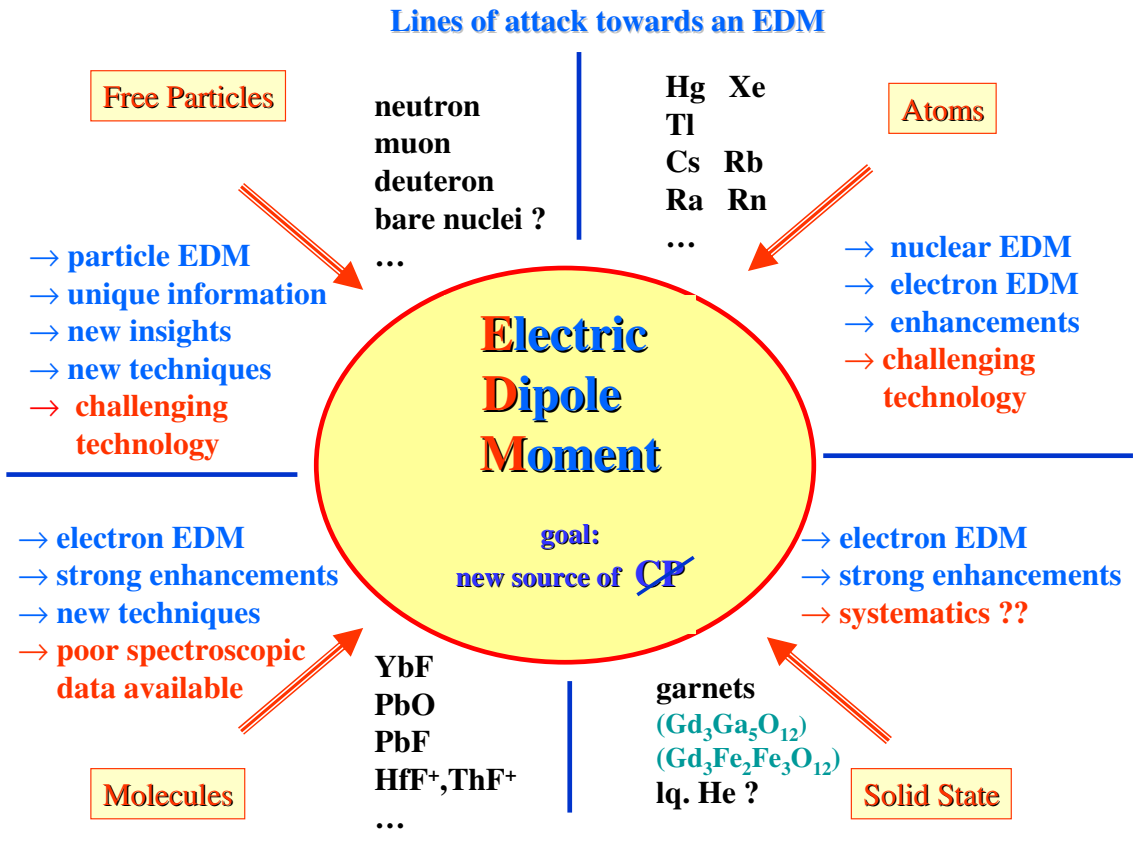

Figure 1: The experimental searches for an EDM follow a number of significantly different lines.

2.2 Time Reversal and CP

CP violation as observed first in the neutral Kaon decays can be described with a single phase factor in the Cabbibo-Kobayashi-Maskawa formalism [11]. Because of its possible relation to the observed matter-antimatter asymmetry in the universe, CP violation has attracted a lot of attention. [1] CP violation as described in the SM is however not sufficient to explain the excess of baryons. This provides a strong motivation to search for yet unknown sources CP symmetry violation. It is in particular a major driving force behind theEDM searches going on at present.

[1] A. Sakharov [12] has suggested that the observed dominance of matter could be explained via CP-violation in the early universe in a state of thermal non-equilibrium and with baryon number violating processes. We note here that the existence of additional sources of CP-Violation is not a necessary condition to explain the matter-antimatter asymmetry. Other viable routes could lead through CPT violation and there without the need of thermal non-equilibrium [13].

EDMs have been searched for in various systems with different sensitivities (Table 1). [3, 14–18]. Distinctively different precision experiments to search for a EDM are under way in many different system.A large number of ideas for significant improvements have been made public. Still, the electron and the neutron get the largest attention of experimental groups, although besides tradition there is little which singles out these systems. Nevertheless, there is a large number of efforts in the USA and in Europe using different approaches which all have unique promising features.

In composed systems, i.e. molecules, atoms or nuclei, fundamental particle dipole moments of constituents can be significantly enhanced [14]. For the electron significant enhancement factors are planned to be exploited such as those associated with the large internal electric fields in polar molecules [19].

The physical systems investigated fall in six groups (see Fig. 1), i.e.

(i) 'point' particles (e, μ, τ),

(ii) nucleons (n, p),

(iii) nuclei (^{2}H, ^{223}Fr, ...),

(iv) atoms (Hg, Xe, Tl, Cs, Rn, Ra,...) and

(v) molecules (TlF, YbF, PbO,HfF^+, ThF^+ ...),

where each investigated object has its own particular advantages. Among the methods employed are

(i) Classical approaches using optical spectroscopy of atoms and molecules in cells, as well as atomic and molecular beams or with contained cold neutrons,

(ii) Modern atomic physics techniques such as atomic and ion traps, fountains and interference techniques;

(iii) Innovative approaches involving radioactive species, storage rings, particles in condensed matter (garnets, superfluid helium) , nuclear spin masers [20], and a few more.

From an unbiased point of view there is no preferred system to search for an EDM. In fact, many different systems need to be examined in order to be able to extract unambiguous information on the nature of EDMs, because depending on the underlying yet unknown processes different systems have in general quite significantly different susceptibility to acquire an EDM through a particular mechanism (see Figure 2). As a first approach an EDM may be considered an "intrinsic property" of an elementary particle as we know them, because the mechanism causing an EDM is not accessible at present. However, an EDM can also arise from CP-odd forces between the constituents under observation, e.g. between nucleons in nuclei or between nuclei and

electrons. Such EDMs could be much higher [31] than such expected for elementary particles originating within the presently popular New Physics models.

Particle	Limit/Measurement [e cm]	Reference	SM limit [factor to go]	possible New Physics [factor to go]
e	$< 1.6 \times 10^{-27}$	[21]	10^{11}	≤ 1
μ	$< 2.8 \times 10^{-19}$	[22]	10^{8}	≤ 200
τ	$(-2.2 < d_\tau < 4.5) \times 10^{-17}$	[23]	10^{7}	≤ 1700
n	$< 2.9 \times 10^{-26}$	[24]	10^{4}	≤ 60
p	$(-3.7 \pm 6.3) \times 10^{-23}$	[25]	10^{7}	$\leq 10^{5}$
Λ^0	$(-3.0 \pm 7.4) \times 10^{-17}$	[26]	10^{11}	10^{9}
$\nu_{e,\mu}$	$< 2 \times 10^{-21}$	[27]		
ν_τ	$< 5.2 \times 10^{-17}$	[28]		
Hg-atom	$< 2.1 \times 10^{-28}$	[29]	$\leq 10^{5}$	various

Table 1: Some actual limits on EDMs and the improvement factors necessary in experiments to reach SM predictions. For electrons, neutrons and muons the region where speculative models have predicted a finite value for an EDM can be reached with presently proposed experiments in the near future. There is a number of new ongoing activities, e.g. in neutral and charged molecules or radioactive atoms, which have no reported limit yet. However, they are similarly promising.

3 Some New Developments in the Field of EDM Searches

The highly active field of EDM searches has very recently seen a plurality of novel ideas. Theoretical work has made very clear that one needs a number of measurements in various systems, in order to identify underlying mechanisms of CP-Violation and EDM generation, once the existence of an EDM has been proven. On the experimental side, novel ideas led to new activities in systems not investigated so far. Among those are in particular radioactive atoms and charged particles. The latter had been excluded by the community for several decades, because of a misinterpretation of the role of the Lorentz force, which only recently could be convincingly cleared up [14,30].

3.1 Radioactive Systems

New facilities around the world make more short-lived radioactive isotopes available for experiments. Of particular interest for EDM searches is the Ra atom. This atom has has as a unique feature in heavy atoms rather close lying states of opposite

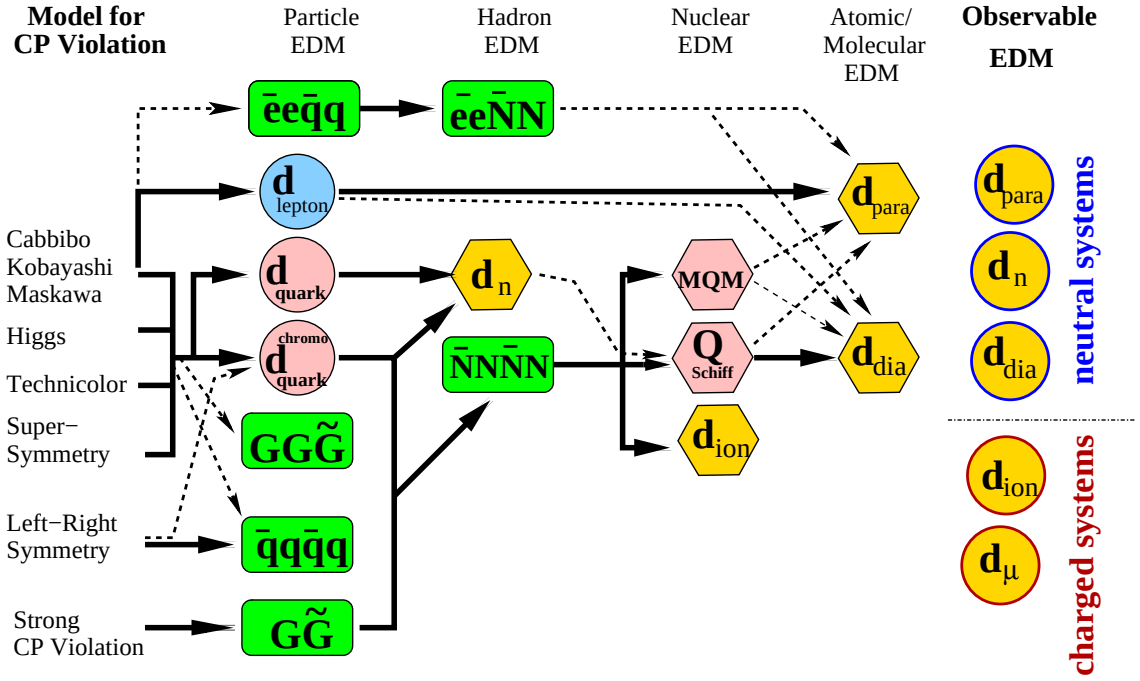

Figure 2: A variety of theoretical speculative models exists in which an EDM could be induced through different mechanisms or a combination of them into fundamental particles and composed systems for which an EDM would be experimentally accessible.

parity. This accidental almost degeneracy of the $7s7p^3P_1$ and $7s6d^3D_2$ states has led to the prediction of a significant enhancement for an electron EDM [32] - much higher than for any other atomic system. An additional advantage of Ra arises from the fact, that for many of its isotopes their nuclei fall are within in a region where (dynamic) octupole deformation occurs, which also enhances the effect of a nucleon EDM substantially, i.e. by some two orders of magnitude [33]. From a technical point of view the Ra atomic levels of interest for an experiment are well accessible spectroscopically and the isotopes can be produced in sufficient quantities in nuclear reactions. The advantage of an accelerator based Ra experiment is apparent, because nuclear EDMs are only possible nuclei with spin and all Ra isotopes with no-vanishing nuclear spin are relatively short-lived [34]. Recently most significant progress towards a Radium EDM experiment has been reported from the Argonne National Laboratory, USA, where successfully a small number of some 10 Ra atoms from an atomic beam source could be stored in a magneto-optical trap (MOT) [35]. Plans were reported to search for a ground state end hence nuclear EDM using a far off resonance optical trap. Activities towards the excited state EDM of the Ra atoms are under way at

KVI , Groningen, The Netherlands [34, 36, 37].

The generic statistical sensitivity of an EDM experiment is given by

$$\delta d = \frac{\hbar}{P\varepsilon T\sqrt{N\tau}E}, \tag{1}$$

where P is the polarization, ε the efficiency, T the measurement time, N the flux of particles, τ the spin coherence time and E the applied electric field. With typical values achievable in most experiments ($P \approx 1, \varepsilon \approx 1, N = 10^6/s, \tau \approx 1s, E = 10^5 V/cm$) one gets $\delta d \approx 7 \cdot 10^{-29} e\,cm$ in a day ($T = 10^5 s$). Therefore statistics is not expected to be a serious problem even with exotic and radioactive systems. However, one should note that systematic effects must be expected the more severe limitations and therefore they need to be in the center of the attention.

3.2 Searches for EDMs in charged Particles

A very novel idea was introduced recently for measuring an EDM of charged particles directly. For such experiments the high motional electric field is exploited, which charged particles at relativistic speed experience in a magnetic storage ring. In such a setup the Schiff theorem can be circumvented (which had excluded charged particles from experiments due to the Lorentz force acceleration), because of the non-trivial geometry of the problem [14]. With an additional radial electric field in the storage region the spin precession due to the magnetic moment anomaly can be compensated, if the effective magnetic anomaly a_{eff} is small, i.e. $a_{eff} << 1$ [38].

The method was first considered for muons. For longitudinally polarized muons injected into the ring an EDM would express itself as a spin rotation out of the orbital plane. This can be observed as a time dependent (to first order linear in time) change of the above/below the plane of orbit counting rate ratio. For the possible muon beams at the future J-PARC facility in Japan a sensitivity of 10^{-24} e cm is expected [30, 39]. Other than for most other EDM searches, in such an experiment the possible muon flux is a major limitation. For models with nonlinear mass scaling of EDM's such a muon EDM experiment would already be more sensitive to some certain new physics models than the present limit on the electron EDM [40]. For certain Left-Right symmetric models a value of d_μ up to 5×10^{-23} e cm would be possible. An experiment carried out at a more intense muon source could provide a significantly more sensitive probe to CP violation in the second generation of particles without strangeness. [2]

[2] A New Physics (non-SM) contribution a_μ^{NP} to the muon magnetic anomaly and a muon EDM d_μ are real and imaginary part of a single complex quantity related through $d_\mu = 3 \times 10^{-22} \times (a_\mu^{NP}/(3 \times 10^{-9})) \times \tan\Phi_{CP} e\,cm$ with a yet unknown CP violating phase Φ_{CP}. The problems around the SM model value for a_μ [41], which cause difficulties for the interpretation of the recent muon g-2 experiment in terms of limits for or indications of New Physics, make a search for d_μ attractive as an important alternative, as the SM value is negligible for the foreseeable future.

The deuteron is the simplest known nucleus. Here an EDM could arise not only from a proton or a neutron EDM, but also from CP-odd nuclear forces [42]. It was shown very recently [31] that the deuteron can be in certain scenarios significantly more sensitive than the neutron . The situation is evident for the case of quark chromo-EDMs, where the EDMs induced into deuteron and neutron are $d_{\mathcal{D}} = -4.67\, d_d^c + 5.22\, d_u^c$ and $d_n = -0.01\, d_d^c + 0.49\, d_u^c$; i.e. the deutron could have a much higher sensitivity to quark chromo-EDMs arising from the proton-neutron interaction within the deuteron. It should be noted that because of its rather small magnetic anomaly the deuteron is a particularly interesting candidate for a ring EDM experiment and a proposal with a sensitivity of 10^{-27} e cm exists [43]. In this case scattering off a target will be used to observe a spin precession. As possible sites of an experiment the Brookhaven National Laboratory (BNL), and KVI are considered. A further novel approach concerns the search for an electron EDM in charged molecular ions such as HfF^+ and ThF^+ where the advantage of easy trapping for ions and the strong enhancement factors for electron EDMs in polar molecules are combined [44]. The EDM experiments directly using charged particles are still in the exploratory and feasibility study phase, however, the progress reports are very encouraging.

4 T-violation Searches other than EDMs

There are many more possibilities to find T-violation besides through searches for EDMs. Among the presently ongoing activities certain correlation observables in nuclear β-decays offer excellent opportunities to find new sources of CP violation [16, 17, 45, 46]. In β-neutrino correlations the 'D'-coefficient [45] (for spin polarized nuclei) offer a high potential to observe new interactions in a region of potential New Physics which is less accessible by EDM searches. However, the 'R'-coefficient [45] (observation of β-particle polarization) would explore the same areas as present EDM searches or β-decay asymmetry measurements. Such experiments are underway at a number of laboratories worldwide [46].

5 Conclusions

There is a large field of searches for EDMs on a variety of systems. They all are well motivated and have unique and robust discovery potentials. Novel ideas have emerged in the recent past to use yet not studied systems and new experimental approaches, which have emerged in the recent past offer excellent opportunities to complement the more traditional experimental approaches on neutron-, atom- and electron-EDMs. Any successful search in the future will have to be complemented by experiments on other systems in order to pin down eventually the mechanisms leading to the observed

EDMs. The highest predicted values in beyond SM speculative theories are well within reach of presently ongoing and planned experiments.

This work has been supported by the Dutch Stichting voor Fundamenteel Onderzoek der Materie (FOM) in the framework of the research programme 48 (TRIμP).[3]

Bibliography

[1] W.-M. Yao et al., Journal of Physics **G 33**, 1 (2006)

[2] T.D. Lee and C.N. Yang, Phys. Rev. **98**, 1501 (1955)

[3] I.B. Khriplovich and S.K. Lamoreaux, "CP Violation Without Strangeness", Springer, Berlin (1997)

[4] A. Czarnecki and W. Marciano, Int.J.Mod.Phys. **A13**, 2235 (1998)

[5] W.C. Haxton and C.E. Wieman, Ann.Rev.Nucl.Part.Sci. **21**, 261 (2001); see also: J. Sapirstein and K.T. Cheng, physics/0409147 (2004) and refrences therein.

[6] D. Armstrong et al, Eur.Phys.J. **A24S2**, 155 (2005)

[7] S.N. Atutov et al., Hyperfine Interactions **146-147**, 83 (2003)

[8] E. Gomez et al., physics/0412073 (2004)

[9] N. Fortson, in: "Parity Violation in Atoms and Polarized Electron Scattering", B. and M.Bouchiat (eds.), World Scientific, Singapore, p. 244 (1999)

[10] J. Sapirstein and K.T. Cheng, physics/0409147 (2004)

[11] J.W. Cronin, Rev.Mod.Phys. **53**, 373 (1981); M. Neubert, Int.J.Mod. Phys. **A11**, 4173 (1996); O. Long, hep-ex/0412047 (2004)

[12] A. Sakharov,JETP **5**, 32 (1967); M. Trodden, Rev.Mod.Phys. **71**, 1463 (1999)

[13] O. Bertolami et al., Phys.Lett. **B395** 178 (1996)

[14] P.G.H. Sandars, Contemp. Phys. **42**, 97 (2001)

[15] Y. Semertzidis, Proceedings SIGHAD03 Workshop, Pisa, Italy, hep-ex/0401016 (2004)

[3] This conference review of recent developments in the field of EDM searches draws significantly on earlier write-ups [18, 46].

[16] K. Jungmann et al., in: "NuPECC Long Range Plan 2004", M.N. Harakeh et al. (eds.), (2004)

[17] T. Akesson et al., hep-ph/0609216 (2006)

[18] K. Jungmann, physics/0501154 (2005)

[19] M.G. Kozlov and D. DeMille, Phys.Rev.Lett. **89**, 133001 (2002); D. Kawall et al., Phys.Rev.Lett.**92**, 13307 (2004)

[20] A. Yoshimi et al., Hyperfine Interactions **159**, 401 (2005)

[21] B.C. Regan et. al., Phys. Rev. Lett., **88**, 071805 (2002)

[22] R. McNabb et al., hep-ex/0407008 (2004)

[23] K. Inami et. al., Phys. Lett. B, **551**, 16 (2002)

[24] C.A. Baker et. al., Phys. Rev. Lett, **97**, 131801 (2006)

[25] D. Cho et. al., Phys. Rev. Lett., **63**, 2559 (1989)

[26] L. Pondrom et. al., Phys. Rev. D, **23**, 814 (1981)

[27] F. del Aguila and M. Sher, Phys. Lett. B, **252**, 116 (1990)

[28] R. Escribano and E. Masso, Phys. Lett. B, **395**, 369 (1997)

[29] M. Romalis, W. Griffith and N. Fortson,Phys.Rev.Lett. **86**, 2505 (2001)

[30] F.J.M. Farley et al., Phys. Rev. Lett. **93**, 052001 (2004)

[31] C.P Liu and R.G.E. Timmermans, Phys.Rev.C **70**, 055501(2004); see also: O. Lebedev et al., Phys. Rev. D **70**, 016003 (2004)

[32] V. Dzuba et al., Phys. Rev. A **63**, 062101 (2001)

[33] J. Engel, this volume; J. Engel et al.,Phys. Rev. **C 68**, 025501 (2003)

[34] K. Jungmann, Acta Phys. Pol., **33** 2049 (2002)

[35] J.R. Guest et al., Phys.Rev.Lett. **98** , 093001 (2007)

[36] E. Traykov et al., Nucl.Instrum.Meth. **A572**, 580 (2007); G.P. Berg G.P. Berg et al., Nucl.Instrum.Meth. **A560**, 169 (2006)

[37] L. Willmann et al., physics/0602022 (2006)

[38] I.B. Khriplovich, Phys.Lett. **B444**, 98 (1998)

[39] Y. Semertzidis et al., J-PARC Letter of Intent L22 (2003)

[40] K.S. Babu, B. Dutta and R. Mohapatra, Phys.Rev.Lett. **85** 5064 (2000); B. Dutta and R. Mohapatra, Phys. Rev. **D68** (2003) 113008

[41] G.W. Bennett et al., Phys. Rev. **D 73**, 072003 (2006) G.W. Bennett et al., Phys. Rev. Lett.**92**, 168102 (2004) see also: Phys. Rev. Lett. **89**,101804 (2002) and H.N. Brown et al., Phys.Rev.Lett.**86**, 2227 (2001)

[42] J. Hisano, hep-ph/0410038 (2004)

[43] Y. Semertzidis et al., AIP Conf. Proc. **698**, 200 (2004); see also: Y.F. Orlov et al., Phys.Rev.Lett. **96**, 214802 (2006)

[44] L. Sinclair et al., APS AMO March Meeting 2007, N32.00001 (2007); E. Cornell, at Lepton Moments III International Symposium, Cape Cod (2007)

[45] P. Herczeg, Prog. Part. and Nucl. Phys. **46**, 413 (2001); N. Severijns et al., Rev. Mod. Phys. **78**, 991 (2006)

[46] K. Jungmann, Nucl.Phys.**A751**, 87 (2005) and K. Jungmann, Eur.Phys.J.**A25**, 677 (2005)

CKM

CKM

New evaluation of CKM Matrix and Unitarity Triangle parameters

Achille Stocchi
Laboratoire de l'Accélérateur Linéaire,
IN2P3-CNRS et Université de Paris-Sud,
Orsay Cedex, France
on behalf of the **UT***fit Coll.* [1]

1 Introduction

The analysis of the Unitarity Triangle (UT) is one of the key places where the flavour sector of the Standard Model (SM) can be tested with great precision, hence it provides a powerful and maybe unique opportunity to look for sizeable effects beyond the SM. In fact, the successes of the B factories - even well beyond the original expectations - and recently of the Tevatron in the B_s^0 sector, have provided the UT analysis with a rich set of measurements, thus allowing for a precise determination of the parameters of the Cabibbo-Kobayashi-Maskawa (CKM) matrix and, more importantly, for non trivial checks of the internal consistency of the SM flavour picture.

In this paper we will start showing the present knowledge of the Unitarity Triangle fit in the Standard Model and we will continue presenting the status of the Unitarity Triangle analysis beyond the Standard Model using a model independent parametrization of the New Physics effects in $|\Delta F| = 2$ processes. For these analyses we make use of the most recent determinations of theoretical and experimental parameters (updated to Summer 2006). The results and the plots presented in this paper can be found at the URL http://www.utfit.org, where they are continuously updated.

2 Unitarity Triangle in the Standard Model

Before the B factories came into play, UT fits were performed by only using measurements of the sides and of the indirect CP violation parameter ϵ_K of neutral Kaon system. The B factories in few years of measurements completely changed the scenario by providing determinations of all the UT angles, in particular the long awaited

[1] M. Bona, M. Ciuchini, E. Franco, V. Lubicz, G. Martinelli, F. Parodi, M. Pierini, P. Roudeau, C. Schiavi, L. Silvestrini, V. Sordini, A. Stocchi, V. Vagnoni

β from $b \to c\bar{c}s$ modes, but also - quite unexpectedly since the penguin pollution in the $B^0 \to \pi^+\pi^-$ decay mode became evident - the α angle. Even more surprisingly, the B factories have been able to close the circuit by providing measurements of the γ angle, even if with large errors so far.

Here below we briefly describe the most relevant measurements entering our SM UT fit:

- The rates of charmed and charmless semileptonic B decays which allow to measure the ratio $|V_{ub}| \,/\, |V_{cb}|$.
- The mass difference between the light and heavy mass eigenstates of the $B^0 - \overline{B}^0$ system Δm_d.
- The mass difference of the $B_s^0 - \overline{B}_s^0$ system Δm_s, compared to Δm_d, $\Delta m_d / \Delta m_s$.
- The ε_K parameter, which measures CP violation in the neutral kaon system.
- β from $b \to c\bar{c}s$ modes and from $B^0 \to D^0\pi^0$.
- The angle α, that can be obtained from the $B \to \pi\pi$ and $B \to \rho\rho$ decays, assuming the SU(2) flavour symmetry and neglecting the contributions of electroweak penguins. It can also be obtained using a time-dependent analysis of $B \to (\rho\pi)^0$ decays on the Dalitz plane. The combination of the BaBar and Belle results including all the three methods gives already a quite precise measurement; just restricting to the SM solution, we get $\alpha = (92 \pm 7)^\circ$ at 68% probability.
- The angle γ that can be extracted from the tree-level decays $B \to DK$, using the fact that a charged B can decay into a $D^0(\overline{D}^0)K$ final state via a $V_{cb}(V_{ub})$ mediated process. CP violation occurs if the D^0 and the $\overline{D}^0$ decay to the same final state. The same argument can be applied to $B \to D^*K$ and $B \to DK^*$ decays. Three methods have been proposed: the Gronau-London-Wyler method (GLW), which consists in reconstructing the neutral D meson in a CP eigenstate: $B^\pm \to D^0_{CP^\pm}K^\pm$, the Atwood-Dunietz-Soni method (ADS), which consists in forcing the $\overline{D}^0$ (D^0) meson, coming from the Cabibbo-suppressed (Cabibbo-allowed) $b \to u$ ($b \to c$) transition to decay into the Cabibbo-allowed (Cabibbo-suppressed) $K\pi$ final state - thus looking at the interference between two amplitudes of similar size; the Dalitz method, consisting in studying the interference between the $b \to u$ and the $b \to c$ transitions using the Dalitz plot of D mesons reconstructed into three-body final states (such as $D^0 \to K_s\pi^-\pi^+$). The advantage of this last method is that the full sub-resonance structure of the three-body decay is considered, including interferences such as those used for GLW and ADS methods plus additional interferences due to the overlap

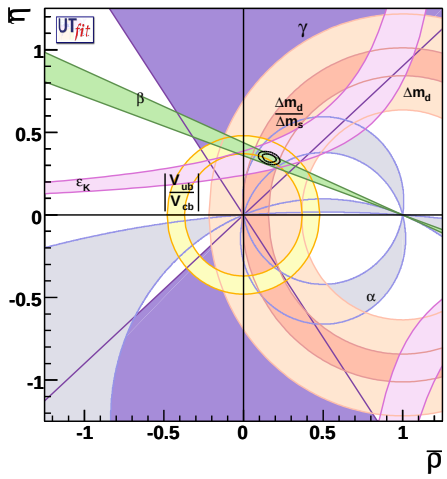

Figure 1: Determination of $\overline{\rho}$ and $\overline{\eta}$ from constraints on $|V_{ub}|\,/\,|V_{cb}|$, Δm_d, Δm_s, ε_K, β, γ, and α. 68% and 95% total probability contours are shown, together with 95% probability regions from the individual constraints.

between broad resonances in some regions of the Dalitz plot. The combination of the BaBar and Belle analyses, including all the three methods, yields the two-fold result $\gamma = (82 \pm 19)^\circ \cup (-98 \pm 19)^\circ$ at 68% probability.

For more details on the SM analysis see [1] (for similar work see [2]). In Tab. 1 we summarize the values of the relevant input parameters used in the SM fit, as well as the output of the fit including all the constraints. A graphical view of the fit result in the $(\overline{\rho}, \overline{\eta})$ plane is shown in Fig. 1. From the plot it is clearly visible how impressive the success of the CKM picture is in describing CP violation in the SM: all the various measurements do agree in constraining the apex of the UT at an astonishing level. However, by looking in more detail at Fig. 1, it is interesting to note that the 95% probability regions depicted by the $\sin 2\beta$ and $|V_{ub}|\,/\,|V_{cb}|$ constraints, two of the most precise ones used in the fit, show just a bare agreement. In particular, in our analysis we find that while the experimental value of $\sin 2\beta$ is in good agreement with the rest of the fit, the same does not hold for $|V_{ub}|\,/\,|V_{cb}|$, which is rather on the high side. It can be shown that this is due to a large value of the inclusive determination of $|V_{ub}|$. Unless this discrepancy should be considered as a hint of NP, it has to be explained by the uncertainties of the theoretical approaches needed to determine $|V_{ub}|$ [3].

Parameter	Value	Gaussian (σ)	Uniform (half-width)
λ	0.2258	0.0014	-
$\|V_{cb}\|$(excl.)	41.3×10^{-3}	1.0×10^{-3}	1.8×10^{-3}
$\|V_{cb}\|$(incl.)	41.6×10^{-3}	0.7×10^{-3}	-
$\|V_{ub}\|$(excl.)	35.0×10^{-4}	4.0×10^{-4}	-
$\|V_{ub}\|$(incl.)	44.9×10^{-4}	3.3×10^{-4}	-
Δm_d	0.507 ps^{-1}	0.005 ps^{-1}	-
Δm_s	17.77 ps^{-1}	0.12 ps^{-1}	-
$f_{B_s}\sqrt{\hat{B}_{B_s}}$	262 MeV	35 MeV	-
$\xi = \frac{f_{B_s}\sqrt{\hat{B}_{B_s}}}{f_{B_d}\sqrt{\hat{B}_{B_d}}}$	1.23	0.06	-
$\hat{B}_K$	0.79	0.04	0.08
ε_K	2.280×10^{-3}	0.013×10^{-3}	-
f_K	0.160 GeV		fixed
Δm_K	0.5301 $\times 10^{-2}$ ps^{-1}		fixed
$\sin 2\beta$	0.675	0.026	-
$\overline{m}_t$	163.8 GeV	3.2 GeV	-
$\overline{m}_b$	4.21 GeV	0.08 GeV	-
$\overline{m}_c$	1.3 GeV	0.1 GeV	-

Parameter	Output	Parameter	Output
$\overline{\rho}$	0.163 ± 0.028	$\overline{\eta}$	0.344 ± 0.016
$\alpha[^\circ]$	92.7 ± 4.2	$\beta[^\circ]$	22.2 ± 0.9
$\gamma[^\circ]$	64.6 ± 4.2	Δm_s [ps^{-1}]	17.77 ± 0.12
$\sin 2\beta$	0.701 ± 0.022	Imλ_t [10^{-5}]	13.8 ± 0.7
$V_{ub}[10^{-3}]$	3.68 ± 0.14	$V_{cb}[10^{-2}]$	4.16 ± 0.06
$V_{td}[10^{-3}]$	8.50 ± 0.27	$\|V_{td}/V_{ts}\|$	0.208 ± 0.007
R_b	0.381 ± 0.014	R_t	0.904 ± 0.028

Table 1: Top: values of the relevant inputs used in the SM UT fit. The inputs from the α and γ measurements are not shown since we make use of the experimental likelihoods (see text). Bottom: SM UT fit results.

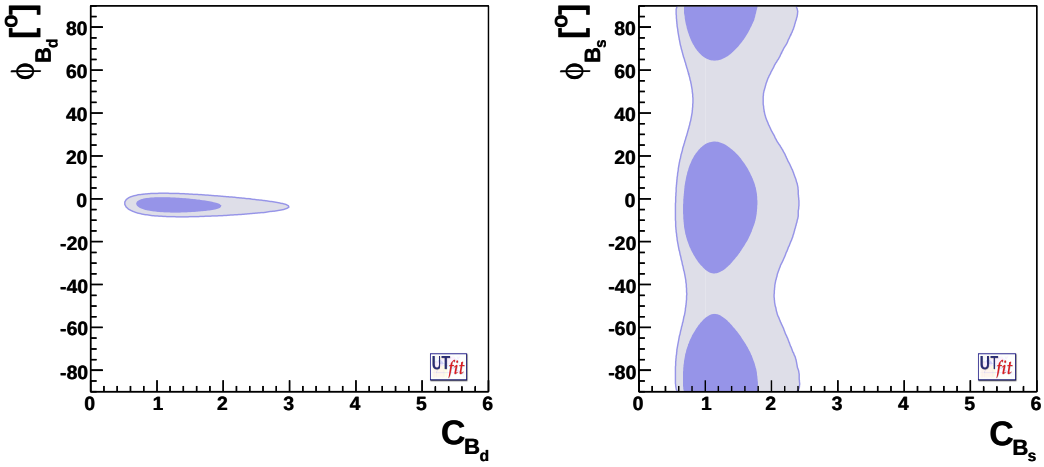

Figure 2: Bounds on the $C_{B_q} - \phi_{B_q}$ planes, from the NP generalized UT fit: 68% and 95% probability regions.

3 New Physics Analysis

Since the mixing processes are described by a single amplitude, they can be parameterized without loss of generality in terms of two parameters quantifying the difference of the amplitude with respect to the SM one. In the case of $B_q^0 - \overline{B}_q^0$ mixing we define

$$C_{B_q}\, e^{2i\phi_{B_q}} = \frac{\langle B_q^0 | H_{\rm eff}^{\rm full} | \overline{B}_q^0 \rangle}{\langle B_q^0 | H_{\rm eff}^{\rm SM} | \overline{B}_q^0 \rangle}\,, \qquad (q = d, s)$$

where $H_{\rm eff}^{\rm SM}$ includes only the SM box diagrams, while $H_{\rm eff}^{\rm full}$ includes also the NP contributions. In the absence of NP, we have that $C_{B_q} = 1$ and $\phi_{B_q} = 0$. The experimental quantities determined from the $B_q^0 - \overline{B}_q^0$ mixings are related to their SM counterparts and the NP parameters by the following relations:

$$\Delta m_q^{\rm exp} = C_{B_q} \Delta m_q^{\rm SM}\,,\ \beta^{\rm exp} = \beta^{\rm SM} + \phi_{B_d}\,,$$
$$\alpha^{\rm exp} = \alpha^{\rm SM} - \phi_{B_d}\,,\ \beta_s^{\rm exp} = \beta_s^{\rm SM} - \phi_{B_s}.$$

For the $K^0 - \overline{K}^0$ mixing is instead convenient to introduce a single parameter:

$$C_{\epsilon_K} = \frac{{\rm Im}[\langle K^0 | H_{\rm eff}^{\rm full} | \overline{K}^0 \rangle]}{{\rm Im}[\langle K^0 | H_{\rm eff}^{\rm SM} | \overline{K}^0 \rangle]}\,,$$

which implies the following relation for the measured value of ε_K:

$$\varepsilon_K^{\rm exp} = C_{\epsilon_K}\, \varepsilon_K^{\rm SM}.$$

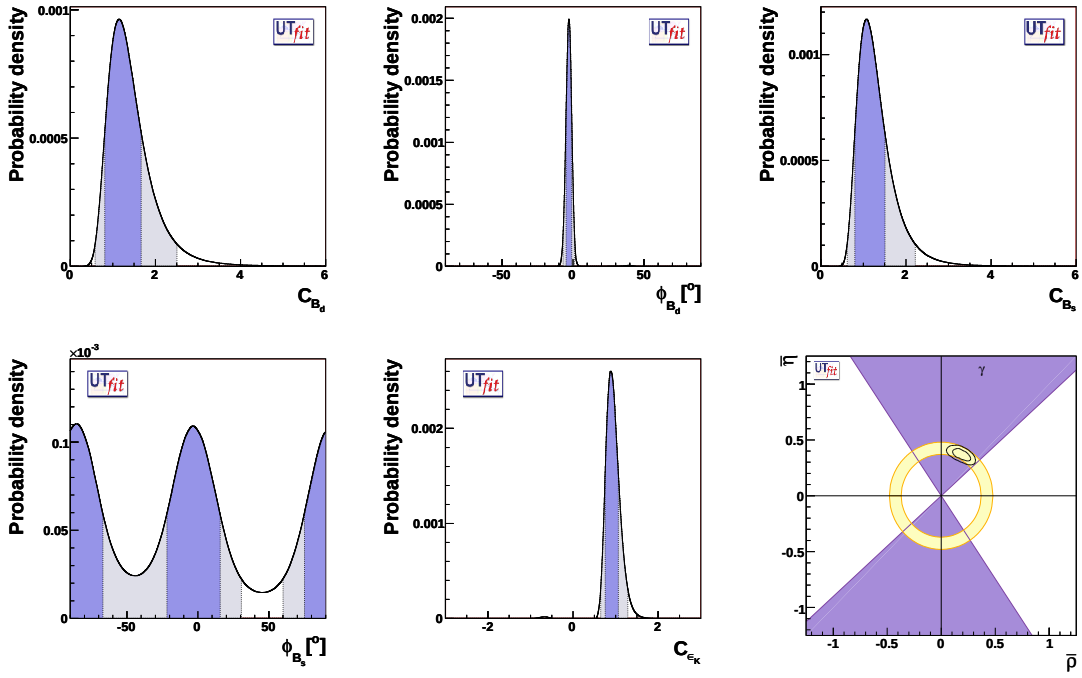

Figure 3: 1D distributions showing the constraints on ϕ_{B_q}, C_{B_q} and C_{ϵ_K} coming from the NP generalized analysis. The bottom-right plot shows instead the 68% and 95% confidence contours in the $\overline{\rho} - \overline{\eta}$ plane as resulting from the NP generalized fit, superimposed to the 95% confidence regions determined by the $|V_{ub}|/|V_{cb}|$ and γ constraints only.

Δm_K is not considered since the long distance effects are not well under control. With these definitions, NP effects which enter the present analysis are parameterized in terms of 5 real quantities: C_{B_d}, ϕ_{B_d}, C_{B_s}, ϕ_{B_s} and C_{ϵ_K}.

The results of the fit are summarized in Tab. 2. For more details on the NP analysis see [4]. For other recent works on the same subject see [5]. The bounds on the two ϕ_B vs C_B planes are given in Fig. 2. The distributions for C_{B_q}, ϕ_{B_q} and C_{ϵ_K} are shown in Fig. 3, and in the same figure also the fit result in the $\overline{\rho} - \overline{\eta}$ plane is depicted. We see that the *non-standard* solution for the UT with its vertex in the third quadrant, which was present in previous analyses, is now absent thanks to the improved value of $A_{\rm SL}$ by the BaBar Collaboration [6] and to the measurement of $A_{\rm CH}$ by the D0 Collaboration [7]. Furthermore, the measurement of Δm_s strongly constrains C_{B_s}, so that it is already known better than C_{B_d}. Finally, A_{CH} and $\Delta\Gamma_s$ provide the first relevant constraints on ϕ_{B_s}.

Parameter	Output	Parameter	Output	Parameter	Output
C_{B_d}	1.24 ± 0.43	$\phi_{B_d}[^\circ]$	-3.0 ± 2.0	C_{B_s}	1.15 ± 0.36
$\phi_{B_s}[^\circ]$	$(-3 \pm 19) \cup (94 \pm 19)$	C_{ϵ_K}	0.91 ± 0.15		
$\overline{\rho}$	0.87 ± 0.056	$\overline{\eta}$	0.370 ± 0.036	$\alpha[^\circ]$	92 ± 9
$\beta[^\circ]$	24.4 ± 1.8	$\gamma[^\circ]$	63 ± 8	$\mathrm{Im}\lambda_t[10^{-5}]$	14.8 ± 1.4
$V_{ub}[10^{-3}]$	4.00 ± 0.24	$V_{cb}[10^{-2}]$	4.15 ± 0.07	$V_{td}[10^{-3}]$	8.39 ± 0.59
$\lvert V_{td}/V_{ts}\rvert$	0.205 ± 0.015	R_b	0.416 ± 0.026	R_t	0.896 ± 0.061
$\sin 2\beta$	0.752 ± 0.040	$\sin 2\beta_s$	0.039 ± 0.004		

Parameter	Output	Parameter	Output	Parameter	Output
$\overline{\rho}$	0.153 ± 0.030	$\overline{\eta}$	0.347 ± 0.018	$\alpha[^\circ]$	91.3 ± 4.8
$\beta[^\circ]$	22.3 ± 0.9	$\gamma[^\circ]$	66.3 ± 4.8	$\sin 2\beta_s$	0.037 ± 0.002

Table 2: Top: determination of UT and NP parameters from the NP generalized fit. Bottom: determination of UUT parameters from the constraints on α, β, γ, $|V_{ub}/V_{cb}|$, and $\Delta m_d/\Delta m_s$ (UUT fit).

4 Universal Unitarity Triangle

In the context of Minimal Flavour Violation (MFV) extensions of the SM [8, 9], it is possible to use the so called Universal Unitarity Triangle (UUT) construction in order to determine the parameters of the CKM matrix independently of NP effects [10]. For this purpose one has to use all the constraints from tree-level processes and from the angle measurements, as well as the $\Delta m_d/\Delta m_s$ ratio, which in MFV scenarios are NP-free. Instead, ϵ_K, Δm_d and Δm_s may receive NP contributions, because of the shifts δS_0^K and δS_0^B of the Inami-Lim functions in the K-$\overline{K}$ and $B_{d,s}$-$\overline{B}_{d,s}$ mixings. With only one Higgs doublet or at small $\tan\beta$ these two contributions are forced to be equal. Instead, for large $\tan\beta$, the two quantities are in general different. In both cases, one can use the output of the UUT given in Tab. 2 and graphically represented in Fig. 4 to constrain $\delta S_0^{K,B}$. We get $\delta S_0 = \delta S_0^K = \delta S_0^B = -0.16 \pm 0.32$ for small $\tan\beta$, while for large $\tan\beta$ we obtain $\delta S_0^B = 0.05 \pm 0.67$ and $\delta S_0^K = -0.18 \pm 0.37$. These bounds can be translated into lower bounds on the MFV scale [11]: $\Lambda > 5.5$ TeV at 95% probability for small $\tan\beta$ and $\Lambda > 5.1$ TeV at 95% probability for large $\tan\beta$.

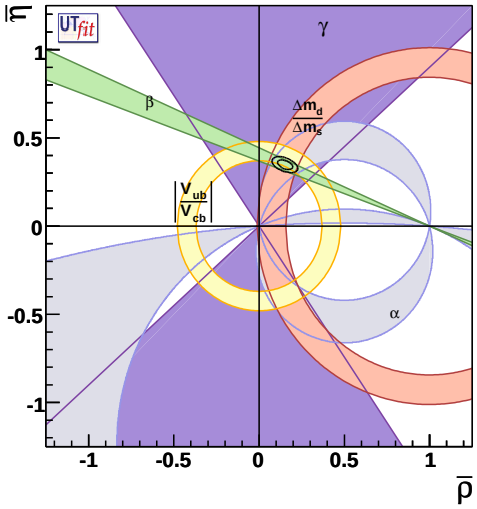

Figure 4: Determination of $\overline{\rho}$ and $\overline{\eta}$ from the constraints on α, β, γ, $|V_{ub}/V_{cb}|$, and $\Delta m_d/\Delta m_s$ (UUT fit).

5 Conclusions

In this paper we have presented updated analyses of the Unitarity Triangle in the Standard Model and beyond, using all the relevant measurements available from the B factories and the Tevatron. Despite the great number of measurements employed in the fit, and the remarkable precision achieved with some of them, the SM is still showing an impressive degree of consistency.

We have performed an analysis with a model-independent approach able to describe general extensions of the SM with loop-mediated contributions to FCNC processes. We have shown how the redundant set of measurements nowadays available allow for a simultaneous determination of the CKM parameters, together with the NP contributions to $|\Delta F| = 2$ processes in the K^0, B^0 and B_s^0 sectors.

Furthermore, we have performed a Universal Unitarity Triangle analysis, showing that it is possible to constrain the UUT parameters with excellent accuracy. In this way, we have been able to put limits on new scale in Minimal Flavour Violation scenarios, in the large and small $\tan\beta$ scenarios, up to about 5-6 TeV.

Bibliography

[1] M. Bona *et al.* [UTfit Collaboration], JHEP **0507**, 028 (2005), [arXiv:hep-ph/0501199]; M. Ciuchini *et al.*, JHEP **0107** (2001) 013 [arXiv:hep-ph/0012308].

[2] J. Charles *et al.*, Eur. Phys. J. C **41** (2005) 1 [hep-ph/0406184]; updates at http://ckmfitter.in2p3.fr/.

[3] M. Bona *et al.* [UTfit Collaboration], [arXiv:hep-ph/0606167].

[4] M. Bona *et al.* [UTfit Collaboration], JHEP **0603**, 080 (2006), [arXiv:hep-ph/0509219];

[5] Z. Ligeti, M. Papucci and G. Perez, Phys. Rev. Lett. **97** (2006) 101801 [arXiv:hep-ph/0604112]; Y. Grossman, Y. Nir and G. Raz, arXiv:hep-ph/0605028; F. J. Botella, G. C. Branco and M. Nebot, arXiv:hep-ph/0608100.

[6] B. Aubert *et al.* [BABAR Collaboration], Phys. Rev. Lett. **96** (2006) 251802 [arXiv:hep-ex/0603053].

[7] D0 Collaboration, D0 Conference note 5189; see also G. Borissov, "D0 results on CP violation phase in B_s system". ICHEP06, Moscow (Russia)

[8] M. Blanke *et al.*, arXiv:hep-ph/0604057.

[9] G. Isidori and P. Paradisi, arXiv:hep-ph/0605012.

[10] A. J. Buras *et al.*, Phys. Lett. B **500**, 161 (2001) [arXiv:hep-ph/0007085].

[11] G. D'Ambrosio *et al.*, Nucl. Phys. B **645**, 155 (2002) [arXiv:hep-ph/0207036].

Recent results on V_{us} from KLOE, KTeV and NA48

Venelin Kozhuharov
Atomic Physics Department,
Faculty of Physics, University of Sofia
5 J. Bourchier Str., Sofia, BULGARIA [1]

1 Introduction

The flavour structure in the quark sector of the Standard Model is described by the CKM matrix [1], [2]. Its unitarity leads to a number of relations for its elements and in particular for the first raw:

$$|V_{ud}|^2 + |V_{us}|^2 + |V_{ub}|^2 = 1 \tag{1}$$

Since $V_{ub} \cong 4 \times 10^{-3}$ the contribution of the last term could be neglected at the current level of uncertainty in V_{ud} and V_{us}. This approximation gives $V_{us} = \sin\theta_c$ as originally suggested by Cabibbo.

The most precise value of V_{ud} comes from the super-allowed $0^+ \rightarrow 0^+$ beta transitions between nuclei and V_{us} is usually calculated from the branchings of the kaon semileptonic decays. Going back to PDG 2004 [3] $V_{us} = 0.2195 \pm 0.0025$ and $V_{ud} = 0.9738 \pm 0.0005$ giving a deviation from unitarity at the level of 2.3σ where the contribution from the uncertainties of V_{ud} and V_{us} in the final error are almost equal.

In the last few years a significant progress in the kaon physics has been made by three experiments - KLOE, KTeV and NA48. The reflection of their results to the extraction of V_{us} is subject of this review.

KTeV at the Main Injector (Fermilab) [5] and NA48 at SPS (CERN) [6] are fixed target experiments and exploit similar techniques of kaon decays in flight. Both consist of a spectrometer system measuring the charged particles momentum and a calorimetry system used for measurement of the energy of photons and electrons. The calorimetry system also provides a way to distinguish between the different type of charged particles through their interactions with matter. A muon veto system is placed at the end of each detector complex. The primary purpose of both experiments

[1] Also JINR Dubna, 141980, Dubna, Moscow Region, RUSSIA

was to measure the direct CP violation parameter ϵ'/ϵ in the neutral kaon system [4]. In 2003 NA48 modified its setup in order to study charged kaon decays.

KLOE experiment [7] is situated at $DA\Phi NE$, the Frascati ϕ factory, where e^-e^- beams collide with a center of mass energy at the ϕ meson mass (1020 MeV). With a probability of $\approx 83\%$ ϕ decays into neutral or charged kaons, anticolinear in the ϕ center of mass (almost true also in the laboratory system). The presence of $K_{L/S}$ ($K^{\pm}$) tags $K_{S/L}$ ($K^{\mp}$). KLOE detector has 2π symmetry, the momentum of the decay products is measured by a magnetic spectrometer which is followed by an elecromagnetic calorimeter.

2 Kaon semileptonic decays

Within the Standard Model $K \to \pi l \nu$ (so called $Kl3$) decay appear as a tree level process of $s \to u$ transition. The inclusive branching ratios of all four modes (K^0e3, $K^0\mu3$, $K^{\pm}e3$ and $K^{\pm}\mu3$) could be written conveniently in the form

$$Br(K_{l3(\gamma)}) = \frac{G_F^2 M_K^5 S_{EW}}{128\pi^3/\tau_K} I_K C^2 (1+\delta_{EM}^I) \times |V_{us} f_+^{K\pi}(0)|^2 \tag{2}$$

where G_F is the Fermi constant, M_K and τ_K are the corresponding kaon mass and lifetime, S_{EW} is the the short distance electroweak enhancement factor, $S_{EW} \cong 1 + \frac{2\alpha}{\pi}(1-\frac{\alpha_s}{4\pi}) \times log\frac{M_Z}{M_\rho} = 1.023$ [8], C is the Klebsh-Gordon coefficient , $C = 1$ for K^0 and $C = \sqrt{\frac{1}{2}}$ for $K^{\pm}$, δ_{EM}^I represents the long-distance electromagnetic correction [9,10], $f_+^{K\pi}(0)$ is the value of the vector form-factor at zero transferred momentum and I_K is the phase space integral dependent on the mode and the shape of the form-factor.

The values of S_{EW}, δ_{EM}^I and $f_+^{K\pi}(0)$ are calculated theoretically while the rest could be obtained from experimental measurements.

2.1 Form factors

The kaon form factors are defined as [11]

$$\langle \pi(q)| s\gamma_\mu u |K(p)\rangle = f_+^{K\pi}(t) \times (p+q) + f_-^{K\pi}(t) \times (p-q) \tag{3}$$

where $t = (p-q)^2$ is the transferred momentum. Instead of the couple f_+, f_- usually another set of form-factors is used $f_+(t)$ and $f_0(t) = f_+(t) + \frac{t}{M_K^2 - M_\pi^2} f_-(t)$ inspired by the VMD model. The dependence of the transferred momentum could be written as

$$f_{+,0}^{K\pi}(t) = f_+^{K\pi}(0)(1+\delta f_{+,0}(t)) \tag{4}$$

It is convenient to express the charged kaon form factor by the neutral one $|f_+^{K^+\pi^0}(0)|^2 = (1+\delta_{SU2}) \times |f_+^{K^0\pi^-}(0)|^2$. The SU2 breaking parameter is obtained within the Chiral

Perturbation Theory, $\delta_{SU2} = 0.046 \pm 0.004$ [9, 12]. $f_+(0)$ was calculated for the first time in the 80s [12]

$$f_+(0) = 0.961 \pm 0.008. \tag{5}$$

However more recent analysis give higher values $f_+(0) = (0.981 \pm 0.012)$ [10]. Another result $f_+(0) = (0.960 \pm 0.009)$ comes from lattice QCD [13] which is consistent with (5). Since $f_+(0)$ enters directly in the calculation of V_{us} a clarification of this problem is highly desirable. In this review (5) is used.

The term $\delta f_{+,0}(t)$ enters in the phase space integral calculation and is subject to different parametrization. The Taylor expansion gives

$$\delta f_{+,0}(t) = \lambda'_{+,0}\frac{t}{M_\pi^2} + \frac{1}{2}\lambda_{+,0}"\frac{t^2}{M_\pi^4}. \tag{6}$$

while within the VMD model $f_{+,0}$ correspond to vector or scalar meson exchange and are parametrized by the mass of the pole:

$$\delta f_{+,0}(t) = \frac{M_{V,S}^2}{M_{V,S}^2 - t} - 1 \tag{7}$$

In both cases the unknown parameters are determined experimentally. If in equation (6) the quadratic term is neglected then the shape of the form factor is given only by its slope λ_+. The three collaborations have studied the form factors in the case of $K_L \to \pi^0 e\nu$ decays and the results can be summarized in the following table:

	λ'_+	$\lambda_+"$	λ_+	Pole mass
NA48 [14]	0.0280 ± 0.0024	0.0004 ± 0.0009	0.0288 ± 0.0012	859 ± 18
KTeV [15]	0.0217 ± 0.0020	0.0029 ± 0.0008	0.0283 ± 0.0006	881 ± 7.1
KLOE [16]	0.0255 ± 0.0018	0.0014 ± 0.0008	0.0286 ± 0.0006	870 ± 9.2

The values agree in the case of linear and pole parametrization but there is a discrepancy for the necessity of a quadratic term in (6). Recently the KTeV collaboration has performed a new calculation of the phase space integral with a reduced model uncertainty, $I_{K0e3} = 0.10262 \pm 0.00032$ [17]. For the rest of the phase-space integrals we use $I_{K0\mu3} = 0.06777 \pm 0.00053$ with the KTeV quadratic form factor parametrization, $I_{K^\pm e3} = 0.1060 \pm 0.0008$ and $I_{K^\pm\mu3} = 0.0702 \pm 0.0005$ with the ISTRA+ measurement of the form factors [18]. A 0.7% error is added to account for the difference between the quadratic and the pole parametrization of the form-factors.

2.2 Kaon lifetime

During the last year two new measurements of the K_L lifetime have been published by KLOE. One of them is obtained from the the proper time distribution of $K_L \to 3\pi^0$

decays [19], giving $\tau_{KL} = (50.92 \pm 0.30)ns$. The second method produces a result for the lifetime as a byproduct of the measurement of the major K_L branching fraction imposing the condition that their sum should be unity [20]. The result is $\tau_{KL} = (50.72 \pm 0.37)ns$, independent of the previous measurement. The combined value including also the only previous measurement in the 70s is $\tau_{KL} = (51.01 \pm 0.20)ns$. For the K_S lifetime the PDG [22] average is used.

Concerning the charged kaons a new preliminary result for the $K^{\pm}$ lifetime has been presented by KLOE $\tau_{K\pm} = (1.2367 \pm 0.0078) \times 10^{-8}s$ [21]. For the moment the PDG average $\tau_{K\pm} = (1.2385 \pm 0.0025) \times 10^{-8}s$ is used and we are waiting for the final result.

2.3 Branching ratios

For a long time the branching ratios of the kaon semileptonic decays were fixed in the PDG due to the lack of new measurements. The BNL result for $Br(K^+e3) = (5.13 \pm 0.10)\%$ [23] published in 2003 was in disagreement with the PDG 2002 value ($Br(K^+e3) = (4.87 \pm 0.06)\%$) [24] and initiated a lot of experimental activity.

All six major K_L branching fractions have been measured by KTeV determining their ratios of decay rates [25]. The results for $Br(K_Le3)$ and $Br(K_L\mu3)$ are

$$Br(K_L \to \pi^{\pm}e^{\mp}\nu) = (40.67 \pm 0.11)\% \quad (8)$$

$$Br(K_L \to \pi^{\pm}\mu^{\mp}\nu) = (27.01 \pm 0.09)\% \quad (9)$$

KLOE has also measured the dominant K_L branchings [20] as mentioned above obtaining for the semileptonic decays

$$Br(K_L \to \pi^{\pm}e^{\mp}\nu) = (40.07 \pm 0.15)\% \quad (10)$$

$$Br(K_L \to \pi^{\pm}\mu^{\mp}\nu) = (26.98 \pm 0.15)\% \quad (11)$$

Apart from the K_L KLOE has studied K_Se3 decays [26]. Using $K_S \to \pi^+\pi^-$ for normalization channel the result is four times more precise than the previous value:

$$Br(K_S \to \pi^{\pm}e^{\mp}\nu) = (7.046 \pm 0.091)\% \quad (12)$$

The NA48 experiment has measured the ratio of the branching ratios of K_Le3 and all two track events [27]. In this way $Br(K_Le3) = R_e(1.0048 - Br(K_l3\pi^0)$, where $Br(K_L3\pi^0)$ is the external input. Using the measured $R_e = 0.4978 \pm 0.0035$ and the current PDG value for $Br(K_L3\pi^0) = (19.69 \pm 0.26)\%$ the result for the K_Le3 branching is

$$Br(K_L \to \pi^{\pm}e^{\mp}\nu) = (40.22 \pm 0.31)\% \quad (13)$$

Preliminary results for the charged semileptonic decays have also been presented by NA48 [28], [29] and KLOE [21]

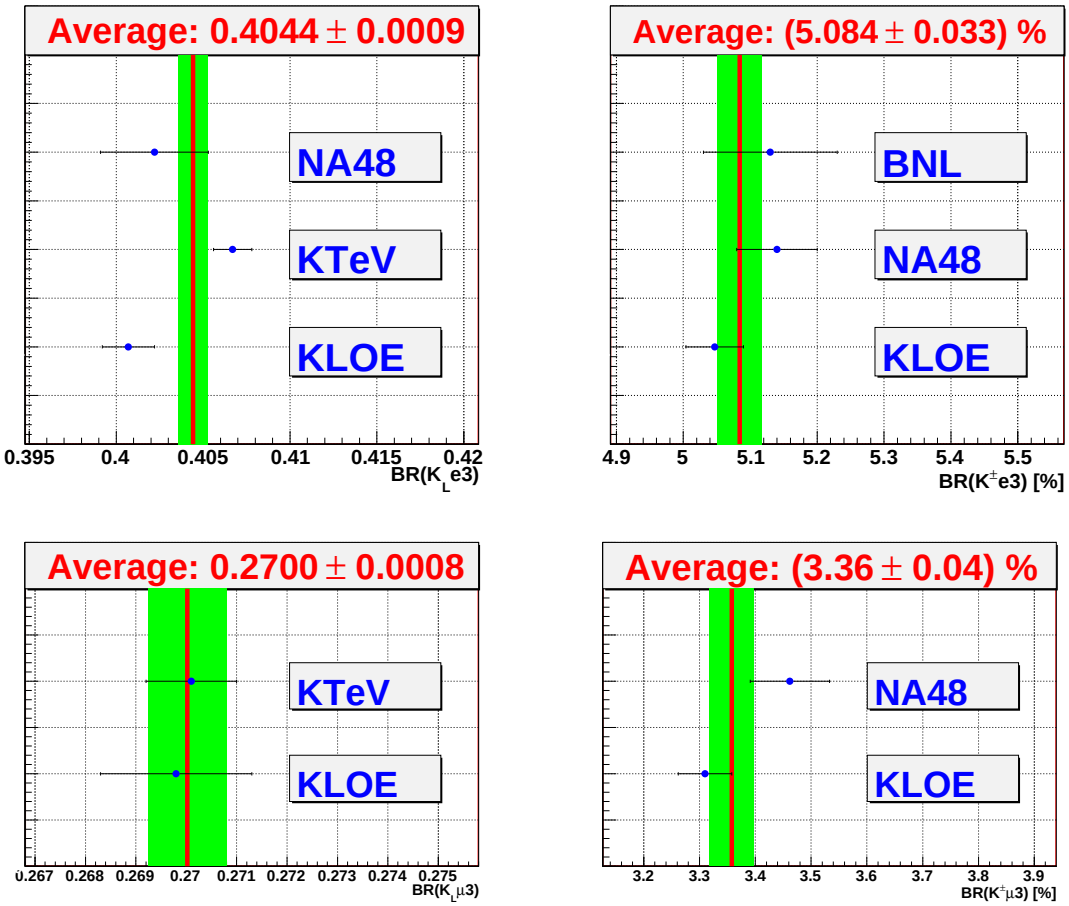

Figure 1: Recent measurements of the kaon semileptonic branching ratios. $Br(K_S \to \pi^{\pm} e^{\mp} \nu) = (7.046 \pm 0.091)\%$

NA48

$$Br(K^{\pm} \to \pi^0 e^{\pm} \nu) = (5.14 \pm 0.06)\% \quad (14)$$
$$Br(K^{\pm} \to \pi^0 \mu^{\pm} \nu) = (3.46 \pm 0.07)\% \quad (15)$$

KLOE

$$Br(K^{\pm} \to \pi^0 e^{\pm} \nu) = (5.047 \pm 0.043)\% \quad (16)$$
$$Br(K^{\pm} \to \pi^0 \mu^{\pm} \nu) = (3.310 \pm 0.048)\% \quad (17)$$

which confirm the discrepancy with the PDG observed by BNL.

This ten new measurements of the kaon semileptonic branching ratios together with the BNL result for $Br(K^{\pm}e3)$ are averaged depending on the decay mode and

are shown on Figure 1 (apart from $Br(K_S e3)$, measured only by KLOE). As can be seen they show very good consistency.

2.4 V_{us} from kaon semileptonic decays

Combining all the inputs mentioned above the values for $V_{us} \times f_+(0)$ from the different modes together with the average are shown of Figure 2.

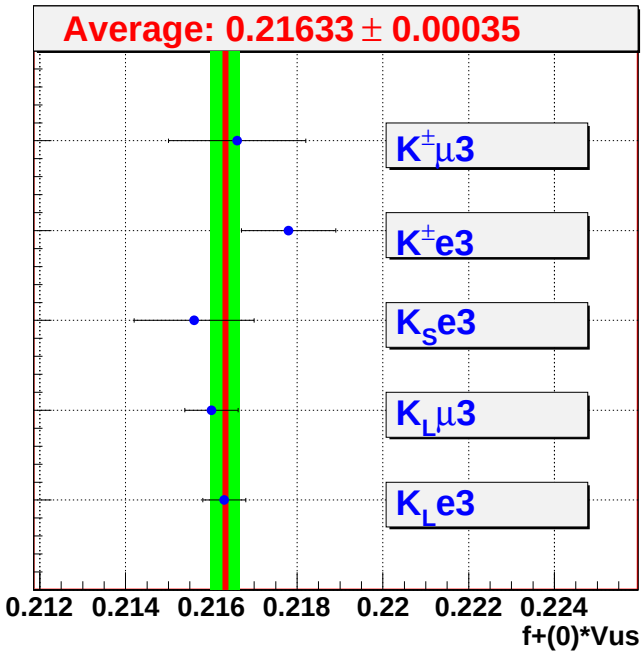

Figure 2: The experimentally measured quantity $V_{us} \times f_+(0)$ from kaon semileptonic decays

The precision on the combined measurement of $V_{us} \times f_+(0)$ is approximately 0.16%. Using for $f_+(0)$ the value obtained by Leutwyler and Roos the result for V_{us} is

$$V_{us} = 0.2251 \pm 0.0019 \tag{18}$$

where the dominant contribution to the error comes from the uncertainty of $f_+(0)$.

3 V_{us} from $Kl2$ decays

A complementary way to extract V_{us} is to use the ratio of the branching ratios of the pion and the kaon leptonic decays [30]. It can be written as

$$\frac{Br(K^{\pm} \to \mu^{\pm}\nu(\gamma))}{Br(\pi^{\pm} \to \mu^{\pm}\nu(\gamma))} = \frac{|V_{us}|^2}{|V_{ud}|^2}\frac{f_K^2}{f_\pi^2} \times \frac{\tau_K}{\tau_\pi}\frac{M_K(1-\frac{M_\mu^2}{M_K^2})^2}{M_\pi(1-\frac{M_\mu^2}{M_\pi^2})^2} \times \frac{1+\frac{\alpha}{\pi}C_K}{1+\frac{\alpha}{\pi}C_\pi} \tag{19}$$

where $\tau_{K,\pi}$ and $f_{K,\pi}$ are the meson lifetimes and decay constants correspondingly and $C_{K,\pi}$ parametrize the electroweak correction. Using the new measurement of $Br(K^{\pm} \to \mu^{\pm}\nu(\gamma)) = (63.66 \pm 0.17)\%$ from KLOE [31] and the lattice QCD calculation of f_K/f_π [32] we get $|V_{us}|/|V_{ud}| = 0.2286^{+0.0026}_{-0.0014}$ which together with the measurement of V_{ud} [33] gives

$$V_{us} = 0.2223^{+0.0026}_{-0.0014} \tag{20}$$

The accuracy of the result is comparable to (18). The dominant error comes from the uncertainty on the ratio f_K/f_π.

4 Conclusions

The values of V_{us} extracted from kaon semileptonic decays and from $K\mu 2$ decay agree. The average is

$$V_{us} = 0.2241 \pm 0.0015. \tag{21}$$

Using $V_{ud} = 0.97377(27)$ we have

$$|V_{ud}|^2 + |V_{us}|^2 = 0.9985 \pm 0.0009. \tag{22}$$

This result is compatible with the Standard Model and the unitarity of the CKM matrix.

Acknowledgements

I would like to thank prof. dr. Leandar Litov for the valuable help during the preparation of this review and the Joint Institute for Nuclear Research - Dubna for the sponsorship.

Bibliography

[1] N. Cabibbo, Phys. Rev. Lett. **10** (1963) 531.

[2] M. Kobayashi and T. Maskawa, Prog. Th. Phys. **49** (1973) 652.

[3] S. Eidelman, *et al.*, Phys. Lett. **B 592** (2004) 1

[4] A. Lai *et al.* [NA48 Collaboration], Eur. Phys. J. C **22** (2001) 231
A. Alavi-Harati *et al.* [KTeV Collaboration], Phys. Rev. D **67** (2003) 012005 [Erratum-ibid. D **70** (2004) 079904]

[5] http://kpasa.fnal.gov:8080/public/ktev.html

[6] http://na48.web.cern.ch/NA48/

[7] http://www.lnf.infn.it/kloe/

[8] W. J. Marciano, A. Sirlin, Phys. Rev. Lett. **71** (1993) 3629

[9] V. Cirigliano, M. Knecht, H. Neufeld, H. Rupertsberger and P. Talavera, Eur. Phys. J. C **23** (2002) 121 [arXiv:hep-ph/0110153].

[10] V. Cirigliano, H. Neufeld and H. Pichl, Eur. Phys. J. C **35** (2004) 53

[11] H. W. Fearing, E. Fischbach, J. Smith, Phys. Rev. D **2** (1970) 542.

[12] H. Leutwyler and M. Roos, Z. Phys. C **25** (1984) 91.

[13] D. Becirevic *et al.*, Nucl. Phys. B **705** (2005) 339

[14] A. Lai *et al.* [NA48 Collaboration], Phys. Lett. B **604** (2004) 1

[15] T. Alexopoulos *et al.* [KTeV Collaboration], Phys. Rev. D **70** (2004) 092007

[16] F. Ambrosino *et al.* [KLOE Collaboration], Phys. Lett. B **636** (2006) 166

[17] E. Abouzaid *et al.* [KTeV Collaboration], Phys. Rev. D **74** (2006) 097101

[18] O. P. Yushchenko *et al.*, Phys. Lett. B **589** (2004) 111

[19] F. Ambrosino *et al.* [KLOE Collaboration], Phys. Lett. B **626** (2005) 15

[20] F. Ambrosino *et al.* [KLOE Collaboration], Phys. Lett. B **632** (2006) 43

[21] R. Versaci [By KLOE Collaboration], arXiv:hep-ex/0701008.

[22] W.-M. Yao, *et al.*Journal of Physics G **33** (2006) 1

[23] A. Sher *et al.*, Phys. Rev. Lett. **91** (2003) 261802

[24] K. Hagiwara *et al.*, Physical Review **D 66** (2002) 010001

[25] T. Alexopoulos *et al.* [KTeV Collaboration], Phys. Rev. D **70** (2004) 092006

[26] F. Ambrosino *et al.* [KLOE Collaboration], Phys. Lett. B **636** (2006) 173

[27] A. Lai *et al.* [NA48 Collaboration], Phys. Lett. B **602** (2004) 41

[28] L. Litov [NA48 Collaboration], arXiv:hep-ex/0501048.

[29] A. Dabrowski, presented at KAON 2005 Workshop

[30] W. J. Marciano, Phys. Rev. Lett. **93** (2004) 231803

[31] F. Ambrosino *et al.* [KLOE Collaboration], Phys. Lett. B **632** (2006) 76

[32] C. Bernard *et al.* [MILC Collaboration], arXiv:hep-lat/0609053.

[33] W. J. Marciano and A. Sirlin, Phys. Rev. Lett. **96** (2006) 032002

Heavy Hadron Decays

Heavy Hadron Decays

Hadronic D Decays and Dalitz Analyses

David G. Cassel
Laboratory for Elementary-Particle Physics
Cornell University
Ithaca, NY 14853 USA

1 Introduction

Recently several factors converged to ignite a renaissance in charm physics. These factors include:

- the need for precision measurements from the charm sector to interpret quantitatively CP violation results from the beauty sector,
- technical and computational developments in Lattice QCD that led to precise calculations that can face precision experimental challenges in the charm sector,
- discovery of new – generally unanticipated – charm meson states (*e.g.*, $D^*_{s0}(2317)$ and $D_{s1}(2460)$), and
- substantial increases in the precision and reach of charm decay measurements due to production of much larger charm data sets (particularly at CESR, KEKB, and PEP II) and excellent detectors in the experiments at these facilities.

In this report I describe recent results in hadronic decays of the stable D mesons (D^0, D^+, and D_s) and Dalitz analyses of resonance structure in their hadronic decays. These results come from experiments at electron-positron colliders (BaBar, Belle, and CLEO-c) and fixed target experiments (E791 and FOCUS).

2 Absolute D^0 and D^+ Branching Fractions

CLEO is providing new precise measurements of absolute D^0 and D^+ branching fractions using D^+ and D^0 decays from $e^+e^- \to \psi(3770) \to D^+D^-$ or $D^0\overline{D}^0$. The mass of the $\psi(3770)$ is below the threshold for $D\overline{D}\pi$ decays, so no additional pions are produced. Furthermore, the multiplicities of D^0 and D^+ decays are low, so events are extremely clean. CLEO measures leptonic, semileptonic, and key hadronic branching fractions using a double tagging technique pioneered by MARK III [1,2]. Most other D branching fractions [3] are measured relative to a reference mode, usually $D^0 \to K^-\pi^+$ or $D^+ \to K^-\pi^+\pi^+$. CLEO has published absolute branching fractions for key Cabibbo-Favored Decays (CFD) to hadrons obtained from 56 pb^{-1}of data [4]. I report

here a preliminary update from 281 pb^{-1} of data; this is the first public presentation of these results. Some other branching ratios utilizing the 281 pb^{-1} data sample have been published or submitted for publication.

The MARK III double tag technique derives absolute branching fractions from measurements of Single Tag (ST) and Double Tag (DT) yields. In ST events, the $D(\overline{D})$ is reconstructed in a specific final state, while the decay products of the $\overline{D}(D)$ are not observed, *e.g.*, $D \to i$ and $\overline{D} \to \overline{X}$. In DT events, both the D and the $\overline{D}$ are reconstructed in specific final states, *e.g.*, $D \to i$ and $\overline{D} \to \overline{\jmath}$. ST and DT yields are given by $N_i = N_{D\overline{D}}\,\mathcal{B}_i\,\epsilon_i$, $N_{\overline{\jmath}} = N_{D\overline{D}}\,\mathcal{B}_{\overline{\jmath}}\,\epsilon_{\overline{\jmath}}$, and $N_{i\overline{\jmath}} = N_{D\overline{D}}\,\mathcal{B}_i\,\mathcal{B}_{\overline{\jmath}}\,\epsilon_{i\overline{\jmath}}$, respectively, where: i and $\overline{\jmath}$ are the decay modes of the D and $\overline{D}$, respectively; $\mathcal{B}_i$, and $\mathcal{B}_{\overline{\jmath}}$ are the corresponding branching fractions; ϵ_i, $\epsilon_{\overline{\jmath}}$, and $\epsilon_{i\overline{\jmath}}$ are the ST and DT efficiencies for these modes; N_i, $N_{\overline{\jmath}}$, and $N_{i\overline{\jmath}}$ are the corresponding ST and DT yields; and $N_{D\overline{D}}$ is the number of $D^0\overline{D}^0$ or D^+D^- events produced in the experiment. Branching fractions and $N_{D\overline{D}}$ can then be obtained from

$$\mathcal{B}_i = \frac{N_{i\overline{\jmath}}}{N_{\overline{\jmath}}}\,\frac{\epsilon_{\overline{\jmath}}}{\epsilon_{i\overline{\jmath}}} \quad \text{and} \quad N_{D\overline{D}} = \frac{N_i N_{\overline{\jmath}}}{N_{i\overline{\jmath}}}\,\frac{\epsilon_{i\overline{\jmath}}}{\epsilon_i \epsilon_{\overline{\jmath}}}$$

where $\epsilon_{\overline{\jmath}}$ is the efficiency for detecting $\overline{D} \to \overline{\jmath}$ ST events, and CP symmetry has been assumed so $\mathcal{B}_{\overline{\imath}} = \mathcal{B}_i$. Obviously the luminosity is not required to determine $\mathcal{B}_i$ or $N_{D\overline{D}}$, but the cross section for $e^+e^- \to \psi(3770) \to D\overline{D}$ can be determined from $N_{D\overline{D}}$ and the luminosity. Furthermore, $\epsilon_{i\overline{\jmath}} \approx \epsilon_i\epsilon_{\overline{\jmath}}$ so the branching fractions and number of events obtained by this method are relatively insensitive to uncertainties in the efficiencies.

CLEO utilizes a χ^2 fit [5] that obtains all D^0 and D^+ branching fractions, as well as the numbers of $D^0\overline{D}^0$ and D^+D^- events from a simultaneous fit to all ST and DT D^0 and D^+ yields. All statistical and systematic uncertainties and their correlations are properly taken into account in this fit.

Candidate D or $\overline{D}$ mesons are selected using mode-dependent requirements on $\Delta E \equiv E(D) - E_0$, the difference between the measured energies $E(D)$ of the candidate and the beam energy E_0. Then ST and DT yields are obtained from fits to beam constrained mass M_{BC} distributions, where the beam energy E_0 is substituted for the measured energy $E(D)$ of a D or $\overline{D}$ candidate. Substitution of E_0 for $E(D)$ improves substantially the mass resolution of the D candidates. The M_{BC} distributions for the DT events are illustrated in Figure 1. Clearly these M_{BC} distributions are very clean with little background. Summed over all modes, the yields obtained from the CLEO-c 281 pb^{-1} sample are 230,225 ST and $13,575 \pm 120$ DT $D^0\overline{D}^0$ events, and 167,086 ST and $8,867 \pm 97$ DT D^+D^- events. With these yields, systematic errors dominate; to be conservative for these preliminary results, most systematic errors are essentially the same as those determined for the 56 pb^{-1} results. Intensive study of the systematic uncertainties are underway and CLEO expects to be able to substantially improve most of them.

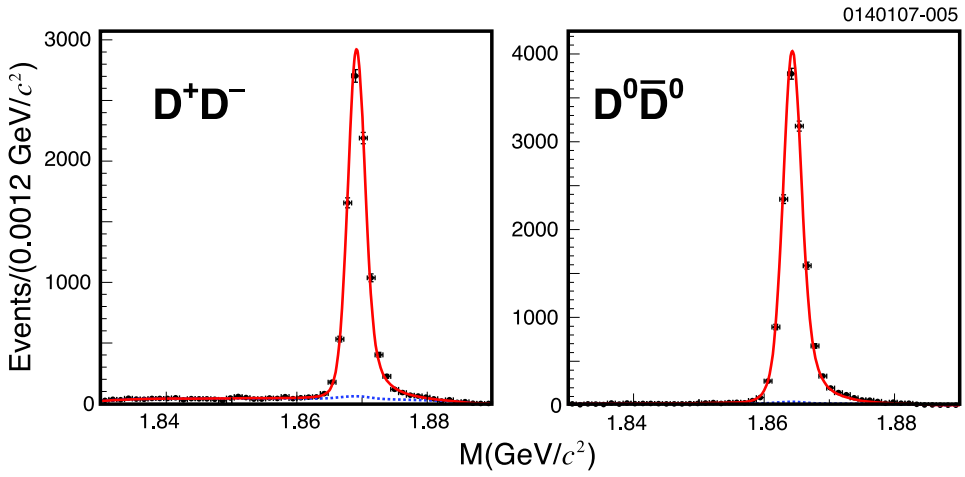

Figure 1: Histograms of M_{BC} distributions of D and $\overline{D}$ candidates in double-tag events from 281 pb^{-1} of CLEO-c $\psi(3770)$ data; (left) D^+D^- DT candidates and (right) $D^0\overline{D}^0$ candidates.

Mode	$\mathcal{B}$ (%)
$D^0 \to K^-\pi^+$	$3.87 \pm 0.04 \pm 0.08$
$D^0 \to K^-\pi^+\pi^0$	$14.6 \pm 0.1 \pm 0.4$
$D^0 \to K^-\pi^+\pi^+\pi^-$	$8.3 \pm 0.1 \pm 0.3$
$D^+ \to K^-\pi^+\pi^+$	$9.2 \pm 0.1 \pm 0.2$
$D^+ \to K^-\pi^+\pi^+\pi^0$	$6.0 \pm 0.1 \pm 0.2$
$D^+ \to K^0_S\pi^+$	$1.55 \pm 0.02 \pm 0.05$
$D^+ \to K^0_S\pi^+\pi^0$	$7.2 \pm 0.1 \pm 0.3$
$D^+ \to K^0_S\pi^+\pi^+\pi^-$	$3.13 \pm 0.05 \pm 0.14$
$D^+ \to K^+K^-\pi^+$	$0.93 \pm 0.02 \pm 0.03$

Table 1: Preliminary CLEO results for hadronic D^0 and D^+ branching fractions, with their statistical and systematic errors. These results come from 281 pb^{-1} of CLEO-c $\psi(3770)$ data, with conservative systematic errors.

The preliminary CLEO results for three D^0 and six D^+ hadronic decay modes are given in Table 1 and compared to PDG04 [6] averages in Figure 2. It is clear that the preliminary CLEO results are substantial improvements over previous measurements. PDG04 averages were used for the comparison because CLEO-c 56 pb^{-1} results were included in the PDG06 averages. Final State Radiation (FSR) is included in the

CLEO-c Monte Carlo (MC) simulations for determining efficiencies. If FSR had not been included in the simulations the branching fractions would decrease by $\lesssim 2\%$. Most other measurements of hadronic D branching fractions did not take FSR into account.

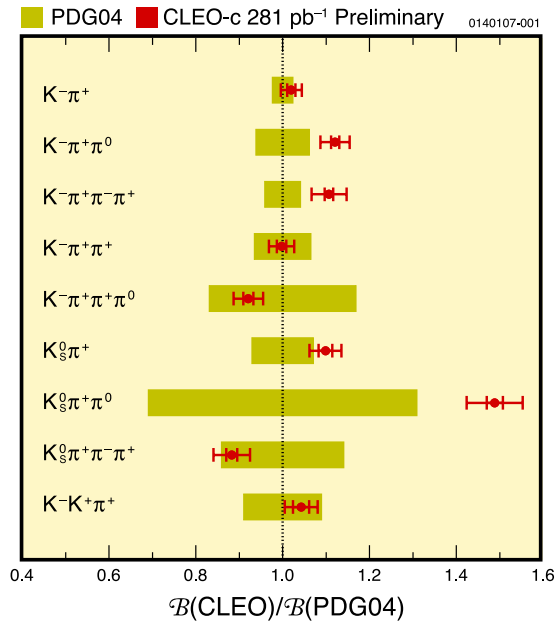

Figure 2: Ratio $\mathcal{B}$(CLEO)/$\mathcal{B}$(PDG04) of preliminary CLEO-c hadronic D^0 and D^+ branching fractions to the 2004 PDG averages. The widths of the PDG bars correspond to the errors in those averages. The CLEO-c points have statistical and systematic error bars.

3 Cabibbo Suppressed D^0 and D^+ Decays

3.1 Singly-Cabibbo-Suppressed D^0 and D^+ Decays to Pions

Using the full 281 pb^{-1} $\psi(3770)$ data sample, CLEO measured Singly-Cabibbo-Suppressed Decays (SCSD) of D^0 and D^+ to multipion final states [7]. The M_{BC} distributions are illustrated in Figure 3. The branching fractions in Table 2 were obtained from measurements of $\mathcal{B}(D^0 \to n(\pi))/\mathcal{B}(D^0 \to K^-\pi^+)$ and $\mathcal{B}(D^+ \to n(\pi))/\mathcal{B}(D^+ \to K^-\pi^+\pi^+)$. The reference branching fractions used to determine the reported multipion branching fractions were $\mathcal{B}(D^0 \to K^-\pi^+) = (3.84 \pm 0.07)\%$ and $\mathcal{B}(D^+ \to K^-\pi^+\pi^+) = (9.4 \pm 0.3)\%$. These were obtained by averaging the

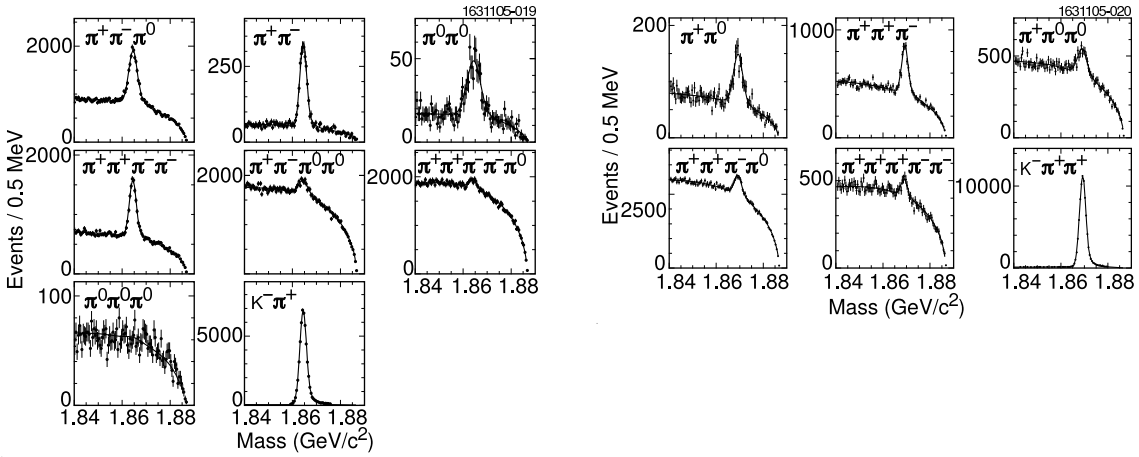

Figure 3: Histograms of M_{BC} for (plots on the left) of $D^0 \to (n)\pi$ events and (plots on the right) $D^+ \to (n)\pi$ from the 281 pb^{-1} $\psi(3770)$ CLEO-c data sample. Histograms of M_{BC} for the reference modes $D^0 \to K^-\pi^+$ and $D^+ \to K^-\pi^+\pi^+$ are included with the $D \to n(\pi)$ histograms on the left and right, respectively.

Mode	CLEO-c $\mathcal{B}$ (10^{-3})	PDG04 $\mathcal{B}$ (10^{-3})
$\pi^+\pi^-$	$1.39 \pm 0.04 \pm 0.03$	1.38 ± 0.05
$\pi^0\pi^0$	$0.79 \pm 0.05 \pm 0.04$	0.84 ± 0.22
$\pi^+\pi^-\pi^0$	$13.2 \pm 0.2 \pm 0.5$	11 ± 4
$\pi^+\pi^-\pi^+\pi^-$	$7.3 \pm 0.1 \pm 0.3$	7.3 ± 0.5
$\pi^+\pi^-\pi^0\pi^0$	$9.9 \pm 0.6 \pm 0.7$	—
$\pi^+\pi^-\pi^+\pi^-\pi^0$	$4.1 \pm 0.5 \pm 0.2$	—
$\pi^+\pi^0$	$1.25 \pm 0.06 \pm 0.08$	1.33 ± 0.22
$\pi^+\pi^+\pi^-$	$3.35 \pm 0.10 \pm 0.20$	3.1 ± 0.4
$\pi^+\pi^0\pi^0$	$4.8 \pm 0.3 \pm 0.4$	—
$\pi^+\pi^+\pi^-\pi^0$	$11.6 \pm 0.4 \pm 0.7$	—
$\pi^+\pi^-\pi^+\pi^-\pi^+$	$1.60 \pm 0.18 \pm 0.17$	1.82 ± 0.25

Table 2: CLEO branching fractions for D^0 and D^+ decays to multiple pions.

56 pb^{-1} CLEO-c results and the PDG04 averages. These new CLEO measurements are compared to the PDG04 [6] averages in Figure 4.

As described in Section 3.4, BaBar has also reported a measurement of $\mathcal{B}(D^+ \to$

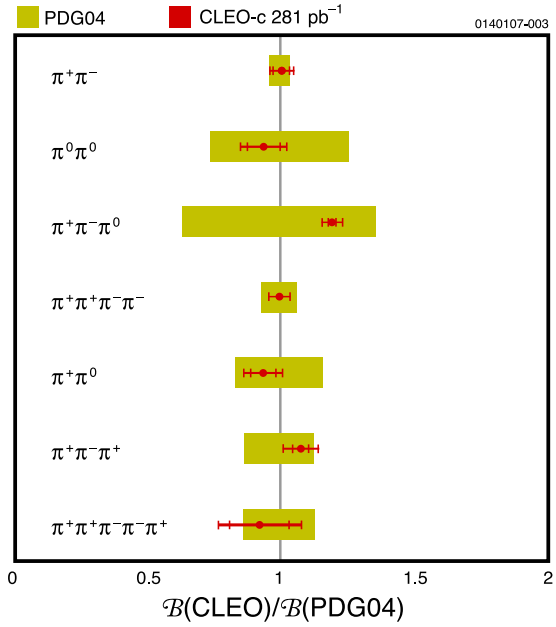

Figure 4: Ratio $\mathcal{B}$(CLEO)/$\mathcal{B}$(PDG06) of CLEO-c measurements of $D \to n(\pi)$ branching fractions to the 2006 PDG averages. The widths of the PDG bars correspond to the errors in those averages.

$\pi^+\pi^0$) along with the first observation of the Doubly-Cabibbo-Suppressed-Decay (DCSD) branching fraction $\mathcal{B}(D^+ \to K^+\pi^0)$. The BaBar result for the ratio of $\mathcal{B}(D^+ \to \pi^+\pi^0)$ to the reference branching fraction $\mathcal{B}(D^+ \to K^-\pi^+\pi^+)$ is in excellent agreement with the CLEO measurement.

The ratio of the isospin amplitudes A_0 and A_2 for $D \to \pi\pi$ decay and their phase difference can be determined from the values of $\mathcal{B}(\pi^+\pi^-)$, $\mathcal{B}(\pi^0\pi^0)$, and $\mathcal{B}(\pi^+\pi^0)$ and the D^0 and D^+ decay widths [8]. Only $I = 0$ and 2 states are allowed for a two pion system, since an isovector state is forbidden. Using D lifetimes from PDG04 [6] and the branching fractions in Table 2, CLEO finds $A_2/A_0 = 0.420 \pm 0.014 \pm 0.001$ and the relative phase $\delta = (86.4 \pm 2.8 \pm 3.3)^\circ$. In contrast to the isospin amplitudes in $K \to \pi\pi$ decays, the two isospin amplitudes in $D \to \pi\pi$ decay are comparable [8]. Furthermore, the large phase difference between the two amplitudes indicates that final state interactions are important.

Searches for η and ω in multipion D^0 and D^+ decays

Untangling the resonant substructure of these decays with more than two pions would require systematic Dalitz analyses. However, searches for ηs and ωs among the decay pions is a first step in this direction. The technique used is illustrated in Figure 5,

where three-pion invariant masses, $M(\pi^+\pi^-\pi^0)$ are plotted for D or $\overline{D}$ candidates within the original ΔE requirement and in sidebands. Although combinatorial backgrounds are large, there are significant signals above background peaks in: $\eta\pi^0$ in $D^0 \to \pi^+\pi^-\pi^0\pi^0$, $\eta\pi^+$ in $D^+ \to \pi^+\pi^+\pi^-\pi^0$, and $\omega\pi^+\pi^-$ in $D^0 \to \pi^+\pi^-\pi^+\pi^-\pi^+$. The branching fractions for these three channels and 90% UL confidence intervals for the other three modes are given in Table 3. The branching fractions for $\eta\pi^+$ and $\omega\pi^+\pi^-$ are significant fractions of the total branching fractions for the parent decays.

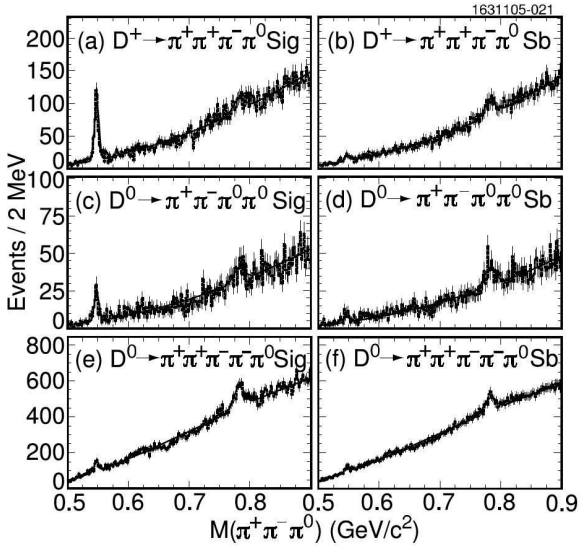

Figure 5: $M(\pi^+\pi^-\pi^0)$ distributions for multipion D^+ and D^0 decays from CLEO-c data.

Mode	$\mathcal{B}$ (10^{-3})	PDG04 $\mathcal{B}$ (10^{-3})
$\eta\pi^0$	$0.62 \pm 0.14 \pm 0.05$	—
$\eta\pi^+$	$3.61 \pm 0.25 \pm 0.26$	3.0 ± 0.6
$\eta\pi^+\pi^-$	< 1.9 (90% CL)	—
$\omega\pi^0$	< 0.26 (90% CL)	—
$\omega\pi^+$	< 0.34 (90% CL)	—
$\omega\pi^+\pi^-$	$1.7 \pm 0.5 \pm 0.2$	—

Table 3: Branching fractions and upper limits for η and ω production in multipion D^0 and D^+ decays from CLEO-c data.

3.2 Singly-Cabibbo-Suppressed Decays from BaBar and Belle

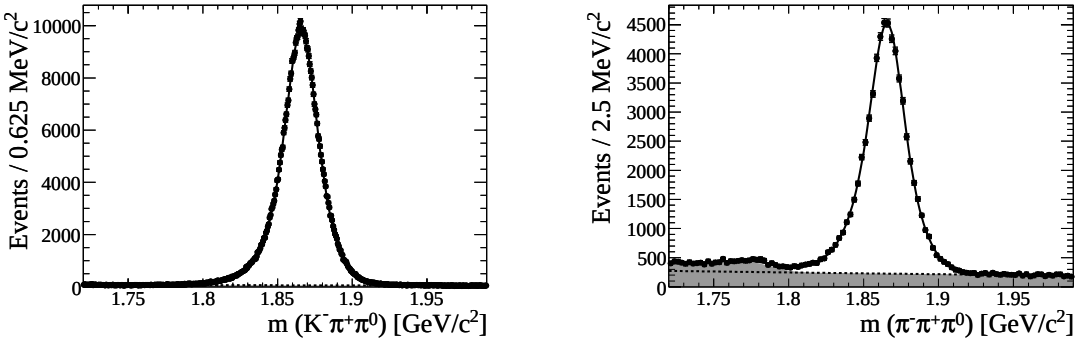

Figure 6: BaBar data for (left) $D^0 \to K^-\pi^+\pi^0$ decays and (right) $D^0 \to \pi^+\pi^-\pi^0$ decays. [9, 10]

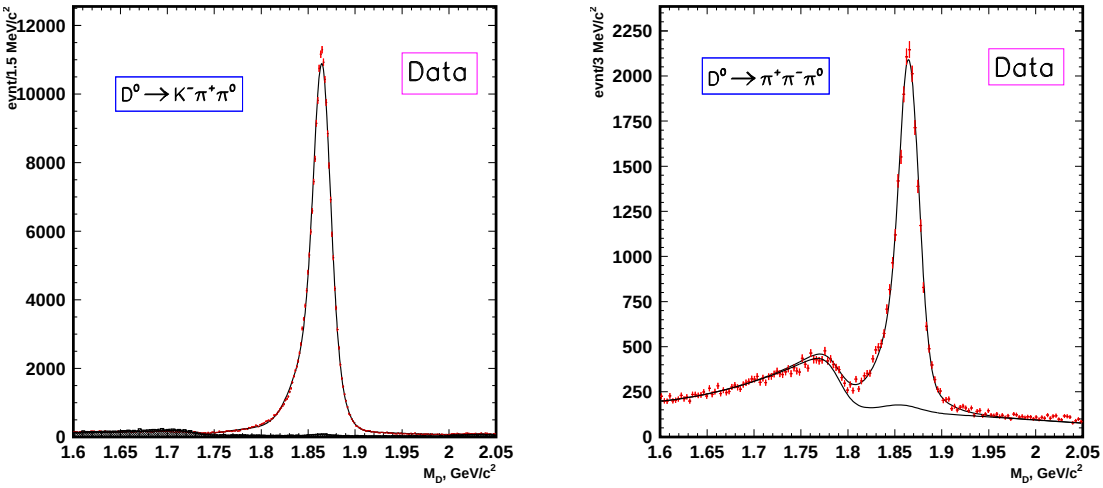

Figure 7: Belle data for (left) $D^0 \to K^-\pi^+\pi^0$ decays and (right) $D^0 \to \pi^+\pi^-\pi^0$ decays.

BaBar [11] and Belle [12] have used their enormous data samples to measure precisely the ratio $\mathcal{B}(D^0 \to \pi^+\pi^-\pi^0)/\mathcal{B}(D^0 \to K^-\pi^+\pi^0)$ of a singly-Cabibbo-suppressed hadronic decay to a similar Cabibbo-favored hadronic decay. The BaBar and Belle data are illustrated in Figures 6 and 7, respectively. The invariant masses of D candidates are used in these analyses, since these data were taken at the $\Upsilon(4S)$ where many $D\overline{D}$ channels with multipions are open (rather than only the $D^0\overline{D}^0$ and D^+D^-

channels at the $\psi(3770)$) so beam-constrained masses cannot be used. Therefore the mass resolutions are substantially worse in the BaBar and Belle data, than in the corresponding CLEO-c data (compare Figures 6 and 7 with Figure 5. However, signal to background ratios in the BaBar and Belle data are substantially better than the corresponding ratio in the CLEO-c data. The results of the three measurements are given in Table 4. Some of the strengths and weaknesses of these measurements are apparent from the yields, errors, and luminosities in the table. Note that the Cabibbo suppression of $\mathcal{B}(D^0 \to \pi^+\pi^-\pi^0)$ is about a factor of 10 relative to $\mathcal{B}(D^0 \to K^-\pi^+\pi^0)$, which is the D^0 hadronic decay mode with the largest branching fraction.

	Yield	$\mathcal{B}(D^0 \to \pi^+\pi^-\pi^0)/\mathcal{B}(D^0 \to K^-\pi^+\pi^0)$	Luminosity
BaBar	$60,426 \pm 343$	$(10.59 \pm 0.06 \pm 0.13) \times 10^{-2}$	232 fb^{-1}
Belle	$22,803 \pm 203$	$(9.71 \pm 0.09 \pm 0.30) \times 10^{-2}$	357 fb^{-1}
CLEO-c	$10,834 \pm 164$	$(9.01 \pm 0.18 \pm 0.39) \times 10^{-2}$	281 pb^{-1}
	$\mathcal{B}(D^0 \to K^-K^+\pi^0)/\mathcal{B}(D^0 \to K^-\pi^+\pi^0)$		
BaBar	$10,773 \pm 122$	$(2.37 \pm 0.03 \pm 0.04) \times 10^{-2}$	232 fb^{-1}
CLEO II	151 ± 42	$(0.95 \pm 0.26) \times 10^{-2}$	2.7 fb^{-1}

Table 4: Measurements of SCSDs from BaBar, Belle, and CLEO. The Belle result is preliminary, while the BaBar and CLEO results have been published. The CLEO-c branching ratio is calculated from measured ratios of both $\mathcal{B}(D^0 \to \pi^+\pi^-\pi^0)$ and $\mathcal{B}(D^0 \to K^-\pi^+\pi^0)$ to $\mathcal{B}(D^0 \to K^-\pi^+)$, without taking correlations into account. Proper use of correlations would reduce the systematic error.

In the same analysis BaBar measured $\mathcal{B}(D^0 \to K^-K^+\pi^0)/\mathcal{B}(D^0 \to K^-\pi^+\pi^0)$. The data are illustrated in Figure 8 and the result is included in Table 4. The BaBar result is significantly larger and much more precise than a previous CLEO result from a much smaller data sample [13].

3.3 Multi-Kaon Modes from FOCUS

FOCUS studied D^0 decays to final states with two or three charged or neutral kaons [15, 16]. The data for the reference mode $D^0 \to K^0_S\pi^+\pi^-$ and two of the neutral kaon signal modes are illustrated in Figure 9 and the ratios of signal branching fractions to the reference branching fraction are given in Table 5. This is the first observation of the modes $D^0 \to K^0_S K^0_S K^\pm\pi^\mp$, which are combined to one branching fraction. The table also includes a measurement of the branching ratio $\mathcal{B}(D^0 \to K^-K^+\pi^+\pi^-)/\mathcal{B}(D^0 \to K^-\pi^+\pi^+\pi^-)$. This branching ratio was measured in a sep-

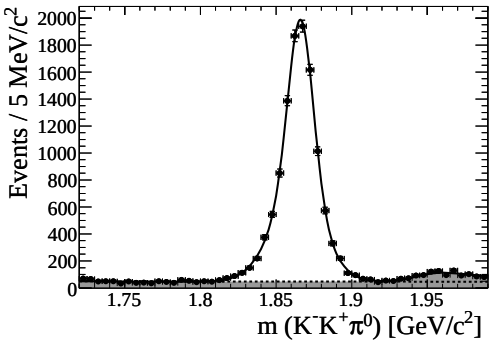

Figure 8: BaBar data for $D^0 \to K^-K^+\pi^0$ decays. [9, 10]

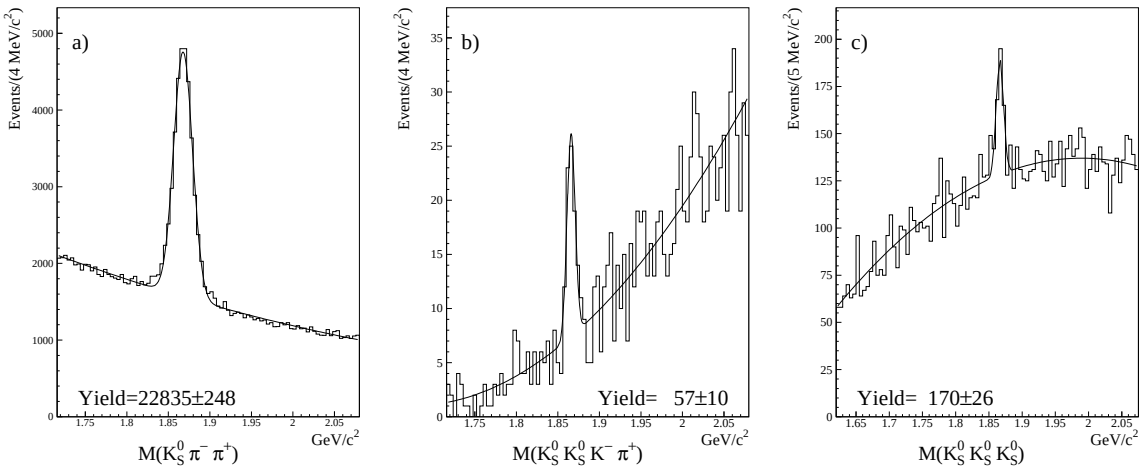

Figure 9: FOCUS data for (left) $D^0 \to K^0_S\pi^+\pi^-$ decays, (middle) $D^0 \to K^0_SK^0_SK^\pm\pi^\mp$ decays, and (right) $D^0 \to K^0_SK^0_SK^0_S$ decays [14].

arate FOCUS analysis of resonant substructure in the the four-body decay $D^0 \to K^-K^+\pi^+\pi^-$ described in Section 6.3.

From the table it is evident that Cabibbo-suppression, relative to the Cabibbo-favored reference mode, is on the order of a factor of 100 for the two-kaon decay modes. However, the Cabibbo-favored decays to three kaons are suppressed by comparable factors. Presumably this is due to the necessity of popping an $s\overline{s}$ quark-antiquark pair to produce the additional two kaons.

Mode	FOCUS $\mathcal{B}_{\rm mode}/\mathcal{B}_{\rm ref}$ (%)	
$D^0 \to K^0\overline{K}^0$	$1.44 \pm 0.32 \pm 0.16$	SCSD
$D^0 \to K^0_S K^0_S \pi^+\pi^-$	$2.08 \pm 0.35 \pm 0.21$	SCSD
$D^0 \to K^0_S K^0_S K^\pm \pi^\mp$	$1.06 \pm 0.19 \pm 0.10$	CF
$D^0 \to K^0_S K^0_S K^0_S$	$1.79 \pm 0.27 \pm 0.26$	CF
$D^0 \to K^-K^+\pi^+\pi^-$	$2.95 \pm 0.11 \pm 0.08$	SCSD

Table 5: FOCUS branching fractions for Cabibbo favored (CF) decays and singly-Cabibbo suppressed D^0 decays to multiple kaons. For the neutral kaon modes, the reference branching fraction is $\mathcal{B}(D^0 \to \overline{K}^0\pi^+\pi^-)$, while the reference branching fraction for the charged kaon mode is $\mathcal{B}(D^0 \to K^-\pi^+\pi^+\pi^-)$.

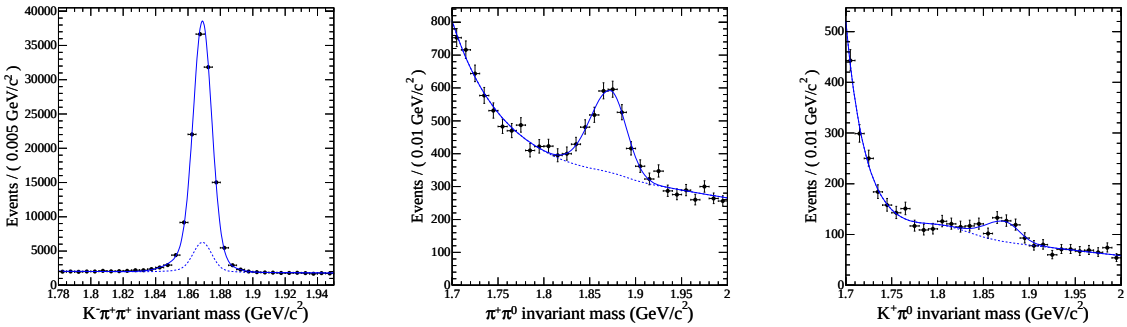

Figure 10: BaBar data for (left) $D^+ \to K^-\pi^+\pi^+$ decays, (middle) $D^+ \to \pi^+\pi^0$ decays, and (right) $D^+ \to K^+\pi^-$ decays. [10, 17]

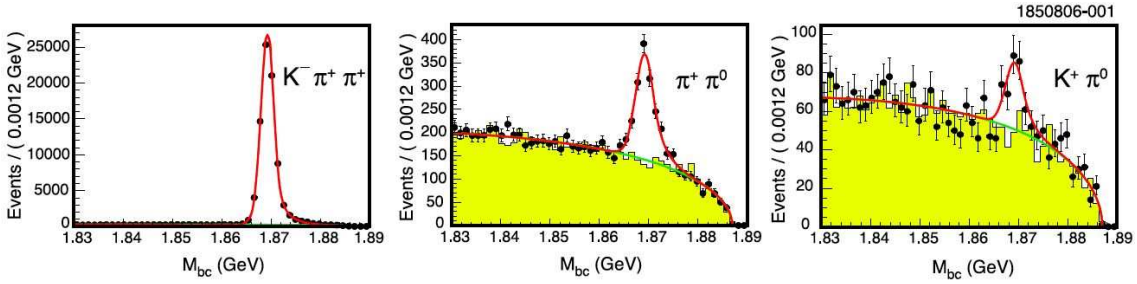

Figure 11: CLEO-c data for (left) $D^+ \to K^-\pi^+\pi^+$ decays, (middle) $D^+ \to \pi^+\pi^0$ decays, and (right) $D^+ \to K^+\pi^-$ decays.

3.4 The Doubly-Cabibbo-Suppressed Decay $D^+ \to K^+\pi^-$

BaBar has reported the first observation of the DCSD $D^+ \to K^+\pi^0$ [18] and the precise measurement of a branching ratio for the SCSD decay $D^+ \to \pi^+\pi^0$ mentioned in Section 3.1. The BaBar data are illustrated in Figure 10, and the CLEO data [19] for the same modes are illustrated in Figure 11. Note that the mass range of the CLEO data is much narrower than the mass range of the BaBar data, illustrating the improvements in mass resolution gained by being able to use beam-constrained masses instead of invariant mass. The ratios of the signal branching fractions $\mathcal{B}(D^+ \to \pi^+\pi^0)$ and $\mathcal{B}(D^+ \to K^+\pi^0)$ of the signal modes to reference branching fraction $\mathcal{B}(D^+ \to K^-\pi^+\pi^+)$ are given in Table 6. BaBar's ability to use tighter cuts on their enormous data sample to compensate for the better mass resolution of the CLEO-c data is evident from the figures and results. The Cabibbo suppression of the $D^+ \to K^+\pi^0$ mode is close to a factor of 5.

	$D^+ \to \pi^+\pi^0$ (SCSD)	$D^+ \to K^+\pi^0$ (DCSD)
	$\mathcal{B}_{\rm mode}/\mathcal{B}_{\rm ref}$	$\mathcal{B}_{\rm mode}/\mathcal{B}_{\rm ref}$
BaBar	$(1.33 \pm 0.11 \pm 0.09) \times 10^{-2}$	$(2.68 \pm 0.50 \pm 0.26) \times 10^{-3}$
CLEO-c	$(1.33 \pm 0.07 \pm 0.06) \times 10^{-2}$	$(2.40 \pm 0.38 \pm 0.16) \times 10^{-3}$

Table 6: The ratios of the branching factions for the SCSD decay $D^+ \to \pi^+\pi^0$ and the DCSD decay $D^+ \to K^+\pi^0$ from BaBar and CLEO-c, to the branching fraction for the reference mode $D^+ \to K^-\pi^+\pi^+$. The CLEO-c result for $D^+ \to \pi^+\pi^0$ is from the SCSD analysis in Section 3.1.

3.5 Comparison of $D \to K^0_S\pi$ and $D \to K^0_L\pi$ Decay Rates

Cabibbo-Favored and Doubly-Cabibbo-Suppressed amplitudes contribute to the decay $D \to K^0\pi$. The observed final states are $D \to K^0_S\pi$ and $D \to K^0_L\pi$, and Bigi and Yamamoto pointed out that interference between CF and DCS amplitudes can lead to different rates for $D \to K^0_S\pi$ and $D \to K^0_L\pi$ [20]. CLEO has measured preliminary branching fractions for these decays by fully reconstructing $D \to K^0_S\pi$ decays and reconstructing $D \to K^0_L\pi$ decays using missing masses [21]. The CLEO data for $D \to K^0_L\pi$ decays are illustrated in Figure 12. The preliminary results given in Table 7 are reported in terms of the ratio $R(D)$ defined by:

$$R(D) \equiv \frac{\mathcal{B}(D \to K^0_S\pi) - \mathcal{B}(D \to K^0_L\pi)}{\mathcal{B}(D \to K^0_S\pi) + \mathcal{B}(D \to K^0_L\pi)}$$

The measured value of $R(D^+)$ is consistent with zero, while $R(D^0)$ is significantly larger than zero. U-spin and SU(3) predict [22] $R(D^0) = 2\tan^2(\theta_c)$ giving $R(D^0) = 0.109 \pm 0.001$, which is in good agreement with the experimental result. On the other hand, $R(D^+)$ is not so simple because internal spectator diagrams contribute to both $D^+ \to \overline{K}^0\pi^+$ and $D^+ \to K^0\pi^+$, but external diagrams contribute to the former and annihilation diagrams contribute to the latter.

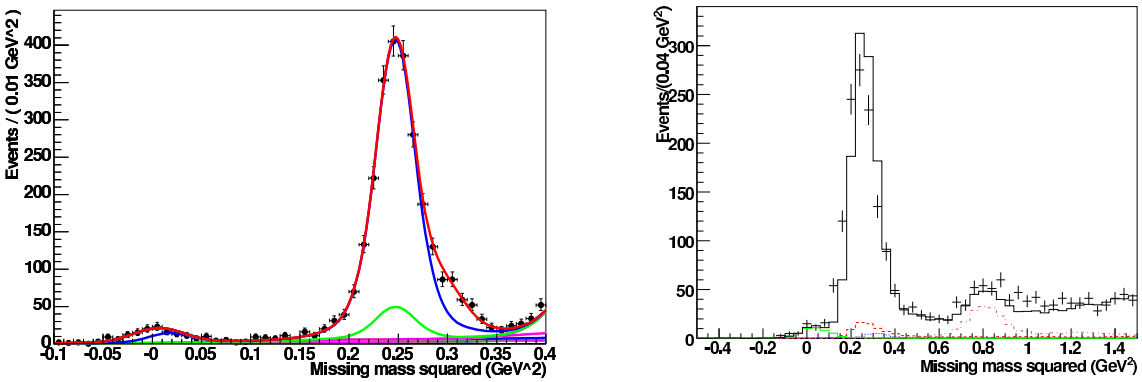

Figure 12: CLEO data for (left) $D^0 K^0_L \pi^0$ decays and (right) $D^+ \to K^0_L \pi^+$ decays.

$R(D^+)$	$0.030 \pm 0.023 \pm 0.025$
$R(D^0)$	$0.122 \pm 0.024 \pm 0.030$

Table 7: CLEO-c Preliminary measurements of the normalized branching fraction differences between $D \to K^0_L\pi$ decays and $D \to K^0_S\pi$ decays.

4 Absolute D_s Branching Fractions

Previously, absolute D_s branching fractions have not been well known, primarily due to difficulties of determining the total number of D_s mesons produced in the experiment [23,24]. CLEO has now addressed this problem with a double tag measurement of absolute D_s branching fractions in e^+e^- collisions just above the $D_s^{\pm}D_s^{*\mp}$ threshold [25].

4.1 The D_s Production Cross Section

Although measurements of the e^+e^- annihilation cross section, $\sigma(e^+e^-)$, at energies above $E_{cm} = 3.8$ GeV have existed for some time [3], little was known about the

composition of the final states. In order to find a favorable point for studying DT $D_s^{\pm}\overline{D}_s^{\mp}$ events, CLEO scanned that region with integrated luminosities of ~ 5 pb^{-1} per point and fast turnaround of results for feedback. After the scan, more luminosity was accumulated at or near $E_{cm} = 4.17$ GeV where the cross section for $D_s^{\pm}D_s^{*\mp}$ production peaks with $\sigma(e^+e^- \to D_s^{\pm}D_s^{*\mp}) \approx 0.9$ nb. Preliminary measurements [25] of cross sections for producing various $D\overline{D}$, $D\overline{D}^*$, and $D^*\overline{D}^*$ pairs are illustrated in Figure 13. CLEO used a total of 195 pb^{-1} of data at $E_{cm} = 4.17$ GeV in the analysis of D_s decays described below.

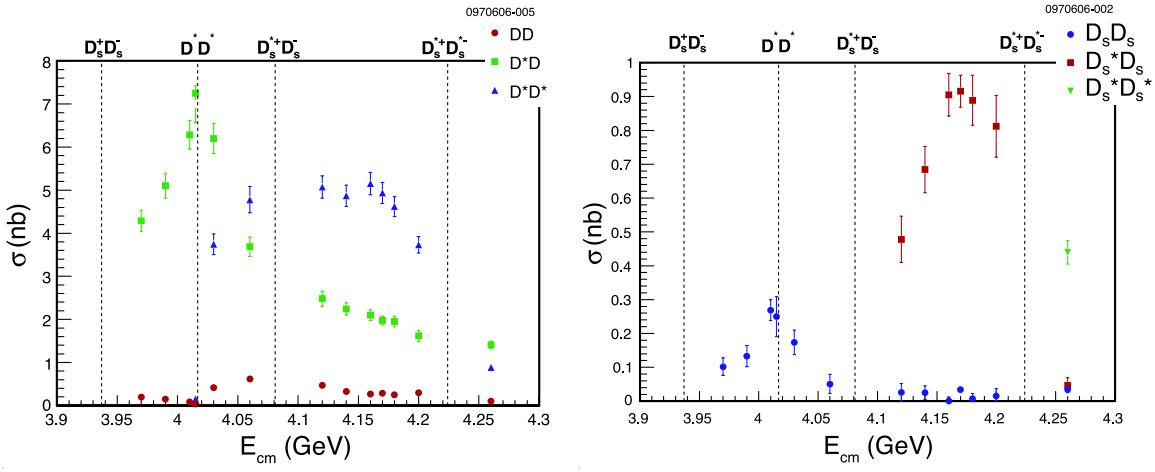

Figure 13: Preliminary CLEO-c cross sections for production of (left) $D^{(*)}\overline{D}^{(*)}$ and (right) $D_s^{+(*)}D_s^{-(*)}$ above the threshold for $D\overline{D}$ production in e^+e^- annihilation. In each graph thresholds are indicated by the vertical dashed lines.

4.2 Analysis of $D_s^{\pm}D_s^{*\mp}$ Events

CLEO chose to ignore the γ or π^0 from D_s^* decay to avoid the low efficiency for detecting the low energy γ or π^0 and the uncertainties in the efficiency for detecting either one of them. Instead, CLEO selects $D_s^{\pm}D_s^{*\mp}$ events using the invariant mass $M(D_s)$ of the D_s candidates and their beam-constrained mass M_{BC}, which is actually a proxy for momentum of the candidate. The M_{BC} distribution for the D_s candidates that were produced directly in the annihilation is relatively narrow, while the M_{BC} distribution for D_s candidates resulting from D_s^* decay is much broader. This is illustrated in Figure 14. Neither distribution is centered exactly on the D_s mass, because the beam energy is not exactly the energy of either the direct D_s or the average energy of the D_s from D_s^* decay.

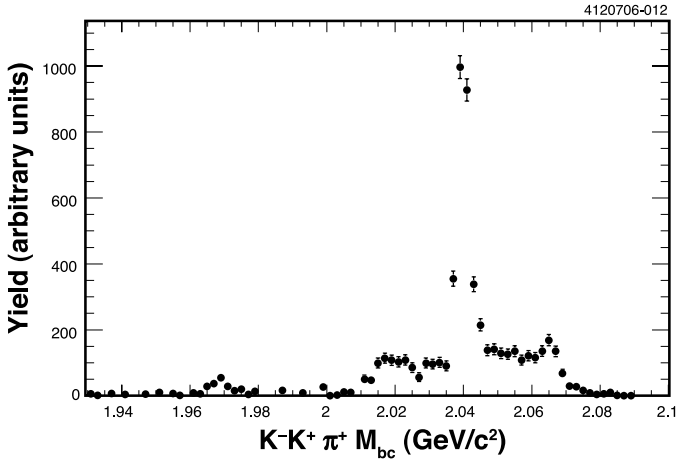

Figure 14: Histogram of M_{BC} for $D_s^+ \to K^-K^+\pi^+$ events from CLEO-c data. The narrow peak at the $M_{BC} = 2.04$ GeV is from $D_s^\pm$ produced directly, while the broad peak from $M_{BC} \approx 2.01$ GeV to $M_{BC} \approx 2.07$ GeV is from $D_s^\pm$ produced in $D_s^{*\pm}$ decay.

CLEO determines single-tag yields by fitting $M(D_s)$ distributions for candidates that pass a very loose cut on M_{BC}. Double-tag yields are determined by counting the numbers of events in signal regions in the $M(D_s^-)$ vs. $M(D_s^+)$ plane, and subtracting backgrounds determined from the numbers of events in sideband regions. These procedures are illustrated for $D_s^\pm \to K^-K^+\pi^\pm$ candidates in Figure 15.

The χ^2 fit [5] procedure used in the measurements of absolute D^0 and D^+ branching fractions is applied to the ST and DT yields for six D_s decay modes. Preliminary absolute branching fractions obtained from this analysis are given in Table 8, and these branching fractions are compared to the PDG06 averages in Figure 16. The preliminary CLEO-c results are clearly significantly more precise than the PDG06 averages. CLEO has an additional 130 pb^{-1} of data at this energy to be analyzed. These data will be included in the publication of the 195 pb^{-1} data sample.

Belle measures $\mathcal{B}(D_s^+ \to K^-K^+\pi^+)$ by applying a clever partial reconstruction technique to $e^+e^- \to D_s^{*\pm}D_{s1}^\mp(2536)$ events [26] that produces double tag data samples. A total of 552.3 fb^{-1} of data taken at the $\Upsilon(4S)$ were used in this analysis. In the first tag, the D_{s1} is fully reconstructed in the $D_{s1} \to D^*K$ mode, while only the γ from $D_s^* \to D_s\gamma$ is observed. In the second tag, the D_s^* is fully reconstructed in the decay chain $D_s^{*\pm} \to D_s^\pm\gamma$ followed by $D_s^\pm \to K^-K^+\pi^\pm$, while only the kaon from $D_{s1} \to D^*K$ is observed. Signal yields are determined by fitting missing mass distributions for the particles that are not reconstructed. The yields from the first tag are proportional to the branching fractions for the D^* decay chain, while the yields from the second tag are proportional to the branching fraction for $D_s^\pm \to K^-K^+\pi^\pm$. Hence, $\mathcal{B}(D_s^+ \to K^-K^+\pi^+)$ can be obtained from the ratio of the second tag yield

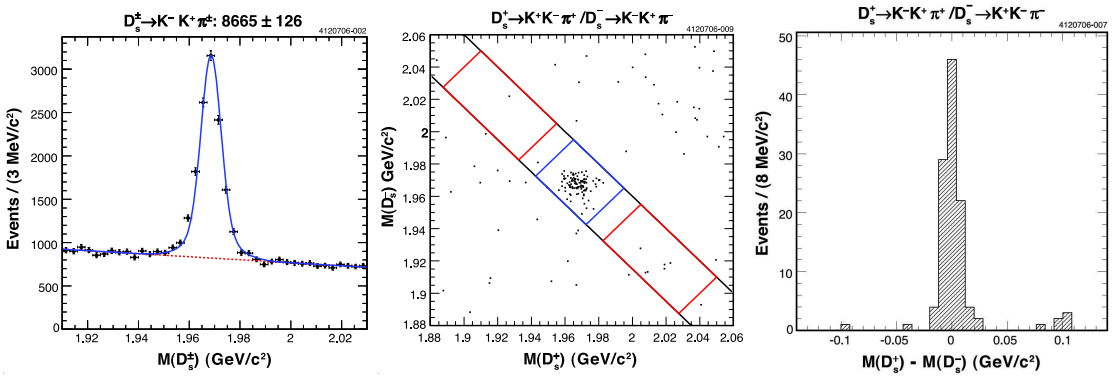

Figure 15: Plots illustrating the CLEO-c $D_s^{\pm}$ decay data: (left) the invariant mass distribution for single-tag $D_s^{\pm} \to K^-K^+\pi^{\pm}$ candidates, (middle) two-dimensional histogram of $M(D_s^-)$ vs. $M(D_s^+)$ for double-tag $D_s^{\pm} \to K^-K^+\pi^{\pm}$ candidates, (right) the mass difference $M(D_s^+) - M(D_s^-)$ for double-tag $D_s^{\pm} \to K^-K^+\pi^{\pm}$ candidates. In the two-dimensional histogram, the narrow (blue) box around the mass peak illustrates the signal region, and the two wider (red) boxes further away from the peak illustrate the sideband region.

D_s^+ Mode	$\mathcal{B}$ (%)
$K_S K^+$	$1.50 \pm 0.09 \pm 0.05$
$K^-K^+\pi^+$	$5.57 \pm 0.30 \pm 0.19$
$K^-K^+\pi^+\pi^0$	$5.62 \pm 0.33 \pm 0.51$
$\pi^+\pi^+\pi^-$	$1.12 \pm 0.08 \pm 0.05$
$\pi^+\eta$	$1.47 \pm 0.12 \pm 0.14$
$\pi^+\eta'$	$4.02 \pm 0.27 \pm 0.30$

Table 8: Preliminary absolute branching fractions for six hadronic $D_s^{\pm}$ decay modes measured by CLEO-c.

to the first tag yield, using known branching fractions for the D^* decay chain, and efficiencies.

The preliminary Belle and CLEO-c results are compared in Table 9 to each other and to the PDG06 [3] average. With its large error, the PDG 06 value is consistent with the Belle and CLEO-c results. However, the more precise Belle and CLEO-c are not very consistent with each other. Hence, more work will be required to be confident that we know absolute D_s^+ branching fractions.

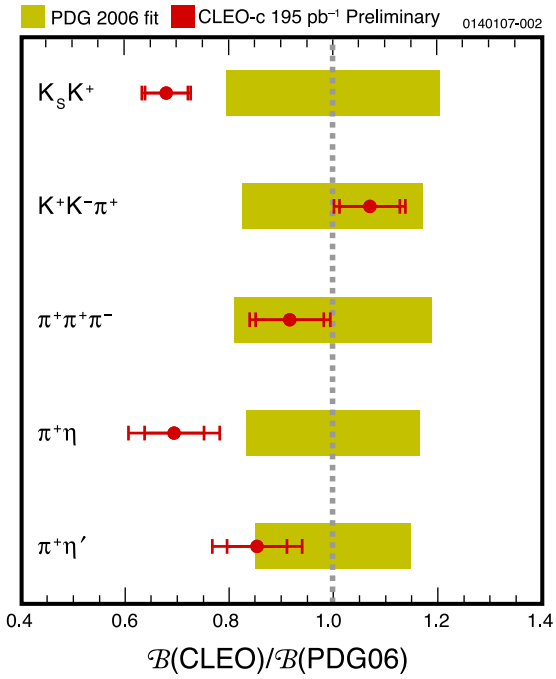

Figure 16: The ratios $\mathcal{B}$(CLEO)/$\mathcal{B}$(PDG06) of preliminary CLEO-c hadronic D_s^+ branching fractions to the PDG06 averages. The widths of the PDG bars correspond to the errors in the averages.

	$\mathcal{B}(D_s^+ \to K^-K^+\pi^+)$ (%)
Belle Preliminary	$4.0 \pm 0.4 \pm 0.4$
CLEO-c Preliminary	$5.57 \pm 0.30 \pm 0.19$
PDG06	5.2 ± 0.9

Table 9: Comparison of preliminary Belle and CLEO-c measurements of the absolute branching fraction for $D_s^+ \to K^-K^+\pi^+$ decay with the PDG06 average.

4.3 Partial $D_s^+ \to K^-K^+\pi^+$ Branching Fractions

The branching fraction of the decay chain $D_s^+ \to \phi\pi^+ \to K^-K^+\pi^+$ is one of the largest D_s^+ branching fractions, and – indeed – it was the decay sequence that provided the first observation of the D_s^+. A branching fraction called $\mathcal{B}(D_s^+ \to \phi\pi^+)$ has often been used as the reference branching fraction for D_s decays. As in the D_s^+ discovery, it is usually derived from a narrow mass cut around the ϕ peak in the $M(K^+K^-)$ distribution in $D_s^+ \to K^-K^+\pi^+$ events.

However, E687 [27] has published and FOCUS [28] has reported significant contributions from $f_0(980)$ (or $a_0(980)$) in the $\phi\pi$ region of the $D_s^+ \to K^-K^+\pi^+$ Dalitz plot. Figure 17 illustrates the invariant K^+K^- mass distribution for $D_s^+ \to K^-K^+\pi^+$ events. A noticeable contribution (presumably scalar) is visible under the ϕ peak in in this distribution. These contributions from other processes constitute approximately 5% of the total yield in a reasonable mass range in $M(K^-K^+)$ around the ϕ mass, M_ϕ. These contributions, which are not from $D_s^+ \to \phi\pi^+$ decays, are comparable to current CLEO-c errors for partial branching fractions obtained using a narrow mass cut around M_ϕ. Hence, it is now difficult to make a case for identifying such a partial branching fraction with $\mathcal{B}(D_s^+ \to \phi\pi^+)$. In response to this dilemma, CLEO now reports partial branching fractions, $\mathcal{B}_{\Delta M} \equiv \mathcal{B}(D_s^+ \to K^-K^+\pi^+)$ with $|M(K^-K^+) - M_\phi| < \Delta M$ MeV/c^2. Preliminary CLEO-c measurements with $\Delta M = 10$ and 20 MeV/c^2 are given in Table 10. I advocate using partial branching fractions like these for the reference branching fractions for other D_s^+ decays. As D_s^+ branching fraction measurements become more precise, I hope that we can reach agreement on a reasonable choice for a D_s^+ reference branching fraction for most other decays that is not called $\mathcal{B}(D_s^+ \to \phi\pi^+)$, even though it has non-negligible contributions from other resonances in the $K^-K^+\pi^+$ Dalitz plot.

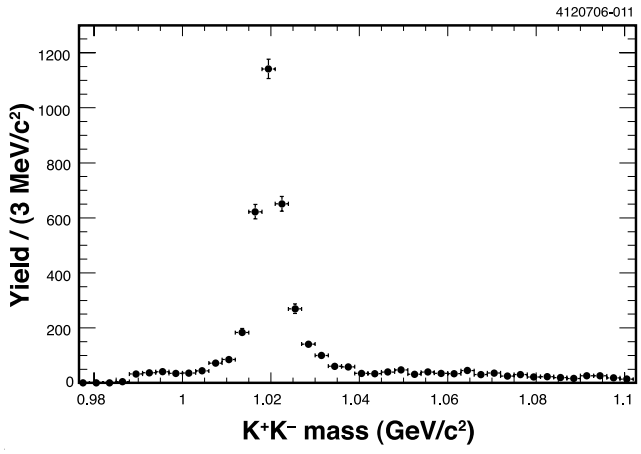

Figure 17: The invariant mass distribution $M(K^+K^-)$ for $D_s^+ \to K^-K^+\pi^+$ candidates in CLEO-c data.

5 Inclusive D^0, D^+, and D_s Decays to $s\overline{s}$

CLEO has measured branching fractions for inclusive D^0, D^+, and D_s decays to ηX, $\eta' X$, and ϕX [29]. Due to the $s\overline{s}$ content of η, η', and ϕ, we expect that the inclusive branching fraction for D_s decays to these particles would be larger than the

	$\mathcal{B}_{\Delta M}$ (%)
$\mathcal{B}_{10}$	$1.98 \pm 0.12 \pm 0.09$
$\mathcal{B}_{20}$	$2.25 \pm 0.13 \pm 0.12$
PDG06	1.77 ± 0.44

Table 10: Preliminary partial branching fractions $\mathcal{B}_{\Delta M} \equiv \mathcal{B}(D_s^+ \to K^-K^+\pi^+)$ with $|M(K^-K^+) - M_\phi| < \Delta M$ MeV/c^2 measured by CLEO. The PDG06 result is determined from $\mathcal{B}(\phi \to K^-K^+)$ and reported $\mathcal{B}(D_s^+ \to \phi\pi^+)$ values.

branching fractions for corresponding D^0 and D^+ decays. CLEO fully reconstructs one D in a favorable mode used in the absolute measurements of hadronic branching fractions. Selection criteria for these D decay candidates include requirements on ΔE (see Section 2). Then CLEO searches for η, η' and ϕ in the decay products from the other D. For this analysis, CLEO utilizes 281 pb^{-1} of $\psi(3770)$ data for D^0 and D^+ decays and 195 pb^{-1} of data at $E_{cm} \approx 4.17$ GeV for D_s decays.

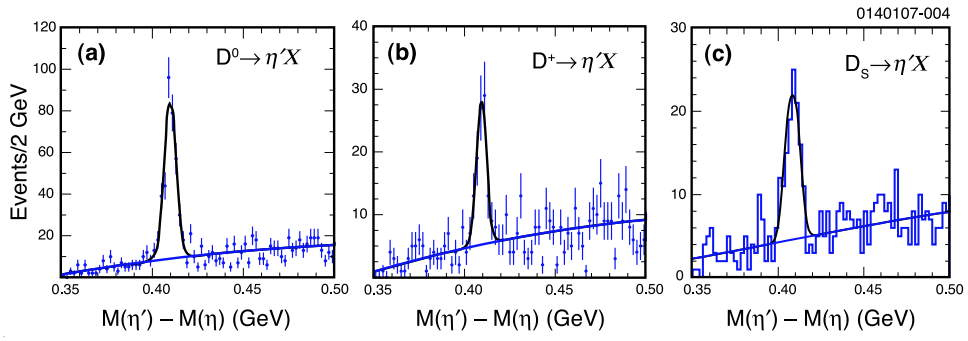

Figure 18: Histograms of the mass differences between η' and η candidates with $\eta' \to \eta\pi^+\pi^-$ with $\eta \to \gamma\gamma$: (a) candidates for $D^0 \to \eta' X$ decay, (b) candidates for $D^+ \to \eta' X$ decay, and (c) candidates for $D_s \to \eta' X$ decay.

Figure 18 illustrates the data used to determine the inclusive $\eta' X$ signal yields. For these inclusive modes, CLEO uses distributions in $M(\eta') - M(\eta)$, the difference between the invariant masses of the η' candidate and the η candidate in its decay chain. Similar distributions for $M(\eta)$ and $M(\phi)$ are used to determine the signal yields for ηX and ϕX. Fitted yields from ΔE sidebands are then subtracted from the signal yields. The resulting inclusive branching fractions are given in Table 11. These results lead to several qualitative observations including:

- η's and ϕs are relatively rare in D^0 and D^+ decay,

- ηs with their lower mass and larger light quark content are produced at substantially higher rates in D^0 and D^+ decays than η' and ϕ,
- the ϕ rate in D_s decay is much higher than it is in D^0 and D^+ decay, and
- the higher ϕ rates in D_s decay can be used to separate D_s from D^0 and D^+ at $\Upsilon(5S)$ and hadron colliders.

CLEO has already used the observation in the last bullet to study the B_s fraction in the final states in $\Upsilon(5S)$ decay [30].

Mode	$\mathcal{B}(D^0)$ (%)	$\mathcal{B}(D^+)$ (%)	$\mathcal{B}(D_s^+)$ (%)
ηX	$9.5 \pm 0.4 \pm 0.8$	$6.3 \pm 0.5 \pm 0.5$	$23.5 \pm 3.1 \pm 2.0$
$\eta' X$	$2.48 \pm 0.17 \pm 0.21$	$1.04 \pm 0.16 \pm 0.09$	$8.7 \pm 1.9 \pm 0.8$
ϕX	$1.05 \pm 0.08 \pm 0.07$	$1.03 \pm 0.10 \pm 0.07$	$16.1 \pm 1.2 \pm 1.1$

Table 11: Branching fractions for inclusive $D \to s\overline{s}X$ decays measured by CLEO.

6 Dalitz Analyses of Hadronic D Decays

In the last decade, large samples of hadronic D decays have been available to the E791 and FOCUS collaborations from fixed target experiments at Fermilab, and to the CLEO, BaBar, and Belle collaborations from e^+e^- collider experiments. Dalitz analyses of these data samples have enabled new insights into the resonant substructure of multibody hadronic D decays. Historically, simply disentangling the resonant substructure has been the major emphasis of these studies. More recently Dalitz analyses of D decays have been stimulated by the possibility that the results can be used to determine the CKM matrix angles γ or ϕ_3.

6.1 Dalitz Analyses of $D^+ \to \pi^+\pi^+\pi^-$ Decays

It has long been understood that several $\pi^+\pi^-$ resonances are likely to contribute to the resonant substructure of $D^+ \to \pi^+\pi^+\pi^-$ decay. These include $\rho^0(770)$, $f_0(980)$, $f_2(g)$, and possible other higher resonances. On the other hand, there has been evidence (not always conclusive) that a lower mass S-wave $\pi^+\pi^-$ state called the σ^0 might exist and might contribute to $D^+ \to \pi^+\pi^+\pi^-$ decay. Finding proof for or against the existence of this state and its contribution to $D^+ \to \pi^+\pi^+\pi^-$ decays has been a major concern of Dalitz analyses of this final state.

The choice of the theoretical model used to fit the Dalitz plot has complicated interpretation of these analyses. The isobar model, in which the decay amplitude is written as a sum of Breit-Wigner resonances for the various contributions, is perhaps

the simplest to interpret [31,32]. However, there are technical difficulties with broad and overlapping resonances in this approach. In principle the K-matrix formalism overcomes many of these difficulties [33], and analyses using it have begun to appear [34]. However, there is relatively little experience with the K-matrix formalism in Dalitz analyses of charm decay.

Dalitz Analysis of $D^+ \to \pi^+\pi^+\pi^-$ Decays from E791

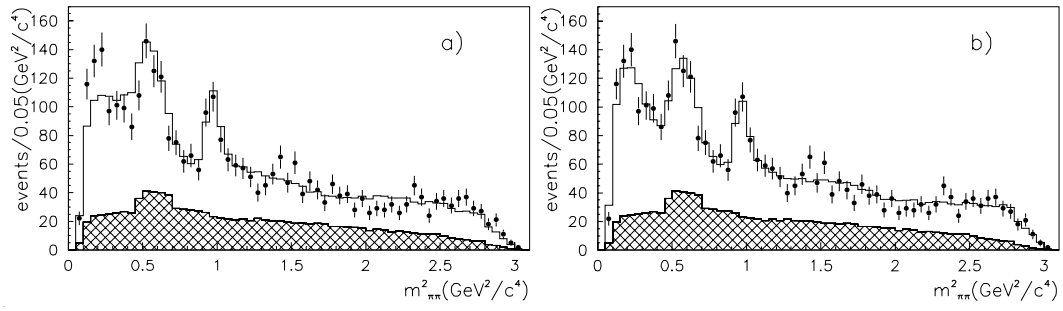

Figure 19: Dalitz plot projections of the E791 data and fits for $D^+ \to \pi^+\pi^+\pi^-$ on the squares of invariant $\pi\pi$ masses: (a) for the fit without a low mass scalar contribution and (b) for the fit with a low mass scalar contribution. The histograms for the two $\pi^+\pi^-$ combinations are summed, and the shaded histograms are the background contributions. [10,35]

The E791 Dalitz analysis of $D^+ \to \pi^+\pi^+\pi^-$ decays utilizes 1,686 candidates produced in 500 GeV/c π^--nucleon interactions [31]. In their isobar model they included contributions from the established resonances $\rho^0(770)$, $f_0(980)$, $f_2(1270)$, $f_0(1370)$, and $\rho^0(1450)$, and a non-resonant contribution. The projection of the fit with these resonances onto the $m^2_{\pi^+\pi^-}$ axis is illustrated in Figure 19(a). Clearly the fit does not represent well the data in the low mass region, $m^2_{\pi^+\pi^-} \approx 0.25$ GeV/c^2. Figure 19(b) shows that the fit is much closer to the data when E791 includes a low mass scalar σ^0 contribution. The fit fractions obtained by E791 are given in Table 12. It is interesting to note that the σ^0 contribution has the largest fit fraction.

Dalitz Analysis of $D^+ \to \pi^+\pi^+\pi^-$ Decays from CLEO

CLEO reported a preliminary Dalitz analysis of $D^+ \to \pi^+\pi^+\pi^-$ decay [36] using an isobar model similar to the one used by E791. The CLEO-c data sample included 4,100 events with a signal to noise ratio of about two to one. Projections on the isobar fit on the $m^2_{\pi^+\pi^-}$ and $m^2_{\pi^+\pi^+}$ axes are illustrated in Figure 20. The preliminary CLEO results are also listed in Table 12. Except for the $\rho(770)\pi^+$ contribution, the results of the two fits are in good agreement.

	CLEO (%)	E791 (%)
$\sigma^0\pi^+$	41.8 ± 2.9	46.3 ± 9.2
$\rho^0\pi^+$	20.0 ± 2.5	33.6 ± 3.9
$f_0(980)\pi^+$	4.1 ± 0.9	6.2 ± 1.4
$f_2(1270)\pi^+$	18.2 ± 2.7	19.4 ± 2.5
$f_0(1370)\pi^+$	2.6 ± 1.9	2.3 ± 1.7
$f_0(1500)\pi^+$	3.4 ± 1.3	—
Non Res	< 3.5	7.8 ± 6.6
$\rho(1450)\pi^+$	< 2.4	7.8 ± 0.6

Table 12: Fit fraction results of isobar Dalitz fits from E791 and CLEO for contributions to $D^+ \to \pi^+\pi^+\pi^-$ decays. The E791 results were published, while the CLEO results are preliminary.

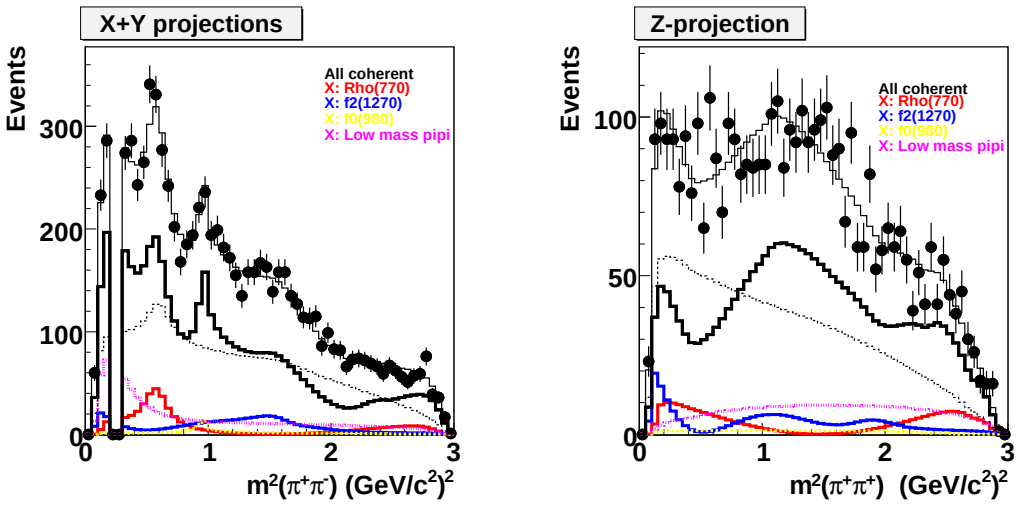

Figure 20: Preliminary Dalitz plot projections on the squares of invariant $\pi\pi$ masses of the CLEO-c data and fits for $D^+ \to \pi^+\pi^+\pi^-$: (left) projections on the $\pi^+\pi^-$ invariant mass squared axis and (right) projections on the $\pi^+\pi^+$ invariant mass squared axis. The empty bin at $m^2_{\pi^+\pi^-} = 0.25$ GeV/c^2 is due to a K^0_S mass cut.

Dalitz Analysis of $D^+ \to \pi^+\pi^+\pi^-$ Decays from FOCUS

FOCUS reported [34] a Dalitz analysis performed on 1,527 $D^+ \to \pi^+\pi^+\pi^-$ decay candidates. In the fit to the data, FOCUS included a nonresonant contribution, traditional isobar Breit-Wigner terms for $\rho^0(770)$ and $f_2(1270)$ contributions, and an

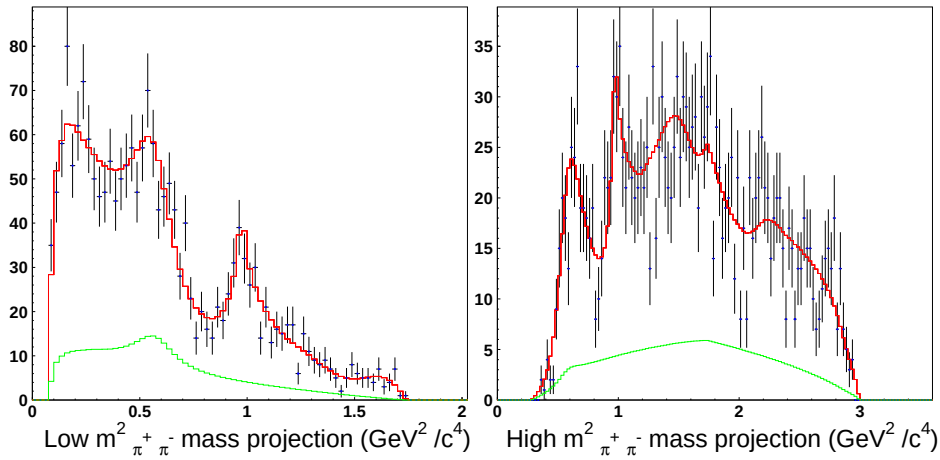

Figure 21: Dalitz plot projections of the FOCUS data and fits for $D^+ \to \pi^+\pi^+\pi^-$ on the squares of invariant $\pi\pi$ masses: (a) projections on the low-mass $\pi^+\pi^-$ combination and (b) projections on the high-mass $\pi^+\pi^-$ combination. [37]

S-wave contribution. The S-wave contribution is not represented as a sum of scalar resonance contributions; it is represented by a K-matrix parameterization with five pole contributions. The projections of the high and low mass combinations of the FOCUS data and fits on the $m^2_{\pi^+\pi^-}$ axis are illustrated in Figure 21. Perhaps the most illuminating comparisons of the FOCUS results with E791 and CLEO are the fit fractions of the $\rho^0(770)$ and $f_2(1270)$ contributions, which are 30.8±3.9 and 11.7±1.9, respectively. Although there is qualitative agreement among the three experiments, a comprehensive understanding of the resonant substructure of $D^+ \to \pi^+\pi^+\pi^-$ will require substantially larger data samples and a better understanding of the strengths and weaknesses of the isobar and K-matrix formalisms.

6.2 Dalitz Analyses that Contribute to Measuring γ or ϕ_3

Utilization of Dalitz analyses of D^0 decays [38–40] to enable measurements of the CKM angle γ or ϕ_3 is one of the more surprising and interesting applications of these analyses. These techniques for measuring[1] γ utilize $B^\pm \to \hat{D}^{0(*)}K^\pm$ decays, where $\hat{D}^0$ can be D^0 or $\overline{D}^0$ and the superscript $(*)$ denotes either D or D^*. The core idea [41] is that the decay can be either Cabibbo favored (*e.g.*, $B^- \to D^0K^-$) or doubly Cabibbo suppressed (*e.g.*, $B^- \to \overline{D}^0K^-$). If the D^0 and $\overline{D}^0$ decay to the same final state (*e.g.*, $\hat{D}^0 \to K^0_S\pi^+\pi^-$) the amplitudes for these two decays can interfere. The phase of the interference term includes γ and a strong phase; the former changes

[1]To simplify notation, I will use γ for either γ or ϕ_3, or both.

sign between B^- and B^+ decays, while the latter does not. Hence, this interference can generate a direct CP violation, a difference between the rates of $B^+ \to \hat{D}^{0(*)}K^+$ and $B^- \to \hat{D}^{0(*)}K^-$ decays. However, amplitude ratios and the strong phase in the D decay are required to determine γ from a measured $B^\pm$ decay rate asymmetry, and these parameters can be determined in a Dalitz analysis of D^0 or $\overline{D}^0$ decays to the appropriate final state.

Dalitz Analyses of $D \to K^0_S\pi^+\pi^-$ Decays to Measure γ

Recently, Babar [38] and Belle [39] analyzed the Dalitz plot for $\hat{D}^0 \to K^0_S\pi^+\pi^-$ decays in $B^\pm \to \hat{D}^{0(*)}K^\pm$ decays. For the Dalitz analyses, Belle utilized 262,000 signal events from a 357 fb^{-1} data sample, and Babar utilized 81,500 signal events from 91.5 fb^{-1} of data. The purity of each final $\hat{D}^0$ data samples was approximately 97%. Both groups fit their Dalitz plots with isobar models; BaBar fit 16 two-body states and Belle fit 18 two-body states, and the BaBar states are a subset of the Belle states. The projections of the data and fits on the Dalitz plot axes from the Belle and Babar are illustrated in Figures 23 and 22, respectively. Due to the enormous data samples, the errors on the data points are very small. The ability of the fits to match the data so well is remarkable. The fit fractions for the four most prominent resonant contributions are given in Table 13. Once again these analyses demonstrate that high quality charm decay measurements can be derived from the enormous BaBar and Belle data samples.

From these analyses, Belle finds $\phi_3 = 53^\circ\ ^{+15^\circ}_{-18^\circ} \pm 3^\circ \pm 9^\circ$ and Babar finds $\gamma = 70^\circ \pm 31^\circ\ ^{+12^\circ}_{-10^\circ}\ ^{+14^\circ}_{-11^\circ}$, where the third errors are estimates of the uncertainties in the Dalitz decay models. Within the large statistical errors there is good agreement between the two results. Since the statistical errors are larger than the systematic errors, there is room for improvement from the data that the two collaborations have not used in these analyses.

State	BaBar (%)	Belle (%)
$K^*(892)^+\pi^-$	58.6	61.2
$K^0_S\rho^0$	22.4	21.6
$K^0_S\sigma$	9.3	9.8
Non Res	7.3	9.7

Table 13: The fit fractions for the four most prominent resonant contributions to $\hat{D}^0 \to K^0_S\pi^+\pi^-$ obtained by BaBar and Belle.

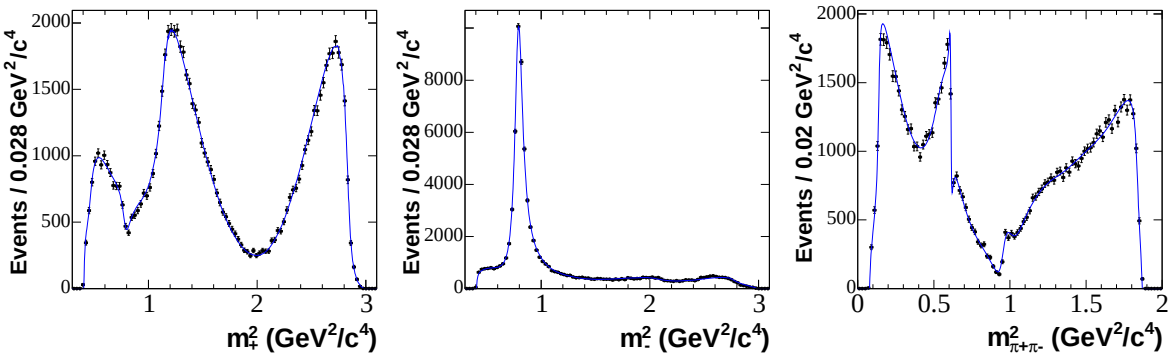

Figure 22: Dalitz plot projections on the squares of invariant masses of the BaBar data and fits for $D \to K^0_S\pi^+\pi^-$: (left) projections on the $K^0_S\pi^+$ invariant mass squared axis, (middle) projections on the $K^0_S\pi^-$ invariant mass squared axis, and (right) projections on the $\pi^+\pi^-$ invariant mass squared axis. [10, 42]

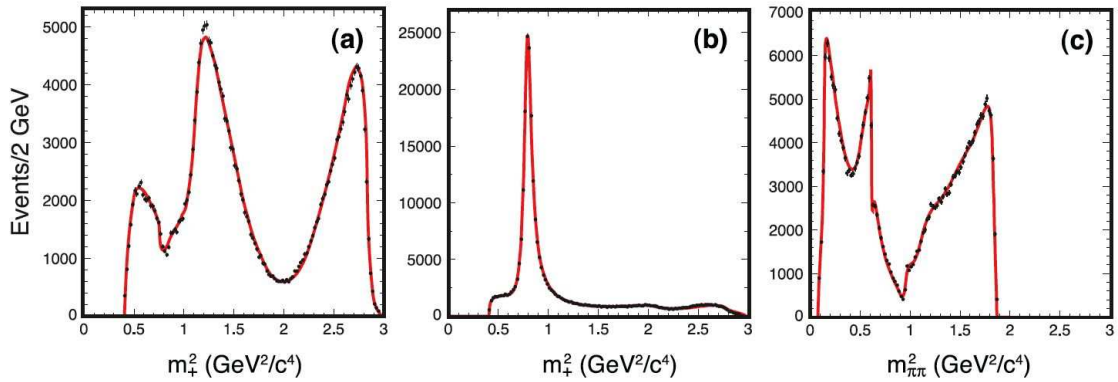

Figure 23: Dalitz plot projections on the squares of invariant masses of the Belle data and fits for $D \to K^0_S\pi^+\pi^-$: (a) projections on the $K^0_S\pi^+$ invariant mass squared axis, (b) projections on the $K^0_S\pi^-$ invariant mass squared axis, and (c) projections on the $\pi^+\pi^-$ invariant mass squared axis. [10, 43]

Dalitz Analysis of $D^0 \to K^+K^-\pi^0$ Decays to Measure γ

CLEO has studied the Dalitz plot of $D^0 \to K^+K^-\pi^0$ decays [40], which can also be used to measure γ in $B^\pm \to \hat{D}^0K^\pm$ decays. The relative complex amplitude for $D^0 \to K^{*+}K^-$ and $D^0 \to K^{*+}K^-$ decays is required to determine γ. This relative amplitude is the same as that for the two decays $D^0 \to K^{*-}K^+$ and $\overline{D}^0 \to K^{*+}K^-$ (and their charge conjugates) assuming CP conservation in these $\hat{D}^0$ decays. CLEO found 735 $D^0 \to K^-K^+\pi^0$ candidates in 9.0 fb^{-1} of data taken with the CLEO III

detector. The Dalitz plot for the events were fit with 13 resonance components and a flat non resonant component. Four of these components, K^{*+}, K^{*-}, ϕ and non-resonant had the largest fit fractions. The projections of the fit on the three mass-squared axes are illustrated in Figure 24. The relative complex amplitude for the $K^{*\pm}K^{\mp}$ decays is defined by,

$$r_D e^{i\delta_D} \equiv \frac{a_{K^{*-}K^+}}{a_{K^{*+}K^-}} e^{i(\delta_{K^{*-}K^+} - \delta_{K^{*+}K^-})}$$

where the a's are the real parts of the amplitudes and the δ's are the phase shifts. The results for r_D and δ_D are $r_D = 0.52 \pm 0.05 \pm 0.04$ and $\phi_D = 332^\circ \pm 8^\circ \pm 11^\circ$.

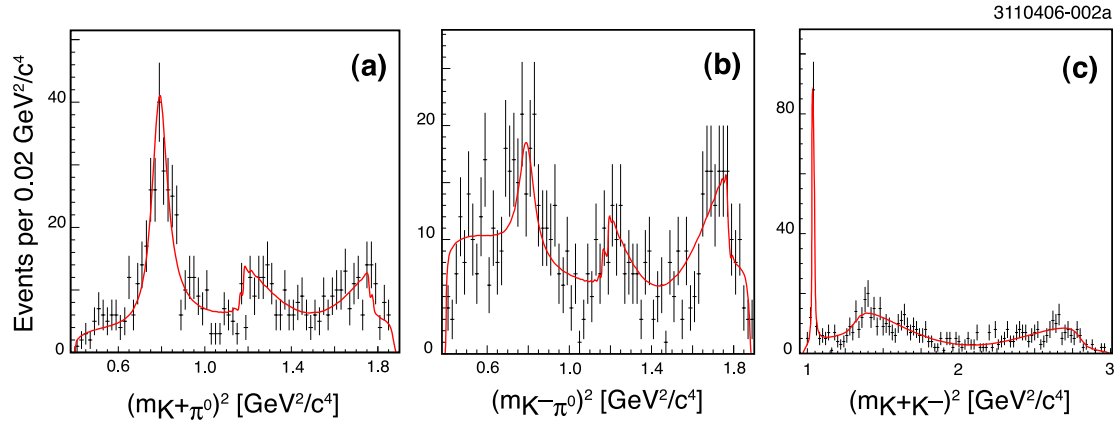

Figure 24: Dalitz plot projections on the squares of invariant masses of the CLEO-c data and fits for $D^0 \to K^+K^-\pi^0$: (a) projections on the $K^+\pi^-$ invariant mass squared axis, (b) projections on the $K^-\pi^0$ invariant mass squared axis, and (c) projections on the K^+K^- invariant mass squared axis.

6.3 Analysis of $D^0 \to K^+K^-\pi^+\pi^-$ Decays from FOCUS

A study of resonant substructure in $D^0 \to K^+K^-\pi^+\pi^-$ decay [16] from FOCUS is the only substantial effort to study resonances in four-body charm decays. After all cuts, FOCUS obtained 1279 ± 48 $D^0 \to K^+K^-\pi^+\pi^-$ events above a modest background. A total of 10 resonant/decay contributions were considered in the analysis; three of these were $K_1(1270)K^-$ where the K_1 decayed to states with other resonances, $\rho^0(770)K^+$, $K_0^*(1430)\pi^+$, and $K^*(890)\pi^+$. The results of the fits projected onto invariant mass axes are illustrated in Figure 25. The fit fractions for the largest components are given in Table 14.

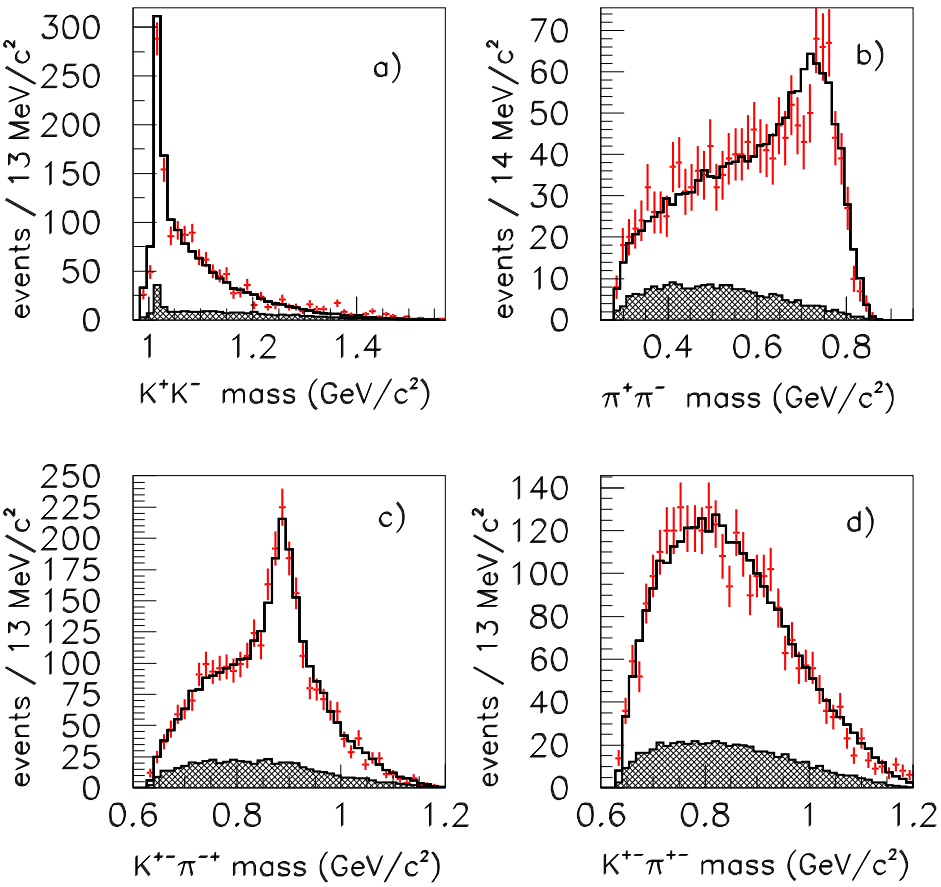

Figure 25: Two-body invariant mass distributions from the FOCUS Collaboration's study the four-body decay $D^0 \to K^+K^-\pi^+\pi^-$. [44]

Mode	Fit Fraction (%)
$K_1(1270)^+K^-$	$33 \pm 6 \pm 4$
$K_1(1400)^+K^-$	$22 \pm 3 \pm 4$
$\phi\rho^0$	$29 \pm 2 \pm 1$
$K^*(1400)^0K^+\pi^-$	$11 \pm 1 \pm 1$
$f_0(980)\pi^+\pi^-$	$15 \pm 3 \pm 2$

Table 14: Fit fractions for the largest components in the FOCUS Dalitz analysis of $D^0 \to K^+K^-\pi^+\pi^-$ decays.

7 Summary and Conclusions

The large data samples and high-quality detectors of the BaBar, Belle, and CLEO-c experiments have led to substantial advances in precision and discovery reach of charm physics. The CLEO Collaboration, operating the CLEO-c detector in the charm threshold region, is measuring absolute D hadronic branching fractions with unprecedented precision.

CLEO reports preliminary results for D^0 and D^+ absolute branching fractions obtained from 281 pb^{-1} of $e^+e^- \to \psi(3770) \to D^+D^-$ or $D^0\overline{D}^0$ data. These results are limited by systematic errors that are as low as $\lesssim 3\%$. CLEO expects to reduce these systematic errors via an ongoing effort. At this level of precision, final state radiation, whose effects are $\lesssim 2\%$, must be considered. This is an interesting problem for the Particle Data Group, since most measurements of branching fractions do not take FSR into account.

CLEO also reports preliminary results for hadronic D_s branching fractions from 195 pb^{-1} of e^+e^- annihilation data taken near $E_{cm} = 4.17$ GeV, which is just above the $D_s^{\pm}D_s^{*\mp}$ threshold. These results, with errors generally below 10%, are a substantial improvement over previous measurements, although they are limited by statistics. CLEO has an additional 130 pb^{-1} of data at this energy to be analyzed, and plans to take more data at this energy in the future. The resonant substructure of the $D_s \to K^-K^+\pi^+$ decay mode is becoming an issue, since one of the contributions to this mode is $D_s \to \phi\pi^+$, which has often been used as a reference branching faction for other D_s decays. There appears to be a significant contribution ($\sim 5\%$) from scalar resonances in a reasonable region in the $M(K^+K^-)$ mass distribution around the ϕ peak. Since the error of the CLEO measurements of $\mathcal{B}(D_s \to K^-K^+\pi^+)$ are comparable to the scalar contribution under the ϕ, we need to define a new reference branching fraction for D_s decays

In addition to the measurements of Cabibbo-favored branching fractions mentioned in the previous paragraphs, many new and accurate measurements of singly- and doubly-Cabibbo-suppressed branching fractions are appearing. BaBar, Belle, and CLEO-c are active in these analyses. By utilizing their enormous data samples, BaBar and Belle are starting to dominate measurements of the ratios of branching fractions to reference-mode branching fractions.

There is substantially increased activity in the Dalitz analyses of hadronic final states of D decays. However, there are serious ambiguities in these analyses due to uncertainties in how to specify the amplitude for the resonant contributions. For example, E791, FOCUS, and CLEO have all reported Dalitz analyses of $D^+ \to \pi^+\pi^+\pi^-$. E791 and CLEO utilize a standard isobar parameterization of the decay amplitude, while FOCUS uses a K-matrix description which has some theoretical advantages. From these three experiments there is general agreement on the main resonant contributions to this decay, but there is important disagreement on the details, particularly

on the presence of a σ scalar contribution to the decay. Developing a consensus on the proper treatment of resonant substructure with multiple overlapping states will become even more important as the larger data samples with higher purity become available.

BaBar and Belle report Dalitz analyses of $D \to K^0_S\pi^+\pi^-$ decays as byproducts of their studies of $B^\pm \to \hat{D}^{0(*)}K^\mp$ decays to measure the CKM angle γ or ϕ_3. These collaborations are able to select enormous data samples with high purity from tagged B decays. CLEO reports a Dalitz analysis of $D^0 \to K^+K^-\pi^0$ decays which can also be used in a determination of γ or ϕ_3.

FOCUS reported the first analysis of the resonant substructure of a four-body hadronic charm decay, $D^0 \to K^+K^-\pi^+\pi^-$. This result on a relatively modest data sample demonstrates that analyses of resonant substructure of charm decays to four or more bodies is a fertile field of research.

In the near future, we can look forward to many more exciting and precise results from the charm sector from the BaBar, Belle, and CLEO collaborations. In the slightly farther future, we expect that the BESIII experiment operating in the charm threshold region at the BEPCII e^+e^- storage ring in Beijing will open a new frontier in the precision and reach of charm decay experiments.

Acknowledgements

I am delighted to acknowledge the contributions of my CLEO and CESR colleagues whose effort produced the CLEO results reported here and many other important measurements in the heavy flavor sector over the years. This report is based upon work supported by the National Science Foundation under Cooperative Agreement No. 0202078. It is a pleasure to acknowledge the generous hospitality of Prof. S. Paul and the staff of HQL06, and the cooperation of the editors of the proceedings.

Bibliography

[1] R. M. Baltrusaitis *et al.* [MARK-III Collaboration], Phys. Rev. Lett. **56**, 2140 (1986).

[2] J. Adler *et al.* [MARK-III Collaboration], Phys. Rev. Lett. **60**, 89 (1988).

[3] W. M. Yao *et al.* [Particle Data Group], J. Phys. G **33**, 1 (2006).

[4] Q. He *et al.* [CLEO Collaboration], Phys. Rev. Lett. **95**, 121801 (2005) [Erratum-ibid. **96**, 199903 (2006)] [arXiv:hep-ex/0504003].

[5] W. M. Sun, Nucl. Instrum. Meth. A **556**, 325 (2006) [arXiv:physics/0503050].

[6] S. Eidelman *et al.* [Particle Data Group], Phys. Lett. B **592**, 1 (2004).

[7] P. Rubin *et al.* [CLEO Collaboration], Phys. Rev. Lett. **96**, 081802 (2006) [arXiv:hep-ex/0512063].

[8] M. Selen *et al.* [CLEO Collaboration], Phys. Rev. Lett. **71**, 1973 (1993)

[9] Reprinted figure with permission from Ref. [11]. Copyright 2006 by the American Physical Society.

[10] Readers may view, browse, and/or download material for temporary copying purposes only, provided these uses are for noncommercial personal purposes. Except as provided by law, this material may not be further reproduced, distributed, transmitted, modified, adapted, performed, displayed, published, or sold in whole or in part, without prior written permission from the American Physical Society.

[11] B. Aubert *et al.* [BABAR Collaboration], Phys. Rev. D **74**, 091102 (2006) [arXiv:hep-ex/0608009].

[12] [BELLE Collaboration], BELLE-CONF-0608, [arXiv:hep-ex/0610062].

[13] D. M. Asner *et al.* [CLEO Collaboration], Phys. Rev. D **54**, 4211 (1996).

[14] Reprinted from Ref. [15], Copyright 2005, with permission from Elsevier

[15] J. M. Link *et al.* [FOCUS Collaboration], Phys. Lett. B **607**, 59 (2005) [arXiv:hep-ex/0410077].

[16] J. M. Link *et al.* [FOCUS Collaboration], Phys. Lett. B **610**, 225 (2005) [arXiv:hep-ex/0411031].

[17] Reprinted figure with permission from Ref. [18]. Copyright 2006 by the American Physical Society.

[18] B. Aubert *et al.* [BABAR Collaboration], Phys. Rev. D **74**, 011107 (2006) [arXiv:hep-ex/0605044].

[19] S. A. Dytman *et al.* [CLEO Collaboration], Phys. Rev. D **74**, 071102 (2006) [Erratum-ibid. D **74**, 079904 (2006)] [arXiv:hep-ex/0609008].

[20] I. I. Y. Bigi and H. Yamamoto, Phys. Lett. B **349**, 363 (1995) [arXiv:hep-ph/9502238].

[21] Q. He *et al.* [CLEO Collaboration], CLEO CONF 06-11, [arXiv:hep-ex/0607068].

[22] J. L. Rosner, Phys. Rev. D **74**, 057502 (2006) [arXiv:hep-ph/0607346].

[23] M. Artuso *et al.* [CLEO Collaboration], Phys. Lett. B **378**, 364 (1996).

[24] B. Aubert *et al.* [BaBar Collaboration], Phys. Rev. D **71**, 091104 (2005) [arXiv:hep-ex/0502041].

[25] N. E. Adam *et al.* [CLEO Collaboration], CLEO CONF 06-13, submitted to ICHEP06, [arXiv:hep-ex/0607079].

[26] K. Abe [Belle Collaboration], BELLE-CONF-0612, submitted to ICHEP06, [arXiv:hep-ex/0701053].

[27] P. L. Frabetti *et al.* [E687 Collaboration], Phys. Lett. B **351**, 591 (1995).

[28] S. Malvezzi, AIP Conf. Proc. **549**, 569 (2002).

[29] G. S. Huang [CLEO Collaboration], Phys. Rev. D **74**, 112005 (2006) [arXiv:hep-ex/0610008].

[30] G. S. Huang *et al.* [CLEO Collaboration], Phys. Rev. D **75**, 012002 (2007) [arXiv:hep-ex/0610035].

[31] E. M. Aitala *et al.* [E791 Collaboration], Phys. Rev. Lett. **86**, 770 (2001) [arXiv:hep-ex/0007028].

[32] S. Kopp *et al.* [CLEO Collaboration], Phys. Rev. D **63**, 092001 (2001) [arXiv:hep-ex/0011065].

[33] M. R. Pennington, Int. J. Mod. Phys. A **21**, 5503 (2006) [arXiv:hep-ph/0608016].

[34] J. M. Link *et al.* [FOCUS Collaboration], Phys. Lett. B **585**, 200 (2004) [arXiv:hep-ex/0312040].

[35] Reprinted figure with permission from Ref. [31]. Copyright 2001 by the American Physical Society.

[36] G. Bonvicini *et al.* [CLEO Collaboration], CLEO CONF 06-14, [arXiv:hep-ex/0607069].

[37] Reprinted from Ref. [34], Copyright 2004, with permission from Elsevier

[38] B. Aubert *et al.* [BABAR Collaboration], Phys. Rev. Lett. **95**, 121802 (2005) [arXiv:hep-ex/0504039].

[39] A. Poluektov *et al.* [Belle Collaboration], Phys. Rev. D **73**, 112009 (2006) [arXiv:hep-ex/0604054].

[40] C. Cawlfield *et al.* [CLEO Collaboration], Phys. Rev. D **74**, 031108 (2006) [arXiv:hep-ex/0606045].

[41] For references to the theoretical literature, see Refs. [38–40].

[42] Reprinted figure with permission from Ref. [38]. Copyright 2005 by the American Physical Society.

[43] Reprinted figure with permission from Ref. [39]. Copyright 2006 by the American Physical Society.

[44] Reprinted from Ref. [16], Copyright 2005, with permission from Elsevier

Spectroscopy and Decay of B Hadrons at the Tevatron

Manfred Paulini
for the CDF and DO Collaboration
Carnegie Mellon University
Department of Physics
Pittsburgh, PA 15213, U.S.A.

1 Introduction

Traditionally, B physics has been the domain of e^+e^- machines operating on the $\Upsilon(4S)$ resonance or the Z^0 pole. But the UA 1 Collaboration has already shown that B physics is feasible at a hadron collider environment (see for example Ref. [1]). The first signal of fully reconstructed B mesons at a hadron collider has been published by the CDF Collaboration in 1992 [2]. CDF reconstructed a handful of $B^+ \to J/\psi K^+$ events in a data sample of 2.6 pb^{-1} taken during the Tevatron Run 0 at the end of the 1980's. Since then experimental techniques improved significantly. Especially with the development of high precision silicon vertex detectors, the study of B hadrons is now an established part of the physics program at hadron colliders.

The CDF and DO experiments can look back to an already successful B physics program during the 1992-1996 Run I data taking period (for a review of B physics results from, for example, CDF in Run I see Ref. [3]). Nowadays, B physics results from a hadron collider are fully competitive with the e^+e^- B factories. As discussed later in this review, with the operation of a hadronic track trigger, CDF reconstructs fully hadronic B decay modes without leptons in the final state. In many cases, the measurements performed at the Tevatron Collider are complementary to the B factories. For example, no B_s^0 mesons or baryons containing b quarks are produced on the $\Upsilon(4S)$ resonance.

B hadrons not produced at the B factories are the topics of this review. We discuss the spectroscopy of excited B states (B^{**}, B_s^{**}) and the observation of the Σ_b baryon at the Tevatron. The second part of this review discusses the decays of B hadrons and measurements of branching fractions. We focus on charmless two-body decays of $B \to h^+h^-$. We end this article by summarizing our finding in the conclusions.

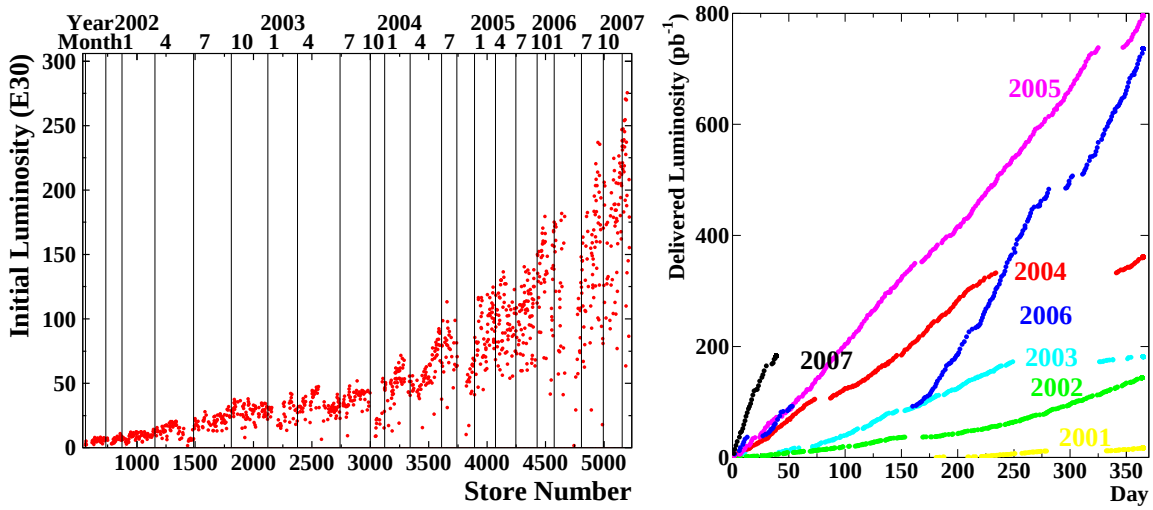

Figure 1: Tevatron (left) initial store luminosity from 2002-2006 and (right) delivered luminosity per calendar year.

2 The Tevatron with the CDF & DO Experiments

The Fermilab accelerator complex has undergone a major upgrade in preparation for Tevatron Run II. The centre-of-mass energy has been increased to 1.96 TeV as compared to 1.8 TeV during Run I and the Main Injector, a new 150 GeV proton storage ring, has replaced the Main Ring as injector of protons and anti-protons into the Tevatron. The present bunch crossing time is 396 ns with a 36×36 $p\overline{p}$ bunch operation. The luminous region of the Tevatron beam has an RMS of $\sim$30 cm along the beamline (z-direction) with a transverse beamwidth of about 25-30 μm.

The initial Tevatron luminosity steadily increased from 2002 to 2006 as shown in Figure 1(left). By the end of 2006, the peak luminosity reached by the Tevatron is $> 25 \cdot 10^{31}$ cm^{-2}s^{-1}. The increase in accelerator performance throughout Run II can also be seen by the delivered luminosity per calendar year as displayed in Figure 1(right). The total integrated luminosity delivered by the Tevatron to CDF and DO at the end of 2006 is $\sim$2.2 fb^{-1} with about 1.8 fb^{-1} recorded to tape by each the CDF and DO experiments. However, most results presented in this review use about 1 fb^{-1} of data.

The CDF detector improvements for Run II [4] were motivated by the shorter accelerator bunch spacing and the increase in luminosity by an order of magnitude. All front-end and trigger electronics has been significantly redesigned and replaced. A DAQ upgrade allows the operation of a pipelined trigger system. CDF's tracking system was completely renewed for Run II. It consists of a Central Outer Tracker (COT)

with 30 200 sense wires arranged in 96 layers, between 40 and 137 cm in radius, organized into eight alternating axial and $\pm 2^\circ$ stereo super-layers. The transverse momentum resolution is $\sigma_{p_T}/p_T \simeq 0.15\% \, p_T/(\mathrm{GeV}/c)$. The specific energy loss by ionization ($\mathrm{d}E/\mathrm{d}x$) of charged particles in the COT is measured from the amount of charge collected by each wire. The Run II silicon vertex detector consists of seven double sided layers and one single sided layer mounted on the beam pipe covering a total radial area from 1.5-28 cm. The silicon vertex detector covers the full Tevatron luminous region and allows for standalone silicon tracking up to a pseudo-rapidity $|\eta|$ of 2. The forward calorimeters have been replaced by a new scintillator tile based plug calorimeter which gives good electron identification up to $|\eta| = 2$. The upgrades to the muon system almost double the central muon coverage and extend it up to $|\eta| \sim 1.5$. The most important improvements for B physics in Run II are a Silicon Vertex Trigger (SVT) and a Time-of-Flight (ToF) system with a resolution of about 100 ps. The later employs 216 three-meter-long scintillator bars located between the outer radius of the COT and the superconducting solenoid. The Time-of-Flight system is most beneficiary for the identification of kaons with a $2\,\sigma$-separation between π and K for $p < 1.6$ GeV/c.

The DO detector also went through a major upgrade before the beginning of Run II [5]. The inner tracking system was completely replaced and includes a new Silicon tracker surrounded by a Scintillating Fiber tracker, both of which are enclosed in a 2 Tesla solenoidal magnetic field. Pre-shower counters are located before the uranium/liquid-argon calorimeter to improve the electron and photon identification. The already excellent muon system has been further improved by adding more shielding to reduce beam background. The Run II DO detector has excellent tracking and lepton acceptance. Tracks with pseudo-rapidity as large as 2.5-3.0 ($\theta \approx 10^\circ$) and transverse momentum p_T as low as 180 MeV/c can be reconstructed. The muon system can identify muons within $|\eta| < 2.0$. The minimum p_T of the reconstructed muons varies as a function of η. In most of the results presented, muons were required to have $p_T > 2$ GeV/c.

2.1 Triggers for B Physics

The total inelastic $p\overline{p}$ cross section at the Tevatron is about three orders of magnitude larger than the b quark production cross section. The CDF and DO trigger system is therefore the most important tool for finding B decay products. In addition, the cross section for b quark production is steeply falling. It drops by almost two orders of magnitude between a b quark p_T of about 8 GeV/c and 25 GeV/c. To find B decay products in hadronic collisions, it is desirable to go as low as possible in the decay products transverse momentum, exploiting as much as possible of the steeply falling b cross section. Of course, the limiting factor is the bandwidth of the experiment's data acquisition system.

In Run I, all B physics triggers at CDF and DO were based on leptons including single and dilepton triggers. In Run II, both experiments still exploit heavy flavour decays which have leptons in the final state. Identification of dimuon events down to very low momentum is possible, allowing for efficient $J/\psi \to \mu^+\mu^-$ triggers. As a consequence, both experiments are able to fully reconstruct B decay modes involving J/ψ's. Both experiments also use inclusive lepton triggers designed to accept semileptonic $B \to \ell\nu_\ell X$ decays. DO has an inclusive muon trigger with excellent acceptance, allowing them to accumulate very large samples of semileptonic decays. The CDF semileptonic triggers require an additional displaced track associated with the lepton, providing cleaner samples with smaller yields.

In addition, the CDF detector has the ability to select events based upon track impact parameter. The Silicon Vertex Trigger gives CDF access to purely hadronic B decays and makes CDF's B physics program fully competitive with the one at the e^+e^- B factories. The hadronic track trigger is the first of its kind operating successfully at a hadron collider. It works as follows: With a fast track trigger at Level 1, CDF finds track pairs in the COT with $p_T > 1.5$ GeV/c. At Level 2, these tracks are linked into the silicon vertex detector and cuts on the track impact parameter (e.g. $d > 100$ μm) are applied. The SVT track impact parameter resolution is about 50 μm including a 33 μm contribution from the transverse beam spreading. The original motivation for CDF's hadronic track trigger was to select $B^0 \to \pi\pi$ decays to be used for CP violation studies. With the different B trigger strategies above, the Collider experiments are able to trigger and reconstruct large samples of heavy flavour hadrons.

3 Spectroscopy

3.1 Study of Orbitally Excited B Mesons

The spectroscopy of excited meson states containing b quarks is not well studied. Only the stable 0^- ground states B^+, B^0 and B_s^0 and the excited 1^- state B^* are established [6]. Quark models predict the existence of two wide (B_0^* and B_1^*) and two narrow (B_1^0 and B_2^{0*}) bound P-states [7]. The wide states decay through an S-wave and therefore have a large width of a couple of hundred MeV/c^2, which makes it difficult to distinguish such states from combinatoric background. The narrow states decay through a D-wave ($L = 2$) and thus should have a small width of around 1 MeV/c^2 [8, 9]. Almost all previous observations [10, 11] of the narrow P-states B_1 and B_2^{0*} have been made indirectly using inclusive or semi-exclusive B decays which prevented the separation of both states and a precise measurement of their properties. In contrast, the masses, widths and decay branching fractions of these states are predicted with good precision by the theoretical models [8, 9].

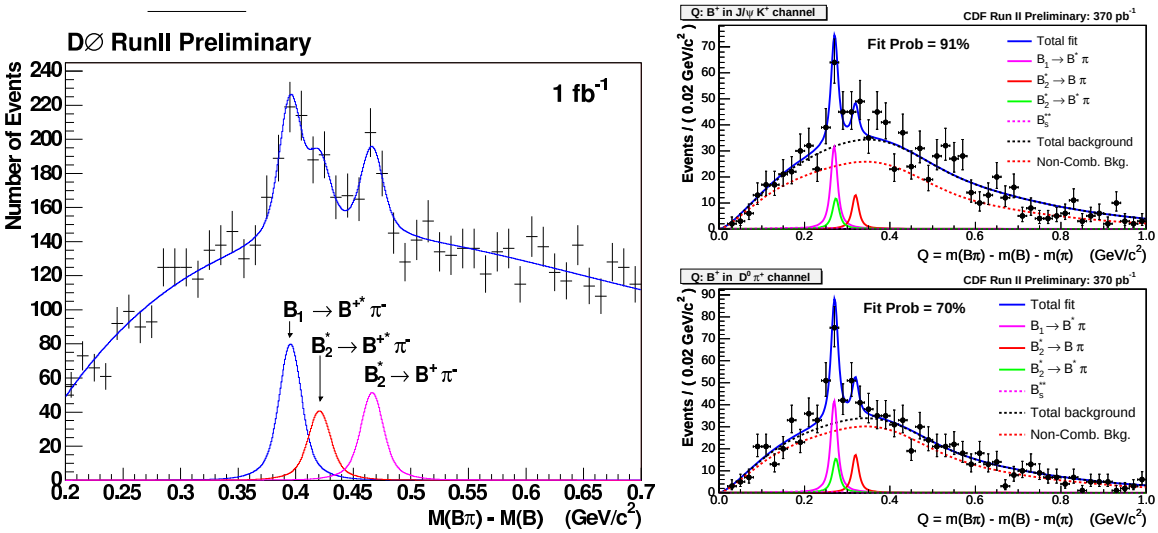

Figure 2: Result of the fit to the B^{**} mass difference (left) $\Delta m = m(B\pi) - m(B)$ from DO and (right top) $Q = m(B\pi) - m(B) - m(\pi)$ from CDF in the $B^+ \to J/\psi K^+$ channel and (right bottom) in the $B^+ \to D^0\pi^+$ mode.

B_1^0 and B_2^{0*} candidates are reconstructed in the following decay modes: $B_1^0 \to B^{*+}\pi^-$ with $B^{*+} \to B^+\gamma$ and $B_2^{0*} \to B^{*+}\pi^-$ with $B^{*+} \to B^+\gamma$ as well as $B_2^{0*} \to B^+\pi^-$. In both cases the soft photon from the B^* decay is not reconstructed resulting in a shift of about 46 MeV/c^2 in the mass spectrum. DO reconstructs the B^+ candidates in the fully reconstructed mode $B^+ \to J/\psi K^+$ with $J/\psi \to \mu^+\mu^-$ while CDF selects B^+ mesons in addition through the $B^+ \to D^0\pi^+$ mode with $D^0 \to K^-\pi^+$. The CDF analysis is based on 360 pb^{-1} of data resulting in a $B^+ \to J/\psi K^+$ signal of 1867 ± 64 events and 2182 ± 54 candidates in the $B^+ \to D^0\pi^+$ channel. The DO measurement employs 1 fb^{-1} of Run II data and finds a signal peak of $16\,219 \pm 180$ events attributed to the decay $B^+ \to J/\psi K^+$.

DO presents their measured mass distribution as $\Delta m = m(B\pi) - m(B)$ as shown in Figure 2(left), while CDF plots $Q = m(B\pi) - m(B) - m(\pi)$ as displayed in Fig. 2(right top) and (right bottom). Clear signals for the narrow excited B states are observed: CDF reconstructs 80 ± 18 events in $B^+ \to J/\psi K^+$ and 106 ± 20 events in the $B^+ \to D^0\pi^+$ channel while DO observes a total of 504 ± 80 candidates for the narrow B^{**} states. The measured masses are reported as $m(B_1^0) = 5720.8 \pm 2.5 \pm 5.3$ MeV/c^2 and $m(B_2^{0*}) - m(B_1^0) = 25.2 \pm 3.0 \pm 1.1$ MeV/c^2 from DO, while CDF quotes $m(B_1^0) = 5734 \pm 3 \pm 2$ MeV/c^2 and $m(B_2^{0*}) = 5738 \pm 5 \pm 1$ MeV/c^2. Clearly these preliminary results are not in good agreement. CDF currently works on an update of their analysis using 1 fb^{-1} of data.

3.2 Observation of Orbitally Excited B_{sJ} Mesons

The properties of $\langle b\overline{s}\rangle$ excited meson states and the comparison with properties of excited states in the $\langle b\overline{u}\rangle$ and $\langle b\overline{d}\rangle$ systems provide good tests of various models of quark bound states. These models [7, 8, 12] predict the existence of two wide resonances (B^*_{s0} and B^*_{s1}) and two narrow (B^0_{s1} and B^{0*}_{s2}) bound P-states. The wide states decay through an S-wave and therefore have a large width of a couple of hundred MeV/c^2. This makes it difficult to distinguish such states from combinatoric background. The narrow states decay through a D-wave ($L = 2$) and therefore should have a small width of around 10 MeV/c^2 [9]. If the mass of the B_{sJ} ($J = 1, 2$) is large enough, then the main decay channel should be $B^{(*)}K$ as the $B^0_s\pi$ decay mode is not allowed by isospin conservation. Previous observations [10] of the narrow B_{sJ} P-states have been made indirectly preventing the separation of both states.

B^0_{s1} and B^{0*}_{s2} candidates are reconstructed in the following decay modes: $B^0_{s1} \to B^{*+}K^-$ with $B^{*+} \to B^+\gamma$ and $B^{0*}_{s2} \to B^{*+}K^-$ with $B^{*+} \to B^+\gamma$ as well as $B^{0*}_{s2} \to B^+K^-$. In both cases the soft photon from the B^* decay is not reconstructed resulting in a shift in the mass spectrum. DO reconstructs the B^+ candidates in the fully reconstructed mode $B^+ \to J/\psi K^+$ with $J/\psi \to \mu^+\mu^-$ while CDF selects B^+ mesons in addition through the $B^+ \to D^0\pi^+$ mode with $D^0 \to K^-\pi^+$. The CDF and DO measurements are each based on 1 fb^{-1} of Run II data. The CDF analysis finds $\sim 31\,000$ $B^+ \to J/\psi K^+$ events and $\sim 27\,200$ candidates in the $B^+ \to D^0\pi^+$ channel. DO uses a signal of $16\,219 \pm 180$ B^+ events from the decay $B^+ \to J/\psi K^+$. Both experiments present their measured mass distribution in the quantity $Q = m(BK) - m(B) - m(K)$ as displayed in Figure 3(left) and (right).

A clear signal at $Q \sim 67$ MeV/c^2 is observed by CDF and DO (see Fig. 3), which is interpreted as the B^{0*}_{s2} state. CDF reconstructs 95 ± 23 events in the peak at $Q = 67.0$ MeV/c^2 while DO reports 135 ± 31 events at $Q = 66.4 \pm 1.4$ MeV/c^2. In addition, CDF observes 36 ± 9 events in a peak at $Q \sim 10.7$ MeV/c^2 which is interpreted as first evidence for the B^0_{s1} state. The measured masses are reported as $m(B^{0*}_{s2}) = 5839.1 \pm 1.4 \pm 1.5$ MeV/c^2 from DO, while CDF quotes $m(B^0_{s1}) = 5829.4 \pm 0.2 \pm 0.6$ MeV/c^2 and $m(B^{0*}_{s2}) = 5839.6 \pm 0.4 \pm 0.5$ MeV/c^2. The results from CDF and DO are in good agreement.

3.3 Observation of Σ_b Baryons

Until recently only one bottom baryon, the Λ^0_b, has been directly observed. At present the CDF collaboration has accumulated the world's largest data sample of bottom baryons, due to a combination of two factors – the CDF displaced track trigger, and the ~ 1 fb^{-1} of integrated luminosity delivered by the Tevatron. Using a sample of fully reconstructed $\Lambda^0_b \to \Lambda^+_c\pi^-$ candidates collected with the displaced track trigger, CDF searched for the decay $\Sigma^{(*)\pm}_b \to \Lambda^0_b\pi^\pm$.

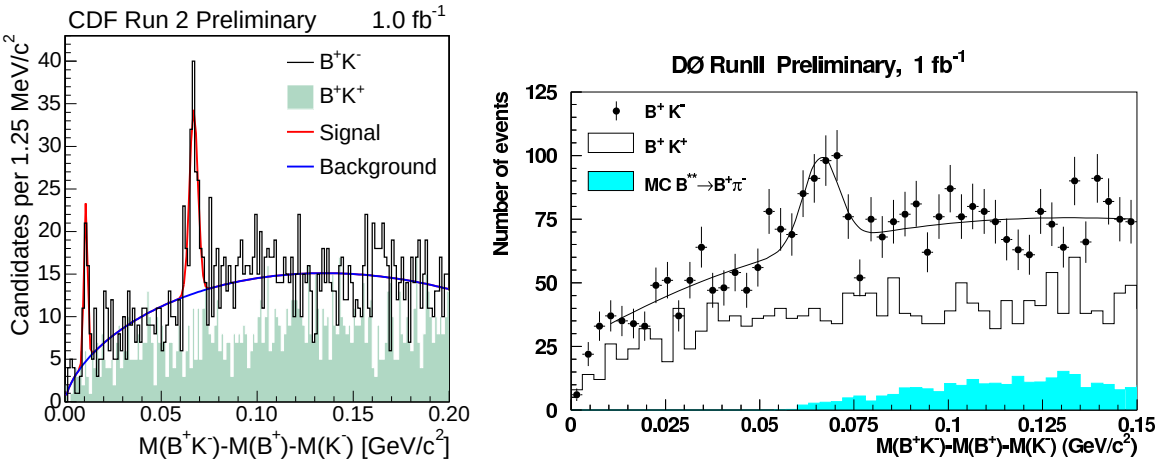

Figure 3: Result of the fit to the B^{**}_{sJ} mass difference $Q = m(BK) - m(B) - m(K)$ from (left) CDF and (right) DO.

The QCD treatment of quark-quark interactions significantly simplifies if one of the participating quarks is much heavier than the QCD confinement scale $\Lambda_{\rm QCD}$. In the limit of $m_Q \to \infty$, where m_Q is the mass of the heavy quark, the angular momentum and flavour of the light quark become good quantum numbers. This approach, known as Heavy Quark Effective Theory (HQET), thus views a baryon made out of one heavy quark and two light quarks as consisting of a heavy static color field surrounded by a cloud corresponding to the light diquark system. In SU(3) the two quarks are in diquark form $\overline{3}$ and 6 according to the decomposition $3 \otimes 3 = \overline{3} \oplus 6$, leading to a generic scheme of baryon classification. Diquark states containing quarks in an antisymmetric flavour configuration, $[q_1, q_2]$, are called Λ-type whereas states with diquarks containing quarks in a flavour symmetric state, $\{q_1, q_2\}$, are called Σ-type.

In the Σ-type ground state the light diquark system has isospin $I = 1$ and $J^P = 1^+$. Together with the heavy quark this leads to a doublet of baryons with $J^P = \frac{1}{2}^+$ (Σ_b) and $J^P = \frac{3}{2}^+$ (Σ_b^*). The ground state Σ-type baryons decay strongly to Λ-type baryons by emitting pions. In the limit $m_Q \to \infty$, the spin doublet $\{\Sigma_b, \Sigma_b^*\}$ would be exactly degenerate since an infinitely heavy quark does not have a spin interaction with a light diquark system. As the heavy quark is not infinitely massive, there will be a small mass splitting between the doublet states and there is an additional isospin splitting between the $\Sigma_b^{(*)-}$ and $\Sigma_b^{(*)+}$ states [13]. There exist a number of predictions for the masses and isospin splittings of these states using HQET, non-relativistic and relativistic potential models, $1/{\rm N}_c$ expansion, sum rules and lattice QCD. References [13, 14] contain some of the existing theoretical estimates, while

Σ_b property	Expected value [MeV/c^2]
m(Σ_b) - m(Λ_b^0)	180 - 210
$m(\Sigma_b^*) - m(\Sigma_b)$	10 - 40
$m(\Sigma_b^-) - m(\Sigma_b^+)$	5 - 7
$\Gamma(\Sigma_b)$, $\Gamma(\Sigma_b^*)$	$\sim$8, $\sim$15

Table 1: General range of theoretical predictions for the $\Sigma_b^{(*)\pm}$ states from References [13, 14].

Table 1 summarizes the range of predictions. The natural width of Σ_b baryons is expected to be dominated by single pion transitions. Decays of the type $\Sigma_{c,b} \to \Lambda_{c,b}\gamma$ are expected to have significantly smaller ($\sim$ 100 keV/c^2) partial widths than the single pion transition, and are thus negligible. The partial width of the P-wave one-pion transition thus depends on the available phase space.

In analogy with the B meson hadronization chain, in this analysis events are separated into "same charge" or SC and "opposite charge" or OC combinations. As the Λ_b^0 is neutral, the charge of the soft pion track determines the charge of the Σ_b baryon, and there will be Σ_b signals for both positive and negative pions. SC (OC) is defined as events where the Σ_b pion has the same (opposite) charge as the pion from the Λ_b^0 decay. With these definitions, the SC distribution contains all $\Sigma_b^{(*)-}$ and $\overline{\Sigma}_b^{(*)-}$ candidates while OC contains $\Sigma_b^{(*)+}$ and $\overline{\Sigma}_b^{(*)+}$.

The present analysis is based on events collected by the CDF detector from 2002 through February 2006, with an integrated luminosity of $\mathcal{L} = 1070 \pm 60$ pb^{-1}. Events collected on the two track trigger are used to reconstruct the decay chain $\Lambda_b^0 \to \Lambda_c^+\pi,\ \Lambda_c^+ \to pK^-\pi^+$. CDF reconstructs a Λ_b^0 yield of approximately 2800 candidates in the signal region $m(\Lambda_b^0) \in [5.565, 5.670]$ GeV/c^2, with the Λ_b^0 mass plot shown in Figure 4.

To separate out the resolution on the mass of each Λ_b^0 candidate, CDF searches for narrow resonances in the mass difference distribution of $Q = m(\Lambda_b^0\pi) - m(\Lambda_b^0) - m_\pi$. Unless explicitly stated, Σ_b refers to both the $J = \frac{1}{2}$ ($\Sigma_b^\pm$) and $J = \frac{3}{2}$ ($\Sigma_b^{*\pm}$) states. There is no transverse momentum cut applied to the pion from the Σ_b decay, since these tracks are expected to be very soft. In order to perform an unbiased search, the cuts for the Σ_b reconstruction are optimized first with the Σ_b signal region blinded. From theoretical predictions the Σ_b signal region is chosen as $30 < Q < 100$ MeV/c^2, while the upper and lower sideband regions of $0 < Q < 30$ MeV/c^2 and $100 < Q < 500$ MeV/c^2 represent the Σ_b background. The signal for the optimization is taken from a PYTHIA Monte Carlo Σ_b sample, with the decays $\Sigma_b \to \Lambda_b^0\pi,\ \Lambda_b^0 \to \Lambda_c^+\pi^-,\ \Lambda_c^+ \to pK^-\pi^+$ forced.

The backgrounds under the Λ_b^0 signal region in the Λ_b^0 mass distribution will

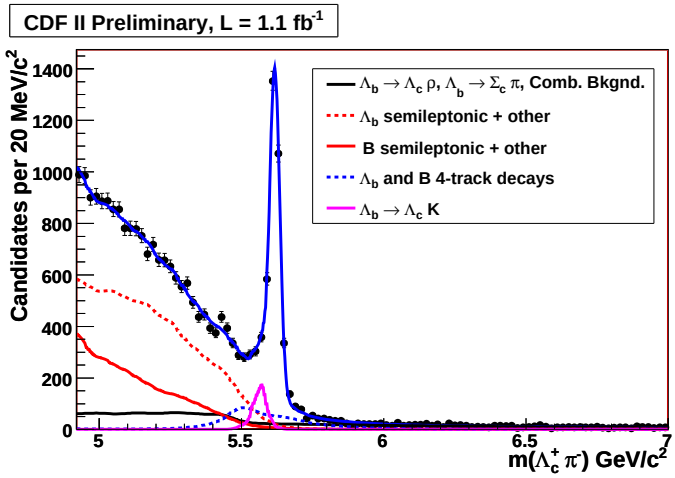

Figure 4: Fit to the invariant mass of $\Lambda_b^0 \to \Lambda_c^+ \pi^-$ candidates. The solid blue line is the total fit, while the primary background sources are listed in the legend.

also be present in the Σ_b Q-distribution. The primary sources of background are Λ_b^0 hadronization and underlying event, hadronization and underlying event of other B meson reflections and combinatorial background underneath the Λ_b^0 peak. The percentage of each background component in the Λ_b^0 signal region is derived from the Λ_b^0 mass fit, and is determined as 86% Λ_b^0 signal, 9% backgrounds and 5% combinatorial background. Other backgrounds (*e.g.* from 5-track decays where one track is taken as the π_{Σ_b} candidate) are negligible, as confirmed in inclusive single-b-hadron Monte Carlo samples.

Upon unblinding the Q signal region, there is an excess observed in data over predicted backgrounds. The excess over background is shown in Table 2. CDF performs a simultaneous unbinned likelihood fit to SC and OC data. To the already described background components, four peaks are added, one for each of the expected Σ_b states. Each peak is a sum of two Breit-Wigner shapes, each convoluted with two Gaussian resolution functions. The detector resolution has a dominant narrow core and a small broader shape describing the tails where the PDF for each peak takes both into account. Due to low statistics, CDF constrains $m(\Sigma_b^{*+}) - m(\Sigma_b^+)$ and $m(\Sigma_b^{*-}) - m(\Sigma_b^-)$ to be the same. The results of the fit are given in Tab. 3 and displayed in Fig. 5(left).

All systematic uncertainties on the mass difference measurements are small compared to their statistical errors. The systematic errors from the tracking sources are determined by comparing the mean and the width of the peak in $m(D^{*+}) - m(D^0)$ between data and Monte Carlo simulation split up in several regions of track p_T. The

Sample	Data events	Bkg events	Data excess over bkg
Same charge	416	268	148
Opposite charge	406	298	108

Table 2: Summary of the number of events in the Q signal region ($Q \in$ [0.03, 0.1] GeV/c^2) for data and predicted background.

Parameter	Value	Parabolic Error	MINOS Errors
$Q(\Sigma_b^+)$ (MeV/c^2)	48.4	2.02	(+2.02, -2.29)
$Q(\Sigma_b^-)$ (MeV/c^2)	55.9	0.963	(+0.990, -0.959)
$Q(\Sigma_b^*)$ - $Q(\Sigma_b)$ (MeV/c^2)	21.3	1.93	(+2.03, -1. 94)
Σ_b^+ events	29	12.0	(+12.4, -11.6)
Σ_b^- events	60	14.3	(+14.8, -13.8)
Σ_b^{*+} events	74	16.8	(+17.2, -16.3)
Σ_b^{*-} events	74	17.8	(+18.2, -17.4)
-ln(Likelihood)	-24553.5	–	–

Table 3: Fit parameters and error values from the fit to data. Positive and negative errors are quoted separately as the error range is asymmetric.

largest discrepancy of the D^{*+} peak is 0.06 MeV/c^2 which is taken as the systematic error for all four peaks. The discrepancy in the mass resolution could be as large as 20%. The effect of a broader resolution is evaluated via a sample of Toy Monte Carlo experiments. The remaining systematics come from assumptions made in the fit to the data, such as the use of fixed background shapes. For the parameters associated with an individual systematic uncertainty, Toy MC samples are generated where these parameters are varied. The sample is then fit with both the default fit and the fit with varied parameters. The difference between fit parameter values in the varied fit and the default fit is caused by the systematic variation and constitutes the associated systematic error.

To evaluate the significance of the measurement, the null hypothesis is tested. The data is fit with no signal and with the standard fit using four peaks. Then the likelihood ratio is computed as $LR = L_1/L_2$, where L_2 is the four signal peak hypothesis and L_1 is the corresponding hypothesis with no peaks. The result of this fit is shown in Figure 5(right) and a likelihood ratio of $\sim 10^{-19}$ is obtained indicating the observation of the $\Sigma_b^{(*)\pm}$ states.

To summarize, the lowest lying charged $\Lambda_b^0\pi$ resonant states are observed in 1 fb^{-1} of data collected by the CDF detector. These are consistent with the lowest lying charged $\Sigma_b^{(*)\pm}$ baryons. The Q values of Σ_b^- and Σ_b^+, and the Σ_b^*-Σ_b mass difference,

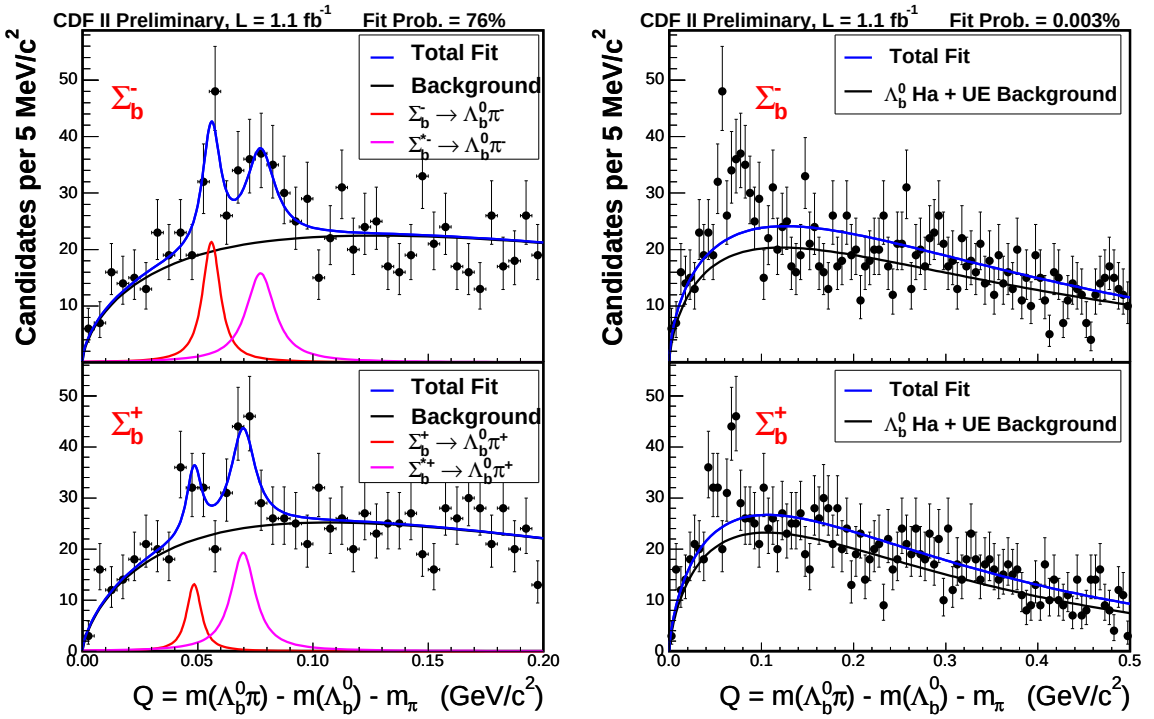

Figure 5: (left) Simultaneous fit to the Σ_b states and (right) with an alternate signal description assuming no signal is present (null hypothesis).

are measured to be:
- $m(\Sigma_b^-) - m(\Lambda_b^0) - m(\pi) = 55.9 \pm 1.0$ (stat) ± 0.1 (syst) MeV/c^2,
- $m(\Sigma_b^+) - m(\Lambda_b^0) - m(\pi) = 48.4^{+2.0}_{-2.3}$ (stat) ± 0.1 (syst) MeV/c^2,
- $m(\Sigma_b^{*-}) - m(\Sigma_b^-) = m(\Sigma_b^{*+}) - m(\Sigma_b^+) = 21.3^{+2.0}_{-1.9}$ (stat) $^{+0.4}_{-0.2}$ (syst) MeV/c^2.

Using the best CDF mass measurement for the Λ_b^0 mass, which is $m(\Lambda_b^0) = 5619.7 \pm 1.2$ (stat) ± 1.2 (syst) MeV/c^2, the absolute mass values and number of events are:
- $m(\Sigma_b^+) = 5808^{+2.0}_{-2.3}$ (stat) ± 1.7 (syst) MeV/c^2, N$(\Sigma_b^+) = 29^{+12.4}_{-11.6}$ (stat) $^{+5.0}_{-3.4}$ (syst),
- $m(\Sigma_b^-) = 5816^{+1.0}_{-1.0}$ (stat) ± 1.7 (syst) MeV/c^2, N$(\Sigma_b^-) = 60^{+14.8}_{-13.8}$ (stat) $^{+8.4}_{-4.0}$ (syst),
- $m(\Sigma_b^{*+}) = 5829^{+1.6}_{-1.8}$ (stat) ± 1.7 (syst) MeV/c^2, N$(\Sigma_b^{*+}) = 74^{+17.2}_{-16.3}$ (stat) $^{+10.3}_{-5.7}$ (syst),
- $m(\Sigma_b^{*-}) = 5837^{+2.1}_{-1.9}$ (stat) ± 1.7 (syst) MeV/c^2, N$(\Sigma_b^{*-}) = 74^{+18.2}_{-17.4}$ (stat) $^{+15.6}_{-5.0}$ (syst).

4 Decay of B Hadrons

In this Section we focus on a new CDF result involving the branching fractions and time-integrated direct CP asymmetries for B^0 and B_s^0 decay modes into pairs of charmless charged hadrons $B \to h^+h^-$.

4.1 Results from Charmless Two-Body Decays $B \to h^+h^-$

The decay modes of B mesons into pairs of charmless pseudo-scalar mesons are effective probes of the quark-mixing matrix (CKM) and sensitive to potential new physics effects. The large production rate of B hadrons at the Tevatron allows measuring such decays in new modes, which are important to supplement our understanding of B meson decays. The still unobserved $B_s^0 \to K^-\pi^+$ decay mode could be used to measure the angle γ [15] of the CKM unitarity triangle and its CP asymmetry could be a powerful model-independent test of the source of direct CP violation in the B meson system [16]. This may provide useful information to solve the current discrepancy between the asymmetries observed in the neutral and charged B modes [17]. The $B_s^0 \to \pi^+\pi^-$ and $B^0 \to K^+K^-$ decay channels proceed only through annihilation diagrams, which are currently poorly known and constitute a source of significant uncertainty in many theoretical calculations [18, 19]. A measurement of both modes would allow a determination of the strength of penguin-annihilation diagrams [20].

Data Selection

CDF analysed a sample (integrated luminosity $\mathcal{L} \sim 1$ fb^{-1}) of pairs of oppositely charged particles with $p_T > 2$ GeV/c and $p_T(1) + p_T(2) > 5.5$ GeV/c, used to form $B_{(s)}^0$ meson candidates. In addition, the trigger required a transverse opening-angle $20^\circ < \Delta\phi < 135^\circ$ between the two tracks, to reject background from particle pairs within the same jet and from back-to-back jets. In addition, both charged particles are required to originate from a displaced vertex with a large impact parameter d_0 ($100\ \mu\text{m} < d_0 < 1$ mm), while the $B_{(s)}^0$ meson candidate is required to be produced in the primary $\overline{p}p$ interaction ($d_0(B) < 140\ \mu$m) and to have traveled a transverse distance $L_{xy}(B) > 200\ \mu$m.

In the offline analysis, an unbiased optimization procedure determines a tightened selection on track-pairs fit to a common decay-vertex. CDF chooses selection cuts minimizing directly the expected uncertainty (through several pseudo-experiments) of the physics observables to be measured. CDF decided to use two different sets of cuts, optimizing separately the measurements of $\mathcal{A}_{CP}(B^0 \to K^+\pi^-)$ and $\mathcal{B}(B_s^0 \to K^-\pi^+)$. For the latter, the sensitivity for discovery and limit setting [21] was optimized rather than the statistical uncertainty on the particular observational parameter, since this mode had not yet been observed. It is verified that the former set of cuts is also adequate to measure other decay rates of the larger yield modes ($B^0 \to \pi^+\pi^-$, $B_s^0 \to K^+K^-$), while the latter, tighter set of cuts, is well suited to measure the decay rates and CP asymmetries related to the rare modes ($B_s^0 \to \pi^+\pi^-$, $B^0 \to K^+K^-$, $\Lambda_b^0 \to p\pi^-$, $\Lambda_b^0 \to pK^-$).

In addition to tightening the trigger cuts in the offline analysis, other discriminating variables such as the isolation of the $B_{(s)}^0$ meson and the information provided by the 3D reconstruction capability of the CDF tracking system are used,

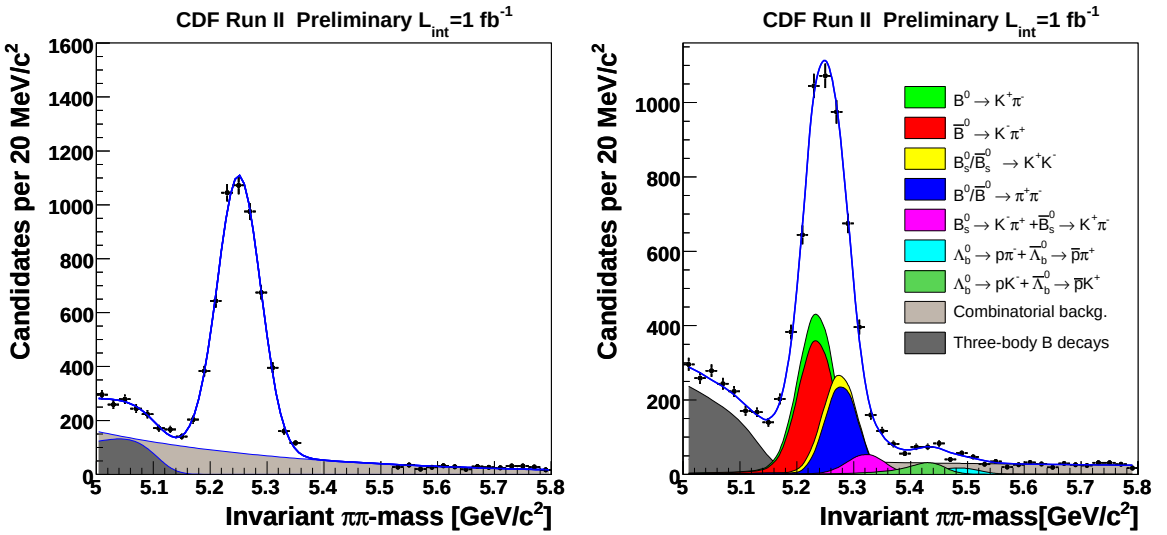

Figure 6: (left) Invariant mass distribution of $B \to h^+h^-$ candidates passing all selection requirements optimized to measure $\mathcal{B}(B_s^0 \to K^-\pi^+)$, using the pion mass assumption for both decay products. The cumulative projections of the likelihood fit for each mode are overlaid in (right).

allowing a great improvement in the signal purity. Isolation is defined as $I(B) = p_T(B)/[p_T(B) + \sum_i p_T(i)]$, in which the sum runs over every other track within a cone of radius one in the $\eta - \phi$ space around the $B^0_{(s)}$ meson flight-direction. By requiring $I(B) > 0.5$ the background is reduced by a factor four while keeping almost 80% of the B signal. The 3D silicon tracking allows to resolve multiple vertices along the beam direction and to reject fake tracks reducing the background by another factor of two, with small inefficiency on the signal. The resulting $\pi\pi$ invariant mass distribution shown in Figure 6(left) display a clean signal of $B \to h^+h^-$ decays. In spite of a good mass resolution (≈ 22 MeV/c^2), the various $B \to h^+h^-$ modes overlap into an unresolved mass peak.

Fit of Sample Composition

The resolution in invariant mass and in particle identification is not sufficient for separating individual decay modes on an event-by-event basis. Therefore CDF performs an unbinned maximum likelihood fit, combining kinematic and particle identification information, to statistically determine the contribution of each mode and the CP asymmetries. For the kinematic portion, CDF uses three loosely correlated observables to summarize the information carried by all possible values of invariant mass

of the B candidate, resulting in different mass assignments to the two outgoing particles. These are: (a) the mass $m_{\pi\pi}$ calculated with the charged pion mass assignment to both particles, (b) the signed momentum imbalance $\alpha = (1 - p_1/p_2)q_1$, where p_1 (p_2) is the lower (higher) of the particle momenta, and q_1 is the sign of the charge of the particle of momentum p_1, and (c) the scalar sum of the particle momenta $p_{tot} = p_1 + p_2$. Using these three variables, the mass of any particular mode m_{12} can be written as:

$$m_{12}^2 = m_{\pi\pi}^2 - 2m_\pi^2 + m_1^2 + m_2^2 - 2\sqrt{p_1^2 + m_\pi^2}\sqrt{p_2^2 + m_\pi^2} - 2\sqrt{p_1^2 + m_1^2}\sqrt{p_2^2 + m_2^2}, \quad (1)$$

$$p_1 = \frac{1 - |\alpha|}{2 - |\alpha|}\, p_{tot}, \qquad p_2 = \frac{1}{2 - |\alpha|}\, p_{tot}, \quad (2)$$

where m_1 (m_2) is the mass of the lower (higher) momentum particle. For simplicity Eq. (1) is written as a function of p_1 and p_2 instead of α and p_{tot} but in the likelihood fit it is used as a function of α and p_{tot}.

Particle identification (PID) information is summarized by a single observable κ for each track defined as

$$\kappa = \frac{\mathrm{d}E/\mathrm{d}x - \mathrm{d}E/\mathrm{d}x(\pi)}{\mathrm{d}E/\mathrm{d}x(K) - \mathrm{d}E/\mathrm{d}x(\pi)}. \quad (3)$$

With the chosen observables, the likelihood contribution of the i^{th} event is written as:

$$\mathcal{L}_i = (1 - b)\sum_j f_j \mathcal{L}_j^{\mathrm{kin}} \mathcal{L}_j^{\mathrm{PID}} + b\left(f_{\mathrm{A}} \mathcal{L}_{\mathrm{A}}^{\mathrm{kin}} \mathcal{L}_{\mathrm{A}}^{\mathrm{PID}} + (1 - f_{\mathrm{A}})\mathcal{L}_{\mathrm{E}}^{\mathrm{kin}} \mathcal{L}_{\mathrm{E}}^{\mathrm{PID}}\right) \quad (4)$$

where:

$$\mathcal{L}_j^{\mathrm{kin}} = R(m_{\pi\pi} - \mathcal{M}_j(\alpha, p_{tot}), \alpha, p_{tot}) P_j(\alpha, p_{\mathrm{tot}}), \quad (5)$$

$$\mathcal{L}_{\mathrm{A}}^{\mathrm{kin}} = \mathrm{A}(m_{\pi\pi}|c_2, m_0) P_{\mathrm{A}}(\alpha, p_{\mathrm{tot}}), \quad (6)$$

$$\mathcal{L}_{\mathrm{E}}^{\mathrm{kin}} = e^{c_1 m_{\pi\pi}} P_{\mathrm{E}}(\alpha, p_{\mathrm{tot}}), \quad (7)$$

$$\mathcal{L}_{j(\mathrm{E,A})}^{\mathrm{PID}} = F_{j(\mathrm{E,A})}(\kappa_1, \kappa_2, \alpha, p_{\mathrm{tot}}). \quad (8)$$

The index 'A(E)' labels the physical (combinatorial) background-related quantities, the index j runs over the twelve distinguishable $B \to h^+h^-$ and $\Lambda_b^0 \to ph$ modes (Fig. 7), and f_j are their respective fractions, to be determined by the fit together with the total background fraction b and with the fraction of the physical (combinatorial) background $f_{A(E)}$. The conditional probability density $R(m_{\pi\pi} - \mathcal{M}_j(\alpha, p_{tot}), \alpha, p_{tot})$ is the mass resolution function of each mode j when the correct mass is assigned to both tracks. In fact, the average mass $\mathcal{M}_j(\alpha, p_{tot})$ is the value of $m_{\pi\pi}$ obtained from Eq. (1) by setting the appropriate particle masses for each decay mode j. Making a simple variable change, $R(m_{\pi\pi} - \mathcal{M}_j(\alpha, p_{tot}), \alpha, p_{tot}) = R(m_j - m_{B^0(B_s^0, \Lambda_b^0)}, \alpha, p_{tot})$ is obtained where m_j is the invariant mass computed with the correct mass assignment

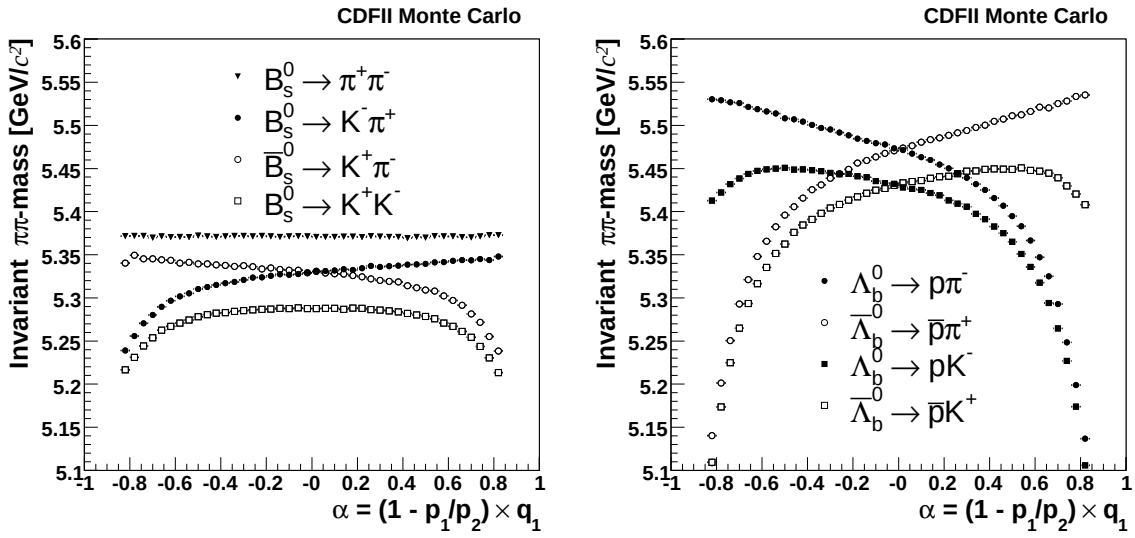

Figure 7: Average $m_{\pi\pi}$ vs α for simulated samples of (left) B_s^0 and (right) Λ_b^0 candidates, where self-tagging final states ($K^+\pi^-$ and $K^-\pi^+$, ph^- and $\overline{p}h^+$) are treated separately. The corresponding plots for the B^0 are similar to B_s^0 but shifted for the mass difference.

to both particles for each mode j. R is parameterized using the detailed detector simulation [22]. To take into account non-Gaussian tails due to the emission of photons in the final state, CDF includes in the simulation soft photon emission of particles in agreement with recent QED calculations [23]. CDF checks the quality of the mass resolution model using about 500K $D^0 \to K^-\pi^+$ decays as shown in Figure 8(left). The mass line-shape of the $D^0 \to K^-\pi^+$ peak is fitted fixing the signal shape from the model, only allowing to vary the background function. CDF obtains good agreement between data and simulation. In Eq. (5) the nominal B^0, B_s^0 and Λ_b^0 masses as measured by CDF [24] are used in order to cancel common systematic uncertainties. The background mass distribution is determined in the fit by varying the parameters c_1, c_2 and m_0 in Eq. (6,7). The probability $P_j(\alpha, p_{tot})$ is the joint probability distribution of (α, p_{tot}) and is parameterized for each mode j by a product of polynomial and exponential functions fitted to Monte Carlo samples produced by a detailed detector simulation [22]. The background function $P_{\mathrm{A(E)}}$ is obtained from the mass sidebands of the data.

A sample of 1.5M $D^{*+} \to D^0\pi^+ \to [K^-\pi^+]\pi^+$ decays, where the D^0 decay products are identified by the charge of the D^{*+} pion, was used to calibrate the $\mathrm{d}E/\mathrm{d}x$ response over time and over the entire tracking volume, and to determine the F func-

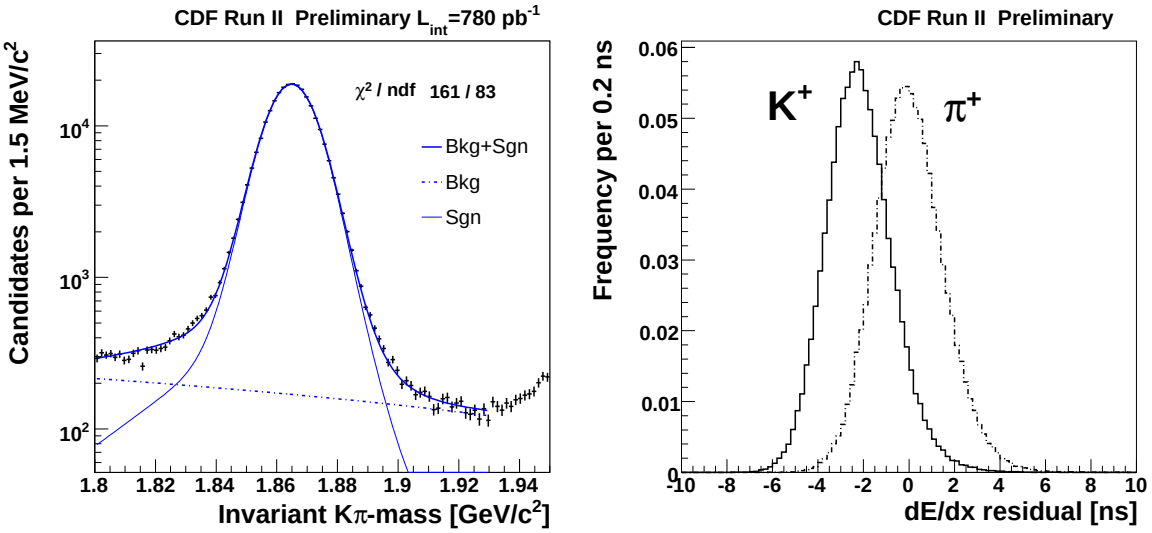

Figure 8: Tagged $D^0 \to K^-\pi^+$ decays from $D^{*+} \to D^0\pi^+ \to [K^-\pi^+]\pi^+$. (left) Check of the mass line shape template performing a 1-dimensional binned fit where the signal mass line shape is completely fixed from the model. (right) Distribution of $\mathrm{d}E/\mathrm{d}x$ (mean COT pulse-width) around the average pion response for calibration samples of kaons (left) and pions (right).

tions in Eq. (8). Using a $> 95\%$ pure D^0 sample, CDF obtains a $1.4\,\sigma$ separation between kaons and pions as shown in Fig. 8(right), corresponding to an uncertainty on the measured fraction of each class of particles that is just 60% worse than the uncertainty attainable with ideal separation. The background term in Eq. (8) is similar to the signal terms, but allows for independent pion, kaon, proton, and electron components, which are free to vary independently. Muons are indistinguishable from pions with the available $\mathrm{d}E/\mathrm{d}x$ resolution.

Fit Results

CDF performs two separate fits. The first one uses the cuts optimized to measure the direct $\mathcal{A}_{CP}(B^0 \to K^+\pi^-)$ and the second one is optimized to measure $\mathcal{B}(B_s^0 \to K^-\pi^+)$. Significant signals are seen for the $B^0 \to \pi^+\pi^-$, $B^0 \to K^+\pi^-$, and $B_s^0 \to K^+K^-$ modes, previously observed by CDF [25]. Three new rare modes are observed for the first time: $B_s^0 \to K^-\pi^+$, $\Lambda_b^0 \to p\pi^-$ and $\Lambda_b^0 \to pK^-$, while no evidence is obtained for the $B_s^0 \to \pi^+\pi^-$ and $B^0 \to K^+K^-$ decay channels.

To convert the yields returned from the fit into relative branching fractions, CDF applies corrections for efficiencies of trigger and offline selection requirements for the

different decay modes. The relative efficiency corrections between various modes do not exceed 20%. Most corrections are determined from the detailed detector simulation [22], with some exceptions which are measured using data. A momentum-averaged relative isolation efficiency between B_s^0 and B^0 mesons of 1.07 ± 0.11 is determined from fully-reconstructed samples of $B_s^0 \to J/\psi\,\phi$, $B_s^0 \to D_s^-\pi^+$, $B^0 \to J/\psi\,K^{*0}$, and $B^0 \to D^-\pi^+$. The lower specific ionization of kaons with respect to pions in the drift chamber is responsible for a $\simeq 5\%$ lower efficiency to reconstruct a kaon. This effect is measured in a sample of $D^+ \to K^-\pi^+\pi^+$ decays triggered with the two track trigger, using the unbiased third track. The only correction needed by the direct CP asymmetries $\mathcal{A}_{CP}(B^0 \to K^+\pi^-)$ and $\mathcal{A}_{CP}(B_s^0 \to K^-\pi^+)$ is a $\leq 0.6\%$ shift due to the different probability for K^+ and K^- to interact with the tracker material. This correction uses a sample of 1M prompt $D^0 \to K^-\pi^+$ decays reconstructed and selected with the same criteria as the $B \to h^+h^-$ decays. Assuming the Standard Model expectation $\mathcal{A}_{CP}(D^0 \to K^-\pi^+) = 0$, the difference between the number of reconstructed $D^0 \to K^-\pi^+$ decays and $\overline{D}^0 \to K^+\pi^-$ provides a measurement of the detector-induced asymmetry between $K^+\pi^-$ and $K^-\pi^+$ final states. Since CDF uses the same fit technique developed for the $B \to h^+h^-$ decays, this measurement provides also a robust check on all possible charge asymmetry biases of the detector and $\mathrm{d}E/\mathrm{d}x$ parameterizations.

The $B_s^0 \to K^+K^-$ and $B_s^0 \to \pi^+\pi^-$ modes require a special treatment, since they contain a superposition of the flavour eigenstates of the B_s^0 meson. Their time evolution might differ from the one of the flavour-specific modes if the width difference $\Delta\Gamma_s$ between the B_s^0 mass eigenstates is significant. The current result is derived under the assumption that both modes are dominated by the short-lived B_s^0 component, that means $\Gamma_s = \Gamma_d$, and $\Delta\Gamma_s/\Gamma_s = 0.12 \pm 0.06$ [26, 27]. The latter uncertainty is included in estimating the overall systematic uncertainty.

The dominant contributions to the systematic uncertainty are as follows. The statistical uncertainty on the isolation efficiency (B_s^0 modes), the uncertainty on the $\mathrm{d}E/\mathrm{d}x$ calibration and parameterization and the uncertainty of the combinatorial background model. The first one is the larger systematics of all measurements with the meson B_s^0 in the initial state except for $\mathcal{A}_{CP}(B_s^0 \to K^-\pi^+)$. This uncertainty is preliminary and conservative, a significant improvement is expected for the final results. The second one, due to $\mathrm{d}E/\mathrm{d}x$, is a large systematics of all measurements, although the parameterization of the specific ionization $\mathrm{d}E/\mathrm{d}x$ is very accurate. The fit of the sample composition is very sensitive to the PID information. The third systematic error is due to the statistical uncertainty of the possible combinatorial background models and it is a dominant systematics for the observables of the rare modes. Smaller systematic uncertainties are assigned for the trigger efficiencies, physical background shapes and kinematics, and the B meson masses and lifetimes.

The measured relative branching fractions are listed in Table 4, where f_d and f_s indicate the respective production fractions of B^0 and B_s^0 mesons from the fragmen-

Mode	N_{signal}	Quantity	Measurement	$\mathcal{B}$ $[10^{-6}]$
$B^0 \to K^+\pi^-$	4045 ± 84	$\mathcal{A}_{CP}(B^0)$	$-0.086 \pm 0.023 \pm 0.009$	
$B^0 \to \pi^+\pi^-$	1121 ± 63	$\frac{\mathcal{B}(B^0\to\pi^+\pi^-)}{\mathcal{B}(B^0\to K^+\pi^-)}$	$0.259 \pm 0.017 \pm 0.016$	$5.10 \pm 0.33 \pm 0.36$
$B_s^0 \to K^+K^-$	1307 ± 64	$\frac{f_s}{f_d}\frac{\mathcal{B}(B_s^0\to K^+K^-)}{\mathcal{B}(B^0\to K^+\pi^-)}$	$0.324 \pm 0.019 \pm 0.041$	$24.4 \pm 1.4 \pm 4.6$
$B_s^0 \to K^-\pi^+$	$230 \pm 34 \pm 16$	$\frac{f_s}{f_d}\frac{\mathcal{B}(B_s^0\to K^-\pi^+)}{\mathcal{B}(B^0\to K^+\pi^-)}$	$0.066 \pm 0.010 \pm 0.010$	$5.0 \pm 0.75 \pm 1.0$
		$\mathcal{A}_{CP}(B_s^0)$	$0.39 \pm 0.15 \pm 0.08$	
		$\mathcal{A}_{\Gamma}(B_s^0)$	$-3.21 \pm 1.60 \pm 0.39$	
$B_s^0 \to \pi^+\pi^-$	$26 \pm 16 \pm 14$	$\frac{f_s}{f_d}\frac{\mathcal{B}(B_s^0\to\pi^+\pi^-)}{\mathcal{B}(B^0\to K^+\pi^-)}$	$0.007 \pm 0.004 \pm 0.005$	$0.53 \pm 0.31 \pm 0.40$ (< 1.36 @ 90% CL)
$B^0 \to K^+K^-$	$61 \pm 25 \pm 35$	$\frac{\mathcal{B}(B^0\to K^+K^-)}{\mathcal{B}(B^0\to K^+\pi^-)}$	$0.020 \pm 0.008 \pm 0.006$	$0.39 \pm 0.16 \pm 0.12$ (< 0.7 @ 90% CL)
$\Lambda_b^0 \to pK^-$	$156 \pm 20 \pm 11$	$\frac{\mathcal{B}(\Lambda_b^0\to p\pi^-)}{\mathcal{B}(\Lambda_b^0\to pK^-)}$	$0.66 \pm 0.14 \pm 0.08$	
$\Lambda_b^0 \to p\pi^-$	$110 \pm 18 \pm 16$			

Table 4: Results on data sample optimized to measure $\mathcal{A}_{CP}(B^0 \to K^+\pi^-)$ (top) and $\mathcal{B}(B_s^0 \to K^-\pi^+)$ (bottom). Absolute branching fractions are normalized to the world-average values $\mathcal{B}(B^0 \to K^+\pi^-) = (19.7 \pm 0.6) \times 10^{-6}$, $f_s = (10.4 \pm 1.4)\%$ and $f_d = (39.8 \pm 1.0)\%$ [17]. We use $\mathcal{A}_{CP}(B^0) = \frac{\mathcal{B}(\overline{B}^0\to K^-\pi^+)-\mathcal{B}(B^0\to K^+\pi^-)}{\mathcal{B}(\overline{B}^0\to K^-\pi^+)+\mathcal{B}(B^0\to K^+\pi^-)}$, $\mathcal{A}_{CP}(B_s^0) = \frac{\mathcal{B}(\overline{B}_s^0\to K^+\pi^-)-\mathcal{B}(B_s^0\to K^-\pi^+)}{\mathcal{B}(\overline{B}_s^0\to K^+\pi^-)+\mathcal{B}(B_s^0\to K^-\pi^+)}$ and $\mathcal{A}_{\Gamma}(B_s^0) = \frac{f_d}{f_s}\frac{\Gamma(\overline{B}^0\to K^-\pi^+)-\Gamma(B^0\to K^+\pi^-)}{\Gamma(\overline{B}_s^0\to K^+\pi^-)-\Gamma(B_s^0\to K^-\pi^+)}$. The first quoted uncertainty is always statistical, the second is systematic.

tation of b quarks in $\overline{p}p$ collisions. An upper limit is also quoted for modes in which no significant signal is observed [28]. The absolute branching fraction results listed are obtained by normalizing the data to the world-average of $\mathcal{B}(B^0 \to K^+\pi^-)$ [17].

CDF reports the first observation of three new rare charmless decays $B_s^0 \to K^-\pi^+$, $\Lambda_b^0 \to p\pi^-$ and $\Lambda_b^0 \to pK^-$ with a significance respectively of 8.2σ, 6σ and 11.5σ. The significance includes both statistical and systematic uncertainty. The statistical uncertainty to evaluate the significance is estimated using several pseudo-experiments with no contributions from rare signals.

The rate of the newly observed mode $\mathcal{B}(B_s^0 \to K^-\pi^+) = (5.0 \pm 0.75 \pm 1.0) \cdot 10^{-6}$ is in agreement with the latest theoretical expectation [29] which is lower than previous predictions [18, 30]. CDF measures for the first time in the B_s^0 meson system the direct CP asymmetry $\mathcal{A}_{CP}(B_s^0 \to K^-\pi^+) = 0.39 \pm 0.15 \pm 0.08$. This value favors a large CP violation in B_s^0 mesons, on the other hand it is also compatible with zero. Ref. [16] suggests a robust test of Standard Model expectations versus new physics comparing the direct CP asymmetries in the $B_s^0 \to K^-\pi^+$ and $B^0 \to K^+\pi^-$ decay modes. Using HFAG input [17], CDF measures $\frac{\Gamma(\overline{B}^0\to K^-\pi^+)-\Gamma(B^0\to K^+\pi^-)}{\Gamma(B_s^0\to K^-\pi^+)-\Gamma(\overline{B}_s^0\to K^+\pi^-)} = 0.84 \pm 0.42 \pm 0.15$ (where Γ is the decay width) in agreement with the Standard

Model expectation of one. Assuming that the relationship above yields one and using as input the branching fraction $\mathcal{B}(B_s^0 \to K^-\pi^+)$ measured in this analysis, the world average for $\mathcal{A}_{CP}(B^0 \to K^+\pi^-)$ and the $\mathcal{B}(B^0 \to K^+\pi^-)$ [17], the expected value for $\mathcal{A}_{CP}(B_s^0 \to K^-\pi^+) \approx 0.37$ is estimated in agreement with the CDF measurement.

The rate of the mode $\mathcal{B}(B_s^0 \to K^+K^-) = (24.4 \pm 1.4 \pm 4.6) \cdot 10^{-6}$ is in agreement with the latest theoretical expectation [31, 32] and with the previous CDF measurement [25]. An improved systematic uncertainty is expected for the final analysis of the same sample. The results for the B^0 meson are in agreement with world average values [17]. The measurement $\mathcal{A}_{CP}(B^0 \to K^+\pi^-) = -0.086 \pm 0.023 \pm 0.009$ is the world's second best measurement and the significance of the new world average $A_{CP}^{avg}(B^0 \to K^+\pi^-) = -0.095 \pm 0.013$ moved from 6σ to 7σ. CDF updates the upper limits and quotes also the absolute branching fractions of the currently unobserved annihilation-type modes: $B^0 \to K^+K^-$ and $B_s^0 \to \pi^+\pi^-$. The rate $\mathcal{B}(B^0 \to K^+K^-) = (0.39 \pm 0.16 \pm 0.12) \cdot 10^{-6}$ has the same uncertainty as the current measurements [17], while the $B_s^0 \to \pi^+\pi^-$ upper limit (already the world's best limit [25]) is improved by a factor of 1.3, approaching the expectations from recent calculations [19,33]. CDF also reports the first observation of two new baryon charmless modes $\Lambda_b^0 \to p\pi^-$ and $\Lambda_b^0 \to pK^-$, and measures $\mathcal{B}(\Lambda_b^0 \to p\pi^-)/\mathcal{B}(\Lambda_b^0 \to pK^-) = 0.66 \pm 0.14 \pm 0.08$ in agreement with expectations from Ref. [34].

5 Summary

We review recent result on heavy quark physics focusing on Run II measurements of B hadron spectroscopy and decay at the Tevatron. A wealth of new B physics measurements from CDF and DO has been available. These include the spectroscopy of excited B states (B^{**}, B_s^{**}) and the observation of the Σ_b baryon. The discussion of the decays of B hadrons and measurements of branching fractions focuses on charmless two-body decays of $B \to h^+h^-$. We report several new B_s^0 and Λ_b^0 decay channels.

Acknowledgments

I would like to thank the organizers of this stimulating meeting for an excellent conference. I also thank my colleagues from the CDF and DO collaboration for their help in preparing this talk as well as these proceedings. I also would like to thank Ann, Emma and Helen, a constant source of inspiration and support, for their continuous understanding about the life of a traveling particle physicist. This work was supported in part by the U.S. Department of Energy under Grant No. DE-FG02-91ER40682.

Bibliography

[1] N. Ellis and A. Kernan, Phys. Rept. **195** (1990) 23.

[2] F. Abe *et al.* [CDF Collaboration], Phys. Rev. Lett. **68** (1992) 3403.

[3] M. Paulini, Int. J. Mod. Phys. A **14** (1999) 2791 [arXiv:hep-ex/9903002].

[4] D. Acosta *et al.* [CDF Collaboration], Phys. Rev. D **71** (2005) 032001 [arXiv:hep-ex/0412071].

[5] V. M. Abazov *et al.* [D0 Collaboration], Nucl. Instrum. Meth. A **565** (2006) 463 [arXiv:physics/0507191].

[6] W. M. Yao *et al.* [Particle Data Group], J. Phys. G **33** (2006) 1.

[7] E. J. Eichten, C. T. Hill and C. Quigg, Phys. Rev. Lett. **71** (1993) 4116 [arXiv:hep-ph/9308337].

[8] D. Ebert, V. O. Galkin and R. N. Faustov, Phys. Rev. D **57**, 5663 (1998) [Erratum-ibid. D **59**, 019902 (1999)] [arXiv:hep-ph/9712318].

[9] N. Isgur, Phys. Rev. D **57** (1998) 4041.

M. Di Pierro and E. Eichten, Phys. Rev. D **64** (2001) 114004 [arXiv:hep-ph/0104208].

[10] R. Akers *et al.* [OPAL Collaboration], Z. Phys. C **66** (1995) 19.

[11] P. Abreu *et al.* [DELPHI Collaboration], Phys. Lett. B **345** (1995) 598.

D. Buskulic *et al.* [ALEPH Collaboration], Z. Phys. C **69** (1996) 393.

R. Barate *et al.* [ALEPH Collaboration], Phys. Lett. B **425** (1998) 215.

A. A. Affolder *et al.* [CDF Collaboration], Phys. Rev. D **64** (2001) 072002.

[12] A. F. Falk and T. Mehen, Phys. Rev. D **53** (1996) 231 [arXiv:hep-ph/9507311].

[13] J. L. Rosner, Phys. Rev. D **75** (2007) 013009 [arXiv:hep-ph/0611207].

[14] D. P. Stanley and D. Robson, Phys. Rev. Lett. **45**, 235 (1980).

D. P. Stanley and D. Robson, Phys. Rev. D **21**, 3180 (1980).

J. L. Basdevant and S. Boukraa, Z. Phys. C **30** (1986) 103.

A. Martin and J. M. Richard, Phys. Lett. B **185**, 426 (1987).

W. Y. P. Hwang and D. B. Lichtenberg, Phys. Rev. D **35** (1987) 3526.

W. Kwong, J. L. Rosner and C. Quigg, Ann. Rev. Nucl. Part. Sci. **37**, 325 (1987).

J. G. Korner, M. Kramer and D. Pirjol, Prog. Part. Nucl. Phys. **33** (1994) 787 [arXiv:hep-ph/9406359].

K. C. Bowler *et al.* [UKQCD Collaboration], Phys. Rev. D **54**, 3619 (1996) [arXiv:hep-lat/9601022].

E. Jenkins, Phys. Rev. D **54**, 4515 (1996) [arXiv:hep-ph/9603449].

N. Mathur, R. Lewis and R. M. Woloshyn, Phys. Rev. D **66**, 014502 (2002) [arXiv:hep-ph/0203253].

C. Albertus, J. E. Amaro, E. Hernandez and J. Nieves, Nucl. Phys. A **740**, 333 (2004) [arXiv:nucl-th/0311100].

D. Ebert, R. N. Faustov and V. O. Galkin, Phys. Rev. D **72**, 034026 (2005) [arXiv:hep-ph/0504112].

[15] M. Gronau and J. L. Rosner, Phys. Lett. B **482** (2000) 71 [arXiv:hep-ph/0003119].

[16] H. J. Lipkin, Phys. Lett. B **621** (2005) 126 [arXiv:hep-ph/0503022].

[17] E. Barberio *et al.* [Heavy Flavor Averaging Group (HFAG)], arXiv:hep-ex/0603003.

[18] M. Beneke and M. Neubert, Nucl. Phys. B **675** (2003) 333 [arXiv:hep-ph/0308039].

[19] Y. D. Yang, F. Su, G. R. Lu and H. J. Hao, Eur. Phys. J. C **44** (2005) 243 [arXiv:hep-ph/0507326].

[20] A. J. Buras, R. Fleischer, S. Recksiegel and F. Schwab, Nucl. Phys. B **697** (2004) 133 [arXiv:hep-ph/0402112].

[21] G. Punzi, *In the Proceedings of PHYSTAT2003: Statistical Problems in Particle Physics, Astrophysics, and Cosmology, Menlo Park, California, 8-11 Sep 2003, pp MODT002* [arXiv:physics/0308063].

[22] E. Gerchtein and M. Paulini, *Proceedings of 2003 Conference for Computing in High-Energy and Nuclear Physics (CHEP 03), La Jolla, California, 24-28 Mar 2003, pp TUMT005* [arXiv:physics/0306031].

[23] E. Baracchini and G. Isidori, Phys. Lett. B **633** (2006) 309 [arXiv:hep-ph/0508071].

[24] D. Acosta *et al.* [CDF Collaboration], Phys. Rev. Lett. **96** (2006) 202001 [arXiv:hep-ex/0508022].

[25] A. Abulencia *et al.* [CDF Collaboration], Phys. Rev. Lett. **97** (2006) 211802 [arXiv:hep-ex/0607021].

[26] M. Beneke, G. Buchalla, C. Greub, A. Lenz and U. Nierste, Phys. Lett. B **459** (1999) 631 [arXiv:hep-ph/9808385].

[27] A. Lenz, arXiv:hep-ph/0412007.

[28] G. J. Feldman and R. D. Cousins, Phys. Rev. D **57** (1998) 3873 [arXiv:physics/9711021].

[29] A. R. Williamson and J. Zupan, Phys. Rev. D **74** (2006) 014003 [Erratum-ibid. D **74** (2006) 03901] [arXiv:hep-ph/0601214].

[30] X. Q. Yu, Y. Li and C. D. Lu, Phys. Rev. D **71** (2005) 074026 [Erratum-ibid. D **72** (2005) 119903] [arXiv:hep-ph/0501152].

[31] S. Descotes-Genon, J. Matias and J. Virto, Phys. Rev. Lett. **97** (2006) 061801 [arXiv:hep-ph/0603239].

[32] S. Baek, D. London, J. Matias and J. Virto, JHEP **0612** (2006) 019 [arXiv:hep-ph/0610109].

[33] Y. Li, C. D. Lu, Z. J. Xiao and X. Q. Yu, Phys. Rev. D **70** (2004) 034009 [arXiv:hep-ph/0404028].

[34] R. Mohanta, A. K. Giri and M. P. Khanna, Phys. Rev. D **63** (2001) 074001 [arXiv:hep-ph/0006109].

Lifetimes and oscillations of heavy mesons

Alexander Lenz
Institut für theoretische Physik
Universität Regensburg
D-93040 Regensburg - Germany

1 Abstract

We review the theoretical status of the lifetime ratios τ_{B^+}/τ_{B_d} and τ_{B_s}/τ_{B_d} and of the mixing quantities ΔM_s, $\Delta\Gamma_s$ and ϕ_s. We show that the ratio $\Delta\Gamma_s/\Delta M_s$ can be determined with almost no non-perturbative uncertainties. Finally we explain how this precise determination of the standard model values can be used to find possible new physics contributions in ΔM_s, $\Delta\Gamma_s$, $\Delta\Gamma_s/\Delta M_s$ and a_{fs}^s. Combining the latest experimental bounds on these quantities one already gets some hints for new physics contributions.

2 Introduction

Inclusive decays (see e.g. [1] or [2] and references therein) and lifetimes of heavy mesons can be calculated within the framework of the so-called heavy quark expansion (HQE) [3,4]. In this approach the decay rate is calculated in an expansion in inverse powers of the heavy b-quark mass.

$$\Gamma = \Gamma_0 + \frac{\Lambda^2}{m_b^2}\Gamma_2 + \frac{\Lambda^3}{m_b^3}\Gamma_3 + \dots \tag{1}$$

Γ_0 represents the decay of a free heavy b-quark, according to this contribution all b-mesons have the same lifetime. The first correction arises at order $1/m_b^2$, they are due to the kinetic and the chromomagnetic operator. At order $1/m_b^3$ the spectator quark gets involved in the weak annihilation and Pauli interference diagrams [3, 5]. This contributions are numerically enhanced by a phase space factor of $16\pi^2$. Each of the Γ_i contains perturbatively calculable Wilson coefficients and non-perturbative parameters, like decay constants or bag parameters. Unfortunately the theoretical predictions for the decay constants vary over a wide range: quenched lattice determinations for f_{B_s} tend to give values of $\mathcal{O}(200)$ MeV, while recent unquenched calculations with 2+1 dynamical light flavors give values around 260 MeV - for a

more detailed discussion see [6–8]. Since lifetime differences depend quadratically on the decay constants, going from 200 MeV to 260 MeV results in an increase of 70%. Here clearly theoretical progress is necessary to pin down the error on the decay constants considerably.

In view of several new theoretical and experimental developments we update the numbers present in the literature (see e.g. [9]).

3 Lifetimes

The lifetime ratio of two heavy mesons can be written as

$$\frac{\tau_1}{\tau_2} = 1 + \frac{\Lambda^3}{m_b^3}\left(\Gamma_3^{(0)} + \frac{\alpha_s}{4\pi}\Gamma_3^{(1)} + \ldots\right) + \frac{\Lambda^4}{m_b^4}\left(\Gamma_4^{(0)} + \frac{\alpha_s}{4\pi}\Gamma_4^{(1)} + \ldots\right) + \ldots \qquad (2)$$

If one neglects small isospin or SU(3) violating effects one has no $1/m_b^2$ corrections [1] and a deviation of the lifetime ratio from one starts at order $1/m_b^3$.

3.1 τ_{B^+}/τ_{B_d}

The leading term $\Gamma_3^{(0)}$ has been determined in [3, 10]. For a quantitative treatment of the lifetime ratios NLO QCD corrections are mandatory - $\Gamma_3^{(1)}$ has been determined in [11, 12]. Subleading effects of $\mathcal{O}(1/m_b)$ turned out to be negligible [13]. The matrix elements of the arising four-quark operators have been determined in [14]. Using the result from [11]

$$\begin{aligned}\frac{\tau(B^+)}{\tau(B_d^0)} - 1 \;&=\; \tau(B^+)\,\left[\Gamma(B_d^0) - \Gamma(B^+)\right] \qquad (3)\\ &=\; 0.0325\,\frac{\tau(B^+)}{1.653\,\text{ps}}\left(\frac{|V_{cb}|}{0.04}\right)^2\left(\frac{m_b}{4.8\text{GeV}}\right)^2\left(\frac{f_B}{200\text{MeV}}\right)^2 \times \\ &\quad \Big[\,(1.0\pm0.2)\,B_1 \;+\; (0.1\pm0.1)\,B_2 \;-\; (18.4\pm0.9)\,\epsilon_1 \;+\; (4.0\pm0.2)\,\epsilon_2\,\Big] + \delta_{1/m}\end{aligned}$$

one gets with the matrix elements from Becirevic [14] ($B_1 = 1.10 \pm 0.20$; $B_2 = 0.79 \pm 0.10$; $\epsilon_1 = -0.02 \pm 0.02$; $\epsilon_2 = 0.03 \pm 0.01$) and the values $V_{cb} = 0.0415$, $m_b = 4.63$ GeV and $f_B = 216$ MeV [15]:

$$\left[\frac{\tau(B^+)}{\tau(B_d^0)}\right]_{\text{NLO}} \;=\; 1.063 \pm 0.027\,, \qquad (4)$$

[1] In the case of $\tau_{\Lambda_b}/\tau_{B_d}$ these effects are expected to be of the order of 5%.

which is in excellent agreement with the experimental number [16, 17]

$$\left[\frac{\tau(B^+)}{\tau(B_d^0)}\right] \;=\; 1.071 \pm 0.009\,. \tag{5}$$

From Eq. (3) one clearly sees that a precise knowledge of the color octet bag parameters ϵ_1 and ϵ_2 - these parameters are of order $1/N_c$ - is mandatory since their coefficients are numerically enhanced. Here clearly more work has to be done.

3.2 τ_{B_s}/τ_{B_d}

In the lifetime ratio τ_{B_s}/τ_{B_d} a cancellation of weak annihilation contributions arises, that differ only by small SU(3)-violation effects. One expects a number that is close to one [10, 12, 18, 19]

$$\frac{\tau(B_s)}{\tau(B_d)} \;=\; 1.00 \pm 0.01\,. \tag{6}$$

This expectation is confirmed by experiment [17, 20]

$$\frac{\tau(B_s)}{\tau(B_d)} \;=\; 0.957 \pm 0.027\,, \tag{7}$$

although more precise experimental numbers would be very desirable.

3.3 $\tau_{B_c^+}$

The lifetime of the doubly heavy meson B_c has been investigated in [21]

$$\tau(B_c) \;=\; 0.52^{+0.18}_{-0.12}\,\text{ps}\,. \tag{8}$$

In addition to the b-quark now also the c-charm quark can decay, giving rise to the biggest contribution to the total decay rate. The current experimental number [22]

$$\tau(B_c) \;=\; 0.469 \pm 0.027\,\text{ps} \tag{9}$$

agrees nicely with the theoretical prediction, but it has much smaller errors. Here clearly some theoretical improvements are necessary to pin down the error.

4 Mixing Parameters

In this section we briefly investigate the status of the mixing parameters. For a more detailed review we refer the interested reader to [7].
The mixing of the neutral B-mesons is described by the off diagonal elements Γ_{12} and

M_{12} of the mixing matrix. Γ_{12} stems from the absorptive part of the box diagrams - only internal up and charm quarks contribute, while M_{12} stems from the dispersive part of the box diagram, therefore being sensitive to heavy internal particles like the top quark or heavy new physics particles. By diagonalizing the mixing matrix we obtain the physical eigenstates B_H and B_L with defined masses (M_H, M_L) and defined decay rates (Γ_H, Γ_L) in terms of the flavor eigenstates $B_s = (\overline{b}s)$ and $\overline{B}_s = (b\overline{s})$:

$$B_H := p\, B + q\, \overline{B}\,, \qquad B_L := p\, B - q\, \overline{B} \qquad \text{with } |p|^2 + |q|^2 = 1\,. \tag{10}$$

The calculable quantities $|M_{12}|$, $|\Gamma_{12}|$ and $\phi = \arg(-M_{12}/\Gamma_{12})$ can be related to three observables:

- **Mass difference:**

$$\Delta M := M_H - M_L = 2|M_{12}| \left(1 + \frac{1}{8}\frac{|\Gamma_{12}|^2}{|M_{12}|^2}\sin^2\phi + ...\right) \tag{11}$$

  $|M_{12}|$ is due to heavy internal particles in the boxdiagrams like the top-quark or SUSY-particles.

- **Decay rate difference:**

$$\Delta\Gamma := \Gamma_L - \Gamma_H = 2|\Gamma_{12}|\cos\phi \left(1 - \frac{1}{8}\frac{|\Gamma_{12}|^2}{|M_{12}|^2}\sin^2\phi + ...\right) \tag{12}$$

  $|\Gamma_{12}|$ is due to light internal particles: particles, like the up- and the charm-quark. It is therefore very insensitive to new physics contributions.

- **Flavor specific/semileptonic CP asymmetries:**
  A decay $B_q \to f$ is called flavor specific, if the decays $\overline{B}_q \to f$ and $B_q \to \overline{f}$ are forbidden and if no direct CP violation occurs, i.e. $|\langle f|B_q\rangle| = |\langle \overline{f}|\overline{B}_q\rangle|$. Some examples are $B_s \to D_s^- \pi^+$ or $B_q \to X l \nu$ (therefore the name semileptonic CP asymmetry). The flavor specific CP asymmetry is defined as

$$\begin{aligned} a_{fs} &= \frac{\Gamma\left(\overline{B}_q(t) \to f\right) - \Gamma\left(B_q(t) \to \overline{f}\right)}{\Gamma\left(\overline{B}_q(t) \to f\right) + \Gamma\left(B_q(t) \to \overline{f}\right)} = -2\left(\left|\frac{q}{p}\right| - 1\right) \\ &= \mathrm{Im}\frac{\Gamma_{12}}{M_{12}} = \frac{\Delta\Gamma}{\Delta M}\tan\phi\,. \end{aligned}$$

4.1 Mass difference

Calculating the box diagram with internal top quarks one obtains

$$M_{12,q} = \frac{G_F^2}{12\pi^2}(V_{tq}^* V_{tb})^2 M_W^2 S_0(x_t) B_{B_q} f_{B_q}^2 M_{B_q} \hat{\eta}_B \tag{13}$$

The Inami-Lim function $S_0(x_t = \overline{m}_t^2/M_W^2)$ [23] is the result of the box diagram without any gluon corrections. The NLO QCD correction is parameterized by $\hat{\eta}_B \approx 0.84$ [24]. The non-perturbative matrix element of the operator $Q = (\bar{b}q)_{V-A}(\bar{b}q)_{V-A}$ is parameterized by the bag parameter B and the decay constant f_B

$$\langle \overline{B_q}|Q|B_q\rangle = \frac{8}{3} B_{B_q} f_{B_q}^2 M_{B_q} \,. \tag{14}$$

Using the conservative estimate $f_{B_s} = 240 \pm 40$ MeV [7] and the bag parameter B from JLQCD [25] we obtain

$$\Delta M_s = 19.3 \pm 6.4 \pm 1.9\,\mathrm{ps}^{-1} \tag{15}$$

The first error stems from the uncertainty in f_{B_s} and the second error summarizes the remaining theoretical uncertainties. The determination of ΔM_d is affected by even larger uncertainties because here one has to extrapolate to the small mass of the down-quark. The ratio $\Delta M_s/\Delta M_d$ is theoretically better under control since in the ratio of the non-perturbative parameters many systematic errors cancel.

This year also ΔM_s was measured, leading to the pleasant situation of having very precise experimental numbers at hand [20, 26, 27]

$$\Delta M_d = 0.507 \pm 0.004\,\mathrm{ps}^{-1}\,, \tag{16}$$
$$\Delta M_s = 17.77 \pm 0.12\,\mathrm{ps}^{-1}\,. \tag{17}$$

To be able to distinguish possible new physics contributions to ΔM_s from QCD uncertainties much more precise numbers for f_{B_s} are needed.

4.2 Decay rate difference and flavor specific CP asymmetries

In order to determine the decay rate difference of the neutral B-mesons and flavor specific CP asymmetries a precise determination of Γ_{12} is needed. With the help of the HQE Γ_{12} can be written as

$$\Gamma_{12} = \frac{\Lambda^3}{m_b^3}\left(\Gamma_3^{(0)} + \frac{\alpha_s}{4\pi}\Gamma_3^{(1)} + \ldots\right) + \frac{\Lambda^4}{m_b^4}\left(\Gamma_4^{(0)} + \frac{\alpha_s}{4\pi}\Gamma_4^{(1)} + \ldots\right) + \ldots \tag{18}$$

The leading term $\Gamma_3^{(0)}$ was determined in [28]. The numerical and conceptual important NLO-QCD corrections ($\Gamma_3^{(1)}$) were determined in [29–31]. Subleading $1/m$-corrections, i.e. $\Gamma_4^{(0)}$ were calculated in [19,32] and even the Wilson coefficients of the $1/m^2$-corrections ($\Gamma_5^{(0)}$) were calculated and found to be small [33].

Besides the already known operator Q in the calculation of Γ_{12} three additional operators arise $\tilde{Q}, Q_S$ and $\tilde{Q}_S$. The tilde stands for a color rearrangement and index S corresponds to a S-P Dirac structure instead of the V-A-structure. $Q = \tilde{Q}$ and it

can be shown [7,19,29] that a certain combination of Q, Q_S and $\tilde{Q}_S$ is suppressed by powers of $1/m_b$ and α_s

$$\tilde{Q} = Q \quad \text{and} \quad R_0 = Q_S + \alpha_1 \tilde{Q}_S + \frac{\alpha_2}{2} Q = \mathcal{O}\left(\frac{1}{m_b}, \alpha_s\right) \tag{19}$$

with $\alpha_i = 1 + \mathcal{O}(\alpha_s)$, for more details see [7]. In the literature [19,28–31] always $\tilde{Q}_S$ was eliminated - with the help of Eq. (19) - and one was left with the operator basis $\{Q, Q_S\}$, which we call in the following the *old basis*. Working in the old basis one finds several serious drawbacks:

- An almost complete cancellation of the coefficient of the operator Q takes place, while the operator Q_S is dominant. So in the ratio $\Delta\Gamma_s/\Delta M_s$ the only coefficient that is free of non-perturbative uncertainties is numerically negligible.
- The $1/m$ corrections are abnormally large - all contributions have the same sign.
- The α_s-corrections and the remaining μ-dependence is unexpectedly large.

In [7] it was found, that expressing Γ_{12} in terms of the *new basis* $\{Q, \tilde{Q}_S\}$ one gets a result, that is free of the above shortcomings. The change of the basis corresponds to throwing away certain contributions of $\mathcal{O}(\alpha_s^2)$ and $\mathcal{O}(\alpha_s/m_b)$, which is beyond the calculated accuracy. For our new determination of Γ_{12} we also use the $\overline{\text{MS}}$-scheme [34], besides the pole scheme for the b-quark mass. Moreover we sum up logarithms of the form $z \ln z$ - with $z = m_c^2/m_b^2$ - to all orders, following [11] and of course we have to include also subleading CKM-structures to determine a_{fs}, as done in [30,31].

In the old basis one obtains

$$\Delta\Gamma_s = \left(\frac{f_{B_s}}{240\,\text{MeV}}\right)^2 \left[0.002B + 0.094B'_S - \left(0.033 B_{\tilde{R}_2} + 0.019 B_{R_0} + 0.005 B_R\right)\right] , \tag{20}$$

$$\frac{\Delta\Gamma_s}{\Delta M_s} = 10^{-4} \cdot \left[0.9 \quad + 40.9\frac{B'_S}{B} - \left(14.4\frac{B_{\tilde{R}_2}}{B} + 8.5\frac{B_{R_0}}{B} + 2.1\frac{B_R}{B}\right)\right] \tag{21}$$

with

$$\langle \overline{B_s} | Q_S | B_s \rangle = -\frac{5}{3} B'_S f_{B_s}^2 M_{B_s} , \quad B'_X := B_X \frac{M_{B_s}^2}{\left(\overline{m}_b + \overline{m}_s\right)^2} . \tag{22}$$

In Eq. (21) we have explicitly shown the dependence on the dominant $1/m$ operators R_2 and R_0 (see [7,19] for the definition). The remaining power corrections are summarized in the coefficient of B_R. One clearly sees that the cancellation in the coefficient of B leads to the undesirable situation, that the only coefficient in $\Delta\Gamma/\Delta M$ that is free of non-perturbative uncertainties is negligible.

This changes however dramatically if one uses the new basis

$$\Delta\Gamma_s = \left(\frac{f_{B_s}}{240\,\text{MeV}}\right)^2 \left[0.105B + 0.024\tilde{B}'_S - \left(0.030B_{\tilde{R}_2} - 0.006B_{R_0} + 0.003B_R\right)\right] \tag{23}$$

$$\frac{\Delta\Gamma_s}{\Delta M_s} = 10^{-4}\cdot\left[46.2 \quad + 10.6\frac{B'_S}{B} - \left(13.2\frac{B_{\tilde{R}_2}}{B} - 2.5\frac{B_{R_0}}{B} + 1.2\frac{B_R}{B}\right)\right] \tag{24}$$

with

$$\langle\overline{B_s}|\tilde{Q}_S|B_s\rangle = \frac{1}{3}\tilde{B}'_S f_{B_s}^2 M_{B_s}\,. \tag{25}$$

Now the dominant part of $\Delta\Gamma/\Delta M$ can be determined without any hadronic uncertainties!
Using the non-perturbative parameters from [25, 35], we obtain the following final numbers (see [7] for the complete list of the numerical input parameters)

$$\Delta\Gamma_s = (0.096 \pm 0.039)\ \text{ps}^{-1} \quad \Rightarrow \quad \frac{\Delta\Gamma_s}{\Gamma_s} = \Delta\Gamma_s\cdot\tau_{B_d} = 0.147 \pm 0.060\,, \tag{26}$$

$$a^s_{fs} = (2.06 \pm 0.57)\cdot 10^{-5}\,, \tag{27}$$

$$\frac{\Delta\Gamma_s}{\Delta M_s} = (49.7 \pm 9.4)\cdot 10^{-4}\,, \tag{28}$$

$$\phi_s = 0.0041 \pm 0.0008 = 0.24^\circ \pm 0.04\,. \tag{29}$$

The composition of the theoretical error of $\Delta\Gamma$ is compared for the use of the old and the new basis in Fig. (1). The by far dominant error comes from the decay constant f_{B_s}, followed by the uncertainty due to the power suppressed operator $\tilde{R}_2$ and the remaining μ-dependence. In this case the theoretical improvement due to the change of basis is somehow limited by the huge uncertainty due to f_{B_s}, which is the same in both bases.

This changes if one looks at the composition of the theoretical error of $\Delta\Gamma/\Delta M$ in Fig. (2). Since now f_{B_s} cancels the dominant error comes from the uncertainty due to the power suppressed operator $\tilde{R}_2$ and the remaining μ-dependence.

One clearly sees that the change of the basis resulted in a considerable reduction of the theoretical error , almost a factor 3 in the case of $\Delta\Gamma_s/\Delta M_s$!
To improve our theoretical knowledge of the mixing quantities further one needs more precise values of the non-perturbative parameters, like the decay constants or the power suppressed operators. If accurate non-perturbative parameters are available one might think about NNLO calculations (α_s^2 or α_s/m_b-corrections) to reduce the remaining μ-dependence.

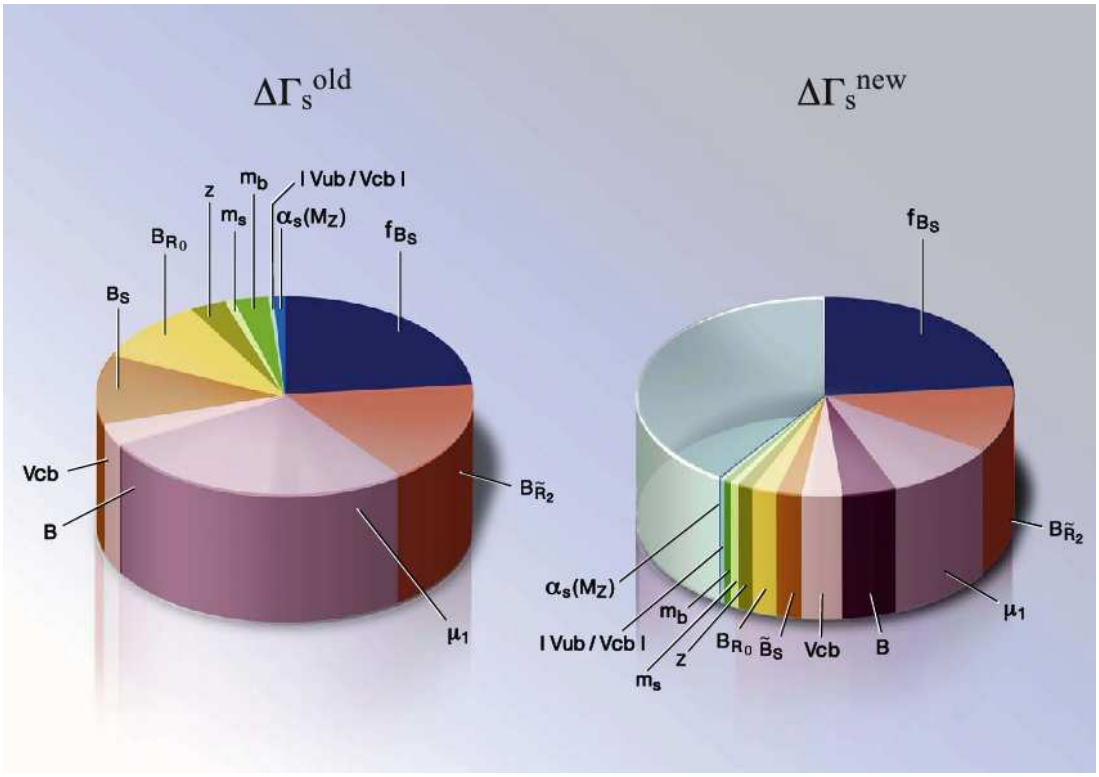

Figure 1: Error budget for the determination of $\Delta\Gamma_s$ in the old and the new basis.

4.3 New Physics

New physics (see e.g. [36]) is expected to have almost no impact on Γ_{12} but it can change M_{12} considerably. Therefore one can write

$$\Gamma_{12,s} = \Gamma_{12,s}^{\rm SM}\,, \qquad M_{12,s} = M_{12,s}^{\rm SM}\cdot\Delta_s\,; \qquad \Delta_s = |\Delta_s| e^{i\phi_s^\Delta} \tag{30}$$

With this parameterisation the physical mixing parameters can be written as

$$\Delta M_s = 2|M_{12,s}^{\rm SM}|\cdot|\Delta_s| \tag{31}$$

$$\Delta\Gamma_s = 2|\Gamma_{12,s}|\cdot\cos\left(\phi_s^{\rm SM}+\phi_s^\Delta\right) \tag{32}$$

$$\frac{\Delta\Gamma_s}{\Delta M_s} = \frac{|\Gamma_{12,s}|}{|M_{12,s}^{\rm SM}|}\cdot\frac{\cos\left(\phi_s^{\rm SM}+\phi_s^\Delta\right)}{|\Delta_s|} \tag{33}$$

$$a_{fs}^s = \frac{|\Gamma_{12,s}|}{|M_{12,s}^{\rm SM}|}\cdot\frac{\sin\left(\phi_s^{\rm SM}+\phi_s^\Delta\right)}{|\Delta_s|} \tag{34}$$

Now we combine the current experimental knowledge about the mixing parameters to find out whether B_s-mixing is described by the standard model alone, or whether

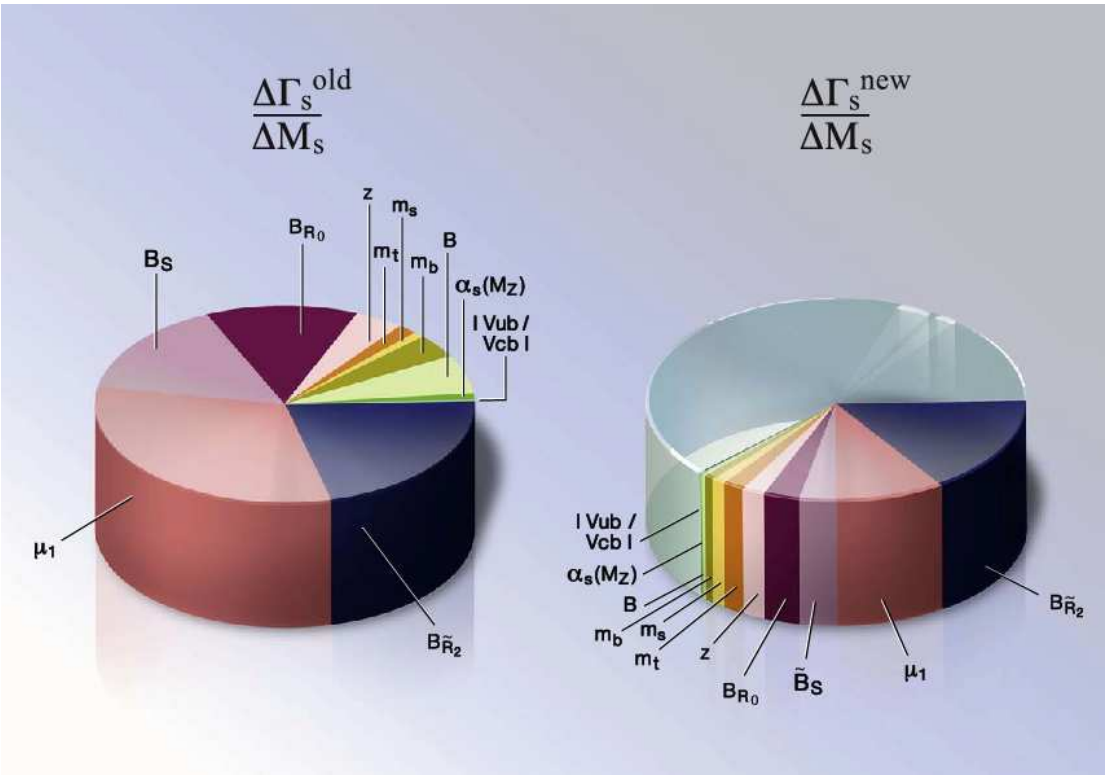

Figure 2: Error budget for the determination of $\Delta\Gamma_s/\Delta M_s$ in the old and the new basis.

we already get some signals of new physics contributions.
The mass difference ΔM_s is now known very precisely [26, 27]

$$\Delta M_s \;=\; 17.77 \pm 0.10_{(\text{syst})} \pm 0.07\,_{(\text{stat})}\,\text{ps}^{-1} \qquad \text{CDF.} \tag{35}$$

For the remaining mixing parameters in the B_s-system only experimental bounds are available. The width difference $\Delta\Gamma_s/\Gamma_s$ was investigated at ALEPH, BELLE, CDF, D0 by analyzing the decays $B_s \to D_s^{(*)+} + D_s^{(*)-}$ [37], $B_s \to J/\Psi + \phi$ [38] and $B_s \to K^+ + K^-$ [39] and the flavor specific lifetime of the B_s meson [40]. A recent combination of all these results yields [41]

$$\Delta\Gamma_s \;=\; 0.097 \pm 0.042\,\text{ps}^{-1}\,, \tag{36}$$

$$\frac{\Delta\Gamma_s}{\Delta M_s} \;=\; (56 \pm 24) \times 10^{-4}\,. \tag{37}$$

Except the angular analysis $B_s \to J/\Psi + \phi$ all other determinations are affected by some drawbacks, described in [7]. Moreover the D0 collaboration has updated their

results [38] for the decay $B_s \to J/\Psi + \phi$ in [17, 26, 42] using 1fb$^-$1 of data. Setting the value of the mixing phase ϕ_s to zero they obtain [17, 26, 42]

$$\Delta\Gamma_s = 0.12 \pm 0.08^{+0.03}_{-0.04}\,\mathrm{ps}^{-1}\,, \tag{38}$$

allowing for a non-zero value of the mixing phase ϕ_s they get

$$\Delta\Gamma_s = 0.17 \pm 0.09 \pm 0.03\,\mathrm{ps}^{-1}\,, \tag{39}$$

$$\phi_s = -0.79 \pm 0.56 \pm 0.01\,. \tag{40}$$

In the following we will for $\Delta\Gamma_s$ and ϕ_s only use the numbers from Eq. (39) and Eq. (40).

The semileptonic CP asymmetry in the B_s system has been determined directly in [43] and found to be

$$a_{sl}^{s,\mathrm{direct}} = (24.5 \pm 19.3 \pm 3.5) \cdot 10^{-3}\,. \tag{41}$$

Moreover the semileptonic CP asymmetry can be extracted from the same sign dimuon asymmetry that was measured in [44] to be

$$a_{sl} = (-2.8 \pm 1.3 \pm 0.9) \cdot 10^{-3}\,. \tag{42}$$

Updating the numbers in [45, 46] one sees that

$$a_{sl} = (0.582 \pm 0.030)\; a_{sl}^d + (0.418 \pm 0.047)\; a_{sl}^s \tag{43}$$

In [45,46] the experimental bound for a_{sl}^d was used to extract from Eq.(42) and Eq.(43) a bound on a_{sl}^s. Due to the huge experimental uncertainties in a_{sl}^d this strategy resulted in a large error on a_{sl}^s. Since in the B_d-system there is not much room left for new physics contributions, we think it is justified to use the theoretical number of a_{sl}^d. Using $a_{sl}^d = -\,(0.48 \pm 0.12) \cdot 10^{-3}$ we get from Eq.(42), Eq.(43) and Eq.(42) already a nice bound

$$a_{sl}^{s,\mathrm{dimuon}} = (-6.0 \pm 3.2 \pm 2.2) \cdot 10^{-3}\,. \tag{44}$$

Combining this number with the direct determination [43] we get our final experimental number for the semileptonic CP asymmetries

$$a_{sl}^s = (-5.2 \pm 3.2 \pm 2.2) \cdot 10^{-3}\,. \tag{45}$$

Now we combine these experimental numbers with the theoretical errors to extract bounds in the imaginary Δ_s-plane by the use of Eqs. (31), (32), (33) and (34), see Fig. (3).

The comparison of experiment and standard model expectation for ΔM_s, $\Delta\Gamma_s$, ϕ_s, $\Delta\Gamma_s/\Delta M_s$ and a_{sl}^s presented in figure 3 already shows some hints for deviations from the standard model.

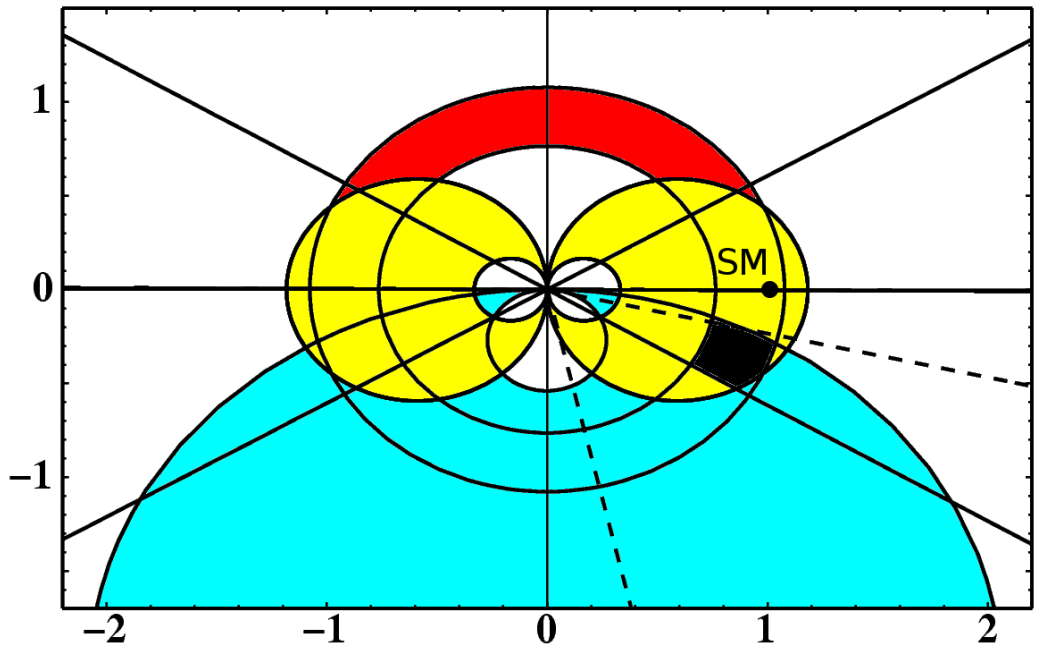

Figure 3: Current experimental bounds in the complex Δ_s-plane. The bound from ΔM_s is given by the red (dark-grey) ring around the origin. The bound from $\Delta\Gamma_s/\Delta M_s$ is given by the yellow (light-grey) region and the bound from a^s_{fs} is given by the light-blue (grey) region. The angle ϕ_s^Δ can be extracted from $\Delta\Gamma_s$ (solid lines) with a four fold ambiguity - one bound coincides with the x-axis! - or from the angular analysis in $B_s \to J/\Psi\phi$ (dashed line). If the standard model is valid all bounds should coincide in the point (1,0). The current experimental situation shows a small deviation, which might become significant, if the experimental uncertainties in $\Delta\Gamma_s$, a^s_{sl} and ϕ_s will go down in near future.

5 Conclusion and outlook

Theoretical predictions of the lifetimes of heavy mesons are in excellent agreement with the experimental numbers. We do not see any signal of possible duality violations. To become more quantitative in the prediction of τ_{B^+}/τ_{B_d} the non-perturbative estimates of the bag parameters B_1, B_2 and ϵ_1, ϵ_2 have to be improved. For τ_{B_s}/τ_{B_d} more precise experimental numbers are needed, while in the case of τ_{B_c} theoretical progress is mandatory.
The theoretical uncertainty in the mixing parameter ΔM is completely dominated by the decay constant. We have presented a method (see [7] for more details) to reduce the theoretical error in $\Delta\Gamma$, $\Delta\Gamma/\Delta M$ and a_{fs} considerably. This relatively clean standard model predictions can be used to look for new physics effects in B_s-mixing. From the currently available experimental bounds on $\Delta\Gamma_s$ and a_{fs} one already gets some hints for deviations from the standard model. This situation will improve dramatically as soon as more data are available.

For a further reduction of the theoretical uncertainty in $\Delta\Gamma$ a much higher accuracy than currently available on the decay constants is necessary. If this problem is solved or if one looks at quantities like $\Delta\Gamma/\Delta M$ and a_{fs} where the dependence on f_B cancels, then the dominant uncertainty comes from the unknown matrix elements of the power suppressed operators. Here any non-perturbative estimate would be very desirable. If accurate non-perturbative parameters are available one might think about NNLO calculations (α_s^2 or α_s/m_b-corrections) to reduce the remaining μ-dependence.

I would like to thank the organizers of HQL2006 for the invitation and Uli Nierste for the pleasant collaboration.

Bibliography

[1] A. Lenz, U. Nierste and G. Ostermaier, Phys. Rev. D **56** (1997) 7228 [arXiv:hep-ph/9706501]; A. Lenz, U. Nierste and G. Ostermaier, Phys. Rev. D **59** (1999) 034008 [arXiv:hep-ph/9802202]; A. Lenz, arXiv:hep-ph/0011258; O. Buchmüller, these proceedings; T. Mannel, these proceedings.

[2] M. Battaglia *et al.*, arXiv:hep-ph/0304132.

[3] M. A. Shifman and M. B. Voloshin, in: *Heavy Quarks* ed. V. A. Khoze and M. A. Shifman, Sov. Phys. Usp. **26** (1983) 387; M. A. Shifman and M. B. Voloshin, Sov. J. Nucl. Phys. **41** (1985) 120 [Yad. Fiz. **41** (1985) 187]; M. A. Shifman and M. B. Voloshin, Sov. Phys. JETP **64** (1986) 698 [Zh. Eksp. Teor. Fiz. **91** (1986) 1180];

[4] J. Chay, H. Georgi and B. Grinstein, Phys. Lett. B **247** (1990) 399; I. I. Bigi, N. G. Uraltsev and A. I. Vainshtein, Phys. Lett. B **293** (1992) 430 [Erratum-ibid. B **297** (1992) 477]; I. I. Y. Bigi, M. A. Shifman, N. G. Uraltsev and A. I. Vainshtein, Phys. Rev. Lett. **71** (1993) 496 [arXiv:hep-ph/9304225]; B. Blok, L. Koyrakh, M. A. Shifman and A. I. Vainshtein, "Differential distributions in semileptonic decays of the heavy flavors in Phys. Rev. D **49** (1994) 3356 [Erratum-ibid. D **50** (1994) 3572] [arXiv:hep-ph/9307247]; A. V. Manohar and M. B. Wise, Phys. Rev. D **49** (1994) 1310 [arXiv:hep-ph/9308246].

[5] B. Guberina, S. Nussinov, R. D. Peccei and R. Ruckl, Phys. Lett. B **89** (1979) 111; N. Bilic, B. Guberina and J. Trampetic, Nucl. Phys. B **248** (1984) 261; B. Guberina, R. Ruckl and J. Trampetic, Z. Phys. C **33** (1986) 297.

[6] V. Lubicz, these proceedings.

[7] A. Lenz and U. Nierste, arXiv:hep-ph/0612167.

[8] T. Onogi, arXiv:hep-lat/0610115.

[9] A. Lenz, arXiv:hep-ph/9906317; M. Beneke and A. Lenz, J. Phys. G **27** (2001) 1219 [arXiv:hep-ph/0012222]; A. Lenz and S. Willocq, J. Phys. G **27** (2001) 1207; A. Lenz, arXiv:hep-ph/0107033; A. Lenz, arXiv:hep-ph/0412007.

[10] I. I. Y. Bigi, B. Blok, M. A. Shifman, N. Uraltsev and A. I. Vainshtein, arXiv:hep-ph/9401298; I. I. Y. Bigi, arXiv:hep-ph/9508408; M. Neubert and C. T. Sachrajda, Nucl. Phys. B **483** (1997) 339 [arXiv:hep-ph/9603202].

[11] M. Beneke, G. Buchalla, C. Greub, A. Lenz and U. Nierste, Nucl. Phys. B **639** (2002) 389 [arXiv:hep-ph/0202106].

[12] E. Franco, V. Lubicz, F. Mescia and C. Tarantino, Nucl. Phys. B **633** (2002) 212 [arXiv:hep-ph/0203089].

[13] A. Lenz and U. Nierste, unpublished, e.g. talk at Academia Sinica 2003; F. Gabbiani, A. I. Onishchenko and A. A. Petrov, Phys. Rev. D **70** (2004) 094031 [arXiv:hep-ph/0407004].

[14] M. Di Pierro and C. T. Sachrajda [UKQCD Collaboration], Nucl. Phys. B **534** (1998) 373 [arXiv:hep-lat/9805028]; D. Becirevic, arXiv:hep-ph/0110124.

[15] A. Gray *et al.* [HPQCD Collaboration], Phys. Rev. Lett. **95** (2005) 212001 [arXiv:hep-lat/0507015].

[16] W. M. Yao *et al.* [Particle Data Group], J. Phys. G **33** (2006) 1.

[17] A. Cano, these proceedings.

[18] Y. Y. Keum and U. Nierste, Phys. Rev. D **57** (1998) 4282 [arXiv:hep-ph/9710512].

[19] M. Beneke, G. Buchalla and I. Dunietz, Phys. Rev. D **54** (1996) 4419 [arXiv:hep-ph/9605259].

[20] http://www.slac.stanford.edu/xorg/hfag/index.html

[21] C. H. Chang, S. L. Chen, T. F. Feng and X. Q. Li, Phys. Rev. D **64** (2001) 014003 [arXiv:hep-ph/0007162]; V. V. Kiselev, A. E. Kovalsky and A. K. Likhoded, Nucl. Phys. B **585** (2000) 353 [arXiv:hep-ph/0002127]. A. Y. Anisimov, I. M. Narodetsky, C. Semay and B. Silvestre-Brac, Phys. Lett. B **452** (1999) 129 [arXiv:hep-ph/9812514]. M. Beneke and G. Buchalla, Phys. Rev. D **53** (1996) 4991 [arXiv:hep-ph/9601249].

[22] A. Abulencia *et al.* [CDF Collaboration], Phys. Rev. Lett. **97** (2006) 012002 [arXiv:hep-ex/0603027]. D0 Collaboration, D0 conference note 4539

[23] T. Inami and C. S. Lim, Prog. Theor. Phys. **65** (1981) 297 [Erratum-ibid. **65** (1981) 1772].

[24] A. J. Buras, M. Jamin and P. H. Weisz, Nucl. Phys. B **347** (1990) 491.

[25] S. Aoki *et al.* [JLQCD Collaboration], Phys. Rev. Lett. **91** (2003) 212001 [arXiv:hep-ph/0307039].

[26] S. Menzemer, these proceedings.

[27] A. Abulencia *et al.* [CDF Collaboration], arXiv:hep-ex/0609040; A. Abulencia [CDF - Run II Collaboration], Phys. Rev. Lett. **97** (2006) 062003 [arXiv:hep-ex/0606027]; V. M. Abazov *et al.* [D0 Collaboration], Phys. Rev. Lett. **97** (2006) 021802 [arXiv:hep-ex/0603029].

[28] J.S. Hagelin, Nucl. Phys. **B193**, 123 (1981); E. Franco, M. Lusignoli and A. Pugliese, Nucl. Phys. **B194**, 403 (1982); L.L. Chau, Phys. Rep. **95**, 1 (1983); A.J. Buras, W. Słominski and H. Steger, Nucl. Phys. **B245**, 369 (1984); M.B. Voloshin, N.G. Uraltsev, V.A. Khoze and M.A. Shifman, Sov. J. Nucl. Phys. **46**, 112 (1987); A. Datta, E.A. Paschos and U. Türke, Phys. Lett. **B196**, 382 (1987); A. Datta, E.A. Paschos and Y.L. Wu, Nucl. Phys. **B311**, 35 (1988).

[29] M. Beneke, G. Buchalla, C. Greub, A. Lenz and U. Nierste, Phys. Lett. B **459** (1999) 631 [arXiv:hep-ph/9808385].

[30] M. Beneke, G. Buchalla, A. Lenz and U. Nierste, Phys. Lett. B **576** (2003) 173 [arXiv:hep-ph/0307344].

[31] M. Ciuchini, E. Franco, V. Lubicz, F. Mescia and C. Tarantino, JHEP **0308** (2003) 031 [arXiv:hep-ph/0308029].

[32] A. S. Dighe, T. Hurth, C. S. Kim and T. Yoshikawa, Nucl. Phys. B **624** (2002) 377 [arXiv:hep-ph/0109088].

[33] A. Lenz and U. Nierste, to appear.

[34] W. A. Bardeen, A. J. Buras, D. W. Duke and T. Muta, Phys. Rev. D **18** (1978) 3998.

[35] D. Becirevic, V. Gimenez, G. Martinelli, M. Papinutto and J. Reyes, JHEP **0204** (2002) 025 [arXiv:hep-lat/0110091].

[36] A. Weiler, these proceedings; T. Iijima, these proceedings; C. Tarantino, these proceedings; R. Fleischer, these proceedings.

[37] R. Barate *et al.* [ALEPH Collaboration], Phys. Lett. B **486** (2000) 286; CDF collaboration, conference note 7925, http://www-cdf.fnal.gov; D0 collaboration, conference note 5068, http://www-do.fnal.gov/; K. Ikado [Belle Collaboration], eConf **C060409** (2006) 003 [arXiv:hep-ex/0605068]; A. Drutskoy, arXiv:hep-ex/0605110; M. Paulini, these proceedings.

[38] D. Acosta *et al.* [CDF Collaboration], Phys. Rev. Lett. **94** (2005) 101803 [arXiv:hep-ex/0412057]; D0 collaboration, conference note 5052, http://www-do.fnal.gov/.

[39] D. Tonelli [CDF Collaboration], eConf **C060409** (2006) 001 [arXiv:hep-ex/0605038];

A. Abulencia [CDF Collaboration], arXiv:hep-ex/0607021.

[40] [Heavy Flavor Averaging Group (HFAG)], arXiv:hep-ex/0603003; V. M. Abazov *et al.* [D0 Collaboration], arXiv:hep-ex/0604046.

[41] R. Van Kooten, eConf **C060409** (2006) 031 [arXiv:hep-ex/0606005].

[42] D0 collaboration, conference note 5144, http://www-do.fnal.gov/.

[43] D0 collaboration, conference note 5143, http://www-do.fnal.gov/.

[44] V. Abazov [D0 Collaboration], "Measurement of the CP-violation parameter of B0 mixing and decay with p arXiv:hep-ex/0609014.

[45] D0 collaboration, conference note 5189, http://www-do.fnal.gov/.

[46] Y. Grossman, Y. Nir and G. Raz, Phys. Rev. Lett. **97** (2006) 151801 [arXiv:hep-ph/0605028].

Lattice QCD, Flavor Physics and the Unitarity Triangle Analysis

Vittorio Lubicz
Dipartimento di Fisica, Università di Roma Tre and INFN Sezione di Roma Tre
Via della Vasca Navale 84
I-00146 Rome, ITALY

Lattice QCD has always played a relevant role in the studies of flavor physics and, in particular, in the Unitarity Triangle (UT) analysis. Before the starting of the B factories, this analysis relied on the results of lattice QCD simulations to relate the experimental determinations of semileptonic B decays, $K-\overline{K}$ and $B_{d,s}-\overline{B}_{d,s}$ mixing to the CKM parameters. In the last years much more information has been obtained from the direct determination of the UT angles from non-leptonic B decays. In this talk, after a presentation of recent averages of lattice QCD results, we compare the outcome of the "classical" UT analysis (**UT***lattice*) with the analysis based on the angles determinations (**UT***angles*). We discuss the role of the different determinations of V_{ub}, and show that current data do not favour the value measured in inclusive decays. Finally we show that the recent measurement of Δm_s, combined with Δm_d and ε_K, allows a quite accurate extraction of the values of the hadronic parameters, $\hat{B}_K$, $f_{Bs}\,\hat{B}_{Bs}^{1/2}$ and ξ. These values, obtained "experimentally" by assuming the validity of the Standard Model, are compared with the theoretical predictions from lattice QCD.

1 Introduction

Lattice QCD has always played a relevant role in the history of the UT fit since the very beginning. At the time when the B factories had not started yet, the "classical" UT analysis relied on the results of lattice QCD simulations to relate the experimental studies of semileptonic B decays, $B_{d,s}-\overline{B}_{d,s}$ and $K-\overline{K}$ mixing to the CKM parameters. Despite the lattice results were mostly obtained in the quenched approximation at that time, and some of the experimental determinations were still rather rough, these analyses allowed to reach at least three important results for flavor physics in the Standard Model (SM): i) the amount of indirect CP violation observed in kaon mixing (ε_K) was shown to be fully consistent with the expectation based on the CKM mechanism of CP violation; ii) and iii) quite accurate predictions for $\sin 2\beta$ and Δm_s were obtained.

Predictions of $\sin 2\beta$ exist since more than 15 years, see Fig. 1 (left): the first indication of a large value of this parameter, namely $\sin 2\beta > 0.55$, dates back to 1992 [1]. In 1995, the prediction $\sin 2\beta = 0.65 \pm 0.12$ was derived [2]. Five years later, when direct measurements were not available yet, we obtained the more accurate estimate $\sin 2\beta = 0.698 \pm 0.066$ [3]. These results are in remarkable agreement with the present experimental average, $\sin 2\beta = 0.675 \pm 0.026$ [4].

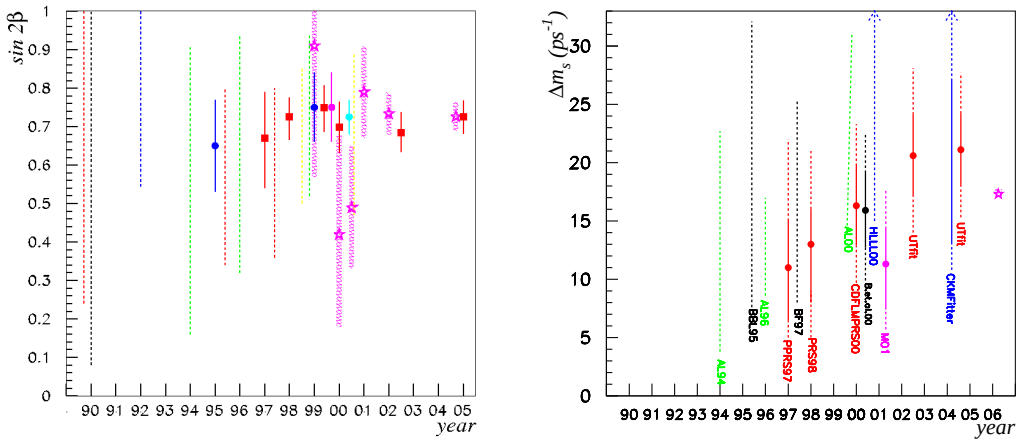

Figure 1: *Evolution of the predictions for* $\sin 2\beta$ *(left) and* Δm_s *(right) over the years. The corresponding experimental determinations are indicated by larger bands and stars. See [5, 6] for the full list of original references*

.

A similar situation holds for Δm_s. A precise indirect determination of Δm_s from the other constraints of the UT fit was available since 1997: $\Delta m_s \in [6.5, 15.0]$ ps^{-1} at 68% probability and $\Delta m_s < 22$ ps^{-1} at 95% probability [7]. A compilation of the predictions for Δm_s by various collaborations as a function of time is shown in Fig. 1 (right). As can be seen from the plot, even in recent years, and despite the improved measurements, in some approaches [8, 9] the predicted range was very large (or corresponds only to a lower bound [8]). An upgraded version of our SM "prediction" for Δm_s obtained from the full UT fit is $\Delta m_s = (18.4 \pm 2.4)$ ps^{-1} [5], in remarkable agreement with the direct measurement $\Delta m_s = (17.77 \pm 0.12)$ ps^{-1} [10]. In Fig. 2 we show the compatibility plot for Δm_s, which illustrates the agreement, at better than $1\,\sigma$ level, of the measured value with the SM expectation.

In the last years, we got much more information on the UT from the direct determinations of the angles α, β and γ, obtained at the B factories from the studies of CP asymmetries in non-leptonic B decays. In the following we will call the ensemble of these measurements **UT***angles*: they allow a determination of $\overline{\rho}$ and $\overline{\eta}$ independently of

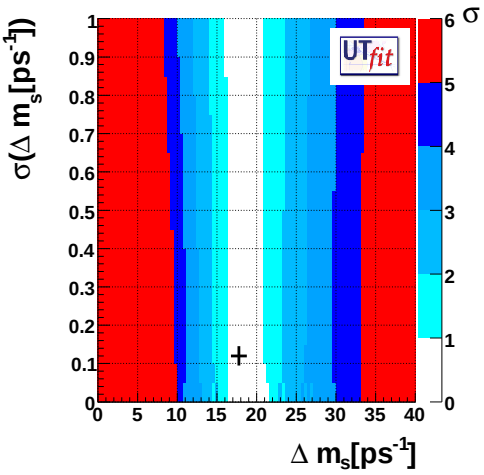

Figure 2: *Compatibility plot of the measured value* $\Delta m_s = (17.77 \pm 0.12)$ ps^{-1} *with the SM expectation from the other constraints of the UT fit.*

the hadronic parameters computed on the lattice. The precision in constraining $\overline{\rho}$ and $\overline{\eta}$ from the **UT***angles* is by now comparable to that obtained from the lattice-related constraints, denoted as **UT***lattice*. The latter include the determination of $|V_{ub}|\,/\,|V_{cb}|$ from semileptonic B decays, ϵ_K, Δm_d and Δm_s.

In this talk, after a presentation of recent averages of lattice QCD results, we will compare the outcome of the **UT***lattice* and **UT***angles* analyses. We will discuss the role played by the different determinations of V_{ub} and show that the value measured in inclusive decays is not favoured by the data. Finally, we will show that the recent measurement of the B_s-meson mixing amplitude Δm_s, combined with Δm_d and ϵ_K, allows a quite accurate extraction of the values of the hadronic matrix elements relevant for $K - \overline{K}$ and $B_{s,d} - \overline{B}_{s,d}$ mixing. Assuming the validity of the SM, we determine these hadronic quantities from the experimental data and compare them with recent lattice calculations. The content of this talk is mostly based on Ref. [6], but we take here the opportunity to update the results by taking into account the most recent experimental findings [5].

2 Averages of Lattice QCD results

Lattice QCD is the theoretical tool of choice to compute hadronic quantities. Being only based on first principles, it does not introduce additional free parameters besides the fundamental couplings of QCD, namely the strong coupling constant and the quark masses. In addition, the systematic uncertainties affecting the results of lattice

calculations can be systematically reduced in time, with the continuously increasing availability of computing power and the development of new algorithms and improved theoretical techniques.

In spite of the appealing features of the lattice approach, the accuracy currently reached in the determination of the hadronic matrix elements is typically still at the level of 10-15%. So far, the main limiting factor for achieving an improved precision has been the lack of sufficient computing power, which has often prevented the possibility of performing "full QCD" simulations and forced the introduction of the quenched approximation. In this approximation an error is introduced which, besides being process dependent, is also difficult to reliably estimate.

Most of the lattice calculations relevant to B-physics used so far the quenched approximation. There are few exception in which $N_f = 2$ dynamical quarks are included in the QCD vacuum fluctuations [11]- [14] and only a single calculation with $N_f = 2 + 1$ [15] [1]. A similar situation holds for the lattice studies of $K - \overline{K}$ mixing. Only three unquenched calculations of the kaon parameter B_K have been produced so far, one including $N_f = 2$ dynamical quarks [16] and two with $N_f = 2 + 1$ [17, 18].

It is important to emphasise that the quenched results, in spite of being unsatisfactory for having been obtained with unrealistic $N_f = 0$, have the advantage that the whole methodology of extracting the desired information from the simulation has been developed and understood, the procedure of non-perturbative renormalization has been implemented, and the whole plethora of results have been checked by many different groups, using various versions of the gauge and fermionic lattice actions. In a number of cases even the continuum extrapolation has been shown to be smooth. The unquenched studies, on the other hand, are sound for being unquenched (although the dynamical quarks are still much heavier than the physical up and down quarks). However, the consequences of the so called fourth-root trick implemented with the staggered fermion formulation are not clear, the non-perturbative renormalization in most of the cases is not carried out, and the results have not been checked yet by different groups. In this respect, unquenching is still a work in progress. At the same time, it is should be noted that the capability of decreasing significantly the values of the simulated light quark masses in recent unquenched calculations has allowed to largely reduce the uncertainty associated with the chiral extrapolation. Particularly relevant cases, in this respect, are the determinations of the pseudoscalar decay constant f_B and of the ratio ξ [15]. For all these reasons it is important to take into account, when producing averages of lattice QCD results, the outcome of the several more recent lattice calculations. The average lattice values that are being used in the

[1] The "+1" indicates that an heavier strange quark is included in the sea, besides the two degenerate up and down quarks

UT analysis, for the quantities relevant to K- and B-physics, are:

$$\begin{aligned}
&\hat{B}_K = 0.79 \pm 0.04 \pm 0.081001[19], \\
&f_{Bs}\hat{B}_{Bs}^{1/2} = 262 \pm 35 \ \text{MeV} \quad , \quad \xi = 1.23 \pm 0.06, \\
&f_{Bd} = 189 \pm 27\,\text{MeV} \quad , \quad f_{Bs} = 230 \pm 30\,\text{MeV}1001[20].
\end{aligned} \tag{1}$$

3 UT*lattice*, UT*angles* and role of $|V_{ub}|$

In Fig. 3 we show the results of the UT fit as obtained from the lattice-related constraints, UT*lattice*, the direct determinations of the UT angles, UT*angles*, and the full analysis [5, 6]. The corresponding determinations of $\overline{\rho}$ and $\overline{\eta}$, as derived

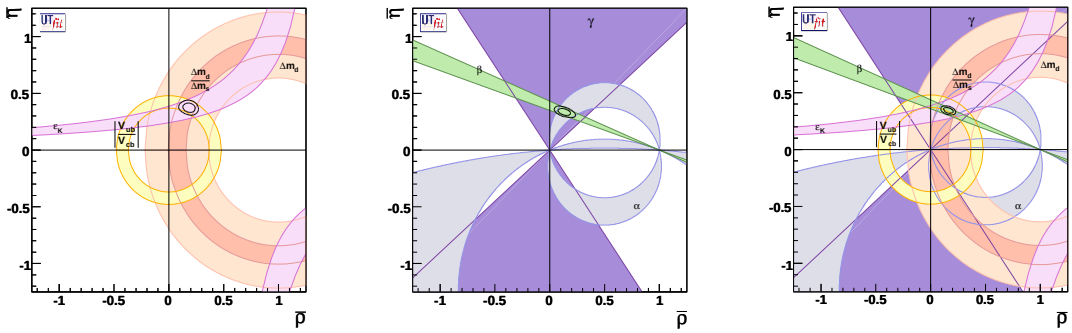

Figure 3: *Determination of $\overline{\rho}$ and $\overline{\eta}$ from* UT*lattice (left),* UT*angles (center) and the full UT (right) analyses. The 68% and 95% total probability contours are shown, together with the 95% probability regions from the individual constraints.*

independently from the UT*lattice* and UT*angles* analyses, are

$$\begin{aligned}
&\textbf{UT}\textit{lattice} && \textbf{UT}\textit{angles} \\
&\overline{\rho} = 0.188 \pm 0.036 \quad , && \overline{\rho} = 0.134 \pm 0.039 \\
&\overline{\eta} = 0.371 \pm 0.027 \quad , && \overline{\eta} = 0.335 \pm 0.020 \ .
\end{aligned} \tag{2}$$

We firstly note that the errors have comparable sizes, i.e. the two analyses have reached at present a comparable level of accuracy. It is also interesting to observe that the UT*angles* fit, based on the direct determination of the UT angles, does not rely at all on theoretical calculation of the hadronic matrix elements, for which there was a long debate about the treatment of values and error distributions [21]. In the UT*angles* analysis, the treatment of theoretical errors is not an issue.

The results in eq. (2) also show the existence of a tension between the values of $\overline{\rho}$ and $\overline{\eta}$ obtained from the two analyses. This is also illustrated by the effects of the

various constraints in the full UT fit, shown in the right plot of Fig. 3. It mainly appears to be a tension between the (presently quite accurate) measurement of $\sin 2\beta$ and the constraint coming from the determination of $|V_{ub}|$ from semileptonic B decays. The poor agreement is also evidenced by the comparison between the experimental value $\sin 2\beta = 0.675(26)$ and the value obtained by using all the other constraints in the UT fit, i.e. $\sin 2\beta = 0.759(37)$. The compatibility plot of $\sin 2\beta$, presented in Fig. 4, shows that this tension is indeed at the $2\,\sigma$ level.

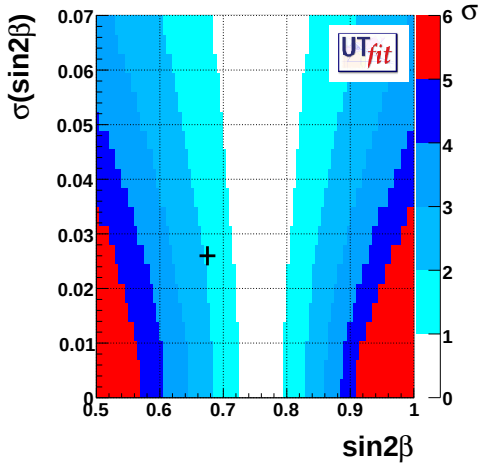

Figure 4: *Compatibility plot of the experimental value of* $\sin 2\beta$ *and the prediction from the rest of the UT fit.*

In order to further investigate where the tension comes from, it is worth recalling that there is a systematic difference between the exclusive and inclusive determination of $|V_{ub}|$ (the inclusive values are always larger than the exclusive ones). Current averages and errors are:

$$\begin{aligned} |V_{ub}|^{\text{excl.}} &= (35.0 \pm 4.0) \times 10^{-4} \\ |V_{ub}|^{\text{incl.}} &= (44.9 \pm 3.3) \times 10^{-4} \end{aligned} \tag{3}$$

These determinations also rely on non-perturbative hadronic quantities: the semileptonic form factors for exclusive semileptonic B decays and the HQET parameters $\overline{\Lambda}$, λ_1 and λ_2, for inclusive ones. While the form factors are determined from lattice QCD calculations and QCD sum rules, the HQET parameters are extracted, together with $|V_{ub}|$, directly the from the fits of the experimental data. In this latter case, however, a certain amount of model dependence has to be introduced, and various approaches (BLNP [22], DGE [23], BLL [24]) are currently considered. The systematic difference

between the exclusive and inclusive determination of $|V_{ub}|$ might be explained by the uncertainties of the theoretical approaches.

In Fig. 5 we show the compatibility plot between the direct determinations of $|V_{ub}|$ from exclusive and inclusive analyses and the rest of the fit. While the exclusive

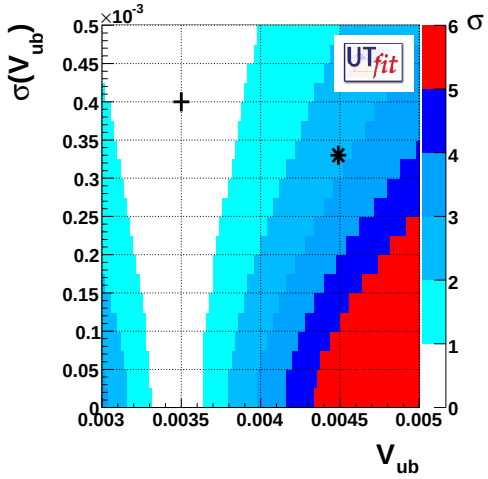

Figure 5: *Compatibility plot between the direct determinations of* $|V_{ub}|$ *from exclusive (cross) and inclusive (star) analyses and the rest of the UT fit.*

determination is in remarkable agreement with the expectation from the UT analysis in the SM, the inclusive value of $|V_{ub}|$ shows a deviation which is almost at the $3\,\sigma$ level. Our analysis suggests that, although both the exclusive and inclusive results are still compatible, there could be some problem with the theoretical calculations, and/or with the estimate of the uncertainties, of inclusive $b \to u$ semileptonic decays. In order to clearly solve this tension, an effort should be made to increase the precision of lattice QCD determinations of the form factors of $B \to \pi$ and $B \to \rho$ semileptonic decays, providing all of them in the unquenched case, with low light quark masses and studying the continuum limit of the relevant form factors. Note that this tension among exclusive and inclusive calculations is a peculiarity of $|V_{ub}|$, since the inclusive and exclusive determinations of $|V_{cb}|$ are in much better agreement.

4 Constraints on lattice parameters

Assuming the validity of the SM, the constraints in the $\overline{\rho}$-$\overline{\eta}$ plane from **UT***angles* and semileptonic B decays, combined with the measurements of Δm_d, Δm_s and ϵ_K, allow the "experimental" determination of several hadronic quantities which were previously taken from lattice QCD calculations. This approach has the advantage that

the extracted values of $\hat{B}_K$ and of the B mixing parameters $f_{Bs,d}\,\hat{B}^{1/2}_{Bs,d}$ (or equivalently $f_{Bs}\,\hat{B}^{1/2}_{Bs}$ and ξ) can be compared directly with the theoretical predictions from lattice QCD.

Besides $\hat{B}_K$, $f_{Bs}\,\hat{B}^{1/2}_{Bs}$ and ξ, we can also extract the values of the leptonic decay constants f_B and f_{Bs} from the fit, using in addition the lattice values of the B mixing parameters, $\hat{B}_{Bd} = \hat{B}_{Bs} = 1.28 \pm 0.05 \pm 0.09$ [20]. With respect to the decay constants, the lattice calculations of the B-parameters are typically affected by smaller uncertainties, since some sources of systematic errors (like those related to the determination of the lattice scale and to chiral logs effects) are either absent or largely reduced. Moreover, quenched and unquenched estimates of the B parameters are found to be quite consistent within each others.

The results for $\hat{B}_K$, $f_{Bs}\,\hat{B}^{1/2}_{Bs}$, ξ, f_B and f_{Bs} extracted from the UT fit are presented in Tab. 1, together with the average values from lattice QCD calculations [19,20] also given in eq. (1). The agreement between the two determinations is remarkable. On the one hand, this comparison provides additional evidence of the spectacular success of the SM in describing flavor physics. On the other hand, the results given in Tab. 1 illustrate the accuracy and the reliability reached at present by lattice QCD calculations. The allowed probability regions in the B_K vs. ξ, $f_{Bs}\hat{B}^{1/2}_{Bs}$ vs. B_K and $f_{Bs}\hat{B}^{1/2}_{Bs}$ vs. ξ planes derived from the UT fit are shown in Fig. 6, together with the results from lattice QCD calculations.

The UTfit determination of $f_{Bs}\,\hat{B}^{1/2}_{Bs}$ has an accuracy of about 2%, which reflects the precision reached in the experimental determination of Δm_s. This uncertainty on $f_{Bs}\,\hat{B}^{1/2}_{Bs}$ is by far smaller than the one reached by lattice QCD calculations. On the other hand, the errors on the UTfit and lattice QCD determinations of $\hat{B}_K$ and ξ have comparable size, leaving in these cases the opportunity for further improvement of the theoretical calculations.

It is worth recalling that the phenomenological extraction of the hadronic parameters and the comparison with lattice results assumes the validity of the SM and it is meaningful in this framework only. A similar strategy could be followed in any given extension of the SM when enough experimental information is available. In general, however, a model-independent UT analysis beyond the SM cannot be carried out without some "a priori" theoretical knowledge of the relevant hadronic parameters.

	$\hat{B}_K$	$f_{Bs}\,\hat{B}^{1/2}_{Bs}$ (MeV)	ξ	f_{Bd} (MeV)	f_{Bs} (MeV)
UT fit	0.75 ± 0.09	261 ± 6	1.24 ± 0.08	187 ± 13	231 ± 9
LQCD	$0.79 \pm 0.04 \pm 0.08$	262 ± 35	1.23 ± 0.06	189 ± 27	230 ± 30

Table 1: *Comparison between determinations of the hadronic parameters from the UT fit and the averages from lattice QCD calculations (eq. (1)).*

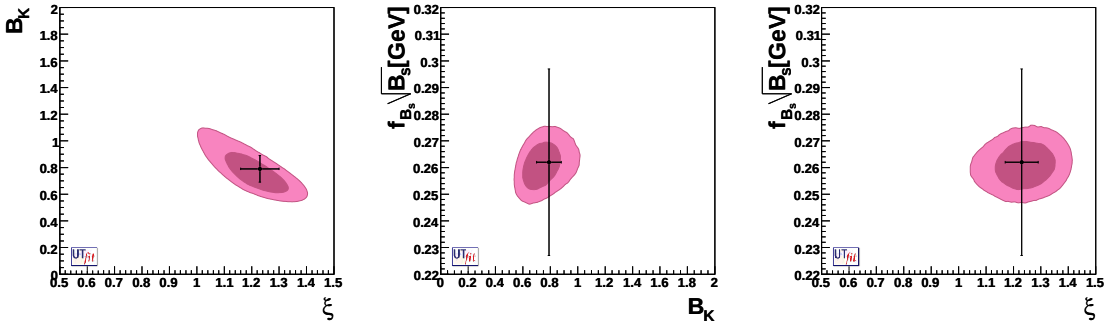

Figure 6: *Two-dimensional constraints in the B_K vs. ξ, $f_{Bs}\sqrt{\hat{B}_s}$ vs. B_K and $f_{Bs}\sqrt{\hat{B}_s}$ vs. ξ planes, using the* **UT***angles result for the CKM matrix and the experimental information on ε_K, Δm_d and Δm_s. The error bars show the results from lattice QCD calculations.*

For this reason, the error in the calculation of the hadronic matrix elements affects the uncertainties in the determination of the New Physics parameters [25, 26], which is at present one of the main motivations for the studies of flavor physics.

5 Conclusions

The recent precise determination of Δm_s by the CDF Collaboration allows a substantial improvement of the accuracy of the UT fit. Thanks to this measurement, it is possible to extract from the experiments the value of the relevant hadronic parameters, assuming the validity of the SM. The results of this fit turn out to be in remarkable agreement with the theoretical predictions of lattice QCD. It is also remarkable that the measurement of Δm_s, combined with all the information coming from the UT fit, allows the determination of $f_{Bs}\,\hat{B}_{Bs}^{1/2}$ with an accuracy of about 2% ($f_{Bs}\,\hat{B}_{Bs}^{1/2} = 261 \pm 6$ MeV).

The only exception to the general consistency of the UT fit is given by the inclusive semileptonic $b \to u$ decays, the analysis of which relies on the parameters of the shape function and other model-dependent assumptions. We observed that the present determination of $|V_{ub}|$ using inclusive methods is disfavoured by all other constraints almost at the $3\,\sigma$ level. This can come either from the fact that the central value of $|V_{ub}|$ from inclusive decays is too large, or from the smallness of the estimated error, or both. We think that it is worth investigating whether the theoretical uncertainty of the inclusive analysis has been realistically estimated. At the same time, an effort should be done for a substantial improvement of the theoretical and experimental accuracy in the extraction of $|V_{ub}|$ from exclusive decays. Indeed in the future a

confirmation of these results, with smaller errors, might reveal the presence of New Physics in the generalised UT analysis [26].

I warmly thank the organisers for the very pleasant and stimulating atmosphere of the conference. I am indebted to all my friends of the **UT***fit* Collaboration, with which most of the results presented in this talk have been obtained.

Bibliography

[1] M. Lusignoli, L. Maiani, G. Martinelli and L. Reina, Nucl. Phys. B **369** (1992) 139.

[2] M. Ciuchini, E. Franco, G. Martinelli, L. Reina and L. Silvestrini, Z. Phys. C **68** (1995) 239 [arXiv:hep-ph/9501265].

[3] M. Ciuchini *et al.*, JHEP **0107** (2001) 013 [arXiv:hep-ph/0012308].

[4] M. Hazumi, plenary talk at the ICHEP'06 conference, `http://ichep06.jinr.ru/reports/2_hazumi_ichep2006.ppt`

[5] The **UT***fit* Collaboration, `http://www.utfit.org`

[6] M. Bona *et al.* [UTfit Collaboration], JHEP **0610** (2006) 081 [arXiv:hep-ph/0606167].

[7] P. Paganini, F. Parodi, P. Roudeau and A. Stocchi, Phys. Scripta **58** (1998) 556 [arXiv:hep-ph/9711261].

[8] A. Hocker, H. Lacker, S. Laplace and F. Le Diberder, Eur. Phys. J. C **21** (2001) 225 [arXiv:hep-ph/0104062].

[9] J. Charles *et al.* [CKMfitter Group], Eur. Phys. J. C **41** (2005) 1 [arXiv:hep-ph/0406184].

[10] A. Abulencia *et al.* [CDF Collaboration], Phys. Rev. Lett. **97** (2006) 242003 [arXiv:hep-ex/0609040].

[11] A. Ali Khan *et al.* [CP-PACS Collaboration], Phys. Rev. D **64** (2001) 054504 [arXiv:hep-lat/0103020].

[12] S. Aoki *et al.* [JLQCD Collaboration], Phys. Rev. Lett. **91** (2003) 212001 [arXiv:hep-ph/0307039].

[13] A. Ali Khan *et al.* [CP-PACS Collaboration], Phys. Rev. D **64** (2001) 034505 [arXiv:hep-lat/0010009].

[14] C. Bernard *et al.* [MILC Collaboration], Phys. Rev. D **66** (2002) 094501 [arXiv:hep-lat/0206016].

[15] A. Gray *et al.* [HPQCD Collaboration], Phys. Rev. Lett. **95** (2005) 212001 [arXiv:hep-lat/0507015].

[16] Y. Aoki *et al.*, Phys. Rev. D **72** (2005) 114505 [arXiv:hep-lat/0411006].

[17] E. Gamiz, S. Collins, C. T. H. Davies, G. P. Lepage, J. Shigemitsu and M. Wingate [HPQCD Collaboration], Phys. Rev. D **73** (2006) 114502 [arXiv:hep-lat/0603023].

[18] D. J. Antonio *et al.*, arXiv:hep-ph/0702042.

[19] C. Dawson, PoS **LAT2005** (2005) 007.

[20] S. Hashimoto, Int. J. Mod. Phys. A **20** (2005) 5133 [arXiv:hep-ph/0411126].

[21] M. Battaglia *et al.*, arXiv:hep-ph/0304132.

[22] B. O. Lange, M. Neubert and G. Paz, Phys. Rev. D **72**, 073006 (2005) [arXiv:hep-ph/0504071].

[23] J. R. Andersen and E. Gardi, JHEP **0601**, 097 (2006) [arXiv:hep-ph/0509360].

[24] C. W. Bauer, Z. Ligeti and M. E. Luke, Phys. Rev. D **64**, 113004 (2001) [arXiv:hep-ph/0107074].

[25] M. Bona *et al.* [UTfit Collaboration], JHEP **0603** (2006) 080 [arXiv:hep-ph/0509219].

[26] M. Bona *et al.* [UTfit Collaboration], Phys. Rev. Lett. **97** (2006) 151803 [arXiv:hep-ph/0605213].

Hadronic B decays

M. Beneke
Institut für Theoretische Physik E, RWTH Aachen
Sommerfeldstr. 28
D - 52074 Aachen, Germany

I briefly summarize the factorization approach to hadronic B decays emphasizing theoretical results that have become available recently. The discussion of its application to data is abridged, and only the determination of $\gamma = (71 \pm 5)^\circ$ from time-dependent CP asymmetries is included in some detail.

1 Introduction

Many observables at the B factories are connected with branching fractions, CP asymmetries and polarization of exclusive, hadronic B decays. They provide access to the flavour and spin structure of the weak interaction, but a straightforward interpretation is usually obscured by the strong interaction. In technical terms, the difficult (long-distance) part of the strong interaction resides in the matrix elements $\langle f|O_i|\overline{B}\rangle$, where O_i is an operator in the effective weak interaction Lagrangian.

Systematic approaches to hadronic B decays are based on expansions in small parameters. The two available options exploit approximate flavour symmetries (expansion parameter m_q/Λ, m_q a light quark mass), or the large energy transfer in B decays (expansion parameter Λ/m_b), resulting in two frameworks – "SU(3)" and "Factorization" – that could hardly be different methodically and technically. In practice, both frameworks are implemented only at the leading order, and additional assumptions are usually necessary (neglecting "small" amplitudes; estimating Λ/m_b corrections). Despite this restriction, there has been much progress by applying and working out these theories over the past few years. In the following I focus on the factorization approach. Furthermore, f will be assumed to be a charmless, two-body, meson final state; the mesons are assumed to be pseudoscalar or vector mesons from the ground state nonet.

2 Theory of hadronic decays (factorization)

The starting point is the investigation of Feynman diagrams with external collinear lines (energetic, massless lines with momenta nearly parallel to one of the two final state mesons, M_1 or M_2), one nearly on-shell heavy-quark line, and soft lines

(representing the light degrees of freedom in the $\overline{B}$ meson). The simultaneous relevance of collinear and soft configurations implies three relevant scales: m_b, $\sqrt{m_b\Lambda}$, and Λ. In the heavy-quark limit the first two are perturbative, and only the third is long-distance. Factorization amounts to showing that the long-distance contributions to the matrix elements $\langle [c1][c2]|O_i|[s]\rangle$ are actually contained in the simpler matrix elements $\langle [c1]|(\overline{q}b)(0)|[s]\rangle$ (form factors), $\langle [ci]|\overline{q}(x)q(0)|0\rangle$, and $\langle 0|\overline{q}(x)b(0)|[s]\rangle$ (light-cone distribution amplitudes). It is then assumed that if this holds perturbatively to all orders for all quark-gluon matrix elements, then it does for the hadronic matrix elements.

Factorization in a similar form was first applied to B decays in [1] as a phenomenological approximation akin to the vacuum saturation approximation for the four-quark operator matrix elements relevant to $B\overline{B}$ mixing. Intuitively, factorization might work, because the partons that eventually form the meson M_2 that does not pick up the spectator quark escape the $\overline{B}$ remnant as an energetic, low-mass, colour-singlet system, and hadronize far away and therefore independently from the remnant. This qualitative argument was given in [2] for the decay $\overline{B}_d \to D^+\pi^-$. In [3] it was shown to hold for charmless decays, where the disruption of the B meson is much more violent, and a calculational framework was provided, in which the phenomenological factorization approach was contained as a leading-order approximation. At the same time, the next-to-leading order corrections were computed.

The new factorization formula included a new mechanism, spectator-scattering, where a hard-collinear interaction with the soft remnant takes place. Thanks to the development of soft-collinear effective theory (SCET), this mechanism is now much better understood. In the following I sketch the rederivation of the factorization formula in SCET [4–6].

Integrating out fluctuations on the scale m_b at leading power in the Λ/m_b expansion amounts to an analysis of the structure of hard subgraphs with external hard-collinear, collinear and soft lines. Those identified as leading are then calculated perturbatively in $\alpha_s(m_b)$. Formulated as an operator matching equation from QCD to $\mathrm{SCET_I}$, the result of this analysis reads

$$O_i \;=\; \left[\overline{\chi}^{(0)}(tn_-)\chi^{(0)}\right] * \Big(C_i^{\mathrm{I}}(t)\left[\overline{\xi}h_v\right] + C_i^{\mathrm{II}}(t,s) * \left[\overline{\xi}\,\not{A}_\perp(sn_+)h_v\right]\Big). \qquad (1)$$

Remarks: (a) The short-distance coefficient C_i^{I} incorporates corrections to naive factorization. The second term describes spectator-scattering with its own short-distance coefficient C_i^{II}. (b) The second term is a leading contribution despite the fact that the corresponding operator is suppressed in dimensional and $\mathrm{SCET_I}$ power counting. This follows by extension of the power-counting analysis of [5]. (c) The meson M_2 factorizes already below the scale m_b [6], since $\mathrm{SCET_I}$ does not contain interactions between the $\chi^{(0)}$ fields and the collinear-1 and soft fields. It follows that at leading power in the heavy-quark expansion, the strong interaction phases originate from the

short-distance coefficients $C_i^{\rm I,II}$ at the hard scale. (d) The result above must be modified to account for a non-factorizing effect when the final state contains an $\eta^{(\prime)}$ meson. This effect is explained in [7], but appears to have been missed in the SCET rederivation of the factorization theorem for mesons with flavour-singlet components [8]. Taking the hadronic matrix element of (1) gives

$$\langle M_1 M_2|O_i|\overline{B}\rangle \;=\; \Phi_{M_2}(u) * \Big(T^{\rm I}(u)\, F^{BM_1}(0) + C^{\rm II}(\tau,u) * \Xi^{BM_1}(\tau,0)\Big), \qquad (2)$$

where I have reintroduced the full QCD form factor $F^{BM_1}(0)$ resulting in a slight modification of the short-distance coefficients. $\Xi^{BM_1}(\tau,0)$ denotes a new, unknown, non-local form factor, which depends on the convolution variable τ.

The different implementations of factorization can be distinguished broadly by their treatment of the different factors in (2). In the PQCD approach [9] the form factors $F^{BM_1}(0)$ and $\Xi^{BM_1}(\tau,0)$ are assumed to be short-distance dominated, and claimed to be calculable in a generalized factorization framework ($k_\perp$-factorization). All four quantities, $T^{\rm I}, C^{\rm II}, F^{BM_1}(0), \Xi^{BM_1}(\tau,0)$ have been calculated at leading order. Recently, some next-to-leading order (NLO) corrections to $T^{\rm I}$ have been included. In the QCD factorization approach [3] it is assumed that the standard heavy-to-light form factors receive a leading soft contribution, and are therefore not calculable. However, $\Xi^{BM_1}(\tau,0)$ is dominated by perturbative hard-collinear interactions, and factorizes further into light-cone distribution amplitudes (see below). In the BBNS implementation of QCD factorization, $F^{BM_1}(0)$ is a phenomenological input (usually from QCD sum rules). The other three quantities, $T^{\rm I}, C^{\rm II}, \Xi^{BM_1}(\tau,0)$ have been calculated at the next-to-leading order. In the BPRS implementation [6] the use of perturbation theory at the hard-collinear scale $\sqrt{m_b\Lambda}$ is avoided, and both form factors are fit to hadronic B decay data. This approach is restricted to leading-order in the short-distance coefficients, since only then does the unknown form factor $\Xi^{BM_1}(\tau,0)$ enter the equations through a single moment. There is another difference between BBNS and BPRS, who claim that (1) is not valid for diagrams with internal charm quark loops. (This should be distinguished from [10], which speculates about large power corrections from charm loops or annihilation.) I believe that the theoretical arguments leading to this conclusion are wrong [11]. For phenomenology, the important consequence from treating charm loop diagrams as non-perturbative is that the penguin amplitudes must be determined from data, such that no CP asymmetry can be predicted from theory alone. Since the tree amplitudes are also determined from data (namely, through the two form factors; the phase of C/T is automatically zero in a leading-order treatment), the BPRS approach has much more in common with amplitude fits to data than with QCD/SCET calculations.

The QCD factorization argument is completed by noting that the non-local SCET$_{\rm I}$ form factor $\Xi^{BM_1}(\tau,0)$ factorizes into light-cone distribution amplitudes, when the

hard-collinear scale $\sqrt{m_b \Lambda}$ is integrated out [5]. Inserting

$$\Xi^{BM_1}(\tau, 0) = J(\tau; \omega, v) * \Phi_B(\omega) * \Phi_{M_1}(v) \tag{3}$$

into (2) results in the original QCD factorization formula with the additional insight that the spectator-scattering kernel $T^{\rm II} = H^{\rm II} * J$ factorizes into a hard and hard-collinear kernel. The development of SCET was crucial to identify the operators and precise matching prescriptions that make the calculation of higher-order corrections to spectator-scattering feasible.

3 Higher-order calculations

On the calculational side one of the main efforts over the past few years has been the calculation of one-loop corrections to spectator-scattering, which formally represents a next-to-next-to-leading contribution in the QCD factorization approach. This programme is now complete. The hard-collinear correction to J has been calculated in [12–14]; the hard correction to $H^{\rm II}$ in [15, 16] for the tree amplitudes and in [17] for the QCD penguin and electroweak penguin amplitudes. (An earlier calculation of the QCD penguin contribution [18] disagrees with [17].) The main results are summarized as follows: (a) The convolution integrals are convergent, which establishes factorization of spectator-scattering at the one-loop order. (b) Perturbation theory works for spectator-scattering, including perturbation theory at the hard-collinear scale. (c) The correction enhances the colour-suppressed tree amplitude, and reduces the colour-allowed one. This improves the description of the tree-dominated decays to pions and ρ mesons. (d) The correction to the colour-allowed QCD penguin amplitude is negligible. Thus there is no essential change in the predictions of branching fractions and CP asymmetries of penguin-dominated decays.

The evaluation of the colour-suppressed tree amplitude gives [17]

$$\begin{aligned} a_2(\pi\pi) &= 0.18 - [0.15 + 0.08i]_{\rm NLO} \\ &\quad + \left[\frac{r_{\rm sp}}{0.485}\right] \Big\{ [0.12]_{\rm LO} + [0.05 + 0.05i]_{\rm NLO} + [0.07]_{\rm tw3} \Big\}. \end{aligned} \tag{4}$$

Here $r_{\rm sp} = (9 f_{M_1} \hat{f}_B)/(m_b F^{BM_1}(0) \lambda_B)$ defines a combination of hadronic parameters that normalizes the spectator-scattering effect. Eq. (4) shows the importance of computing quantum corrections: the naive factorization value 0.18 is nearly canceled by the 1-loop vertex correction calculated in [3]. It now appears that the colour-suppressed tree amplitude is generated by spectator-scattering. It is not excluded that $r_{\rm sp}$ is a factor of two larger than 0.485, in which case a_2 becomes rather large. My interpretation of the pattern of the $\pi\pi$, $\pi\rho$ and $\rho\rho$ branching fractions is that spectator-scattering is important [19]. On the other hand, the large direct CP

asymmetry in $\overline{B}_d \to \pi^+\pi^-$ cannot be explained by known radiative corrections, and remains a problem.

Next-to-leading order corrections have recently been implemented in the PQCD approach for the first time [20]. More precisely, the 1-loop kernel $T^{\rm I}$ from the QCD factorization approach is used as a short-distance coefficient for the subsequent tree-level PQCD calculation. The numerical impact is again strongest on the colour-suppressed tree amplitude, C. But while this correction ($-[0.15 + 0.08i]_{\rm NLO}$ in (4)) results in a near cancellation of the naive factorization term in the QCD factorization approach, it provides an enhancement of C by a factor of several in [20]. This resolves the πK puzzle in the PQCD approach.

I am rather sceptical about the possibility to perform accurate calculations in the PQCD approach. A complete NLO calculation in the PQCD approach requires a calculation of all one-loop spectator-scattering diagrams (similar to [15–17]) rather than the 1-loop BBNS kernels. The calculation of $T^{\rm I}$ is done with on-shell external lines, but when the vertex diagram appears as a subdiagram in a larger diagram with hard-collinear exchanges, the external lines of the subdiagram can be far off-shell. Hence T^I is not the appropriate quantity to be used. The numerical differences between (4) and [20] despite the same input $T^{\rm I}$ can be traced to the choice of scales. The one-loop correction to $T^{\rm I}$ makes the result less sensitive to variations of the renormalization scale in the Wilson coefficients, but only for scales larger than about 1.5 GeV, below which perturbation theory breaks down. Factorization shows that the scale of the Wilson coefficients should be of order m_b. However, in the PQCD approach the scales m_b and $\sqrt{m_b\Lambda}$ are not distinguished, and the Wilson coefficients are evaluated at very low scales (to 500 MeV), where perturbation theory is not reliable. An unphysical enhancement of the Wilson coefficients at small scales is also the origin of the large penguin and annihilation amplitude in the PQCD approach. Yet a variation of the renormalization scale is not included in theoretical error estimates.

4 Power-suppressed effects

Power corrections to the QCD penguin amplitudes are essential for a successful phenomenology within the factorization framework. The most important Λ/m_b effect is the scalar QCD penguin amplitude $r_\chi a_6$. Fortunately, the bulk contribution to this amplitude appears to be calculable, although its factorization properties are not yet understood. This power correction is responsible for the differences between PP, PV and VV final states and the $\eta^{(\prime)}K^{(*)}$ final states [7]. The calculated pattern is in very good agreement with experimental data.

The second most important power correction is presumably weak annihilation. I emphasize "presumably", since there is no unambiguous empirical evidence of any weak annihilation contribution in charmless decays, and only upper limits can be

derived. The theoretical difficulty with power corrections is reflected in the different treatments of annihilation. In PQCD it is calculable and large. In the BBNS implementation of factorization it is represented by a phenomenological parameter [21], not very large, but it makes the calculation of CP asymmetries uncertain. In the BPRS implementation it is neglected together with all power corrections. This is phenomenologically viable, since the charm penguin amplitude is fit to data anyway. Some weak annihilation amplitudes have been calculated with light-cone QCD sum rules [22]; the result is compatible with the BBNS parameterization.

It is not difficult to write down the power-suppressed operators in SCET [23]. The problem is that the factorization formula involves convolutions, which usually turn out to be divergent at the endpoints, making the result meaningless. The inadequacy of SCET in addressing this well-known problem in hard-exclusive scattering was pointed out in various forms in [5,24], but no solution was offered. In the recent paper [25] it is proposed that endpoint divergences can be eliminated by a new type of factorization ("zero-bin"). This would be a breakthrough; however, I do not see how "zero-bin" factorization could possibly be correct, since it cuts off the endpoint contributions without defining the appropriate non-perturbative objects that would represent the endpoint region. Thus, the new factorization-scale dependence is not consistently canceled.

To explain this I compare the treatment of a certain weak annihilation diagram in "zero-bin" factorization [26] with the BBNS parameterization [19, 21]. In the first method, the divergent integral $\alpha_s \int_0^1 dx\, \phi_{M_2}(x)/\overline{x}^2$ is interpreted as

$$-\phi'_{M_2}(1) \cdot \alpha_s \ln \frac{m_B}{\mu_-} + F, \tag{5}$$

in the second as

$$-\phi'_{M_2}(1) \left(1 + \varrho_A e^{i\varphi_A}\right) \cdot \alpha_s \ln \frac{m_B}{\Lambda} + F, \tag{6}$$

where

$$F \equiv \alpha_s \int_0^1 dx\, \frac{\phi_{M_2}(x) + \overline{x}\phi'_{M_2}(1)}{\overline{x}^2} \tag{7}$$

is a finite, subtracted integral. In [26] μ_- is taken to be of order m_b, thus the first term in (5) is of order α_s and perturbative. The endpoint contribution is effectively set to zero, but the dependence on the arbitrary factorization scale μ_- is not canceled. A candidate non-perturbative parameter for the endpoint contribution could be $\phi'_{M_2}(1)$, but this object is not defined in SCET, so a field-theoretical definition of the method is missing. The second expression (6) looks similar, but now there is a large endpoint logarithm, and $\alpha_s \ln m_B/\Lambda$ is of order 1. The endpoint contribution is considered to be non-perturbative, and is parameterized by the complex quantity $\varrho_A e^{i\varphi_A}$. It is again the absence of a field-theoretical definition of this quantity that makes the

BBNS parameterization a phenomenological model. Expression (6) is clearly a more conservative treatment of the problem than (5).

It is evident that in the absence of a field-theoretical definition of the zero-bin subtraction method, the statement that "annihilation is real and calculable" is wishful thinking (I share the wish.); it also contradicts the QCD sum rule calculation [22]. My strong criticism (prompted by strong claims) is not to mean that the problem of endpoint factorization is not important. To the contrary, its solution is prerequisite to further progress in SCET.

5 Phenomenology (omitted)

There is not enough space to discuss the factorization calculations of branching fractions and CP asymmetries and the comparison with data. I focus on the calculation of the CP-violating S parameters and the determination of γ in the following section. A very brief summary of the other topics discussed in the talk reads:

- The global comparison of all $B \to PP, PV$ data with scenario S4 of [19] remains impressively good, including CP asymmetries, but there are persistent exceptions. The same is true for the PQCD [20,30] and BPRS [8,31] approaches.
- An enhancement of the electroweak penguin amplitude to explain the πK system is no longer compelling. The difference between the CP asymmetries in $\pi^0 K^\pm$ and $\pi^\mp K^\pm$ seems to require an enhancement of the colour-suppressed tree amplitude, which cannot be explained by factorization.
- There exist interesting effects [27,28] in $B \to VV$ decays, which motivate further polarization studies. See [29] for a comprehensive analysis of these decays.

6 Determination of γ from S_f

The time-dependent CP asymmetries S_f in tree-dominated $\Delta D = 1$ decays are particularly suited [19, 21] to determine the CKM phase γ (or α; I assume that β is determined experimentally) in the framework of QCD factorization, since hadronic uncertainty enters only in the penguin correction; the dependence on strong phases is reduced, because it arises only through $\cos\delta$; the sensitivity to γ is maximal near $\gamma \sim 70°$.

Figure 1 shows that for $f = (\pi\pi, \pi\rho, [\rho\rho]_L)$ and measurements $S_f = (-0.59 \pm 0.09, 0.03 \pm 0.09, -0.06 \pm 0.18)$ (HFAG averages), one obtains (ignoring a second solution that does not lead to consistent results) $\gamma = (70^{+13}_{-10}, 69 \pm 7, 73 \pm 8)°$. The three determinations are in agreement with each other, resulting in the average $\gamma = (71 \pm 5)°$. See [19, 29] for details.

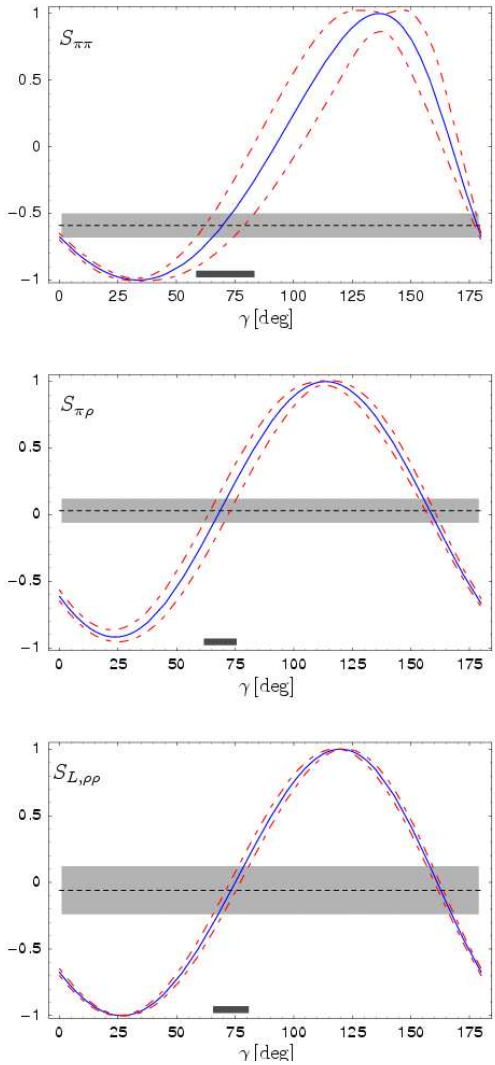

Figure 1: CKM phase γ from S_f with $f = (\pi\pi, \pi\rho, [\rho\rho]_L)$.

7 Conclusion

The subject of hadronic decays has been and still is a very fertile ground for developing new theoretical concepts in heavy flavour physics. A lot has been learned about hadronic dynamics. Moreover, γ is by now known rather well from charmless decays. There should be some way to include this information in the CKM fits.

Bibliography

[1] D. Fakirov and B. Stech, Nucl. Phys. B **133** (1978) 315.

[2] J. D. Bjorken, Nucl. Phys. Proc. Suppl. **11** (1989) 325.

[3] M. Beneke, G. Buchalla, M. Neubert and C. T. Sachrajda, Phys. Rev. Lett. **83**, 1914 (1999) [hep-ph/9905312]; Nucl. Phys. B **591**, 313 (2000) [hep-ph/0006124].

[4] J. Chay and C. Kim, Nucl. Phys. B **680** (2004) 302 [hep-ph/0301262].

[5] M. Beneke and T. Feldmann, Nucl. Phys. B **685** (2004) 249 [hep-ph/0311335].

[6] C. W. Bauer, D. Pirjol, I. Z. Rothstein and I. W. Stewart, Phys. Rev. D **70** (2004) 054015 [hep-ph/0401188].

[7] M. Beneke and M. Neubert, Nucl. Phys. B **651** (2003) 225 [hep-ph/0210085].

[8] A. R. Williamson and J. Zupan, Phys. Rev. D **74** (2006) 014003 [hep-ph/0601214].

[9] Y. Y. Keum, H. N. Li and A. I. Sanda, Phys. Rev. D **63** (2001) 054008 [hep-ph/0004173].

[10] M. Ciuchini, et al., Phys. Lett. B **515** (2001) 33 [hep-ph/0104126].

[11] M. Beneke, G. Buchalla, M. Neubert and C. T. Sachrajda, Phys. Rev. D **72** (2005) 098501 [hep-ph/0411171]; M. Beneke, Int. J. Mod. Phys. A **21** (2006) 642 [hep-ph/0509297].

[12] R. J. Hill, T. Becher, S. J. Lee and M. Neubert, JHEP **0407** (2004) 081 [hep-ph/0404217]; T. Becher and R. J. Hill, JHEP **0410** (2004) 055 [hep-ph/0408344].

[13] G. G. Kirilin, [hep-ph/0508235].

[14] M. Beneke and D. Yang, Nucl. Phys. B **736** (2006) 34 [hep-ph/0508250].

[15] M. Beneke and S. Jäger, Nucl. Phys. B **751** (2006) 160 [hep-ph/0512351].

[16] N. Kivel, [hep-ph/0608291].

[17] M. Beneke and S. Jäger, hep-ph/0610322.

[18] X. q. Li and Y. d. Yang, Phys. Rev. D **72** (2005) 074007 [hep-ph/0508079].

[19] M. Beneke and M. Neubert, Nucl. Phys. B **675**, 333 (2003), [hep-ph/0308039].

[20] H. n. Li, S. Mishima and A. I. Sanda, Phys. Rev. D **72** (2005) 114005 [hep-ph/0508041].

[21] M. Beneke, G. Buchalla, M. Neubert and C. T. Sachrajda, Nucl. Phys. B **606** (2001) 245 [hep-ph/0104110].

[22] A. Khodjamirian, T. Mannel, M. Melcher and B. Melic, Phys. Rev. D **72**, 094012 (2005) [hep-ph/0509049].

[23] T. Feldmann and T. Hurth, JHEP **0411**, 037 (2004) [hep-ph/0408188].

[24] T. Becher, R. J. Hill, B. O. Lange and M. Neubert, Phys. Rev. D **69**, 034013 (2004) [hep-ph/0309227]; T. Becher, R. J. Hill and M. Neubert, Phys. Rev. D **69**, 054017 (2004) [hep-ph/0308122].

[25] A. V. Manohar and I. W. Stewart, [hep-ph/0605001].

[26] C. M. Arnesen, Z. Ligeti, I. Z. Rothstein and I. W. Stewart, [hep-ph/0607001].

[27] A. L. Kagan, Phys. Lett. B **601** (2004) 151 [hep-ph/0405134].

[28] M. Beneke, J. Rohrer and D. Yang, Phys. Rev. Lett. **96** (2006) 141801 [hep-ph/0512258].

[29] M. Beneke, J. Rohrer and D. Yang, [hep-ph/0612290].

[30] H. n. Li and S. Mishima, Phys. Rev. D **74** (2006) 094020 [hep-ph/0608277].

[31] C. W. Bauer, I. Z. Rothstein and I. W. Stewart, Phys. Rev. D **74** (2006) 034010 [hep-ph/0510241].

Measurements of the Top Quark at the Tevatron Collider

Lucio Cerrito
on behalf of the CDF and D⊘ Collaborations
Particle Physics Research Centre
Department of Physics
Queen Mary, University of London
E1 4NS London, U.K.

1 Introduction

We present recent preliminary measurements of the top-antitop pair production cross section and determinations of the top quark pole mass, performed using the data collected by the CDF and D⊘ Collaborations at the Tevatron Collider([1]). In the lepton plus jets final state, with semileptonic B decay, the pair production cross section has now been measured at CDF using ∼760 pb^{-1} of proton-antiproton collisions at a centre-of-mass energy of $\sqrt{s}$=1.96 TeV. A measurement of the production cross section has also been made with ∼1 fb^{-1} of data in the all-jets final state by the CDF Collaboration. The mass of the top quark has now been measured using ∼1 fb^{-1} of collision data using all decay channels of the top quark pair, yielding the most precise measurements of the top mass to date.

Top quarks are produced at the Tevatron Collider predominantly in pairs of top-antitop via quark-antiquark scattering (∼85%) and gluon-gluon fusion (∼15%). The decay of top quarks proceeds before hadronization almost exclusively as $t \to Wb$, therefore it is common to classify the final state of a $t\bar{t}$ event according to the decay modes of the W bosons. The decay channels are labelled as: *dilepton*, when both W's from the top pair decay leptonically, *lepton plus jets* when one the W's decays leptonically and the second decays hadronically, and *all hadronic*, when both W's decay hadronically. The identification of b quarks in jets is made either through the measurement of a displaced secondary vertex in the event (due to the long lifetime of B-hadrons), or through the detection of a muon or electron from the semileptonic decay of B-hadrons.

[1]The Tevatron is a proton-antiproton synchrotron accelerator producing collisions at a centre-of-mass energy of 1.96 TeV (Run II) in two locations (CDF and D⊘). The Tevatron operated until 1998 (Run I) at a centre-of-mass energy of 1.8 TeV.

The measurement of the $t\bar{t}$ production cross section provides a test of the theory of Quantum Chromo Dynamics (QCD), while the comparison of the measurements from different decay channels allows probing both the production and decay mechanism described by the standard model (SM). At $\sqrt{s}$=1.96 TeV, the predicted $t\bar{t}$ cross section is $\sigma_{t\bar{t}} = 6.8^{+0.7}_{-0.9}$ pb for a top mass (M_t) of 175 GeV/c^2 [1]. The top quark mass, on the other hand, is a crucial ingredient of the SM and its precision measurement, combined with the independent measurement of the mass of the W boson, allows predicting the SM Higgs boson mass.

2 Top Quark Pair Production Cross Section

2.1 Lepton plus jets events with soft muon b-tagging

This analysis is based on data corresponding to an integrated luminosity of ∼760 pb^{-1}, collected with the CDF II detector [2–5] between March 2002 and September 2005. The data are collected with an inclusive lepton trigger that required an electron (muon) with $E_T > 18$ GeV ($P_T > 18$ GeV/c) [6]. From the inclusive lepton dataset we select events offline with a reconstructed isolated electron E_T (muon P_T) greater than 20 GeV, missing $E_T > 20$ GeV and at least 3 jets with $E_T > 15$ GeV. Background events, predominantly due to QCD production of W bosons with multiple jets, are rejected in the first instance using the total event energy $H_T > 200$ GeV (H_T is the scalar sum of the electron E_T, muon P_T, missing E_T and jet E_T for jets with $E_T > 8$ GeV and $|\eta| < 2.4$). To further enhance the top quark signal against background events, we identify events with one or more b-jets by searching inside jets for semileptonic decays of B-hadrons into muons (with $P_T > 3$ GeV/c, $\Delta R < 0.6$ from a jet axis). From 85 candidate $t\bar{t}$ events and 27.3±2.5 expected background events, and considering the detector acceptance and event selection efficiency, we determine a cross section of $7.8\pm1.7(\text{stat})^{+1.1}_{-1.0}(\text{syst})$ pb. The result is in good agreement with our previous measurement [7], which used an integrated luminosity of ∼200 pb^{-1} or about 1/4th of the presently analysed dataset.

2.2 All hadronic events

This analysis is performed using ∼1.0 fb^{-1} of $p\bar{p}$ collisions at $\sqrt{s}$=1.96 TeV, selected with a multijet trigger. The trigger requires at least four calorimeter clusters with $E_T \geq 15$ GeV and a total transverse energy exceeding 175 GeV. Candidate $t\bar{t}$ events are required to have between 6 and 8 jets with $E_T > 15$ GeV and $|\eta| < 2.0$, and jets must be separated in $\eta - \phi$ by $\Delta R \geq 0.5$. Due to the low signal (S) to background (B) ratio after the trigger and topoligical selections defined above, a neural network (NN) based kinematical selection is applied. The NN is a Multilayer perceptron (MLP [8]), a feed-forward network with an input layer, hidden layers and an output layer.

The inputs to the NN include variables such as the total and sub-leading transverse energy, centrality, aplanarity and dijet and trijet masses [9]. The single output node provides the variable NN_{out} on which we base the selection. The final additional requirement is that at least one jet has a displaced secondary vertex (called a tag), compatible with the presence of one or more b-jets in the event. The best selection cut on NN_{out} is determined considering the total expected signal and background and maximising $\Delta(B+S)/S$. We observe 1233 tags from within the selected sample, with a background expectation of 846±37 tags. The excess of tags with respect to the background is ascribed to the $t\bar{t}$ production and from this excess we measure a production cross section of: 8.3±1.0(stat)±0.5(lum)$^{+2.0}_{-1.5}$(syst) pb.

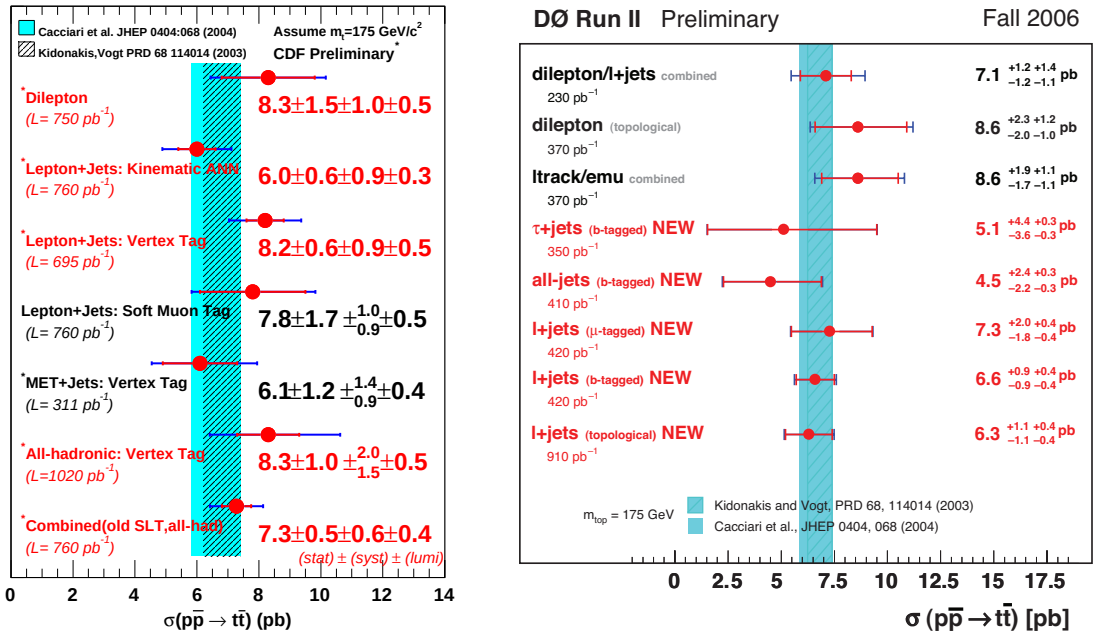

(a) (b)

Figure 1: Preliminary measurements of the $t\bar{t}$ production cross section at $\sqrt{s}$=1.96 TeV measured by (a):CDF and (b): D⊘.

2.3 Overview of $t\bar{t}$ production cross section measurements

The overview of preliminary measurements of the $t\bar{t}$ production cross section at the Tevatron is shown in Figure 1 for the CDF experiment (a) and for the D⊘ experiment (b). The measurements analyse datasets corresponding to integrated luminosity between ∼200 pb^{-1} and ∼1 fb^{-1}. A systematic uncertainty of about 6%, on the knowledge of the integrated luminosity of the samples, is common to all measurements for

each experiment. All the results are in good agreement with the SM calculation, and the measured cross section averaged over different decay channels has now reached a similar accuracy (∼12%) to the theoretical prediction. Moreover, the measured cross section appears, within the current uncertainties, in good agreement among the different decay channels.

3 Top Quark Pole Mass

3.1 Dilepton events

The dilepton channel, consisting of the decays $t\bar{t} \to \bar{b}\ell^-\overline{\nu}_\ell b\ell'^+\nu'_\ell$, has a small branching fraction but allows measurements which are less reliant on the calibration of the jet energies than measurements in channels with hadronic W decays. This analysis is based on an integrated luminosity of ∼1.0 fb^{-1} collected with the CDF II detector between March 2002 and March 2006. Top candidate events are selected by requiring two leptons, both with $E_T > 20$ GeV ($P_T > 20$ GeV/c form muons) and at least one of which is isolated ([2]). Candidate events must also have at least two jets with $E_T > 15$ GeV, measured within $|\eta|$ <2.5. We also require candidate events to have $\not\!\!E_T > 25$ GeV and, in events with $\not\!\!E_T < 50$ GeV, that the $\not\!\!E_T$ vector is at least 20° from the closest lepton or jet. In order to extract maximum information from the sample, we adapt in this analysis a technique based on leading-order production cross section and a parametrized description of the jet energy resolution. Per-event likelihoods in top mass are combined to construct a joint likelihood from which the top quark mass (M_t) is determined. The total expression for the probability of a given pole mass for a specific event can be written as:

$$P(x|M_t) = \frac{1}{N}\int d\Phi_8 |\mathcal{M}_{t\bar{t}}(p;M_t)|^2 \prod_{\text{jets}} W(p,j)W(p_T,U)f_{\text{PDF}}(q_1)f_{\text{PDF}}(q_2), \quad (1)$$

where the integral is over the entire six-particle phase space, q is the vector of incominig parton-level quantities, p is the vector of resulting parton-level quantities: lepton and quark momenta. The functions W are called transfer functions, and parametrise the probability of measuring a detector-level observable (j, U) given a parton-level observable (p, p_T). Finally, $|\mathcal{M}_{t\bar{t}}(p;M_t)|$ is the $t\bar{t}$ production matrix element as defined in [10, 11]. Background events are taken into account by constructing a generalized per-event probability which includes terms for each background, calculated with a differential cross section similar to Equation 1. After calibrating the technique with Monte Carlo simulations of the experiment, we measure:

[2] An isolated lepton is one for which no more than 10% extra energy is measured in a cone of $\Delta R \equiv \sqrt{(\Delta\phi)^2 + (\Delta\eta)^2} \leq 0.4$ around the lepton

$M_{\rm top}$=164.5±3.9(stat)±3.9(syst) GeV/c^2. The single largest source of systematic uncertainty comes from the uncertainty in the jet energy calibration (±3.5 GeV/c^2). Other significant systematic uncertainties are due to the Monte Carlo modeling of $t\bar{t}$ production and decay, and the modeling of the background events.

3.2 Lepton plus jets events

This analysis is a preliminary measurement of the top quark mass from the lepton plus jets decay channel using ∼940 pb^{-1} of data collected from March 2002 to February 2006 with the CDF II detector. Events are selected requiring a single, high-transverse energy (greater than 20 GeV), well-isolated lepton, large missing energy from the neutrino (greater than 20 GeV), and exactly four central jets with high transverse energy (greater than 15 GeV, $|\eta| < 2.0$), two from the b quarks and two from the hadronic W. Of these jets we require at least one to be identified as originating from a vertex displaced from the primary vertex. In order to reject most non-W background, we further require the axis between missing transverse energy and leading jet, $\Delta\phi$, not be collinear for the lowest values of missing transverse energy passing our selection. The method to determine the top quark mass is similar to the one described in Section 3.1 for dilepton events, whereby we create a likelihood for each event by combining a signal probability with a background probability. However, in this analysis the combined likelihood describes, and is maximised for, not only the top quark mass but also the jet energy scale (JES, an overall multiplicative factor to the jet energy measurements), and the fraction of events consistent with the signal hypothesis. The JES systematic uncertainty is measured constraining the mass of the W from the two untagged jets to 80.4 GeV/c^2, and we assume the JES determined for the W-jets also applies to b-jets. An additional systematic uncertainty is included to take into account the difference between the JES determined from the hadronic decaying W, and the proper b-jets energy scale. Simulated samples with different top quark masses as input are used to validate and calibrate the anaysis method. The extracted top mass is found to be unbiased with respect to the top quark mass for which the input events were generated. From 166 events passing our selection requirements we measure: $M_{\rm top}$=170.9±2.2(stat+JES)±1.4(syst) GeV/c^2. The quoted systematic error include uncertainties on the Monte Carlo modeling of $t\bar{t}$ production and decay, the detector response, and the modeling of background events.

3.3 All hadronic events

This analysis is performed using ~ 1 fb^{-1} of $p\overline{p}$ collisions at $\sqrt{s} = 1.96$ TeV collected with the CDF II detector. The technique used is based on a comparison, through likelihood maximization, of the top invariant mass distribution in data with a Monte Carlo simulation of the top signal and background events. The event selection is

described in Section 2.2. We define a quantity (χ^2) as a function of one free parameter, the top mass itself, and use the first 6 jets in order of decreasing E_T to fully reconstruct the event. Of the possible permutations of jet assignments compatible with the $t\overline{t}$ decay chain, we choose the one with the lowest χ^2. The χ^2 contains two terms which constrain the light quark jets to form the two W masses. Then a third jet four-momentum is added in order to form two objects closely spaced in the unknown mass. An additional term is added to account for the uncertainties on jet momentum measurements. The definition is thus as follows:

$$\begin{aligned}\chi^2 &= \frac{(m_{jj_1}-m_W)^2}{\Gamma_W^2}+\frac{(m_{jj_2}-m_W)^2}{\Gamma_W^2}+\frac{(m_{jjj_1}-m_t)^2}{\Gamma_t^2} \\ &+\frac{(m_{jjj_2}-m_t)^2}{\Gamma_t^2}+\sum_{i=1}^{N}\frac{(p_i^{\rm fit}-p_i^{\rm data})^2}{\sigma_i^2},\end{aligned} \tag{2}$$

where m_{jj} is the invariant mass of the dijet, m_{jjj} is the invariant mass of the trijet, $m_W = 80.4$ GeV/c^2 and Γ_W=2.1 GeV/c^2 the W boson mass and width, Γ_t=1.5 GeV/c^2 and m_t the free parameter, with the constraint that the mass of the two top quarks be equal. The distribution of invariant mass for background events is derived from the data using the sample before the b-tagging request, and is then corrected for the presence of top events. Given a model for signal and background mass templates, we use a likelihood function to determine the mass of the top quark that best describes the data, as well as extracting the number of signal (n_s) and background (n_b) tags in the sample. We measure $n_s = 334 \pm 33$ and $n_b = 573 \pm 26$ tags and the top quark mass of M_t=174.0±2.2(stat)±4.8(syst) GeV/c^2. Systematic uncertiainties are largely due to the uncertainty on the jet energy measurements (±4.5 GeV/c^2), with smaller contributions (≤1.0 GeV/c^2) from the Monte Carlo modeling of the top signal and the detector response.

3.4 Overview and combination of the top quark mass measurements

The recent preliminary measurements of the top quark mass at CDF, together with the measurements of the D⊘ experiment, are summarized in Figure 2 [12]. The plot includes published measurements from Tevatron data in Run I (1992-1996) and preliminary measurments in Run II, in all three decay channels of the top quark pair. The measurements in the different channels are reasonably consistent with each other. The combination of the measurements, taking into account the statistical and systematical uncertainties and their correlations, yields the preliminary world average mass of the top quark: M_t=171.4±1.2(stat)±1.8(syst) GeV/c^2, which corresponds to a total uncertainty of 2.1 GeV/c^2. The precision on the mass measurement is limited

by the systematic uncertainties, which are dominated by the calibration of the jet energy measurements.

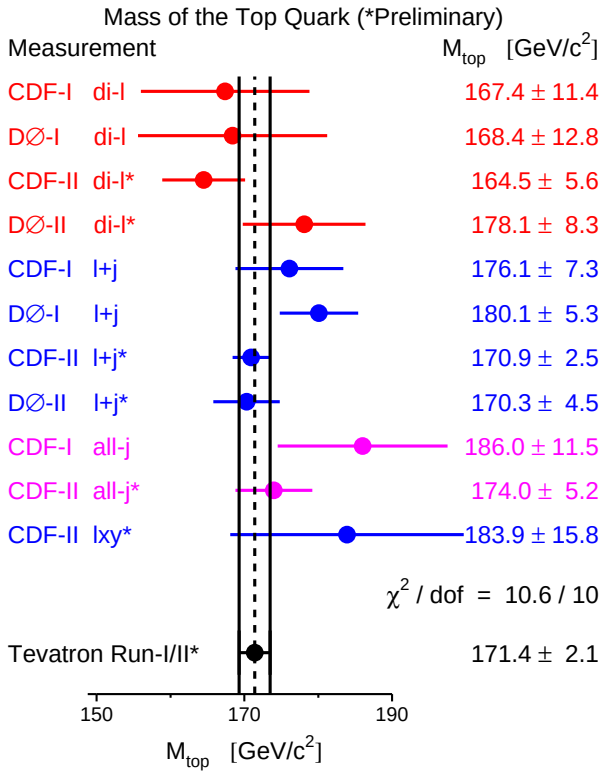

Figure 2: Summary of the measurements included in the world average mass of the top quark.

4 Conclusions

We have presented recent preliminary measurements of the top quark pair production cross section and the top quark mass at the Tevatron Collider. All recent measurements are now using $\sim$1 fb^{-1} of proton-antiproton collision data at a center-of-mass energy of $\sqrt{s} = 1.96$ TeV. All $t\bar{t}$ cross section measurements are in good agreement with the SM calculation, and the precision of the CDF average cross section is approaching the theoretical accuracy of $\sim \pm 12\%$. The world average mass of the top quark is: M_t=171.4$\pm$1.2(stat)$\pm$1.8(syst) GeV/c^2 and is therefore now known with an accuracy of 1.2%. The systematic uncertainty, which limits the precision to the mass measurement, is expected to improve as larger data sets are collected at the Tevatron

Collider. It can be reasonably expected that with the full Run II data set the top quark mass could be known to better than 1%.

Bibliography

[1] M.Cacciari, S.Frixione, G.Ridolfi, M.L.Mangano and P.Nason, JHEP 0404(2004) 68.

[2] F. Abe *et al.*, Nucl. Instrum. Methods Phys. Res. A 271, 387 (1988).

[3] D. Amidei, *et al.*, Nucl. Instrum. Methods Phys. Res. A 350, 73 (1994).

[4] F. Abe *et al.*, Phys Rev. D 52, 4784 (1995).

[5] P. Azzi *et al.*, Nucl. Instrum. Methods Phys. Res. A 360, 137 (1995).

[6] The transverse momentum, P_T, is the projection of a particle's momentum onto the plane perpendicular to the beam axis. The pseudorapidity, η, is defined as: $-\ln \tan(\theta/2)$, where θ is the polar angle with respect to the direction of the proton beam. The missing transverse energy, $\not\!\!E_T$, is the transverse component of the energy imbalance in the calorimeter, and is identified with the undetected neutrino's transverse momenta.

[7] D. Acosta *et al.*, Phys. Rev. D 72, 032002, 2005.

[8] See http://schwind.home.cern.ch/schwind/talks/ITseminar/index.htm and http://www.fynu.ucl.ac.be/users/c.delaere/level2/MLP for a description of MLP.

[9] For a description of these variables see F. Abe *et al.*, Phys. Rev. Lett. 79, 1992 (1997).

[10] G. Mahlon, S. Parke, Phys. Lett. B 411, 173 (1997).

[11] G. Mahlone, S. Parke, Phys. Rev. D 55, 7249 (1996).

[12] The Tevatron Electroweak Working Group, FERMILAB-TM-2355-E, hep-ex/0608032 (2006).

Charm and beauty structure of the proton

Riccardo Brugnera[1]
Dipartimento di Fisica dell'Universitá di Padova and
INFN Sezione di Padova
E-mail:riccardo.brugnera@pd.infn.it

1 Introduction

Heavy quarks production is an important testing ground for quantum chromodynamics (QCD), because QCD calculations are expected to be reliable if a hard scale is present in the process. In heavy quarks production a hard scale is provided by the quark mass. Moreover heavy quarks production can give direct access to the gluon density in the proton due to the fact that it proceeds, in QCD, almost exclusively via photon-gluon fusion, where a photon from the incoming electron interacts with a gluon in the proton giving an heavy quark-anti-quark pair. Results will be shown both for deep-inelastic scattering (DIS), where the virtuality of the exchanged boson Q^2 is large, and photo-production, where the Q^2 is equal to zero. Various experimental techniques are used in order to select charm and beauty events, ranging from the measurement of D^* cross section to impact parameter analyses. The results are found to be compatible with the predictions of perturbative QCD (pQCD).

This paper is organized as follows. The relevant features of the HERA collider and of the H1 and ZEUS detectors are described in section 2. In section 3, an introduction to the physics of heavy quarks production in ep collisions is given. The sections 4 and 5 illustrate the tagging methods and the experimental results for the charm quark, while 6 and 7 do the same for the beauty quark. The charm and beauty structure functions are presented in section 8. The results obtained for the gluon polarization by the COMPASS Collaboration are described in section 9. Finally the conclusions are drawn in section 10.

2 The HERA collider and its two multipurpose experiments: H1 and ZEUS

HERA is the first ep collider and consists of two separate rings of circumference 6.3 km, one a warm magnet electron (or positron) ring with maximum energy 30 GeV and

[1]On behalf of the H1 and ZEUS Collaborations.

the other a superconducting magnet proton ring of maximum energy 920 GeV. The rings are brought together at four intersection regions, two of them are occupied by the experiments H1 and ZEUS. The HERA life can be divided in two parts: HERA-I from 1992 to 2000 and HERA-II from 2003 to the middle of 2007. During the first period, HERA worked with $e^{\pm}$ beam of 27.5 GeV while the energy of the proton beam was raised from 820 GeV to 920 GeV. The beam spot had the dimension of 150×30 μm^2 and the integrated luminosity collected by each experiments was about 130 pb^{-1}. At the end of 2000 there was a long shutdown, in which both HERA and the two experiments made important upgrades. In 2003 HERA started its functioning and it is to foreseen to work up to the middle of 2007. During the HERA-II period the energies of the lepton and proton beams remained unchanged: 27.5 GeV and 920 GeV respectively. A reduced beam spot (80×20 μm^2) and more reliable beams operation have enhanced a lot the delivered luminosity to the experiments ($\sim$ 180 pb^{-1} per experiment from 2003 to 2005). In Fig. 1 the integrated luminosities per period are shown as function of the day of the run.

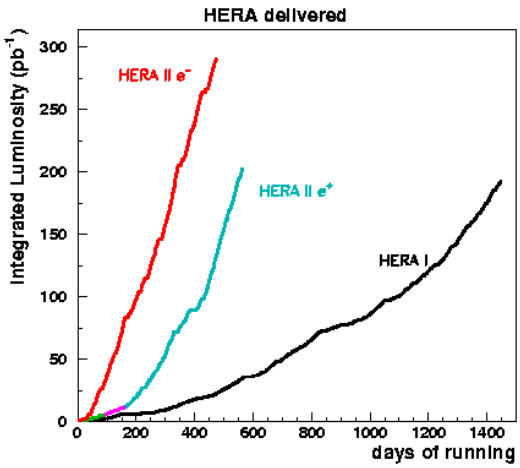

Figure 1: The integrated luminosity delivered by HERA, subdivided into HERA-I period and HERA-II, versus the days of running. The HERA-II period is furthermore divided in HERA-II with electrons (HERA-II e^-) and HERA-II with positrons (HERA-II e^+).

The H1 [1] and ZEUS [2] detectors are general purpose detectors with nearly hermetic calorimetric coverage. They are designed in order to investigate all aspects of high energy ep collisions. In particular both the scattered electron and the hadronic system in a hard ep interaction are measured. They are differentiated principally by the choices made for the calorimetry. The H1 collaboration has stressed electron identification and energy resolution, while the ZEUS Collaboration has put its

emphasis on optimizing calorimetry for the hadronic measurements. The detector designs reflect these different emphases. The H1 detector has a large diameter magnet encompassing the main liquid argon calorimeter, while the ZEUS detector has chosen a uranium-scintillator sampling calorimeter with equal response to electrons and hadrons. Cross sectional view of the H1 and ZEUS detectors are presented in Fig. 2 and 3 respectively.

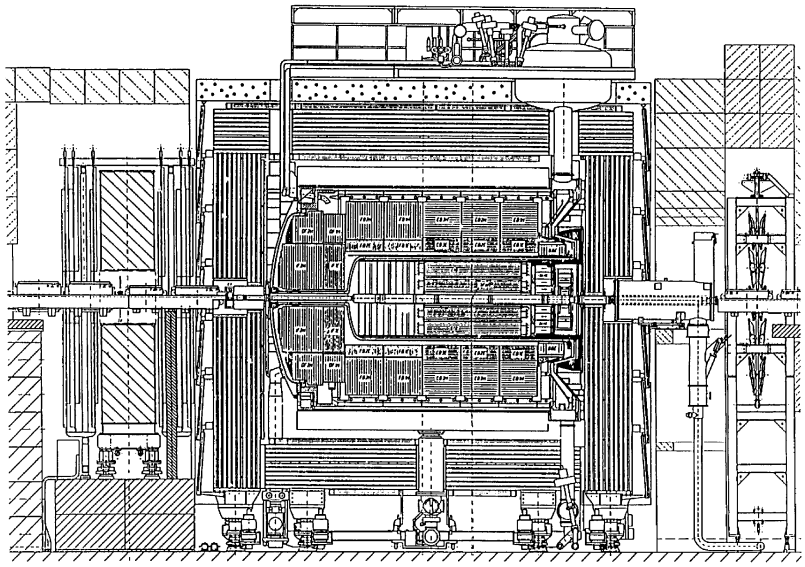

Figure 2: Cross sectional view of the H1 detector.

3 Production of Heavy Quarks in ep collisions

In pQCD, at leading order (LO), two distinct classes of processes contribute to the production of heavy quarks (charm and beauty) in ep collisions at HERA. In direct-photon processes (Fig. 4a), the photon emitted from the electron enters the hard process $\gamma g \to Q\overline{Q}$ directly. In resolved-photon processes (Fig. 4b to 4d), the photon fluctuates into a hadronic state before the hard interaction and acts as a source of partons, one of which takes part in the hard interaction. Resolved photon processes are expected to contribute significantly in the photo-production regime, in which the photon is quasi-real, and to be suppressed towards higher Q^2.

Next-to-leading order (NLO) calculations in several schemes are available [3, 4]. In DIS regime, all approaches assume that Q^2 and heavy quark mass m_Q provide a hard enough scale to allow the applicability of pQCD and to garantee the validity of the factorization theorem. In photo-production regime the hard scale is given by

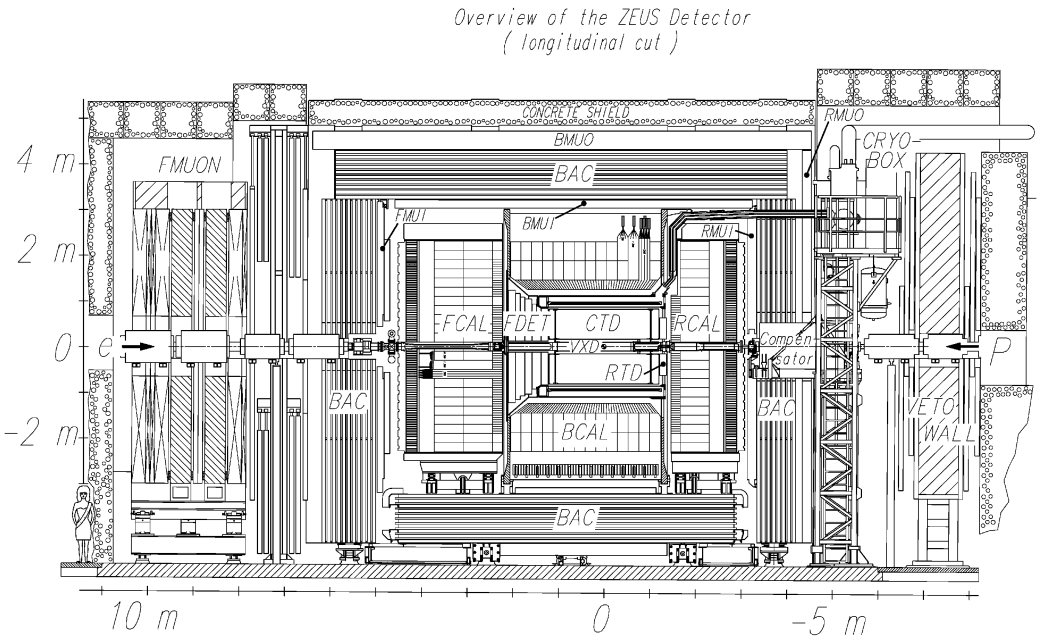

Figure 3: Cross sectional view of the ZEUS detector.

the transverse momentum of the heavy quark $p_{t,Q}$ and m_Q. In the fixed-order, or "massive", scheme [2], u, d, s are the only active flavours in the structure functions of the proton and photon. The heavy quarks are assumed to be produced only at perturbative level via photon-gluon fusion. This scheme is expected to work well in regions where $p^2_{t,Q} \sim m^2_Q$ (if in photo-production regime) or where $Q^2 \sim m^2_Q$ (if in DIS regime). At higher transverse momenta or Q^2, calculations based on this scheme can break down due to large logarithms $\sim ln(p^2_{t,Q}/m^2_Q)$ ($\sim ln(Q^2/m^2_Q)$). In this case the resummed, or "massless", scheme [3] [5] should be applicable. In this scheme, charm and beauty are regarded as active flavours (massless partons) in the structure functions of the proton and photon and are fragmented from massless partons into massive hadrons after the hard process. There are also calculations[4] which tempt to treat the heavy quarks correctly for all Q^2. Therefore, at low Q^2, an heavy quark is produced dynamically through the boson-gluon fusion process, whereas, at high Q^2, heavy quark parton densities are introduced. The transition between the two extremes is treated in different way by different authors [6].

[2]The scheme is often referred to as fixed flavour number scheme (FFNS).
[3]The scheme is often referred as the zero mass variable flavour number scheme (ZMVFNS).
[4]The scheme is commonly referred to as variable flavour number scheme (VFNS).

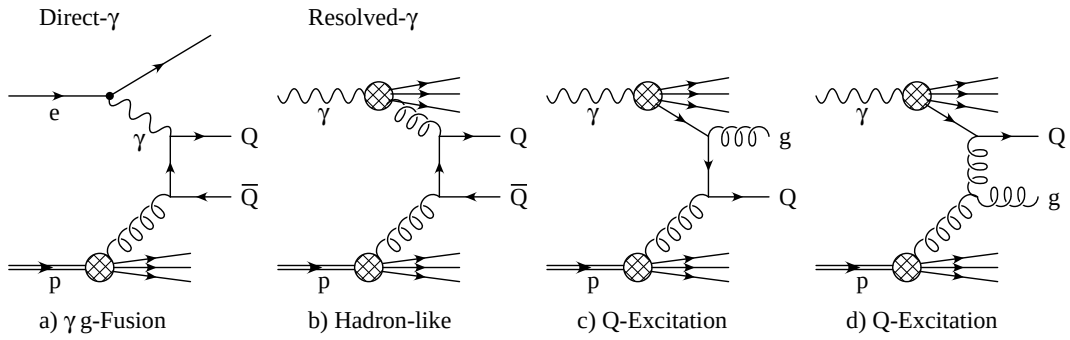

Figure 4: Heavy Quarks production processes in leading order pQCD.

4 Charm production: tagging methods

The main method used for charm tagging is the identification of the D^* mesons using the decay channel $D^{*+} \to D^0\pi_s^+$ with the subsequent decay $D^0 \to K^-\pi^+$, where π_s refers to the low momentum π in the decay. The decay particles of the D^* meson are reconstructed in the central detector, usually without particle identification. In Fig. 5 it is shown a distribution of the mass difference $\Delta M = M(K\pi\pi_s) - M(K\pi)$ from the ZEUS Collaboration. A clear signal is seen around the nominal value $M(D^*) - M(D^0)$. In order to mantain under control the combinatorial background, various cuts are made on the p_t of the tracks and on the energy of the event. Of course also other charmed hadrons were identified and analyzed, such as D^+, D_s, Λ_c, but with less statistics. Finally, the sistematic use of the vertex detectors, first implemented in H1 and now also in ZEUS, is changing dramatically the perspective of the physical analysis in the charm sector as it already happened in the beauty one (see section 6 and 7).

5 Charm production: experimental results

The status of the charm analysis can be summarized by the two plots of Fig. 6, where the differential D^* cross section as a function of the pseudo-rapidity[5] of the D^* mesons, $\eta(D^*)$ on the left, and the differential D^* cross sections as a function of Q^2 on the right are shown [7].

The plot on the left of Fig. 6 shows the good agreement between the ZEUS and H1 data. The bands in both plots represent the NLO predictions using the HVQDIS program [8], the widths of the bands correspond to the uncertainties in the mass

[5]The pseudo-rapidity η corresponding to a polar angle θ (measured respect to the positive z-axis, corresponding to the the incoming proton beam direction) is given by η = -ln tan(θ/2).

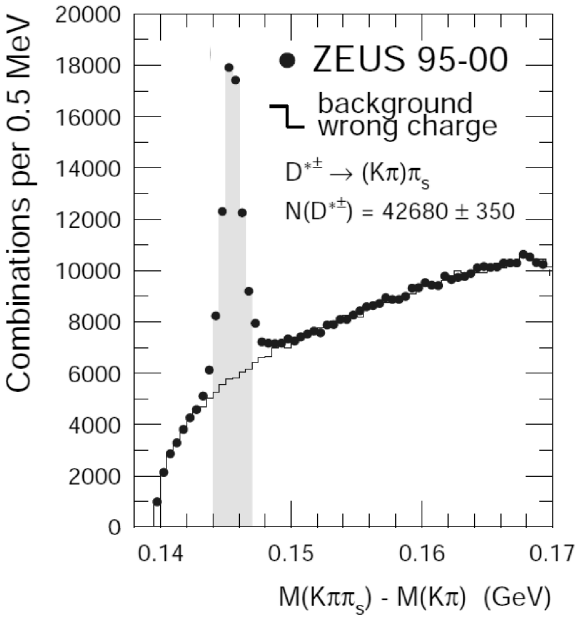

Figure 5: The distribution of the mass difference, $\Delta M = M(K\pi\pi_s) - M(K\pi)$, for D^* candidates. The $D^{*\pm}$ candidates (dots) are shown compared to the wrong charge combinations (histogram). The shaded region shows the signal region. The number of D^* mesons is determined by subtracting the wrong charge background.

of the charm, in the renormalization and factorization scales, in the proton parton density functions and in the fragmentation. Rather remarkable is the fact that the $d\sigma/dQ^2$ data are well described by NLO calculations over five orders of magnitude. Some discrepancies between data and theory are seen in photoproduction: D^* photoproduction cross sections [9] as function of the transverse momentum, $p_T(D^*)$, and $\eta(D^*)$ show that the predictions from NLO QCD are too low for $p_T(D^*) > 3$ GeV and $\eta(D^*) > 0$. Part of this deficit may be due to hadronisation effects. The predictions for single jet and dijet production accompanied by a D^* meson should have smaller uncertainties from these effects. For that aim the following correlations were studied: the difference in the azimuthal angle, $\Delta\phi(D^*,\text{jet})$, between the D^* and a jet not containing the D^* meson and those between the two jets of highest transverse energy, $\Delta\phi^{jj}$, and the squared transverse momentum of the dijet system, $(p_T^{jj})^2$. For the LO $2 \to 2$ process, the two jets, or the D^* and a jet not containing the D^* meson, are produced back-to-back with $\Delta\phi = \pi$ and very low p_T. Large deviations from these values may come from higher-order QCD effects. In Fig. 7 the differential cross section as function of the $\Delta\phi(D^*,\text{jet})$ is shown, a large fraction of the produced D^*+jet combinations deviates from back-to-back configuration indicating the importance of higher order contributions. The available NLO calculations (massive FMNR [4] and

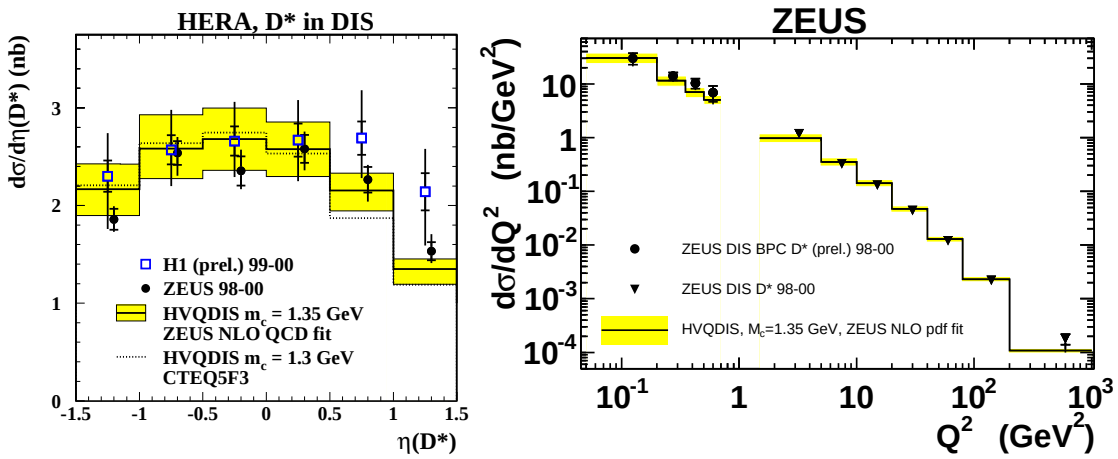

Figure 6: On the left, differential D^* cross sections as a function of $\eta(D^*)$, filled points from the ZEUS experiment and empty squares from the H1 experiment. The bands are the NLO predictions of HVQDIS. On the right, differential D^* cross sections as a function of Q^2 for low Q^2 (dots) and from results on D^* production in DIS (triangle) compared to the NLO predictions from HVQDIS. The data come from the ZEUS Collaboration.

ZMVFNS [10]) underestimate significantly the observed cross sections in the region $\Delta\phi(D^*,\text{jet}) < 120^o$. The cross section $d\sigma/d\Delta\phi^{jj}$, see Fig. 8, is reasonable reproduced by the NLO predictions in the direct-enriched region, that is $x_\gamma^{obs} > 0.75$[6] , although the data exhibit a somewhat harder distribution. In the resolved-enriched region, $x_\gamma^{obs} < 0.75$, the data exhibit a harder spectrum than for $x_\gamma^{obs} > 0.75$. The NLO prediction of the cross section for $x_\gamma^{obs} < 0.75$ has a significantly softer distribution compared to the data. The low- x_γ^{obs} region is more sensitive to higher-order topologies not present in the massive NLO prediction. The predictions from PYTHIA MC [11] reproduce neither the shape nor the normalisation of the data for low and high x_γ^{obs}. However, the predictions from the HERWIG MC [12] give an excellent description of the shapes of all distributions, although the normalisation is underestimated by a factor of 2.5. The fact that a MC programme incorporating parton showers can successfully describe the data whereas the NLO QCD prediction cannot indicates that the QCD calculation requires higher orders. Matching of parton showers with NLO calculations such as in the MC@NLO programme [13], which is not currently available for the processes studied here, should improve the description of the data.

[6] x_γ^{obs} represents the fraction of the photon momentum partecipating to the hard scattering.

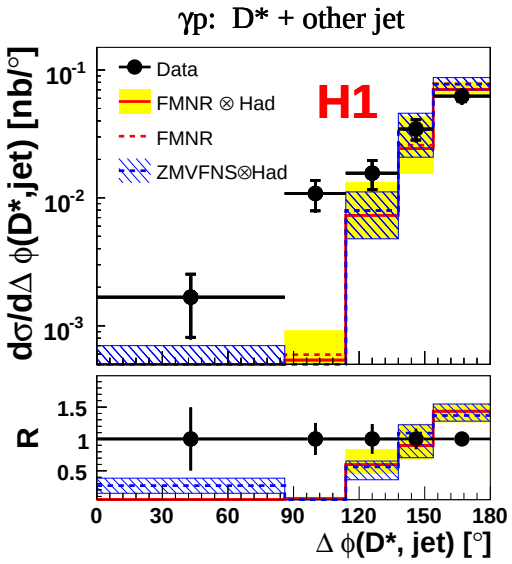

Figure 7: D^*+jet cross sections as function of $\Delta\phi(D^*,\text{jet})$ compared with the predictions of the NLO calculations FMNR and ZMVFNS.

6 Beauty production: tagging methods

The H1 and ZEUS Collaborations have presented measurements in which the events containing beauty are identified in the following manners: using high p_T leptons (mainly muons) from semileptonic b-decays, or using the impact parameters of all tracks coming from secondary decay vertices (inclusive lifetime tag analysis), or finally using double tagged events ($D^* + \mu$, $\mu\mu$).

In the first method, the transverse momentum p_T^{rel} of the muon with respect to the axis of the associated jets exhibits a much harder spectrum for muons from b-decays than for the other sources. Sometime, in order to enhance the signal to noise ratio also the signed impact parameter δ of the muon track with respect to the primary event vertex is used, this quantity reflects the lifetime of the particle from which the muon decays. The relative contributions from b, c and light quarks are determined by a fit to the p_T^{rel} distribution or to a combined fit to the p_T^{rel} and δ distributions using the shapes of Monte Carlo b, c and light quarks distributions as templates.

In the second method, the track selection requires full silicon vertex detector information. From the measured impact parameter δ a lifetime significance $S = \delta/\sigma_\delta$ is calculated. Two independent distributions are constructed. S_1 is the significance distribution of tracks in events with exactly one selected tracks. S_2 contains the significances of the tracks with the second highest significance for events with two or more selected tracks. Events in which the tracks with the first and second highest

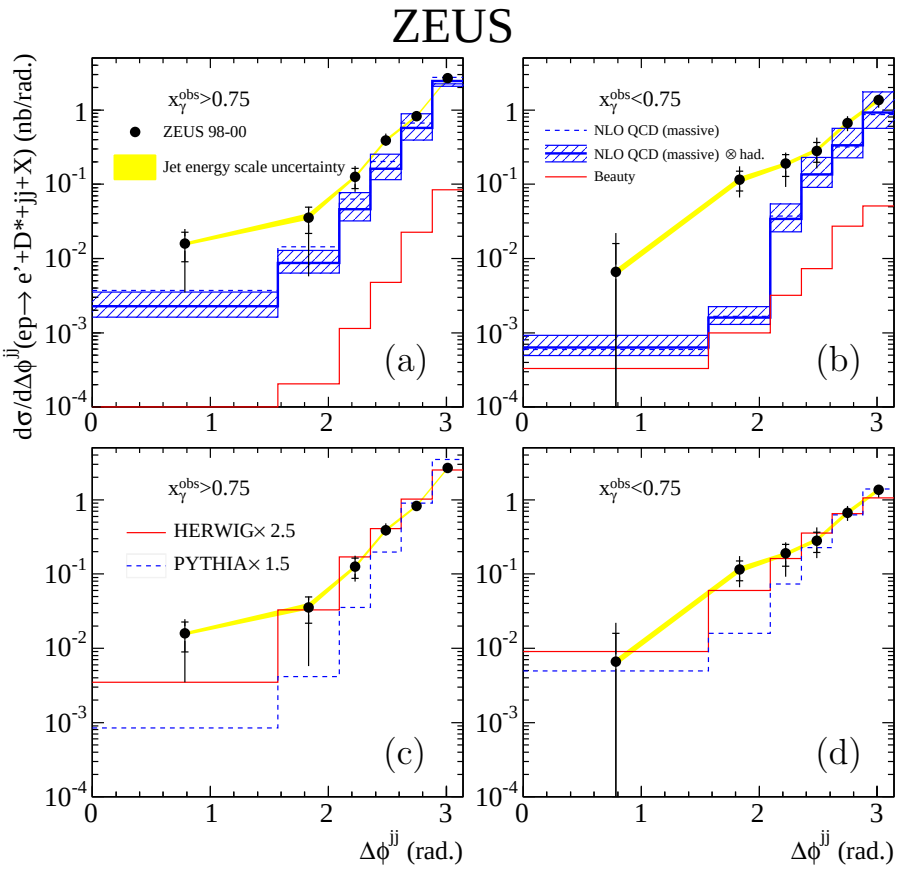

Figure 8: Cross section for the process $ep \rightarrow e + D^* + jj + X$ separated into (a,c) direct enriched ($x_\gamma^{obs} > 0.75$) and (b,d) resolved enriched ($x_\gamma^{obs} < 0.75$). The data (solide dots) are compared (a,b) to the massive QCD prediction with (solid line) and without (dotted line) hadronisation corrections applied. The theoretical uncertainties (hatched band) come from the change in scales simultaneously with the change in charm mass. The beauty component is also shown (lower histogram). The data are also compared (c,d) with HERWIG (solid line) and PYTHIA (dashed line) MC predictions multiplied by the indicated factors. The data come from the ZEUS Collaboration.

absolute significance have different signs are removed from the S_2 distribution. The subtracted significance distributions are obtained by bin-wise subtraction of the numbers of entries on the negative side from those on the positive side. The subtraction method substantially reduces the systematic uncertainties due to track and vertex resolutions. The relative contributions from b, c and light quarks are determined from a fit to the subtracted S_1 and S_2 distributions and the total number of events,

using the shapes of Monte Carlo b, c and light quarks distributions as templates.

In the third method, doubled tagged events, events are selected containing at least one reconstructed D^* and at least one muon, $D^* + \mu$, or two muons in the final state ($\mu\mu$). In order to suppress the various types of backgrounds the charge and angle correlations of the D^* with respect to the muon and of the two muons are exploited. These double tagged measurements extend to significantly lower centre-of mass energies of the $b\bar{b}$ system than measurements based on leptons and/or jets with high transverse momentum. Furthermore, these double tagged events permit to test higher order QCD effects. For instance, in the photon-gluon rest frame the angle between the heavy quarks is 180^o at leading order, but at NLO it can differ significantly from this value due to hard gluon radiation.

7 Beauty production: experimental results

Differential measurements from H1 and ZEUS are available for beauty production in photoproduction and DIS [14], [15] using the lepton+jet(s) tag method. Figure 9 shows the differential photoproduction cross sections as a function of the muon transverse momentum (on the left) and of the pseudo-rapidity for the process $ep \rightarrow eb\bar{b}X \rightarrow ejj\mu$. The H1 and ZEUS data, which are in reasonable agreement when they are compared in the same phase space region (see the $d\sigma/d\eta^\mu$ plot on the right side), are compared to a NLO calculation in the massive scheme [4]. The NLO calculations describe the ZEUS data well. Comparing with the H1 data, the NLO calculations predict a less steep behaviour for the $d\sigma/dp_t^\mu$ and is lower than the H1 data in the lower momentum bin by roughly a factor of 2.5; at higher transverse momenta better agreement is observed. In DIS (data not shown), the total cross section measurements made by the H1 and ZEUS Collaborations are somewhat higher than the predictions. The observed excess is pronounced at large muon pseudo-rapidities, low values of Q^2 and muon transverse momentum.

As said in section 6, using double tagged events [16, 17] it is possible to measure the b production up to very low p_t values. In Fig. 10 the differential cross sections as a function of the muon transverse momentum p_T^μ (plot on the left) and the muon pseudo-rapidity η^μ (plot on the right), for muons from b decays in dimuon events and restricted to the phase space $p_t^\mu > 1.5$ GeV and -2.2$< \eta^\mu < 2.5$ for both muons are shown. Very good agreement is observed with the PYTHIA+RAPGAP [18] predictions scaled by a factor 1.95 (histogram). Apart from the normalization, the leading parton shower approach yields a good description of the corresponding physics processes within the entire accessible phase space. The data are also compared to the absolute NLO prediction in the massive scheme convoluted with the hadronization from PYTHIA MC (shaded band). Again, good agreement in shape is observed, with a tendency to underestimate the data normalisation. A potential trend for in-

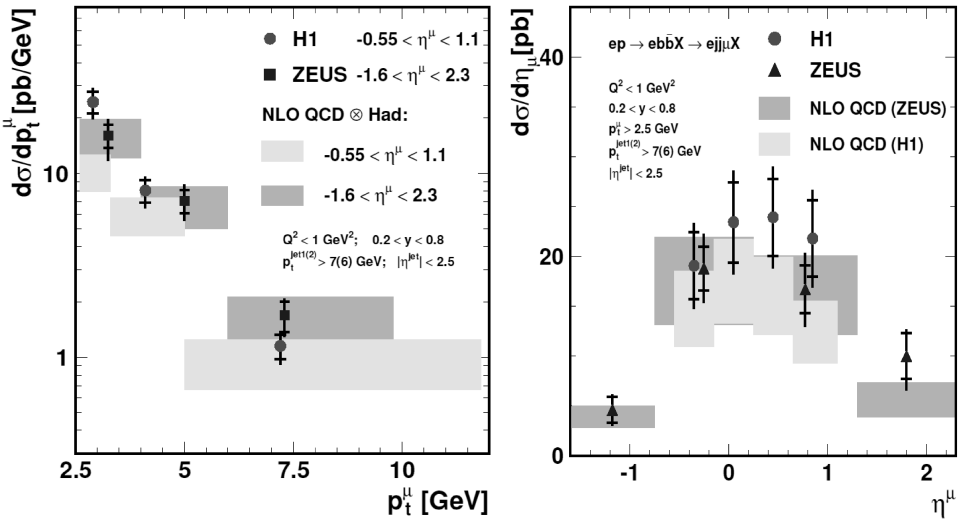

Figure 9: Differential cross sections as a function of the muon transverse momentum p_T^μ (on the left) and the muon pseudo-rapidity η^μ (on the right), for muons coming from b decays in dijet events. The two sets of data coming from the H1 and ZEUS experiments were measured in different phase space regions. The full error bars are the quadratic sum of the statistical (inner part) and systematic uncertainties. The bands represent the NLO predictions convoluted with their uncertaintites obtained by varying the b-quark mass and the renormalization and factorization scales.

creasing data/theory deviations towards low p_t and/or high η, suggested by other measurements as said before, is not supported.

Exploiting the experimental possibilities offered by its microvertex detector, H1 has measured charm and beauty photoproduction using events with two or more jets at high transverse momentum [19]. In this analysis events containing heavy quarks are distinguished from light quark events by the long lifetime of c and b flavoured hadrons, which lead to the displacements of tracks from the primary vertex (see section 6). This analysis provides the first simultaneous measurement of charm and beauty in photoproduction, extending to larger values of transverse jet momentum than previous measurements. In Fig. 11 the measured differential cross sections for charm (plot on the left) and beauty (plot on the right) as functions of the transverse momentum of the leading jet $p_t^{jet_1}$ are shown. Both charm and beauty data are reasonbly well described in shape both by the Monte Carlo simulations (PYTHIA and CASCADE[7] [20]) and the NLO QCD (FMNR) calculations. For charm, the

[7]The CASCADE program implements the k_t-factorisation approach instead of the usual collinear factorisation approach. In the $\gamma g^* \to Q\overline{Q}$ matrix element, which takes the heavy quark mass into account, the incoming gluon is treated off mass-shell and can have a finite transverse momentum.

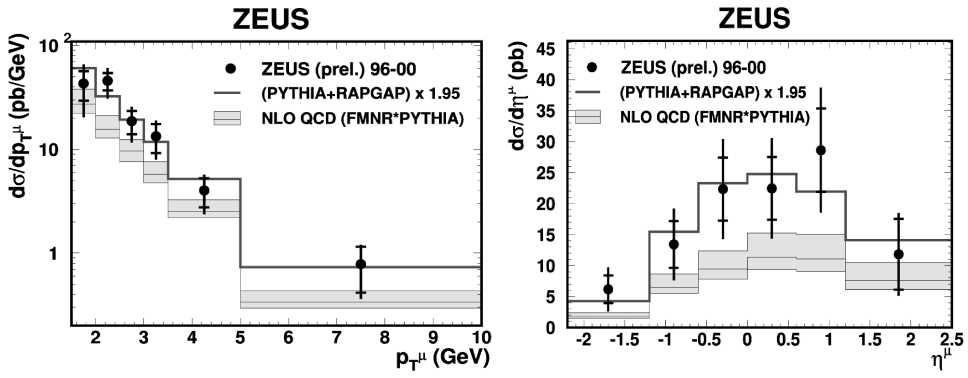

Figure 10: Differential cross sections as a function of the muon transverse momentum p_T^μ (on the left) and the muon pseudo-rapidity η^μ (on the right), for muons from b decays in dimuon events. Data come from the ZEUS experiment. The full error bars are the quadratic sum of the statistical (inner part) and systematic uncertainties. The data are compared to the NLO QCD predictions (shaded band) and to the MC predictions (histogram).

NLO QCD calculation is somewhat lower than the measurement but still in reasonable agreement within the theoretical errors, for beauty the disagreement is slightly higher. The MC's predict a normalisation which is similar to that of FMNR. The bulk of the disagreement between data and NLO calculation, especially for the beauty, is observed in the region of small values of x_γ^{obs} where the prediction lies below the data. Restricting the data to $x_\gamma^{obs} > 0.85$, a significant improvement can be obtained: the charm cross sections are in good agreement with the NLO QCD calculation both in normalisation and shape, the beauty cross sections are also reasonably well described.

The major part of the results shown in this section were obtained in the photoproduction regime ($Q^2 < 1$ GeV^2), and they differ greatly due to different experimental cuts, different tagging-methods. It is difficult to compare each other and also to extract a general message from the comparison between data and NLO QCD calculations. In order to overcome these difficulties the various measured cross sections were translated to b-quark differential cross sections as a function of the quark transverse momentum, $d\sigma(ep \to bX)/dp_T^b$, in the pseudo-rapidity range $|\eta^b| < 2$. In Fig. 12 the so extrapolated differential cross sections are shown and compared with the NLO QCD (FMNR) calculations (shaded band). The data are in reasonable agreement between them, they tend to be somewhat higher than the predictions, the disagreement is concentrated at low and medium values of p_T^b, at high values there is a nice agreement.

The calculations are performed at LO, higher order QCD corrections are simulated with initial state parton showers.

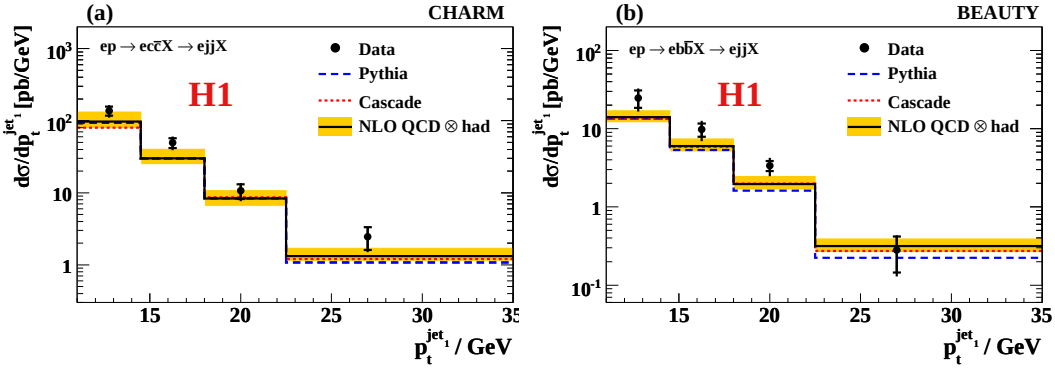

Figure 11: Differential charm (on the left) and beauty (on the right) photoproduction cross sections $d\sigma/dp_t^{jet_1}$ for the process $ep \to e(c\overline{c}$ or $b\overline{b})X \to ejjX$. The full error bars are the quadratic sum of the statistical (inner part) and systematic uncertainties. The solid lines indicate the prediction from a NLO QCD calculation, corrected for hadronisation effects, and the shaded band shows the estimated uncertainty. The absolute predictions from PYTHIA (dashed lines) and CASCADE (dotted lines) are also shown.

8 The charm and beauty structure functions

The structure functions more frequently studied (F_2 and xF_3) are inclusive objects and thus contain contributions from both valence and sea quarks. The H1 and ZEUS detectors have the ability to provide identification of a particular quark flavour opening so the possibility of studying the contribution of that flavour to F_2. This is particularly important in the case of heavy flavours, as they are likely produced in the hard scattering and not in the subsequent hadronisation of the struck parton. In other words very precise theoretical predictions can be done as explained in the section 3. Due to the fact that at order α_s heavy quark production in DIS occurs through boson-gluon fusion process (see Fig. 4), this process involves the gluon density xg directly so it gives an experimental handle on this quantity.

$F_2^{c\overline{c}}$ is calculated from the measured charm cross sections as follows:

- The cross section for $c\overline{c}$ is calculated from the D^* cross section [21] (extrapolated to the full phase space) using:

$$\sigma(ep \to ec\overline{c}X) = \frac{1}{2}\frac{\sigma(ep \to eD^*X)}{P(c \to D^*)} \tag{1}$$

  where $P(c \to D^*)$ is the probability that a charm quark will produce a D^* meson (about 25%). As said in the sections 4 and 6, the advent of the micro-vertex detectors has permitted to distinguish events containing heavy quarks

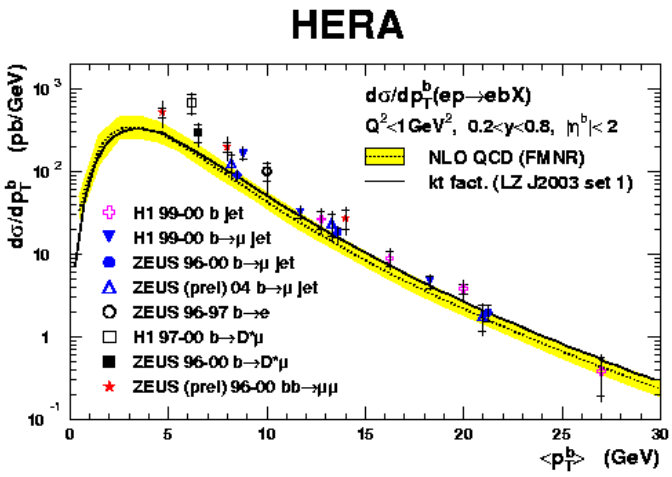

Figure 12: Differential cross section for b-quark production as a function of the b-quark transverse momentum p_T^b for b-quark pseudo-rapidity $|\eta^b| < 2$ and for $Q^2 < 1$ GeV^2, $0.2 < y < 0.8$. The various points show results from the H1 and ZEUS Collaborations using different b-tag methods. The full error bars are the quadratic sum of the statistical (inner part) and systematic uncertainties. The dashed line shows the NLO QCD prediction with the theoretical uncertainty shown as the shaded band. The continuous line shows the k_t factorization predictions from CASCADE MC.

from light quark events by the long lifetimes of c and b flavoured hadrons, which lead to displacements of tracks from the primary vertex. Furthermore the results can be obtained in kinematic regions where there is little extrapolation needed to the full phase space and so the model dependent uncertainty due to the extrapolation is small. These measurements were done by the H1 Collaboration [22].

- Finally $F_2^{c\bar{c}}$ is related to $ep \to ec\bar{c}X$ cross-section by:

$$\frac{d^2\sigma(c\bar{c})}{dxdQ^2} = \frac{2\pi\alpha^2}{Q^4 x}((1+(1-y)^2)F_2^{c\bar{c}} - y^2 F_L^{c\bar{c}}), \qquad (2)$$

where the small contribution from $F_L^{c\bar{c}}$ is calculated from QCD, while xF_3 is neglected due to the fact that the measurements are made at small Q^2.

In Fig. 13 (plot on the left) all the data about $F_2^{c\bar{c}}$ are shown as function of x at Q^2 values between 2 and 500 GeV^2. The various data sets, obtained with different techniques, are in good agreement between them. The structure function $F_2^{c\bar{c}}$ shows a rise with decreasing x at constant values of Q^2. The rise becomes steeper at higher Q^2. The data are compared to calculations using the recent ZEUS NLO fit [23],

in which the parton densities in the proton are parameterized by performing fits to inclusive DIS measurements from ZEUS and fixed-target experiments. The prediction describes the data well for all Q^2 and x except for the lowest Q^2, where some difference is observed. In Fig. 13 (plot on the right) the ratio $F_2^{c\bar{c}}/F_2$ is shown as function of x at fixed values of Q^2. The charm contribution to F_2 rises from 10% to 30% as Q^2 increases and x decreases. The strong rise of $F_2^{c\bar{c}}$ at low values of x is similar to that of the gluon density and thus supports the hypothesis that charm production is dominated by the boson-gluon fusion mechanism.

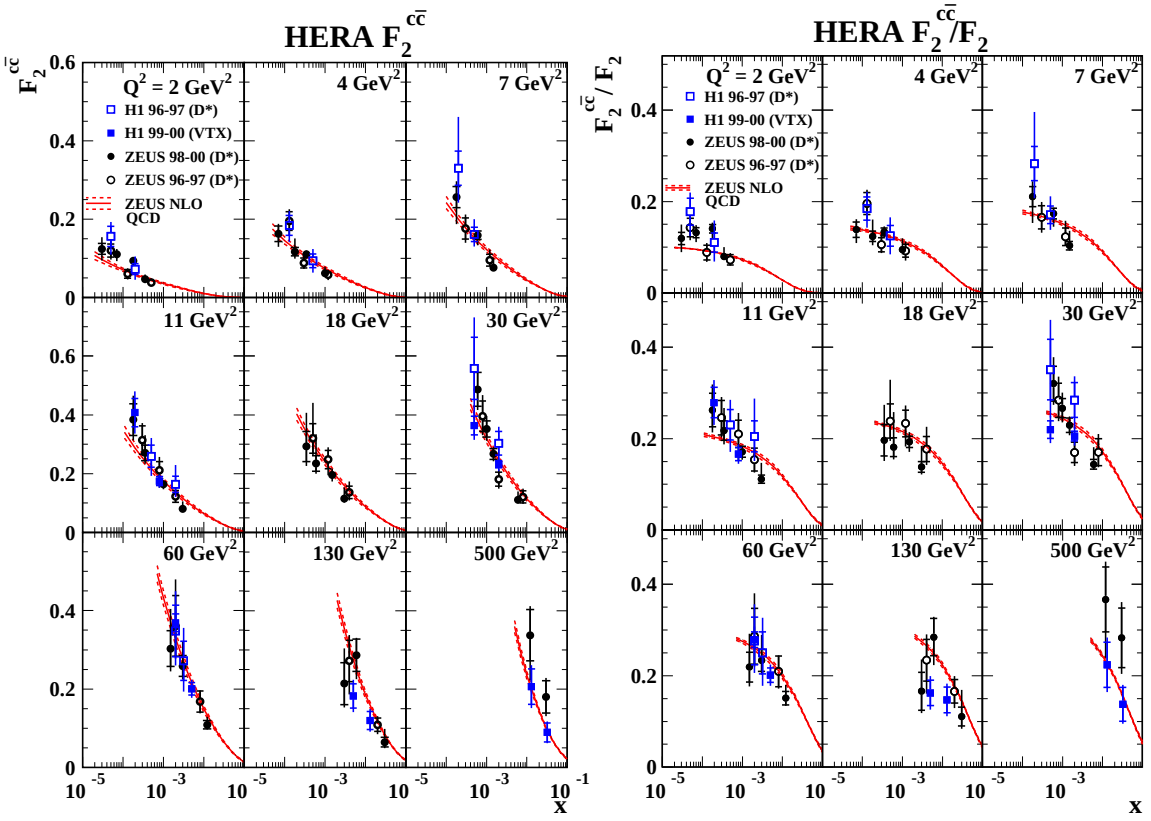

Figure 13: On the left plot, the measured $F_2^{c\bar{c}}$ at Q^2 values between 2 and 500 GeV^2 as a function of x is shown while on the right plot the measured ratio $F_2^{c\bar{c}}/F_2$. Data from the H1 and ZEUS experiments using different charm tagging are shown. The data are shown with statistical uncertainties (inner bars) and statistical and systematic uncertainties added in quadrature (outer bars). The curves represent the ZEUS NLO fit.

Using the help of the micro-vertex detector it was possible to measure the structure function $F_2^{b\bar{b}}$ [22] in a similar manner to those depicted for the $F_2^{c\bar{c}}$. The measurement of the b cross section (and so of $F_2^{b\bar{b}}$) is particularly challenging since b events comprise

only a small fraction (typically $< 5\%$) of the total cross section. In Fig. 14 the measured $F_2^{b\bar{b}}$ (by the H1 Collaboration) is shown as function of Q^2. The measurement shows positive scaling violations which increase with decreasing of x. The data are compared with the variable flavour number scheme QCD predictions from MRST [24] and CTEQ [25] at NLO and a recent calculation at NNLO [26]. The predictions are found to describe the data reasonably well. The beauty contribution to F_2, in the present kinematic range, increases rapidly with Q^2 from 0.4% at $Q^2 = 12$ GeV^2 to 1.5% at $Q^2 = 60$ GeV^2.

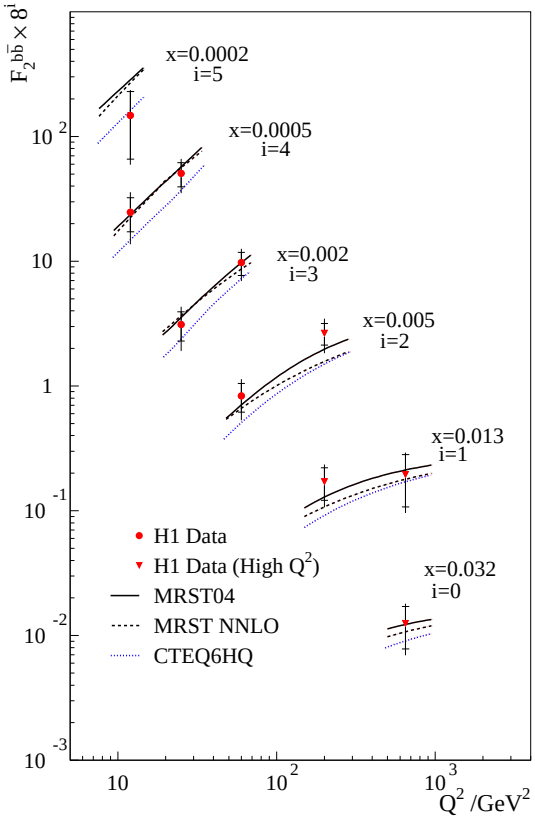

Figure 14: The measured $F_2^{b\bar{b}}$ shown as function of Q^2 for various x values. The inner error bars show the statistical errors, the outer error bars represent the statistical and systematic errors added in quadrature. The prediction of QCD are also shown.

9 Polarized gluon distribution

In this section, results obtained by the COMPASS Collaboration [27] on the determination of the polarized gluon distribution Δg using the open charm processes in polarized deep inelastic scattering are presented. Formally, one may write for the spin of the proton:

$$\frac{1}{2} = \frac{1}{2}\Delta\Sigma + \Delta g + < L_z >, \tag{3}$$

where $\Delta\Sigma$ is the contribution from the quarks and antiquarks, Δg from the gluons and the last term the mean contribution of any orbital angular momentum of the constituents. While for $\Delta\Sigma$ the situation starts to be solid, the challenge remains to measure Δg and $< L_z >$. The COMPASS experiment at CERN is a facility for spectroscopy and spin physics using hadron and muon beams from the SpS with a variety of targets and a range of sophisticated detectors for analyzing the final state. With a wide range of particle identification devices, the measurement of Δg through the boson-gluon fusion production of $c\overline{c}$ pairs is a primary aim. This first measurement was performed by scattering a positive muon polarized beam at 160 GeV on a solid polarized target. COMPASS has searched for D^o mesons in the decay $D^o \to K^-\pi^+$. To reduce background the neutral D's was also tagged by requiring them to come from the decay $D^{*+} \to D^o\pi^+$. In the measurement there is no reconstruction of the D^o vertex, all the reconstruction is based on the determination of the invariant mass and in the identification of the kaon through the RICH detector. The result is $\Delta g/g = -0.57 \pm 0.41(\text{stat})$ at a x value of the gluon equal to 0.15 and at a $Q^2 = 13$ GeV^2; the systematic error is smaller than the statistical one. In Fig. 15 the gluon polarization $\Delta g/g$ as a function of x at fixed Q^2 is shown. The points represent the present LO analyses of hadron helicity asymmetries (mainly from high p_T hadrons). The result from open charm obtained by COMPASS is also shown (star symbol). It is smaller than - but still compatible with - zero. COMPASS performed a NLO fits to the spin-dependent structure function $g_1(x, Q^2)$ world data. Two about equally good solutions for $\Delta g(x, Q^2)$ were found, one with a positive and one with a negative first moment ΔG.

10 Conclusions

In the previous pages, part of the results obtained by the H1 and ZEUS Collaborations in the field of heavy flavours has been summarized. We have seen that their charm and beauty data are in satisfactory agreement. In photo-production regime, beauty and charm data are in general agreement with the NLO predictions, even if beauty data are partially slightly higher. Charm production gives a large contribution to the inclusive DIS cross section: it was measured with good precision in a large part of phase space, NLO QCD calculations describe the data within accuracy. The first $F_2^{b\overline{b}}$

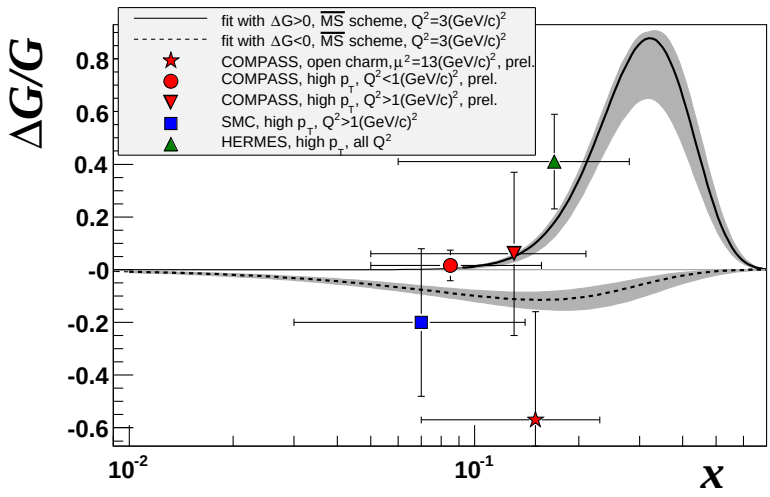

Figure 15: Gluon polarization $\Delta g/g$ as a function of x at $Q^2 = Q_0^2$ obtained by NLO QCD fits (bands) and from LO analyses of hadron helicity asymmetries (symbols).

measurement was also shown. All the presented results come from the HERA-I period, much more will come using all the statistics from HERA-II period. In the polarized DIS field the new preliminary result on $\Delta g/g$ from the COMPASS Collaboration using open charm was shown. The measurement, considered the most model-independent tool to study gluon-polarisation, still suffers from big statistical uncertainties, they will be highly reduced using the large amount of data that COMPASS will collect in the near future.

Bibliography

[1] H1 Collab., I. Abt et al., Nucl. Instrum. Meth. A **386**, 310 (1997).

[2] ZEUS Collab., U. Holm (ed.), *The ZEUS Detector*. Status Report (unpublished), DESY (1993), available on http://www-zeus.desy.de/bluebook/bluebook.html.

[3] E. Laenen et al., Phys. Lett. B **291**, 325 (1992);
E. Laenen et al., Nucl. Phys. B **392**, 162 (1993);
E. Laenen et al., Nucl. Phys. B **392**, 229 (1993);
S. Riemersma, J. Smith and W.L. van Neerven, Phys. Lett. B **347**, 143 (1995);
B.W. Harris and J. Smith, Nucl. Phys. B **452**, 109 (1995);
B.W. Harris and J. Smith, Phys. Lett. B **353**, 535 (1995) [Erratum-ibid B **359**, 423 (1995)];

M.A. Aivazis et al., Phys. Rev. D **50**, 3102 (1994);
J.C. Collins, Phys. Rev. D **58**, 094002 (1998).

[4] S. Frixione et al., Phys. Lett. B **348**, 633 (1995);
S. Frixione et al., Nucl. Phys. B **454**, 3 (1995).

[5] J. Binnewies, B.A. Kniehl and G. Kramer, Z. Phys. C **76**, 677 (1997);
B.A. Kniehl, G. Kramer and M. Spira, Z. Phys. C **76**, 689 (1997);
J. Binnewies, B.A. Kniehl and G. Kramer, Phys. Rev. D **58**, 014014 (1998).

[6] H. L. Lai and W. K. Tung, Z. Phys. C **74**, 463 (1997);
R. S. Thorne, J. Phys. G **25**, 1307 (1999);
A. Chuvakin et al., Eur. Phys. J. C **18**, 547 (2001);
R. S. Thorne and R. G. Roberts, Eur. Phys. J. C **19**, 339 (2001).

[7] ZEUS Collab., S. Chekanov et al., Phys. Rev. D **69**, 0120004 (2004);
ZEUS Collab., *Measurement of D^* meson production in deep inelastic ep scattering at low Q^**, abstract:265, submitted to the XII International Symposium on Lepton-Photon Interactions at High Energy, 30 June - 5 July 2005, Uppsala, Sweden;
H1 Collab., *Inclusive $D^{*\pm}$ meson and associated dijet production in deep-inelastic scattering*, abstract: 5-0163, submitted to the 32nd International Conference on High Energy Physics, ICHEP04, 16 August - 22 August 2004, Beijing, China.

[8] B.W. Harris and J. Smith, Phys. Rev. D **57**, 2806 (1998).

[9] ZEUS Collab., J. Breitweg et al., Eur. Phys. C **6**, 67 (1999);
ZEUS Collab., S. Chekanov et al., Nucl. Phys. B **729**, 492 (2005);
H1 Collab., A. Aktas et al., DESY-06-110, submitted to Eur. Phys. J. C.

[10] B. A. Kniehl, *Hadron Production in Hadron Hadron and Lepton Hadron Collisions*, in *14th Topical Conference on Hadron Collider Physics*, eds. M. Erdmann and T. Mueller, pp. 161-170. Springer, Heidelberg, 2003;
G. Heinrich and B.A. Kniehl, Phys. Rev. D **70**, 094035 (2004).

[11] T. Sjostrand et al., Comp. Phys. Comm. **135**, 238 (2001).

[12] G. Marchesini et al., Preprint Cavendish-HEP-99/17 (1999).

[13] S. Frixione and B.R. Webber, JHEP **0206**, 029 (2002);
S. Frixione, P. Nason and B.R. Webber, JHEP **0308**, 007 (2003).

[14] H1 Collab., C. Adloff et al., Phys. Lett. B **467**, 156 (1999);
H1 Collab., A. Aktas et al., Eur. Phys. J. C **41**, 453 (2005).

[15] ZEUS Collab., S. Chekanov et al., Phys. Rev. D **70**, 012008 (2004);
ZEUS Collab., S. Chekanov et al., Phys. Lett. B **599**, 173 (2004).

[16] H1 Collab., A. Aktas et al., Phys. Lett. B **621**, 56 (2005);
ZEUS Collab., S. Chekanov et al., DESY-06-166, submitted to Eur. Phys. J. C.

[17] ZEUS Collab., S. Chekanov et al., *Measurement of beauty production from dimuon events at HERA*, abstract:269, submitted to the XII International Symposium on Lepton-Photon Interactions at High Energy, 30 June - 5 July 2005, Uppsala, Sweden.

[18] H. Jung, Comp. Phys. Comm. **86**, 147 (1995).

[19] H1 Collab., A. Aktas et al., DESY-06-039, accepted by Eur. Phys. J. C.

[20] H. Jung and G.P. Salam, Eur. Phys. J. C **19**, 351 (2001);
H. Jung, Comp. Phys. Comm. **143**, 100 (2002).

[21] H1 Collab., C. Adloff et al., Z. Phys. C **72**, 593 (1996);
ZEUS Collab., J. Breitweg et al., Phys. Lett. B **407**, 402 (1997);
H1 Collab., C. Adloff et al., Nucl. Phys. B **545**, 21 (1999);
ZEUS Collab., J. Breitweg et al., Eur. Phys. J. C **12**, 35 (2000);
H1 Collab., C. Adloff et al., Phys. Lett. B **528**, 199 (2002);
ZEUS Collab., S. Chekanov et al., Phys. Rev. D **59**, 012004 (2004).

[22] H1 Collab., A. Aktas et al., Eur. Phys. J. C **40**, 349 (2005);
H1 Collab., A. Aktas et al., Eur. Phys. J. C **45**, 23 (2006).

[23] ZEUS Collab., S. Chekanov et al., Phys. Rev. D **67**, 012007 (2003).

[24] A.D. Martin et al., Eur. Phys. J. C **39**, 155 (2005).

[25] S. Kretzer et al., Phys. Rev. D **69**, 114005 (2004).

[26] R.S. Thorne, Phys. Rev. D **73**, 054019 (2006).

[27] See the web site http://wwwcompass.cern.ch/ for any detail.

Neutrinos

Neutrinos

Theory and Phenomenology of Neutrino Mixing

Carlo Giunti
INFN, Sezione di Torino,
and
Dipartimento di Fisica Teorica, Università di Torino,
Via P. Giuria 1, I–10125 Torino, Italy

Abstract

We review some fundamental aspects of the theory of neutrino masses and mixing. The results of neutrino oscillation experiments are interpreted as evidence of three-neutrino mixing. Implications for the mixing parameters and the neutrino masses are discussed, with emphasis on the connection with the measurements of the absolute values of neutrino masses in beta decay and neutrinoless double-beta decay experiments and cosmological observations.

1 Introduction to Neutrino Masses

In the Standard Model (SM) neutrinos are massless. This is due to the fact that, in the SM, neutrinos are described by the left-handed chiral fields ν_{eL}, $\nu_{\mu L}$, $\nu_{\tau L}$ only. Since the corresponding right-handed fields ν_{eR}, $\nu_{\mu R}$, $\nu_{\tau R}$ do not exist in the SM, a Dirac mass term,

$$\mathcal{L}^{\mathrm{D}} = \sum_{\alpha,\beta=e,\mu,\tau} \overline{\nu_{\alpha L}}\, M^{\mathrm{D}}_{\alpha\beta}\, \nu_{\beta R} + \mathrm{H.c.}\,, \tag{1}$$

is precluded. Here M^{D} is a complex 3×3 mass matrix (see Refs. [1–4]). On the other hand, the other elementary fermions (quarks and charged leptons) are described by left-handed and right-handed chiral fields, which allow them to have Dirac-type masses after the spontaneous electroweak symmetry breaking $\mathrm{SU(2)}_L \times \mathrm{U(1)}_Y \to \mathrm{U(1)}_Q$ generated by the Higgs mechanism. Note that the off-diagonal terms in the Dirac mass matrix M^{D} violate the conservation of the lepton numbers L_e, L_μ and L_τ, whereas the total lepton number $\mathrm{L} = \mathrm{L}_e + \mathrm{L}_\mu + \mathrm{L}_\tau$ is conserved.

In 1937 Ettore Majorana [5] discovered that a massive neutral fermion can be described by a two-component spinor, which is simpler than a four-component Dirac spinor. The fundamental difference of a Majorana fermion with respect to a Dirac fermion is that for a Majorana fermion the particle and antiparticle states coincide. In other words, charge conjugation does not have any effect on a Majorana fermion

field. Since charge conjugation inverts the chirality, in the SM there are three right-handed neutrino fields $(\nu_{\alpha L})^C \equiv \nu_{\alpha R}^C$, for $\alpha = e, \mu, \tau$. In the Majorana theory, the right-handed neutrino fields in Eq. (1) are identified with the corresponding charge-conjugated right-handed neutrino fields ν_{eR}^C, $\nu_{\mu R}^C$, $\nu_{\tau R}^C$, leading to the Majorana mass term[1]

$$\mathcal{L}_L^{\mathrm{M}} = \frac{1}{2} \sum_{\alpha,\beta=e,\mu,\tau} \overline{\nu_{\alpha L}} \, (M_L^{\mathrm{M}})_{\alpha\beta} \, \nu_{\beta R}^C + \mathrm{H.c.} \,, \tag{2}$$

with a complex symmetric 3×3 mass matrix M_L^{M} (see Refs. [1–4]). Although allowed by the field content of the SM, this Majorana mass term is forbidden by the gauge symmetries of the SM. It could be generated by the Vacuum Expectation Value (VEV) of a Higgs triplet, which is absent in the SM. Note that the Majorana mass term $\mathcal{L}_L^{\mathrm{M}}$ violates the conservation of the total lepton number L by two units.

Summarizing, the field content and the gauge symmetries of the SM hinder the existence of the Dirac and Majorana mass terms in Eqs. (1) and (2). This prediction of the SM is in contradiction with the experimental evidence of neutrino oscillations, which are due to neutrino masses and mixing (see Refs. [1–4, 6–10]). Therefore, it is necessary to extend the SM in order to describe the real world.

The simplest extension of the SM consists in the introduction of the three right-handed neutrino fields ν_{eR}, $\nu_{\mu R}$, $\nu_{\tau R}$, which are singlets under the gauge symmetries of the SM. In this way, the neutrino fields become similar to the other elementary fermion fields, which have both left-handed and right-handed components. The Dirac mass term in Eq. (1) can be generated by the same Higgs mechanism which generates the Dirac masses of charged leptons and quarks. However, a surprise arises: the Majorana mass term for the right-handed neutrino fields,

$$\mathcal{L}_R^{\mathrm{M}} = \frac{1}{2} \sum_{\alpha,\beta=e,\mu,\tau} \overline{\nu_{\alpha L}^C} \, (M_R^{\mathrm{M}})_{\alpha\beta} \, \nu_{\beta R} + \mathrm{H.c.} \,, \tag{3}$$

is invariant under the gauge symmetries of the SM and, hence, allowed. Therefore, the seemingly innocuous introduction of right-handed neutrino fields leads to fundamental new physics: Majorana neutrino masses and the existence of processes with $|\Delta \mathrm{L}| = 2$.

In general, in a model with left-handed and right-handed neutrino fields, the neutrino mass term is of the Dirac-Majorana type $\mathcal{L}^{\mathrm{D+M}} = \mathcal{L}^{\mathrm{D}} + \mathcal{L}_R^{\mathrm{M}}$, which can be written as

$$\mathcal{L}^{\mathrm{D+M}} = \frac{1}{2} \begin{pmatrix} \overline{\nu_L} & \overline{\nu_L^C} \end{pmatrix} \begin{pmatrix} 0 & M^{\mathrm{D}} \\ (M^{\mathrm{D}})^T & M_R^{\mathrm{M}} \end{pmatrix} \begin{pmatrix} \nu_R^C \\ \nu_R \end{pmatrix} + \mathrm{H.c.} \,, \tag{4}$$

where $\nu_L^T = \begin{pmatrix} \nu_{eL}^T & \nu_{\mu L}^T & \nu_{\tau L}^T \end{pmatrix}$ and $\nu_R^T = \begin{pmatrix} \nu_{eR}^T & \nu_{\mu R}^T & \nu_{\tau R}^T \end{pmatrix}$. In the mass matrix, the 3×3 block which would correspond to M_L^{M} is set to zero because $\mathcal{L}_L^{\mathrm{M}}$ is forbidden by

[1] The additional factor 1/2 is put by hand in order to avoid double counting in the derivation of the field equations using the canonical Euler-Lagrange prescription.

the gauge symmetries of the SM, as explained above. Since the Dirac mass matrix M^{D} is generated by the Higgs mechanism of the SM, its elements are proportional to the VEV of the Higgs doublet, $v_{\mathrm{SM}} = \left(\sqrt{2}G_{\mathrm{F}}\right)^{-1/2} = 246\,\mathrm{GeV}$, where G_{F} is the Fermi constant. Hence, the elements of M^{D} are expected to be at most of the order of $10^2\,\mathrm{GeV}$. This constraint is expressed by saying that they are "protected" by the gauge symmetries of the SM. On the other hand, since the Majorana mass term of the right-handed neutrino fields is invariant under the gauge symmetries of the SM, the elements of M_R^{M} are not protected by the SM gauge symmetries. In other words, from the SM point of view, the elements of M_R^{M} could have arbitrarily large values. If M_R^{M} is generated by the Higgs mechanism at a high-energy scale of new physics beyond the SM, the elements of M_R^{M} are expected to be of the order of such new high-energy scale, which could be as high as a grand-unification scale of about $10^{15}\,\mathrm{GeV}$. In this case, the total mass matrix can be approximately diagonalized by blocks, leading to a light 3×3 mass matrix

$$M_{\mathrm{light}} \simeq M^{\mathrm{D}} \, (M_R^{\mathrm{M}})^{-1} \, M^{\mathrm{D}T} \,, \tag{5}$$

and a heavy 3×3 mass matrix $M_{\mathrm{heavy}} \simeq M_R^{\mathrm{M}}$. The three light and the three heavy masses are given, respectively, by the eigenvalues of M_{light} and M_{heavy}. Therefore, there are three heavy neutrinos which are practically decoupled from the low-energy physics in our reach and three light neutrinos whose masses are suppressed with respect to the elements of the Dirac mass matrix M^{D} by the small matrix factor $(M_R^{\mathrm{M}})^{-1} \, M^{\mathrm{D}T}$. This is the famous see-saw mechanism [11–14], which explains naturally the smallness of the three light neutrino masses. It is important to note that the see-saw mechanism predicts that massive neutrinos are Majorana particles, leading to the existence of new measurable phenomena with $|\Delta \mathrm{L}| = 2$. The most accessible is neutrinoless double-β decay (see section 3.3).

The see-saw mechanism is a particular case (see Ref. [15]) of the following general argument [16] in favor of Majorana massive neutrinos as a general consequence of new physics beyond the SM at a high-energy scale Λ. The most general effective low-energy Lagrangian can be written as

$$\mathcal{L}_{\mathrm{eff}} = \mathcal{L}_{\mathrm{SM}} + \frac{\Omega_5}{\Lambda} + \frac{\Omega_6}{\Lambda^2} + \dots \,, \tag{6}$$

where $\mathcal{L}_{\mathrm{SM}}$ is the SM Lagrangian. The additional non-SM terms contain the field operators Ω_5, Ω_6, ..., which have energy dimension larger than four, as indicated by the index. These operators contain SM fields only. Furthermore, they are constrained to be invariant under the SM gauge symmetries, because the new high-energy theory by which they are generated is an extension of the SM. They are not included in $\mathcal{L}_{\mathrm{SM}}$, because they are not renormalizable (similarly to the Fermi Lagrangian, which is the effective non-renormalizable Lagrangian of weak interactions for energies much

smaller than $v_{\rm SM}$). Since each Lagrangian term must have energy dimension equal to four, the non-SM terms in Eq. (6) are suppressed by appropriate negative powers of the high-energy scale Λ. The less-suppressed non-SM term is the 5-D operator

$$\Omega_5 = \sum_{\alpha\beta} g_{\alpha\beta} \left(L^T_{\alpha L} \, \sigma_2 \, \Phi \right) \mathcal{C}^\dagger \left(\Phi^T \, \sigma_2 \, L_{\beta L} \right) + \text{H.c.} \,, \tag{7}$$

where $L_{\alpha L}$, Φ, $\mathcal{C}$ and σ_i are, respectively, the left-handed lepton doublets ($\alpha = e, \mu, \tau$), the Higgs doublet, the charge-conjugation matrix and the Pauli matrices ($i = 1, 2, 3$). At the electroweak symmetry breaking, Ω_5 generates a Majorana mass term of the type in Eq. (2), with the mass matrix

$$(M^{\rm M}_L)_{\alpha\beta} = \frac{v^2_{\rm SM}}{\Lambda} \, g_{\alpha\beta} l\bar{l} v_{\rm SM} = 246 \, \text{GeV} \,. \tag{8}$$

Hence, the neutrino masses are naturally suppressed by the very small ratio $v_{\rm SM}/\Lambda$ with respect to the masses of the charged leptons and quarks, which are proportional to $v_{\rm SM}$. It is remarkable that the 5-D operator in Eq. (7) is unique, in contrast to the multiplicity of 6-D operators (see Ref. [17]), which include operators for nucleon decay. Hence, Majorana neutrino masses provide the most accessible window on new physics beyond the SM.

2 Three-Neutrino Mixing

The mass matrix of the three light neutrinos (either Dirac or Majorana) can be diagonalized through the unitary transformation

$$\nu_{\alpha L} = \sum_{k=1}^{3} U_{\alpha k} \, \nu_{kL} \,, \tag{9}$$

where U is the 3×3 unitary mixing matrix. An important consequence of neutrino mixing is the existence of neutrino flavor oscillations, which depend on the elements of the mixing matrix and on the squared-mass differences $\Delta m^2_{kj} \equiv m^2_k - m^2_j$. Neutrino oscillations have been observed (see Refs. [2–4, 7–10]) in solar and reactor neutrino experiments ($\nu_e \to \nu_{\mu,\tau}$), with a squared-mass difference [9]

$$\Delta m^2_{\rm SOL} = 7.92 \, (1 \pm 0.09) \times 10^{-5} \, \text{eV}^2 \quad [2\sigma] \,, \tag{10}$$

and in atmospheric and accelerator neutrino experiments ($\nu_\mu \to \nu_\tau$), with a squared-mass difference [18]

$$\Delta m^2_{\rm ATM} = 2.6 \left(1^{+0.14}_{-0.15} \right) \times 10^{-3} \, \text{eV}^2 \quad [2\sigma] \,. \tag{11}$$

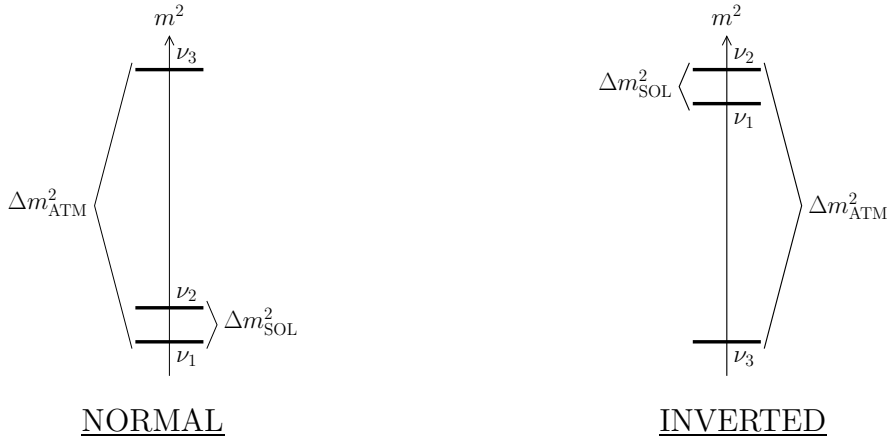

Figure 1: The two three-neutrino schemes allowed by the hierarchy $\Delta m^2_{\rm SOL} \ll \Delta m^2_{\rm ATM}$.

Hence, there is a hierarchy of squared-mass differences:

$$\Delta m^2_{\rm ATM} \simeq 30\, \Delta m^2_{\rm SOL}\,. \tag{12}$$

This hierarchy is easily accommodated in the framework of three-neutrino mixing, in which there are two independent squared-mass differences. We label the neutrino masses in order to have

$$\Delta m^2_{\rm SOL} = \Delta m^2_{21}\,, \tag{13}$$

$$\Delta m^2_{\rm ATM} \simeq |\Delta m^2_{31}| \simeq |\Delta m^2_{32}|\,. \tag{14}$$

The two possible schemes are illustrated in Fig. 1. They differ by the sign of $\Delta m^2_{31} \simeq \Delta m^2_{32}$.

Information on neutrino mixing is traditionally obtained from the analysis of the experimental data in the framework of an effective two-neutrino mixing scheme, in which oscillations depend on only one squared-mass difference (Δm^2) and one mixing angle (ϑ). This approximation is allowed [19] by the smallness of $|U_{e3}|$, which is the only element of the mixing matrix which affects both the solar-reactor and atmospheric-accelerator oscillations, as illustrated in Fig. 2. In fact, solar and reactor experiments have observed the disappearance of electron neutrinos, which depends only on the elements of the mixing matrix which connect ν_e with the three massive neutrinos: U_{e1}, U_{e2} and U_{e3}. On the other hand, the hierarchy of squared-mass differences in Eq. (12) implies that ν_1 and ν_2 are practically the same in atmospheric and accelerator oscillations and contribute through $|U_{\alpha1}|^2 + |U_{\alpha2}|^2 = 1 - |U_{\alpha3}|^2$. Hence these oscillations depend only on the third column of the elements of the mixing matrix.

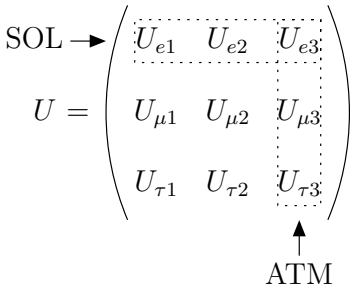

Figure 2: Schematic description of the contributions of the elements of the mixing matrix to solar (SOL) and atmospheric (ATM) neutrino oscillations.

The smallness of $|U_{e3}|$ is known from the results of the CHOOZ and Palo Verde experiments (see Ref. [20]), leading to [18]

$$|U_{e3}|^2 = 0.008^{+0.023}_{-0.008} \qquad [2\sigma]\,. \tag{15}$$

In this case, in the standard parameterization of the mixing matrix (see Ref. [4]), we have $|U_{e3}|^2 = \sin^2\vartheta_{13}$, the effective mixing angle measured in solar and reactor experiment is approximately equal to ϑ_{12} and the effective mixing angle measured in atmospheric and accelerator experiment is approximately equal to ϑ_{23}. An analysis of the data yields large values for ϑ_{12} and ϑ_{23} [9, 18]:

$$\sin^2\vartheta_{12} = 0.314\left(1^{+0.18}_{-0.15}\right) \qquad [2\sigma]\,, \tag{16}$$

$$\sin^2\vartheta_{23} = 0.45\left(1^{+0.35}_{-0.20}\right) \qquad [2\sigma]\,. \tag{17}$$

The mixing angle ϑ_{23} is close to maximal ($\pi/4$). The mixing angle ϑ_{12} is large, but less than maximal.

From the determination of the mixing angles, it is possible to reconstruct the allowed ranges for the elements of the mixing matrix: at 2σ we have

$$|U|_{2\sigma} \simeq \begin{pmatrix} 0.78 - 0.86 & 0.51 - 0.61 & 0.00 - 0.18 \\ 0.21 - 0.57 & 0.41 - 0.74 & 0.59 - 0.78 \\ 0.19 - 0.56 & 0.39 - 0.72 & 0.62 - 0.80 \end{pmatrix}. \tag{18}$$

One can see that all the elements of the mixing matrix are large, except $|U_{e3}|$, for which we have only an upper bound.

A mixing matrix of the type in Eq. (18), with two large mixing angles (ϑ_{12} and ϑ_{23}), is called "bilarge". Several future experiments are aimed at a measurement of the small mixing angle ϑ_{13} (see Ref. [21]), whose finiteness is crucial for the existence of CP violation in the lepton sector, for the possibility to measure matter effects with

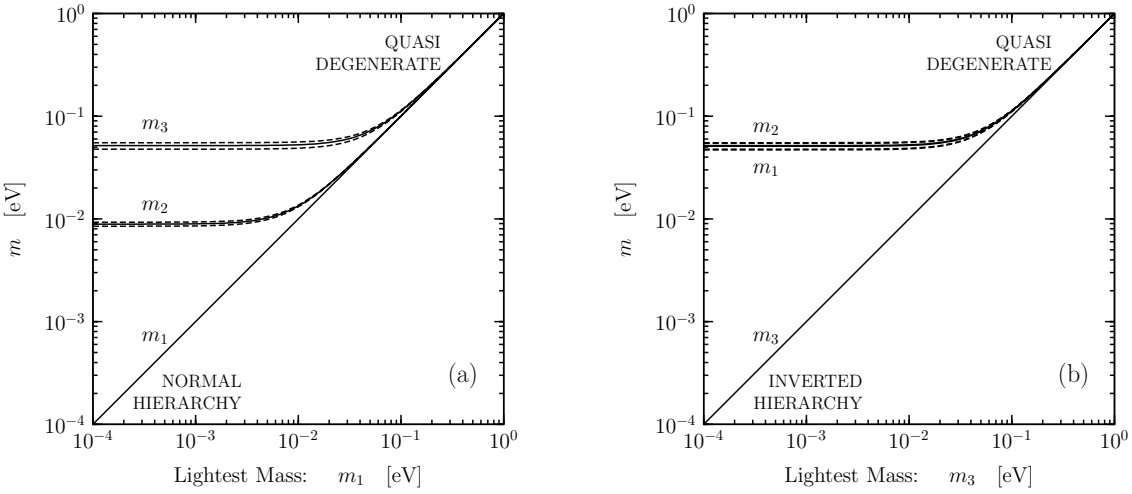

Figure 3: Values of neutrino masses as functions of the lightest mass, m_1 in the normal scheme (a) and m_3 in the inverted scheme (b). Solid lines correspond to the best-fit. Dashed lines enclose 2σ ranges.

future neutrino beam passing through the Earth and for the possibility to distinguish the normal and inverted schemes in future oscillation experiments.

As a first approximation, it is instructive to consider $\vartheta_{13} = 0$. In this case, the mixing matrix is given by

$$U = \begin{pmatrix} c_{\vartheta_{12}} & s_{\vartheta_{12}} & 0 \\ -s_{\vartheta_{12}} c_{\vartheta_{23}} & c_{\vartheta_{12}} c_{\vartheta_{23}} & s_{\vartheta_{23}} \\ s_{\vartheta_{12}} s_{\vartheta_{23}} & -c_{\vartheta_{12}} s_{\vartheta_{23}} & c_{\vartheta_{23}} \end{pmatrix} , \tag{19}$$

where $c_{\vartheta_{ij}} \equiv \cos\vartheta_{ij}$ and $s_{\vartheta_{ij}} \equiv \sin\vartheta_{ij}$. Choosing the attractive values

$$\sin^2\vartheta_{12} = \frac{1}{3} , \qquad \sin^2\vartheta_{23} = \frac{1}{2} , \tag{20}$$

which are within the ranges in Eqs. (16) and (17), we have the so-called "tri-bimaximal" mixing matrix [22]

$$U = \begin{pmatrix} \sqrt{2/3} & 1/\sqrt{3} & 0 \\ -1/\sqrt{6} & 1/\sqrt{3} & 1/\sqrt{2} \\ 1/\sqrt{6} & -1/\sqrt{3} & 1/\sqrt{2} \end{pmatrix} . \tag{21}$$

The name is due to the fact that the magnitudes of all the elements of the second column are equal (trimaximal mixing) and the third column have only two finite elements, which have the same magnitude (bimaximal mixing).

In the approximation in Eq. (19), we have

$$\nu_e = c_{\vartheta_{12}} \nu_1 + s_{\vartheta_{12}} \nu_2 , \tag{22}$$

which is a two-neutrino mixing relation. In oscillations, electron neutrinos can transform in the orthogonal state

$$\nu_\perp = -s_{\vartheta_{12}}\nu_1 + c_{\vartheta_{12}}\nu_2 = c_{\vartheta_{23}}\nu_\mu - s_{\vartheta_{23}}\nu_\tau \,. \tag{23}$$

Hence, The state in which solar and reactor electron neutrinos transform is a superposition of ν_μ and ν_τ determined by the atmospheric mixing angle ϑ_{23}. The closeness of ϑ_{23} to maximal mixing implies an approximate equal amount of ν_μ and ν_τ. If one further takes into account that the SNO experiment measured a suppression of about 1/3 of the solar ν_e flux for $E \gtrsim 6\,\text{MeV}$, it follows that the flux of high-energy solar neutrinos on the Earth is composed of an approximately equal amount of ν_e, ν_μ and ν_τ.

3 The Absolute Scale of Neutrino Masses

Since neutrino oscillations depend on the differences of the squared neutrino masses, other types of experiments are needed in order to determine the absolute values of neutrino masses. However, what is really unknown from the results of neutrino oscillation experiments is only one mass, since the other masses can be determined from the known difference of the squared neutrino masses. In the three-neutrino mixing schemes in Fig. 1, it is convenient to choose as unknown the lightest mass (m_1 in the normal scheme and m_3 in the inverted scheme) and plot the masses as shown in Fig. 3. One can see that, in the normal scheme, if m_1 is small, there is a normal mass hierarchy $m_1 \ll m_2 \ll m_3$. On the other hand, in the inverted scheme, if m_3 is small, there is a so-called "inverted mass hierarchy" $m_3 \ll m_1 \lesssim m_2$, since m_1 and m_2 are separated by the small solar mass splitting. In both schemes, the three neutrino masses are quasi-degenerate for

$$m_3 \gtrsim m_2 \gtrsim m_1 \gg \sqrt{\Delta m^2_{\text{ATM}}} \simeq 5 \times 10^{-2}\,\text{eV}\,. \tag{24}$$

In the next three subsections, we discuss the tree most efficient methods for the determination of the absolute scale of neutrino masses: β decay, cosmological observations and neutrinoless double-β decay.

3.1 Beta Decay

The measurement of the energy spectrum of electrons emitted in nuclear β decay provides a robust kinematical measurement of the effective electron neutrino mass.

Let us consider first, for simplicity, a massive electron neutrino without mixing. In this case, the differential decay rate in allowed[2] β-decays is proportional to the

[2]Allowed β-decays are characterized by the independence of the nuclear matrix element from the electron energy.

square of the Kurie function

$$K(T) = \left[(Q-T) \sqrt{(Q-T)^2 - m_{\nu_e}^2} \right]^{1/2} , \tag{25}$$

where $Q = M_i - M_f - m_e$ (M_i and M_f are, respectively, the masses of the initial and final nuclei and m_e is the electron mass) and $T = E_e - m_e$ is the electron kinetic energy. If $m_{\nu_e} = 0$, the Kurie function is a decreasing linear function of T, going to zero at the so-called "end-point" of the spectrum, $T = Q$, as illustrated by the dotted line in Fig. 4 for tritium β decay. A small electron neutrino mass affects the electron spectrum near the end-point, which shifts to $T = Q - m_{\nu_e}$, as shown by the dashed line in Fig. 4. Therefore, in practice, information on the value of the neutrino mass is obtained looking for a distortion of the Kurie plot with respect to the linear function near the end-point. Using this technique, the Mainz tritium experiment [23] obtained the most stringent upper bound on the electron neutrino mass:

$$m_{\nu_e} < 2.3\,\text{eV} \quad [95\%\,\text{CL}]\,. \tag{26}$$

The Troitzk tritium experiment [24] obtained the comparable bound $m_{\nu_e} < 2.5\,\text{eV}$ [95% CL]. The main reason why tritium β-decay experiments are the most sensitive to the electron neutrino mass is that tritium β-decay has one of the smallest Q-values among all known β-decays. Since the relative number of events occurring in an interval of energy ΔT below the end-point is proportional to $(\Delta T/Q)^3$, a small Q-value is desirable for a maximization of the fraction of decay events that occur near the end-point of the spectrum. Moreover, tritium β-decay is a superallowed transition between mirror nuclei[3] with a relatively short half-life (about 12.3 years), which implies an acceptable number of observed events during the experiment lifetime. Another advantage of tritium β-decay is that the atomic structure is less complicated than those of heavier atoms, leading to a more accurate calculation of atomic effects.

In the case of neutrino mixing, the Kurie function is given by

$$K(T) = \left[(Q-T) \sum_{k=1}^{3} |U_{ek}|^2 \sqrt{(Q-T)^2 - m_k^2} \right]^{1/2} . \tag{27}$$

This is a function of 5 parameters, the three neutrino masses and two mixing parameters (the unitarity of the mixing matrix implies that $\sum_{k=1}^{3} |U_{ek}|^2 = 1$). The main characteristics of the distortion of the Kurie function with respect to the linear function corresponding to massless neutrinos are:

[3]Superallowed transitions are allowed transitions between nuclei belonging to the same isospin multiplet. Mirror nuclei are pairs of nuclei which have equal numbers of protons and neutrons plus an extra proton in one case and an extra neutron in the other. In this case, the overlap of the initial and final nuclear wave functions is close to one, leading to a large nuclear matrix element.

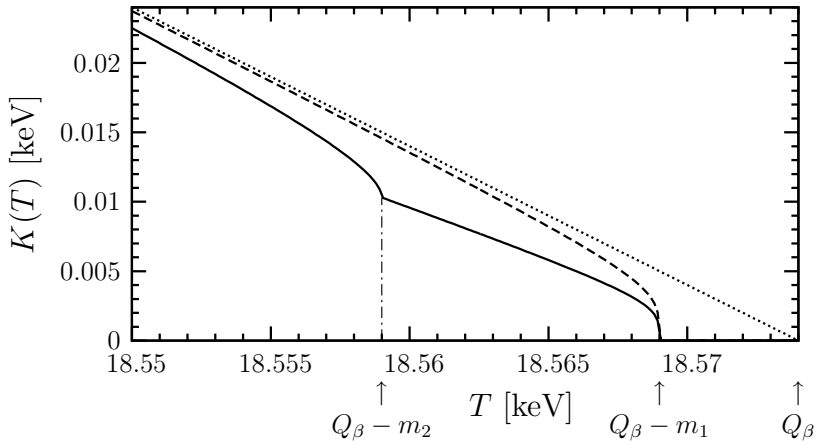

Figure 4: Kurie plot for tritium β decay. Dotted line: the linear Kurie function for $m_{\nu_e} = 0$. Dashed line: Kurie function in Eq. (25) for $m_{\nu_e} = 5\,\text{eV}$. Solid line: Kurie function in Eq. (27) for two-neutrino mixing with $m_1 = 5\,\text{eV}$, $m_2 = 15\,\text{eV}$ and $\vartheta = \pi/4$.

(a) A shift of the end-point of the spectrum from $T = Q$ to $T = Q - m_{\text{lht}}$, calling ν_{lht} the lightest massive neutrino component of ν_e (if $U_{e3} = 0$, $\nu_{\text{lht}} = \nu_1$ in both the normal and inverted schemes; otherwise, $\nu_{\text{lht}} = \nu_1$ in the normal scheme and $\nu_{\text{lht}} = \nu_3$ in the inverted scheme).

(b) Kinks at the electron kinetic energies $T_k = Q - m_k$, for $\nu_k \neq \nu_{\text{lht}}$, with corresponding strength determined by the value of $|U_{ek}|^2$.

This behavior of the Kurie function is illustrated by the solid line in Fig. 4, which describes the case of two-neutrino mixing ($U_{e3} = 0$) with $m_1 = 5\,\text{eV}$, $m_2 = 15\,\text{eV}$ and $\vartheta = \pi/4$ ($|U_{e1}|^2 = |U_{e2}|^2 = 1/2$).

If, in the future, effects of the neutrino masses will be discovered in tritium or other β-decay experiments, a precise analysis of the data may reveal kinks of the Kurie function due to mixing of the electron neutrino with more than one massive neutrino. In this case, the data will have to be analyzed using Eq. (27).

However, so far tritium experiments did not find any effect of the neutrino masses and their data have been analyzed in terms of the one-generation Kurie function in Eq. (25), leading to the upper bound in Eq. (26). How this result can be interpreted in the framework of three-neutrino mixing, in which Eq. (27) holds? The exact expression of $K(T)$ in Eq. (27) cannot be reduced to the one-generation Kurie function in Eq. (25). In order to achieve such a reduction in an approximate way, one must note that, if an experiment does not find any effect of the neutrino masses, its resolution for the measurement of $Q_\beta - T$ is much larger than the values of the neutrino masses.

Considering $m_k l\bar{l} Q_\beta - T$, we have

$$\begin{aligned} K^2 &= (Q-T)^2 \sum_k |U_{ek}|^2 \sqrt{1 - \frac{m_k^2}{(Q-T)^2}} \simeq (Q-T)^2 \sum_k |U_{ek}|^2 \left[1 - \frac{1}{2} \frac{m_k^2}{(Q-T)^2} \right] \\ &= (Q-T)^2 \left[1 - \frac{1}{2} \frac{m_\beta^2}{(Q-T)^2} \right] \simeq (Q-T)^2 \sqrt{1 - \frac{m_\beta^2}{(Q-T)^2}} \\ &= (Q-T) \sqrt{(Q-T)^2 - m_\beta^2} \,, \end{aligned} \tag{28}$$

with m_β given by

$$m_\beta^2 = \sum_k |U_{ek}|^2 m_k^2 \,. \tag{29}$$

The approximate expression of $K(T)$ in terms of m_β is the same as the expression in Eq. (25) of the one-generation Kurie function in terms of m_{ν_e}. Therefore, m_β can be considered as the effective electron neutrino mass in β-decay. In the case of three-neutrino mixing, the upper bound in Eq. (26) must be interpreted as a bound on m_β:

$$m_\beta < 2.3 \, \text{eV} \quad [95\% \, \text{CL}] \,. \tag{30}$$

If the future experiments do not find any effect of neutrino masses, they will provide more stringent bounds on the value of m_β.

In the standard parameterization of the mixing matrix, we have

$$m_\beta^2 = c_{12}^2 \, c_{13}^2 \, m_1^2 + s_{12}^2 \, c_{13}^2 \, m_2^2 + s_{13}^2 \, m_3^2 \,. \tag{31}$$

Although neutrino oscillation experiments do not give information on the absolute values of neutrino masses, they give information on the squared-mass differences Δm_{21}^2 and Δm_{31}^2 and on the mixing angles ϑ_{12} and ϑ_{13} (see Eqs. (10), (11), (15), (16) and (17)). As shown in Fig. 3, the values of the neutrino masses can be determined as functions of the lightest mass (m_1 in the normal scheme and m_3 in the inverted scheme). Therefore, also m_β can be considered as a function of the lightest mass, as shown in Fig. 5. The middle solid lines correspond to the best fit and the extreme solid lines delimit the 2σ allowed range. We have also shown with dashed lines the best-fit and 2σ ranges of the neutrino masses (same as in Fig. 3), which help to understand their contribution to m_β.

From Fig. 5 one can see that, in the case of a normal mass hierarchy (normal scheme with $m_1 l\bar{l} m_2 l\bar{l} m_3$), the main contribution to m_β is due to m_2 or m_3 or both, because the upper limit for m_β is larger than the upper limit for m_2. In the case of an inverted mass hierarchy (inverted scheme with $m_3 l\bar{l} m_1 \lesssim m_2$), m_β has practically the same value as m_1 and m_2. In the case of a quasi-degenerate spectrum, m_β coincides with the approximately equal value of the three neutrino masses in both the normal and inverted schemes.

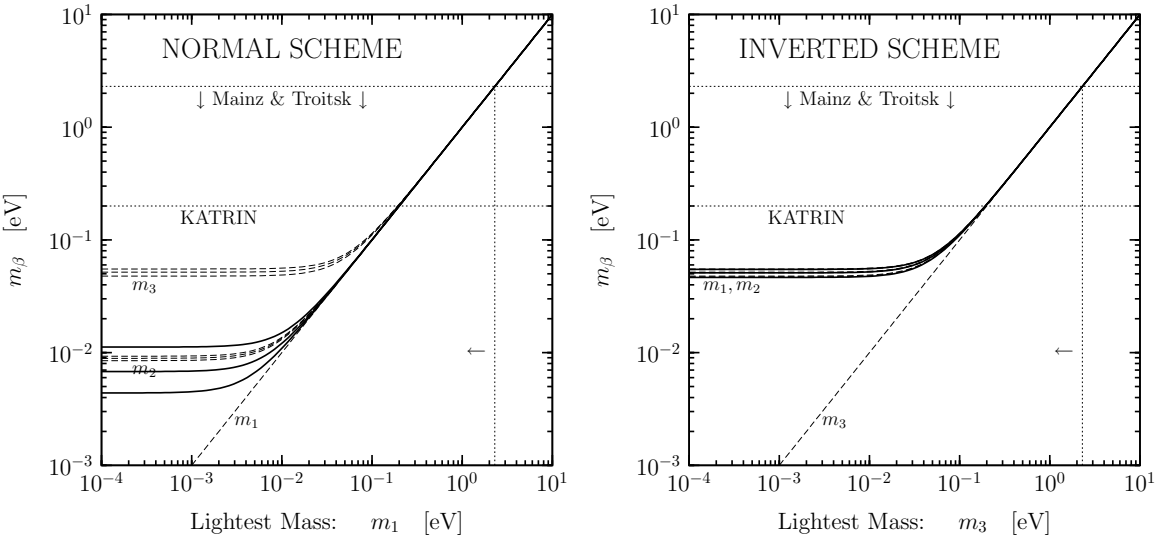

Figure 5: Effective neutrino mass m_β in tritium β-decay experiments as a function of the lightest mass (m_1 in the normal scheme and m_3 in the inverted scheme; see Fig. 1). Middle solid lines correspond to the best-fit values of the oscillation parameters. Extreme solid lines enclose 2σ ranges. Dashed lines show the best-fit values and 2σ ranges of individual masses. In the inverted scheme, the best-fit values and 2σ ranges of m_1 and m_2 are practically the same and coincide with the best-fit value and 2σ range of m_β.

Figure 5 shows that the present experiments and the future KATRIN experiment [25], with an expected sensitivity of about 0.2 eV, give information on the absolute values of neutrino masses in the quasi-degenerate region in both the normal and inverted schemes. From the Mainz upper bound in Eq. (26), for the individual neutrino masses we obtain

$$m_k < 2.3\,\text{eV} \quad [95\%\,\text{CL}]\,, \tag{32}$$

with $k = 1, 2, 3$.

One can note from Fig. 5 that the allowed ranges of m_β in the normal and inverted schemes in the case of a mass hierarchy are quite different and non overlapping: the lower limit for m_β in the inverted scheme is about 4.7×10^{-2} eV, whereas the upper limit for m_β in the normal scheme is about 1.1×10^{-2} eV. If future experiments find an upper bound for m_β which is smaller than about 4.7×10^{-2} eV, the inverted scheme will be excluded, leaving the normal scheme as the only possibility.

Figure 5 shows also that β-decay experiments will not have to improve indefinitely for finding the effects of neutrino masses: the ultimate sensitivity is set at about 4×10^{-3} eV, which is the lower bound for m_β in the case of a normal mass hierarchy.

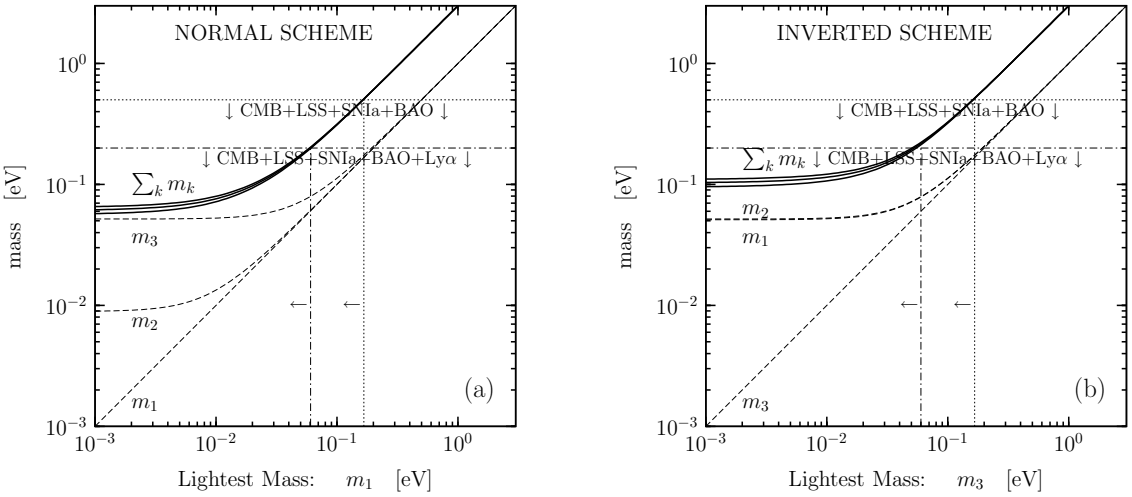

Figure 6: Sum of neutrino masses in the two schemes of three-neutrino mixing indicated by neutrino oscillation data, as a function of the lightest mass (m_1 in the normal scheme in (a) and m_3 in the inverted scheme in (b)). The three solid lines represent the best-fit and 2σ uncertainty band obtained from the squared-mass differences in Eqs. (10) and (11). The two horizontal dotted lines represent the approximate cosmological upper bound range in Eq. (33), and the two vertical dotted lines give the corresponding upper bound range for the lightest mass. The dashed curves show the three individual masses.

Of course, when some β-decay experiment will reveal the effects of neutrino masses, a more complicated analysis using the expression of $K(T)$ in Eq. (27) will be needed. In that case, it may be possible to distinguish between the normal and inverted schemes even if both are allowed (i.e. $m_\beta \gtrsim 4.7 \times 10^{-2}\,\text{eV}$).

3.2 Cosmological Bounds on Neutrino Masses

If neutrinos have masses of the order of 1 eV, they constitute a so-called "hot dark matter", which suppresses the power spectrum of density fluctuations in the early universe at "small" scales, of the order of 1–10 Mpc (see Ref. [26]). The suppression depends on the sum of neutrino masses $\sum_k m_k$.

Recent high precision measurements of density fluctuations in the Cosmic Microwave Background (WMAP) and in the Large Scale Structure distribution of galaxies (2dFGRS, SDSS), combined with other cosmological data, led to stringent upper limits on $\sum_k m_k$, of the order of a fraction of eV [18, 27–29]. The most crucial type of data are the so-called Lyman-α forests, which are absorption lines in the spectra of high-redshift quasars due to intergalactic hydrogen clouds with dimensions of the order of 1–10 Mpc. Unfortunately, the interpretation of Lyman-α data may suffer

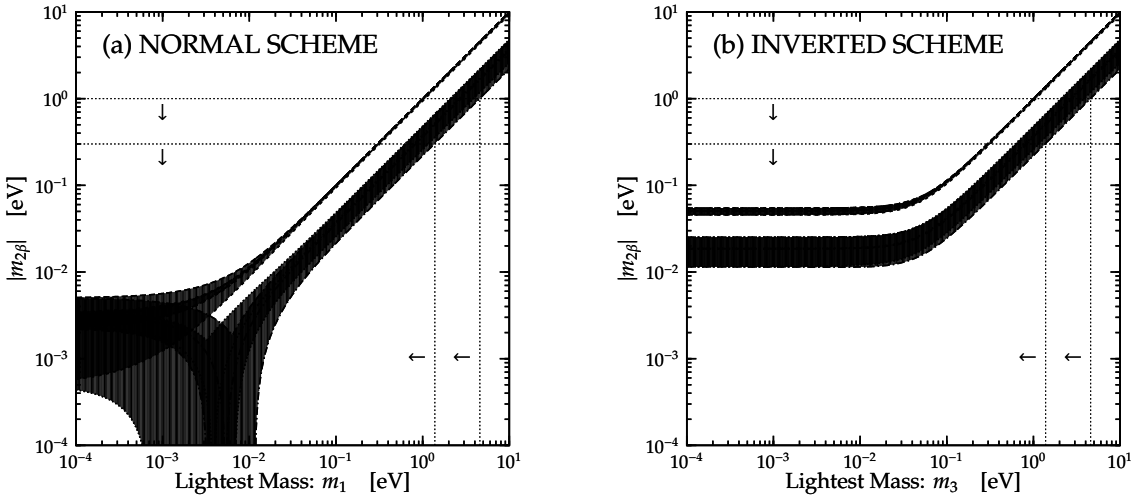

Figure 7: Absolute value $|m_{2\beta}|$ of the effective Majorana neutrino mass in $2\beta_{0\nu}$ decay as a function of the lightest mass m_1 in the normal scheme (a) and m_3 in the inverted scheme (b). The white areas in the strips need CP violation. The two horizontal dotted lines correspond to the extremes of the upper bound range in Eq. (38). The two vertical dotted lines show the corresponding upper bounds for m_1 (a) and m_3 (b).

from large systematic uncertainties. Summarizing the different limits obtained in Refs. [18, 27–29], we estimate an approximate 2σ upper bound

$$\sum_k m_k \lesssim 0.2 - 0.5\,\text{eV}\,, \tag{33}$$

with the extremes reached with or without Lyman-α data. These limits are shown in Fig. 6, where we have plotted the value of $\sum_k m_k$ as a function of the unknown value of the lightest mass, using the values of the squared-mass differences in Eqs. (10) and (11). One can see that cosmological measurements are starting to explore the interesting region in which the tree neutrinos are not quasi-degenerate. In the future, the inverted scheme can be excluded by an upper bound of about $9 \times 10^{-2}\,\text{eV}$ on the sum of neutrino masses.

3.3 Neutrinoless Double-Beta Decay

Neutrinoless double-β decay ($2\beta_{0\nu}$) is a very important process, because it is not only sensitive to the absolute value of neutrino masses, but mainly because it is allowed only if neutrinos are Majorana particles [30, 31]. The observation of neutrinoless double-β decay would represent a discovery of a new type of particles, Majorana particles. This would be a fundamental improvement in our understanding of nature.

Neutrinoless double-β decays are processes of the type $\mathcal{N}(A,Z) \to \mathcal{N}(A,Z\pm2) + e^\mp + e^\mp$, in which no neutrino is emitted, with a change of two units of the total lepton number. These processes are forbidden in the Standard Model. The $2\beta_{0\nu}$ half-life of a nucleus $\mathcal{N}$ is given by (see Refs. [32–35])

$$[T^{0\nu}_{1/2}(\mathcal{N})]^{-1} = G^{\mathcal{N}}_{0\nu} \, |\mathcal{M}^{\mathcal{N}}_{0\nu}|^2 \, \frac{|m_{2\beta}|^2}{m_e^2} \,, \tag{34}$$

where $G^{\mathcal{N}}_{0\nu}$ is the phase-space factor, $\mathcal{M}^{\mathcal{N}}_{0\nu}$ is the nuclear matrix element and

$$m_{2\beta} = \sum_{k=1}^{3} U_{ek}^2 \, m_k \tag{35}$$

is the effective Majorana mass. The phase space factor can be calculated with small uncertainties (see, for example, Table 3.4 of Ref. [32] and Table 6 of Ref. [33]).

In spite of many experimental efforts, so far no experiment observed an unquestionable signal[4]. The most stringent bound has been obtained in the Heidelberg-Moscow ^{76}Ge experiment [41]:

$$T^{0\nu}_{1/2}(^{76}\mathrm{Ge}) > 1.9 \times 10^{25} \, \mathrm{y} \qquad [90\% \, \mathrm{CL}] \,. \tag{36}$$

The IGEX experiment [42] obtained the comparable limit $T^{0\nu}_{1/2}(^{76}\mathrm{Ge}) > 1.57 \times 10^{25}\,\mathrm{y}$ [90% CL]. For the future, many new $2\beta_{0\nu}$ experiments are planned and under preparation (see Refs. [35, 43]), since the quest for the Majorana nature of neutrinos is of fundamental importance.

The extraction of the value of $|m_{2\beta}|$ from the data has unfortunately a large systematic uncertainty, which is due to the large theoretical uncertainty in the evaluation of the nuclear matrix element $\mathcal{M}_{0\nu}$ (see Refs. [34, 35]). In the following, we will use as a possible range for the nuclear matrix element $|\mathcal{M}_{0\nu}|$ the interval which covers the results of reliable calculations listed in Tab. 2 of Ref. [35]:

$$1.5 \lesssim |\mathcal{M}^{^{76}\mathrm{Ge}}_{0\nu}| \lesssim 4.6 \,, \tag{37}$$

which corresponds to an uncertainty of a factor of 3 for the determination of $|m_{2\beta}|$ from $T^{0\nu}_{1/2}(^{76}\mathrm{Ge})$. Using the range (37), the upper bound (36) implies ($G^{^{76}\mathrm{Ge}}_{0\nu} = 6.31 \times 10^{-15}\,\mathrm{y}^{-1}$)

$$|m_{2\beta}| \lesssim 0.3 - 1.0 \, \mathrm{eV} \,. \tag{38}$$

Figure 7 shows the allowed range for $|m_{2\beta}|$ as a function of the unknown value of the lightest mass, using the values of the oscillation parameters in Eqs. (10), (11), (15),

[4] There is a claim of an observation of the $2\beta^-_{0\nu}$ decay of ^{76}Ge with $T^{0\nu}_{1/2}(^{76}\mathrm{Ge}) = 1.19^{+1.00}_{-0.17} \times 10^{25}\,\mathrm{y}$ [36,37]. However, this measurement is rather controversial [38–40]. The issue can only be settled by future experiments (see Ref. [35]).

(16) and (17). One can see that, in the region where the lightest mass is very small, the allowed ranges for $|m_{2\beta}|$ in the normal and inverted schemes are dramatically different. This is due to the fact that in the normal scheme strong cancellations between the contributions of m_2 and m_3 are possible, whereas in the inverted scheme the contributions of m_1 and m_2 cannot cancel, because maximal mixing in the $1-2$ sector is excluded by solar data ($\vartheta_{12} < \pi/4$ at 5.8σ [44]). On the other hand, there is no difference between the normal and inverted schemes in the quasi-degenerate region, which is probed by the present data. From Fig. 7 one can see that, in the future, the normal and inverted schemes may be distinguished by reaching a sensitivity of about $10^{-2}\,\text{eV}$.

4 Conclusions

The results of neutrino oscillation experiments have shown that neutrinos are massive particles, there is a hierarchy of squared mass differences and the mixing matrix is bilarge i.e. with two large and one small mixing angles.

From the theoretical point of view, it is very likely that massive neutrinos are Majorana particles, with a small mass connected to new high-energy physics beyond the Standard Model by a see-saw type relation. An intense experimental effort is under way in the search for neutrinoless double-β decay, which is the most accessible signal of the Majorana nature of massive neutrinos.

Since neutrino oscillations depend on the differences of the squared neutrino masses, the absolute scale of neutrino masses is still not known, except for upper bounds obtained in β decay and neutrinoless double-β decay experiments and through cosmological observations.

The measurement of the effective electron neutrino mass in β decay experiments is robust but very difficult. The future KATRIN experiment [25] will reach a sensitivity of about $0.2\,\text{eV}$.

Cosmological observations have already pushed the upper limit for the sum of the neutrino masses at a few tenths of eV, in the interesting region in which the tree neutrinos are not quasi-degenerate. Significant improvements are expected in the near future (see Ref. [26]), with the caveat that cosmological information on fundamental physical quantities depend on the assumption of a cosmological model and on the interpretation of astrophysical observations.

Let us finally mention that we have not considered the indication of $\overline{\nu}_\mu \to \overline{\nu}_e$ transitions, found in the LSND experiment [45]. This signal is under investigation in the MiniBooNE experiment at Fermilab [46]. This check is important, because a confirmation of the LSND signal could require an extension of the three-neutrino mixing scheme (see Refs. [2, 7]).

Bibliography

[1] S.M. Bilenky and S.T. Petcov, Rev. Mod. Phys. 59 (1987) 671.

[2] S.M. Bilenky, C. Giunti and W. Grimus, Prog. Part. Nucl. Phys. 43 (1999) 1, hep-ph/9812360.

[3] S.M. Bilenky et al., Phys. Rept. 379 (2003) 69, hep-ph/0211462.

[4] C. Giunti and M. Laveder, hep-ph/0310238.

[5] E. Majorana, Nuovo Cim. 14 (1937) 171.

[6] S.M. Bilenky and B. Pontecorvo, Phys. Rept. 41 (1978) 225.

[7] M. Gonzalez-Garcia and Y. Nir, Rev. Mod. Phys. 75 (2003) 345, hep-ph/0202058.

[8] M. Maltoni et al., New J. Phys. 6 (2004) 122, hep-ph/0405172.

[9] G.L. Fogli et al., hep-ph/0506083.

[10] A. Strumia and F. Vissani hep-ph/0606054.

[11] P. Minkowski, Phys. Lett. B67 (1977) 421.

[12] T. Yanagida, Workshop on the Baryon Number of the Universe and Unified Theories, Tsukuba, Japan, 13-14 Feb 1979.

[13] M. Gell-Mann, P. Ramond and R. Slansky, In 'Supergravity', p. 315, edited by F. van Nieuwenhuizen and D. Freedman, North Holland, Amsterdam.

[14] R.N. Mohapatra and G. Senjanovic, Phys. Rev. Lett. 44 (1980) 912.

[15] G. Altarelli and F. Feruglio, Phys. Rept. 320 (1999) 295, hep-ph/9905536.

[16] S. Weinberg, Phys. Rev. Lett. 43 (1979) 1566.

[17] G. Costa and F. Zwirner, Riv. Nuovo Cim. 9N3 (1986) 1.

[18] G. Fogli et al., hep-ph/0608060.

[19] S.M. Bilenky and C. Giunti, Phys. Lett. B444 (1998) 379, hep-ph/9802201.

[20] C. Bemporad, G. Gratta and P. Vogel, Rev. Mod. Phys. 74 (2002) 297, hep-ph/0107277.

[21] A. Blondel et al., hep-ph/0606111.

[22] P.F. Harrison, D.H. Perkins and W.G. Scott, Phys. Lett. B530 (2002) 167, hep-ph/0202074.

[23] C. Kraus et al., Eur. Phys. J. 40 (2005) 447, hep-ex/0412056.

[24] V.M. Lobashev et al., Phys. Lett. B460 (1999) 227.

[25] KATRIN, L. Bornschein et al., eConf C030626 (2003) FRAP14, hep-ex/0309007, XIII Physics in Collision Conference(PIC03), Zeuthen, Germany, June 2003.

[26] J. Lesgourgues and S. Pastor, Phys. Rept. 429 (2006) 307, astro-ph/0603494.

[27] A. Goobar et al., JCAP 0606 (2006) 019, astro-ph/0602155.

[28] WMAP, D. Spergel et al., astro-ph/0603449.

[29] U. Seljak, A. Slosar and P. McDonald, astro-ph/0604335.

[30] J. Schechter and J.W.F. Valle, Phys. Rev. D25 (1982) 2951.

[31] E. Takasugi, Phys. Lett. B149 (1984) 372.

[32] M. Doi, T. Kotani and E. Takasugi, Prog. Theor. Phys. Suppl. 83 (1985) 1.

[33] J. Suhonen and O. Civitarese, Phys. Rept. 300 (1998) 123.

[34] O. Civitarese and J. Suhonen, Nucl. Phys. A729 (2003) 867, nucl-th/0208005.

[35] S.R. Elliott and J. Engel, J. Phys. G30 (2004) R183, hep-ph/0405078.

[36] H.V. Klapdor-Kleingrothaus et al., Mod. Phys. Lett. A16 (2001) 2409, hep-ph/0201231.

[37] H. Klapdor-Kleingrothaus et al., Phys. Lett. B586 (2004) 198, hep-ph/0404088.

[38] F. Feruglio, A. Strumia and F. Vissani, Nucl. Phys. B637 (2002) 345, hep-ph/0201291.

[39] C.E. Aalseth et al., Mod. Phys. Lett. A17 (2002) 1475, hep-ex/0202018.

[40] A. Bakalyarov et al., Phys. Part. Nucl. Lett. 2 (2005) 77, hep-ex/0309016.

[41] H.V. Klapdor-Kleingrothaus et al., Eur. Phys. J. A12 (2001) 147.

[42] IGEX, C.E. Aalseth et al., Phys. Rev. D65 (2002) 092007, hep-ex/0202026.

[43] C. Aalseth et al., hep-ph/0412300.

[44] J.N. Bahcall, M.C. Gonzalez-Garcia and C. Pena-Garay, JHEP 08 (2004) 016, hep-ph/0406294.

[45] LSND, A. Aguilar et al., Phys. Rev. D64 (2001) 112007, hep-ex/0104049.

[46] M. Sorel, hep-ex/0602018.

Majorana Neutrinos

Fernando Ferroni
Department of Physics
Università di Roma La Sapienza & INFN Sezione di Roma
I-00185 Roma, ITALY

1 Introduction

Mysteries about neutrinos are several and of different nature. We know that they are neutral particles with an extraordinary little mass compared to the one of all the others. Although they are massive we have not succeeded yet in measuring their mass. We do not know if the neutrino is a particle different from its antiparticle or rather as hypothesized [1] by Majorana in 1937 they are the same particle. Majorana observed that the minimal description of spin 1/2 particles involves only two degrees of freedom and that such a particle, absolutely neutral, coincides with its antiparticle. If the Majorana conjecture holds then it will be possible to measure an extremely fascinating and rare process that takes the name of Neutrinoless Double Beta Decay (0ν DBD). The net effect of this ultra rare process will be to transform two neutrons in a nucleus into two protons and simultaneously to emit two electrons. Since no neutrinos will be present in the final state the sum of the energy of the two electrons will be a line. The rate of this yet unobserved phenomenon will also allow a determination, although not precise, of the neutrino mass. A set of pioneering experiments [2] has been performed for this search. With the exception of one, all of them resulted into a negative observation. The one claiming a positive evidence [3] (about 4σ) has not fully convinced the community and it is waiting for a possible confirmation. A new generation of experiments is in preparation [4] for challenging this difficult problem. In this paper, one of them will be described in some detail. It is CUORE [5], a concept extrapolated from a running prototype (CUORICINO [6]) that will be functional around 2010 with a sensitivity such to be able to probe the inverted hierarchy region as described by the most recent analyses [8] of the global neutrino data.

2 Majorana Neutrinos and Double Beta Decay

Neutrinoless double-beta decay is an old subject. What is new is the fact that, recently, neutrino oscillation experiments have unequivocally demonstrated that neutrinos have mass and that the neutrino mass eigenstates mix. Indeed the massive

nature of neutrinos is a key element in resurrecting the interest for the Majorana conjecture. The difference between Dirac neutrinos and Majorana ones is shown in Fig. 1. The practical possibility to test the Majorana nature of neutrinos is indeed

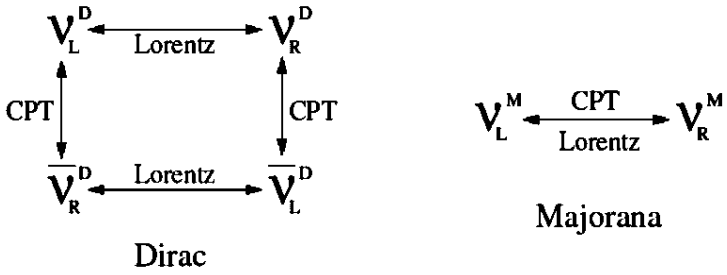

Figure 1: Dirac and Majorana neutrinos

in detecting the process shown in Fig. 2, the Double Beta Decay (DBD) without emission of neutrinos.

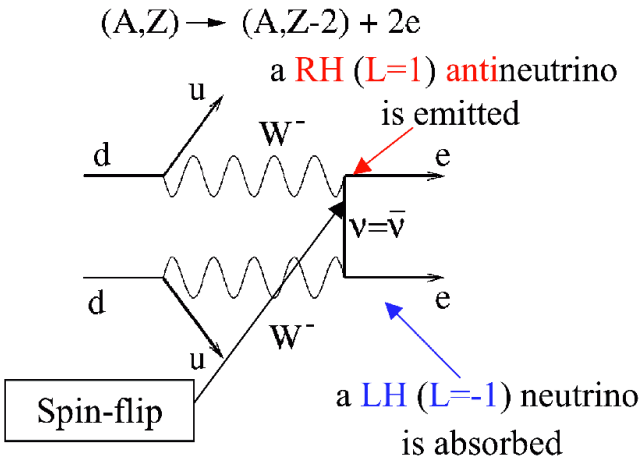

Figure 2: Neutrinoless Double Beta Decay diagram

Although the possibility [7] for this process was pointed out by W. Furry far in the past the experimental search looked just impossible. The key element for the process to occur is in fact in the helicity flip needed. As long as the neutrino was thought to be massless this could just not happen. Nowadays we know that this is indeed possible. The discriminant between Dirac and Majorana neutrinos is in the lepton flavour conservation, required by Dirac and violated by Majorana. So that the observation of neutrinoless DBD would be the proof of the Majorana conjecture. The oscillation

experiments have yielded valuable information on the mixing angles and on the mass differences of the three eigenstates. They cannot, however, determine the scale of the neutrino mass, which is fixed by the lightest neutrino mass eigenvalue. This can only be directly determined by beta decay end point spectral shape measurements, or in the case of Majorana neutrinos, by the observation and measurement of the neutrinoless double-beta decay half-life. The oscillation experiments yield values for the mixing angles and mass differences accurate enough to allow the prediction of a range of values of the effective mass of the Majorana electron neutrino. As a function of the oscillation parameters indeed we find that

$$m_{\beta\beta} = \Sigma m_{\nu_k} U_{ek}^2 = cos^2\theta_{13}(m_1 cos^2\theta_{12} + m_2 e^{2i\alpha} sin^2\theta_{12}) + m_3 e^{2i\beta} sin^2\theta_{13}$$

According to most theoretical analyses of of present neutrino experiment results, next-generation DBD experiments with mass sensitivities of the order of 10 meV may find the Majorana neutrino if its mass spectrum is of the quasi- degenerate type or it exhibits inverted hierarchy.

3 Experimental techniques

The DBD are extremely rare processes. In the two neutrino decay mode their half-lives range from $T_{1/2} \simeq 10^{18} y$ to 10^{25} y. The rate for this process will go as

$$1/\tau = G(Q, Z)|M_{nucl}|^2 m_{\beta\beta}^2$$

// The first factor (phase space) that goes like Q^5 is easily calculated. The second (nuclear matrix element) is hard to compute. Several calculation made under different approaches exist and they differ as much as two order of magnitude. The experimental investigation of these phenomena requires a large amount of DBD emitter, in low-background detectors with the capability for selecting reliably the signal from the background. The sensitivity of an experiment will go as $S^{0\nu} \propto a(\frac{MT}{b\Delta E})^{1/2}\epsilon$. Isotopic abundance (a) and efficiency (ϵ) will make you gain linearly, while mass (M) and time (T) only as the square root. Also background level (b) and energy resolution (ΔE) behaves as a square root. In the case of the neutrinoless decay searches, the detectors should have a sharp energy resolution, or good tracking of particles, or other discriminating mechanisms. There are several natural and enriched isotopes that have been used in experiments with tens of kilograms. Some of them could be produced in amounts large enough to be good candidates for next generation experiments. The choice of the emitters should be made also according to its two-neutrino half-life (which could limit the ultimate sensitivity of the neutrinoless decay), according also to its nuclear factor-of-merit and according to the experimental sensitivity that the detector can achieve. The element has to be chosen amongst the one in the following table 3.

Isotope	$Q_{\beta\beta}$ (MeV)	Isotopic abundance (%)
^{48}Ca	4.271	0.0035
^{76}Ge	2.039	7.8
^{82}Se	2.995	9.2
^{96}Zr	3.350	2.8
^{100}Mo	3.034	9.6
^{116}Cd	2.802	7.5
^{128}Te	0.868	31.7
^{130}Te	2.533	34.5
^{136}Xe	2.479	8.9
^{150}Nd	3.367	5.6

Figure 3: Candidate elements for 0ν DBD

Double beta decay experiments can be divided into two main categories (see Fig. 4): measurement with source being separate from the detector and measurement with a detector that also acts as the source.

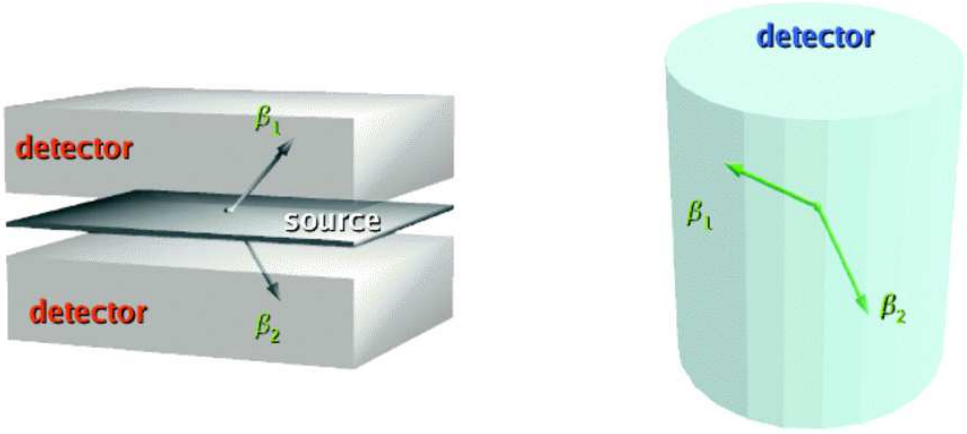

Figure 4: Schematics of main DBD detector types

When the source is the same as the detector (calorimetric type) , source mass is maximized while materials that could potentially contribute to the background is minimized. Also energy resolution can be optimized. However the absence of topological signature does not allow to reject on the event-by-event basis the background coming from photons. Conversely the other type of detectors (spectrometer type) can optimize the background rejection although at the cost of a reduced mass, a complicate geometry and a comparatively worse energy resolution. Bolometers belong to the

calorimetric category. At low temperatures (the operating temperature for CUORICINO is 8 mK), the heat capacity of crystals is proportional to the cube of the ratio of the operating and Debye temperatures. The energy released in a single particle interaction within the crystal is clearly measurable as change in temperature of the entire crystal by using neutron transmutation doped (NTD) germanium thermistors which are optimized to operate at these temperatures.

A number of experiments are currently at various stages of development to probe the degenerate and into the inverted mass hierarchy region of the neutrino mass spectrum.

All of them are needed since it is imperative to carry out double beta decay searches in multiple isotopes, both to improve the nuclear matrix calculations necessary to extract the effective neutrino mass, and to ensure that the observation of a line at the expected energy is not a result of a yet unknown radioactivity line.

4 CUORICINO and CUORE

Cryogenic bolometers, with their excellent energy resolution, flexibility in material, and availability in high purity of material of interest, are excellent detectors for search for neutrinoless double beta decay. Kilogram-size single crystals (cubic crystals of 5cm side) for TeO_2 are now available and utilized in CUORICINO in an array for a total detector mass of 40 kg. CUORICINO results from a total exposure of 8.38 kg-yr of

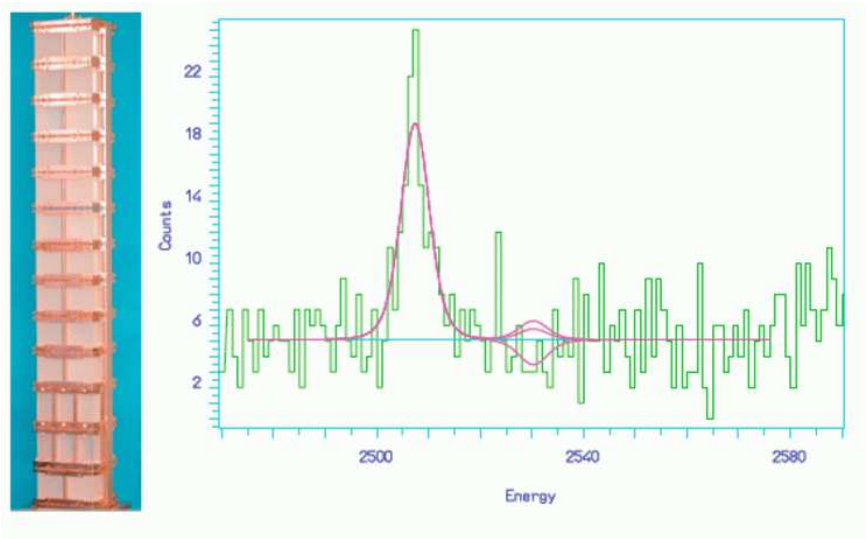

Figure 5: CUORICINO sketch (left) and results (right)

^{130}Te (Fig. 5) show no evidence for a peak at 2530 keV, the expected Q-value for for

^{130}Te. The absence of any excess events above backgrounds in the region of interest gives a limit of $T_{1/2} \geq 2.4 \times 10^{24}$ yr(90%) C.L. on the 0ν decay rate of ^{130}Te. This corresponds to an effective neutrino mass of $m_{\beta\beta} \leq 0.18 - 0.94$ eV, the range reflecting the spread in nuclear matrix element calculations. The background measured in the region of interest is 0.18 ± 0.01 counts/keV/kg/yr. CUORE (Cryogenic Underground Observatory for Rare Events), to be located at the Gran Sasso National Laboratory of INFN (LNGS) , at a depth of 3400 m.w.e., will consist of 988 bolometers of TeO_2 crystals, with a total mass of 740 kg. Because of the high isotopic abundance (34%), 204 kg of ^{130}Te will be available for the relevant process without isotopic enrichment, a virtue that eliminates the requirement for the very expensive process needed in all of the other proposed next generation experiments, making CUORE both timely and significantly less expensive than other experiments. CUOREÕs modular design (see Fig. 6) and flexibility of cryogenic detector will also allow future searches in other isotopes of interest.

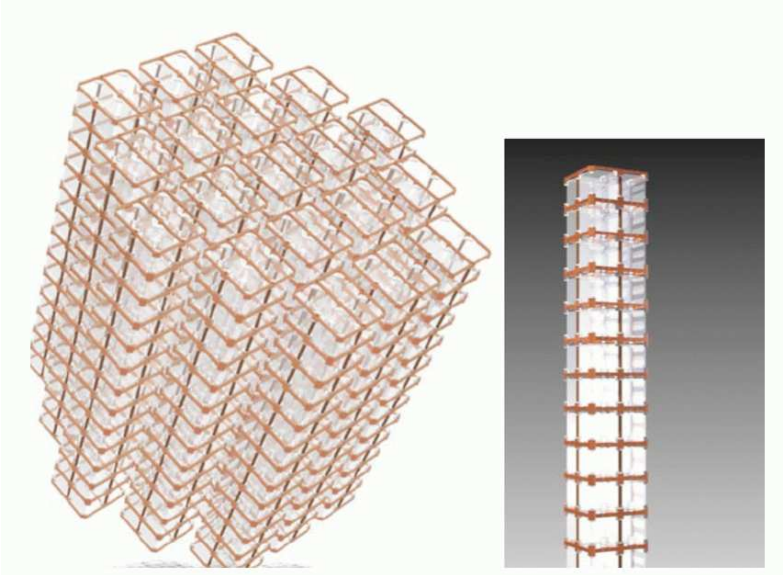

Figure 6: CUORE design

The extrapolation from CUORICINO results to CUORE expectation is based on the following facts:

- a total mass 20 times larger
- a running time 10 times longer
- an energy resolution 50% better

- a background 20 times smaller

The major challenge in obtaining the desired sensitivity is the reduction of the background rate. This task can be accomplished in three main ways: 1) By reducing the amount of material (Cu in our case) surrounding the crystals. 2) By a proper cleaning procedure of all the materials that will be in contact or will ÒseeÓ the crystals. 3) By finding a veto procedure to eliminate unwanted signals coming from outside the bolometer. The results so far available from the CUORICINO understanding, the dedicated *R&D* performed in a dedicated cryogenic facility running at LNGS and the MonteCarlo simulations indicate that a factor 10 has been already secured. The sensitivity, in term of neutrino mass and taking into account the entire set of matrix elements calculation available, is $m_{\beta\beta} \approx 19 - 100$ meV.

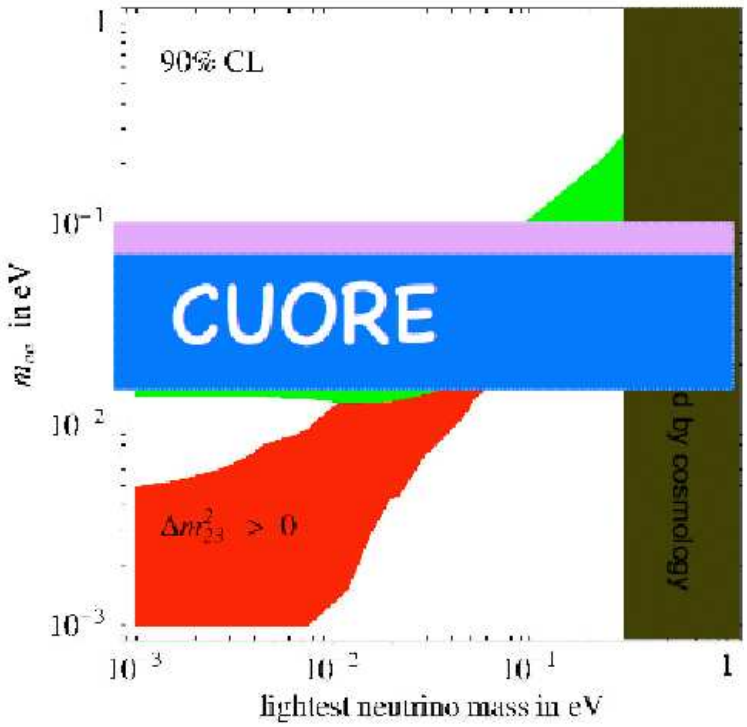

Figure 7: CUORE projected sensitivity to $m_{\beta\beta}$

5 Conclusion

Neutrino physics is one of the leading field of the high energy research today. One of the top question that has to be answered is about the Dirac or Majorana nature of

neutrino mass. The neutrino-less double beta decay search is the only experimental line that can answer this fundamental question and that might possibly be the sole chance to provide a measure of neutrino mass. Cryogenic bolometer, with its flexibility in material choice and the ability to scale up to the ton- scale makes it an ideal technology for large-scale detector for double-beta physics experiments. CUORICINO is currently running as the most sensitive experiment. Much of the technology has been tested for CUORE that will start taking data in 2010 with much a larger mass. The sensitivity of CUORE will allow probing a good portion of the mass region predicted in case of inverted hierarchy. The proof of the Majorana nature of the neutrinos might be achieved by CUORE together with a determination of the neutrino mass scale.

6 Acknowledgments

I am deeply indebted to Prof. E. Fiorini and all my colleagues in CUORE. The list of their names is found in [5].

Bibliography

[1] E. Majorana, Il Nuovo Cimento, **14**, 171, (1937).

[2] See for example presentations at NeutrinoÕ06 by M. Hirsch, F. Simkovic, S. Elliott, and A. Barabash.

[3] H. V. Klapdor-Kleingrothaus et al., Nucl. Instrum. Meth., **A522**, 371 (2004).

[4] Ph. Adamson et al., EoI in the SuperNemo double beta decay program, 2004; I. Abt et al., GERDA Technical Proposal, 2005; C.E. Alseth et al., The proposed Majorana ^{76}Ge double beta decay experiment, Nucl. Phys. Proc. Suppl., **138**, 217 (2005); H. Ejiri et al., Double Beta Decays and solar neutrinos with ^{100}Mo, 2005; D. Akimov et al., EXO: An Advanced Enriched Xenon double-beta decay Observatory, Nucl. Phys. Proc. Suppl., **138**, 224 (2005).

[5] R. Ardito et al., hep-ex/0501010.

[6] R. Alessandrello et al., Nucl. Phys. Proc. Suppl., **87**, 78 (2000).

[7] W. H. Furry, Phys. Rev., **56**, 1184 (1939)

[8] A. Strumia and F. Vissani, Nucl. Phys. **B276**, 294 (2005).
G. L. Fogli et al., Prog. Part. Nucl. Phys. , **57**, 742 (2006).

Astrophysical Neutrinos at Low Energies

Lothar Oberauer
Physikdepartment E15
TU München
85748 Garching, Germany

1 Solar Neutrinos

The measurement of the total flux of solar neutrinos in the GALLEX, GNO [1], and SAGE [2] experiments was a milestone in understanding the basics of the pp-fusion cycle in the center of the sun. Furthermore it was the first evidence for physics beyond the standard model as astrophysical explanations for the observed deficit on the solar ν_e flux were ruled out. Now, after SNO [3] and the reactor experiment KamLAND [4] it is known, that neutrinos oscillate. For the first time neutrino flavor transition has been measured by SNO with an accuracy of about 7 sigma. The survival probability of the high energy solar ^{8}B-neutrinos has been determined to be $(34 \pm 4)\%$. In GALLEX and GNO the survival probability for all solar neutrinos was measured to be $(55 \pm 5)\%$. This difference is a clear hint for matter effects inside the sun as it was predicted by the MSW-mechanism [5]. Low energy solar neutrinos are driven by vacuum oscillations, whereas neutrinos with $E_\nu >$MeV are dominated by matter enhanced flavor transitions. The corresponding oscillations parameter are: $\delta m^2_{21} = m^2_2 - m^2_1 = (+7.9 \pm 0.7)\, eV^2$ and $tan^2\Theta = (0.45 \pm 0.05)$. Solar neutrino spectroscopy revealed a positive sign of δm^2_{21}, because otherwise the MSW effect would not work. Therefore we know that $m_2 > m_1$. It is amazing how experiments which were primary designed to solve astrophysical problems shed light on intrinsic neutrino parameter which could not be approached otherwise.

Future of solar neutrino spectroscopy

Up to now solar neutrino spectroscopy for the high energetic ^{8}B-branch has been performed. The main goal for next future experiments like BOREXINO [6] and KamLAND [7] is the measurement of the monoenergetic ^{7}Be-neutrino flux and neutrinos from other sources in the low energy range. An accuracy of 10% in the measurement of the ^{7}Be-ν rate would lead to a 1% precision for the pp-neutrino flux stemming from the primary $p+p \rightarrow^2 D+\nu_e$ fusion reaction, by taking into account the solar luminosity. As the theoretical uncertainty of the neutrino flux from this branch is also in the

1% range, precise tests of solar models would become possible. In addition the first determination of the CNO-branch would be of major astrophysical interest. Recent results from the LUNA experiment on the $^{14}N(p,\gamma)^{15}O$ fusion reaction [8] lowered the CNO-neutrino flux prediction by a factor ∼2. This would imply an increase for the estimation of the age of globular clusters by 0.7 to 1 Gy.

Measuring the ^{7}Be-flux can be used also to search for new neutrino interactions [9]. In the standard picture including neutrino oscillations a ^{7}Be-neutrino event rate due to elastic scattering on electrons ($\nu + e^- \rightarrow \nu + e^-$) of about 30 counts per day is expected in BOREXINO with a fiducial volume of $110\,m^3$ of liquid scintillator. The recoil electrons from the reaction above will give rise to a sharp Compton-like edge in the energy distribution at 660 keV. Flavor changing neutral current interaction should alter this rate significantly towards lower values.

Besides low energy solar neutrinos BOREXINO is aiming for measuring terrestrial neutrinos as well as neutrinos from European reactors. Here the inverse beta reaction $\overline{\nu}_e + p \rightarrow e^+ + n$ would be used, taking advantage from the delayed coincidence method provided by the prompt positron signal and delayed neutron capture ($n + p \rightarrow^2 D + \gamma$, $E_\gamma = 2.2$ MeV). This clear signature is extremely helpful to reject background events. Between 30 and about 60 counts per year are expected from both sources, depending mainly on geophysical models. The maximal energy of terrestrial neutrinos, stemming from beta decays in the U- and Th-chains, is about 3 MeV, whereas the reactor neutrino spectrum ends at about 8 MeV. Hence, the contributions from both sources can be separated simply by their energy distributions. The measurement of terrestrial neutrinos will reveal information about the content of U and Th in the Earth, while the reactor neutrinos can be used to probe the KamLAND result.

In addition BOREXINO would register about 100 events in case a supernova explosion of type II will happen in the center of our galaxy. With an artificial neutrino source a search for a neutrino magnetic moment will be performed. In 2006 the detector was filled with water and first Cherenkov-events due to high energy accelerator neutrinos from CERN have been observed. Several purification methods have been tested in the "Counting Test Facility" (CTF). With the CTF new limits on the $\overline{\nu}_e$-flux from the sun have been established [10]. Only one background event have been found in a measuring period of about 2 years. It is planned to fill BOREXINO with liquid scintillator in the beginning of 2007 and to start data taking in the same year.

2 Atmospheric Neutrinos

The first evidence for neutrino oscillations came from the Super-Kamiokande (SK) Collaboration in 1998. Atmospheric neutrinos are decay products of pions, kaons (and the generated muons) which are produced in collisions of primary cosmic ray particles with nuclei of the upper atmosphere. Therefore the ratio R of muon neutrinos to elec-

tron neutrinos is expected to be $R = (\nu_\mu + \overline{\nu}_\mu)/(\nu_e + \overline{\nu}_e)$ 2. The atmospheric neutrino problem had been under investigation since the 1980's by various experiments, e.g. by the water Cherenkov detectors Kamioka and IMB, who reported $R_{measured}/R_{theory}$ 0.6 and by the iron calorimeters NUSEX and FREJUS who observed $R_{measured}/R_{theory}$ 1. The situation became clearer after 1996 when the 50kton water cerenkov detector Super-Kamiokande [11] started operating and eventually collected enough statistics to perform a zenith angle analysis of the observed electron neutrino and muon neutrino events (In the SK-I data set over 11000 events are used in the oscillation analysis). The zenith angle is defined as the angle between the zenith direction and the direction of the observed neutrino. It turned out that while the number of downward muon events is as expected, the number of upward muon events is significantly reduced. The number of electron events both upward and downward behaves as expected. Because the zenith angle of an event corresponds to the distance L of the neutrino traveled between its creation and detection, the oscillation probability of a neutrino which depends on L, will also depend on the zenith angle. The Super-Kamiokande zenith angle distributions for muon events are in excellent agreement with the neutrino oscillation hypothesis. All observations are compatible with the assumption of $\nu_\mu \rightarrow \nu_\tau$ oscillations. The possibility of $\nu_\mu \rightarrow \nu_e$ oscillations was ruled out by the reactor experiment Chooz [12], and oscillations into sterile neutrinos are disfavoured by the observations of neutral current events in SuperKamiokande as expected in the $\nu_\mu \rightarrow \nu_\tau$ szenario. In addition oscillations into sterile neutrinos would lead to matter effects which would generate different spectral distributions compared to those which have been observed. The oscillation hypothesis is confirmed by a recent L/E analysis of the SuperKamiokande data as well as by the accelerator experiments K2K [13] and Minos [14].

3 Supernova Neutrinos

Solar neutrino physics opened the window to astrophysical observations where neutrinos are used as probes. Indeed the basic idea of thermal nuclear fusion as source for stellar energies was proven by detecting solar neutrinos and in future important details about the pp- and the CNO-cycle may be revealed by new experiments in this field. The first neutrino signal outside of our solar system, even outside from our galaxy was observed in February 1987 when a blue giant star in the Large Magellanic Cloud exploded as a supernova type II at a distance of about 50kpc (ca. 150 light years). In total 19 neutrino events were recorded in two large water Cherenkov detectors (Kamioka, Japan, and IMB, USA) within a time window of about 20 seconds [15]. This observation allowed for the first time to measure the energy release of a gravitational collapse, as about 99% of the total gravitational energy is emitted in neutrinos. In spite of the small number of events the basic idea about the mechanism

of a supernova of this nature (i.e. SN-type II) was confirmed. With running detectors, like SuperKamiokande, a supernova type II explosion in our galaxy would be accompanied by a neutrino signal of about 15,000 events. Hence, the development of a gravitational collapse could be followed in great detail. In order to measure flavor dependent fluxes different nuclei as target for neutrino are proposed. In LENA (Low Energy Neutrino Astronomy) a large liquid scintillator detector (total mass around 50kt) is proposed to serve as detector for supernova neutrinos [16]. Here neutrino interactions on protons as well as on ^{12}C could be used which would allow to disentangle the flavor composition of a supernova burst in time and energy. Besides large liquid scintillator detectors water Cherenkov tanks with huge target masses close to 1 Mt (e.g. Hyperkamiokande in Japan, MEMPHIS in Europe, UNO in the USA) as well as 100 kt liquid Argon devices are proposed for future Supernova neutrino detection. The Argon detector GLACIER would open the possibility to detect the electron neutrino content with great statistics. In Europe physicists are working together in the LAGUNA [17] project (Large Apparatus for Grand Unification and Neutrino Astronomy) to explore the physical potential and the technical feasibility of all three approaches.

From all past supernova type II explosions in our universe one expects a low background of relic supernova neutrinos. Up to now only upper limits on the flux of those SNR-neutrinos (electron anti-neutrinos; detection via $\overline{\nu}_e p \rightarrow e^+ n$) are reported. In LENA or in a modified SuperKamiokande detector (Gd-loaded water) the detection of SNR-ν could succeed. After 10 years of measurement with LENA the spectral shape of the SNR-$\overline{\nu}_e$ flux could be determined in the energy window between 10 MeV and 30 MeV and details about gravitational collapses as well as the star formation in the early universe would be explored [16]. The lower energy limit is due to the world wide neutrino emission in nuclear power plants, whereas the upper bound is given by the background of atmospheric neutrinos.

This work was partly supported by the Deutsche Forschungsgemeinschaft DFG within the Sonderforschungsbereich SFB 375 Astro- Particle Physics.

Bibliography

[1] M. Altmann et al. (GNO coll.), Phys.Lett. B **616** 174 (2005).

[2] J.N. Abdurashitov et al. (SAGE coll.), Phys. Rev. Lett. **83** 4686 (1999).

[3] B. Aharmim et al. (SNO coll.), Phys. Rev. C **72** 055502 (2006).

[4] T. Araki et al. (KamLAND coll.), Phys. Rev. Lett. **94** 081801 (2005).

[5] L. Wolfenstein, Phys. Rev. **D17**, 2369 (1978); S.P. Mikheev and A. Yu. Smirnov, Sov. J. Nucl. Phys. **42**, 913 (1985).

[6] G. Alimonti et al. (BOREXINO coll.), Astropart. Phys. **16** 205 (2002).

[7] A. Suzuki, for the KamLAND coll., 3rd International Workshop on NO-VE: Neutrino Oscillations in Venice: 50 Years after the Neutrino Experimental Discovery, Venice, Italy, 7-10 Feb (2006).

[8] D. Bemmerer et al. (LUNA coll.), Euro. Phys. J. **A27** 161 (2005).

[9] A. Friedland et al., Phys.Rev. **D70** 111301 (2004).

[10] M. Balata et al. (BOREXINO coll.), Eur. Phys. J. **C47** 21 (2006).

[11] Y. Fukuda et al., (SuperKamiokande coll.), Phys. Rev. Lett. **81** 1562 (1998).

[12] M. Apollonio et al., (Chooz coll.), Phys. Lett. **B 420** 397 (1998).

[13] K. Nishikawa, Nucl. Phys. B (Proc. Suppl.) **118** 129 (2003).

[14] D.G. Michael et al., (MINOS coll.), Phys. Rev. Lett. **97** 191801 (2006).

[15] K. Sato, H. Suzuki, Phys. Rev. Lett. **58** 2722 (1987).

[16] M. Wurm et al., Phys. Rev. **D75** 023007 (2007).

[17] J.E. Campagne et al., (LAGUNA coll.) to be published (2007).

Neutrinos; Opportunities and Strategies in the Future

Hisakazu Minakata
Department of Physics
Tokyo Metropolitan University
Hachioji, Tokyo 192-0397, Japan

1 Introduction

Neutrino physics, in particular its experimental part, has been extremely successful in the last 10 years. It would be worthwhile to look it back on this occasion as a prologue to our discussion on the future. In 1998 the Super-Kamiokande atmospheric neutrino observation confirmed [1] the smoking gun evidence for atmospheric neutrino anomaly seen in the deficit of the rate and in the zenith angle distribution of ν_μ induced events in the Kamiokande experiment [2]. It was the first evidence for mass-induced neutrino oscillation.[1] The evidence for neutrino oscillation was readily confirmed by the first long-baseline (LBL) accelerator neutrino experiment K2K [6] using man-made ν_μ beam. In this sense, the first corner stone was placed in the 2-3 sector of the lepton flavor mixing matrix, the MNS matrix [5]. It established surprisingly that the mixing angle θ_{23} is large, which may even close to the maximal, refuting the prejudice of small flavor mixing angles deeply rooted among theorists at that time.

On the other hand, there have been great amount of efforts in the solar neutrino observation pioneered by Davis with his ^{37}Cl experiment in sixties which was developed in close collaboration with the devoted theorist [7]. In the last 20 years the field has been enriched by participation by Kamiokande, Ga, Super-Kamiokande, and SNO experiments [8]. In particular, the latter two experiments were united to the confirm the particle physics nature of the solar neutrino problem, the evidence for solar neutrino flavor transformation [9]. Later SNO *in situ* confirmed the evidence [10]. I would like to note here that the deficit of the ^{8}B flux obtained by Davis in his ^{37}Cl experiment [11], though suffered from stubborn skepticism for more than 30 years, was convincingly confirmed by the SNO charged current (CC) measurement. The

[1]The history of theory of neutrino oscillation is somewhat involved. In 1957 Pontecorvo [3] discussed $\nu \leftrightarrow \overline{\nu}$ oscillation in close analogy to $K^0 \leftrightarrow \overline{K}^0$ oscillation [4]. In 1962 Maki, Nakagawa, and Sakata [5] first pointed out the possibility of neutrino flavor transformation, the phenomenon established experimentally only recently as described here.

beautiful finale of the solar neutrino problem came with KamLAND [12] which identified its cause as due to the mass-induced neutrino oscillation which clearly pinned down the large mixing angle (LMA) MSW solar neutrino solution [13]. The particular significance of the KamLAND result in this context, so called the KamLAND massacre (of non-standard scenarios), was emphasized by many people with detailed analysis for example in [14]. The resultant mixing angle θ_{12} turned out to be large, but not maximal.

Finally, several experiments, Super-Kamiokande [15], KamLAND [16], K2K [17], and MINOS [18], observed the oscillatory behavior, thereby established the phenomenon of mass-induced neutrino oscillation. At this moment, it constitutes the first and the unique evidence for physics beyond the Standard Model.

What is the next? The most common answer, which I also share, is to explore the unknown 1-3 sector, for which the only knowledge we have is the upper bound on θ_{13} [19,20]. Discovery of leptonic CP violation must throw light on tantalizing mystery of interrelationship between quarks and leptons. The discussion of the quark-lepton correspondence which can be traced to early sixties [21], and in a modern context presented in a compelling form with the anomaly cancellation in Standard Model [22] strongly suggests that they have common roots. It is also possible that the Kobayashi-Maskawa type CP violation [23] in the lepton sector might be related to CP violation at high energies which is required for leptogenesis [24] to work. See, e.g., [25] and the references cited therein for this point.

Despite the great progress in our understanding mentioned above we do have many important unanswered questions. The list includes, for example, the followings: What is the origin of neutrino masses and mixing? What is the reason for disparity between small quark and large lepton mixings? Is there underlying quark-lepton symmetry, or quark-lepton complementarity? Is there flavor symmetry which includes quarks and leptons? I am sure that many more questions exist. These points are discussed in depth in a recent review [26].

The new stage of neutrino physics may also be characterized as beginning of the era of precision measurement of lepton mixing parameters. Testing the various theoretical ideas proposed to understand the uncovered structure mentioned above requires accurate determination of mixing parameters. For example, to test the quark-lepton complementarity [27, 28] experimentally, one needs to improve accuracies for θ_{12} determination from the current one, $\simeq 12\%$ for $\sin^2\theta_{12}$, to the one comparable to the Cabibbo angle, $\sim 1\%$ [29]. It will be discussed in Sec. 9.

I must admit that the scope of my discussions is quite limited; The crucially important issues such as absolute neutrino mass, nature of neutrinos (Majorana vs. Dirac), Majorana CP violation and leptogenesis are not covered. Moreover, it covers only a part of the things that should be addressed for exploring unknowns done by the future LBL experiments, that is, concrete ways of how to determine the mixing parameters with the next generation conventional ν_μ superbeam [30, 31] and reactor

experiments. Yet, conventional superbeam experiments are extremely interesting because, in principle, they can be done in the next 10-15 years without long-term R&D effort.

Here is a composition of this long report. First of all, I intend to be pedagogical in writing this report; I met with many brilliant young people in "World Summit in Galapagos" [32], and a broad class of audiences who are keenly interested in neutrino physics in "Heavy Quarks and Leptons" [33]. It is a pity if this manuscript is entirely unreadable to them. In Sec. 2, we review how the atmospheric parameters Δm^2_{32} and θ_{23} are determined. In Sec. 3, we explain how θ_{13} can be measured and briefly review the reactor and the accelerator methods. In Sec. 4, we provide a simple understanding of the interplay between the vacuum and the matter effect by introducing the bi-probability plot. In Sec. 5, we mention two alternative strategies of how to measure CP violation and give some historical remarks on how the thoughts on measuring leptonic CP violation were evolved. In Sec. 6, we explain in a simple terms the cause of the parameter degeneracy by using the bi-probability plot. It is an important topics for precision measurement of the lepton mixing parameters because the degeneracy acts as a notorious obstacle to it. In Sec. 7, we discuss how the eight-fold parameter degeneracy can be resolved *in situ* by using "T2KK", the Tokai-to-Kamioka-Korea setting. In Sec. 8, we describe an alternative method for solving a part of the degeneracy called the θ_{23} octant degeneracy by combining reactor and accelerator experiments. In Sec. 9, we discuss, by taking a concrete example, how theoretical/phenomenological hypothesis can be confronted to experiments. In Sec. 10, we give a concluding remark.

2 Atmospheric parameters; Δm^2_{31} and θ_{23}

"Bread and butter" in the coming era of precision measurement of lepton mixing parameters is the accurate determination of the atmospheric parameters, Δm^2_{31} and θ_{23}. It will be carried out by the accelerator disappearance experiments which measures energy spectrum modulation of muon neutrinos. Ignoring terms proportional to Δm^2_{21} and θ_{13}, the disappearance probability in vacuum can be written as

$$P(\nu_\mu \to \nu_\mu) \;=\; 1 - \sin^2 2\theta_{23} \sin^2\Big(\frac{\Delta m^2_{31} L}{4E}\Big) \qquad (1)$$

In view of (1), very roughly speaking, the position and the depth of the dip corresponding to the first oscillation maximum, $\Delta_{31} \equiv \frac{\Delta m^2_{31} L}{4E} = \pi/2$, tell us Δm^2_{31} and $\sin^2 2\theta_{23}$, respectively.

The current limits on these parameters from the SK atmospheric neutrino observation are $1.5 \times 10^{-3}\mathrm{eV}^2 < \Delta m^2_{31} < 3.4 \times 10^{-3}\mathrm{eV}^2$ and $\sin^2 2\theta_{23} > 0.92$ at 90% CL [1]. K2K, the first accelerator LBL experiment obtained the similar results,

$1.9 \times 10^{-3}\mathrm{eV}^2 < \Delta m^2_{31} < 3.5 \times 10^{-3}\mathrm{eV}^2$ at 90% CL though the sensitivity to θ_{23} is much worse, $\sin^2 2\theta_{23} < 0.6$ [34]. The currently running MINOS experiment [18] aims at determining Δm^2_{31} to $\simeq 6\%$ level, and $\sin^2 2\theta_{23}$ to $\simeq 8\%$ level, both at 90% CL. The next generation LBL experiment T2K [35] is expected to improve the sensitivity to $\simeq 2\%$ level for Δm^2_{31} excluding systematics, and $\simeq 1\%$ level for $\sin^2 2\theta_{23}$ including systematics, both at 90% CL [36]. These numbers are cross checked in various occasions [37, 38]. The US project NOνA [39] will also have the similar sensitivities. These accuracies are quite essential to resolve the parameter degeneracy (see Sec. 6) to achieve the goal of precision determination of the lepton mixing parameters.

3 θ_{13}

To reach the goal of seeing leptonic CP violation, we have to clear the first hurdle, knowing the value of θ_{13}. What is the most appropriate way to measure the parameter? To answer the question we consider the neutrino oscillation channel which involve ν_e, otherwise θ_{13} would not be contained in leading order. There are two candidate channels; $\nu_e \to \nu_e$ and $\nu_\mu \to \nu_e$ (or, $\nu_e \to \nu_\mu$). In our discussion that follows, $\nu_e \to \nu_\tau$ is the same as $\nu_e \to \nu_\mu$.

We note that $P(\nu_e \to \nu_e)$ probed at energy/baseline appropriate to atmospheric Δm^2 scale consists of interference terms between amplitudes $A(\nu_e - \nu_3 \to \nu_3 - \nu_e)$ and $A(\nu_e - \nu_1 \to \nu_1 - \nu_e) + A(\nu_e - \nu_2 \to \nu_2 - \nu_e)$. Then, obviously $|U_{e3}|^2$ is involved in the disappearance probability. On the other hand, in the appearance channel $\nu_\mu \to \nu_e$, the oscillation probability contains interference terms between amplitudes $A(\nu_\mu - \nu_3 \to \nu_3 - \nu_e)$ and $A(\nu_\mu - \nu_1 \to \nu_1 - \nu_e) + A(\nu_\mu - \nu_2 \to \nu_2 - \nu_e)$. Then, the appearance channel looks to be advantageous because only a single power of $|U_{e3}|$ is involved. But, it is untrue; When there is a hierarchy in Δm^2, $\Delta m^2_{21} \overline{ll} \Delta m^2_{31}$, unitarity tells us that these two terms nearly cancel, leaving another power of $|U_{e3}|$. As a consequence, $P(\nu_\mu \to \nu_e)$ is also proportional to $|U_{e3}|^2$. Hence, there are two comparably good ways to measure θ_{13}; the reactor and the accelerator methods which measure $P(\nu_e \to \nu_e)$ and $P(\nu_\mu \to \nu_e)$, respectively. Let us describe them one by one.

Before getting into the task we give here the explicit expressions of oscillation probabilities. For $\overline{\nu}_e$ disappearance channel it reads (see e.g., erratum in [40])

$$\begin{aligned} 1 - P(\overline{\nu}_e \to \overline{\nu}_e) &= \sin^2 2\theta_{13} \sin^2 \left(\frac{\Delta m^2_{31} L}{4E} \right) \\ &- \frac{1}{2} s^2_{12} \sin^2 2\theta_{13} \sin \left(\frac{\Delta m^2_{31} L}{2E} \right) \sin \left(\frac{\Delta m^2_{21} L}{2E} \right) \\ &+ \left[c^4_{13} \sin^2 2\theta_{12} + s^2_{12} \sin^2 2\theta_{13} \cos \left(\frac{\Delta m^2_{31} L}{2E} \right) \right] \sin^2 \left(\frac{\Delta m^2_{21} L}{4E} \right) \end{aligned} \quad (2)$$

For the appearance channel, we use the $\nu_\mu(\overline{\nu}_\mu) \to \nu_e(\overline{\nu}_e)$ oscillation probability with

first-order matter effect [41]

$$\begin{aligned} P[\nu_\mu(\overline{\nu}_\mu) \;\to\; & \nu_{\rm e}(\overline{\nu}_e)] \\ = \;& \sin^2 2\theta_{13} s_{23}^2 \left[\sin^2\left(\frac{\Delta m_{31}^2 L}{4E}\right) - \frac{1}{2} s_{12}^2 \left(\frac{\Delta m_{21}^2 L}{2E}\right) \sin\left(\frac{\Delta m_{31}^2 L}{2E}\right) \right. \\ & \left. \pm \left(\frac{4Ea}{\Delta m_{31}^2}\right) \sin^2\left(\frac{\Delta m_{31}^2 L}{4E}\right) \mp \frac{aL}{2} \sin\left(\frac{\Delta m_{31}^2 L}{2E}\right) \right] \\ + \;& 2J_r \left(\frac{\Delta m_{21}^2 L}{2E}\right) \left[\cos\delta \sin\left(\frac{\Delta m_{31}^2 L}{2E}\right) \mp 2\sin\delta \sin^2\left(\frac{\Delta m_{31}^2 L}{4E}\right) \right] \\ + \;& c_{23}^2 \sin^2 2\theta_{12} \left(\frac{\Delta m_{21}^2 L}{4E}\right)^2, \end{aligned} \tag{3}$$

where the terms of order $s_{13}\left(\frac{\Delta m_{21}^2}{\Delta m_{31}^2}\right)^2$ and $aLs_{13}\left(\frac{\Delta m_{21}^2}{\Delta m_{31}^2}\right)$ are neglected. In Eq. (3), $a \equiv \sqrt{2} G_F N_e$ [13] where G_F is the Fermi constant, N_e denotes the averaged electron number density along the neutrino trajectory in the earth, J_r ($\equiv c_{12}s_{12}c_{13}^2 s_{13} c_{23} s_{23}$) denotes the reduced Jarlskog factor, and the upper and the lower sign $\pm$ refer to the neutrino and anti-neutrino channels, respectively. In both of the oscillation probabilities, $P(\overline{\nu}_e \to \overline{\nu}_e)$ and $P(\nu_\mu \to \nu_e)$, the leading atmospheric oscillation terms have the common factor $\sin^2 2\theta_{13}$, in agreement with the discussion given above. The last term in Eq. (3) is the solar scale oscillation term, which will be important for resolving the θ_{23} degeneracy.

3.1 Reactor measurement of θ_{13}

It was proposed [40,42] that by using identical near and far detectors which is placed close to and at around ∼1 km from the reactor, respectively, one can search for non-zero θ_{13} to a region of $\sin^2 2\theta_{13} \sim 0.01$. An advantage of the reactor θ_{13} experiments is their cost effectiveness which stems from that the beam is intense enough (and furthermore free!) and low in energy to allows relatively compact detectors placed at baselines much shorter than those of accelerator experiments. Intensive efforts over several years from these proposals entailed the various projects in world wide as described in [43]. By now a few projects have already been approved, or are close to the status [44–46].

Scientific merit of the reactor measurement of θ_{13} is that it provides pure measurement of θ_{13} without being affected by other mixing parameters, as emphasized in [40]. It implies, among other things, that it can help resolving the θ_{23} octant degeneracy as pointed out in [40], and recently demonstrated in detail in [38]. On the other hand, the same property may be understood as "shortcoming" of the reactor experiment, if one want to search for leptonic CP violation. It is known that ν_e ($\overline{\nu}_e$) disappearance probability has no sensitivity to δ even in matter with arbitrary profile with negligible

higher order correction [47]. We note, however, that reactor θ_{13} experiment can be combined with accelerator appearance measurement to uncover CP violation [48].

3.2 Accelerator measurement of θ_{13}

In contrast to the reactor experiments accelerator measurement of θ_{13} is "contaminated" (or enriched) by the other mixing parameters, in particular by δ in the case of low energy superbeam experiments. The sensitivity to θ_{13} therefore depends upon δ in a significant way. Though it sounds like drawback of the accelerator method, it in turn means that the LBL θ_{13} experiments can be upgraded to search for leptonic CP violation. (This is why and how the low-energy superbeam was originally motivated in [30].) There exist an approved experiment T2K [35] using the 0.75 MW neutrino beam from J-PARC, and a competitive proposal of NOνA [39] which uses NuMI beam line in Fermilab. The sensitivity to θ_{13}, is roughly speaking, up to $\sin^2 2\theta_{13} \sim 0.01$. However, the better knowledge of background rejection and the systematic errors are required to make the number more solid. Though less sensitive, MINOS [18] and OPERA [49] have some sensitivities to θ_{13}.

If θ_{13} is really small, $\sin^2 2\theta_{13} < 0.01$, probably we need new technology to explore the region of θ_{13}. The best candidates are neutrino factory [50] or the beta beam [51]. For them we refer [52] for overview and for extensive references.

4 Vacuum vs. matter effects

To proceed further, we need some knowledges on neutrino oscillation in matter. There are several ways to simply understand the matter effect in neutrino oscillations. One is to use perturbative approach [41,53]. The other is to rely on Cervera *et al.* formula [55] which applies to higher matter densities. The most important reason why we want to understand the feature of vacuum-matter interplay in neutrino oscillation is that they tend to mix and confuse with each other. For the early references which took into account the matter effect which inevitably comes in into LBL CP violation search, see e.g., [41, 53–55].

Probably, the simplest way to understand the matter effect as well as CP phase effect is to rely on the CP trajectory diagram in $P(\nu_\mu \to \nu_e)$ and $P(\overline{\nu}_\mu \to \overline{\nu}_e)$ space, for short, the bi-probability plot [56]. It is given in Fig. 1. By writing the bi-probability diagram one can easily understand the relative importance of CP and the matter effects in a pictorial way; Magnitude of effect of CP violating phase δ is represented as the size of the ellipses, while that of the matter effect can be read off as a separation between the two ellipses with positive (blue ellipse) and negative (red ellipse) sign of Δm^2_{31}. The distance from the origin to the ellipse complex represents $s^2_{23} \sin^2 2\theta_{13}$. We mention that the bi-probability plot can be extended to the one which includes

T violation in which the charming relations between probabilities called the CP-CP and the T-CP relations are hidden [57, 58].

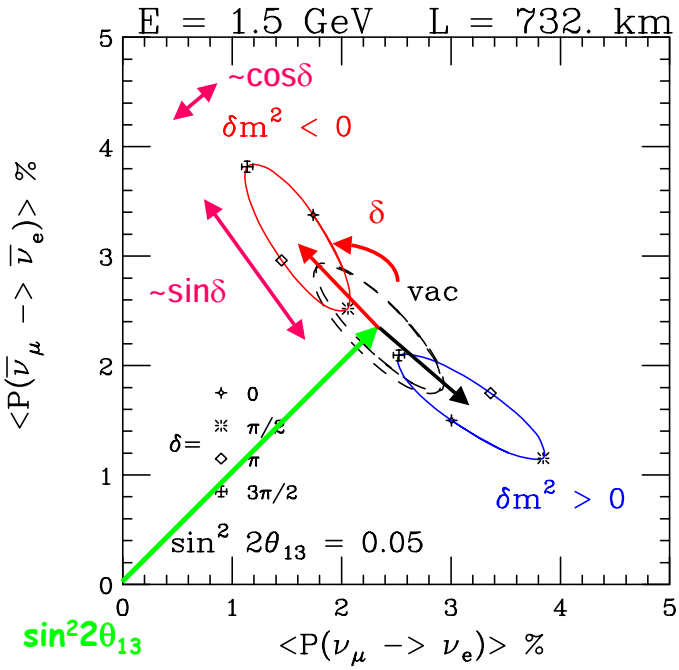

Figure 1: A P- $\overline{P}$ bi-probability plot with experimental parameters corresponding to NuMI off-axis project is presented for the purpose of exhibiting characteristic features of the neutrino oscillations relevant for low-energy superbeam experiments. Namely, it can disply competing three effects, CP violating and CP conserving effects due to δ as well as the matter effects in a compact fashion. For more detailed description of its properties, see [56]. The art work is done by Adam Para.

5 CP violating phase δ

If θ_{13} is not too small and is within reach by the next generation reactor or LBL experiments, the door is open to search for leptonic CP violation using conventional superbeam. When people started to think about the possibility of observing CP violation there were two alternative ways to approach the goal, high-energy vs. low-energy options, as described in [59]. The high-energy option, the majority at that time, is based on the idea of neutrino factory [50] which utilizes intense neutrino beam from muon storage ring. Because background can be suppressed to a very small level due to clean detection of high-energy muons, the sensitivity to θ_{13} and δ can be

extremely good. We do not quote the number here because its re-examination by taking into account the possibility of lowering the threshold is ongoing in the context of neutrino factory International Scoping Study [60], which should be available soon.

The low-energy option is based on very simple fact that the effect of CP phase δ is large at low energies [30, 54]. What is good in the low-energy option is that it can be realized with conventional ν_μ superbeam. It opens the possibility that the CP violation search can be pursued by relying on known beam technology with no need of an extensive R&D efforts, and is doable in the next 10-15 years if we can enjoy generous governmental support. On the other hand, ν_e appearance search with conventional ν_μ beam inevitably has the intrinsic problem of background, not only of the beam origin but also due to the neutral current (NC) π^0 in the case of water Cherenkov detectors. Despite the potential difficulties, the possibility of experimental search for leptonic CP violation became the realistic option when LOI of the T2K experiment with optimistic conclusion was submitted [35].

Unfortunately, the optimism in the early era was challenged by several potential obstacles. First of all, reducing the systematic error to a required level, a few % level, is a tremendous task. Good news is that several experiments are going on, or to be done, to measure hadron production [61, 62] and neutrino nucleus interaction cross sections [63]. Other difficulties include, for example: the possibility that CP violation could be masked by the unknown sign of Δm^2_{31}, or in more general context the presence of parameter degeneracy [56, 65, 66] which can obscure the CP violation, which will be the topics of the next section.

6 Parameter degeneracy

Since sometime ago people recognized that measurement of $P(\nu_\mu \to \nu_e)$ and $P(\overline{\nu}_\mu \to \overline{\nu}_e)$ at a particular energy, no matter how accurate they are, allows multiple solutions of θ_{13} and δ, the problem of parameter degeneracy. The nature of the degeneracy can be understood as the intrinsic degeneracy [65], which is duplicated by the unknown sign of Δm^2 [56], and the possible octant ambiguity of θ_{23} [66] if it is not maximal. For an overview of the resultant eight-fold parameter degeneracy, see e.g., [67, 68].

It is in fact easy to understand the cause of the parameter degeneracy if we use the bi-probability plot. Look at Fig. 2. Suppose that your experimentalist friend gives you the measurement point denoted as an open circle in Fig. 2. Then, it is evident that you can draw two ellipses, as shown in blue solid lines in Fig. 2, that pass through the observed point, which implies the existence of two solutions of θ_{13} and δ. The two-fold ambiguity is usually called the intrinsic degeneracy. If we are ignorant of the neutrino mass hierarchy, i.e., the sign of Δm^2_{31}, the two more ellipses can be drawn, as shown by the red dashed line in Fig. 2; duplication of the solution by the unknown mass hierarchy. Altogether one has four-fold parameter degeneracy.

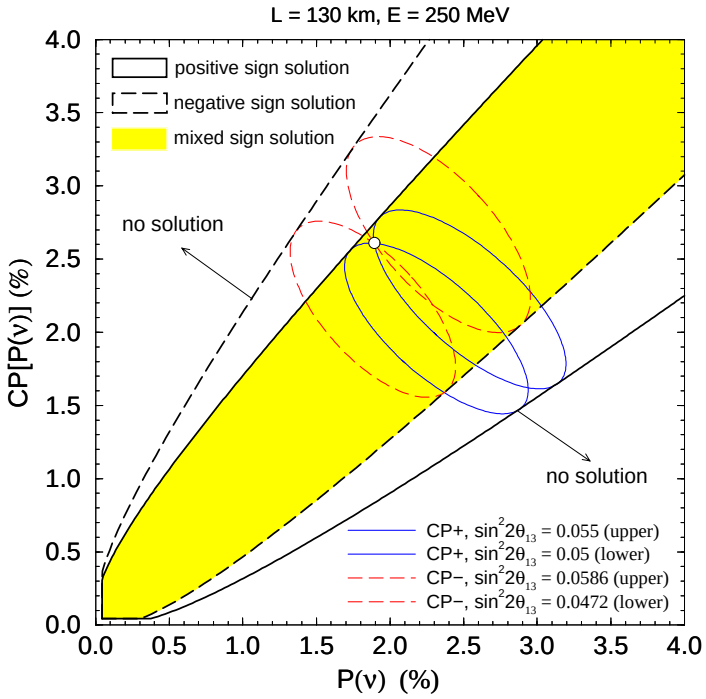

Figure 2: An example of the degenerate solutions for the CERN-Frejius project in the $P(\nu) \equiv P(\nu_\mu \to \nu_e)$ verses $CP[P(\nu)] \equiv P(\overline{\nu}_\mu \to \overline{\nu}_e)$ plane. Between the solid (dashed) lines is the allowed region for positive (negative) Δm^2_{31} and the shaded region is where solution for both signs are allowed. The solid (dashed) ellipses are for positive (negative) Δm^2_{31} and they all meet at a single point. This is the CP parameter degeneracy problem. We have used a fixed neutrino energy of 250 MeV and a baseline of 130 km. The mixing parameters are fixed to be $|\Delta m^2_{13}| = 3 \times 10^{-3} eV^2$, $\sin^2 2\theta_{23} = 1.0$, $\Delta m^2_{12} = +5 \times 10^{-5} eV^2$, $\sin^2 2\theta_{12} = 0.8$ and $Y_e \rho = 1.5$ g cm^{-3}. The figure is taken from [68].

Unfortunately, it is not the end of the story. If θ_{23} is not maximal, we are enriched with another degeneracy, the θ_{23} octant degeneracy. The ν_μ disappearance measurement of $P(\nu_\mu \to \nu_\mu)$ gives a value of $\sin^2 2\theta_{23}$. It then allows two solutions of θ_{23} if $\theta_{23} \neq \pi/4$, $s^2_{23} = \frac{1}{2}\left[1 \pm \sqrt{1 - \sin^2 2\theta_{23}}\right]$, one in the first octant and the other in the second octant. Since this is "orthogonal" to the intrinsic and the sign Δm^2_{31} degeneracies with four solutions of θ_{13} and δ, the total eight-fold degeneracy results.

Prior to the systematic discussion of how to solve the degeneracy we want to mention about the simplest method of solving the $\theta_{13} - \delta$ degeneracy. By tuning the beam energy to the "shrunk ellipse limit" [69] the degeneracy can be reduced to the two-fold one, $\delta \leftrightarrow \pi - \delta$. Notice that there is no confusion between CP violation and

CP conservation even in the presence of this degeneracy.

7 Resolving the eight-fold parameter degeneracy

It is known that degeneracy of neutrino oscillation parameters acts as a severe limiting factor to the precision determination of θ_{13}, θ_{23}, and δ. It is particularly true for the θ_{23} octant degeneracy [37]. Expecting the era of precision measurement in the next 10-30 years, it is the time that the formulation of the well defined strategy for exploring the whole structure of the lepton flavor mixing is of immense need.

Toward the goal, I explain in detail how the degeneracy can be resolved by using a concrete setting, which is called "T2KK". It is an acronym for Tokai-to-Kamioka-Korea two detector complex, an upgraded next project to T2K phase I for exploring the whole structure of lepton flavor mixing [70, 71]. It utilizes two half a megaton (0.27 Mton fiducial volume) water Cherenkov detectors one in Kamioka (295 km) and the other in somewhere in Korea ($\sim$1000 km) which receive ν_μ and $\overline{\nu}_\mu$ superbeam of 4 MW from J-PARC facility. We assume 4 years of running with each neutrino and antineutrino mode. For further details of T2KK, please consult to the original manuscripts [70, 71]. For a broader view of T2KK including wider class of detector options and locations, see the web page of the workshops which are focused on this project [72]. Though T2KK is *not* the unique way of resolving the eight-fold parameter degeneracy it is nice to have a concrete project to solve all the degeneracy *in situ*; It provides the bottom line understanding on how it can be lifted, and the lesson may be useful to think about alternative ways.

How does T2KK solve the 8-fold parameter degeneracy? In a nutshell, the setting can resolve the three kind of degeneracies in the following ways:

- The intrinsic degeneracy; Spectrum information solves the intrinsic degeneracy.
- The sign-Δm^2 degeneracy; Difference in the earth matter effect between the intermediate (Kamioka) and the far (Korea) detectors solves the sign-Δm^2 degeneracy.
- The θ_{23} octant degeneracy; Difference in solar Δm^2 oscillation effect (which is proportional to c_{23}^2) between the intermediate and the far detectors solves the θ_{23} octant degeneracy.

Let me explain these points one by one.

7.1 Intrinsic degeneracy

First look at Fig. 3 in which the sensitivities for resolving the intrinsic degeneracy by the Tokai-to-Kamioka phase II (T2K II) setting [35] (left panel) and the Kamioka-

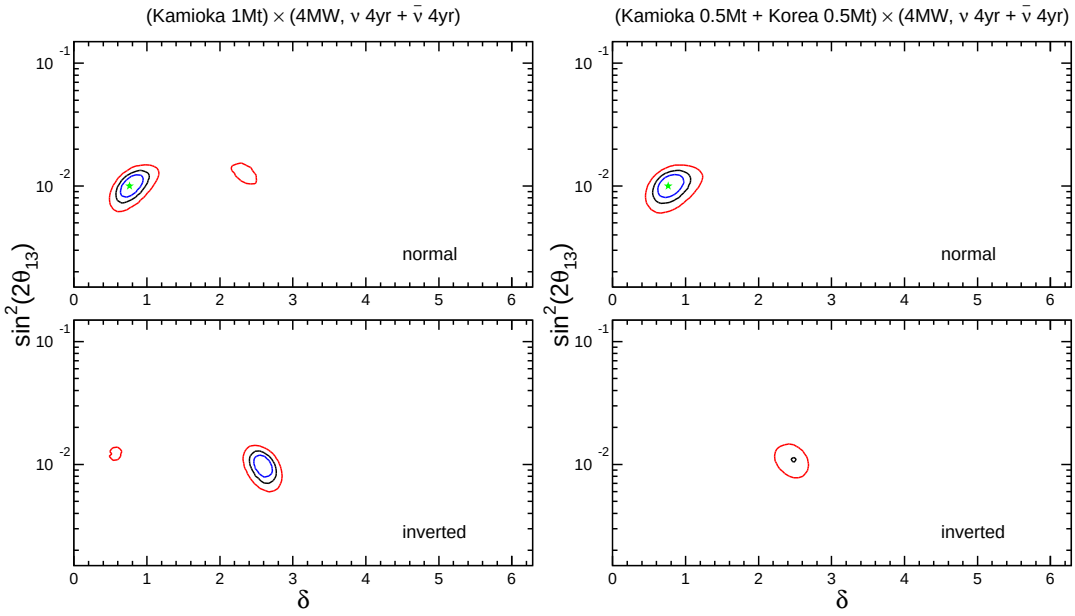

Figure 3: The region allowed in $\delta - \sin^2 2\theta_{13}$ space by 4 years of neutrino and antineutrino running in T2K II (left panel), and the Kamioka-Korea two detector setting (right panel). They are taken from the supplementary figures behind the reference [70] to which the readers are referred for details of the analysis. Notice that the standard setting in T2K II, 2 (6) years of neutrino (antineutrino) running, leads to a very similar results (as given in [73]) to the one presented in the left panel of this figure. The true solutions are assumed to be located at ($\sin^2 2\theta_{13}$ and δ) = (0.01, $\pi/4$) with positive sign of Δm^2_{31}, as indicated as the green star. The intrinsic and the Δm^2_{31}-sign clones appear in the same and the opposite sign Δm^2_{31} panels, respectively. Three contours in each figure correspond to the 68% (blue line), 90% (black line) and 99% (red line) C.L. sensitivities, respectively.

Korea two detector setting (right panel) are presented. Figure 3 is taken from supplementary figures prepared for the study reported in [70], in which the details of the analysis are described. In the left panel of Fig. 3 it is shown that the intrinsic degeneracy in (assumed) each mass hierarchy is almost resolved by the T2K II setting at the particular set of values of the mixing parameters as indicated in the caption. Since the matter effect plays minor role in the T2K II setting it is likely that the spectral information is mainly responsible for lifting the intrinsic degeneracy.

In the right panel of the same figure it is exhibited that the intrinsic degeneracy is completely resolved by the T2KK setting at the same values of the mixing parameters, indicating power of the two detector method [74]. Namely, the comparison between the intermediate and the far detectors placed at the first and the second oscillation

maxima, respectively, supersedes a single detector measurement in Kamioka with the same total volume in spite of much less statistics in the Korean detector.

7.2 Sign-Δm^2 degeneracy

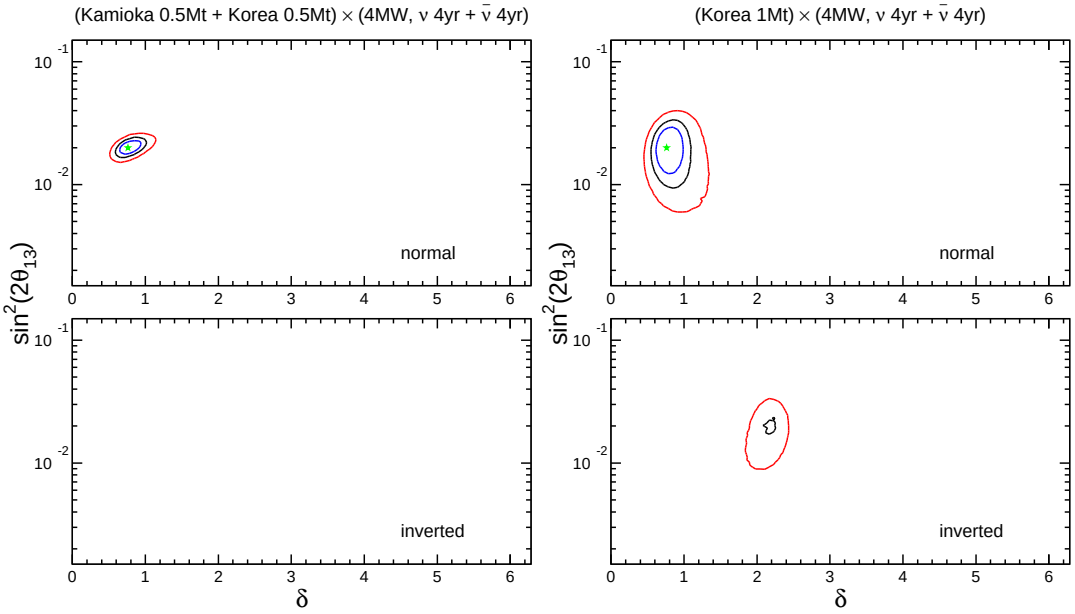

Figure 4: The similar sensitivity plot as in Fig. 3. Left panel is for T2KK and the right panel for a single 0.54 megaton detector placed in Korea.

It should be noted that the sign-Δm^2 degeneracy is also lifted though incompletely by the Kamioka-Korea setting as indicated in the right-lower panel of Fig. 3. It is well known that the interference effect between the vacuum and the matter effects depends upon the mass hierarchy, i.e., the sign of Δm^2_{31}, and many people have been proposed to utilize it to resolve the mass hierarchy.

But, it is not the whole story here. To indicate this point the sensitivities for the two settings are compared in Fig. 4. One is T2KK (left panel) and the other is the case of single 0.54 megaton detector placed in Korea (right panel). It should be noticed that a single detector in Korea with the same total volume fails to resolve the sign-Δm^2 degeneracy which is completely lifted by T2KK at the particular values of the mixing parameters. Again, the sensitivity is enhanced by comparing the yields of the two identical detectors.

The fact that the T2KK setting can resolve the four-fold degeneracy by the spectrum analysis and comparison between the two detectors is explained by plotting the energy dependences of the appearance probabilities in Fig. 5.

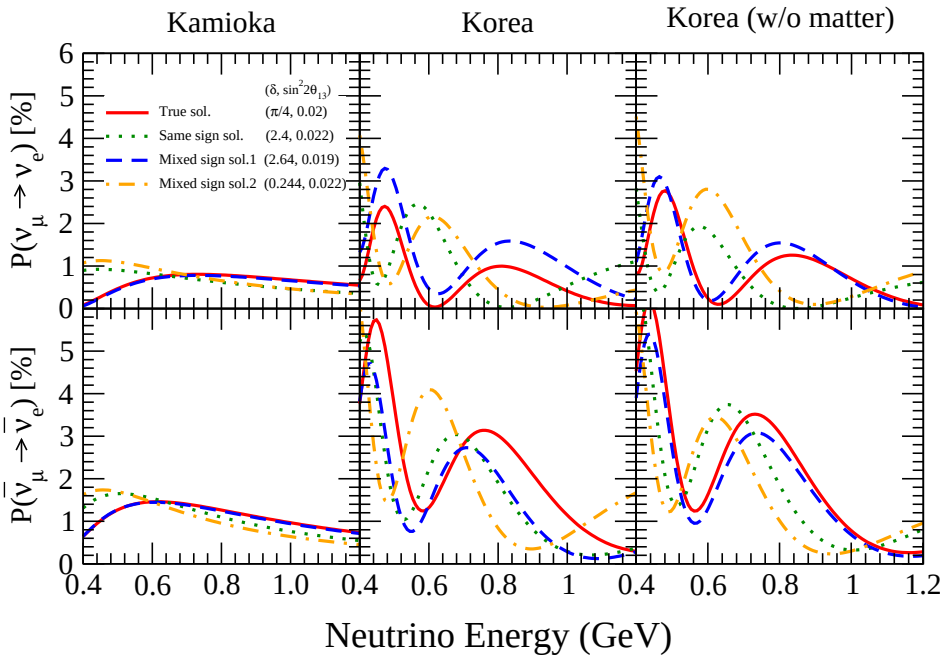

Figure 5: Neutrino oscillation probabilities corresponding to a four-fold degenerate solutions obtained by measurement in Kamioka by the rate only analysis are plotted as a function of neutrino energy. Left panels: appearance probabilities in Kamioka. Middle panels: appearance probabilities in Korea. Right panels: appearance probabilities in Korea, but without the matter effect.

7.3 θ_{23} octant degeneracy

The θ_{23} octant degeneracy arise because accelerator disappearance and appearance measurement determine $\sin^2 2\theta_{23}$ and the combination $s^2_{23}\sin^2 2\theta_{13}$, respectively, but not s^2_{23} itself. Therefore, it is hard to resolve in the accelerator experiments using conventional ν_μ beam. See [38] for an explicit analytic treatment of this point.

One way to solve the θ_{23} octant degeneracy is to utilize the solar Δm^2 oscillation term. This is the principle used by the atmospheric neutrino method for resolving the octant degeneracy [75–77]. Since the solar term, the last term in Eq. (3), depend upon c^2_{23} (not s^2_{23}) the degeneracy can be lifted. The next question is if it can be distinguished from the rest of the atmospheric oscillation terms. Fortunately, the answer seems to be yes because of the clear difference in energy dependence, as shown in Fig. 6. Note that the figure is the inverted hierarchy version of Fig. 2 in [71], and behavior of the solar term compared to the atmospheric ones is very similar to in the

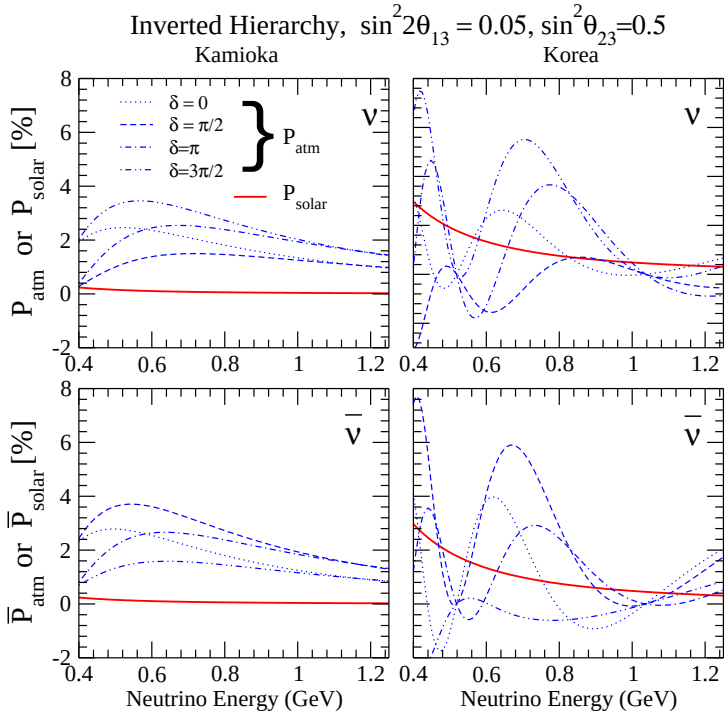

Figure 6: The energy dependence of the solar term (red solid line) is contrasted with the ones of atmospheric plus interference terms in the ν_e appearance oscillation probabilities with various values of CP phase δ; $\delta = 0$ (dotted line), $\delta = \pi/2$ (dashed line), $\delta = \pi$ (dash-dotted line), and $\delta = 3\pi/2$ (double-dash-dotted line). The neutrino mass hierarchy is assumed to be the inverted one. For the corresponding figure of the normal mass hierarchy, see [71].

case of the normal hierarchy.

7.4 Decoupling between the degeneracies

In passing, we briefly comment on the problem of decoupling between the degeneracies. For a fuller treatment, see [71]. The question is as follows: People sometimes discuss how to solve the degeneracy A without worrying about the degeneracy B, and vise versa. Is this a legitimate procedure? We want to answer to this question in the positive under the environment that the matter effect can be treated as a perturbation.

To resolve the degeneracy one has to distinguish between the values of the oscillation probabilities with the two different solutions corresponding to the degeneracy.

We define the probability difference

$$\begin{aligned}\Delta P^{ab}(\nu_\alpha \to \nu_\beta) &\equiv P\left(\nu_\alpha \to \nu_\beta; \theta_{23}^{(a)}, \theta_{13}^{(a)}, \delta^{(a)}, (\Delta m^2_{31})^{(a)}\right) \\ &- P\left(\nu_\alpha \to \nu_\beta; \theta_{23}^{(b)}, \theta_{13}^{(b)}, \delta^{(b)}, (\Delta m^2_{31})^{(b)}\right), \end{aligned} \tag{4}$$

as a measure for it where the superscripts a and b label the degenerate solutions. Suppose that we are discussing the degeneracy A. The decoupling between the degeneracies A and B holds if ΔP^{ab} defined in (4) for the degeneracy A is invariant under the replacement of the mixing parameters corresponding to the degeneracy B, and vice versa.

The best example of the decoupling is given by the one between the θ_{23} octant and the sign-Δm^2 degeneracies. Therefore, let us describe it here, leaving discussions on other cases to [71]. One can easily compute $\Delta P^{1st-2nd}(\nu_\mu \to \nu_e)$ for the θ_{23} octant degeneracy by using (3). It consists of the solar and the solar-atmospheric interference terms, with over-all factor of $\cos 2\theta_{23}$ because of the property $J_r^{1st} - J_r^{2nd} = \cos 2\theta_{23}^{1st} J_r^{1st}$ in leading order in $\cos 2\theta_{23}$. The remarkable feature of $\Delta P^{1st-2nd}(\nu_\mu \to \nu_e)$ is that the leading-order matter effect terms drops out completely.

Now, we notice the key feature of $\Delta P^{1st-2nd}(\nu_\mu \to \nu_e)$; It is invariant under the transformations $\Delta m^2_{31}) \to -\Delta m^2_{31}$ and $\delta \to \pi - \delta$, which exchanges the two sign-Δm^2 degenerate solutions, the invariance which holds in the presence of the solar term. It means that resolution of the θ_{23} degeneracy can be executed without knowing the mass hierarchy in experimental set up which allows perturbative treatment of matter effect.

Next, we examine the inverse problem; Does the determination of mass hierarchy decouple from resolution of the θ_{23} degeneracy? One can compute in the similar way $\Delta P^{norm-inv}$ for the sign-Δm^2 degeneracy. Because the exchange of two sign-Δm^2 degenerate solutions is the approximate symmetry of the vacuum oscillation probability [56], most of the vacuum terms drops out. We observe that $\Delta P^{norm-inv}(\nu_\mu \to \nu_e)$ is invariant under transformation $\theta_{23}^{1st} \to \theta_{23}^{2nd}$ and $\theta_{13}^{1st} \to \theta_{13}^{2nd}$, because its θ_{13} and θ_{23} dependences are through the combination $\sin^2 2\theta_{13} s^2_{23}$. Therefore, resolution of the mass hierarchy can be carried out independently of which solution of the θ_{23} degeneracy is realized in nature.

We mention here that the decoupling argument can be generalized to include the other pair of degeneracies as done in [71].

7.5 Analysis results

Since the space is quite limited, we directly go to the results of our analysis. The original analysis in [70] has been re-examined with an improved code which takes into account a difference between beam profiles in the intermediate and the far detectors, and the inclusion of the muon disappearance channel [71]. In Fig. 7, and in Fig. 8, the

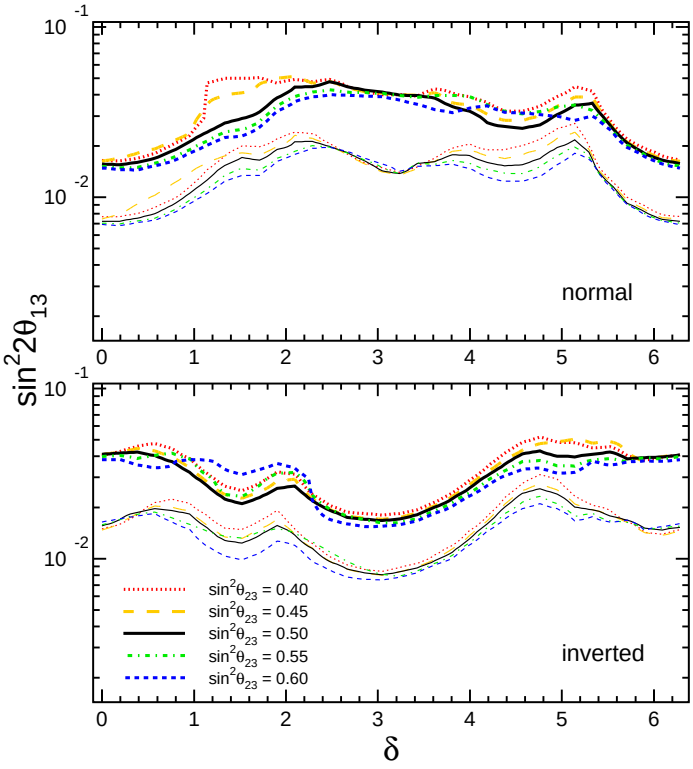

Figure 7: 2(thin lines) and 3(thick lines) standard deviation sensitivities to the mass hierarchy determination for several values of $\sin^2 2\theta_{23}$ (red dotted, yellow long-dashed, black solid, green dash-dotted, and blue short-dashed lines show the results for $\sin^2\theta_{23} = 0.40$, 0.45, 0.50, 0.55 and 0.60, respectively). The sensitivity is defined in the plane of $\sin^2 2\theta_{13}$ versus CP phase δ. The top and bottom panels show the cases for positive and negative mass hierarchies, respectively. Taken from [71].

results of re-analysis for the mass hierarchy resolution and CP violation, respectively, are presented. Figure 7 shows that the sensitivity to the mass hierarchy depends very weakly to θ_{23}, as expected by the decoupling argument given in [71]. The same argument suggests that they obey the scaling behavior; the curves falls to a single curve if plotted by $s^2_{23}\sin^2 2\theta_{13}$. The sensitivity greatly improves the one possessed by the original T2K II setup and is competitive to other similar projects. See [70] for comparison between the performances of T2KK and T2K II setting.

The θ_{23}-independence of the CP sensitivity is even more prominent, as shown in Fig. 8. This feature is again consistent with the decoupling argument. The sensitivity to CP violation is similar to that of the T2K II setting except for at large θ_{13} region where the T2KK sensitivity surpasses that of the T2K II. It is due to the fact that the identical two-detector setting solves the degeneracies. We emphasize that the CP

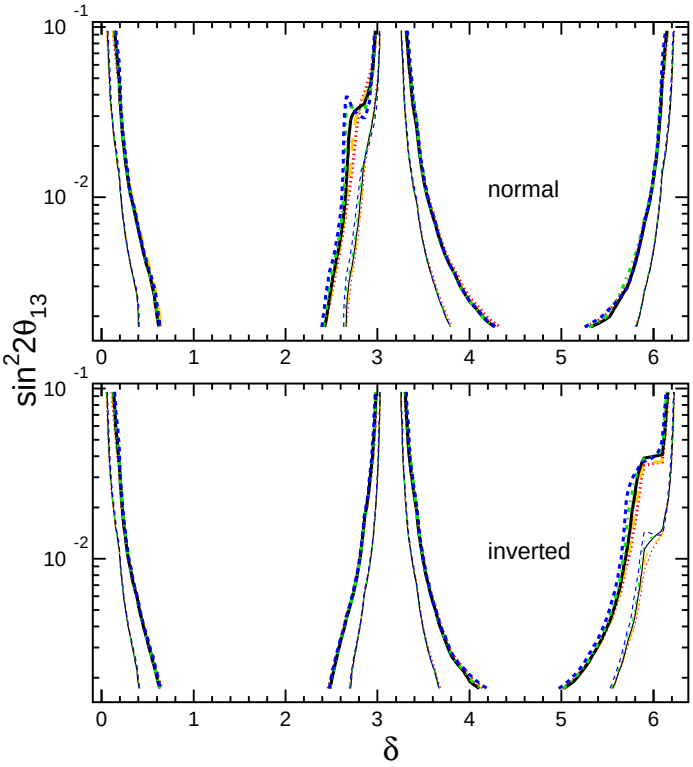

Figure 8: Sensitivities to the CP violation, $\sin\delta \neq 0$. The meaning of the lines and colors are identical to that in Fig. 7. Taken from [71].

sensitivity of T2KK setting at the large θ_{13} region seems to be the largest among the similar proposals including neutrino factory.

In Fig. 9, the sensitivity to the θ_{23} octant degeneracy is presented. From this figure, we conclude that the experiment we consider here is able to solve the octant ambiguity, if $\sin^2\theta_{23} < 0.38\,(0.42)$ or $> 0.62\,(0.58)$ at 3 (2) standard deviation CL. Roughly speaking, the sensitivity is independent of θ_{13} and the mass hierarchy. The dependence of this sensitivity on the CP phase δ is a mild one as one can see by comparing the left and the right panels of Fig. 9, providing another evidence for decoupling.

As discussed in detail in [38], the θ_{23} degeneracy is the difficult one to solve only by the accelerator experiments. Though the argument is still true, T2KK circumvents it because it has sensitivity to the solar term. Yet, the sensitivity is quite limited if plotted in s^2_{23} plane, as one can observe in Fig. 9. Nonetheless, we stress that it is not easy to supersede the sensitivity presented in Fig. 9. For example, T2KK's sensitivity is slightly better than the one by the atmospheric neutrino method based on 3 years observation in Hyper-Kamiokande reported in [76].

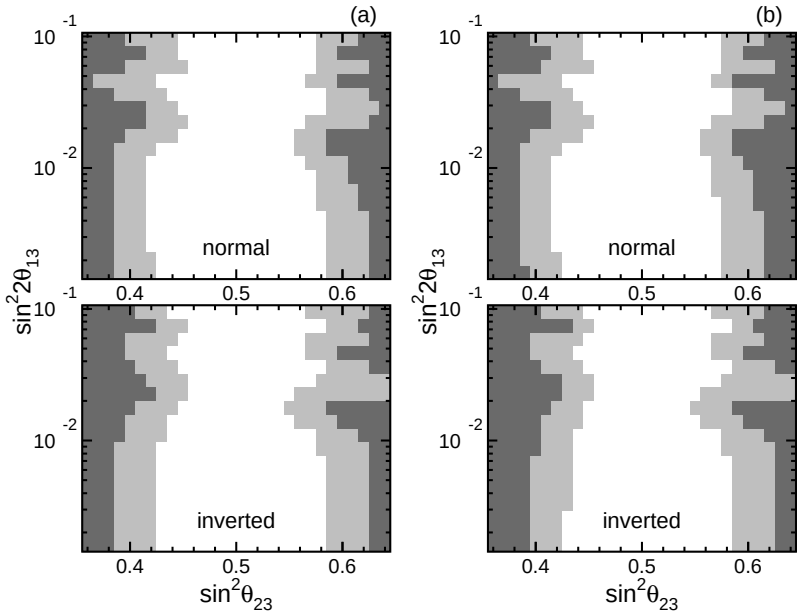

Figure 9: 2 (light gray area) and 3 (dark gray area) standard deviation sensitivities to the θ_{23} octant degeneracy for 0.27 Mton detectors both in Kamioka and Korea [71]. 4 years running with neutrino beam and another 4 years with anti-neutrino beam are assumed. In (a), the sensitivity is defined so that the experiment is able to identify the octant of θ_{23} for any values of the CP phase δ. In (b), it is defined so that the experiment is able to identify the octant of θ_{23} for half of the CP δ phase space.

We emphasize that our estimates of sensitivities for the mass hierarchy resolution, CP violation, and the θ_{23} octant degeneracy are based on the known technology for rejecting NC induced background in water Cherenkov detectors. Moreover, we have used a conservative value of 5% for most of the systematic errors [70, 71]. Therefore, our results can be regarded as the robust bottom-line sensitivities achievable by conventional superbeam experiments. Of course, there may be ways to improve the sensitivities over the current T2KK design.

At the end of this section, we should mention that the method explored in this article is by no means unique. With regard to the sign-Δm^2 (mass hierarchy) degeneracy we note that other methods include the one which utilize atmospheric neutrinos [78], supernova neutrinos [79,80], neutrino-less double beta decay [81], and ν_e and ν_μ disappearance channels [82–84]. We have already mentioned about the θ_{23} octant degeneracy, and a further comment follows immediately below.

8 Reactor-Accelerator method for θ_{23} octant degeneracy

Detecting the solar oscillation effect is not the unique way of resolving the θ_{23} octant degeneracy. The alternative methods proposed include, in addition to the already mentioned atmospheric neutrino method, the reactor accelerator combined method [38, 40], and the atmospheric accelerator combined method [85].

Here, we explain the reactor-accelerator combined method. The principle is again very simple; The reactor measurement can pick up one of the solutions of θ_{13} because it is a pure measurement of θ_{13}, the possibility first explored in [40]. This principle is explained in Fig. 10 which are taken from [38]. This reference gives a detailed quantitative analysis of the sensitivity achievable by the accelerator-reactor combined method. The upper (lower) four panels of Fig. 10 describe the process of how the θ_{23} octant degeneracy can be resolved for the case where the true value of $\sin^2\theta_{23} = 0.458$ (0.542), corresponding to $\sin^2 2\theta_{23} = 0.993$. The other input mixing parameters are given as $\Delta m^2_{31} = 2.5 \times 10^{-3}$ eV^2, $\sin^2 2\theta_{13} = 0.1$ and $\delta = 0$, $\Delta m^2_{21} = 8.0 \times 10^{-5}$ eV^2, $\sin^2\theta_{12} = 0.31$ (the input values of $\sin^2 2\theta_{13}$ and $\sin^2\theta_{23}$ are indicated by the symbol of star in the plot). (a) The regions enclosed by the solid and the dashed curves are allowed regions only by the results of appearance and disappearance accelerator measurement, respectively. (b) The regions that remain allowed when results of appearance and disappearance measurement are combined. (c) The regions allowed by reactor measurement. (d) The regions allowed after combining the results of appearance and disappearance accelerator experiments with the reactor measurement. The exposures for accelerator are assumed to be 2 (6) years of neutrino (anti-neutrino) running with 4 MW beam power with Hyper-Kamionande whose fiducial volume is 0.54 Mt, whereas for the reactor we assume an exposure of 10 GW·kt·yr. The case of optimistic systematic error is taken.

In Fig. 11 presented is the region in $\sin^2 2\theta_{13} - \sin^2\theta_{23}$ space where the θ_{23} octant degeneracy can be resolved. The upper and the lower figures in Fig. 11 are with a relatively pessimistic and an optimistic systematic errors, respectively, as indicated in the figures. For definition of the errors and details of the analysis procedure, see [38]. By comparing Fig. 11 with Fig. 9, we observe that the sensitivity achievable by the reactor-accelerator combined method surpasses that of T2KK in large θ_{13} region, $\sin^2 2\theta_{13} > 0.03 - 0.05$, the critical value very dependent of the systematic errors.

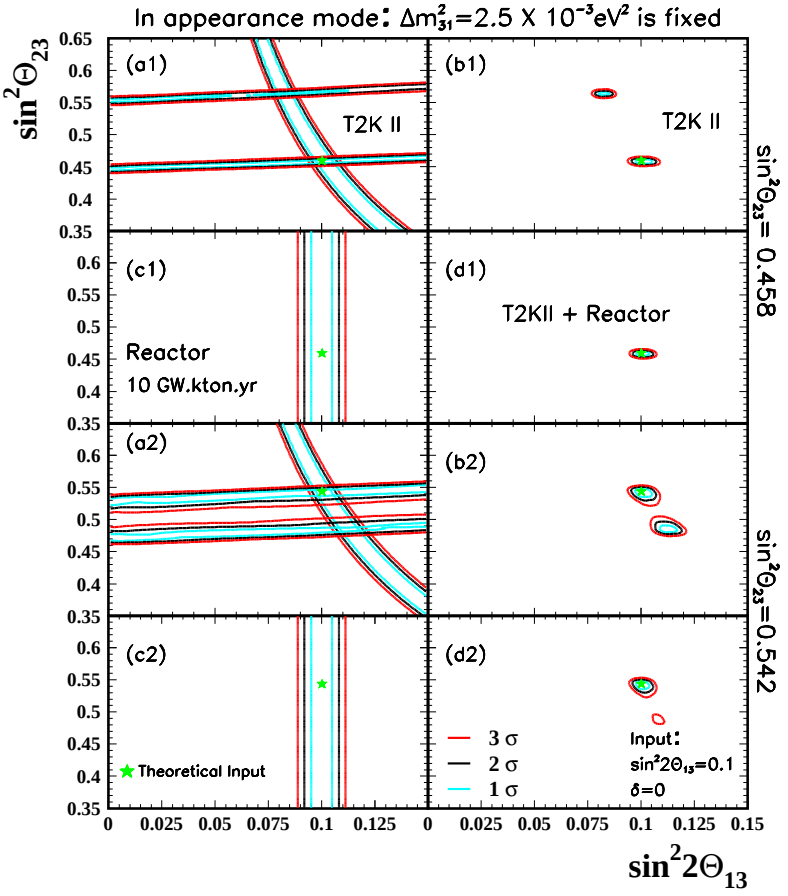

Figure 10: The principle of reactor-accelerator method for resolving θ_{23} degeneracy is explained in a pictorial way. For details, see the text.

9 How to proceed; Confrontation of theoretical ideas to experiments

In the bottom-up approach to the origin of neutrino mass and the mixing it is important to test various phenomenologically motivated ideas experimentally. In this article we discuss only one example, the quark-lepton complementarity (QLC) [27]. and briefly mention about the $\mu \leftrightarrow \tau$ exchange symmetry. An extensive list of the relevant references for the $\mu \leftrightarrow \tau$ symmetry, which is too long to quote in this manuscript, may be found in [26, 38].

The empirically suggested relation

$$\theta_{12} + \theta_C = \frac{\pi}{4}, \tag{5}$$

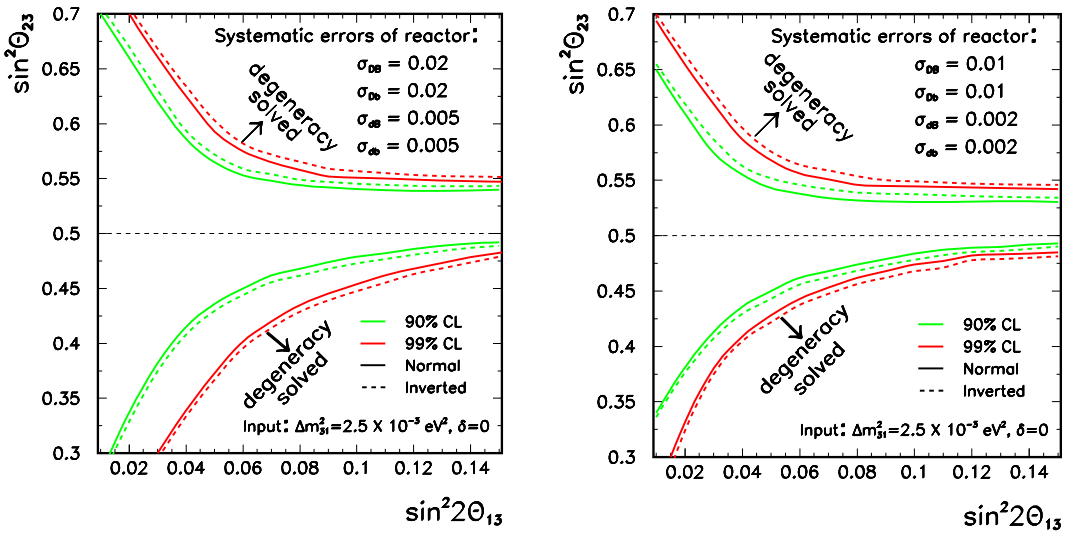

Figure 11: The region in $\sin^2 2\theta_{13} - \sin^2\theta_{23}$ space where the θ_{23} octant degeneracy can be resolved at 90% (thin green) and 99% (thick red) CL [38]. The left and the right panels are for the (relatively) conservative and the optimistic systematic errors, as indicated in the figures. The solid (dashed) curve is for the case of taking the normal (inverted) hierarchy to perform the fit, assuming the normal hierarchy as input.

with θ_C being the Cabibbo angle is under active investigation [28] and is dubbed as the QLC relation. If not accidental, it may suggest a new way of thinking on how quarks and leptons are unified. It may have extension to the 2-3 sector, $\theta_{23}^{(lepton)} + \theta_{23}^{(quark)} = \frac{\pi}{4}$.

We now discuss how the relation (5) can be tested experimentally. Since the Cabibbo angle is measured in an enormous precision as emphasized earlier, the real problem is to what accuracy the solar angle θ_{12} can be measured experimentally. At this moment there exist two approaches to measure θ_{12} accurately. The first one is a natural extension of the method by which θ_{12} is determined today, namely, combining the solar and the KamLAND experiments. The other one is to create a dedicated new reactor experiment with detector at around the first oscillation maximum of reactor neutrino oscillation, "SADO" (see below). Let me briefly explain about the basic ideas behind them one by one.

9.1 Solar-KamLAND method

Combining the solar and the KamLAND experiments is powerful, assuming CPT invariance, because solar neutrino measurement is good at constraining θ_{12} and KamLAND determines with high precision the other parameter Δm^2_{21}. The feature makes the analysis of the solar neutrino parameter determination essentially 1-dimensional.

Experiments	$\delta s^2_{12}/s^2_{12}$ at 68.27% CL	$\delta s^2_{12}/s^2_{12}$ at 99.73% CL
Solar+ KL (present)	8 %	26 %
Solar+ KL (3 yr)	7 %	20 %
Solar+ KL (3 yr) + pp (1%)	4 %	11 %
54 km		
SADO for 10 GWth·kt·yr	4.6 % (5.0 %)	12.2 % (12.9 %)
SADO for 20 GWth·kt·yr	3.4 % (3.8 %)	8.8 % (9.5 %)
SADO for 60 GWth·kt·yr	2.1 % (2.4 %)	5.5 % (6.2 %)

Table 1: Comparisons of fractional errors of the experimentally determined mixing angle, $\delta s^2_{12}/s^2_{12} \equiv \delta(\sin^2\theta_{12})/\sin^2\theta_{12}$, by current and future solar neutrino experiments and KamLAND (KL), obtained from Tables 3 and 8 of Ref. [89], versus that by $\mathrm{SADO_{single}}$, which means to ignore all the other reactors than Kashiwazaki-Kariwa, obtained at 68.27% and 99.73% CL for 1 DOF in [90]. The numbers in parentheses are for $\mathrm{SADO_{multi}}$, which takes into account all 16 reactors all over Japan.

The former characteristics is particularly clear from the fact that the ratio of CC to NC rates in SNO directly measures $\sin^2\theta_{12}$ in the LMA solution. The current data allows accuracy of determination of $\sin^2\theta_{12}$ of about $\simeq 12\%$ (2 DOF) (the last reference in [8].) Further progress in measurement in SNO and KamLAND may improve the accuracy by a factor of ~ 2 but not too much beyond that.

If one wants to improve substantially the accuracy of θ_{12} determination, the existing solar neutrino experiments are not quite enough. Measurement of low-energy pp and ^{7}Be neutrinos is particularly useful by exploring vacuum oscillation regime. Fortunately, varying proposal for such low energy solar neutrino measurement are available in the world [86]. Measurement of ^{7}Be neutrinos is attempted in Borexino [87] and in KamLAND [88].

The improvement that is made possible by these additional measurement is thoroughly discussed by Bahcall and Peña-Garay [89]. Since the vacuum oscillation is the dominant mechanism at low energies measuring pp neutrino rate gives nothing but measurement of $\sin^2 2\theta_{12}$. On the other hand, ^{7}Be neutrino may carry unique informations of oscillation parameters due to its characteristic feature of monochromatic energy. The solar-KamLAND method will allow us to determine $\sin^2\theta_{12}$ to 4% level at 1σ CL [89]. In the upper panels of Table 1, we tabulate the sensitivities (1 DOF) currently obtained and expected by the future measurement.

9.2 SADO; Several-tens of km Antineutrino DetectOr

Though natural and profitable as a dual-purpose experiment for both θ_{12} and solar flux measurement the solar-KamLAND method is not the unique possibility for reaching

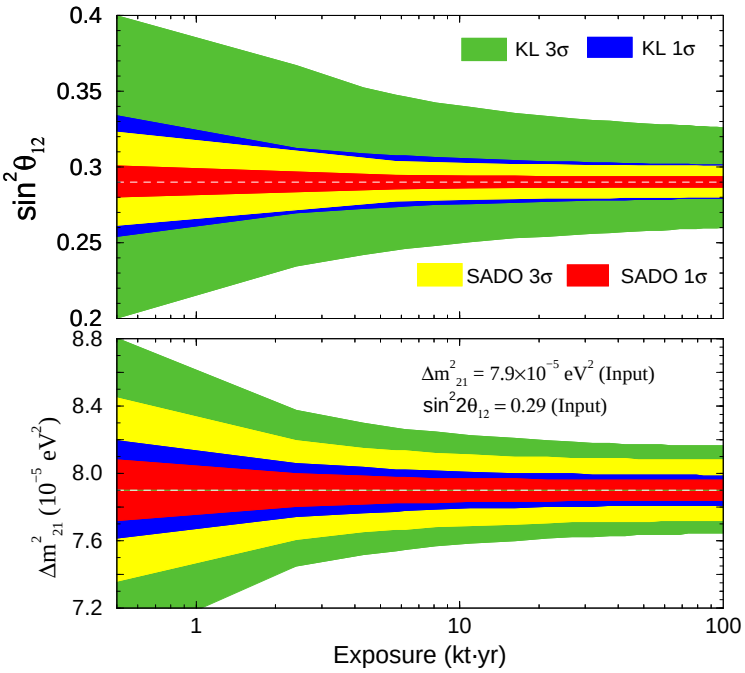

Figure 12: Accuracies of determination of $\sin^2\theta_{12}$ (upper panel) and Δm^2_{21} (lower panel) reachable by KamLAND and SADO (both 1 DOF) are compared with the same systematic error of 4% [91]. The geo-neutrino contribution was switched off.

the region of the highest sensitivity for θ_{12}. The most traditional way of measuring mixing angles at the highest possible sensitivities is either to tune beam energy to the oscillation maximum (for example [35] which is for $\sin^2 2\theta_{23}$), or to set up a detector at baseline corresponding to it as employed by various reactor experiments to measure θ_{13} [40, 43]. It is also notable that the first proposal of prototype superbeam experiment for detecting CP violation [30] entailed in a setup at around the first oscillation maximum.

For θ_{12} the latter method can be applied to reactor neutrinos and in fact a concrete idea for possible experimental setup for dedicated reactor θ_{12} is worked out in detail [90, 91]. See also [92] for the related proposals with reactor neutrinos. The type of experiment is dubbed in [90] as "SADO", an acronym of *Several-tens of km Antineutrino DetectOr* because of the range of baseline distance appropriate for the experiments. It is a very feasible experiment because it does not require extreme reduction of the systematic error to 1% level, as required in the θ_{13} measurement mentioned above. As is demonstrated in [90] reduction of the systematic error to 4% level would be sufficient if no energy spectrum cut at $E_{prompt} = 2.6$ MeV is performed. It should be within reach in view of the current KamLAND error of 6.5% [16]. The

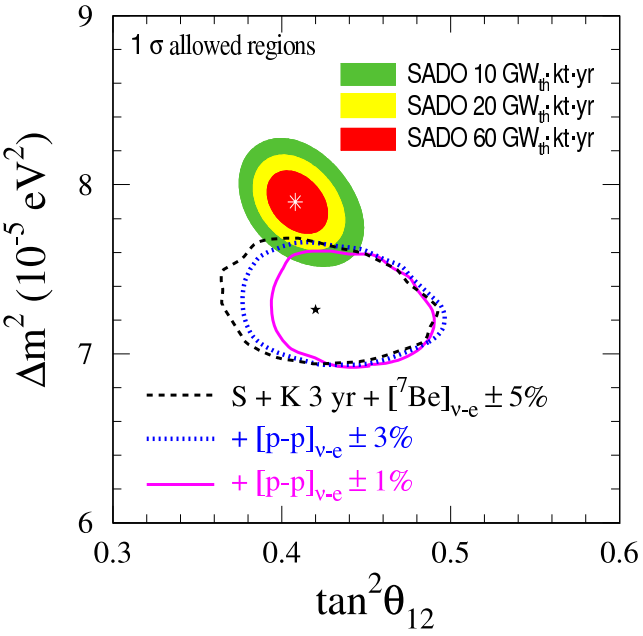

Figure 13: SADO's sensitivity contours are plotted in $\tan^2\theta_{12}$-Δm^2_{21} space and are overlaid on Fig.6 of the roadmap paper [89], in which the sensitivities of solar-KamLAND combined method are presented. The errors are defined both with 2 DOF. Taken from [91].

effect of geo-neutrino background, which then has to be worried about without spectrum cut, is shown to be tolerable even for most conservative choice of geo-neutrino model, the Fully Radiogenic model [90].

The accuracy achievable by the dedicated reactor θ_{12} measurement is quite remarkable. It will reach to 2% level at 1σ CL (1 DOF) for 60 $\mathrm{GW_{th}}\cdot\mathrm{kt}\cdot\mathrm{yr}$ exposure as shown in Table 1. With Kashiwazaki-Kariwa nuclear reactor complex, it corresponds to about 6 years operation for KamLAND size detector. It is notable that possible uncertainties due to the surrounding reactors are also modest, as one can see in Table 1. In Fig. 13 we show in the two-dimensional space spanned by $\tan^2\theta_{12}$ and Δm^2_{21} the contours of sensitivities achievable by the solar-KamLAND method and by the dedicated reactor experiment. Notice that the measurement is not yet systematics dominated and therefore further improvement of the sensitivity is possible by gaining more statistics. If SADO can run long enough it can go beyond the solar-KamLAND method.

9.3 $\mu \leftrightarrow \tau$ symmetry

The $\mu \leftrightarrow \tau$ exchange symmetry is attractive because it predicts $\theta_{13} = 0$ and $\theta_{23} = \pi/4$ in the symmetry limit. For extensive references on this symmetry, see e.g., [26,38,93]. But, since the symmetry is badly broken (note that $m_\tau \simeq 20\ m_\mu$), the predictions $\theta_{13} = 0$ and $\theta_{23} = \pi/4$ cannot be exact. It is important to try to compute deviations from the results obtained in the symmetry limit.

Now, the question is how can we pick up the right one out of the vast majority of the proposed symmetries? One way to proceed is to make clear how symmetry breaking affects the predictions. For example, it is shown in [93] that breaking of the Z_2 symmetry tends to prefer larger deviation from the maximal θ_{23} than vanishing θ_{13}. Such study has to be performed in an extensive way including various symmetries.

If one can make definitive prediction in a class of models on which octant of θ_{23} is chosen when the $\mu \leftrightarrow \tau$ symmetry is broken, one can test such a class of models by resolving the θ_{23} octant degeneracy. We have discussed in Sec. 7 and in Sec. 8 the ways of how it can be carried out.

9.4 Comments on precision measurement of Δm^2

We have explained in Sec. 2 how the atmospheric Δm^2_{32}, which may be better characterized as $\Delta m^2_{\mu\mu}$ [83], can be determined. For various reasons one may want to improve the accuracy of determining Δm^2_{32} to a sub-percent level. Here, we want to remark that unfortunately there is a serious obstacle against it; the problem of absolute energy scale error. See Appendix of [84] for an explicit demonstration of this fact. It comes from the limitation of the accuracy of calibrating the absolute energy of muons in the case of ν_μ disappearance measurement. The current value for the error in Super-Kamiokande is about 2% at GeV region (second reference in [1]) and apparently no concrete idea has been emerged to improve it. It is believed to be a limiting factor in Δm^2_{32} determination in much higher statistics region enabled by T2K II with Hyper-Kamiokande.

We note that there is the unique case which is free from the problem of energy scale error; the recently proposed resonant $\overline{\nu}_e$ absorption reaction enhanced by Mössbauer effect [94]. This method utilizes the recoilless resonant absorption reaction, $\overline{\nu}_e + {}^3$He + orbital $e^- \rightarrow {}^3$H, with monochromatic $\overline{\nu}_e$ beam from the T-conjugate bound state beta decay, ${}^3\mathrm{H} \rightarrow {}^3\mathrm{He} + \text{orbital } e^- + \overline{\nu}_e$. When the source atoms are embedded into a solid the energy width of the beam is estimated to be $\sim 10^{-11}$ eV, which is utterly negligible. If feasible experimentally, the monochromatic nature of the beam may allow accurate measurement of Δm^2_{31} to $\simeq (0.3/\sin^2 2\theta_{13})\%$ at 1σ CL [95]. We emphasize that it gives a very rare chance of achieving a sub-percent level determination of Δm^2_{31}.

10 Conclusion

I have tried to give an overview of neutrino physics emphasizing the experimental activities in the near future. I must admit that this is a personal overview, not mentioning very many important subjects and projects in all over the world, and I have to apologize for that. But, I tried to give a coherent view which largely come from the works I did in the last several years. I feel it appropriate to emphasize that we have learned a lot during the golden era of neutrino physics. But, it seems obvious to me that we have done only a half and new surprises are waiting for us in the future.

I would like to thank all of my collaborators, in particular Takaaki Kajita, Hiroshi Nunokawa, Masaki Ishitsuka, Shoei Nakayama, Renata Zukanovich Funchal, Stephen Parke, Hiroaki Sugiyama, and Shoichi Uchinami for fruitful collaborations and useful discussions. This work was supported in part by the Grant-in-Aid for Scientific Research, No. 16340078, Japan Society for the Promotion of Science.

Bibliography

[1] Y. Fukuda *et al.* [Super-Kamiokande Collaboration], Phys. Rev. Lett. **81**, 1562 (1998) [arXiv:hep-ex/9807003]; Y. Ashie *et al.* [Super-Kamiokande Collaboration], Phys. Rev. D **71**, 112005 (2005) [arXiv:hep-ex/0501064].

[2] K. S. Hirata *et al.* [Kamiokande-II Collaboration], Phys. Lett. B **280**, 146 (1992); Y. Fukuda *et al.* [Kamiokande Collaboration], Phys. Lett. B **335**, 237 (1994).

[3] B. Pontecorvo, Sov. Phys. JETP **7**, 172 (1958) [Zh. Eksp. Teor. Fiz. **34**, 247 (1957)].

[4] M. Gell-Mann and A. Pais, Phys. Rev. **97**, 1387 (1955); A. Pais and O. Piccioni, Phys. Rev. **100**, 1487 (1955).

[5] Z. Maki, M. Nakagawa and S. Sakata, Prog. Theor. Phys. **28**, 870 (1962).

[6] M. H. Ahn *et al.* [K2K Collaboration], Phys. Rev. Lett. **90**, 041801 (2003) [arXiv:hep-ex/0212007].

[7] J. N. Bahcall, Phys. Rev. Lett. **12**, 300 (1964); R. Davis, Phys. Rev. Lett. **12**, 303 (1964).

[8] B. T. Cleveland *et al.*, Astrophys. J. **496**, 505 (1998); Y. Fukuda *et al.* [Kamiokande Collaboration], Phys. Rev. Lett. **77**, 1683 (1996); J. N. Abdurashitov *et al.* [SAGE Collaboration], Phys. Rev. C **60**, 055801 (1999) [arXiv:astro-ph/9907113]; W. Hampel *et al.* [GALLEX Collaboration], Phys. Lett. B **447**, 127 (1999); M. Altmann *et al.* [GNO Collaboration], Phys.

Lett. B **616**, 174 (2005) [arXiv:hep-ex/0504037]; J. Hosaka *et al.* [Super-Kamkiokande Collaboration], Phys. Rev. D **73**, 112001 (2006) [arXiv:hep-ex/0508053]; B. Aharmim *et al.* [SNO Collaboration], Phys. Rev. C **72**, 055502 (2005) [arXiv:nucl-ex/0502021].

[9] Q. R. Ahmad *et al.* [SNO Collaboration], Phys. Rev. Lett. **87**, 071301 (2001) [arXiv:nucl-ex/0106015]; S. Fukuda *et al.* [Super-Kamiokande Collaboration], Phys. Rev. Lett. **86**, 5651 (2001) [arXiv:hep-ex/0103032].

[10] Q. R. Ahmad *et al.* [SNO Collaboration], Phys. Rev. Lett. **89**, 011301 (2002) [arXiv:nucl-ex/0204008]. S. N. Ahmed *et al.* [SNO Collaboration], Phys. Rev. Lett. **92**, 181301 (2004) [arXiv:nucl-ex/0309004].

[11] The first reference in [8].

[12] K. Eguchi *et al.* [KamLAND Collaboration], Phys. Rev. Lett. **90**, 021802 (2003) [arXiv:hep-ex/0212021];

[13] L. Wolfenstein, Phys. Rev. D **17**, 2369 (1978). S. P. Mikheyev and A. Yu. Smirnov, Yad. Fiz. **42**, 1441 (1985) [Sov. J. Nucl. Phys. **42**, 913 (1985)]; Nuovo Cim. C **9**, 17 (1986).

[14] O. G. Miranda, M. A. Tortola and J. W. F. Valle, JHEP **0610**, 008 (2006) [arXiv:hep-ph/0406280].

[15] Y. Ashie *et al.* [Super-Kamiokande Collaboration], Phys. Rev. Lett. **93**, 101801 (2004) [arXiv:hep-ex/0404034].

[16] T. Araki *et al.* [KamLAND Collaboration], Phys. Rev. Lett. **94**, 081801 (2005) [arXiv:hep-ex/0406035].

[17] E. Aliu *et al.* [K2K Collaboration], Phys. Rev. Lett. **94**, 081802 (2005) [arXiv:hep-ex/0411038].

[18] D. G. Michael *et al.* [MINOS Collaboration], arXiv:hep-ex/0607088.

[19] M. Apollonio *et al.* [CHOOZ Collaboration], Phys. Lett. B **420**, 397 (1998) [arXiv:hep-ex/9711002]; *ibid.* B **466**, 415 (1999) [arXiv:hep-ex/9907037]. See also, The Palo Verde Collaboration, F. Boehm *et al.*, Phys. Rev. D **64** (2001) 112001 [arXiv:hep-ex/0107009].

[20] M. H. Ahn *et al.* [K2K Collaboration], Phys. Rev. Lett. **93**, 051801 (2004) [arXiv:hep-ex/0402017].

[21] A. Gamba, R. E. Marshak and S. Okubo, Proc. Nat. Acad. Sci. **45**, 881 (1959); Z. Maki, M. Nakagawa, Y. Ohnuki, and S. Sakata, Prog. Theor. Phys. **23**, 1174 (1960).

[22] C. Bouchiat, J. Iliopoulos and P. Meyer, Phys. Lett. B **38**, 519 (1972).

[23] M. Kobayashi and T. Maskawa, Prog. Theor. Phys. **49**, 652 (1973).

[24] M. Fukugita and T. Yanagida, Phys. Lett. B **174**, 45 (1986).

[25] S. Pascoli, S. T. Petcov and A. Riotto, arXiv:hep-ph/0611338.

[26] R. N. Mohapatra and A. Y. Smirnov, J. Phys. Conf. Ser. **53**, 44 (2006) [arXiv:hep-ph/0603118].

[27] M. Raidal, Phys. Rev. Lett. **93**, 161801 (2004) [arXiv:hep-ph/0404046]; H. Minakata and A. Yu Smirnov, Phys. Rev. D **70**, 073009 (2004) [arXiv:hep-ph/0405088].

[28] For a review in an early stage, see e.g., H. Minakata, arXiv:hep-ph/0505262.

[29] W. M. Yao *et al.* [Particle Data Group], J. Phys. G **33**, 1 (2006).

[30] H. Minakata and H. Nunokawa, Phys. Lett. B **495**, 369 (2000) [arXiv:hep-ph/0004114]; Nucl. Instrum. Meth. A **472**, 421 (2000) [arXiv:hep-ph/0009091].

[31] J. Sato, Nucl. Instrum. Meth. **A472**, 434 (2001) [arXiv:hep-ph/0008056]; B. Richter, arXiv:hep-ph/0008222.

[32] The conference web page; http://www.usfq.edu.ec/phy/

[33] The conference web page; http://hql06.physik.tu-muenchen.de/

[34] M. H. Ahn *et al.* [K2K Collaboration], Phys. Rev. D **74**, 072003 (2006) [arXiv:hep-ex/0606032].

[35] Y. Itow *et al.*, arXiv:hep-ex/0106019. For an updated version, see http://neutrino.kek.jp/jhfnu/loi/loi.v2.030528.pdf

[36] K. Hiraide, Master Thesis, Kyoto University, February 2005 (in Japanese), http://jnusrv01.kek.jp/jhfnu/thesis/

[37] H. Minakata, M. Sonoyama and H. Sugiyama, Phys. Rev. D **70**, 113012 (2004) [arXiv:hep-ph/0406073].

[38] K. Hiraide, H. Minakata, T. Nakaya, H. Nunokawa, H. Sugiyama, W. J. C. Teves and R. Zukanovich Funchal, Phys. Rev. D **73**, 093008 (2006) [arXiv:hep-ph/0601258].

[39] D. S. Ayres *et al.* [NOvA Collaboration], arXiv:hep-ex/0503053.

[40] H. Minakata, H. Sugiyama, O. Yasuda, K. Inoue and F. Suekane, Phys. Rev. D **68**, 033017 (2003) [Erratum-ibid. D **70**, 059901 (2004)] [arXiv:hep-ph/0211111].

[41] J. Arafune, M. Koike and J. Sato, Phys. Rev. D **56** (1997) 3093 [*Erratum-ibid.* D **60** (1997) 119905], [arXiv:hep-ph/9703351].

[42] Y. Kozlov, L. Mikaelyan and V. Sinev, Phys. Atom. Nucl. **66**, 469 (2003) [Yad. Fiz. **66**, 497 (2003)] [arXiv:hep-ph/0109277].

[43] K. Anderson *et al.*, White Paper Report on Using Nuclear Reactors to Search for a Value of θ_{13}, arXiv:hep-ex/0402041.

[44] F. Ardellier *et al.* [Double Chooz Collaboration], arXiv:hep-ex/0606025.

[45] Kyung Kwang Joo, Talk given at Neutrino Oscillation Workshop (NOW2006) Conca Specchiulla, Otranto, Italy, September 9-16, 2006.

[46] Y. f. Wang, arXiv:hep-ex/0610024.

[47] H. Minakata and S. Watanabe, Phys. Lett. **B468**, 256 (1999) [arXiv:hep-ph/9906530].

[48] H. Minakata and H. Sugiyama, Phys. Lett. B **580**, 216 (2004) [arXiv:hep-ph/0309323].

[49] M. Komatsu, P. Migliozzi, and F. Terranova, J. Phys. G **29**, 443 (2003) [arXiv:hep-ph/0210043].

[50] S. Geer, Phys. Rev. D **57**, 6989 (1998) [Erratum-ibid. D **59**, 039903 (1999)] [arXiv:hep-ph/9712290]; A. De Rujula, M. B. Gavela and P. Hernandez, Nucl. Phys. **B547**, 21 (1999) [arXiv:hep-ph/9811390].

[51] P. Zucchelli, Phys. Lett. B **532**, 166 (2002).

[52] M. Apollonio *et al.*, arXiv:hep-ph/0210192; C. Albright *et al.*, arXiv:hep-ex/0008064.

[53] H. Minakata and H. Nunokawa, Phys. Rev. D **57**, 4403 (1998) [arXiv:hep-ph/9705208];

[54] O. Yasuda, Acta Phys. Polon. B **30**, 3089 (1999) [arXiv:hep-ph/9910428].

[55] A. Cervera, A. Donini, M. B. Gavela, J. J. Gomez Cadenas, P. Hernandez, O. Mena and S. Rigolin, Nucl. Phys. B **579**, 17 (2000) [Erratum-ibid. B **593**, 731 (2001)] [arXiv:hep-ph/0002108].

[56] H. Minakata and H. Nunokawa, JHEP **0110**, 001 (2001) [arXiv:hep-ph/0108085]; Nucl. Phys. Proc. Suppl. **110**, 404 (2002) [arXiv:hep-ph/0111131].

[57] H. Minakata, H. Nunokawa and S. J. Parke, Phys. Lett. B **537**, 249 (2002) [arXiv:hep-ph/0204171].

[58] M. Blom and H. Minakata, New J. Phys. **6**, 130 (2004) [arXiv:hep-ph/0404142].

[59] H. Minakata, Nucl. Phys. Proc. Suppl. **100**, 237 (2001) [arXiv:hep-ph/0101231].

[60] International Scoping Study of a Future Neutrino Factory and Super-Beam Facility; http://www.hep.ph.ic.ac.uk/iss/

[61] M. G. Catanesi, Nucl. Phys. Proc. Suppl. **100**, 130 (2001). G. Prior [HARP Collaboration], Nucl. Phys. A **752**, 24 (2005).

[62] R. Raja, Nucl. Instrum. Meth. A **553**, 225 (2005) [arXiv:hep-ex/0501005]; D. Isenhower *et al.* [MIPP Collaboration], arXiv:hep-ex/0609057.

[63] S. Nakayama *et al.* [K2K Collaboration], Phys. Lett. B **619**, 255 (2005) [arXiv:hep-ex/0408134]; M. Hasegawa *et al.* [K2K Collaboration], Phys. Rev. Lett. **95**, 252301 (2005) [arXiv:hep-ex/0506008]; M. O. Wascko [MiniBooNE Collaboration], arXiv:hep-ex/0602050; K. S. McFarland [MINERvA Collaboration], arXiv:physics/0605088; A. A. Aguilar-Arevalo *et al.* [SciBooNE Collaboration], arXiv:hep-ex/0601022.

[64] P. Huber, M. Lindner and W. Winter, Nucl. Phys. B **645**, 3 (2002) [arXiv:hep-ph/0204352].

[65] J. Burguet-Castell, M. B. Gavela, J. J. Gomez-Cadenas, P. Hernandez and O. Mena, Nucl. Phys. B **608**, 301 (2001) [arXiv:hep-ph/0103258].

[66] G. Fogli and E. Lisi, Phys. Rev. **D54**, 3667 (1996) [arXiv:hep-ph/9604415].

[67] V. Barger, D. Marfatia and K. Whisnant, Phys. Rev. D **65**, 073023 (2002) [arXiv:hep-ph/0112119];

[68] H. Minakata, H. Nunokawa and S. Parke, Phys. Rev. D **66**, 093012 (2002) [arXiv:hep-ph/0208163].

[69] T. Kajita, H. Minakata and H. Nunokawa, Phys. Lett. B **528**, 245 (2002) [arXiv:hep-ph/0112345].

[70] M. Ishitsuka, T. Kajita, H. Minakata and H. Nunokawa, Phys. Rev. D **72**, 033003 (2005) [arXiv:hep-ph/0504026].

[71] . Kajita, H. Minakata, S. Nakayama and H. Nunokawa, Phys. Rev. D **75**, 013006 (2007) [arXiv:hep-ph/0609286].

[72] The first workshop: http://newton.kias.re.kr/ hepph/J2K/
The second workshop: http://t2kk.snu.ac.kr/

[73] H. Minakata, arXiv:hep-ph/0604088; Phys. Scripta **127**, 73 (2006).

[74] H. Minakata and H. Nunokawa, Phys. Lett. B **413**, 369 (1997) [arXiv:hep-ph/9706281].

[75] O. L. G. Peres and A. Y. Smirnov, Phys. Lett. B **456**, 204 (1999) [arXiv:hep-ph/9902312]; Nucl. Phys. B **680**, 479 (2004) [arXiv:hep-ph/0309312]; M. C. Gonzalez-Garcia, M. Maltoni and A. Y. Smirnov, Phys. Rev. D **70**, 093005 (2004) [arXiv:hep-ph/0408170].

[76] M. Shiozawa, T. Kajita, S. Nakayama, Y. Obayashi, and K. Okumura, in Proceedings of the RCCN International Workshop on Sub-dominant Oscillation Effects in Atmospheric Neutrino Experiments, Kashiwa, Japan, Dec. 2004, p.57; T. Kajita, Nucl. Phys. Proc. Suppl. **155**, 87 (2006).

[77] S. Choubey and P. Roy, Phys. Rev. D **73**, 013006 (2006) [arXiv:hep-ph/0509197].

[78] T. Kajita, Talk given at Next Generation of Nucleon Decay and Neutrino Detectors (NNN05), Aussois, Savoie, France, April 7-9, 2005. http://nnn05.in2p3.fr/; S. Palomares-Ruiz and S. T. Petcov, Nucl. Phys. B **712**, 392 (2005) [arXiv:hep-ph/0406096]; S. T. Petcov and T. Schwetz, Nucl. Phys. B **740**, 1 (2006) [arXiv:hep-ph/0511277]; R. Gandhi, P. Ghoshal, S. Goswami, P. Mehta and S. Uma Sankar, arXiv:hep-ph/0506145.

[79] A. S. Dighe and A. Y. Smirnov, Phys. Rev. D **62**, 033007 (2000) [arXiv:hep-ph/9907423]; H. Minakata and H. Nunokawa, Phys. Lett. B **504**, 301 (2001) [arXiv:hep-ph/0010240]; C. Lunardini and A. Y. Smirnov, JCAP **0306**, 009 (2003) [arXiv:hep-ph/0302033]. V. Barger, P. Huber and D. Marfatia, Phys. Lett. B **617**, 167 (2005) [arXiv:hep-ph/0501184].

[80] A. S. Dighe, M. T. Keil and G. G. Raffelt, JCAP **0306**, 005 (2003) [arXiv:hep-ph/0303210]; *ibid.* **0306**, 006 (2003) [arXiv:hep-ph/0304150]; R. Tomas,

M. Kachelriess, G. Raffelt, A. Dighe, H. T. Janka and L. Scheck, JCAP **0409**, 015 (2004) [arXiv:astro-ph/0407132].

[81] S. Pascoli, S. T. Petcov and T. Schwetz, Nucl. Phys. B **734**, 24 (2006) [arXiv:hep-ph/0505226]; S. Choubey and W. Rodejohann, Phys. Rev. D **72**, 033016 (2005) [arXiv:hep-ph/0506102].

[82] A. de Gouvea, J. Jenkins and B. Kayser, Phys. Rev. D **71**, 113009 (2005) [arXiv:hep-ph/0503079];

[83] H. Nunokawa, S. J. Parke and R. Zukanovich Funchal, Phys. Rev. D **72**, 013009 (2005) [arXiv:hep-ph/0503283].

[84] H. Minakata, H. Nunokawa, S. J. Parke and R. Zukanovich Funchal, Phys. Rev. D **74**, 053008 (2006) [arXiv:hep-ph/0607284].

[85] P. Huber, M. Maltoni and T. Schwetz, Phys. Rev. D **71**, 053006 (2005) [arXiv:hep-ph/0501037].

[86] M. Nakahata, Talk at the 5th Workshop on "Neutrino Oscillations and their Origin" (NOON2004), February 11-15, 2004, Odaiba, Tokyo, Japan. http://www-sk.icrr.u-tokyo.ac.jp/noon2004/

[87] G. Alimonti *et al.* [Borexino Collaboration], Astropart. Phys. **16**, 205 (2002) [arXiv:hep-ex/0012030].

[88] J. Shirai, Talk given at Neutrino Oscillation Workshop (NOW2006), Conca Specchiulla (Otranto, Lecce, Italy), September 9-16, 2006,

[89] J. N. Bahcall and C. Peña-Garay, JHEP **0311**, 004 (2003) [arXiv:hep-ph/0305159].

[90] H. Minakata, H. Nunokawa, W. J. C. Teves and R. Zukanovich Funchal, Phys. Rev. D **71**, 013005 (2005) [arXiv:hep-ph/0407326];

[91] H. Minakata, H. Nunokawa, W. J. C. Teves and R. Zukanovich Funchal, Nucl. Phys. Proc. Suppl. **145**, 45 (2005) [arXiv:hep-ph/0501250].

[92] A. Bandyopadhyay, S. Choubey, S. Goswami and S. T. Petcov, Phys. Rev. D **72**, 033013 (2005) [arXiv:hep-ph/0410283]; J. F. Kopp, M. Lindner, A. Merle and M. Rolinec, arXiv:hep-ph/0606151; S. T. Petcov and T. Schwetz, arXiv:hep-ph/0607155.

[93] W. Grimus, A. S. Joshipura, S. Kaneko, L. Lavoura, H. Sawanaka and M. Tanimoto, Nucl. Phys. B **713**, 151 (2005) [arXiv:hep-ph/0408123].

[94] R. S. Raghavan, arXiv:hep-ph/0601079.

[95] H. Minakata and S. Uchinami, New J. Phys. **8**, 143 (2006) [arXiv:hep-ph/0602046].

Latest Results from MINOS

David E. Jaffe,
for the MINOS collaboration
Department of Physics
Brookhaven National Laboratory
Upton, NY, USA

Amongst the goals of the MINOS experiment are the test of the $\nu_\mu \to \nu_\tau$ oscillation and the search for sub-dominant $\nu_\mu \to \nu_e$ oscillations. The former proceeds by a ν_μ "disappearance" analysis while the latter would involve the "appearance" of ν_e interactions in a predominantly ν_μ beam.

The disappearance of muon neutrinos is described by

$$P(\nu_\mu \to \nu_\mu) = 1 - \sin^2 2\theta_{23} \sin^2(1.27\Delta m^2_{23} L/E) \quad (1)$$

in the two-flavor approximation where θ_{23} is the angle between the second row and third column of the neutrino mixing matrix, $\Delta m^2_{23} = m^2_2 - m^2_3$ (eV^2), L is the neutrino flight distance in km and E is the neutrino energy in GeV. A generic disappearance experiment compares a measured muon neutrino energy spectrum at a fixed baseline to the known energy spectrum of muon neutrino beam to extract the oscillation parameters $\sin^2 2\theta$ which controls the overall magnitude of the disappearance and Δm^2 which controls the energy dependence.

MINOS is a long baseline neutrino experiment with a near detector (ND) located 1 km from the primary target in the Fermilab NuMI beam line and a far detector (FD) located 735 km away in the Soudan mine in Minnesota approximately 700 meters underground. To produce the neutrino beam, the 120 GeV main injector proton beam impinges upon a $\sim$1 m long segmented graphite target in a $\sim$10 μs spill. Two magnetic focusing horns downstream of the target focus positive mesons into the 675m long decay pipe where $\pi^+ \to \mu^+\nu_\mu$ decays are the dominant mechanism for the production of the neutrino beam. The NuMI target is moveable and the low energy (LE-10) configuration is the most favorable for the oscillation analysis and constitutes $\sim$ 95% of the total exposure. The LE-10 beam is 92.9% ν_μ, 5.8% $\overline{\nu}_\mu$ and 1.3% $\nu_e + \overline{\nu}_e$. The remaining $\sim$5% of the exposure was taken with other configurations for systematic studies. For an exposure of 10^{20} protons-on-target (POT), approximately 390 ν_μ events are expected at the FD in the absence of oscillations.

Both the ND and FD are functionally identical and consist of 2.54 cm thick octagonal steel plates magnetized with a toroidal 1.2 T field interleaved with planes composed of 4.1 cm wide $\times$ 1 cm thick scintillator strips. Alternating U- and V-planes of scintillator are oriented at $\pm 45^\circ$ with respect to the vertical. The ND and

FD contains 282/152 and 484/484 steel/scintillator planes for a mass of 1 and 5.4 kt, respectively. The FD is divided into two equal length super modules.

Muon neutrino charged current (CC) interactions are identified by a long muon track and hadronic activity at the interaction vertex. By contrast, neutral current (NC) interactions often create short, diffuse showers whilst ν_e CC events are characterized by a typical compact electromagnetic shower profile. The neutrino energy is given by the sum of the shower and muon energy. The shower energy resolution is $55\%/\sqrt{(E \text{ GeV})}$ and the muon momentum resolution is 13% based on curvature and 6% based on range for muons that stop in the detector.

The separation of ν_μ CC candidates from the NC background begins with beam and data quality cuts (FD livetime $\approx 99\%$). Candidate events are required to have at least one negatively charged track with a vertex in the fiducial volume ($1 < z(\text{m}) < 5$ and $r(\text{m}) < 1$ at the ND and 0.5(2.0) meter from the front(rear) face of each FD supermodule and $r(\text{m}) < 3.7$). Further separation is provided by use of a 'particle identification' (PID) variable that combines three simulated probability density functions (PDFs) for CC and NC events. The three PDFs are the distribution of event length which is related to the muon momentum, the fraction of the pulse height in the event that is on the track which is related to the event inelasticity and the pulse height per plane on the track which is related to dE/dx. The resulting selection achieves a CC purity of $\sim$97% at both the ND and FD.

To predict the unoscillated FD energy spectrum, an extrapolation method is used that takes into account the two-body pion decay kinematics and the beamline geometry to accomodate the effective point (line) source of neutrinos as seen by the FD (ND). The primary extrapolation method is dubbed the 'beam matrix method' and it, as well as alternative methods, were tested extensively for robustness with simulated data.

Figure 1 shows the predicted FD ν_μ candidate spectrum using the matrix method as well as an alternative method and the data for a total exposure of 1.17×10^{20} POT. The oscillations parameters determined from the fit are $|\Delta m^2_{32}| = (2.74^{+0.44}_{-0.26}) \times 10^{-3}$ eV^2 and $\sin^2 2\theta_{32} = 1.00^{+0.00}_{-0.13}$ where both the statistical and systematic uncertainties are included [1]. The results are compared to previous measurements in Figure 2 and show the improvement in $|\Delta m^2_{32}|$ precision achieved by the MINOS result. The systematic uncertainty is currently $\sim 40\%$ of the statistical uncertainty for $|\Delta m^2_{32}|$ and is largely data driven, thus it is expected to decrease with the accumulation of more data. Hence one expects the $|\Delta m^2_{32}|$ precision to be dominated by statistical uncertainty for the foreseeable future.

A ν_e "appearance" analysis by MINOS has a substantially different character than the disappearance analysis in that it is background dominated. The appearance probability is

$$P(\nu_\mu \to \nu_e) \approx \sin^2\theta_{23} \sin^2 2\theta_{13} \sin^2(1.27\Delta m^2_{23} L/E) \qquad (2)$$

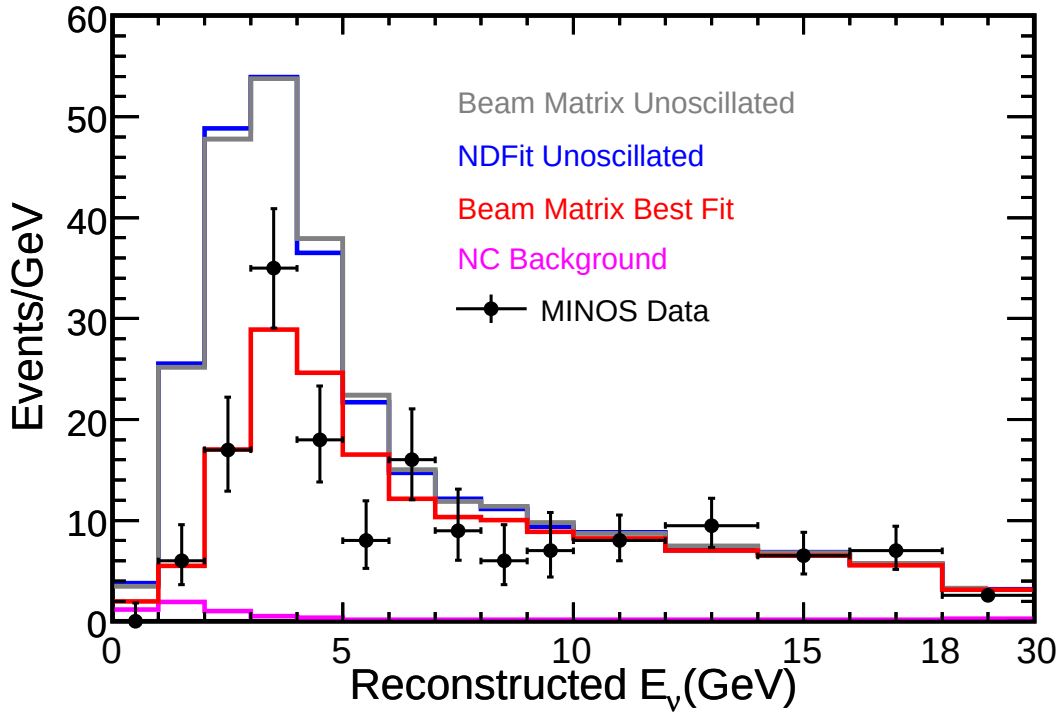

Figure 1: Comparison of the far detector spectrum with predictions for no oscillations for both analysis methods and for oscillations with the best-fit parameters from the beam matrix extrapolation method. The estimated NC background is also shown. The last energy bin contains events between 18-30 Gev.

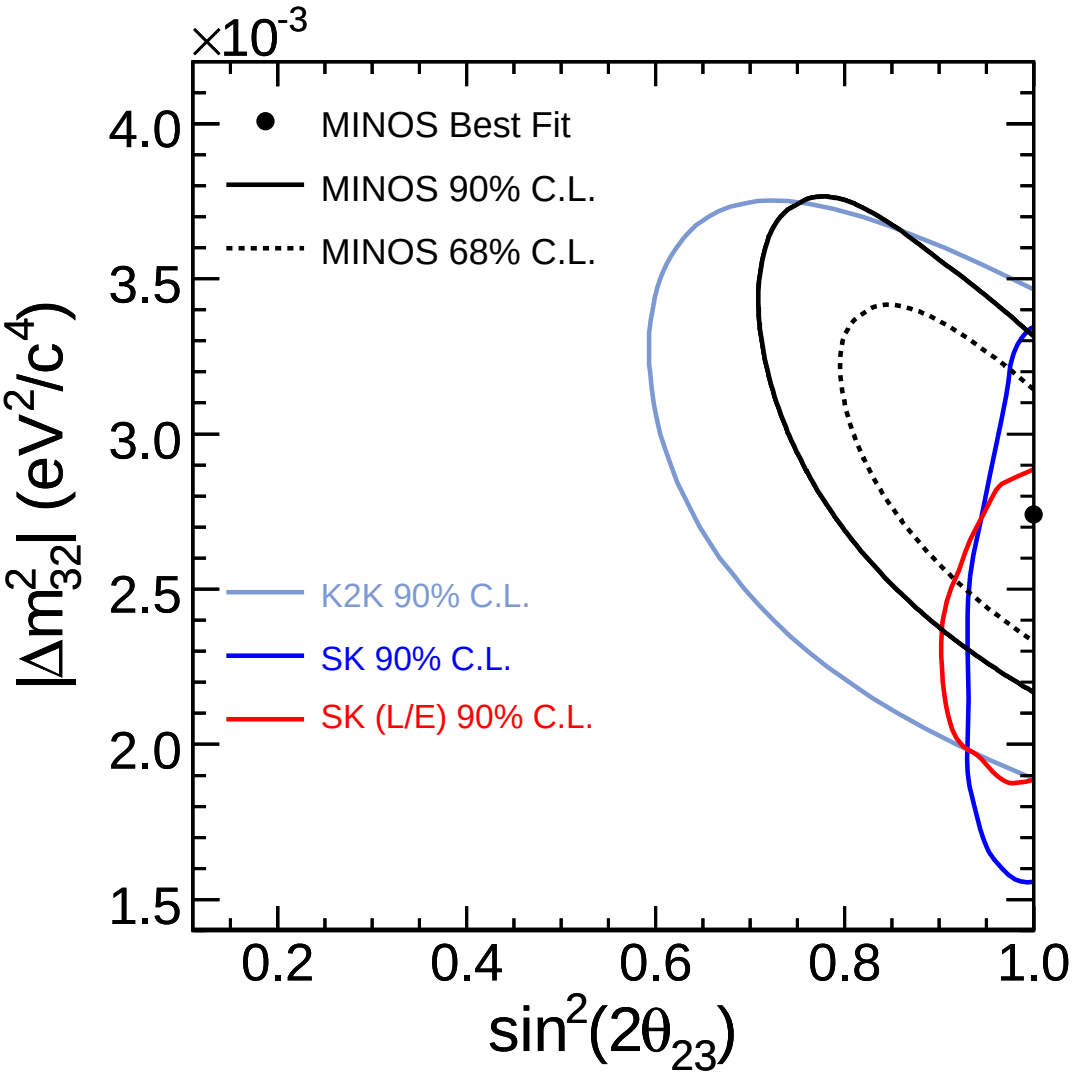

Figure 2: Confidence intervals for the fit to the MINOS data using the beam matrix method including systematic errors. Also shown are the contours from the previous highest precision experiments [2].

and is sensitive to $\sin^2 2\theta_{13}$ for which only an upper limit of 0.17 at 90% CL exists [3]. The ν_e appearance is difficult because the MINOS detector is not optimized for electromagnetic shower detection. Even with relatively sophisticated ν_e candidate selection, the background to signal ratio for $\sin^2 2\theta_{13} = 0.10$ is ≈ 2. Approximately 2/3 of the background is due to NC events where π^0 final states in the hadronic system produce electromagnetic showers. The intrinsic ν_e component of the beam is expected to contribute an additional $\sim 15\%$ of the background. The remaining two components each contribute $\sim 10\%$ and are due to ν_μ CC interactions with an unidentified muon track or to ν_τ CC events that have an electron in the final state.

Given that the ν_e appearance analysis is background-dominated, various techniques have been developed to estimate the background components from the data. Two techniques are under investigation for estimating the NC background. One technique would create "NC" events by removing the reconstructed muon track from ν_μ CC events and reconstructing the "muon-removed" events. The second technique would use data with the magnetic horns turned off to resolve the NC and ν_μ CC background components at the ND. With the horns off, the high energy portion of the neutrino spectrum, which is largely responsible for the NC background, remains whilst the ν_μ CC component produced by the focusing of the horns, is greatly diminished (Figure 1). For the intrinsic ν_e beam component of the background, a technique that exploits the ability to MINOS to distinguish ν_μ and $\overline{\nu}_\mu$ is being investigated. The ν_e beam at low energy is dominated by ν_e from $\mu^+ \to e^+\nu_e\overline{\nu}_\mu$ decays where the μ^+ are the produced by focused π^+ decays. The technique would attempt to resolve the $\sim 10\%$ contribution to the $\overline{\nu}_\mu$ spectrum at the ND by subtracting the estimated contribution to $\overline{\nu}_\mu$ from pion and kaon decays. Assuming the total background can be determined with a $\pm 10\%$ precision, MINOS can achieve a 90% CL sensitivity to $\sin^2 2\theta_{13}$ via ν_e appearance comparable to the current limit with an exposure of 4×10^{20} POT.

In summary, using an exposure of 1.27×10^{20} POT, MINOS has completed a ν_μ disappearance analysis with results $|\Delta m^2_{32}| = (2.74^{+0.44}_{-0.26}) \times 10^{-3}$ eV^2 and $\sin^2 2\theta_{32} = 1.00^{+0.00}_{-0.13}$ consistent with previous results. Prospects for ν_e appearance analysis with the second year of running have been presented.

Bibliography

[1] D.G. Michael *et al.*, Phys.Rev.Lett.**97**, 191801 (2006).

[2] Y.Ashie *et al.*, Phys.Rev.Lett. **93**, 101801 (2004); Y.Ashie *et al.*, Phys.Rev. D**71**, 112005 (2005); E.Aliu *et al.*, Phys.Rev.Lett. **94**, 081802 (2005); M.H.Ahn *et al.*, `hep-ex/0606032`.

[3] M.Apollonio *et al.*, Eur.Phys.J. C **27**, 331 (2003).

Summary Talk

Summary Talk

Shedding light on flavour symmetries with rare decays of quarks and leptons

Gino Isidori
INFN, Laboratori Nazionali di Frascati,
Via E. Fermi 40,
I-00044 Frascati, Italy

1 Introduction

In the last few years there has been a great experimental progress in quark and lepton flavour physics. On the quark side, the two B-factories have been very successful, both from the accelerator and the detector point of view. As a result, all the relevant parameters describing quark-flavour mixing within the Standard Model (quark masses and CKM angles) are now know with good accuracy. Despite this great progress, the overall picture of quark flavour physics is a bit frustrating as far as the search for physics beyond the Standard Model (SM) is concerned. The situation is somehow similar to the flavour-conserving electroweak physics after LEP: the SM works very well and genuine one-loop electroweak effects have been tested with relative accuracy in the 10%–30% range.

The situation of the lepton sector is more uncertain but also more exciting. The discovery of neutrino oscillations has two very significant implications: i) the SM is not complete; ii) there exists new flavour structures in addition to the three SM Yukawa couplings. We have not yet enough information to unambiguously determine how the SM Lagrangian should be modified in order to describe the phenomenon of neutrino oscillations. However, natural explanations point toward the existence of new degrees of freedom with explicit breaking of lepton number at very high energy scales ($\Lambda_{\rm LN} \sim 10^{10}$–$10^{15}$ GeV), in agreement with the expectations of Grand Unified Theories (GUT). As I will discuss in this talk, these insight about non-SM degrees of freedom from neutrino physics are likely to have non-trivial implications in other sectors of the model. In particular, in rare decays of charged leptons and, possibly, in a few rare B and K decays. Interestingly enough, these connections can be derived without specific dynamical assumptions about new physics, but only analysing the flavour-symmetry structure of the theory be means of general Effective Field Theory (EFT) approaches.

2 The SM as EFT and the flavour problem

The SM Lagrangian can be regarded as the renormalizable part of an effective field theory, valid up to some still undetermined cut-off scale Λ above the electroweak scale. Since the SM is renormalizable, we have no direct clues about the value of Λ; however, theoretical arguments based on a natural solution of the hierarchy problem suggest that Λ should not exceed a few TeV. As long as we are interested only in low-energy experiments, the EFT approach to physics beyond the SM is particularly useful. It allows us to analyse all realistic extensions of the model in terms of few unknown parameters (the coefficients of the higher-dimensional operators suppressed by inverse powers of Λ) and to compare the sensitivity to New Physics (NP) of different low-energy observables.

The non-renormalizable operators should naturally induce large effects in processes which are not mediated by tree-level SM amplitudes, such as flavour-changing neutral-current (FCNC) rare processes. Up to now there is no evidence of deviations from the SM in these processes and this implies severe bounds on the effective scale of various dimension-six operators. For instance, the good agreement between SM expectations and experimental determinations of K^0–$\overline{K}^0$ mixing leads to bounds above 10^4 TeV for the effective scale of $\Delta S = 2$ operators, i.e. well above the few TeV range suggested by the Higgs sector. Similar bounds are obtained for the scale of operators contributing to lepton-flavour violating (LFV) transitions in the lepton sector, such as $\mu \to e\gamma$.

The apparent contradiction between these two determinations of Λ is a manifestation of what in many specific frameworks (supersymmetry, technicolour, etc.) goes under the name of *flavour problem*: if we insist with the theoretical prejudice that new physics has to emerge in the TeV region, we have to conclude that the new theory possesses a highly non-generic flavour structure. Interestingly enough, this structure has not been clearly identified yet, mainly because the SM, i.e. the low-energy limit of the new theory, doesn't possess an exact flavour symmetry.

The most reasonable (but also most *pessimistic*) solution to the flavour problem is the so-called *Minimal Flavour Violation* (MFV) hypothesis [1–4]. Under this assumption, which will be discussed in detail in the next sections, flavour-violating interactions are linked to the known structure of Yukawa couplings also beyond the SM. As a result, non-standard contributions in FCNC transitions turn out to suppressed to a level consistent with experiments even for $\Lambda \sim$ few TeV. On the most interesting aspects of the MFV hypothesis is that it can easily be implemented within the general EFT approach to new physics [3, 4]. The effective theories based on this symmetry principle allow us to establish unambiguous correlations among NP effects in various rare decays. These falsifiable predictions are the key ingredients to identify in a model-independent way which are the irreducible sources of breaking of the flavour symmetry.

3 MFV in the quark sector

The pure gauge sector of the SM is invariant under a large symmetry group of flavour transformations: $\mathcal{G}_{\rm SM} = \mathcal{G}_q \otimes \mathcal{G}_\ell \otimes U(1)^5$, where

$$\mathcal{G}_q = {\rm SU}(3)_{Q_L} \otimes {\rm SU}(3)_{U_R} \otimes {\rm SU}(3)_{D_R}, \qquad \mathcal{G}_\ell = {\rm SU}(3)_{L_L} \otimes {\rm SU}(3)_{E_R} \tag{1}$$

nd three of the five $U(1)$ charges can be identified with baryon number, lepton number and hypercharge [1, 3]. This large group and, particularly the SU(3) subgroups controlling flavour-changing transitions, is explicitly broken by the Yukawa interaction

$$\mathcal{L}_Y = \overline{Q}_L \lambda_d D_R H + \overline{Q}_L \lambda_u U_R H_c + \overline{L}_L \lambda_e E_R H + {\rm h.c.} \tag{2}$$

Since $\mathcal{G}_{\rm SM}$ is broken already within the SM, it would not be consistent to impose it as an exact symmetry of the additional degrees of freedom present in SM extensions: even if absent a the tree-level, the breaking of $\mathcal{G}_{\rm SM}$ would reappear at the quantum level because of the Yukawa interaction. The most restrictive hypothesis we can make to *protect* the breaking of $\mathcal{G}_{\rm SM}$ in a consistent way, is to assume that λ_d, λ_u and λ_e are the only source of $\mathcal{G}_{\rm SM}$-breaking also beyond the SM.

To derive the phenomenological consequences of this hypothesis, it is convenient to treat $\mathcal{G}_{\rm SM}$ as an unbroken symmetry of the underlying theory, promoting the λ_i to be dynamical fields with non-trivial transformation properties under $\mathcal{G}_{\rm SM}$

$$\lambda_u \sim (3, \overline{3}, 1)_{{\rm SU}(3)^3_q} , \qquad \lambda_d \sim (3, 1, \overline{3})_{{\rm SU}(3)^3_q} , \qquad \lambda_e \sim (3, \overline{3})_{{\rm SU}(3)^2_\ell} . \tag{3}$$

f the breaking of $\mathcal{G}_{\rm SM}$ occurs at very high energy scales –well above the TeV region where the we expect new degrees of freedom– at low-energies we would only be sensitive to the background values of the λ_i, i.e. to the ordinary SM Yukawa couplings. Employing the EFT language, we then define that an effective theory satisfies the criterion of Minimal Flavour Violation if all higher-dimensional operators, constructed from SM and λ fields, are (formally) invariant under the flavour group $\mathcal{G}_{\rm SM}$ [3].

According to this criterion, one should in principle consider operators with arbitrary powers of the (adimensional) Yukawa fields. However, a strong simplification arises by the observation that all the eigenvalues of the Yukawa matrices are small, but for the top one, and that the off-diagonal elements of the CKM matrix (V_{ij}) are very suppressed. It is then easy to realize that, similarly to the pure SM case, the leading coupling ruling all FCNC transitions with external down-type quarks is [3]:

$$(\Delta^q_{\rm LL})_{i\neq j} = (\lambda_u \lambda_u^\dagger)_{ij} \approx y_t^2 (V_{\rm CKM})^*_{3i} (V_{\rm CKM})_{3j} , \qquad y_t = m_t/v \approx 1 . \tag{4}$$

s a result, within this framework the bounds on the scale of dimension-six FCNC effective operators turn out to be in the few TeV range (see Ref. [5] for updated values). Moreover, the flavour structure of $\Delta^q_{\rm FC}$ implies a well-defined link among

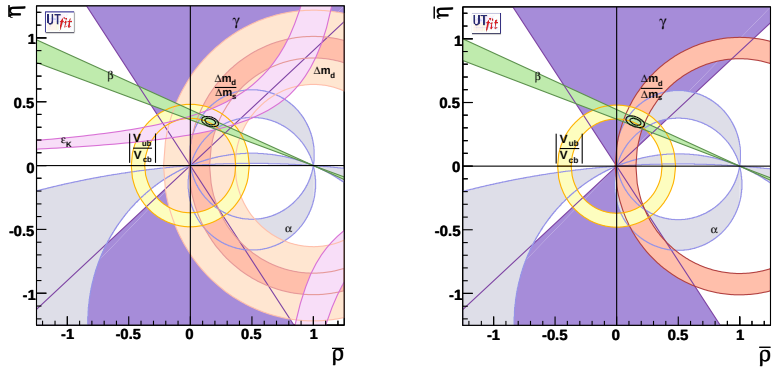

Figure 1: Fit of the CKM unitarity triangle within the SM (left) and in generic extensions of the SM satisfying the MFV hypothesis (right) [5].

possible deviations from the SM in FCNC transitions of the type $s \to d$, $b \to d$, and $b \to s$ (the only quark-level transitions where observable deviations from the SM are expected).

The idea that the CKM matrix rules the strength of FCNC transitions also beyond the SM has become a very popular concept in the recent literature and has been implemented and discussed in several works (see e.g. Ref. [2]). However, it is worth stressing that the CKM matrix represents only one part of the problem: a key role in determining the structure of FCNCs is also played by quark masses (via the GIM mechanism), or by the Yukawa eigenvalues. In this respect, the above MFV criterion provides the maximal protection of FCNCs (or the minimal violation of flavour symmetry), since the full structure of Yukawa matrices is preserved. Moreover, contrary to other approaches, the above MFV criterion is based on a renormalization-group-invariant symmetry argument, which can easily be extended to EFT approaches where new degrees of freedoms (such as extra Higgs doubles, or SUSY partners of the SM fields) are explicitly included.

As shown in Fig. 1, the MFV hypothesis provides a natural (a posteriori) justification of why no NP effects have been observed in the quark sector: by construction, most of the clean observables measured at B factories are insensitive to NP effects in this framework. However, it should be stressed that we are still very far from having proved the validity of this hypothesis from data. Non-minimal sources of flavour symmetry breaking with specific flavour structures, such as those discussed in Ref. [6], are still allowed (even with NP scales in the TeV range). A proof of the MFV hypothesis can be achieved only with a positive evidence of physics beyond the SM exhibiting the flavour pattern (link between $s \to d$, $b \to d$, and $b \to s$) predicted by the MFV assumption.

4 MFV in the lepton sector

Apart from arguments based on the analogy between quarks and leptons, the introduction of a MFV hypothesis for the lepton sector (MLFV) is demanded by a severe fine-tuning problem also in the lepton sector: within a generic EFT approach, the non-observation of $\mu \to e\gamma$ implies an effective NP scale above 10^5 TeV unless the coupling of the corresponding effective operator is suppressed by some symmetry principle.

Since the observed neutrino mass parameters are not described by the SM Yukawa interaction in Eq. (2), the formulation of a MLFV hypothesis is not straightforward. A proposal based on the assumption that the breaking of total lepton number (LN) and lepton flavour are decoupled in the underlying theory has recently been presented in Ref. [4], and further analysed in Ref. [7]. Two independent MLFV scenarios have been identified. They are characterized by the different status assigned to the effective Majorana mass matrix g_ν appearing as coefficient of the $|\Delta L| = 2$ dimension-five operator in the low energy effective theory [8]:

$$\mathcal{L}^\nu_{\rm eff} = -\frac{1}{\Lambda_{\rm LN}}\, g^{ij}_\nu (\overline{L}^{ci}_L \tau_2 H)(H^T \tau_2 L^j_L) + \text{h.c.} \quad \longrightarrow \quad m_\nu = \frac{g_\nu v^2}{\Lambda_{\rm LN}} \tag{5}$$

n the truly minimal scenario (dubbed *minimal field content*), g_ν and the charged-lepton Yukawa coupling (λ_e) are assumed to be the only irreducible sources of breaking of $\mathcal{G}_\ell$, the lepton-flavour symmetry of the low-energy theory.

The irreducible character of g_ν does not hold in many realistic underlying theories with heavy right-handed neutrinos. For this reason, a second scenario (dubbed *extended field content*), with heavy right-handed neutrinos and a larger lepton-flavour symmetry group, $\mathcal{G}_\ell \times {\rm O}(3)_{\nu_R}$, has also been considered. In this extended scenario, the most natural and economical choice about the symmetry-breaking terms is the identification of the two Yukawa couplings, λ_ν and λ_e, as the only irreducible symmetry-breaking structures. In this context, $g_\nu \sim \lambda_\nu^T \lambda_\nu$ and the LN-breaking mass term of the heavy right-handed neutrinos is flavour-blind (up to Yukawa-induced corrections):

$$\begin{aligned} \mathcal{L}_{\rm heavy} &= -\frac{1}{2} M^{ij}_\nu \overline{\nu}^{ci}_R \nu^j_R + \text{h.c.} \qquad M^{ij}_\nu = M_\nu \delta^{ij} \\ \mathcal{L}^{\rm ext}_Y &= \mathcal{L}_Y + i\lambda^{ij}_\nu \overline{\nu}^i_R (H^T \tau_2 L^j_L) + \text{h.c.} \end{aligned} \tag{6}$$

n this scenario the flavour changing coupling relevant to $l_i \to l_j \gamma$ decays reads

$$(\Delta^\ell_{\rm LR})_{\rm MLFV} \;\propto\; \lambda_e \lambda_\nu^\dagger \lambda_\nu \to \frac{m_e}{v}\,\frac{M_\nu}{v^2} U_{\rm PMNS}\, (m_\nu^{1/2})_{\rm diag} H^2 (m_\nu^{1/2})_{\rm diag}\, U^\dagger_{\rm PMNS} \tag{7}$$

where H is an Hermitian-orthogonal matrix which can be parametrized in terms of three real parameters (ϕ_i) which control the amount of CP-violation in the right-handed sector [9]. In the CP-conserving limit, $H \to I$ and the phenomenological

predictions for lepton FCNC decays turns out to be quite similar to the minimal field content scenario [4].

Once the field content of model is extended, there are in principle many alternative options to define the irreducible sources of lepton flavour symmetry breaking (see e.g. Ref. [10] for an extensive discussion). However, the specific choice discussed above has two important advantages: it is predictive and closely resemble the MFV hypothesis in the quark sector. The ν_R's are the counterpart of right-handed up quarks and, similarly to the quark sector, the symmetry-breaking sources are two Yukawa couplings.

The basic assumptions of the MLFV hypotheses are definitely less data-driven with respect to the quark sector. Nonetheless, the formulation of an EFT based on these assumptions is still very useful. As I will briefly illustrate in the following, it allows us to address in a very general way the following fundamental question: how can we detect the presence of new irreducible (fundamental) sources of LF symmetry breaking?

4.1 Phenomenological consequences on LFV decays

Using the MLFV-EFT approach, one can easily demonstrate that –in absence of new sources of LF violation– visible FCNC decays of μ and τ can occur only if there is a large hierarchy between Λ (the scale of new degrees of freedoms carrying LF) and $\Lambda_{\rm LN} \sim M_\nu$ (the scale of total LN violation) [4]. This condition is indeed realized within the explicit extensions of the SM widely discussed in the literature which predict sizable LF violating effects in charged leptons (see e.g. Ref. [11–14]).

More interestingly, the EFT allows us to draw unambiguous predictions about the relative size of LF violating decays of charged leptons (in terms of neutrino masses and mixing angles). At present, the uncertainty in the predictions for such ratios is limited from the poorly constrained value of the 1–3 mixing angle in the neutrino mass matrix (s_{13}) and, to a lesser extent, from the neutrino spectrum ordering and the CP violating phase δ. One of the clearest consequences from the phenomenological point of view is the observation that if $s_{13} \gtrsim 0.1$ there is no hope to observe $\tau \to \mu\gamma$ at future accelerators (see Fig. 2). This happens because the stringent constraints from $\mu \to e\gamma$ already forbid too low values for the effective scale of LF violation. In other words, in absence of new sources of LF violation the most sensitive FCNC probe in the lepton sector is $\mu \to e\gamma$. This process should indeed be observed at MEG [15] for very realistic values of the new-physics scales Λ and $\Lambda_{\rm LN}$. Interestingly enough, this conclusion holds both in the minimal- and in the extended-field-content formulation of the MLFV framework.

The expectation of a higher NP sensitivity of $\mu \to \mu\gamma$ with respect to $\tau \to \mu\gamma$ (taking into account the corresponding experimental resolutions) is confirmed in several realistic NP frameworks. This happens for instance in the MSSM scenarios

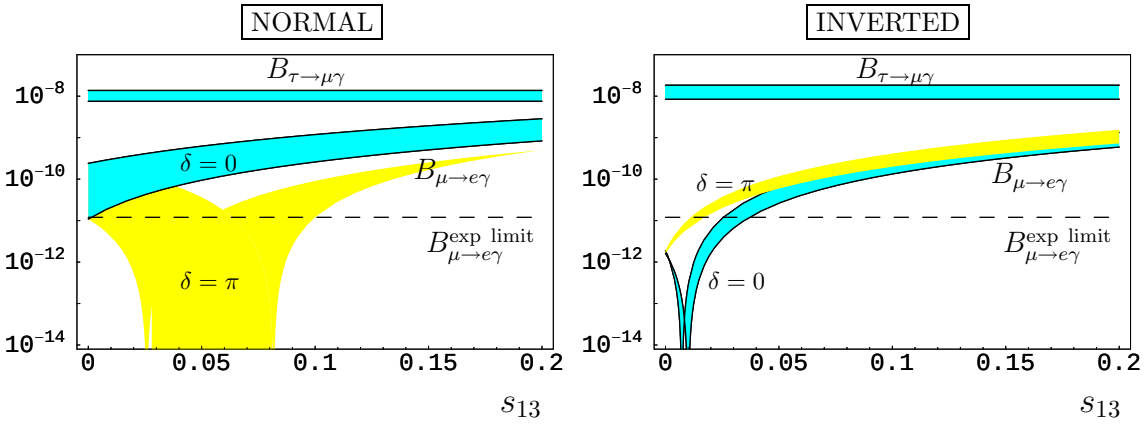

Figure 2: $B_{\tau\to\mu\gamma} = \Gamma(\tau \to \mu\gamma)/\Gamma(\tau \to \mu\nu\overline{\nu})$ compared to the $\mu \to e\gamma$ constraint within MLFV (minimal field content), as a function of the neutrino mixing angle s_{13} [4]. The shading corresponds to different values of the phase δ and the normal/inverted spectrum. The NP scales have been set to $\Lambda_{\rm LN}/\Lambda = 10^{10}$; their variation affects only the overall vertical scale.

analysed in Ref. [12–14] (see Fig. 3) with the exception of specific corners of the parameter space [12].

4.2 Leptogenesis

In the MLFV scenario with extended field content we can hope to generate the observed matter-antimatter asymmetry of the Universe by means of leptogenesis [16]. The viability of leptogenesis within the MLFV framework, which has recently been demonstrated in Ref. [17–19], is an interesting conceptual point: it implies that there are no phenomenological motivations to introduce new sources of flavour symmetry breaking in addition to the four λ_i (the three SM Yukawa couplings and λ_ν).

A necessary condition for leptogenesis to occur is a non-degenerate heavy-neutrino spectrum. Within the MLFV framework, the tree-level degeneracy of heavy neutrinos is lifted only by radiative corrections, which implies a rather predictive/constrained scenario. The most general form of the ν_R mass-splittings has the following structure:

$$\frac{\Delta M_R}{M_R} = c_\nu \left[\lambda_\nu\lambda_\nu^\dagger + (\lambda_\nu\lambda_\nu^\dagger)^T\right] + c^{(1)}_{\nu\nu} \left[\lambda_\nu\lambda_\nu^\dagger\lambda_\nu\lambda_\nu^\dagger + (\lambda_\nu\lambda_\nu^\dagger\lambda_\nu\lambda_\nu^\dagger)^T\right]$$
$$+c^{(2)}_{\nu\nu} \left[\lambda_\nu\lambda_\nu^\dagger(\lambda_\nu\lambda_\nu^\dagger)^T\right] + c^{(3)}_{\nu\nu} \left[(\lambda_\nu\lambda_\nu^\dagger)^T\lambda_\nu\lambda_\nu^\dagger\right] + c_{\nu l} \left[\lambda_\nu\lambda_e^\dagger\lambda_e\lambda_\nu^\dagger + (\lambda_\nu\lambda_e^\dagger\lambda_e\lambda_\nu^\dagger)^T\right] + \dots$$

Even without specifying the value of the c_i, this form allows us to derive a few general conclusions [17]:

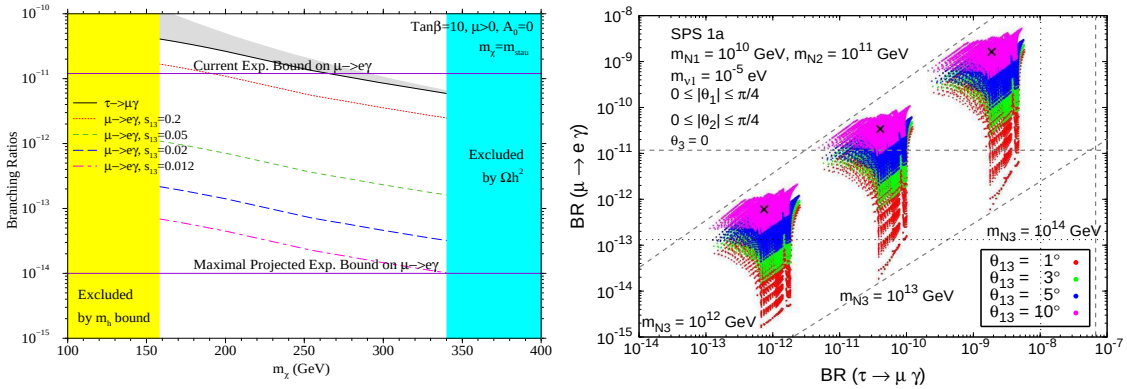

Figure 3: Left: Isolevel curves for $\mathcal{B}(\mu \to e\gamma)$ and $\mathcal{B}(\tau \to \mu\gamma)$ in the MSSM scenario of Ref. [13]. Right: $\mathcal{B}(\mu \to e\gamma)$ vs. $\mathcal{B}(\tau \to \mu\gamma)$ in the MSSM scenario of Ref. [14]

- The term proportional to c_ν does not generate a CPV asymmetry, but sets the scale for the mass splittings: these are of the order of magnitude of the decay widths, realizing in a natural way the condition of resonant leptogenesis.

- The right amount of leptogenesis can be generated even with $\lambda_e = 0$, if all the ϕ_i (the CP-violating parameters of H) are non vanishing. However, since $\lambda_\nu \sim \sqrt{M_\nu}$, for low values of M_ν ($\lesssim 10^{12}$ GeV) the asymmetry generated by the $c_{\nu l}$ term dominates. In this case η_B is typically too small to match the observed value and has a flat dependence on M_ν. At $M_\nu \gtrsim 10^{12}$ GeV the quadratic terms $c^{(i)}_{\nu\nu}$ dominate, determining an approximate linear growth of η_B with M_ν. These two regimes are illustrated in Fig.4.

As shown in in Fig.4, baryogenesis through leptogenesis is viable in MLFV models. In particular, assuming a loop hierarchy between the c_i (as expected in a perturbative scenario) and neglecting flavour-dependent effects in the Boltzmann equations (one-flavour approximation of Ref. [20]), the right size of η_B is naturally reached for $M_\nu \gtrsim 10^{12}$ GeV [17]. As shown in Ref. [18, 19], this lower bound can be weakened by the inclusion of flavour-dependent effects in the Boltzmann equations and/or by the tan β-enhancement of λ_e occurring in two-Higgs doublet models.

From the phenomenological point of view, an important difference with respect to the CP-conserving case is the fact that non-vanishing ϕ_i change the predictions of the LFV decays, typically producing an enhancement of the $\mathcal{B}(\mu \to e\gamma)/\mathcal{B}(\tau \to \mu\gamma)$ ratio. The effect of the new phases is moderate and the CP-conserving predictions are recovered only for $M_\nu \gg 10^{12}$ GeV.

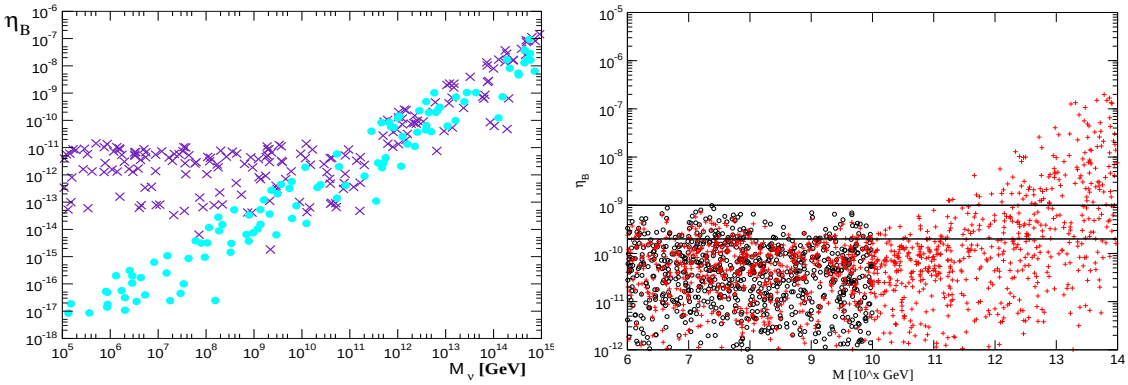

Figure 4: Left: Baryon asymmetry (η_B) as a function of the right-handed neutrino mass scale (M_ν) for $c_{\nu l} = 0$ (cyan circles) and $c_{\nu l} \neq 0$ (violet crosses) in the MLFV framework with extended field content [17]. Right: η_B as a function of M_ν with the inclusion of flavour-dependent effects [18].

5 MFV in Grand Unified Theories

Once we accept the idea that flavour dynamics obeys a MFV principle, both in the quark and in the lepton sector, it is interesting to ask if and how this is compatible with a grand-unified theory (GUT), where quarks and leptons sit in the same representations of a unified gauge group. This question has recently been addressed in Ref. [21], considering the exemplifying case of $\mathrm{SU}(5)_{\mathrm{gauge}}$.

Within $\mathrm{SU}(5)_{\mathrm{gauge}}$, the down-type singlet quarks (d^c_{iR}) and the lepton doublets (L_{iL}) belong to the $\overline{\mathbf{5}}$ representation; the quark doublet (Q_{iL}), the up-type (u^c_{iR}) and lepton singlets (e^c_{iR}) belong to the **10** representation, and finally the right-handed neutrinos (ν_{iR}) are singlet. In this framework the largest group of flavour transformation commuting with the gauge group is $\mathcal{G}_{\mathrm{GUT}} = \mathrm{SU}(3)_{\overline{5}} \times \mathrm{SU}(3)_{10} \times \mathrm{SU}(3)_1$, which is smaller than the direct product of the quark and lepton groups discussed before ($\mathcal{G}_q \times \mathcal{G}_l$). We should therefore expect some violations of the MFV+MLFV predictions, either in the quark sector, or in the lepton sector, or in both.

A phenomenologically acceptable description of the low-energy fermion mass matrices requires the introduction of at least four irreducible sources of $\mathcal{G}_{\mathrm{GUT}}$ breaking. From this point of view the situation is apparently similar to the non-unified case: the four $\mathcal{G}_{\mathrm{GUT}}$ spurions can be put in one-to-one correspondence with the low-energy spurions λ_u,λ_d, λ_e, and λ_ν. However, the smaller flavour group does not allow the diagonalization of λ_d and λ_e (which transform in the same way under $\mathcal{G}_{\mathrm{GUT}}$) in the same basis. As a result, two additional mixing matrices can appear in the expressions for flavour changing rates [21]. The hierarchical texture of the new mixing matrices is known since they reduce to the identity matrix in the limit $\lambda_e^T = \lambda_d$. Taking

into account this fact, and analysing the structure of the allowed higher-dimensional operators, a number of reasonably firm phenomenological consequences can be deduced [21]:

- There is a well defined limit in which the standard MFV scenario for the quark sector is fully recovered: $M_\nu \bar{l} l 10^{12}$ GeV and small $\tan\beta$ (in a two-Higgs doublet case). For $M_\nu \sim 10^{12}$ GeV and small $\tan\beta$, deviations from the standard MFV pattern can be expected in rare K decays but not in B physics.[1] Ignoring fine-tuned scenarios, $M_\nu \gg 10^{12}$ GeV is excluded by the present constraints on quark FCNC transitions. Independently from the value of M_ν, deviations from the standard MFV pattern can appear both in K and in B physics for $\tan\beta \gtrsim m_t/m_b$ (see the next section).

- Contrary to the non-GUT MFV framework, the rate for $\mu \to e\gamma$ (and other LFV decays) cannot be arbitrarily suppressed by lowering the average mass M_ν of the heavy ν_R. This fact can easily be understood by looking at the flavour structure of the relevant effective couplings, which now assume the following form:

$$(\Delta^\ell_{\rm LR})_{\rm MFV-GUT} = \; c_1 \; \lambda_e \lambda_\nu^\dagger \lambda_\nu \; + \; c_2 \; \lambda_u \lambda_u^\dagger \lambda_e \; + \; c_3 \; \lambda_u \lambda_u^\dagger \lambda_d^T \; + \; \ldots \qquad (8)$$

  In addition to the terms involving $\lambda_\nu \sim \sqrt{M_\nu}$ already present in the non-unified case, the GUT group allows also M_ν-independent terms involving the quark Yukawa couplings. The latter become competitive for $M_\nu \lesssim 10^{12}$ GeV and their contribution is such that for $\Lambda \lesssim 10$ TeV the $\mu \to e\gamma$ rate is above 10^{-13} (i.e. within the reach of MEG [15]).

- Improved experimental information on $\tau \to \mu\gamma$ and $\tau \to e\gamma$ are a now a key tool: the best observables to discriminate the relative size of the MLFV contributions with respect to the GUT-MFV ones. In particular, if the quark-induced terms turn out to be dominant, the $\mathcal{B}(\tau \to \mu\gamma)/\mathcal{B}(\mu \to e\gamma)$ ratio could reach values of $\mathcal{O}(10^{-4})$, allowing $\tau \to \mu\gamma$ to be just below the present exclusion bounds.

6 The large $\tan\beta$ scenario

The conclusions discussed in the previous section are very general and holds in most GUT theories. The large $\tan\beta$ regime represents a more specific corner of GUT

[1] The conclusion that K decays are the most sensitive probes of possible deviations from the strict MFV ansatz follows from the strong suppression of the $s \to d$ short-distance amplitude in the SM [$V_{td}V_{ts}^* = \mathcal{O}(10^{-4})$], and goes beyond the hypothesis of an underlying GUT. This is the reason why $K \to \pi\nu\overline{\nu}$ decays, which are the best probes of $s \to d$ $\Delta F = 1$ short-distance amplitudes [22], play a key role in any extension of the SM containing non-minimal sources of flavour symmetry breaking, as confirmed by recent analyses performed in the framework of the Little Higgs model with T parity [23], and in the MSSM with non-minimal A terms [24].

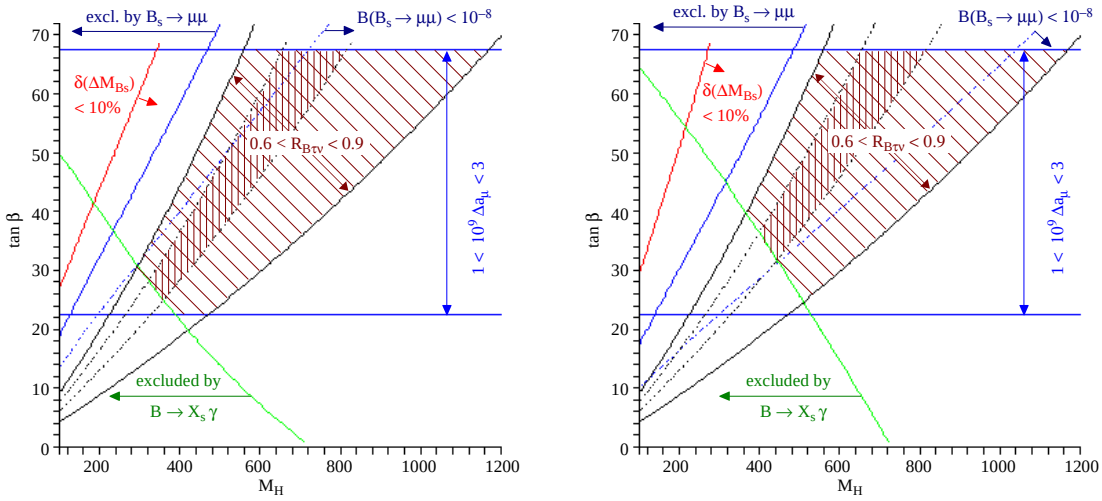

Figure 5: Correlations in the M_H–$\tan\beta$ plane within the MSSM for heavy squarks ($\mu = M_{\tilde{q}} = 2M_{\tilde{\ell}} = 3M_2 \approx 1$ TeV, $A_U = -/+ 1$ TeV in the left/right plot) [30]. $R_{B\tau\nu} = \mathcal{B}(B \to \tau\nu)/\mathcal{B}^{\rm SM}(B \to \tau\nu)$.

models, which is particularly interesting for flavour physics. Tan$\beta = v_u/v_d$, denotes the ratio of the two Higgs vacuum expectation values, which in many extensions of the SM are coupled separately to up- and down-type quarks (consistently with the MFV hypothesis). This parameter controls the overall normalization of the Yukawa couplings. The regime of large $\tan\beta$ [$\tan\beta = \mathcal{O}(m_t/m_b)$] has an intrinsic theoretical interest since it allows the unification of top and bottom Yukawa couplings, as predicted for instance in SO(10).

Since the b-quark Yukawa coupling become $\mathcal{O}(1)$, the large $\tan\beta$ regime is particularly interesting for B physics, even in absence of deviations from the MFV hypothesis. One of the most clear phenomenological consequences is the suppression of the $B \to \ell\nu$ decay rate with respect to its SM expectation [25]. Potentially measurable effects are expected also in $B \to X_s\gamma$, ΔM_{B_s} and, especially, in the helicity-suppressed FCNC decays $B_{s,d} \to \ell^+\ell^-$. The recent experimental evidence of $B \to \tau\nu$ at Belle [26] and Babar [28], the precise ΔM_{B_s} measurement by CDF [28], and the constantly improving bounds on $B_{s,d} \to \ell^+\ell^-$ by both CDF and D0 [29], make this scenario particularly interesting and timing from the phenomenological point if view.

Within the EFT approach where all the high degrees of freedom –but for the Higgs fields– are integrated out [3], we cannot establish well-defined correlations among these observables. However, the scenario becomes quite predictive within a more ambitious EFT: the MSSM with MFV. As recently shown in Ref. [30,31], in the MFV-MSSM with large $\tan\beta$ and heavy squarks, interesting correlations can be established

among the B observables mentioned above and two flavour-conserving observables: the anomalous magnetic moment of the muon and the lower limit on the lightest Higgs boson mass. An illustration of these correlations is shown in Fig. 5.

Present data are far from having established a clear evidence for such scenario (as for any deviation from the SM). Nonetheless, it is interesting to note that this scenario can naturally solve the long-standing $(g-2)_\mu$ anomaly and explain in a natural why the lightest Higgs boson has not been observed yet. Moreover, it predicts visible deviations from the SM in $\mathcal{B}(B \to \tau\nu)$ (most likely a suppression, of at least 10%) and $B_{s,d} \to \ell^+\ell^-$ (most likely a enhancement, up to a factor of 10), which could possibly be revealed in the near future. Finally, the parameter space which leads to these interesting effects can also naturally explain why $\mathcal{B}(B \to X_s\gamma)$ and ΔM_{B_s} are in good agreement with the SM expectations [30].

The observables $\mathcal{B}(B \to \tau\nu)$, $\mathcal{B}(B_{s,d} \to \ell^+\ell^-)$ and $(g-2)_\mu$ can be considered as the most promising low-energy probes of the MSSM scenario with heavy squarks and large $\tan\beta$. Nonetheless, interesting consequences of this scenario could possibly be identified also in other observables. In particular, as pointed out in [32], if the slepton sector contains sizable sources of LFV, we could even hope to observe violations of lepton universality in the $\mathcal{B}(P \to \ell\nu)/\mathcal{B}(P \to \ell'\nu)$ ratios. Deviations from the SM can be $\mathcal{O}(1\%)$ in $\mathcal{B}(K \to e\nu)/\mathcal{B}(K \to \mu\nu)$ [32], and can reach $\mathcal{O}(1)$ and $\mathcal{O}(10^3)$ in $\mathcal{B}(B \to \mu\nu)/\mathcal{B}(B \to \tau\nu)$ and $\mathcal{B}(B \to e\nu)/\mathcal{B}(B \to \tau\nu)$, respectively [30].

7 Conclusions

Rare decays of quarks and leptons provide a unique opportunity to shed more light on the underlying mechanism of flavour mixing. The discovery of neutrino oscillations, which has opened a new era in flavour physics, gives us more hopes in this respect. As we have shown by means of a general EFT approach to physics beyond the SM, under rather general hypothesis (quark-lepton unification and new physics in the TeV range) neutrino oscillations imply the existence of interesting non-standard effects also in rare decays of charged leptons and, possibly, in a few rare B and K decay observables.

The most solid and exciting expectation is a $\mu \to e\gamma$ branching ratio exceeding 10^{-13}, i.e. within the reach of the MEG experiment. In more specific scenarios, we could also observe sizable non-standard effects in rare FCNC τ and K decays and –particularly in the large $\tan\beta$ regime of the MSSM– in the purely leptonic decays of both charged and neutral B mesons.

Acknowledgments

It is a pleasure to thank Vincenzo Cirigliano, Ben Grinsten, Paride Paradisi, Valentina Porretti, and Mark Wise, for the enjoyable collaborations on which this talk is largely based. I also wish to thank organizers of HQL2006 for the invitation to this interesting conference. This work has been supported in part by the EU Contract No. MRTN-CT-2006-035482, "FLAVIAnet".

Bibliography

[1] R. S. Chivukula and H. Georgi, Phys. Lett. B **188** 1987 (99); L. J. Hall and L. Randall, Phys. Rev. Lett. **65**, 2939 (1990).

[2] A. Ali and D. London, Eur. Phys. Jour. C **9**1999687 [hep-ph/9903535]; A. J. Buras *et al.*, Phys. Lett. B **500** 2001 (161) [hep-ph/0007085]; S. Laplace, Z. Ligeti, Y. Nir and G. Perez, Phys. Rev. D **65**, 2002 (094040) [hep-ph/0202010]; A. J. Buras, Acta Phys. Polon. B **34** (2003) 5615 [hep-ph/0310208].

[3] G. D'Ambrosio, G. F. Giudice, G. Isidori and A. Strumia, Nucl. Phys. **B645**, 2002 (155) [hep-ph/0207036].

[4] V. Cirigliano, B. Grinstein, G. Isidori and M. B. Wise, Nucl. Phys. **B728**, 2005 (121) [hep-ph/0507001].

[5] M. Bona *et al.* [UTfit Collaboration], Phys. Rev. Lett. **97** (2006) 151803 [hep-ph/0605213].

[6] T. Feldmann and T. Mannel, hep-ph/0611095.

[7] V. Cirigliano and B. Grinstein, Nucl. Phys. B **752** (2006) 18 [hep-ph/0601111].

[8] S. Weinberg, Phys. Rev. Lett. **43**, 1566 (1979).

[9] S. Pascoli, S. T. Petcov and C. E. Yaguna, Phys. Lett. B **564**, 241 (2003) [hep-ph/0301095].

[10] S. Davidson and F. Palorini, Phys. Lett. B **642**, 72 (2006) [hep-ph/0607329].

[11] R. Barbieri, L. J. Hall and A. Strumia, Nucl. Phys. **B445**, 1995 (219) [hep-ph/9501334].

[12] J. R. Ellis, J. Hisano, M. Raidal and Y. Shimizu, Phys. Rev. D **66** (2002) 115013 [hep-ph/0206110].

[13] A. Masiero, S. Profumo, S. K. Vempati and C. E. Yaguna, JHEP **0403** (2004) 046 [hep-ph/0401138].

[14] S. Antusch, E. Arganda, M. J. Herrero and A. M. Teixeira, JHEP **0611** (2006) 090 [hep-ph/0607263].

[15] M. Grassi [MEG Collaboration], Nucl. Phys. Proc. Suppl. **149** (2005) 369.

[16] M. Fukugita and T. Yanagida, Phys. Lett. B **174**, 45 (1986).

[17] V. Cirigliano, G. Isidori and V. Porretti, Nucl. Phys. B **763** (2007), 228 [hep-ph/0608123].

[18] G. C. Branco, A. J. Buras, S. Jager, S. Uhlig and A. Weiler, hep-ph/0609067.

[19] S. Uhlig, hep-ph/0612262.

[20] S. Blanchet and P. Di Bari, JCAP **0606**, 023 (2006) [hep-ph/0603107].

[21] B. Grinstein, V. Cirigliano, G. Isidori and M. B. Wise, Nucl. Phys. B **763** (2007) 35 [hep-ph/0608123].

[22] For recent reviews see: U. Haisch, hep-ph/0605170; D. Bryman, A. J. Buras, G. Isidori and L. Littenberg, Int. J. Mod. Phys. A **21**, 487 (2006) [hep-ph/0505171]; A. J. Buras, F. Schwab and S. Uhlig, hep-ph/0405132.

[23] M. Blanke *et al.*, JHEP **0701** (2007) 066 [hep-ph/0610298]; C. Tarantino, hep-ph/0702152 (these proceedings).

[24] G. Isidori *et al.*, JHEP **0608** (2006) 064 [hep-ph/0604074].

[25] W. S. Hou, Phys. Rev. D **48** (1993) 2342.

[26] K. Ikado *et al.*, Phys. Rev. Lett. **97** (2006) 251802 [hep-ex/0604018].

[27] B. Aubert *et al.* [BABAR Collaboration], hep-ex/0608019.

[28] A. Abulencia *et al.* [CDF Collaboration], Phys. Rev. Lett. **97** (2006) 062003 [hep-ex/0606027].

[29] R. Bernhard *et al.* [CDF Collaboration], hep-ex/0508058.

[30] G. Isidori and P. Paradisi, Phys. Lett. B **639** (2006) 499 [hep-ph/0605012].

[31] E. Lunghi, W. Porod and O. Vives, Phys. Rev. D **74**, 075003 (2006) [hep-ph/0605177].

[32] A. Masiero, P. Paradisi and R. Petronzio, Phys. Rev. D **74** (2006) 011701 [hep-ph/0511289].

Program

HQL06 Scientific Program

Monday, October 16, 2006

Time	Session	Talk	Speaker
9:15	Opening	Prof. Heckl (Dt. Museum), Prof. Laubereau (Dean), Prof. Hoang (MPI), Prof. Paul (TUM)	
9:45	HQS	New states: ccbar and charmed mesons	Prof. T. Lesiak
10:30	HQS	Recent Results in Bottomonium Physics	T. Pedlar (CLEO)
10:55	Coffee		
11:30	HQS	SELEX results	J. Engelfried (Selex)
11:50	HQS	NRQCD and Quarkonia	N. Brambilla
12:35	HQS	B lifetimes, CPV and rare decays	A. Cano (CDF)
13:05	Lunch		
14:35	HQS	Charmonium Physics with PANDA	J. Ritman
14:55	Kaons	New Results on Neutral Hyperon Decays	R. Wanke
15:20	Kaons	The Search for New Physics in Hyperon Decays with HyperCP	E.C. Dukes
15:45	Kaons	Rare K and B-decays	A. Weiler
16:30	Coffee		
17:05	Kaons	Rare K-decays (KTEV&NA48)	M. Arenton
17:50	Kaons	Ke4 decays and Wigner CUSP	L. Masetti
18:15		End of session	
19:30	Reception	Wirtshaus in der Au, Lilienstr. 51	

Tuesday, October 17, 2006

Time	Session	Talk	Speaker
9:15	Kaons	New Results from KLOE	R. Versaci
9:40	Kaons	KL decays into n p's + gamma	E. Cheu
10:05	Kaons	New results on B_s at CDF	S. Menzemer (CDF)
10:40	LSLD	Global HQE fit to moments in $B \to X_c l\nu$ and in $B \to X_s\gamma$ decays	O. Buchmüller
11:05	Coffee		
11:35	LSLD	Theory of Semileptonic B Decays	T. Mannel
12:20	LSLD	New Physics search in B decays and Super B factories	T Iijima (Belle)
12:45	Lunch		
14:15	LSLD	Charmless B-decays	W. Gradl (BaBar)
15:00	LSLD	Leptonic and Semileptonic D-decays	H. Mahlke (CLEO)
15:30	LSLD	Exclusive s.l. B-decays ($b \to c$)	A.E. Snyder (BaBar)
15:55	Coffee		
16:40	LSLD	Semileptonic $b \to u$ transition	E. Won (Belle)
17:10	LSLD	K and B Physics in the Littlest Higgs Model with T-Parity	C. Tarantino
17:40	LSLD	D decays	S. Fajfer
18:25	LSLD	Review of Charm Mixing	D. Asner (CLEO)
18:50		End of session	

Wednesday, October 18, 2006

Time	Session	Talk	Speaker
9:15	CP	CP-Violation and B physics@LHC	R. Fleischer
10:00	CP	CP-Violation: the Unitarity Triangle angle α	Ch.Touramanis (BaBar)
10:35	Coffee		
11:00	HHD	Hadronic D and Ds decays, including Dalitz plot analyses	D. Cassel (CLEO)
11:30	CP	CP-Violation Angle gamma	H. Yamamoto (Belle)
12:00	CP	$K^+ \to 3\pi$ with Na48/2	G. Lamanna
12:25	CP	Proposal for a new measurement with NA48(/3)	G. Ruggiero
12:50	Lunch		
14:00		Tours start at Deutsches Museum	
19:30		Departure to Dinner from Deutsches Museum	
20:00		Conference dinner: Taxisgarten, Taxisstr. 12	

Thursday, October 19, 2006

Time	Session	Talk	Speaker
9:15	CP	Searches for permanent Electric Dipole Moments	K. Jungmann
9:45	CKM	New evaluation of the CKM-matrix and Unitarity	A. Stocchi
10:15	CKM	New results for Vus from KLOE, KTEV and NA48	V. Kozhuharov
10:45	CP	CP-Violation in B decays - the angle beta	G. Dubois-Felsmann (BaBar)
11:15	Coffee		
11:45	HDD	Spectroscopy, Lifetimes and Decays of B hadrons	M. Paulini (CDF)
12:15	HHD	Lifetimes and oscillations of heavy mesons	A. Lenz
12:40	HHD	Lattice QCD, Flavor Physics and the Unitarity Triangle Analysis	V. Lubicz
13:10	Lunch		
14:35	HHD	Theory of non-leptonic B-decays	M. Beneke
15:05	HHD	Top physics results at the Tevatron	L. Cerrito (CDF)
15:50	HS	Charm & Beauty structure of the proton	R. Brugnera
16:20	Coffee		
17:00	Neutrinos	Theory and Phenomenology of Neutrino Mixing	C. Giunti
17:45	Neutrinos	Majorana Neutrinos	F: Ferroni
18:10	Neutrinos	Astrophysical neutrinos	L. Oberauer
18:35		End of session	

Friday, October 20, 2006

Time	Session	Talk	Speaker
9:15	Neutrinos	Future strategy of neutrino Experiments	H. Minakata
10:00	Neutrinos	Latest results from MINOS	D. Jaffe
10:25	HL	Lepton Flavour Violation and Rare Lepton Decays	T. Mori
10:55	Coffee		
11:30	Closing Talk	Outlook	G. Isidori
12:25		Award for young scientists (best speaker)	
12:35		End of conference	

Participants

HQL06 Participants

	Michaela	Albrecht
	Wolfgang	Altmannshofer
Dr.	Michael	Arenton
Dr.	Arthur	Snyder
Dr.	David	Asner
	Cano	Ay
Prof.	Martin	Beneke
Dr.	Stefano	Bianco
	Monika	Blanke
	Nora	Brambilla
Dr.	Riccardo	Brugnera
Prof.	Gerhard	Buchalla
Dr.	Oliver	Buchmuller
Prof. Dr.	Andrzej	Buras
Dr.	Lucio	Cerrito
Dr.	Elliott	Cheu
Prof.	Brad	Cox
Prof.	Cassel	David
	Anna-Maria	Dinkelbach
Prof.	Helmut	Koch
Dr.	Gregory	Dubois-Felsmann
Prof.	Edmond	Dukes
	Björn	Duling
	Johannes	Eiglsperger
Dr.	Jurgen	Engelfried
	Thorsten	Ewerth
Prof.	Franco	Fabbri
Prof.	Svjetlana	Fajfer
Prof. Dr.	Francisco	Fernandez
Prof.	Fernando	Ferroni
Dr.	Robert	Fleischer
	Karin	Frank
Dr.	Jan Michael	Friedrich
Dr.	Carlo	Giunti
	Stefanie	Grabmueller
Dr.	Wolfgang	Gradl
Dr.	Diego	Guadagnoli
	Florian	Haas

	Hassan	Hassanabadi
Dr.	Andre	Hoang
	Tina	Huber
Prof.	Toru	Iijima
Dr.	Christoph	Ilgner
Dr.	Gino	Isidori
	David	Jaffe
Dr.	Sebastian	Jäger
	Merkel	Jesko
Prof.	Klaus	Jungmann
Dr.	Bernhard	Ketzer
Prof.	Konrad	Kleinknecht
Mr.	Venelin	Kozhuharov
	Roland	Kuhn
Dr.	Gianluca	Lamanna
PD Dr.	Alexander	Lenz
Prof.	Tadeusz	Lesiak
Prof.	Cai-Dian	Lu
Prof.	Vittorio	Lubicz
Prof.	Vera	Luth
Dr.	Hai Long	Ma
Dr.	Hanna	Mahlke
Prof.	Manfred	Paulini
Prof.	Thomas	Mannel
Prof.	Giancarlo	Mantovani
	Lucia	Masetti
	Dmytro	Melnychuk
Dr.	Stephanie	Menzemer
Prof.	Hisakazu	Minakata
Prof.	Toshinori	Mori
	Thiemo	Nagel
	Sebastian	Neubert
Prof.	Lothar	Oberauer
Prof	Stephan	Paul
Dr.	Todd	Pedlar
Prof.	Vladimir	Penev
Prof. Dr.	Klaus	Peters
	Maurizio	Pierini
	Anton	Poschenrieder
	Christoph	Promberger
Dr.	Stefan	Recksiegel

	Carola	Reinke
Prof.	Saurabh	Rindani
Prof.	James	Ritman
Dr.	Giuseppe	Ruggiero
	Sebastian	Schatt
	Felix	Schwab
	David	Straub
	Achille	Stocchi
Dr.	Cecilia	Tarantino
Dr.	Christos	Touramanis
	Robert	Tschirhart
	Selma	Uhlig
Dr.	Roberto	Versaci
Dr.	Rainer	Wanke
	Andreas	Weiler
Prof.	Wolfram	Weise
	Michael	Wick
Dr.	Andreas	Winhart
Prof.	Eunil	Won
Prof.	Hitoshi	Yamamoto
Dr.	Zhou	Yufeng

Pictures

Pictures


DEUTSCHES
MUSEUM


KARL FRIEDRICH GA
OTTO von GUERICKE

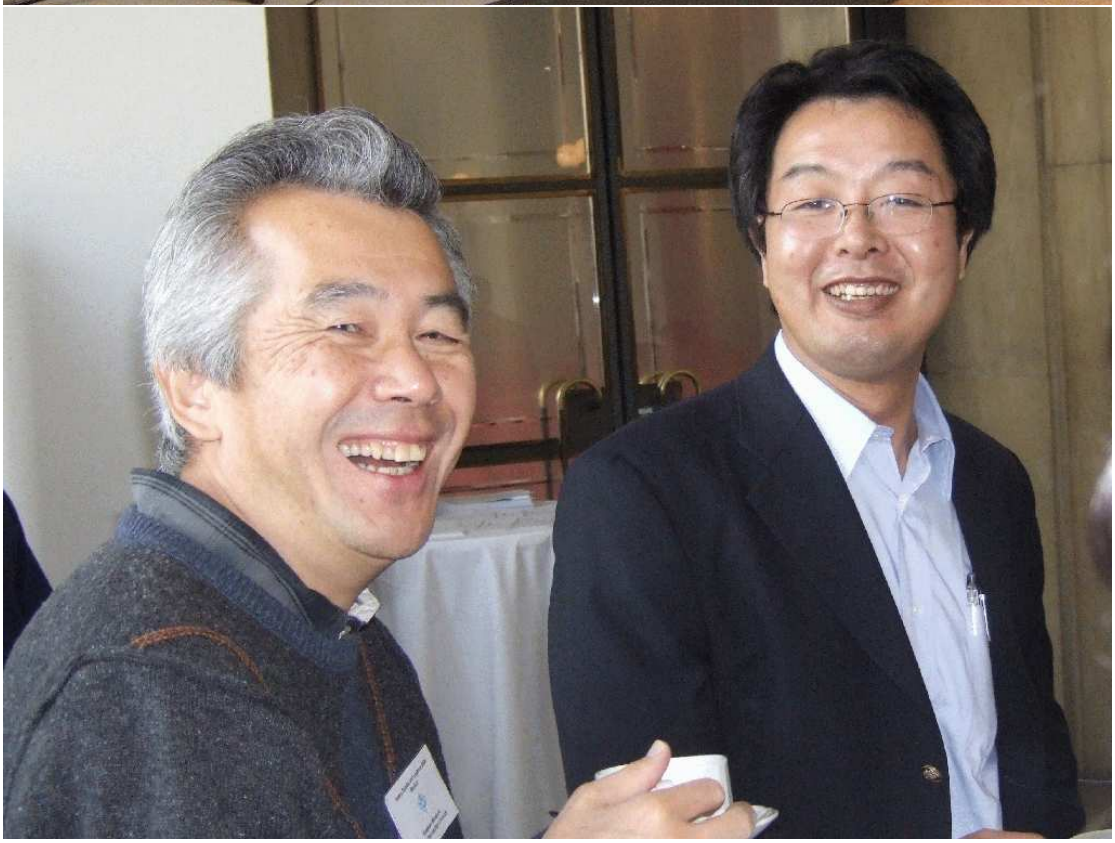


Deutsches Museum
LISE MEITNER
HEINRICH HERTZ


DIE ARCHITEKTEN
DES MUSEUMSBAUTEN


KARL FRIEDRICH GAUSS

Author Index